Physics of Atomic Nuclei, Vol. 64, No. 3, 2001, pp. 365–366. Translated from Yadernaya Fizika, Vol. 64, No. 3, 2001, pp. 419–420.

90th ANNIVERSARY OF A.B. MIGDAL'S BIRTHDAY

Arkadiĭ Benediktovich Migdal (March 11, 1911–February 9, 1991)

Arkadiĭ Benediktovich Migdal, an acclaimed theoretical physicist, would have celebrated his 90th birthday on March 11. Had it not been for the sudden and fatal illness that cut short his life a month before he reached the age of 80, Migdal's creative activity would certainly have continued much longer. Indeed, in the summer of 1990 (that is, just before the first symptoms of the disease revealed themselves), Prof. Migdal was still strong enough to challenge his younger colleagues in the Caucasus mountains, where he spent his vacation.

Arkadiĭ Migdal was born in Lida, a small town in western Byelorussia, but he shortly moved to Leningrad (St. Petersburg), together with his parents. It was in Leningrad where he was fascinated by science. That Migdal came of "nonproletarian" parents was a hovering threat to his scientific career: as a student, he was evicted from the Leningrad University and even had to spend 70 days in jail (a relatively mild penalty for those years of massive repression). Fortunately, Migdal was able to return to the university and to take his first lessons in physics from M.P. Bronshteĭn—a brilliant theoretical physicist, whom his peers compared to L.D. Landau. Those lessons proved to be brief: in 1937, Bronshteĭn was arrested and then executed. For a while, A. Migdal was tutored in Leningrad by V.A. Fock and then moved to Moscow to join L.D. Landau's group as a postgraduate. By that time, A. Migdal had largely matured as a physicist with an original approach to scientific problems. This could be seen from the very first studies of his, which date back to the Leningrad period and which were devoted to neutron–atom interactions. There, Migdal proposed the shakeup method, which has since then been included in textbooks on quantum mechanics and which has found many applications in various realms of physics. In particular, Migdal himself employed this method in theoretically describing the alpha- and beta-decay-induced ionization of atoms.

Migdal's awesome career in physics may be naturally divided into three periods. Over the first period, which extended approximately to the mid-1950s, Migdal tackled a broad diversity of problems in various areas of physics. His earliest studies were devoted to atomic physics and the theory of the nucleus. In 1945, Migdal was appointed head of the theory division at Kurchatov's center for atomic energy. Of his collaborators in the "atomic project," G.I. Budker, V.M. Galitsky, B.T. Geilikman, and S.T. Belyaev later won broad recognition. The research agenda was largely dictated by military needs and included plasma physics and the theory of nuclear reactors. Yet, Migdal was able to give much attention to pure physics: in 1946, he addressed the problem of nuclear photoeffect, where he developed a theory that predicted, among other things, the existence of a giant dipole resonance and which made it possible to estimate its position. It is remarkable that, within Migdal's formalism, which was essentially model-independent, the position of the resonance was expressed solely in terms of the parameters in the Weizsäcker formula. Because of the relative isolation of Soviet science, Western physicists failed to notice and appreciate Migdal's predictions in due time. Shortly after the experimental observation of a giant dipole resonance in 1947, a model description of the phenomenon was proposed by M. Goldhaber and E. Teller, who were wrongly credited as pioneers in the field. It took the physics community considerable time to acknowledge finally Migdal's priority in predicting the giant dipole resonance and in estimating its position.

Yet another outstanding result obtained by Migdal in that period concerns the resonance final-state interaction of slow particles formed in nuclear reactions,

1063-7788/01/6403-0365$21.00 © 2001 MAIK "Nauka/Interperiodica"

which has been known since then as the Migdal–Watson effect. Last but not least, Migdal was able to construct a quantitative description of the phenomenon dubbed the Landau–Pomeranchuk effect and associated with the coherent multiple rescattering of a relativistic particle in matter. It was with great relish that Migdal used to recollect an episode when Prof. I.Ya. Pomeranchuk, whom he held in very high esteem, took off his hat in appreciation of Migdal's accomplishment. The thing is that Landau and Pomeranchuk themselves provided a qualitative picture of coherent rescattering, but they stopped short of quantitatively tackling the problem, deeming that this was impossible. Migdal pledged to do the impossible and succeeded! For this, he had to devise a novel method of quantum kinetic equations. Nowadays, the effect of coherent rescattering plays a key role in our understanding of collisions between ultrarelativistic nuclei, which is based on QCD. That this phenomenon is now referred to as the Landau–Pomeranchuk–Migdal effect duly acknowledges Migdal's contribution to the subject.

The second period of Prof. Migdal's career, albeit rather short (it spans the second half of the 1950s), proved to be rich in remarkable results. Those years saw the emergence and rapid development of a new theoretical approach to problems in condensed-matter physics, that which is based on methods of quantum field theory. Together with his disciples Galitsky and Belyaev, Prof. Migdal made hefty contributions to the subject. Of particular importance are his study of 1957, where he proved the theorem of a jump in the momentum distribution of particles in an arbitrary Fermi system (Migdal's jump), and two studies of 1958. In one of the last two, he, together with Galitsky, developed a theoretical description of Fermi systems in terms of Green's functions, while, in the other, he successfully applied this method to electron–phonon interactions in metals. Since then, these classical results have been cited in all textbooks on the theory of many-body systems. Prof. Migdal's study of 1959, where he applied his original methods to quantify the superfluidity effect on nuclear moments of inertia and where he hypothesized, for the first time (this hypothesis is widely used at present), superfluidity in neutron stars, also belongs to that period.

The aforementioned analysis of nuclear moments of inertia marked a transition to the third period of Prof. Migdal's investigations, which was entirely devoted to nuclear physics. In the early 1960s, Migdal and his pupils were able to develop a quantitative theory of nuclei treated as many-body systems, which has since then been referred to as the theory of finite Fermi systems. These investigations were summarized in a monograph published in 1965 and translated into English in 1967 under the title *Theory of Finite Fermi Systems and Application to Atomic Nuclei* (Interscience, New York). So far, it has been a handbook for many theoretical nuclear physicists worldwide.

In the early 1970s, Prof. Migdal took interest in phenomena induced by strong fields. This led him to studying pionic and isobar degrees of freedom in nuclei. In 1971, he put forth the elegant idea that the ground state of a nucleus might undergo rearrangement giving rise to a Bose condensate of pions modified by nuclear matter (so-called pion condensate). That exciting idea spawned a torrent of studies elsewhere. Migdal and his pupils were the first to realize that, under normal conditions, there is no pion condensate in nuclei. However, the possibility of its formation in the superdense nuclear matter of a neutron star or in high-energy ion–ion collisions has been discussed so far. This idea gave impetus to the construction of a series of heavy-ion accelerators and to an intense development of nuclear physics.

In the 1980s, the focus of Migdal's attention switched to QCD, where, as usual, he addressed the basic problem, that of confinement. Migdal failed to develop a consistent theory of confinement (no such theory has been created so far), but he derived a number of important results, which were highly appraised by QCD pundits.

Migdal was a gifted teacher of physics. At the Moscow Institute of Engineering Physics, where he taught for many years, Prof. Migdal delivered a number of original lecture courses that provided ample material for two broadly known monographs (published by him partly in collaboration with V.P. Krainov): *Approximate Methods in Quantum Mechanics* (Benjamin, New York, 1969) and *Approximate Methods in Physics*.

Toward the end of his life, Migdal often reflected on the philosophic and psychological aspects of science and publicized his ideas on the subject. A passionate and many-sided personality, Migdal showed true talent in anything he was keen on. For example, he shot the first submarine films in the Soviet Union, which won prizes at many contests, and his sculptures were highly appraised by professional artists. He was also a great story teller and easily captivated the attention of any audience.

Migdal's impact on science would not be restricted to his articles and monographs: in fact, he created a robust scientific school, and many of his pupils rose to eminence themselves. Of the people who have contributed to the memorial issues of *Yadernaya Fizika* (*Physics of Atomic Nuclei*), some are lucky to be Migdal's immediate pupils, others are pupils of the pupils, and still others, albeit not directly belonging to his school, were more or less affected by his ideas and personality. So many are the received contributions that three consecutive issues (instead of a single one planned originally) of the journal will be devoted to the memory of Prof. Migdal. In a sense, the physics results reported in these memorial issues may be viewed as part of Migdal's legacy.

E.E. Saperstein

Physics of Atomic Nuclei, Vol. 64, No. 3, 2001, pp. 367–392. Translated from Yadernaya Fizika, Vol. 64, No. 3, 2001, pp. 421–446.

90th ANNIVERSARY OF A.B. MIGDAL'S BIRTHDAY
NUCLEI

Critical Charge in Quantum Electrodynamics

V. S. Popov

Institute of Theoretical and Experimental Physics, Bol'shaya Cheremushkinskaya ul. 25, Moscow, 117259 Russia

Received July 5, 2000

Abstract—The critical nuclear charge Z_{cr} and the critical distance R_{cr} in the system of two colliding heavy nuclei—they are defined as those at which the ground-state level of the electron spectrum descends to the boundary of the lower continuum, with the result that beyond them (that is, for $Z > Z_{cr}$ or $R < R_{cr}$) spontaneous positron production from a vacuum becomes possible—are important parameters in the quantum electrodynamics of ultrastrong Coulomb fields. Various methods for calculating Z_{cr} and R_{cr} are considered, along with the dependence of these quantities on the screening of the Coulomb field of a nucleus by the electron shell of the atom, on an external magnetic field, on the particle mass and spin, and on some other parameters of relevance. The effective-potential method for the Dirac equation and the application of the Wentzel–Kramers–Brillouin method to the Coulomb field for $Z > 137$ and to the two-body Salpeter equation for the quark–antiquark system are discussed. Some technical details in the procedure for calculating the critical distance R_{cr} in the relativistic problem of two Coulomb centers are described. © *2001 MAIK "Nauka/Interperiodica".*

Dedicated to the blessed memory
of Arkadiĭ Benediktovich Migdal
and Mikhail Samuilovich Marinov

Es war … eine Zeit die Riesen brauchte und Riesen zeugte,
Riesen an Denkkraft, Leidenschaft und Character,
an Vielseitigkeit und Gelehrsamkeit.
Friedrich Engels "Dialektik der Natur"[1)]

Mighty, Immense, and Great is the Distant Astral Law …

1. INTRODUCTION

Thirty years ago, there arose interest in the predictions of quantum electrodynamics (QED) in ultrastrong Coulomb fields—in particular, in the effect of spontaneous positron production from a vacuum (see, for example, [1–30] and the review articles [7, 31–39]). A feature peculiar to this process is that it has no bearing on the frequency of an electric field and can occur in the case of an arbitrarily slow (adiabatic) growth of the nuclear charge in the region $Z > Z_{cr}$, a point where it differs from any other positron-production mechanism known so far. Moreover, its probability cannot be computed by perturbation theory,[2)] so that it is necessary to analyze exact solutions to the Dirac equation in an external field.

The problem was formulated by Pomeranchuk and Smorodinsky [40], who considered, as far back as 1945, the energy spectrum of an electron in a Coulomb field with allowance for a finite radius of a nucleus and obtained the first ever estimate for Z_{cr}. After that, however, the problem was not investigated for a long time.

After the year 1969, there appeared a torrent of theoretical studies devoted to this and some other allied problems. Various aspects of spontaneous positron production (as well as of accompanying processes like induced positron production, which is associated with a nonzero frequency of the electric field as the nuclei involved approach; pair conversion in the case of the Coulomb excitation of colliding nuclei; and delta-electron production[3)]) were analyzed in detail both for the case of an isolated superheavy nucleus and for the case where two heavy nuclei such that $Z_1 + Z_2 > Z_{cr}$—for example, uranium nuclei—approach each other. The theoretical description of the structure of the vacuum electron shell of a supercritical ($Z > Z_{cr}$) atom in [7, 15–17] proved to be somewhat out of the ordinary. This range of problems was comprehensively analyzed in the review articles [7, 31–39], where the interested reader can find all necessary details.

[1)] It was ... a time which called for giants and produced giants—giants in power of thought, passion and character, in universality and learning [quoted from Friedrich Engels, *Dialectics of Nature* (Progress Publishers, Moscow, 1982; translated from the German by Clemens Dutt)].

[2)] The probability of spontaneous positron production exhibits a nonanalytic (in the parameter $\zeta = Z\alpha$, α being the fine-structure constant) threshold behavior for $Z \longrightarrow Z_{cr}$ [see Eq. (37) below].

[3)] These accompanying processes must be taken into account in performing relevant experiments. For all these questions, the reader is referred to [7, 10, 21, 25, 39].

1063-7788/01/6403-0367$21.00

The present article, whose objective is less ambitious, is aimed at describing and discussing various methods for calculating the critical nuclear charge Z_{cr} and the critical distance R_{cr} for a collision of two heavy nuclei, as well as at analyzing some equations for the energies of the levels of the electron spectrum in the region $Z \gtrsim Z_{cr}$. The above quantities are basic physical parameters of the problem, which appear in all equations that are used in the theory of spontaneous positron production. At the same time, these questions have not yet received adequate attention in the surveys known to the present author.

In the following, use is made, as a rule, of the system of units where $\hbar = c = m = 1$ (m is the electron mass); distances and ε, the energy of a level, are measured in, respectively, $\hbar/mc = 386.2$ fm and mc^2 units; $\alpha = e^2/\hbar c = 1/137$; and $\zeta = Z\alpha$. The rest energy is included in ε, so that the values of $\varepsilon = 1$ and -1 correspond, respectively, to a free electron at rest (boundary of the upper continuum for solutions to the Dirac equation) and to the boundary of the lower continuum.

This article is dedicated to the memory of Arkadiĭ Benediktovich Migdal (1911–1991) and Mikhail Samuilovich Marinov (1939–2000). Discussions with Arkadiĭ Benediktovich (AB as we called him in a narrow circle of physicists) on various aspects of the QED of strong fields, as well as on a wider range of physical (and not only physical) topics, were always extremely interesting and instructive for me. Recollecting the past, I would like to mention some features that were calling cards of his personality as it remained in my memory. First, it was his desire to understand always the result of any complicated calculations in simple physical terms or on the basis of an appropriate model. Second, it was AB's love for the semiclassical approach, which he knew in minute detail and was able to apply to intricate physics problems (in this connection, see, for example, his remarkable monograph [41]). Third, AB was highly democratic: he would have discussed scientific problems in just the same way with a student and with an academician, while his disapproval of some ideas, which was sometimes expressed very sharply, never became personal (I know this from my own experience). Finally, it was his scientific audacity: for example, AB was not afraid to admit violation of the Pauli exclusion principle for electrons that have descended to the lower continuum [30] and had stubbornly advocated his opinion for quite a long period of time despite the objections and criticism of many Soviet theoretical physicists.[4)] These are the features of AB's scientific style that impressed me most deeply. It would be no wonder to me, however, if such a list as composed by some other contemporary of AB were totally different—is it not true that he was so forceful and diverse a personality that he could be compared (in my opinion) to such creators of the Renaissance period as Geronimo Cardano or Benvenuto Cellini?

I would also like to recollect the discussion on the problem of positron levels that would emerge with increasing Z from the lower continuum. It was in 1970, and it was AB, YaB (Yakov Borisovich Zeldovich), and the present author who participated in this discussion. At that time, AB firmly believed in the existence of such states, while YaB and I questioned this and raised some objections. Our objections annoyed AB, and the discussion became very hot. Finally, Yakov Borisovich said, "Kadya, you have forgotten about the Pauli exclusion principle." The reaction of AB was instantaneous and tempestuous, and everything ended in the following words of Yakov Borisovich: "Kadya, let us finish today at this point, but do not think, please, that I could not answer to you properly and in the same tone, but the presence of Vladimir Stepanovich troubles me somewhat." This scene is still before my eyes, but I do not take courage to go in further details, for this requires greater writing abilities. This episode was reflected in part in the article written by Zeldovich and the present author [7].

Many years of friendship and cooperation connected me with Misha Marinov (some results of our joint work—in particular, those concerning spontaneous positron production—were used in the present article, especially in Section 3), who was a highly educated physicist and who possessed a deep knowledge of mathematics and a great pedagogical talent. I recall with admiration lectures (brilliant in form and excellent in content) on exceptional Lie groups, Cayley octanions, and Grassmann numbers that Misha delivered at the Institute of Theoretical and Experimental Physics (Moscow) shortly after these mathematical constructions (nearly unknown to theoretical physicists at that time) had come into use in the theory of elementary particles.

2. CRITICAL CHARGE OF A NUCLEUS

The discrete spectrum of the energy levels of an electron moving in the Coulomb field of a nucleus falls within the range $-1 \le \varepsilon < 1$. The problem admits an analytic solution in the case of a pointlike charge, where the energy levels are determined by the well-known Sommerfeld fine-structure formula [42]. For example, the energy of the $1s_{1/2}$ ground-state term in the Coulomb field $V(r) = -\zeta/r$ is given by

$$\varepsilon_0(\zeta) = \sqrt{1-\zeta^2}, \quad 0 < \zeta = Z\alpha < 1. \qquad (1)$$

The curve of the $1s$ level terminates at $Z = \alpha^{-1} = 137$ and $\varepsilon_0 = 0$, not reaching the boundary of the lower contin-

[4)] Of course, AB was wrong in this case, but this example is a good illustration of a feature that was peculiar to his personality—the total absence of reverence for commonly recognized authorities.

uum. For the energy-degenerate $ns_{1/2}$ and $np_{1/2}$ states for $\zeta \longrightarrow 1$, we similarly have

$$\varepsilon_n(\zeta) = \frac{n-1}{N_0} + \frac{1}{N_0^3}\sqrt{1-\zeta^2} + O(1-\zeta^2), \qquad N_0 = \sqrt{n^2 - 2n + 2}, \tag{1a}$$

where $n = 0, 1, 2, \ldots$ is the principal quantum number. A formal analytic continuation of $\varepsilon_n(\zeta)$ to the region $Z > 137$ leads to imaginary values of energy and complex-valued wave functions, but this is unsatisfactory from the physical point of view.[5)] The reason behind the emergence of this difficulty can easily be traced with the aid of the effective-potential method [4, 7, 18].

For the sake of simplicity, we begin by considering the case of spherical symmetry, $V = V(r)$. Upon a separation of the variables, the Dirac equation in a central field reduces to a set of differential equations for the radial wave functions $g(r)$ and $f(r)$. The substitution

$$\varphi = W^{-1/2} g, \quad W = 1 + \varepsilon - V(r), \tag{2}$$

where g corresponds to the upper component of the Dirac bispinor [45], recasts these equations into a form similar to the Schrödinger equation but with an effective energy E and an effective potential U. Specifically, we have

$$E = (\varepsilon^2 - 1)/2, \qquad U(r) = \varepsilon V - \frac{1}{2}V^2 + \frac{\kappa(\kappa+1)}{2r^2} + \frac{V''}{4W} + \frac{3}{8}\left(\frac{V'}{W}\right)^2 - \frac{\kappa V'}{2rW}, \tag{3}$$

where the quantum number $\kappa = \mp(j + 1/2)$ corresponds to $j = l \pm 1/2$ states, j and l being, respectively, the total angular momentum of the electron and its orbital angular momentum (for the upper component g). We note that the effective potential U depends on the angular momentum j and on the energy ε of a level and that it takes markedly different forms for ε values close to +1 and –1. For the Coulomb field of a pointlike nucleus, we have

$$U(r) = \begin{cases} \dfrac{j(j+1) - \zeta^2}{2r^2} + \ldots & \text{for} \quad r \longrightarrow 0 \\ -\dfrac{\varepsilon\zeta}{r} + \dfrac{\kappa^2 - \zeta^2 + a}{2r^2} + \ldots & \text{for} \quad r \longrightarrow \infty \end{cases} \tag{4}$$

($a = \kappa$ for $\varepsilon > 1$ and $a = -1/4$ for $\varepsilon = -1$).

At sufficiently large values of the charge Z, a singular attraction that is in inverse proportion to the radius squared and which can lead to collapse into the center [46–49] (a phenomenon well known in quantum mechanics) arises in the effective potential at small distances. In order to demonstrate this, we consider a trial function different from zero only in the region $0 < r < r_0$. In accordance with the Heisenberg uncertainty relation, one has $\langle p^2 \rangle r_0^2 \geq 1/4$, whence it follows that

$$\langle H \rangle = \frac{1}{2}\langle p^2 \rangle + \langle U \rangle \leq \frac{(j+1/2)^2 - \zeta^2}{2r_0^2} + O\left(\frac{1}{r_0}\right), \qquad r_0 \ll 1.$$

For $\zeta > j + 1/2$, the spectrum of the effective Hamiltonian H is not bounded from below, since we have $\langle H \rangle \longrightarrow -\infty$ for $r_0 \longrightarrow 0$. Such a situation corresponds to collapse into the center of forces in classical mechanics and to the emergence of complex eigenvalues in the case of the Dirac equation, but this is precisely what occurs in the latter case [as can be seen from Eqs. (1) and (1a)] upon a formal continuation of the energy spectrum of levels for a pointlike charge to the region $\zeta > 1$.

From the aforesaid, it is clear that the emergence of a singularity in the formulas for $\varepsilon_n(\zeta)$ at $\zeta = 1$ is due to the use of the idealized case of a pointlike charge. This approximation provides a high precision for light nuclei, but it becomes inapplicable at $\zeta > 1$ for the $j = 1/2$ states and at $\zeta > j + 1/2$ for states characterized by the angular momentum j. At such large values of Z, the Dirac equation must be solved with a potential cut off at small distances, whereby the finiteness of nuclear sizes is taken into account. In such a potential,

$$V(r) = \begin{cases} \zeta/r & \text{for} \quad r > r_N \\ \dfrac{\zeta}{r_N} f\left(\dfrac{r}{r_N}\right) & \text{for} \quad 0 < r < r_N, \end{cases} \tag{5}$$

the form of the cutoff function $f(r/r_N)$ is dictated by the electric-charge distribution over the nuclear volume (see Appendix A).

Pomeranchuk and Smorodinsky [40] were the first to notice this. By introducing finite nuclear sizes, they showed that the Dirac equation has a solution over the entire region from $Z = 0$, $\varepsilon = 1$ to $Z = Z_{cr}$, $\varepsilon = -1$ and roughly estimated the critical charge Z_{cr} (however, their estimate proved to be exaggerated). More precise values of Z_{cr} were obtained later in [50, 51]. However, it remained unclear what actually occurs at $Z > Z_{cr}$. For more than 25 years, this problem had not attracted much attention.

A breakthrough occurred in the years 1969 and 1970, when the problem of the critical charge of a nucleus and physical phenomena in the region $Z > Z_{cr}$ became the subject of intensive investigations. First of all, the value of Z_{cr} was calculated precisely for a spherical nucleus. These precise values were obtained independently by two methods. Pieper and Greiner [2] determined the energies of the levels by numerically solving the Dirac equation and found Z_{cr} as the point of intersection of the curve representing the level $\varepsilon_0(\zeta)$ and

[5)] Nonetheless, such a possibility was considered in the literature [43, 44]. There, complex values arise from the absorption boundary condition imposed for $r \longrightarrow 0$.

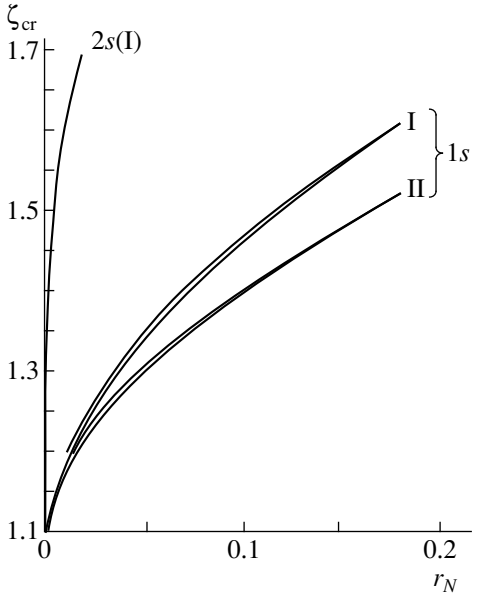

Fig. 1. Critical charge of a nucleus ($\zeta_{cr} = Z_{cr}/137$) for the $1s_{1/2}$ and $2s_{1/2}$ levels (the nuclear radius r_N is given in $\hbar/mc$ = 386 fm units). The cutoff models I and II correspond to the uniform charge distributions over the nuclear surface and volume, respectively. In each pair of close curves, the upper and the lower one represent, respectively, the results of the numerical calculation from [3] and the results obtained with the semiclassical formula (45).

the boundary of the lower continuum (they assumed that the nuclear charge is uniformly distributed over the volume of a sphere of radius $r_N = r_0A^{1/3}$, where r_0 = 1.2 fm and where the dependence of the atomic number A on the nuclear charge was approximated by the formula $A = 63.6 + 1.30Z + 0.00733Z^2$, which was obtained from a dedicated consideration for a region of superheavy nuclei ($100 < Z < 250$).

On the other hand, it was noticed in [3] that solutions to the Dirac equation are strongly simplified at $\varepsilon = -1$. Owing to this, it is possible to derive an equation immediately for Z_{cr}. The result is

$$zK'_{i\nu}(z)/K_{i\nu}(z) = 2\xi, \qquad (6)$$

where $z = \sqrt{8\zeta_{cr}r_N}$, $\nu = 2\sqrt{\zeta_{cr}^2 - \kappa^2}$, $K_{i\nu}(z)$ is a Macdonald function,[6)] and $\xi = \xi(\zeta, \kappa)$ is the logarithmic derivative of the intrinsic wave function at the nuclear boundary [see Eq. (A.2) in Appendix A]. A numerical solution to Eq. (6) was constructed for the case of $r_N = r_0A^{1/3}$ with r_0 = 1.1 fm and $A = 2.6Z$ (these values are typical of heavy nuclei) and for the following two cutoff models:

$$\left.\begin{array}{ll} \text{I} & f(x) \equiv 1 \\ \text{II} & f(x) = (3 - x^2)/2 \end{array}\right\} \quad \text{for} \quad 0 < x \equiv r/r_N < 1.$$

[6)] It is a real-valued function at real ν and $z > 0$, which decreases in proportion to $\exp(-z)$ for $z \longrightarrow \infty$ and which features an infinite number of oscillations for $z \longrightarrow 0$.

Of these, the second corresponds to a constant density of the electric charge in a nucleus. For a few low-lying levels, the results of the calculations based on model II are the following:

$$Z_{cr} = 169(1s_{1/2}), \quad 185(2p_{1/2}), \quad 230(2s_{1/2}), \ldots \qquad (7)$$

(see also Fig. 1). These values are in good agreement with those from [2].

In this connection, there arises the problem of sensitivity of Z_{cr} values to a detailed form of the nuclear-density distribution in superheavy nuclei. This problem can be resolved by comparing the Z_{cr} values as obtained for the cutoff models I and II—the point is that model I assumes that the charge is entirely concentrated on the nuclear surface, while model II corresponds to a uniform electric-charge distribution over the nuclear volume and is therefore quite realistic. Upon going over from model I to model II, the value of the electrostatic potential at the center of a nucleus increases by a factor of 1.5, amounting to $V(0) = 1.5\zeta/r_N \simeq 70mc^2 = 35$ MeV. The corresponding values of ζ_{cr} at r_N = 10 fm are Z_{cr} = 1.271 (I) and 1.243 (II), the difference of Z_{cr} values within models I and II being 3.8 units. From these results alone, we can conclude that less significant modifications (like allowances for the diffuseness of the nuclear boundary, for deviations from a spherical shape of nuclei, and for changes in the relationship between A and Z in superheavy nuclei) would lead to very modest modifications (of not more than one unit) to Z_{cr} (these effects were estimated in [13, 18, 25]). For the critical charge Z_{cr} of a naked nucleus (that is, a nucleus not surrounded by an electron shell), we can take the values in (7).

So far, the nucleus has been considered to be naked—that is, completely deprived of its electron shell. But if it is surrounded by such a shell, the shell electrons reside near the nucleus for some part of the time, screening its charge; as a result, Z effectively becomes smaller, so that Z_{cr} increases. Estimating this effect is especially important in connection with performing experiments to study spontaneous positron production in heavy-ion collisions. Indeed, the total charge of nuclei, $Z_1 + Z_2$, can exceed the critical charge $Z_{cr} \approx 170$ calculated without allowing for screening only by 15–20 units; therefore, an increase in Z_{cr} even by 10 units would considerably complicate an experiment with heavy nuclei available at present.

Since it is very difficult to calculate Z_{cr} in the problem of two centers, the analysis was actually performed for a spherical nucleus. The electron-shell density was taken according to the Thomas–Fermi equation [52]. Although the speed of K-shell electrons is $v \sim c$, the majority of electrons occur at distances of $r \sim 137Z^{-1/3} \gg 1$ from the nucleus, so that the use of the nonrelativistic Thomas–Fermi model is justified. For the screening-induced increase in the critical charge, the results obtained in [11] and [19] for the case of a neutral atom are ΔZ_{cr} = 1.5 and 1.2, respectively. A modest distinction between these two values seems to be due to the

use of the different shapes of the electron-charge distribution within the nucleus in those studies. Moreover, the screening of the nuclear charge was taken into account more correctly in [11] on the basis of the relativistic Hartree–Fock–Slater equation (see [12]), and the value of $Z_{cr} = 173$ was obtained there. Summing the different corrections, we find that, upon a transition from the cutoff model II to a nucleus that has a diffuse boundary and which is surrounded by an electron shell, the Z_{cr} values presented in (7) increase by approximately 3 ± 1 units for the 1*s* and 2*p* states (see Table 1). It is also possible to investigate Z_{cr} as a function of the degree of ionization of the electron shell, $q = (Z - N)/Z$, where N is the total number of electrons in the shell (we have $q = 0$ for a neutral atom and $q = 1$ for a naked nucleus). With allowance for the screening effect, the self-consistent potential for an electron now becomes

$$V_q(r) = -\left(\frac{Z}{r_N} f(r/r_N) + \frac{Z-N}{r_0}\right)e^2 \text{ for } 0 < r < r_N;$$

$$V_q(r) = -\left(\frac{Z}{r} \varphi(x) + \frac{Z-N}{r_0}\right)e^2 \text{ in the region } r_N < r < r_0;$$

and

$$V_q(r) = -(Z-N)e^2/r$$

for $r > r_0$, where $\varphi(x)$ is a solution to the Thomas–Fermi equation for an ion, $x = (128Z/9\pi^2)^{1/3} r/a_B = 0.0425\zeta^{1/3} r$, and r_0 is the radius of a positive ion in the Thomas–Fermi model [52] [here, $r_0 \longrightarrow \infty$ at $q = 0$ ($r_0 \gg r_N$)].

A change in Z_{cr} can be found by perturbation theory [18]. Specifically, we have

$$\delta\zeta_{cr} = \beta^{-1}\langle \delta V\rangle, \quad \langle \delta V\rangle = \int \delta V(r)\rho_{cr}(r) r^2 dr, \quad (8)$$

where $\rho_{cr} = \psi^+\psi$ is the electron-shell density at the critical point and β is the slope of the level [see Eq. (12) below]. Substituting the expression $\delta V = V_q(r) - V_0(r)$ into (8) and considering that the main contribution to the relevant integral comes from the region where $r \sim r_K \ll r_a$ (r_K is the *K*-shell radius, and r_a is the mean radius of the atom), we obtain [53]

$$\Delta Z_{cr}(q) = \Delta Z_{cr}(0) F(q). \quad (9)$$

The correction $\Delta Z_{cr}(0)$ for a neutral atom was found by numerically solving the Dirac equation for $\varepsilon = -1$ and $V(r) = -\zeta r^{-1}\varphi_0(x)$. The results of the calculation are quoted in Table 1; the graph of the function $F(q)$ is depicted in Fig. 2, where we can see that, in the region $q \lesssim 0.5$, this function changes insignificantly—for example, $F(0.5) = 0.907$ [q values around 0.5 correspond to a (Z_1, Z_2, e) quasimolecule arising in a collision of a naked nucleus with a neutral atom, because we usually have $Z_1 \approx Z_2$)]. Thus, the correction for screening in an ion whose degree of ionization is $q \sim 0.5$ is nearly identical to that in a neutral atom. This can easily be understood: with increasing degree q of ionization, the electron shell comes closer to the nucleus, whereby a decrease in the screening shell charge, which is equal to $(1 - q)Z$, is partly compensated. On the other hand, the correction ΔZ_{cr} decreases fast when we go over to a naked nucleus ($q \longrightarrow 1$) since $F(q) \propto (1 - q)^{1/3} \longrightarrow 0$.

Table 1. Critical charge for a spherical nucleus (lowest states with $\kappa = \mp 1$)

	$1s_{1/2}$	$2p_{1/2}$	$2s_{1/2}$	$3p_{1/2}$
$Z_{cr}^{(0)}$	168.8	181.3	232	254
ΔZ_{cr}	1.2	1.1	3.5	3.3
$\Delta Z_{cr}'$	0	1.5	3.1	4.6
$\Delta Z_{cr}''$	0.5	0.6	0.8	1.0
Z_{cr}	170.5	184.5	239	263
ζ_{cr}	1.245	1.346	1.74	1.92
$\langle r\rangle$	0.500	1.27	2.27	5.76
	0.309	0.237	0.552	0.459
$\rho(\zeta = \zeta_{cr})$	1.62	0.333	0.994	0.333

Note: The following notation is used here: $Z_{cr}^{(0)}$ is the critical charge for a naked nucleus with a sharp boundary (cutoff model II); ΔZ_{cr} is the correction for screening in a neutral atom; $\Delta Z_{cr}'$ is the correction for screening by the vacuum shell; $\Delta Z_{cr}''$ is the correction due to the diffuseness of the nuclear boundary; and $\langle r\rangle$ is the mean radius of the electron state in $\hbar/mc$ units: (first row) at $\zeta_{cr}^{(0)} = 1$ (for a pointlike nucleus) and (second row) at $\zeta = \zeta_{cr}$ with allowance for finite nuclear sizes. The parameter ρ is defined in (31) and (B.13).

The calculations presented in [53] also took into account the screening of the nuclear charge by a vacuum shell of a supercritical atom (whose $Z > Z_{cr}$ nucleus attracts such a shell upon positron emission [26, 54]) and the diffuseness of the nuclear boundary. The eventual results of those calculations for Z_{cr} are given in Table 1.

It is interesting to find out how finite nuclear sizes eliminate the singularity of the energy $\varepsilon_0(\zeta)$ at $\zeta = Z\alpha = 1$. Suppose that the cutoff radius r_N is arbitrarily small in relation to the electron Compton wavelength. In the limit $\Lambda = \ln(1/r_N) \gg 1$ (which is of a somewhat academic interest), the energy of the 1*s* level becomes [5, 7]

$$\varepsilon_0(\zeta) = \gamma \coth \Lambda\gamma, \quad \gamma = \sqrt{1 - \zeta^2}. \quad (10)$$

In the region $Z < 137$, $\coth\Lambda\gamma = 1 + \exp(-2\Lambda\gamma) + \ldots$ tends to unity exponentially fast, so that, for $1 - \zeta \gg \Lambda^{-2}$, the energy $\varepsilon_0(\zeta)$ coincides with expression (1) for a pointlike charge and is virtually independent of the way in which the Coulomb potential is cut off within the nucleus. On the other hand, the point $\zeta = 1$ is no longer a singular point for the function $\varepsilon_0(\zeta)$ at $r_N > 0$, and

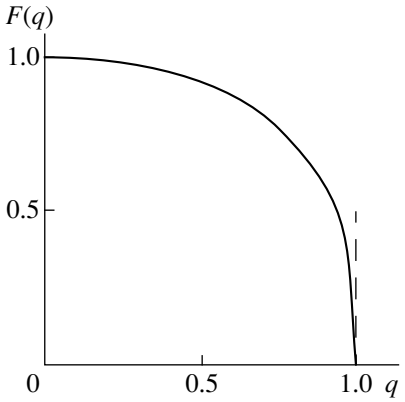

Fig. 2. Graph of the function $F(q)$ in (9) ($q = 1 - N/Z$ is the degree of ionization of the electron shell of a superheavy atom).

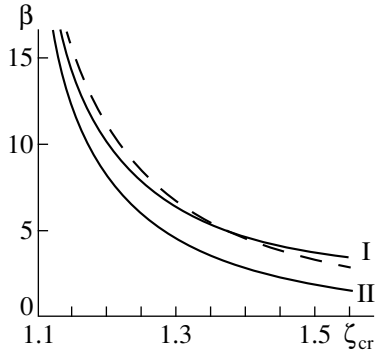

Fig. 3. Slope β of the ground-state level entering the lower continuum: (solid curves) results of the numerical calculation from [4] and (dashed curve) result obtained in the semiclassical approximation [74] for the cutoff model I.

expression (10) can be continued to the region $Z > 137$ with the result

$$\varepsilon_0(\zeta) = \tilde{\gamma}\coth\Lambda\tilde{\gamma}, \quad \tilde{\gamma} = \sqrt{\zeta^2 - 1}. \tag{10a}$$

Expressions (10) and (10a) describe a unified analytic function that, in the vicinity of the point $\zeta = 1$, is expanded in a convergent series in integral powers of $1 - \zeta^2$ as

$$\varepsilon_0(\zeta) = \frac{1}{\Lambda}\left\{1 + \sum_{n=1}^{\infty} 2^{2n}\frac{B_{2n}}{(2n)!}\Lambda^{2n}(1-\zeta^2)^n\right\}, \tag{10b}$$

where B_{2n} are Bernoulli numbers [$B_2 = 1/6$, $B_4 \equiv -1/30$, …, $B_{2n}/(2n)! \approx 2(-1)^{n-1}(2\pi)^{-2n}$ for $n \longrightarrow \infty$]. Expression (10a) has a pole at $\tilde{\gamma} = \pi/\Lambda$,[7] whence we obtain the asymptotic formula

$$\zeta_{cr} = 1 + \frac{\pi^2}{2\Lambda^2} + O(\Lambda^{-3}), \quad \Lambda \gg 1. \tag{11}$$

We can see from this formula that ζ_{cr} as a function of the cutoff radius r_N has a singularity for $r_N \longrightarrow 0$. Therefore, finite nuclear sizes cannot be taken into account by perturbation theory if $Z > 137$. Here, collapse into the center for the Dirac equation with a pointlike Coulomb potential clearly manifests itself.

In the zero-range limit ($r_N = 0$), the curve representing the 1s level reaches the point $\varepsilon = 0$ at $\zeta = 1$ and steeply terminates after that (the derivative is $d\varepsilon_0/d\zeta = -\infty$). This shows that the zero-range approximation is inapplicable to the problem being considered. At the same time, the function $\varepsilon_0(\zeta)$ smoothly intersects the line $\varepsilon = 0$ if $r_N > 0$, showing no singularities there, and enters the lower continuum with a finite slope β:

$$\beta = -\left.\frac{d\varepsilon}{d\zeta}\right|_{\zeta=\zeta_{cr}} = \int v(\mathbf{r})\rho_{cr}d^3r, \qquad \rho_{cr} = \psi_0^2(r)|_{\zeta=\zeta_{cr}} \tag{12}$$

(Fig. 3). Here, we have written the potential in the form $V(\mathbf{r}) = -\zeta v(\mathbf{r})$, assuming that the function v determining the shape of the potential no longer depends on ζ [for the potential in Eq. (5), this holds to a high precision, since the dependence $r_N \propto \zeta^{1/3}$ is rather weak]. The parameter β determines the threshold behavior of the probability of spontaneous positron production [4, 21].

The properties of atomic states for $Z > 137$ were also investigated. Presented below are the formulas for the mean radius of the ground state and for its variance. For a $Z < 137$ pointlike nucleus, we have [see Eqs. (B.2) and (B.9)]

$$\langle r\rangle = (1 + 2\sqrt{1-\zeta^2})/2\zeta, \quad \Delta r = \frac{\langle r\rangle}{(1 + 2\sqrt{1-\zeta^2})^{1/2}}. \tag{13}$$

For the $\kappa = -1$ states (that is, $ns_{1/2}$ states), the results at the boundary of the lower continuum are

$$\langle r\rangle = \frac{(4\zeta_{cr}^2 - 3)(1 + 0.3\zeta_{cr}^2)}{2\zeta_{cr}(2\zeta_{cr}^2 + 3)}, \quad \varepsilon = -1 \tag{14}$$

(see Table 1). For an arbitrary energy of a level, $0 > \varepsilon > -1$, the expression for $\langle r\rangle$ is much more complicated [3]. According to numerical calculations, the mean radius of the ground state decreases monotonically with increasing ζ (see Fig. 5 in [3]), this decrease being especially pronounced when the charge increases from $Z = 137$ to Z_{cr} (compare the corresponding numbers in Table 1); on the contrary, the relative variance $\Delta r/\langle r\rangle$

[7] In fact, this pole is spurious—it is removed in solving the problem more accurately, whereby it is shown that, near the critical point, there is a comparatively narrow region $\zeta_{cr} - \zeta \sim \Lambda^{-3}$, where expression (10a) is inapplicable. The relevant expression for the energy of the level can be found in [5].

increases. The magnetic moment of the electron in a bound state is given by [6]

$$\mu_{cr} \equiv \mu(\zeta = \zeta_{cr}) = 2(4\zeta_{cr}^2 - 3)/3(2\zeta_{cr}^2 + 3), \quad \kappa = -1. \tag{15}$$

In particular, $\mu_{cr} \longrightarrow 2/15 = 0.133$ for $\zeta_{cr} \longrightarrow 1$ and $\mu_{cr} = 0.350 \approx 1/3$ of the Bohr magneton for $\zeta_{cr} = 1.245$ (1*s* ground state).

Equations (13)–(15) can easily be generalized to other states of the discrete spectrum (see Appendix B). Table 1 also quotes the values of the parameter $\rho = w_2/w_1$, which characterizes the relative weight of the lower and the upper component of the Dirac bispinor [see Eq. (B.13)]. Since $\rho \sim 1$, the electron bound state at the boundary of the lower continuum is fully relativistic (as might have been expected).

Equations (6), (14), and (15) have so simple a form owing to the fact that, in the case of the Coulomb field $V(r) = -\zeta/r$, solutions to the Dirac equation at $\varepsilon = -1$ that decrease at infinity are explicitly expressed in terms of a Macdonald function as

$$\begin{aligned} G(r) \equiv rg(r) &= K_{i\nu}(z), \\ F(r) \equiv rf(r) &= \zeta^{-1}(rG' + \kappa G) \\ &= \zeta^{-1}\left[\kappa K_{i\nu}(z) + \frac{1}{2}zK'_{i\nu}(z)\right] \end{aligned} \tag{16}$$

(the normalization factors are omitted here), where $z = 2^{3/2}(\zeta r)^{1/2}$, $\nu = 2(\zeta^2 - \kappa^2)^{1/2}$, $\zeta > |\kappa|$, and the radial wave functions $g(r)$ and $f(r)$ correspond to the definition given in [45], the normalization condition being $\int_0^\infty (G^2 + F^2)dr = 1$ here (in the limit $r_N \longrightarrow 0$, the normalization factor can be calculated explicitly [4, 21]). From (16), it follows that, in the limit $r \longrightarrow \infty$, we have

$$\begin{aligned} G(r) &\approx c_1 r^{-1/4} \exp(-\sqrt{8\zeta_{cr}}r), \\ F(r) &\approx c_2 r^{1/4} \exp(-\sqrt{8\zeta_{cr}}r), \end{aligned} \tag{17}$$

the ratio of the coefficients c_1 and c_2 being $c_1/c_2 = -\sqrt{\zeta_{cr}/2}$. Thus, the electron level that reached the boundary of the lower continuum remains localized (compare with the results given in [1]). At large distances from the nucleus, we then have $F/G \propto \sqrt{\zeta r} \gg 1$ and the electron-shell density decreases exponentially,

$$\begin{aligned} \rho_{cr}(r) &= (G^2(r) + F^2(r))/4\pi r^2 \\ &\approx \text{const} \times r^{-3/2} \exp(-c_3\sqrt{\zeta_{cr}}r), \quad r \longrightarrow \infty, \end{aligned} \tag{17a}$$

with the numerically large coefficient of $c_3 = 2^{5/2} = 5.657$.

A considerable simplification in Eqs. (14)–(16) in relation to the general case of $\varepsilon \neq -1$ may be due to some additional symmetry of the Dirac equation. In this connection, it should be noted that the group of the hidden symmetry of the hydrogen atom (for the nonrelativistic case, it was discovered by Fock [55] and Bargmann [56]; see also [57–62]) was considered in [63–65] for the relativistic Coulomb problem. However, no special analysis has been performed for $\varepsilon = -1$ states at the boundary of the lower continuum.

3. CRITICAL DISTANCE FOR COLLIDING NUCLEI

There are no nuclei with charge $Z \sim Z_{cr} > 170$ in nature, and prospects for synthesizing them are absolutely unclear at present.[8)] It was noted by Gershtein and Zeldovich [1], however, that supercritical electric fields are generated for a short period of time in the case where two ordinary heavy ions (for example two naked uranium nuclei with total charge $Z_1 + Z_2 = 184 > Z_{cr}$) come to each other within a distance R less than the critical distance R_{cr}. Such an experiment is quite feasible, and the corresponding theoretical problem is that of two centers for the Dirac equation. Since the nuclei involved move at nonrelativistic velocities ($v_N/c \approx 1/20$) and since a K electron is relativistic for $Z\alpha \gtrsim 1$, the energies of the electron terms can be calculated in the adiabatic approximation. The charge of each of the colliding nuclei is less than 137, whence it follows that finite nuclear sizes can be taken into account by perturbation theory. Solving the Dirac equation for two pointlike charges at rest that occur at a distance R from each other and which generate the potential

$$V(\mathbf{r}) = -\left(\frac{Z_1\alpha}{r_1} + \frac{Z_2\alpha}{r_2}\right), \quad r_{1,2} = |\mathbf{r} \pm \mathbf{R}/2|, \tag{18}$$

where $r_{1,2}$ are the distances between the electron and the nuclei involved, presents the most serious difficulty in the problem. This problem is much more complicated than the above problem of solving the Dirac equation for a spherical nucleus.

The Schrödinger equation with the potential (18) has received a comprehensive study [67] (it has numerous applications in the theory of molecules, in the physics of muon catalysis, and in some other allied realms). In this case, variables in the nonrelativistic Schrödinger equation are separated in the ellipsoidal coordinates (see [48])[9)]

$$\xi = \frac{r_1 + r_2}{R}, \quad \eta = \frac{r_1 - r_2}{R},$$
$$\xi \geq 1, \quad -1 \leq \eta \leq 1, \quad 0 \leq \varphi \leq 2\pi,$$

[8)] In this connection, mention should be made of the last record in these realms—the formation of $Z = 114$ and $Z = 116$ nuclei in $^{48}Ca + ^{242,244}Pu$ interactions (in all, seven such nuclei have been observed so far). In all probability, these nuclear species lie near the island of stability of superheavy elements—its existence has long since been predicted by theorists (see, for example, [66]). Naturally, this also quickens interest in QED predictions in the region $Z > 137$.

[9)] In the mathematical literature [47, 67], they are more often referred to as prolate spheroidal coordinates.

and the equation reduces to two ordinary differential equations. In going over to the relativistic problem of two Coulomb centers, we run into the following additional difficulties:

(i) Variables are not separated in any of the known systems of orthogonal coordinates.

(ii) Near each of the nuclei, the wave function develops a singularity associated with the term $-(1/2)V^2$ in the effective potential.

(iii) There is a significant spin–orbit interaction, because of which the upper and the lower spinor component of the wave function are on the same order of magnitude at $Z\alpha \sim 1$.

Squaring the Dirac equation at $\varepsilon = -1$, we arrive at the set of equations

$$\begin{aligned} \Delta\psi_1 + U_{11}\psi_1 + U_{12}\psi_2 &= 0, \\ \Delta\psi_2 + U_{21}\psi_1 + U_{22}\psi_2 &= 0, \end{aligned} \tag{19}$$

where the matrix elements U_{ij} depend on r_1 and r_2 and on the parameters R and ζ (see Appendix C). Upon separating the azimuthal angle φ, we obtain a set of second-order partial differential equations on a plane. A direct application of standard finite-difference methods for solving boundary-value problems for elliptic equations to this set is inappropriate because of the presence of singularities. The critical distance R_{cr} was calculated by the Ritz method [14, 27] or by the Kantorovich method (see [22, 23]).[10)] Either method relies on the variational principle. Within the Ritz method, the ψ function is represented as a finite sum $\psi = \sum_n c_n\varphi_n$, where $\{\varphi_n\}$ is a fixed set of basis functions, while c_n are variable constants. Within the Kantorovich method, $\psi = \sum_n d_n(y)\varphi_n(x)$, where d_n are fixed functions of the variable y, while φ_n are variable functions of x. Substituting the ψ function into the quadratic energy functional, one arrives at a bilinear form in the coefficients c_n within the Ritz method or at a functional bilinear in φ_n within the Kantorovich method.

The condition requiring that the energy be minimal leads to a set of linear algebraic equations within the first method or a set of ordinary differential equations for the functions $\varphi_n(x)$ within the second method. In order to achieve a high precision in variational calculations, it is important to choose correctly the variables x and y and the functions $d_n(y)$; in the Ritz method, success depends on the choice of basis functions φ_n.

The following approach was adopted in [22, 23]. We denote by $\rho = \sqrt{x^2 + y^2}$, z, and φ cylindrical coordinates. If the charges of the nuclei are identical, $Z_1 = Z_2 = Z/2$, the wave function of the ground-state term is symmetric under the inversion in the $z = 0$ plane. In addition, we note that, for the ground-state term, the projection of the total angular momentum of the relevant quasimolecule is $J_z = \Lambda + s_z = 1/2$, while the projection of the orbital angular momentum Λ is zero for ψ_1 and unity for ψ_2. Isolating kinematical factors, we can represent the spinor components as

$$\psi_1(\mathbf{r}) = \chi_1(\rho, z), \quad \psi_2(\mathbf{r}) = \frac{\rho z}{R^2}e^{i\varphi}\chi_2(\rho, z), \tag{20}$$

where χ_1 and χ_2 are real-valued functions that are even in z. Instead of ρ and z, we now introduce the variables $x = x(\rho, z)$ and $y = y(\rho, z)$ in such a way that the singular points of Eqs. (19) occur at $x = 0$ and ∞, irrespective of y. For this, it is sufficient that $x \longrightarrow 0$ when $r_1 \longrightarrow 0$ or $r_2 \longrightarrow 0$ and $x \longrightarrow \infty$ when $r_{1,2} \longrightarrow \infty$. The choice of the variable y is not very important—it is only necessary that the variables x and y be independent. Specifically, use was made of the variables

$$x = \xi^2 - \eta^2 = \frac{r_1 r_2}{4R^2}, \quad y = \frac{\eta^2}{\xi^2 - \eta^2} = \frac{(r_1 - r_2)^2}{4r_1 r_2}, \tag{21}$$

which take values in the curvilinear triangle $(x^{-1} - 1)\theta(1 - x) < y < x^{-1}$ on the (x, y) plane. In terms of these variables, we have $V(\mathbf{r}) = -2\zeta R^{-1}\sqrt{(1 + y)/x}$. The trial functions were represented as

$$\chi_1 = \sum_{k=1}^{m}\varphi_k(x)y^{k-1}, \quad \chi_2 = \sum_{k=1}^{n}\varphi_{m+k}(x)y^{k-1}. \tag{22}$$

A minimization of the energy functional leads to the set of $N = m + n$ equations

$$\frac{d}{dx}\left(P\frac{d\varphi}{dx} + R\varphi\right) - Q\varphi - R^T\frac{d\varphi}{dx} = 0,$$

$$\varphi = \begin{pmatrix} \varphi_1 \\ \varphi_2 \\ \vdots \\ \varphi_N \end{pmatrix}, \tag{23}$$

where P, Q, and R are $(N \times N)$ matrices dependent on x. All the coefficients P_{ij}, $Q_{ij}(x)$, and $R_{ij}(x)$ are expressed in terms of elementary functions; by way of example, we indicate that, at $i = j = 1$,

$$P_{11}(x) = x\begin{cases} \sqrt{1+x} - \sqrt{1-x} - \ln\dfrac{1+\sqrt{1+x}}{1+\sqrt{1-x}} & \text{for} \\ 0 < x \le 1 & \\ \sqrt{1+x} - \ln[(1+\sqrt{1+x})/\sqrt{x}] & \text{for} \\ x > 1. & \end{cases} \tag{24}$$

[10)] The idea of reducing a partial differential equation to a set of ordinary differential equations is due to Kantorovich. Solutions to Poisson's and the biharmonic equation were considered in [68] in various regions on a plane, and it was shown there that, as a rule, this method converges faster than the variational Ritz method and is more accurate than it.

The functions P_{ij}, Q_{ij}, and R_{ij} are continuous at the point $x = 1$, together with their first derivatives;[11] it is convenient to calculate them with the aid of the recursion relations from [22]. The boundary conditions for the functions $\varphi_i(x)$ for $x \longrightarrow 0, \infty$ follow from the requirement that the norm of the ψ function be convergent.

The boundary-value problem specified by Eq. (23) has a solution only at specific $R = R_{cr}(Z)$. The functions $\varphi_k(x)$ have a power-law singularity for $x \longrightarrow 0$ and an essential singularity for $x \longrightarrow \infty$. The character of these singularities and the expansions near them immediately follow from Eqs. (23). Introducing the matrix of logarithmic derivatives,

$$Y = \|Y_{ij}(x)\|, \quad \varphi_i' = \sum_{j=1}^{N} Y_{ij}\varphi_j,$$

we reduce the set of Eqs. (23) to the matrix Riccati equation

$$Y' = A - BY - Y^2, \tag{25}$$

where

$$A = P^{-1}(Q - R'), \quad B = P^{-1}(R - R^T + P'). \tag{25a}$$

By numerically solving this equation by the Runge–Kutta method in the intervals (x_0, x_1) and (x_∞, x_1), we determined the matrices $Y_0(x_1)$ and $Y_\infty(x_1)$. The condition of continuity of the function $\varphi_i(x)$ and $\varphi_i'(x)$ at $x = x_1$ leads to the set of homogeneous equations $\{Y_0(x_1) - Y_\infty(x_1)\}\varphi(x_1) = 0$, which has a nontrivial solution under the condition

$$\mathrm{Det}\|Y_0(x_1) - Y_\infty(x_1)\| = 0, \tag{26}$$

whence we can determine R_{cr} at a given charge ζ. In view of Eq. (24), it is natural to choose the matching point at $x_1 = 1$; in numerically solving Eq. (25), it is convenient to make the substitution $t = x^{-1/4}$, $0 < t \le 1$. The choice of the initial points of integration at $x_0 = t_0 = 0.07$ and $x_\infty = t_0^{-4} \approx 4 \times 10^4$ has made it possible to ensure a precision not poorer than 0.15% in calculating $R_{cr}(\zeta)$.

The choice of trial functions in the form (22) will be referred to as an (m, n) approximation. With increasing m or n, the class of trial functions becomes wider and the accuracy of the (m, n) approximation becomes higher, which can be seen from Table 2. The calculations were performed for $(m, n) = (1, 0)$, $(2, 0)$, $(2, 1)$, and $(4, 3)$. The results for the $Z = 90$–100 nuclei are quoted in Table 3.[12] In order to assess the accuracy of various methods, we consider the case of $Z = 92$ (uranium nuclei) in greater detail (see Table 2). In addition to the (m, n) approximations, we present here some more numbers: the R_{cr} value as obtained by the Ritz method [14] and in the monopole approximation (see also Fig. 4), as well as the R_{cr} value deduced in [9] by matching the relevant asymptotic expressions. From Table 2, it can be seen that, with increasing order of the

Table 2. Convergence of the (m, n) approximations in the two-center problem for the Dirac equation

(m, n)	R_{cr}, fm		
	$Z = 184$ (U + U)	$Z = 190$ (U + Cf)	$Z = 200$
(1, 0)	34.7	–	68.1
(2, 0)	37.4	–	72.4
(2, 1)	38.37	50.8	74.4
(4, 3)	38.42	50.9	74.8
According to [24, 25]	36.8	48	–
Asymptotic values from [9]	35.5	46.7	68.2
Monopole approximation [25]	34.1	44.8	64.8

Table 3. Parameters of the $1s\sigma$ electron state at the critical point

$Z_1 = Z_2$	$R_{cr}^{(0)}$		R_{cr}	A_∞	β	ρ
	numerical	asymptotic				
90	31.0	28.7	26.5	2.23	0.807	1.478
92	38.4	35.5	34.3	2.51	0.823	1.426
93	42.4	39.1	38.4	2.66	0.832	1.400
94	46.6	42.8	42.6	2.82	0.840	1.376
95	50.9	46.7	47.0	2.99	0.848	1.353
96	55.4	50.8	51.6	3.17	0.857	1.330
97	60.0	55.0	56.3	3.36	0.865	1.307
98	64.8	59.2	61.0	3.56	0.873	1.286
99	69.7	63.7	66.0	3.76	0.881	1.265
100	74.8	68.2	71.1	3.98	0.888	1.244
114	160.0	143.0	–	3.98	0.888	–
126	255.0	–	–	–	–	–

Note: The distances $R_{cr}^{(0)}$ (for pointlike nuclei) and R_{cr} (with allowance for finite nuclear sizes) are given in fm. The former were obtained from a numerical calculation in [23] and from the asymptotic formula (32). The parameters β and ρ are defined in (30a) and (31), respectively.

[11] The expressions for the coefficients $P_{ij}(x)$, etc., for $x < 1$ differ from those for $x > 1$ because the topology of the surfaces $x(\xi, \eta) = c$ changes at $c = 1$: they are simply connected for $c > 1$ and doubly connected for $0 < c < 1$.

[12] Unfortunately, an algebraic error was made in [22] in calculating the coefficients Q_{13} and Q_{23} in the equations of the (2, 1) approximation [these terms die out at small and large distances from nuclei and do not affect the corresponding asymptotic expressions for $\psi(\mathbf{r})$; therefore, they are poorly controllable]. This error resulted in overestimating the R_{cr} values in the (2, 1) approximation by about 20% (see [23, 24] in this connection); however, it exerts no effect on the (1, 0) and the (2, 0) approximation, where the results from [22] remain valid.

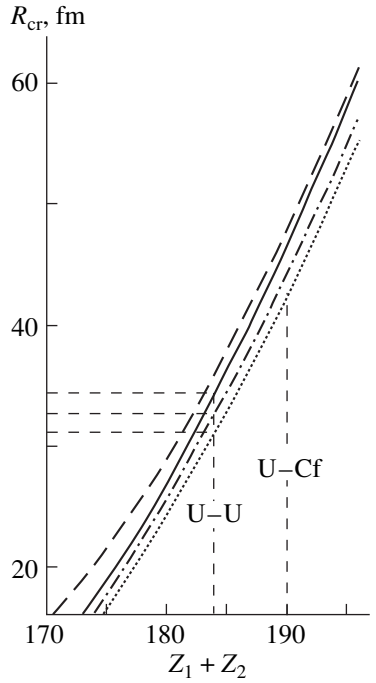

Fig. 4. Critical radius R_{cr} (fm) for the $1s\sigma$ ground-state term according to [25]: (dashed curve) results for naked nuclei at $r_N = 0$, (solid curve) results for naked nuclei with allowance for finite nuclear sizes, (dash-dotted curve) results for the case of 30 electrons in the atomic shell, and (dotted curve) results for the case of 100 electrons in the atomic shell.

(m, n) approximation, the relevant values of R_{cr} increase monotonically {from the variational principle, it follows that the exact value of R_{cr} can only exceed the result obtained in any (m, n) approximation [8, 18]}.

Let us now consider the Ritz method. In these calculations, use was made of a system of the Hilleraas basis functions

$$\psi^m_{nls}(\xi, \eta) = \exp\left(-\frac{\xi - 1}{2a}\right) L_n^m\left(\frac{\xi - 1}{a}\right) P_l^m(\eta)\chi_s, \quad (27)$$

which leads to a fast convergence in the nonrelativistic problem of two centers. However, these functions are finite near the nuclei ($\xi \longrightarrow 1$, $\eta \longrightarrow \pm 1$), whereas an exact solution to the relativistic problem of two centers has a Coulomb singularity:

$$\psi(\mathbf{r}) \propto (\xi^2 - \eta^2)^{-\sigma}, \quad \sigma = 1 - \sqrt{1 - (Z\alpha)^2/4}, \quad Z = Z_1 + Z_2 \quad (28)$$

(in the nonrelativistic limit $Z\alpha \longrightarrow 0$, this singularity disappears). The presence of the singularity impairs convergence of the expansion in the basis $\{\psi^m_{nls}\}$. Within the Kantorovich method, there is no such difficulty, since the functions $\varphi_k(x)$ automatically have the required singularity for $x = \xi^2 - \eta^2 \longrightarrow 0$ [this is ensured by the set of Eqs. (23) itself]. In all probability,

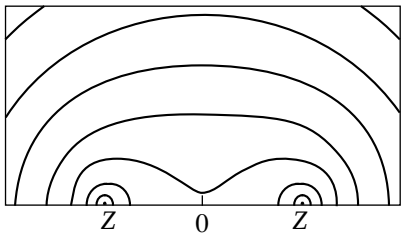

Fig. 5. Density ρ_{cr} for the $1s\sigma$ ground-state term at $Z_1 = Z_2 = 92$. The values of ρ_{cr} for neighboring curves differ by the factor of $10^{1/5}$. The positions of the nuclei are denoted by Z.

this explains the fact that, for $Z = 92$, the R_{cr} value as obtained within the Ritz method with 100 trial functions is close to the result from [22] in the (1, 0) approximation, which involves only one function $\varphi_1(x)$.

It is also possible to compute the electron wave function at the critical point $\zeta = \zeta_{cr}$ and quantities associated with it (see [23] and Appendix C of the present study). Figure 5 shows the density $\rho_{cr}(\mathbf{r}) = \psi^+\psi$ for the $1s\sigma$ state of the U + U quasimolecule at $R = R_{cr}$. Near each nucleus, as well as at large distances from the nuclei, the density $\rho(\mathbf{r})$ is spherically symmetric; that is,

$$\rho_{cr}(\mathbf{r}) \approx \begin{cases} A_0^2 r_i^{2(\sigma-1)}, & r_i \longrightarrow 0 \ (i = 1, 2), \\ A_\infty^2 r^{-3/2} \exp(-\sqrt{32\zeta} r), & r \longrightarrow \infty, \end{cases} \quad (29)$$

where $\sigma = \sqrt{1 - \zeta^2/4}$. The asymptotic coefficients A_0 and A_∞ were computed in [23]. Table 3 gives the values of the coefficient A_∞, which determines the probability of peripheral processes (for example, the probability of atom ionization in a strong electric field).

Near the boundary $\varepsilon = -1$, the energy of the level is

$$\varepsilon(R) = -1 + \beta\frac{R - R_{cr}}{R_{cr}} + O((R - R_{cr})^2). \quad (30)$$

The slope parameter β, which determines the threshold behavior of the cross section for spontaneous positron production [4, 21], can be calculated by the formula

$$\beta = \frac{1}{2}\left(\frac{d\ln R_{cr}}{d\zeta}\right)^{-1} \int \psi^+\left(\frac{1}{r_1} + \frac{1}{r_2}\right)\psi d^3 r, \quad \psi = \begin{pmatrix}\varphi \\ \chi\end{pmatrix}. \quad (30a)$$

The results are quoted in Table 3. For nuclei from the uranium region, β is a nearly linear function of Z (Fig. 6). The values of the parameter

$$\rho = \int \chi^+\chi d^3 r / \int \varphi^+\varphi d^3 r, \quad (31)$$

which characterizes the magnitude of relativistic effects for a bound electron, are also given in Table 3.

Finally, the approximate analytic formula

$$R_{\rm cr}(\zeta) = \zeta^{-1}\exp\left\{\frac{1}{g}\left[\arg\Gamma(1+2ig) - \operatorname{arccot}\frac{g-g'/g}{1+g'}\right]\right\} \quad (32)$$

was obtained in [9] by matching the relevant asymptotic expressions for the problem of two centers.[13] This method is usually quite accurate for shallow levels—this can be easily demonstrated by considering the problem of two delta-function wells at a fixed distance between them (the simplest example of a two-center problem). Therefore, it is natural to apply it to the problem being considered because, here, the effective energy is $E = 0$.

In (32), we set $g = \sqrt{\zeta^2 - 1}$, $g' = \sqrt{4 - \zeta^2}$, and $\zeta = (Z_1 + Z_2)/137$ and denoted by $\arg\Gamma(z)$ that branch of this multifunction for which $g^{-1}\arg\Gamma(1 + 2ig) = -2C + O(g^2)$ for $g \longrightarrow 0$ ($C = 0.5772\ldots$). This simple formula qualitatively reproduces the ζ dependence of the critical distance. It is consistent with expression (11) for $\delta \longrightarrow 0$ and, as can be seen from Tables 2 and 3, has an uncertainty of about 5 to 10% for $Z_1 + Z_2 \lesssim 200$ (as Z increases beyond this value, its accuracy deteriorates, however). Surprisingly, the asymptotic expression (32) agrees, to a percent precision, with the $R_{\rm cr}$ values as calculated with allowance for finite nuclear sizes (see Table 3); therefore, it can be used to obtain a fast estimate of $R_{\rm cr}$.

For the case of scalar particles, a similar approximation was constructed in [8], where the authors also formulated the variational principle for calculating $R_{\rm cr}$. For the case of one spherical nucleus, they found that $Z_{\rm cr}$ satisfies the equation

$$r_N = \frac{1}{2\zeta_{\rm cr}}\exp\left\{\frac{1}{g}\left[\arg\Gamma(1+2ig) - \operatorname{arccot}\left(-\frac{\xi}{g}\right)\right]\right\}, \quad (32a)$$

where $g = \sqrt{\zeta_{\rm cr}^2 - 1}$ and ξ is the same quantity as in Eq. (6). A comparison of expression (32a) with the results of the calculations according to the exact Eq. (6) reveals that, in the region around $r_N \sim 10$ fm, this formula provide $\zeta_{\rm cr}$ to a percent precision.

The last row of Table 2 presents $R_{\rm cr}$ values calculated in the monopole approximation, which corresponds to replacing the potential (18) by its zeroth spherical harmonic:

$$V(\mathbf{r}) \longrightarrow V_0(r) = \frac{1}{4\pi}\int V(r\mathbf{n})\,d\Omega_{\mathbf{n}}. \quad (33)$$

For the two-center problem ($r_N = 0$, $Z_1 = Z_2$), we have $V_0(r) = -2\zeta/R$ for $0 < r < R/2$ and $V_0(r) = -\zeta/r$ for $r > R/2$.

[13] In order to derive this formula, use was made of the fact that an excess over the critical charge is small in actual collisions: $\delta = (Z_1 + Z_2 - Z_{\rm cr})/Z_{\rm cr} \ll 1$ (for example, $\delta = 0.07$ in U + U collisions and $\delta \approx 0.1$ in U + Cf collisions).

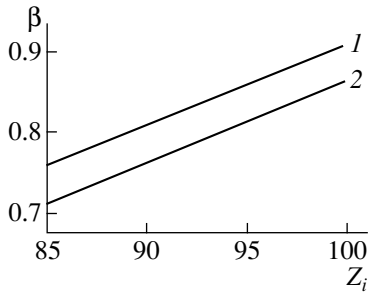

Fig. 6. Slope β of a level in the two-center problem [see Eq. (30)] versus the ion charge Z_i: (straight line *1*) results of the numerical calculation according to formula (30a) and (straight line *2*) results in the WKB approximation [formula (A.7)].

With allowance for finite nuclear sizes and at $Z_1 \neq Z_2$, the expression for $V_0(r)$ is rather cumbersome {see Eq. (29) from [25]}, but numerically solving the Dirac equation presents no serious difficulties because of the spherical symmetry of the potential. It can be seen from Table 2 that, for nuclei from the uranium region, the precision of the monopole approximation is acceptable (about 10%). The critical-distance values obtained in this way in [25] are displayed in Fig. 4 both for naked nuclei and for nuclei with an electron shell featuring 30 and 100 electrons.

So far, we have considered the $1s\sigma$ ground-state term of the relevant quasimolecule. For the next, $2p_{1/2}\sigma$, term, the result in the monopole approximation at $Z_1 = Z_2 = 92$ is $R_{\rm cr} \approx 18$ fm [25], which is close to the sum of the radii of the two nuclei involved. In this case, the deformation of one nucleus by the Coulomb field of the other nucleus becomes sizable, so that the problem ceases to be pure.

4. EFFECTIVE-POTENTIAL METHOD

The effective-potential method [7, 18] is useful for a qualitative analysis of the situation that emerges when a discrete level approaches the boundary of the lower continuum. The method consists in going over from the Dirac equation to the simpler Schrödinger equation featuring an effective energy E and an effective potential U. In general, the relation between the effective potential U and the original potential V directly appearing in the Dirac equation is rather complicated. The relevant expressions are simplified at the boundary of the lower continuum because, there, we are dealing with states at zero (effective) energy ($E = 0$). Equation (3) then takes the form

$$U(r) = -\frac{1}{2}V^2 - V + \frac{\kappa^2 + \kappa}{2r^2} + \frac{1}{4}\nu' - \frac{\kappa\nu}{2r} + \frac{1}{8}\nu^2, \quad (34)$$

where $\nu(r) = -V'/V$ depends only on the form of the original potential $V(r)$. Let us consider some specific examples.

For power-law attractive potentials

$$V(r) = -gr^{-\nu} \quad \text{for} \quad 0 < r < \infty \ (\nu > 0), \tag{35}$$

we have $\nu(r) = \nu/r$; taking into account the Langer correction $1/8r^2$, which improves the accuracy of the semiclassical approximation at small distances [40],[14] we arrive at

$$U(r) = -\frac{g^2}{2r^{2\nu}} + \frac{g}{r^\nu} + \left(\kappa + \frac{1-\nu}{2}\right)^2 \frac{1}{2r^2}. \tag{35a}$$

By way of example, we indicate that, in the case of a Coulomb field, the effective potential has the form

$$U(r) = \frac{\zeta}{r} - \frac{\zeta^2 - \kappa^2}{2r^2} \quad (g = \zeta, \nu = 1) \tag{36}$$

(see Fig. 7). Thus, we conclude that, for ε values close to –1, the effective potential involves a broad Coulomb barrier, owing to which the electron state under analysis is not delocalized when $\varepsilon \longrightarrow -1$; that is, the wave function decreases fast at infinity (compare with the results presented in [1]). For example, relation (17) holds at the critical point $Z = Z_{cr}$. This distinguishes the problem being considered from a typically nonrelativistic situation, where $\psi(r) \sim e^{-\lambda r}$ and $\lambda = \sqrt{2m\varepsilon_b} \longrightarrow 0$ for $\varepsilon_b \longrightarrow 0$ (here, ε_b is the binding energy—that is, the spacing between the level and the boundary of the continuous spectrum).

The presence of a Coulomb barrier in the effective potential affects all features of spontaneous positron production. For $Z > Z_{cr}$, the 1*s* level disappears from the discrete spectrum, going over to the lower continuum.[15] Since $\varepsilon < -1$, the effective energy E is positive, so that there arises the possibility for the level to decay by penetrating through the potential barrier (see Fig. 7).

The penetrability of the barrier in the effective potential determines the probability $\gamma(k)$ of spontaneous positron production. At the threshold ($k \ll 1$, where $k = \sqrt{\varepsilon_0^2 - 1}$ is the emitted-positron momentum), we have [3, 4]

$$\gamma \propto \exp\{-2\pi\zeta[\sqrt{1+k^2}/k - \sqrt{1-\zeta^{-2}}]\} \approx \exp\left(-b\sqrt{\frac{Z_{cr}}{Z - Z_{cr}}}\right) \tag{37}$$

(apart from a preexponential factor), where b is a numerical factor on the order of unity—for example, $b = 1.73$ for model I at $\zeta_{cr} = 1.25$.

For arbitrary $\nu < 2$, the potential in (35a) involves a barrier whose penetrability is exponentially small when $k \longrightarrow 0$. By using the Wentzel–Kramers–Brillouin (WKB) method,[16] one obtains [69, 70]

$$\psi_0(r) \propto [U(r)]^{-1/4} \exp\left\{-\int^r \sqrt{2U(r')}\,dr'\right\} \propto r^{\nu/4} \exp\left(-\frac{\sqrt{8g}}{2-\nu} r^{\frac{2-\nu}{2}}\right), \quad r \longrightarrow \infty, \tag{38}$$

$$\gamma(k) \propto \exp\{-\sqrt{\pi}\Gamma((2-\nu)/2\nu)/\Gamma(\nu^{-1})k^\nu\}. \tag{39}$$

But if $\nu > 2$, the penetrability here is determined by the centrifugal barrier; at the threshold, we therefore have

$$\gamma(k) \propto k^L, \quad L = j + \frac{1}{2}(1 - \nu\,\mathrm{sgn}\kappa).$$

Let us finally consider short-range potentials featuring an exponential tail,

$$V(r) = -gr^{-\nu}\exp(-\mu r), \quad r \longrightarrow \infty. \tag{40}$$

From (34), we find in this case that

$$U(r) = \frac{1}{8}\mu^2 + \frac{(\nu - 2\kappa)\mu}{4r} + O\left(\frac{1}{r^2}\right), \quad \varepsilon = -1; \tag{41}$$

therefore, we have $\psi_0(r) \propto \exp(-\mu r/2)$. Thus, we conclude that a state that descends to the boundary of the lower continuum remains localized in this case as well.

The use of an effective potential proved to be very useful for developing a physical interpretation of electron states occurring in a lower continuum for $Z > Z_{cr}$ [7].

Finally, we would like to comment on higher spin ($s > 1/2$) particles. Solutions to the Proca equation ($s = 1$) in the Coulomb field of a pointlike charge were considered in [71, 72], and it was shown there that, for any $\zeta > 0$, there occurs a collapse into the center. For the attractive potentials $V(r) = -gr^{-n}$ ($n > 0$), the effective

[14] It is well known that, in some cases, semiclassical energy spectra become coincident with exact ones upon introducing this correction.

[15] According to [1], the charge density associated with a single electron is delocalized for $Z \longrightarrow Z_{cr}$. However, the preexponential factor that appears in the asymptotic expression for the wave function, $\psi(r) \propto r^\mu \exp(-\lambda r)$, and which is associated with the Coulomb barrier in the effective potential (36) was disregarded in [1]. Since $\mu = \zeta\varepsilon/\lambda \longrightarrow -\infty$ and $\lambda = \sqrt{1-\varepsilon^2} \longrightarrow 0$ for $\varepsilon \longrightarrow -1$, the factor r^μ compensates for an ever slower decrease of the exponential $\exp(-\lambda r)$ for $r \longrightarrow \infty$, when the level approaches the boundary of the lower continuum (in contrast to the case of $\varepsilon \longrightarrow -1$, where the Coulomb interaction of the electron with the nucleus increases $\langle r \rangle$ in relation to what occurs in the case of a short-range potential). Thus, a bound state at the boundary of the lower continuum remains localized both for electrons [3] and for scalar mesons [4]. Therefore, there are no reasons to expect that the polarization charge of the vacuum increases greatly for $Z \longrightarrow Z_{cr}$ (in the case of fermions, for which the Pauli exclusion principle is operative [7]); this is fully confirmed by the numerical calculations of vacuum polarization that were performed in the 1980s, as well as by those calculations for the vacuum-polarization-induced shifts of levels in heavy atoms up to $Z = 137$ and even up to $Z = 170 \sim Z_{cr}$.

[16] The condition of applicability of the semiclassical approximation [41, 47] is satisfied here: $\frac{d}{dr}(1/p(r)) \propto \nu g^{-1/2} r^{-(2-\nu)/2} \ll 1$ for $r \longrightarrow \infty$.

potential (35) for states characterized by specific values of the total angular momentum j has the form

$$U(r) = -gn\sqrt{j(j+1)}/r^{n+2} + \ldots, \quad r \longrightarrow 0; \quad (42)$$

therefore, collapse into the center occurs here at an arbitrarily small power-law singularity of $V(r)$ at the origin [3]. For the Proca equation, the potential that represents the boundary between regular and singular potentials has the form

$$V(r) = -g\ln\frac{1}{r} + \ldots, \quad r \longrightarrow 0, \quad (43)$$

in which case

$$U(r) = -g\sqrt{j(j+1)}/r^2 + \ldots. \quad (44)$$

For $g < g_{cr} = (j+1/2)^2/\sqrt{j(j+1)}$, this potential is regular, requiring no cutoff; as soon as the coupling constant g exceeds the critical value g_{cr}, it becomes singular (similarly to the Coulomb potential for the Dirac and the Klein–Gordon equation).

5. WENTZEL–KRAMERS–BRILLOUIN METHOD FOR $Z > 137$

It is of interest to apply the semiclassical approximation to the case of a strong Coulomb field. The first attempt along these lines was made by Krainov [73], but he used the WKB method not only in the Coulomb field region ($r > r_N$) but also in the interior of the nucleus, where its accuracy is rather poor. A consistent application of the WKB method to the relativistic Coulomb problem was developed in [74], where the semiclassical wave function was matched with a solution to the Dirac equation in the internal region ($0 < r < r_N$). In practice, it is more convenient to find not ζ_{cr} at a given nuclear radius but the function

$$r_N = \frac{\zeta_{cr}^2 - \kappa^2}{\zeta_{cr}(1+\cosh 2y)},$$

$$y - \tanh y = \frac{1}{2\sqrt{\zeta_{cr}^2 - \kappa^2}} \quad (45)$$

$$\times\left\{\left(n_r + \frac{2l+3}{4}\right)\pi - \operatorname{arccot}\left(\frac{\xi}{\sqrt{\zeta_{cr}^2 - \kappa^2}}\right)\right\},$$

where ξ is the logarithmic derivative of the internal wave function at the boundary of the nucleus (see Appendix A). This formula is convenient for applications, its accuracy is about 1% in the region of radii around $r_N \sim 10$ fm, and it correctly reproduces the dependence of Z_{cr} on the model of cutoff of the Coulomb potential within the nucleus (see Fig. 1). Moreover, its accuracy only improves with increasing r_N or ζ_{cr} [see Fig. 1 and Eq. (A.4)]. For the next, $2s_{1/2}$, level, the precise and the semiclassical curve are indistinguishable on the scale of the figure.

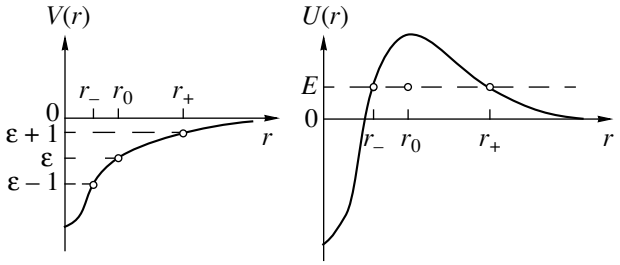

Fig. 7. Original potential $V(r)$ and effective potential $U(r)$ for the relativistic Coulomb problem at $Z \approx Z_{cr}$ [here, $r_\pm$ are the turning points, while $r_0 = (\zeta^2 - \kappa^2)/\zeta$ is the point where the effective potential peaks].

The electron state at the boundary of the lower continuum remains localized [see Eqs. (17) and (29) above]. Therefore, the discrete level for $Z \longrightarrow Z_{cr}$ does not tend to be tangent to the boundary $\varepsilon = -1$, entering the lower continuum with a finite slope β:

$$\varepsilon(\zeta) = -1 + \beta(\zeta_{cr} - \zeta) + \ldots. \quad (46)$$

The value of β is of some interest for the theory [4, 21]. As can be seen from Figs. 3 and 6, the WKB method determines the slope parameter β to a satisfactory precision.

The semiclassical approximation can also be applied to the relativistic two-center problem. Referring the interested reader to [75–77] for details, where the WKB method was consistently developed for $\varepsilon \approx -1$ states of the Dirac equation, we only present here an equation that determines the energies of the electron terms of the quasimolecular system (Z_1, Z_2, e^-) near the boundary $\varepsilon = -1$. Specifically, we have

$$\frac{R_{cr}}{R} = \left[1 - \left(1 + \frac{1-2\kappa}{4\zeta^2}\right)(1+\varepsilon)\right]\phi(x), \quad (47)$$

where

$$x = (1-\rho^2)\left[\varepsilon^2 - 1 + \left(\kappa - \frac{5}{4}\right)\frac{(1+\varepsilon)^2}{\zeta^2}\right]$$

$$\times\left[1 - \left(1 + \frac{1-2\kappa}{4\zeta^2}\right)(1+\varepsilon)\right]^{-2},$$

$$\phi(x) = \exp\left\{\frac{1}{2\sqrt{x}}[(1+\sqrt{x})\ln(1+\sqrt{x})\right.$$

$$\left. -(1-\sqrt{x})\ln(1-\sqrt{x})] - 1\right\}, \quad x > 0,$$

$$\phi(x) = (1-x)^{1/2}\exp\{(\arctan\sqrt{-x}/\sqrt{-x}) - 1\}, \quad x < 0,$$

$\zeta = (Z_1 + Z_2)/137$, and $\rho = |\kappa|/\zeta$ $(0 < \rho < 1)$. At $\varepsilon \approx -1$, we have $x = (1-\rho^2)(\varepsilon^2 - 1) + \ldots$. According to (47), the energy of the term, ε, depends on the ratio R/R_{cr} [this is a corollary of the condition $r_N \ll r \ll r_K$ (where r_K is the K-shell radius), which is satisfied, provided that the

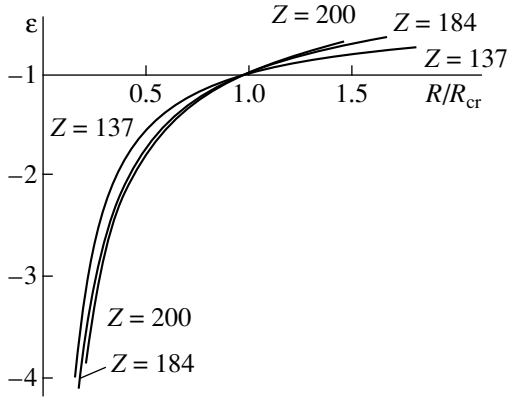

Fig. 8. Energy of the ground-state term in the two-center problem. The values of the total charge $Z = Z_1 + Z_2$ of the nuclei involved are indicated on the curves.

total charge of the two nuclei involved exceeds only slightly the critical charge value, $Z_1 + Z_2 - Z_{cr} \ll Z_{cr}$]. The value R_{cr} itself was calculated separately—for example, by means of the variational method (see Section 3). The results are represented by the curves in Fig. 8.

The possible existence of $Z \gg Z_{cr}$ nuclei (of course, stability of such nuclei can be ensured only by some new mechanism—for example, by the formation of a negative-pion condensate [28]), referred to as supercharged ones, was considered in the literature [29, 78]. We denote by n_κ and N the number of discrete levels characterized by a given value of the quantum number κ that have descended to the lower continuum and the total number of such levels, respectively, and by N_e the number of electrons in the vacuum shell of a supercritial atom (such a shell is formed near a supercritical atom upon positron emission). Obviously, the relations $N = \sum_\kappa n_\kappa$ and $N_e = \sum_\kappa (2j + 1)n_\kappa$ then hold; in the semiclassical approximation, we obtain

$$N = \frac{1}{2}\int_0^\infty (V^2 + 2V)_+ r dr,$$
$$N_e = \frac{4}{3\pi}\int_0^\infty \{(V^2 + 2V)_+\}^{3/2} r^2 dr, \quad (48)$$

where $f_+(r) = f(r)$ if $f(r) \geq 0$ and $f_+(r) = 0$ if $f(r) < 0$. In the case of the potential given by (5), it follows that, for $\zeta \gg 1$, we have

$$N = \frac{1}{2}\zeta^2\left(\ln\frac{\zeta}{r_N} + c_4\right),$$
$$N_e = \frac{4}{3\pi}\zeta^3\left(\ln\frac{\zeta}{r_N} + c_5\right), \quad (49)$$

where c_4 and c_5 are numerical constants on the order of unity that depend on the cutoff model. Figure 9 borrowed from [79] demonstrates that the semiclassical approximation is quite accurate even at relatively small values of $\zeta \gtrsim 2$.

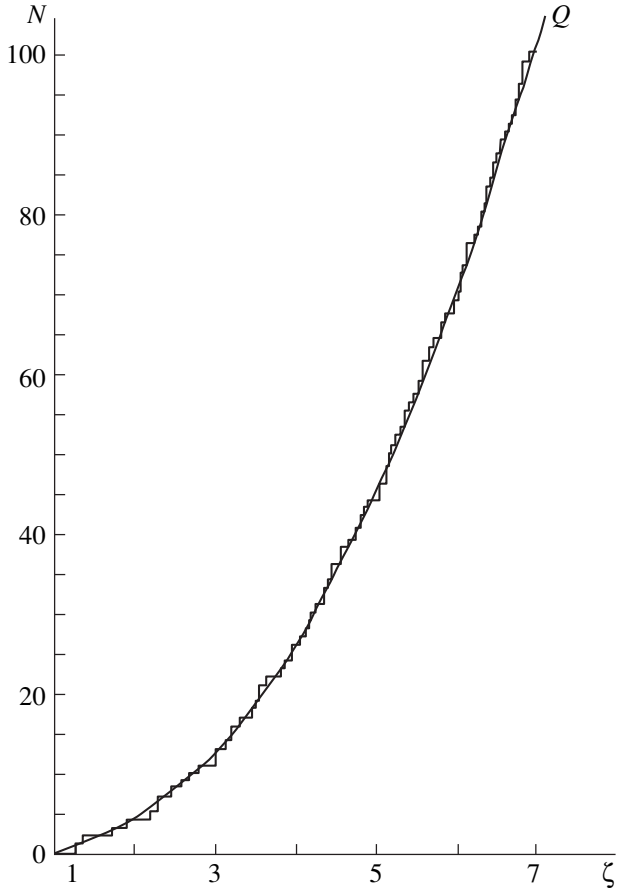

Fig. 9. Number N of levels that have descended to the lower continuum [for the potential (5)]. The stepwise broken line represents a numerical solution to the Dirac equation, while the curve Q was computed according to the semiclassical formula (49).

Equations (48) suggest that the local density of the electron cloud in the vacuum shell of a supercritical atom is $\rho(r) = (V^2 + 2V)^{3/2}/3\pi^2$, and this natural assumption can indeed be rigorously substantiated [54]. This makes it possible to write the relativistic Thomas–Fermi equation [26, 54]

$$\Delta V = -4\pi e^2\left[\frac{1}{3\pi^2}(V^2 + 2V)^{3/2} - n_p(r)\right] \quad (50)$$

(where n_p is the density of protons in a supercritical nucleus), whose solution determines the properties of the electron shell in an atom for $Z \gg 137$.

We will not dwell any more on these questions, referring the interested reader to the aforementioned studies and to the monographs [38, 39, 78]. The only objective here was to demonstrate the efficiency of the WKB method for ultrastrong Coulomb fields.

Table 4. Accuracy of the WKB method for the Salpeter equation (case of massless quarks)

	$n_r = 0$	1	2	3	5	References
$l = 0$	0.9724	0.9958	0.9983	0.9991	0.99953	[83]
	0.9725	0.9959	0.9982	0.99905	–	[84]
$l = 1$	0.9391	0.9743	0.9858	0.9908	0.9952	[83]
	0.9382	0.9744	0.9859	0.9910	–	[84]
$l = 2$	0.9232	0.9590	0.9742	0.9820	0.9897	[83]
$l = 3$	0.9152	0.9478	0.9642	0.9742	–	[84]

Note: Quoted in the table are the meson-mass ratios $M_{n_r l}^{(\mathrm{calc})}/M_{n_r l}$, where $M_{n_r l}$ stands for the results of numerical calculations from [83, 84], while $M_{n_r l}^{(\mathrm{calc})}$ corresponds to the calculation relying on the modified quantization rule from [74] and taking into account relativistic kinematics according to [85].

It should be noted here that the WKB method can be applied to two-particle relativistic wave equations, including the Salpeter equation [80–82] for the quark–antiquark system. In the case of the confining potential $V(r) = \sigma r$ (where σ is the tension of the string between the quark and the antiquark involved) in this Salpeter equation

$$\{\sqrt{\mathbf{p}^2 + m_1^2} + \sqrt{\mathbf{p}^2 + m_2^2} + V(r)\}\psi_n = M_n\psi_n,$$

where $\mathbf{p} = -i\nabla$, m_1 and m_2 are the masses of the quarks (whose spins are disregarded here), and M_n are the meson masses, the semiclassical mass spectrum of mesons agrees, to a percent accuracy, with the spectrum obtained by numerically solving [83, 84] the Salpeter equation (especially for $l \sim 1$ states, including the ground state, for which $n_r = l = 0$). For further details, the reader is referred to [85, 86] (see also Table 4).

6. Z_{cr} FOR OTHER PARTICLE SPECIES

In the case of a Coulomb field, the Klein–Gordon equation has a solution decreasing at infinity,

$$\chi_l(r) = \mathrm{const} \times W_{\mu,\, i\nu/2}(x), \quad -1 \le \varepsilon < 1, \qquad (51)$$

where $x = 2\lambda r$,

$$\lambda = \sqrt{1-\varepsilon^2}, \quad \mu = \zeta\varepsilon/\lambda, \qquad i\nu/2 = \sqrt{(l+1/2)^2 - \zeta^2}, \qquad (51a)$$

and $W_{\mu,\, i\nu/2}$ is the Whittaker function. The energy of the ground-state level in the field of a pointlike charge is

$$\varepsilon_0(\zeta) = \left(\frac{1}{2} + \sqrt{\frac{1}{4} - \zeta^2}\right)^{1/2} = \frac{1}{\sqrt{2}}\left(1 + \sqrt{\frac{1}{2} - \zeta} + \ldots\right), \quad \zeta \longrightarrow \frac{1}{2} \qquad (52)$$

[compare with Eq. (1)]. States that are pure in the orbital angular momentum l now undergo collapse into the center for $\zeta > l + 1/2$. In the limit $\varepsilon \longrightarrow -1$, which corresponds to $\lambda \longrightarrow 0$, $\mu \longrightarrow -\infty$, and $\mu x \longrightarrow -2\zeta r$, the Whittaker function is simplified significantly to become

$$\chi_l(r) = \mathrm{const} \times r^{1/2} K_{i\nu}(\sqrt{8\zeta r}), \qquad \nu = 2\sqrt{\zeta^2 - (l+1/2)^2}. \qquad (53)$$

It can easily be shown that the equation for ζ_{cr} can be written in a unified form for the spin values of $s = 0$ and 1/2; that is,

$$zK'_{i\nu}(z)/K_{i\nu}(z) = 2(s + \xi) - 1, \qquad (54)$$

where $z = \sqrt{8\zeta_{\mathrm{cr}} r_N}$, as in Eq. (6). For the ground state, we have $\nu = 2\sqrt{\zeta_{\mathrm{cr}}^2 - (s+1/2)^2}$ in both cases.

Under the condition $r_N \ll 1/m$, we have $\xi = \zeta\cot\zeta$ for the cutoff model I (see Appendix A), as before. Considering, however, that $mr_N > 1$ for pions, we conclude that the Klein–Gordon equation must be solved exactly in the internal region $r < r_N$. In the simplest case ($l = 0$, cutoff model I), we obtain

$$\xi = \beta\cot\beta, \quad \beta = \sqrt{\zeta(\zeta - 2r_N)}. \qquad (55)$$

Equations (54) and (55) were solved with the aid of a computer [3]. Although $Z_{\mathrm{cr}} = 1/2\alpha = 68.5$ for a pointlike charge in this case, the value of Z_{cr} exceeds 137 even at $r_N \sim 0.1\hbar/mc$ (see Fig. 4 in [3]). A numerical calculation for pions ($\hbar/m_\pi c = 1.41$ fm) yields $Z_{\mathrm{cr}}^{(\pi)} \approx 3300$ [87], which is far beyond any known nucleus.

The situation is similar for muons ($\hbar/m_\mu c = 1.87$ fm). Solving Eq. (6) led to $\zeta_{\mathrm{cr}} = 16.7$ or $Z_{\mathrm{cr}}^{(\mu)} \approx 2300$ for model II and $Z_{\mathrm{cr}}^{(\mu)} \approx 3700$ for model I [69]. Thus, we can see that, for $r_N \ll 1/m$, the numerical value of Z_{cr} depends greatly on the choice of model. It should be emphasized that it was Migdal who suggested the existence of supercharged nuclei with $Z \sim 137^{3/2}$ [29]; however, the theory does not provide definitive results

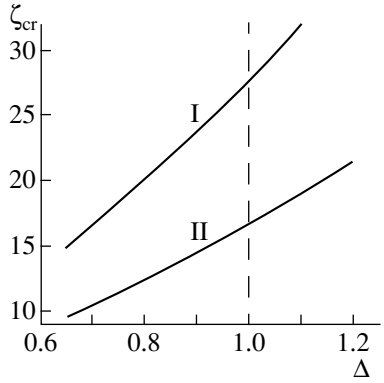

Fig. 10. Critical charge of a nucleus for the muon (the cutoff models I and II were used). For ordinary heavy nuclei, the parameter Δ is equal to unity.

for their density and for the relation between A and Z. Let us assume that $r_N = r_0 A^{1/3}$, where $r_0 = 1.2\delta$ fm and $A/Z = 2.6\xi$, δ and ξ being free parameters (for conventional nuclei, we have $\delta = \xi = 1$). The critical charge $Z_{cr}^{(\mu)}$ depends strongly on the parameter $\Delta = \delta\xi^{1/3}$ (see Fig. 10). It should also be noted that the above values of the critical charge should be treated as a first approximation, since the calculation took no account of the screening of the potential (5) by the electron shell that the naked nucleus attracts from a vacuum upon the spontaneous emission of positrons and their escape to infinity. The inclusion of the screening effect is expected to increase Z_{cr} still further.

Thus, the situation where muon or pion levels in a superheavy nucleus reach the boundary $\varepsilon = -mc^2$ can hardly be realized.

7. MISCELLANEA

Here, we consider some additional questions related to those discussed in Sections 2–6.

1. From Eq. (4), it can be seen that, for $\varepsilon \approx -1$, $\zeta > j + 1/2$ electron states, an effective attraction proportional to $1/r^2$ arises at small distances (for a pointlike charge, it leads to a collapse into the center [46–49]). This attraction, which is a purely relativistic effect, stems from introducing the Coulomb interaction of the electron with the nucleus in a minimal way—that is, through the time component of the 4-potential A_μ. This can be seen from the example of the Klein–Gordon equation alone, which is obtained for a spinless particle from the relation $\mathbf{p}^2 = \varepsilon^2 - m^2$ by means of the substitution $p_\mu \longrightarrow p_\mu - eA_\mu$. The resulting equation

$$\Delta\varphi + [(\varepsilon - V)^2 - m^2]\varphi = 0 \qquad (56)$$

is identical to the Schrödinger equation in form if we set

$$E = (\varepsilon^2 - m^2)/2m, \quad U = \frac{\varepsilon}{m}V - \frac{1}{2m}V^2. \qquad (57)$$

The term $-\frac{1}{2m}V^2$ is dominant at small distances, where $|V(r)| \longrightarrow \infty$ and leads to attraction, irrespective of the sign of $V(r)$. For the spin value of $s = 1/2$, the form of the effective potential becomes more complicated, but it undergoes no significant qualitative changes: the expression for $U(r)$ develops additional terms associated with the particle spin and spin–orbit interaction [see Eqs. (3) and (34) and also Appendix C].

2. If light charged scalar bosons (of mass about m_e) existed in nature, then effects associated with the approach of a discrete level to the boundary $\varepsilon = -mc^2$ would be observable because $Z_{cr} = 68.5$ at $r_N = 0$ for such bosons. However, we have $\hbar/m_\pi c = 1.41$ fm and $m_\pi r_N \gg 1$ for the pion, and Z_{cr} considerably exceeds 137 in this region, as was shown in the preceding section.

A modest (in relation to the case of a pointlike charge) increase in Z_{cr} from $Z_{cr}^{(0)} = 137$ for electrons is associated with the fact that $m_e r_N \sim 0.03 \ll 1$.

3. With increasing potential-well depth, the energy levels ε for bosons and fermions behave differently, which was first discovered by Schiff *et al.* [88], who considered the example of s states in the square well $V(r) = -g\theta(r_0 - r)$ for the Klein–Gordon equation. Namely, the dependence of ε on the coupling constant g in the case of the Klein–Gordon equation is nonmonotonic—there is a backbending, which occurs near $\varepsilon = -1$ if the well is sufficiently wide. At some coupling-constant value $g = g_{cr}$, two levels going from the continuum boundaries $\varepsilon = 1$ and -1 merge, whereupon there arise states characterized by a square-integrable wave function; however, the energies of these states are complex-valued, which is at odds with unitarity. This means that, at $g > g_{cr}$, the single-particle Klein–Gordon Hamiltonian is no longer a self-conjugate operator and has no physical meaning.

A physical interpretation of this phenomenon was given by Migdal [28]: at $g \sim g_{cr}$, there occur the virtual production of charged particle–antiparticle pairs and a strong vacuum polarization, which screens the bare charge g, thereby preventing it from reaching the critical charge g_{cr}. It follows that, in the boson case, the theory must inevitably be multiparticle at $g \sim g_{cr}$. (For electrons, the situation is totally different. Because of the Pauli exclusion principle, there are only two vacancies in the K shell at $Z > Z_{cr} \sim 170$ upon positron emission; therefore, vacuum polarization leads only to a small effect of order α and is unable to prevent the descent of the next levels of the electron spectrum to the lower continuum [7].)

By developing these considerations further, Migdal *et al.* [78] created the theory of pion condensation in nuclear matter and predicted some interesting effects. Unfortunately, no experimental evidence for the existence of a pion condensate in conventional heavy nuclei has been obtained so far.

4. It should be noted that the problem of establishing the character of the motion of levels near the boundary $\varepsilon = -1$ presents considerable difficulties, because its investigation involves analyzing complicated equations. After [88], the problem was addressed in [89–95]; however, some of the results presented in [91, 92] are erroneous. The relativistic generalization of the effective-range expansion for states whose energy is close to the boundary of the lower continuum is a very convenient means for studying this problem [95]. An analysis along these lines reveals [69, 95] that, for the Dirac equation, there are no positron levels that would arise from the lower continuum and which would have a positive derivative $d\varepsilon/d\zeta$. At the same time, there are such levels for the Klein–Gordon equation [88], in which case, for a short-range potential $V(r) = -gv(r)$, two bound states merge at some value $g = g_{cr}$ and $\varepsilon > -1$; for $g > g_{cr}$, the S matrix for this case develops complex poles on the physical sheet. A remarkable property of the Dirac equation is that it does not involve such a difficulty; therefore, the single-particle Dirac equation retains, to some extent, its meaning in the supercritical region $g > g_{cr}$ as well [7].

If the potential $V(r)$ possesses a Coulomb tail for $r \longrightarrow \infty$, the bound state remains localized even at $\varepsilon = -1$ and $\zeta = \zeta_{cr}$ owing to the presence of a barrier in $U(r)$ [see Eq. (17) above]. Therefore, all levels of the discrete spectrum enter the lower continuum at a finite slope $d\varepsilon/d\zeta = -\beta < 0$ (both for the spin of $s = 1/2$ and for the spin of $s = 0$ [4]). Nonetheless, the distinction between the boson and the fermion case still remains at the fundamental level: the S-matrix pole corresponding to a bound state at $Z < Z_{cr}$ goes into the complex plane (for $Z > Z_{cr}$) on the physical sheet at $s = 0$ and on the unphysical sheet at $s = 1/2$.

5. Let us consider the effect of a magnetic field on Z_{cr}. In a magnetic field so strong that the Larmor radius of an electron, $l = \sqrt{\hbar c/eB} = \sqrt{B_0/B}$ (in $\hbar/mc$ units), is less than the mean ground-state radius $\langle r \rangle$, the electron shell is squeezed toward the nucleus in the direction orthogonal to the field **B**, taking a cigarlike shape [96–98]; therefore, the electron effectively undergoes a stronger attraction to the nucleus than in the absence of a field, whereby the critical charge decreases. The condition $l \ll \langle r \rangle$ actually corresponds to $B \gg B_0 = m^2c^3/e\hbar = 4.41 \times 10^{13}$ G (where B_0 is the critical, Schwinger [99], field[17]) peculiar to QED).

The problem being discussed was comprehensively studied in [101]. For a "weak" magnetic field, the reduction of Z_{cr} can be found by perturbation theory. The result is

$$\zeta_{cr}(B) = \zeta_{cr}(0) - \frac{5\pi^2\mu}{6[\ln(1/r_N)]^3}\frac{B}{B_0} + O((B/B_0)^2), \quad (58)$$

where μ is the magnetic moment (15). It follows that, even at $B \sim 0.1B_0 \sim 5 \times 10^{12}$ G, $\Delta Z_{cr} < 1$.

For stronger fields, the dependence $Z_{cr}(B)$ is obtained from the equations derived in [101], which were solved numerically. Presented immediately below are some results referring to the ground state: $Z_{cr} \approx 165$ at $B = B_0$, $Z_{cr} = 96$ at $B = 100B_0$, $Z_{cr} = 92$ (uranium nucleus) at $B = 133B_0 \approx 5.5 \times 10^{15}$ G, and $Z_{cr} = 41$ at $B = 2.4 \times 10^4 B_0 \approx 10^{18}$ G. The next level of the electron spectrum reaches the boundary $\varepsilon = -1$ at $B \sim 1.5 \times 10^{16}$ G if $Z_{cr} = 92$, and so on.

Thus, we conclude that, in the presence of a strong magnetic field, the boundary of the lower continuum can be reached at charge values as small as $Z < 170$—for example, in the case of a naked uranium nucleus or even in the case of lighter nuclei. The above estimates show, however, that this requires magnetic fields of strength not less than the critical one. It should be recalled that maximum magnetic fields achieved so far under laboratory conditions are six orders of magnitude less than that [102, 103].

6. Some authors considered modifications to QED and their effect on spontaneous positron production.[18] In particular, Rafelski *et al.* [107] considered a nonlinear Lagrangian of the Born–Infeld type [108]. For the case of electrostatics, it leads to the energy density

$$w = \frac{E_0^2}{2n}\left[\left(1 + \frac{D^2}{E_0^2}\right)^n - 1\right], \quad (59)$$

where n and E_0 are parameters of the theory—for example, $n = 1$ (or $E_0 \longrightarrow \infty$), $n = 1/2$, and the limiting case of $n = 0$ correspond, respectively, to Maxwell electrodynamics, to Born–Infeld theory, and to Infeld–Hoffmann theory.

We denote by E_B the E_0 value obtained from the condition [108] that the electron mass is entirely of an electromagnetic origin. We then have $E_B = 1.2 \times 10^{18}$ V/cm at $n = 1/2$, in which case $Z_{cr} = 214$ for the $1s$ level [107]. This would naturally dash the hopes for observing spontaneous positron production in experiments with known heavy nuclei. However, the above value of E_0 contradicts experimental data on atomic levels. In order to avoid a conflict with the precisely measured energy differences in the spectra of the ^{82}Pb and ^{100}Fm nuclei, it is necessary to assume [110] that $E_0 > 140E_B \sim 2 \times 10^{20}$ V/cm. As a result, the critical charge can increase by not more than two units.

Here, we will not consider other modifications to QED (see, for example, [111, 112]) that were also discussed in the literature in connection with the effect of spontaneous positron production.

[17] Of course, so strong a field can occur only under extremal conditions (for example, within pulsars [100]).

[18] At present, the predictions of QED are in remarkable agreement with experimental data: in the record case of the electron anomalous magnetic moment, the accuracy is 10^{-12} [104–106]. In this connection, the modifications to QED that are discussed below seem less interesting.

7. The method of linear combinations of atomic orbitals (LCAO), which is known from quantum chemistry, was used in [113] to solve the relativistic two-center problem. For the ground-state term considered in the case of identical charges of the nuclei involved, one can set

$$\psi = a\psi_1 + b\psi_2, \quad a = b = 1/\sqrt{2(1+S)}, \qquad (60)$$

where ψ_1 and ψ_2 are the wave functions of an electron moving in the field of, respectively, the first and the second center, while $S = \langle\psi_1|\psi_2\rangle$ is the overlap integral. The relativistic wave functions of the hydrogen-like atom [45] with an effective charge $Q\alpha < 1$ (which depends on R and Z) were taken for ψ_1 and ψ_2. As a result, an analytic, albeit rather cumbersome, formula was obtained for the ground-state term. This formula makes it possible to calculate $\varepsilon_0(R, Z)$ over a wide region of R and Z. A comparison with the numerical results from [27] shows that the error of this formula is 10% at $Z/2 = 35$ (Br + Br system) and as large as 25% at $Z/2 = 92$. Thus, we can see that, in the region $90 \le Z/2 \le 100$, the accuracy of this approximation is insufficient, so that it is necessary to use a more complicated trial function featuring a greater number of variational parameters than in (60).

8. OPTIMISTIC CONCLUSION

Qu'est-ce qu'optimisme? disait Cacambo. Hélas! dit Candide, c'est la rage de soutenir que tout est bien quand on est mal.

Voltaire "Candide ou l'Optimisme"[19)]

Let us briefly touch upon the currently prevalent experimental situation.

Experiments seeking spontaneous and induced positron production in heavy-ion collisions (at energies close to the height of the Coulomb barrier) were performed at the UNILAC heavy-ion accelerator of GSI (Darmstadt, Germany). There, beams of Pb and U ions of energies 3 to 6 MeV per projectile nucleon were obtained. Even the first experiments [114, 115], which were conducted in the subcritical region ($Z_1 + Z_2 < Z_{cr}$), recorded induced positron production due to the quickly varying (in time) Coulomb field of colliding nuclei (the term "quasiatomic" or "induced" positrons is often used in the literature for this case). The energy spectra of these positrons comply well with the results of theoretical calculations for the process. Of particular interest are the results [116–118] presented by two experimental groups, EPOS and ORANGE, which were named after the magnetic spectrometers that they used. In addition to the theoretically predicted continuous spectrum of positrons, these groups reported the observation of a few relatively narrow positron peaks (of width not greater than 40 keV). Later on, this effect, which was much to the surprise of experimentalists and which was dubbed the Darmstadt effect, was repeatedly tested and refined, and a few tens of events were recorded under the areas of the most pronounced peaks (at $E_{e^+} \approx 255$ and 340 keV). Subsequently, narrow peaks were also observed in the spectrum of electrons recorded in coincidence with positrons and in the total-energy ($E_{e^+} + E_{e^-}$) spectra (see [119–121] and references in the review article by Pokotilovsky [122]), which is puzzling phenomenon indeed.

Naturally, these unusual phenomena inspired keen interest of theorists. In the period from 1985 to 1992, there appeared a few tens of theoretical studies that were devoted to the subject and which put forth various hypotheses, sometimes exotic ones, to explain the Darmstadt effect: the decay of a new particle (axion [123, 124]), composite extended particles, magnetic quasibound states of the e^+e^- system [125], a new phase in the QED vacuum [112], the formation (in heavy-ion collision) of a quasimolecule whose nuclei are at a distance $R < R_{cr}$ for a time period $T \gg R_{cr}/v \sim \hbar/mc^2 \sim 10^{-21}$ s [126, 127], and the capture and cooling of positrons in an expanding open resonator between two Coulomb centers [128]. Without further extending this list, we only note that none of these mechanisms could provide a full and compelling description of all phenomena observed at GSI.

More recently, a critical analysis of these (extremely difficult) experiments and new experiments that collected much vaster statistics revealed that narrow lines in the electron and positron spectra were an experimental error (this was recognized by the authors from GSI themselves [129, 130]), so that no new physics is needed, as has already occurred many times in the history of science, for explaining these phenomena.

It is difficult to say when the Darmstadt experiment will be continued, if at all, and when a detailed comparison of the theory of spontaneous positron production with experimental data will be performed, which would imply a check upon QED and upon the Dirac equation not in the traditional region of high energies and small distances but in the new region of ultrastrong external fields. These experiments are complicated[20)] and expensive, while one should not expect sensational discoveries here. At the same time, such experiments do not require new giant accelerators whose construction

[19)]"What is optimism?" said Cacambo. "Alas!" Candide said, "it is the mania of maintaining that everything is well when we are wretched." [Quoted from *Candide and Other Romances by Voltaire* (Dodd, Mead and Company, New York, 1928; translated from the French by Richard Aldington.]

[20)]The main difficulty here consists in isolating the process of interest among other processes inevitably accompanying it, like induced positron production and the formation of positrons in nuclear processes. Moreover, the spontaneous-positron-production cross section itself is small near the threshold ($E \longrightarrow E_{thr} = 2(Ze)^2/R_{cr}$) [4, 7, 21] because of the Coulomb barrier in (36), which also ensures a localization of the electron state with energy $\varepsilon \le -1$ in the lower continuum. At energies $E \gtrsim 2E_{thr}$, however, this cross section no longer has an exponential smallness.

could ruin the budget of a country: the energy that is necessary to cause the approach of two uranium nuclei within the critical distance of $R_{cr} \approx 35$ fm is 5 to 6 MeV per nucleon, an energy value that has long since been achieved at heavy-ion accelerators available worldwide. Moreover, considerable advances have recently been made in producing beams of heavy ions deprived partly or even completely of their electron shell (it should be recalled [7, 38, 39] that, for spontaneous positron production, it is necessary that an unfilled K-level descend to the lower continuum[21]). All this gives sufficient grounds to regard the future of experimental investigations in these realms of physics with a refrained optimism (at the same time, the above opinion of Voltaire also deserves attention).

The situation can change drastically if $Z \gtrsim 137^{3/2}$ nuclei are discovered some day, which must be surrounded, as the theory indicates, by a dense vacuum shell consisting of electrons that have descended to the lower continuum. The possible existence of such supercharged nuclei (with $A > 10^3$ and $N = Z$) was repeatedly emphasized by Migdal [29, 78, 131–133]. Their stability would be guaranteed owing to the screening of the proton charge by the negative-pion condensate and by electrons distributed within the nucleus:

"For $Z > Z_c \approx (137)^{3/2}$ stable nuclei should exist. At a sufficient value of $Z - Z_c$ such nuclei should be stable with respect to fission" [29].

"For highly charged nuclei, fission instability is most important. Fission stability is possible only if the Coulomb energy is considerably suppressed. This means that the π^- charge should be of the order of Z. As we have shown, $Z_\pi \approx Z$ at $Ze^3 \sim 1$. Thus, the considerable suppression of the Coulomb energy at $Ze^3 \sim 1$ can lead to the stability of supercharged nuclei" [133].

An analysis has revealed that there exist two possible regions of stability of anomalous nuclei—the region of superdense nuclei ($Z \approx N$, $Z \lesssim 10^2$) and the region of superheavy nuclei ($Z \approx N$, $Z \gtrsim 10^3$); here, the electric charge of baryons is fully compensated by the pion condensate and by the electrons …. In the limiting case of $Z \gg 1/e^3 \approx 1600$, the interior of a superheavy nucleus appears to be an electrically neutral plasma formed by baryons, pion-condensate mesons, electrons, and negative muons. For such nuclei, there are no upper bounds on A, so that there can in principle exist stars in the form of a nucleus [78].

These are basic conclusions from those studies on the possible existence of superheavy nuclei in nature. Of course, it should be borne in mind that the modern theory of the nucleus is not celestial mechanics: even the law of interaction between two nucleons in a vacuum has not been established conclusively, nor can an *ab initio* solution to the Schrödinger equation for a heavy nucleus be obtained. Therefore, a theoretical extrapolation from conventional nuclei to the far region around $Z \sim 137^{3/2}$ can hardly be reliable.[22] However, we would like to complete the present discussion with the following words: "Cela est bien dit, répondit Candide; mai il faut cultiver notre jardin" [136].[23]

ACKNOWLEDGMENTS

I am grateful to S.S. Gershtein, B.M. Karnakov, V.D. Mur, and L.B. Okun for looking through the manuscript and for enlightening comments; to Yu.Ts. Oganessian for a discussion on the problem of superheavy elements; to D.N. Voskresensky and E.E. Saperstein for calling my attention to the studies quoted in [134, 135]; to V.I. Lisin and S.G. Pozdnyakov for performing relevant numerical calculations; and to M.N. Markina for assistance in the preparation of the manuscript.

This work was supported in part by the Russian Foundation for Basic Research (project nos. 98-02-17007 and 01-02-1685).

APPENDIX A

Semiclassical Approximation in the Relativistic Coulomb Problem

(a) Let us consider the case of a heavy spherical nucleus. Since we have $r_N \ll \hbar/mc = 1$ in Eq. (5) (at $\zeta = 1.25$, the nuclear radius is $r_N \approx 0.023$), the main contribution to the quantization integral comes from the region $r_N < r < r_0$, where

$$p^2(r) = \frac{g^2}{r^2}\left(1 - \frac{r}{r_0}\right), \quad g = \sqrt{\zeta^2 - \kappa^2}, \qquad r_0 = g^2/2\zeta, \tag{A.1}$$

r_0 being the turning point. The semiclassical wave function corresponding to the upper component of the Dirac

[21] It is worthy of note that spontaneous positron production from a vacuum is possible not only in a collision of two $Z_u > Z_{cr}$ nuclei with unfilled K shells but also in the case where this is so for only one (Z_1) of the nuclei (the second can involve K electrons—this can be for example, a neutral atom of the target nucleus). In the latter case, it is necessary that $Z_1 \geq Z_2$, as follows from a comparison of the molecular terms of the (Z_1, Z_2, e) system at small and at large distances between the nuclei [20, 21].

[22] In this connection, the following comment is in order. Estimates from [28, 131] revealed that there are nuclei close to the pion-condensate instability; in particular, pion condensation may occur in ordinary heavy nuclei. However, a detailed analysis of experimental data (absence of the doubling of the 0^+ and 0^- levels in the ^{208}Pb spectrum, which is known comprehensively; probabilities of single-nucleon slow-pion capture by nuclei; etc.) showed that there is no condensate in nuclei [78, 134]. At present, the variational calculations from [135] indicate that pion condensation is possible in neutron stars [at a density of $\rho \sim (1.5–2.0)\rho_0$, where $\rho_0 \approx 0.15$ nuclon/fm^3 is the normal nuclear density].

[23] "It is well said," replied Candide, "but we must cultivate our gardens." [Quoted from *Candide and Other Romances by Voltaire* (Dodd, Mead and company, New York, 1928; translated from the French by Richard Aldington.]

bispinor has here the form

$$G(r) = [rp(r)]^{-1/2}\sin\left(\int_{r_N}^{r} p(r')dr' + \gamma\right).$$

The phase γ is determined by matching this wave function with the internal wave function at the boundary of the nucleus. The result is

$$g\cot\gamma = \xi + O(r_N/r_0), \quad \xi = \left.\frac{d\ln G(r)}{d\ln r}\right|_{r=r_N} \qquad (A.2)$$

(actually, we have $r_N/r_0 \lesssim 0.1 \ll 1$). For ζ_{cr}, the modified quantization condition [74] yields

$$\int_{r_N}^{r_0}\sqrt{\frac{\zeta_{cr}^2-\kappa^2}{r^2}-\frac{2\zeta_{cr}}{r}} = \left(n_r+\frac{2l+3}{4}\right)\pi-\gamma, \qquad (A.3)$$

$$n_r = 0, 1, 2, \ldots.$$

Upon evaluating the integral, Eq. (A.3) reduces to the form (45). It should be noted that the greater ζ, the higher the degree to which the condition

$$\frac{d}{dr}(1/p(r)) = \frac{1-r/2r_0}{g(1-r/r_0)^{3/2}} \ll 1, \qquad (A.4)$$

which ensures the applicability of the semiclassical approximation, is satisfied (this is so everywhere with the exception of the vicinity of the turning point). This explains the behavior of the curves in Fig. 1.

(b) Let us consider the relativistic problem of two centers. For nuclei from the uranium region, the radius of the K shell is five to ten times as great as R_{cr}; in calculating the energy $\varepsilon(R)$ of the electron term, it is therefore not necessary to know the wave function in the region $r \lesssim R/2$, where the special features of the two-center problem are of importance, but where the ε dependence of $p(r)$ is immaterial. Equation (47) for $\varepsilon(R)$ follows from a comparison of two quantization integrals at close energies. We have

$$\int_{R/2}^{r_t} F(r,\varepsilon)\frac{dr}{r} = \int_{R_{cr}/2}^{r_0} F(r,\varepsilon=-1)\frac{dr}{r}, \qquad (A.5)$$

where $p(r) = r^{-1}F(r,\varepsilon)$ is a semiclassical momentum,

$$F = [a-2br+cr^2+O((1+\varepsilon)^3)]^{1/2},$$
$$a = g^2 = \zeta^2-\kappa^2,$$
$$b = \zeta\left[1-\left(1+\frac{1-2\kappa}{4\zeta^2}\right)(1+\varepsilon)\right], \qquad (A.6)$$
$$c = \varepsilon^2-1+\left(\kappa-\frac{5}{4}\right)\zeta^{-2}(\varepsilon+1),$$

and $r_t = r_0\left[1-\frac{1}{2}(1-\kappa^2/\zeta^2)(1+\varepsilon)+\ldots\right]$ is the position of the turning point at ε values sufficiently close to –1.

In Eq. (47), we have $x = 0$ at $\varepsilon = -1$; the function $\phi(x)$ is given by different formulas for $x > 0$ and $x < 0$, but $x = 0$ is not a singular point for this function: $\phi(x) = 1 - \frac{1}{6}x + O(x^2)$ for $x \longrightarrow 0$. A compact expression for the slope parameter β can be obtained from Eq. (47) [77]. The result is

$$\beta = \frac{3}{2}\left(1+\frac{4\kappa^2-6\kappa+3}{8\zeta^2}\right)^{-1}. \qquad (A.7)$$

In particular $\beta = 12\zeta^2/(8\zeta^2+13)$ for the ground-state term (see straight line *2* in Fig. 6).

(c) The logarithmic derivative ξ appearing in Eqs. (6), (54), (A.2), and (A.3) can be found from the Riccati equation [18]

$$u' - \left(\frac{f'}{f}+\frac{1}{x}\right)u + \frac{u^2}{x} = \frac{\kappa(\kappa+1)}{x} + \kappa\frac{f'}{f} - \zeta^2 x f^2, \qquad (A.8)$$
$$0 < x < 1.$$

We also have $\xi = u(1)$ and $u(0) = |\kappa|$ if $\kappa < 0$ [here, $x = r/r_N$, and $f(x)$ is the cutoff function from Eq. (5)]. For the $\kappa = j + 1/2 > 0$ states, we obtain

$$\xi(\zeta,\kappa) = \zeta^2/[\kappa-\xi(\zeta,-\kappa)]-\kappa. \qquad (A.9)$$

For example, we find for the *ns* levels ($\kappa = -1$) within model I that

$$\xi(\zeta,-1) = \zeta\cot\zeta$$
$$= \sum_{k=0}^{\infty} a_k\zeta^{2k} = 1-\frac{1}{3}\zeta^2-\frac{1}{45}\zeta^4-\frac{2}{945}\zeta^6-\ldots, \qquad (A.10)$$

where $a_k \approx -2/\pi^{2k}$ for $k \longrightarrow \infty$; for $\kappa = -(l+1) < 0$, we have

$$\xi(\zeta,\kappa) = (2l+1)\frac{f_l(\zeta)}{f_{l+1}(\zeta)} - l$$
$$= l+1-\frac{\zeta^2}{2l+3}-\frac{\zeta^4}{(2l+3)^2(2l+5)}+\ldots, \qquad (A.11)$$

while for $\kappa = l > 0$, we use Eq. (A.9). In particular, we find for the $np_{1/2}$ states that

$$\xi(\zeta,1) = \zeta^2-1+\frac{\zeta^3}{\tan\zeta-\zeta}$$
$$= 2-\frac{1}{5}\zeta^2-\frac{1}{175}\zeta^4-\ldots, \qquad (A.12)$$

where l is the orbital angular momentum for the upper component and $f_l(x) = \Gamma(l+1/2)(x/2)^{1/2-l}J_{l-1/2}(x)$, $f_l(0) = 1$. For more realistic cutoff models, it is straightforward to calculate the values of ξ numerically.

Presented below are some useful expansions. Representing the volume charge density in a nucleus as

$$\frac{Z}{4\pi r_N^3}\rho(r/r_N), \quad \int_0^1 \rho(x)x^2dx = 1, \tag{A.13}$$

and setting $\rho(x) = \rho_0 + \rho_1 x + \rho_2 x^2 + \ldots$, we arrive at

$$\begin{aligned} f(x) &= f_0 - \sum_{n=2}^{\infty} \frac{\rho_{n-2}}{n(n+1)}x^n, \\ f_0 &= \int_0^1 \rho(x)x\,dx = \sum_{n=0}^{\infty} \frac{\rho_n}{n+2}. \end{aligned} \tag{A.14}$$

By way of example, we indicate that, for the $\kappa = -1$ states, the result for ξ is

$$\begin{aligned} \xi &= 1 - c_1\zeta^2 - c_2\zeta^4 + \ldots, \\ c_1 &= \sum_{n=0}^{\infty} \frac{(n+6)}{3(n+3)(n+5)}\rho_n. \end{aligned} \tag{A.15}$$

In particular, we find for model II that $\rho(x) = 3\theta(1-x)$, $\rho_0 = 3$, and $\rho_n = 0$ for $n \geq 1$ and that $a_1 = 2/5$, $a_2 = 17/40$, $a_3 = 0.665$, ….

In the case of scalar particles, it is only necessary to replace $\kappa(\kappa+1)$ by $l(l+1)$ in Eq. (A.8) and to discard terms involving $f'(x)$. For the cutoff model I, the value of $\xi(\zeta, l)$ is then coincident with that in (A.11).

APPENDIX B

The energy eigenvalues for the Dirac equation with the pointlike-charge potential $V(r) = -\zeta/r$ are given by [45]

$$\varepsilon_{nj\kappa} = \sqrt{1 - \zeta^2/N^2}, \quad N = \sqrt{q^2 + q\nu + \kappa^2}, \tag{B.1}$$

where $q \equiv n_r = 0, 1, 2, \ldots$ is the radial quantum number; n is the principal quantum number; $\nu = 2\sqrt{\kappa^2 - \zeta^2}$; and $j = 1/2, 3/2, \ldots, n - 1/2$ is the angular momentum. The mean radius of the $|nj\kappa\rangle$ state is [6] is

$$\langle r\rangle_{nj\kappa} = \frac{1}{2\zeta}[(3N^2 - \kappa^2)\varepsilon_{nj\kappa} - \kappa], \quad \zeta < |\kappa|. \tag{B.2}$$

In particular, expression (13) follows from here for the ground-state ($n = N = 1$) level; for the energy-degenerate (at $\zeta < 1$) $2s_{1/2}$ and $2p_{1/2}$ levels, we have[24)]

$$\begin{aligned} \varepsilon_2(\zeta) &= [(1 + \sqrt{1-\zeta^2})/2]^{1/2}, \\ \langle r\rangle &= \frac{1}{2\zeta}(12\varepsilon_2^3 - \varepsilon_2 - \kappa). \end{aligned} \tag{B.3}$$

[24)]It should be emphasized, however, that, at $\zeta \approx 1$, these formulas, as well as those in (1) and (13), are valid to a logarithmic precision [see (10)].

For the $\kappa = \pm 1$ states, there is a square-root singularity at $Z = 137$ [see, for example, Eq. (1a)],

$$\langle r\rangle = \frac{1}{2}\left[\frac{q(3q^2+2)}{\sqrt{q^2+1}} \pm 1\right] + O(\sqrt{1-\zeta^2}), \tag{B.4}$$

where $q = n - 1$ and where the upper (lower) sign refers to the $ns_{1/2}$ ($np_{1/2}$) states.

It is natural to determine the magnetic moment of an electron in a bound state from the relation $\mu = -(\partial\varepsilon/\partial B)_{B\to 0}$, where $\delta\varepsilon = \left\langle -\frac{1}{2}[\mathbf{r}\alpha]\cdot\mathbf{B}\right\rangle$. This yields (in Bohr magneton units) [6]

$$\mu = [1 + (2j+1)\varepsilon]/(2j+2), \quad \kappa < 0, \tag{B.5}$$

and a similar formula for $\kappa > 0$ states.

In the particular case of $\kappa = -n$ (that is, for the $1s_{1/2}$, $2p_{3/2}$, $3d_{5/2}$, etc., states, including the ground state), the relevant formulas are simplified to become

$$\begin{aligned} \varepsilon_n &= \sqrt{1 - \frac{\zeta^2}{n^2}}, \quad \langle r\rangle = \frac{n}{2\zeta}(1 + 2\sqrt{n^2 - \zeta^2}), \\ \mu &= \frac{1 + 2\sqrt{n^2 - \zeta^2}}{2n+1} \end{aligned} \tag{B.6}$$

(the formula for μ was obtained by Breit [137]).

For the ground state of $s = 0$ or $s = 1/2$ particles, the probability-distribution density and its moments are given by

$$\rho(r) = \psi^+\psi = A^2\exp(-2\lambda r)r^{2\eta-2}, \tag{B.7}$$

$$\langle r^\sigma\rangle = 4\pi\int_0^\infty \rho(r)r^{\sigma+2}dr = \frac{\Gamma(2\eta+\sigma+1)}{(2\lambda)^\sigma\Gamma(2\eta+1)}, \tag{B.8}$$

where

$$\lambda = \sqrt{1-\varepsilon^2}, \quad \eta = \varepsilon\zeta/\lambda, \quad A = \sqrt{\frac{2^{2\eta-1}\lambda^{2\eta+1}}{\pi\Gamma(2\eta+1)}},$$

and $\varepsilon = \varepsilon_0(\zeta)$ is the energy of this state. In particular, we have

$$\begin{aligned} \langle r\rangle &= \frac{2\eta+1}{2\lambda}, \quad \Delta r = (\langle r^2\rangle - \langle r\rangle^2)^{1/2} = \frac{\sqrt{2\eta+1}}{2\lambda}, \\ \left\langle\frac{1}{r}\right\rangle &= \frac{\lambda}{\eta}, \quad \langle V\rangle = -\zeta\langle 1/r\rangle = -(1-\varepsilon_0^2)/\varepsilon_0, \\ \langle T\rangle/\langle V\rangle &= -(1+\varepsilon_0)^{-1} \end{aligned} \tag{B.9}$$

($\varepsilon_0 = m + \langle T\rangle + \langle V\rangle$). Thus, the virial theorem $\langle V\rangle = -2\langle T\rangle$ is valid only for $\zeta \ll 1$—that is only in the nonrelativistic case.

Table 5

ζ_{cr}	$\kappa = -1$			$\kappa = 1$		
	ρ	$\langle r \rangle$	μ_{cr}	ρ	$\langle r \rangle$	μ_{cr}
1.00	2.33	0.130	0.133	0.333	0.075	0
1.25	1.61	0.312	0.354	0.333	0.195	0
1.50	1.22	0.447	0.533	0.333	0.300	0

For $s = 1/2$ (electron), we have $\varepsilon_0 = \eta = \sqrt{1-\zeta^2}$ and $\lambda = \zeta$, while, for scalar particles, the results are

$$\varepsilon_0 = \left(\frac{1}{2} + \sqrt{\frac{1}{4} - \zeta^2}\right)^{1/2},$$
$$\lambda = \left(\frac{1}{2} - \sqrt{\frac{1}{4} - \zeta^2}\right)^{1/2}, \quad \eta = \varepsilon_0^2.$$

In the nonrelativistic limit, we arrive at

$$\varepsilon_0(\zeta) = 1 - \frac{\zeta^2}{2} - \frac{a}{8}\zeta^4 + \ldots,$$
$$\lambda = \zeta + \frac{a-1}{8}\zeta^3 + \ldots, \quad \eta = 1 - \frac{a+3}{8}\zeta^2 + \ldots, \tag{B.10}$$

$$A = \sqrt{\frac{\zeta^3}{\pi}}\left[1 - \frac{a+3}{8}\zeta^2 \ln\zeta + O(\zeta^2)\right],$$
$$\langle r \rangle = \frac{3}{2Z}a_B\left(1 - \frac{5a+3}{24}\zeta^2 + \ldots\right), \tag{B.11}$$

where $a = 1$ at $s = 1/2$ and $a = 5$ at $s = 0$, while $a_B = \hbar^2/me^2$ is the Bohr radius.

If $\zeta \geq j + 1/2$, the pointlike-nucleus approximation is no longer applicable to states characterized by the angular momentum j; as a result, the wave functions become much more complicated [3, 5]. At $\varepsilon = -1$, we can use, however, the simpler expressions (16). For $ns_{1/2}$ ($\kappa = -1$) states, this leads to expressions (14) and (15), while, at $\kappa = 1$, we arrive at

$$\langle r \rangle = \frac{3}{40\zeta_{cr}}(4\zeta_{cr}^2 - 3), \quad \mu_{cr} = 0. \tag{B.12}$$

It is interesting to note that, for $\zeta_{cr} \gg 1$, the mean radius behaves identically, $\langle r \rangle = 0.3\zeta_{cr}[1 + O(\zeta_{cr}^{-2})]$, in the two cases ($\kappa = \mp 1$).

We denote by w_1 and w_2 the relative weights of the upper and the lower component of the Dirac bispinor (in other words, the probability that a bound electron has the orbital angular moment l or $l' = 2j - l$),

$$w_1 = \int_0^\infty G^2(r)dr = (1+\rho)^{-1},$$
$$w_2 = \int_0^\infty F^2(r)dr = \frac{\rho}{1+\rho}. \tag{B.13}$$

The parameter $\rho = w_2/w_1$ characterizes the degree to which the electron state being considered is relativistic. To illustrate this, we note that, in the nonrelativistic state ($\rho = \zeta^2/4n^2 \ll 1$), we have $\rho = (q + \sqrt{q^2+1})^{-2}$ at $\zeta = 1$ and

$$\rho = \frac{1}{3}\left[1 + \frac{2\kappa^2 - 3\kappa + 1}{\zeta_{cr}^2}\right] \tag{B.14}$$

for states at the boundary of the lower continuum.

It should be emphasized that these formulas are valid only under the condition $r_N \ll \langle r \rangle$. The numerical values of the parameters for $\varepsilon = -1$ states are quoted in Table 5.

The mean radius $\langle r \rangle$ increases quite fast with increasing ζ_{cr}. This increase is not due to the effect of the internal region $r < r_N$, whose contribution is small. The probability for the electron to reside within the nucleus can be roughly estimated as $w_N \approx (r_N/\langle r \rangle)^3 \sim 10^{-3}$–$10^{-2}$ at $r_N = 10$ fm. In this sense, the situation resembles that in the deuteron, with the difference—a significant one, however—that the electron, which is relativistic here ($\rho \sim 1$), is confined near the nucleus owing to the Coulomb barrier in the effective potential (36). The probability w_N can be calculated more precisely by using the formula

$$w_N = \frac{4\pi A_0^2}{2\eta + 1}(m_e r_N)^{2\eta+1}, \tag{B.15}$$

where A_0 is the asymptotic coefficient in the wave function at the origin. This yields $w_N = 0.02$, 0.019, and 0.037 for the $1s$, $2s$, and $2p_{1/2}$ states, respectively; for two nuclei at the distance $R = R_{cr}$, we have $A_0 = 3.56$ and w_N 3.6(–3) at $Z/2 = 92$ and $A_0 = 1.86$ and $w_N = 1.7(-3)$ at $Z/2 = 100$ (the values of A_0 were borrowed from [23]).

The decrease in the critical distance because of cutting off the Coulomb potential within the nucleus can be computed by the formula

$$R_{cr} = R_{cr}^{(0)}(1 - \beta^{-1}\Delta\varepsilon), \tag{B.16}$$

where $R_{cr}^{(0)}$ is associated with pointlike nuclei (problem of two centers), β is the slope of the level as given by Eq. (30a), and $\Delta\varepsilon$ is the shift of the level upon taking into account finite nuclear sizes.

By perturbation theory, we find

$$\Delta\varepsilon = 2\pi A_0^2 \zeta\gamma^{-1} r_N^{2\gamma} F(\gamma),$$
$$F(\gamma) = 2\gamma\int_0^1 [x^{-1} - f(x)]x^{2\gamma-1}dx, \quad \text{(B.17)}$$

where $\zeta = 2Z\alpha = 2\sqrt{1-\gamma^2}$. The results for the cutoff models I and II are $F(\gamma) = (2\gamma+1)^{-1}$ and $F(\gamma) = 3/(2\gamma+1)(2\gamma+3)$, respectively. A more precise formula for $\Delta\varepsilon$ can be obtained by matching the wave functions at the boundary of the nucleus. In this way, the R_{cr} values quoted in Table 3 were calculated in [23].

APPENDIX C

The Dirac equation for an electron with a static potential $V(\mathbf{r})$ has the form

$$(\boldsymbol{\sigma}\cdot\mathbf{p})\varphi = W\chi, \quad (\boldsymbol{\sigma}\cdot\mathbf{p})\chi = (W-2)\varphi, \quad \text{(C.1)}$$

where $W = 1 + \varepsilon - V$, while φ and χ are, respectively, the upper and the lower bispinor component (here, the potential is not assumed to be spherically symmetric). The substitution $\psi = W^{-1/2}\varphi$ reduces Eqs. (C.1) to the form

$$\Delta\psi + (\varepsilon^2 - 1 - 2U)\psi = 0, \quad \text{(C.2)}$$

$$U = \varepsilon V - \frac{1}{2}V^2 + \frac{1}{4W}\Delta V + \frac{3}{8W^2}(\nabla V)^2 + \frac{1}{2W}[\nabla V\times\mathbf{p}]\cdot\boldsymbol{\sigma}. \quad \text{(C.3)}$$

Here, ψ and the effective potential U are both two-component quantities. For $1 > \varepsilon \geq -1$, $W(\mathbf{r})$ is positive for any attractive potential; therefore, a transition from the set of Dirac equations (C.1) to Eq. (C.2) does not involve singularities.[25] Formally, Eq. (C.2) has the form of the ordinary Schrödinger equation featuring spin–orbit coupling. The difference, however, is that the potential U itself depends (in a rather complicated way) on the energy ε. At the boundary of the lower continuum, $W = -V$, expression (C.3) takes the somewhat simpler form (19). The explicit expressions for the functions $U_{ij}(\mathbf{r})$ can be found in [22].

In calculating the mean radius, the slope of the level at the boundary of the lower continuum, and other similar quantities, it is necessary to normalize the Dirac function. It will now be shown how this can be done without calculating the lower component explicitly. From Eqs. (C.1), we have

$$\chi = W^{-1}(\boldsymbol{\sigma}\cdot\mathbf{p})\varphi = SW^{-1/2}\psi,$$
$$\langle\chi|\chi\rangle = \langle\psi|W^{-1/2}S^+SW^{-1/2}|\psi\rangle, \quad \text{(C.4)}$$

where

$$S = W^{-1}(\boldsymbol{\sigma}\cdot\mathbf{p})W = \boldsymbol{\sigma}\cdot\mathbf{P}, \quad \mathbf{P} = \mathbf{p} - i\mathbf{A},$$
$$\mathbf{A} = \nabla\ln W = -W^{-1}\nabla V,$$
$$S^+S = (\mathbf{P}^+\cdot\mathbf{P}) + i[\mathbf{P}^+\times\mathbf{P}]\cdot\boldsymbol{\sigma}$$
$$= \mathbf{p}^2 + \mathbf{A}^2 - \nabla\mathbf{A} - 2[\mathbf{A}\cdot\mathbf{p}]\times\boldsymbol{\sigma}, \quad \text{(C.5)}$$

and $\mathbf{p} = -i\nabla$. Performing integration by parts and using Eq. (C.2), we arrive at the identity

$$\langle f\psi|\mathbf{p}^2|f\psi\rangle = \int\psi^+\{(\nabla f)^2 + (\varepsilon^2-1)f^2 - (f^2U + Uf^2)\}\psi d^3r, \quad \text{(C.6)}$$

where $f(\mathbf{r})$ is an arbitrary real-valued function (in our case, $f = W^{-1/2}$). Taking into account the relations

$$\nabla\mathbf{A} = -(\mathbf{A}^2 + W^{-1}\nabla V), \quad [\mathbf{p}, W^\alpha] = -i\alpha W^\alpha\mathbf{A},$$
$$W^{-1/2}[\mathbf{A}\times\mathbf{p}]W^{-1/2} = W^{-1}[\mathbf{A}\times\mathbf{p}],$$

and expression (C.3) for the effective potential, we obtain

$$N \equiv \langle\varphi|\varphi\rangle + \langle\chi|\chi\rangle = \int\psi^+\hat{T}\psi d^3r, \quad \text{(C.7)}$$

$$\hat{T} = 2(\varepsilon - V) + \frac{1}{2W^2}\Delta V + \frac{3}{2W^3}(\nabla V)^2 + \frac{1}{W^2}[\nabla V\times\mathbf{p}]\cdot\boldsymbol{\sigma}. \quad \text{(C.8)}$$

Considered immediately below are some cases where the above formulas can be simplified.

(a) For the central field $V = V(r)$, we have

$$[\nabla V\times\mathbf{p}]\cdot\boldsymbol{\sigma} = r^{-1}V'(r)(\mathbf{l}\cdot\boldsymbol{\sigma}) = -(\kappa+1)r^{-1}V'(r)$$

and $\Delta V = V'' + 2r^{-1}V'$. Equation (C.3) then reduces to Eq. (3), while Eq. (C.8) yields

$$N = \int_0^\infty (G^2 + F^2)dr$$
$$\equiv \int_0^\infty \left\{2\left(1 - \frac{1}{W}\right) + \frac{V''}{2W^3} + \frac{3}{2W^4}V'^2 - \frac{\kappa V'}{rW^3}\right\}G^2(r)dr, \quad \text{(C.9)}$$

where $G = rg(r)$ and $F = rf(r)$ are radial wave functions. In [18], this formula was obtained directly for spherically symmetric potentials and was used in the calculations.

[25] In the case of a repulsive potential, $V(\mathbf{r}) > 0$, the function W can vanish and become negative. Instead of (C.2), it is therefore necessary to use the equation that is obtained from the set of Eqs. (C.1) upon the substitution $\chi = (1 - \varepsilon + V)^{-1/2}\psi$.

(b) At the boundary of the lower continuum ($\varepsilon = -1$), we have $W = -V$ and

$$\hat{T} = -2(1+V) + \frac{1}{2V^2}\Delta V - \frac{3}{2V^3}(\nabla V)^2 + \frac{1}{V^2}[\nabla V \times \mathbf{p}]\cdot\boldsymbol{\sigma}. \quad \text{(C.10)}$$

It should be noted that, in the problem of two pointlike Coulomb centers, we can omit, in the above formulas, terms that are proportional to the Laplacian ΔV. In order to demonstrate this, we note that $W \propto r^{-1}$ for $r \longrightarrow 0$; hence, $W^{-\alpha}\Delta V \propto r^{\alpha}\delta(\mathbf{r}) \equiv 0$ for any $\alpha > 0$. The same is true for any system of pointlike charges.

(c) At $\varepsilon = -1$ and $V(r) = -\zeta/r$, we have

$$N = \int_0^\infty (G^2 + F^2)dr = 2\int_0^\infty \left(1 - \frac{2\kappa - 1}{4\zeta^2} - \frac{r}{\zeta}\right)G^2 dr. \quad \text{(C.11)}$$

Similar identities can be obtained for the moments of the electron-density distribution. They are presented here in the simplest (and the most important) case of $\kappa = -1$. Denoting

$$\langle r^\sigma \rangle = \int_0^\infty (G^2 + F^2)r^\sigma dr \Big/ \int_0^\infty (G^2 + F^2)dr,$$

$$\overline{r^\sigma} = \int_0^\infty G^2 r^\sigma \Big/ \int_0^\infty G^2 dr,$$

we obtain

$$\langle r^\sigma \rangle = \left\{\left(\zeta + \frac{\sigma^2 + 4\sigma + 3}{4\zeta}\right)\overline{r^\sigma} - \overline{r^{\sigma+1}}\right\} \Big/ \left(\zeta + \frac{3}{4\zeta} - \bar{r}\right). \quad \text{(C.12)}$$

Thus, the problem reduces to averaging over the upper component $G(r)$ exclusively. For the case of the Coulomb field, we find with the aid of (16) that

$$\overline{r^\sigma} = \frac{\sqrt{\pi}\Gamma(\sigma+1)}{2(8\zeta)^\sigma \Gamma(\sigma + 3/2)}\left|\frac{\Gamma(\sigma + 1 + i\nu)}{\Gamma(1 + i\nu)}\right|^2, \quad \text{(C.13)}$$

$$\sigma > -1.$$

For natural values of σ, the last expression reduces to polynomials:

$$\overline{r^\sigma} = \zeta^{-1} P_\sigma(\zeta),$$

$$P_1 = \frac{1}{3}\zeta^2 - \frac{1}{4}, \quad P_2 = \frac{2}{15}\zeta^3 - \frac{1}{10}\zeta, \quad \text{(C.14)}$$

$$P_3 = \frac{2}{35}\zeta^4 + \frac{1}{35}\zeta^2 - \frac{3}{56}, \ldots.$$

With the aid of (C.14), we can easily deduce Eqs. (14), (15), and (B.12).

REFERENCES

1. S. S. Gershteĭn and Ya. B. Zel'dovich, Zh. Éksp. Teor. Fiz. **57**, 654 (1969) [Sov. Phys. JETP **30**, 358 (1970)]; Lett. Nuovo Cimento **1**, 835 (1969).
2. W. Pieper and W. Greiner, Z. Phys. **218**, 327 (1969).
3. V. S. Popov, Pis'ma Zh. Éksp. Teor. Fiz. **11**, 254 (1970) [JETP Lett. **11**, 162 (1970)]; Yad. Fiz. **12**, 429 (1970) [Sov. J. Nucl. Phys. **12**, 235 (1971)].
4. V. S. Popov, Zh. Éksp. Teor. Fiz. **59**, 965 (1970) [Sov. Phys. JETP **32**, 526 (1971)].
5. V. S. Popov, Zh. Éksp. Teor. Fiz. **60**, 1228 (1971) [Sov. Phys. JETP **33**, 665 (1971)].
6. A. M. Perelomov and V. S. Popov, Yad. Fiz. **14**, 661 (1971) [Sov. J. Nucl. Phys. **14**, 370 (1972)].
7. Ya. B. Zel'dovich and V. S. Popov, Usp. Fiz. Nauk **105**, 403 (1971) [Sov. Phys. Usp. **14**, 673 (1972)].
8. V. S. Popov and T. I. Rozhdestvenskaya, Pis'ma Zh. Éksp. Teor. Fiz. **14**, 267 (1971) [JETP Lett. **14**, 177 (1971)].
9. V. S. Popov, Pis'ma Zh. Éksp. Teor. Fiz. **16**, 355 (1972) [JETP Lett. **16**, 251 (1972)].
10. B. Müller, J. Rafelski, and W. Greiner, Z. Phys. **257**, 62, 183 (1972).
11. G. Soff, B. Müller, and J. Rafelski, Z. Naturforsch. Teil A **29**, 1267 (1974).
12. B. Fricke, W. Greiner, and J. T. Waber, Theor. Chim. Acta **21**, 235 (1971).
13. B. Müller, H. Peitz, J. Rafelski, and W. Greiner, Phys. Rev. Lett. **28**, 1235 (1972).
14. B. Müller, J. Rafelski, and W. Greiner, Phys. Lett. B **47B**, 5 (1973).
15. L. Fulcher and A. Klein, Phys. Rev. D **8**, 2455 (1973).
16. J. Rafelski, B. Müller, and W. Greiner, Nucl. Phys. B **68**, 585 (1974).
17. M. Gyulassy, Phys. Rev. Lett. **33**, 921 (1974); Nucl. Phys. A **244**, 497 (1975).
18. V. S. Popov, Yad. Fiz. **14**, 458 (1971) [Sov. J. Nucl. Phys. **14**, 257 (1972)]; **15**, 1069 (1972) [**15**, 595 (1972)].
19. M. S. Marinov and V. S. Popov, Pis'ma Zh. Éksp. Teor. Fiz. **17**, 511 (1973) [JETP Lett. **17**, 368 (1973)].
20. S. S. Gershtein and V. S. Popov, Lett. Nuovo Cimento **6**, 593 (1973).
21. V. S. Popov, Pis'ma Zh. Éksp. Teor. Fiz. **18**, 53 (1973) [JETP Lett. **18**, 29 (1973)]; Zh. Éksp. Teor. Fiz. **65**, 35 (1973) [Sov. Phys. JETP **38**, 18 (1974)]; Yad. Fiz. **19**, 155 (1974) [Sov. J. Nucl. Phys. **19**, 81 (1974)].
22. M. S. Marinov, V. S. Popov, and V. L. Stolin, Pis'ma Zh. Éksp. Teor. Fiz. **19**, 76 (1974) [JETP Lett. **19**, 49 (1974)]; J. Comput. Phys. **19**, 241 (1975).
23. V. I. Lisin, M. S. Marinov, and V. S. Popov, Phys. Lett. B **69B**, 141 (1977); **91B**, 20 (1980).
24. J. Rafelski and B. Müller, Phys. Lett. B **65B**, 205 (1976).
25. G. Soff, W. Greiner, W. Betz, and B. Müller, Phys. Rev. A **20**, 169 (1979).
26. B. Müller and J. Rafelski, Phys. Rev. Lett. **34**, 349 (1975).

27. B. Müller and W. Greiner, Z. Naturforsch. Teil A **31**, 1 (1976).
28. A. B. Migdal, Zh. Éksp. Teor. Fiz. **61**, 2209 (1971) [Sov. Phys. JETP **34**, 1184 (1972)]; A. B. Migdal, Nucl. Phys. B **52**, 483 (1973).
29. A. B. Migdal, Phys. Lett. B **52B**, 182 (1974).
30. A. B. Migdal, Zh. Éksp. Teor. Fiz. **70**, 411 (1976) [Sov. Phys. JETP **43**, 211 (1976)].
31. S. J. Brodsky, Comments At. Mol. Phys. **4**, 109 (1973).
32. L. B. Okun', Comments Nucl. Part. Phys. **6**, 25 (1974).
33. V. S. Popov, in *Proceedings of the 3rd Physics School of Institute of Theoretical and Experimental Physics* (Atomizdat, Moscow, 1975), Vol. 1, p. 5.
34. J. P. Reinhardt and W. Greiner, Rep. Prog. Phys. **40**, 219 (1977).
35. J. Rafelski, L. P. Fulcher, and A. Klein, Phys. Rep. C **38**, 227 (1978).
36. V. S. Popov, Izv. Akad. Nauk SSSR, Ser. Fiz. **41**, 2577 (1977).
37. V. S. Popov, Preprint ITÉF-169 (Institute of Theoretical and Experimental Physics, Moscow, 1980); Priroda, No. 10, 14 (1981).
38. A. B. Migdal, *Fermions and Bosons in Strong Fields* (Nauka, Moscow, 1978).
39. W. Greiner, B. Müller, and J. Rafelski, *Quantum Electrodynamics of Strong Fields* (Springer-Verlag, Berlin, 1985).
40. I. Pomeranchuk and Ya. Smorodinsky, J. Phys. USSR **9**, 97 (1945); I. Ya. Pomeranchuk, *Collection of Scientific Works* (Nauka, Moscow, 1972), Vol. 2, p. 21.
41. A. B. Migdal, *Qualitative Methods in Quantum Theory* (Nauka, Moscow, 1975; Benjamin, Reading, 1977).
42. A. Sommerfeld, *Atomic Structure and Spectral Lines* (Methuen, London, 1934; Gostekhizdat, Moscow, 1956), Vol. 1.
43. F. L. Scarf, Phys. Rev. **109**, 2170 (1958).
44. S. P. Alliluev, Zh. Éksp. Teor. Fiz. **61**, 15 (1971) [Sov. Phys. JETP **34**, 8 (1972)].
45. A. I. Akhiezer and V. B. Berestetskii, *Quantum Electrodynamics* (Gostekhizdat, Moscow, 1953; Wiley, New York, 1965).
46. K. M. Case, Phys. Rev. **80**, 797 (1950).
47. P. M. Morse and H. Feshbach, *Methods of Theoretical Physics* (McGraw-Hill, New York, 1953), Vol. 2, Chap. 12.
48. L. D. Landau and E. M. Lifshitz, *Course of Theoretical Physics*, Vol. 3: *Quantum Mechanics: Non-Relativistic Theory* (Nauka, Moscow, 1974; Pergamon, New York, 1977).
49. A. M. Perelomov and V. S. Popov, Teor. Mat. Fiz. **4**, 48 (1970).
50. F. G. Werner and J. A. Wheeler, Phys. Rev. **109**, 126 (1958).
51. V. V. Voronkov and N. N. Kolesnikov, Zh. Éksp. Teor. Fiz. **39**, 189 (1960) [Sov. Phys. JETP **12**, 136 (1960)].
52. P. Gombäs, *Die Statistische Theorie des Atoms und ihre Anwendungen* (Springer-Verlag, Vienna, 1949; Inostrannaya Literatura, Moscow, 1951).
53. V. S. Popov, V. L. Eletskiĭ, and M. S. Marinov, Zh. Éksp. Teor. Fiz. **73**, 1241 (1977) [Sov. Phys. JETP **46**, 653 (1977)].
54. A. B. Migdal, V. S. Popov, and D. N. Voskresenskiĭ, Pis'ma Zh. Éksp. Teor. Fiz. **24**, 186 (1976) [JETP Lett. **24**, 163 (1976)]; Zh. Éksp. Teor. Fiz. **72**, 834 (1977) [Sov. Phys. JETP **45**, 436 (1977)].
55. V. A. Fock, Z. Phys. **98**, 145 (1935).
56. V. Bargmann, Z. Phys. **99**, 576 (1935).
57. S. P. Alliluev, Zh. Éksp. Teor. Fiz. **33**, 200 (1957) [Sov. Phys. JETP **6**, 156 (1958)].
58. J. Schwinger, J. Math. Phys. **5**, 1606 (1964).
59. G. Gyorgyi and J. Révai, Zh. Éksp. Teor. Fiz. **48**, 1445 (1965) [Sov. Phys. JETP **21**, 967 (1965)].
60. A. M. Perelomov and V. S. Popov, Zh. Éksp. Teor. Fiz. **50**, 179 (1966) [Sov. Phys. JETP **23**, 118 (1966)].
61. M. Bander and C. Itzykson, Rev. Mod. Phys. **38**, 330, 346 (1966).
62. V. S. Popov, in *Physics of High Energies and Theory of Elementary Particles* (Naukova Dumka, Kiev, 1967), p. 702.
63. M. H. Johnson and B. A. Lippman, Phys. Rev. **78**, 329 (1950).
64. P. C. Martin and R. J. Glauber, Phys. Rev. **109**, 1307 (1958).
65. A. M. Perelomov and V. S. Popov, Dokl. Akad. Nauk SSSR **181**, 320 (1968) [Sov. Phys. Dokl. **13**, 685 (1969)].
66. Yu. Ts. Oganessian *et al.*, Phys. Rev. Lett. **83**, 3154 (1999); Yu. Ts. Oganessian, Preprint No. R7-2000-23, OIYaI (Joint Institute for Nuclear Research, Dubna, 2000); Yad. Fiz. **63**, 1769 (2000) [Phys. At. Nucl. **63**, 1679 (2000)].
67. I. V. Komarov, L. I. Ponomarev, and S. Yu. Slavyanov, *Spheroidal and Coulomb Spheroidal Functions* (Nauka, Moscow, 1976).
68. L. V. Kantorovich and V. I. Krylow, *Approximate Methods of Higher Analysis* (Fizmatgiz, Moscow, 1962; Wiley, New York, 1964).
69. V. S. Popov, V. L. Eletskiĭ, and V. D. Mur, Zh. Éksp. Teor. Fiz. **71**, 856 (1976) [Sov. Phys. JETP **44**, 451 (1976)].
70. A. B. Migdal, A. M. Perelomov, and V. S. Popov, Yad. Fiz. **14**, 874 (1971) [Sov. J. Nucl. Phys. **14**, 488 (1972)]; **16**, 222 (1972) [**16**, 120 (1973)].
71. I. Tamm, Phys. Rev. **58**, 952 (1940).
72. H. C. Corben and J. Schwinger, Phys. Rev. **58**, 953 (1940).
73. V. P. Kraĭnov, Pis'ma Zh. Éksp. Teor. Fiz. **13**, 359 (1971) [JETP Lett. **13**, 255 (1971)].
74. M. S. Marinov and V. S. Popov, Zh. Éksp. Teor. Fiz. **67**, 1250 (1974) [Sov. Phys. JETP **40**, 621 (1975)]; J. Phys. A **8**, 1575 (1975).
75. V. D. Mur, V. S. Popov, and D. N. Voskresenskiĭ, Pis'ma Zh. Éksp. Teor. Fiz. **28**, 140 (1978) [JETP Lett. **28**, 129 (1978)].
76. V. L. Eletskiĭ, D. N. Voskresenskiĭ, and V. S. Popov, Yad. Fiz. **26**, 994 (1977) [Sov. J. Nucl. Phys. **26**, 526 (1977)].
77. V. S. Popov, V. L. Eletsky, V. D. Mur, and D. N. Voskresensky, Phys. Lett. B **80B**, 68 (1978); V. S. Popov *et al.*, Zh. Éksp. Teor. Fiz. **76**, 431 (1979) [Sov. Phys. JETP **49**, 218 (1979)].

78. A. B. Migdal, D. N. Voskresensky, E. E. Saperstein, and M. A. Troitsky, *Pionic Degrees of Freedom of Nuclear Matter* (Nauka, Moscow, 1991).
79. V. L. Eletskiĭ and V. S. Popov, Yad. Fiz. **25**, 1107 (1977) [Sov. J. Nucl. Phys. **25**, 587 (1977)].
80. E. E. Salpeter, Phys. Rev. **87**, 328 (1952).
81. G. 't Hooft, Nucl. Phys. B **75**, 461 (1974).
82. W. Lucha and F. Schöberl, in *Quark Confinement and the Hadron Spectrum* (World Sci., Singapore, 1994), p. 100.
83. P. Cea, P. Colangelo, G. Nardulli, *et al.*, Phys. Rev. D **26**, 1157 (1982); P. Cea, G. Nardulli, and G. Paiano, Phys. Rev. D **28**, 2291 (1983).
84. J. L. Basdevant and S. Boukraa, Z. Phys. C **28**, 423 (1985).
85. B. M. Karnakov, V. D. Mur, and V. S. Popov, Zh. Éksp. Teor. Fiz. **116**, 511 (1999) [JETP **89**, 271 (1999)].
86. V. L. Morgunov, A. V. Nefediev, and Yu. A. Simonov, Phys. Lett. B **459**, 653 (1999).
87. W. Fleischer and G. Soff, Z. Naturforsch. Teil A **39**, 703 (1984).
88. L. I. Schiff, H. Snyder, and J. Weinberg, Phys. Rev. **57**, 315 (1940).
89. G. Calucci and G. C. Ghirardi, Nuovo Cimento A **10**, 121 (1972).
90. B. A. Arbuzov and V. E. Rochev, Teor. Mat. Fiz. **12**, 204 (1972).
91. V. P. Kraĭnov, Zh. Éksp. Teor. Fiz. **64**, 800 (1973) [Sov. Phys. JETP **37**, 406 (1973)].
92. M. Bawin and J. P. Lavine, Nuovo Cimento A **23**, 311 (1974).
93. M. Bawin and J. P. Lavine, Phys. Rev. D **12**, 1192 (1975).
94. A. Klein and J. Rafelski, Phys. Rev. D **11**, 300 (1975); **12**, 1194 (1975).
95. V. D. Mur and V. S. Popov, Teor. Mat. Fiz. **27**, 81, 204 (1976).
96. R. Loudon, Am. J. Phys. **27**, 649 (1959).
97. H. Hasegawa and R. E. Howard, J. Phys. Chem. Solids **21**, 179 (1961).
98. B. B. Kadomtsev, Zh. Éksp. Teor. Fiz. **58**, 1765 (1970) [Sov. Phys. JETP **31**, 945 (1970)].
99. J. Schwinger, Phys. Rev. **82**, 664 (1951).
100. H. Ruder, G. Wunner, H. Herold, and F. Geyer, *Atoms in Strong Magnetic Fields* (Springer-Verlag, Berlin, 1994).
101. V. N. Oraevskiĭ, A. I. Rez, and V. B. Semikoz, Zh. Éksp. Teor. Fiz. **72**, 820 (1977) [Sov. Phys. JETP **45**, 428 (1977)].
102. A. D. Sakharov, R. Z. Lyudaev, E. N. Smirnov, *et al.*, Dokl. Akad. Nauk SSSR **196**, 65 (1971) [Sov. Phys. Dokl. **16**, 1 (1971)].
103. A. D. Sakharov, *Scientific Works* (Tsentrkom, Moscow, 1995).
104. R. van Dyck, Jr., P. Schwinberg, and H. Dehmelt, Phys. Rev. Lett. **59**, 26 (1987).
105. T. Kinoshita, Rep. Prog. Phys. **59**, 1459 (1996).
106. V. W. Hughes and T. Kinoshita, Rev. Mod. Phys. **71**, S133 (1999).
107. J. Rafelski, L. P. Fulcher, and W. Greiner, Phys. Rev. Lett. **27**, 958 (1971); Nuovo Cimento B **13**, 135 (1973).
108. M. Born and L. Infeld, Proc. R. Soc. London, Ser. A **144**, 425 (1934).
109. L. Infeld and B. Hoffmann, Phys. Rev. **51**, 765 (1937).
110. G. Soff, J. Rafelski, and W. Greiner, Phys. Rev. A **7**, 903 (1973).
111. G. Soff, B. Müller, J. Rafelski, and W. Greiner, Z. Naturforsch. Teil A **28**, 1389 (1973).
112. D. G. Caldi and A. Chodos, Phys. Rev. D **36**, 2876 (1987).
113. V. I. Matveev, D. U. Matrasulov, and Kh. Yu. Rakhimov, Yad. Fiz. **63**, 381 (2000) [Phys. At. Nucl. **63**, 318 (2000)].
114. H. Backe *et al.*, Phys. Rev. Lett. **40**, 1443 (1978).
115. G. Kozhuharov *et al.*, Phys. Rev. Lett. **42**, 376 (1979).
116. S. Schweppe *et al.*, Phys. Rev. Lett. **51**, 2261 (1983).
117. M. Clemente *et al.*, Phys. Lett. B **137B**, 41 (1984).
118. T. Cowan *et al.*, Phys. Rev. Lett. **54**, 1761 (1985); **56**, 444 (1986).
119. H. Tsertos *et al.*, Z. Phys. A **326**, 235 (1987).
120. W. Koenig *et al.*, Phys. Lett. B **218**, 12 (1989).
121. P. Salabura *et al.*, Phys. Lett. B **245**, 153 (1990).
122. Yu. N. Pokotilovskiĭ, Fiz. Élem. Chastits At. Yadra **24**, 5 (1993) [Phys. Part. Nucl. **24**, 1 (1993)].
123. A. B. Balantekin, C. Bottcher, M. R. Strayer, and S. J. Lee, Phys. Rev. Lett. **55**, 461 (1985).
124. A. Chodos and L. C. R. Wijewardhana, Phys. Rev. Lett. **56**, 302 (1986).
125. A. O. Barut, Z. Phys. A **336**, 317 (1990).
126. M. Seiwert, W. Greiner, and W. T. Pinkston, J. Phys. G **11**, L21 (1985).
127. S. Schramm *et al.*, Z. Phys. A **323**, 275 (1986).
128. Yu. N. Demkov and S. Yu. Ovchinnikov, Pis'ma Zh. Éksp. Teor. Fiz. **46**, 14 (1987) [JETP Lett. **46**, 14 (1987)].
129. R. Ganz *et al.*, Phys. Lett. B **389**, 4 (1996).
130. GSI–Nachrichten, **2/99**, 8 (1999).
131. A. B. Migdal, O. A. Markin, and I. N. Mishustin, Zh. Éksp. Teor. Fiz. **66**, 443 (1974) [Sov. Phys. JETP **39**, 212 (1974)]; **70**, 1592 (1976) [**43**, 830 (1976)].
132. A. B. Migdal, G. A. Sorokin, O. A. Markin, and I. N. Mishustin, Phys. Lett. B **65B**, 423 (1977); Zh. Éksp. Teor. Fiz. **72**, 1247 (1976) [Sov. Phys. JETP **45**, 654 (1977)].
133. A. B. Migdal, Rev. Mod. Phys. **50**, 107 (1978).
134. A. B. Migdal, E. E. Saperstein, M. A. Troitsky, and D. N. Voskresensky, Phys. Rep. **192**, 179 (1990).
135. A. Akmal, V. R. Pandharipande, and D. J. Ravenhall, Phys. Rev. C **58**, 1804 (1998).
136. *Romans de Voltaire* (Firmin-Didot, Paris, 1887), p. 193.
137. G. Breit, Nature **122**, 649 (1928).

Translated by A. Isaakyan

Physics of Atomic Nuclei, Vol. 64, No. 3, 2001, pp. 393–415. Translated from Yadernaya Fizika, Vol. 64, No. 3, 2001, pp. 447–470.

90th ANNIVERSARY OF A.B. MIGDAL'S BIRTHDAY
NUCLEI

New Method in Bardeen–Cooper–Schrieffer Theory: Triplet Pairing in Superfluid Dense Neutron Matter

V. A. Khodel

Russian Research Centre Kurchatov Institute, pl. Kurchatova 1, Moscow, 123182 Russia

Received July 3, 2000

Abstract—On the basis of the method outlined in the first part of this review, the properties of superfluid dense neutron matter are analyzed in the density region where the spin of a Cooper pair and its total angular momentum are $S = 1$ and $J = 2$, respectively. An analytic solution to the problem of $^3P_2$ pairing in neutron matter is presented. Basic features of the structure and of the energy spectrum of superfluid phases are discussed. Degeneracy that is absolutely dissimilar to that which is associated with the phase transformation of the order parameter in the *S*-pairing problem is a distinct feature of the structure of the aforementioned phases. It appears that one or even a few numbers characterizing the weight of components associated with different values of the projection M of the total angular momentum $J = 2$ of a Cooper pair can be chosen arbitrarily, while the others adjust to them in accordance with universal laws. As a result, the structure of any phase depends neither on the density, nor on the temperature, nor on any other input parameter. The phases found here form two groups degenerate in energy. One of these groups comprises phases for which the sign of the order parameter remains unchanged over the entire Fermi surface, while the other consists of phases whose order parameter has a zero. The energy splitting between the phases from the different groups is calculated analytically as a function of temperature. The relative magnitude of this splitting changes from approximately 3% at $T = 0$ to zero in the vicinity of the critical point T_c. The role of tensor forces in dense neutron matter is analyzed. It is shown that the mixing of the orbital angular momenta $L = 1$ and $L = 3$ of Cooper pairs that is induced by tensor forces completely removes degeneracy peculiar to the $^3P_2$-pairing problem—the number of phases and their structure at a given temperature are tightly fixed, while the energy spectrum of the phases splits completely. *© 2001 MAIK "Nauka/Interperiodica".*

1. INTRODUCTION

This article represents the second part of the review study devoted to applications of the new method proposed some years ago [1] within Bardeen–Cooper–Schrieffer (BCS) theory. The first part [2], which was published two years ago, addressed primarily the problem of *S* pairing. In recent years, however, the attention of theorists and experimentalists switched to the investigation of systems featuring Cooper pairs whose orbital angular momenta differ from zero. There are a few reasons for this. First, pairs in liquid ^{3}He, which is the only superfluid Fermi liquid on the Earth (the critical temperature T_c is about 2.6 mK [3, 4]), have the orbital angular momentum of $L = 1$ [5, 6]. Second, *D* pairing is realized in electron systems of high-temperature superconductors [7]. Third, the dense neutron liquid filling the core of neutron stars is superfluid, as was predicted by A.B. Migdal [8] and as was corroborated by the observations of the damping of sudden variations (glitches) in the velocity of the rotation of pulsars [9–13]. These variations are interpreted as a manifestation of the rearrangement of the vortex structure in a rotating neutron star [14–16]. In its core, the neutron density $\rho = p_F^3/3\pi^2$ (where p_F is the Fermi momentum) is so high that the *S* pairing of neutrons is impossible. Indeed, its existence depends on the sign of the *S*-wave phase for *nn* scattering at typical momenta about p_F. This sign is reversed when the density ρ reaches values of 2 to $2.5\rho_0$, where $\rho_0 = 0.17$ fm^{-3} is an equilibrium nuclear density. Nevertheless, attraction that is responsible for the emergence of a superfluid state is still operative at such Fermi momenta in the *P* wave. It turns out that, upon taking into account the interference between spin–orbit and tensor forces, the triplet channel of spin $S = 1$ and total angular momentum $J = 2$ is favored [17–21]. The objective of the present article is to discuss the phase diagram of superfluid neutron matter at densities and temperatures from the region dominated by pair correlations characterized by these quantum numbers.

It should be noted that, in the analogous *S*-pairing problem, where the order parameter is real-valued, everything reduces to calculating the temperature boundary $T_c(P)$ separating a superfluid and a normal liquid. In the triplet case, however, the situation is different. The order parameter, which is a complicated function of spin and angle, is capable of rearranging; therefore, phase transitions similar to the transition between the *A* and the *B* phase in superfluid ^{3}He are also possible in dense neutron matter.

Mathematical difficulties associated with determining phase-transition points—in a broader sense, the spectrum of superfluid phases—are much more chal-

lenging in the case of triplet pairing than in the case of S pairing. This is the reason why, in the majority of studies devoted to such systems, the authors restrict themselves to investigating the symmetry properties of the order parameter [22, 23], subsequently constructing a phenomenological free-energy functional and solving the relevant Ginzburg–Landau equations. Unfortunately, this approach is applicable only in the vicinity of T_c—it is insufficient for constructing the total phase diagram of the system, so that required information has hitherto been extracted only from numerical calculations [18, 24–27].

In order to compute numerically the phase diagram of superfluid neutron matter with allowance for triplet pairing, it is necessary to solve, with a computer, a set of at least five nonlinear integral equations. Since the energy splitting between different phases is extremely small, this must be done for many points of the (ρ, T) plane and to a rather high degree of precision. Usually, such numerical calculations rely on an iterative procedure, which actually involves choosing some initial state and substituting it on the right-hand side of the set of equations to be solved. The result obtained on the left-hand side is then used in the same way—that is, it is substituted on the right-hand side, and all operations are repeated anew. A weak point of this method is that its convergence often depends on the choice of initial iteration. This is not the whole story, however—the success or failure of the method is also determined, to a considerable extent, by the form of the kernel in the integral equation to which the iterative procedure is applied. From this point of view, the kernel of the BCS equation is one of the most inconvenient because it is singular: at $\Delta = 0$, the relevant integral diverges logarithmically. It is well known that, for singular kernels, many methods devised to simplify procedures for solving the problem in question are inappropriate. In order to improve the accuracy, very elaborate methods are employed—for example, those that rely on constructing an energy functional whose variation leads to the required equation or the required set of equations and on further minimizing this functional on the basis of all latest advancements in the variational approach. Unfortunately, a determination of all minima of a rather complicated energy functional is sometimes plagued by difficulties, especially if the energy landscape is nearly planar, which occurs if the problem at hand is partly or totally degenerate. Below, we will see that, in the case of systems involving $^3P_2$ pairing, we are dealing with such a situation.

That the calculations are extremely cumbersome presents yet another problem of significance. The greater the number of equations to be solved, the lower the rate at which iterations converge and, hence, the higher the requirements for the mathematical algorithms to be used for this. So far, it has been the unwieldiness of the procedure that has been the main obstacle for performing systematic calculations of the order-parameter structure in neutron matter in the entire temperature interval from zero to T_c even in the simplest approximation ignoring the mixing of the $^3P_2$ and $^3F_2$ channels. But we will see below that this mixing plays a crucial role in the calculation of the phase diagram for a superfluid system involving $J = 2$ Cooper pairs.

That iterative procedures are insufficiently accurate and that their implementation requires cumbersome calculations do not exhaust the flaws in this method. A much more hazardous point is that a process starting from an arbitrary initial state can miss some solution, as does indeed frequently occur. For example, only one two-component phase whose order parameter is a superposition of harmonics corresponding to the total-angular-momentum projections of $M = 0, \pm 2$ was found in vast and highly accurate calculations of the properties of superfluid neutron matter in the problem of pure $^3P_2$ pairing [24]. As will be shown in Section 3, there are actually two two-component phases. There exist some more examples of this type. Therefore, it is not surprising that the total spectrum of superfluid phases has not yet been found for any system featuring triplet pairing.

Finally, it is often difficult to interpret and to analyze results obtained within an iterative method, in particular, and within any other numerical method, in general. For example, it could be expected that different interactions would lead to different results for the gap structure, but this is not so in fact. From a comparison of the results presented in [24, 26], it can be seen that the ratio of the calculated energy splitting between different phases to the gap Δ_F takes nearly the same value in the two studies despite significant distinctions between the forms of the interactions used there. Of course, the reason behind this stability can hardly be found without resort to analytic methods similar to those that are used in the theory of second-order phase transitions. In tackling the problems being discussed and some other allied problems, we rely here on the method that was proposed previously in [1] for solving the BCS equation for the gap Δ in the S-pairing problem and which consists in reducing this equation to two virtually independent equations—one for the shape factor and the other for the gap amplitude. It is only necessary to extend this method to the case of triplet pairing.

The ensuing exposition is organized as follows. Sections 2 and 3 are devoted to a detailed description of this procedure implemented in [28]. The results obtained there are used in Section 4 to find the structure and the energy spectrum of the superfluid phases in the problem of pure $^3P_2$ pairing. It is shown that the set of all phases can be partitioned into two groups—one that includes phases whose order parameter has no zeros and the other that comprises phases whose order parameter vanishes at some point. In this problem, the structure of multicomponent phases appears to be degenerate. One (a few in some cases) of the numbers that determine this structure can be chosen arbitrarily,

while the others are determined according to a universal recipe that depends neither on the details of the interaction between the particles involved nor on density and temperature. Only the relative energy splitting of the phases depends on temperature, and only the gap in the spectrum of single-particle excitations, a type of scale factor in the problem, depends on all the remaining factors. In Section 5, the effect of contributions that are induced by tensor forces and which are off-diagonal in the orbital angular momentum of Cooper pairs is investigated within perturbation theory. It is demonstrated that the mixing of the $L = 1$ and $L = 3$ channels completely removes degeneracy peculiar to the $^3P_2$-pairing problem—the number of different superfluid phases and their structure at a given temperature are tightly fixed, while the energy spectrum of the phases splits completely. The resulting structure of the phases shows a low sensitivity to variations of interaction parameters, but it changes sizably with temperature. The last section is devoted to discussing the results obtained in the present study.

2. TRIPLET PAIRING: GENERAL FORMULAS

In superfluid dense neutron matter, the Cooper pair spin is $S = 1$ and the orbital angular momentum L is nonvanishing; therefore, the conventional BCS equation [29]

$$\Delta_{\alpha\beta}(\mathbf{p}) = -\int \mathcal{V}_{\alpha\beta\gamma\delta}(\mathbf{p}, \mathbf{p}_1)\frac{\tanh\frac{E(\mathbf{p}_1)}{2T}}{2E(\mathbf{p}_1)}\Delta_{\gamma\delta}(\mathbf{p}_1)\frac{d^3p_1}{(2\pi)^3}, \quad (1)$$

which involves the interaction block $\mathcal{V}$ that is irreducible in the particle–particle channel—this means that, in this channel, there are no diagrams connected only by two lines—transforms into a set of coupled equations for the components Δ_L^{JM}, which are determined by the expansion

$$\Delta_{\alpha\beta}(\mathbf{p}) = \sum_{J,L,M}\Delta_L^{JM}(p)(G_{LJ}^M(\mathbf{n}))_{\alpha\beta} \quad (2)$$

and which, owing to the T invariance of nuclear forces, satisfy the relation

$$(\Delta_L^{JM}(p))^* = (-1)^{J-M}\Delta_L^{J,-M}(p). \quad (3)$$

In systems featuring tensor interactions, the expansion of the block $\mathcal{V}$ (in neutron matter, it is often replaced by the *nn*-interaction potential) includes matrix elements that are off-diagonal in the angular orbital momentum:

$$\mathcal{V}(\mathbf{p}, \mathbf{p}_1) = 4\pi\sum_{LL'JM}(-1)^{(L-L')/2}\mathcal{V}_{LL'}^J(p, p_1)G_{LJ}^M(\mathbf{n})(G_{L'J}^M(\mathbf{n}_1))^*. \quad (4)$$

In the triplet case, the spin matrix $G_{LJ}^M(\mathbf{n})$, which absorbs entirely the angular and spin dependences, can be written as [24]

$$(G_{LJ}^M(\mathbf{n}))_{\alpha\beta} = \sum_{M_S M_L} C_{\frac{1}{2}\alpha\frac{1}{2}\beta}^{1M_S}C_{1M_SLM_L}^{JM}Y_{LM_L}(\mathbf{n}). \quad (5)$$

The quasiparticle spectrum has the form

$$E(\mathbf{p}) = \sqrt{\xi^2(p) + D^2(\mathbf{p})}, \quad (6)$$

which is more complicated than that in the case of S pairing.

In just the same way as in the S-pairing problem, the single-particle energy $\xi(p)$ of the normal Fermi system is calculated within the effective-mass approximation, $\xi(p) = p_F(p - p_F)/M^*$. As a rule, this approximation provides a high precision since the main contribution to the relevant integrals comes from the region near the Fermi surface. As to the squared gap vector $D^2(\mathbf{p})$, which appears in Eq. (6) and which is given by [24]

$$D^2(\mathbf{p}) = \frac{1}{2}\sum_{LJML_1J_1M_1}(\Delta_L^{JM}(p))^*\Delta_{L_1}^{J_1M_1}(p)S_{LL_1}^{JMJ_1M_1}(\mathbf{n}), \quad (7)$$

it now depends on the direction $\mathbf{n}$ of the relative momentum $\mathbf{p}$. This dependence is contained in the functions

$$S_{LL_1}^{JMJ_1M_1}(\mathbf{n}) = \mathrm{tr}[(G_{LJ}^M(\mathbf{n}))^*G_{L_1J_1}^{M_1}(\mathbf{n})] = \sum_{M_S m m_1}C_{1M_SLm}^{JM}C_{1M_SL_1m_1}^{J_1M_1}Y_{Lm}^*(\mathbf{n})Y_{L_1m_1}(\mathbf{n}), \quad (8)$$

which arise upon summation over the projections of the spin and the orbital angular momentum of the Cooper pair.

By using the normalization condition

$$\int S_{LL_1}^{JMJ_1M_1}(\mathbf{n})d\mathbf{n} = \delta_{J_1J}\delta_{L_1L}\delta_{M_1M}, \quad (9)$$

we can express the averaged gap Δ_F in the spectrum of single-particle excitations at the Fermi surface in terms of the components $\Delta_L^{JM}(p_F)$ as

$$\Delta_F^2 = \int D^2(p = p_F, \mathbf{n})\frac{d\mathbf{n}}{4\pi} = \frac{1}{8\pi}\sum_{LJM}(\Delta_L^{JM}(p_F))^*\Delta_L^{JM}(p_F). \quad (10)$$

In order to find the zeros and the maxima of the gap at the Fermi surface with the aim of analyzing some sym-

metry properties of the order parameter, it is sufficient to know the structure function $d^2(\mathbf{n})$ [28],

$$d^2(\mathbf{n}) = \frac{D^2(p = p_F, \mathbf{n})}{\Delta_F^2}, \quad (11)$$

which is normalized according to (10) by the condition

$$\int d^2(\mathbf{n}) \frac{d\mathbf{n}}{4\pi} = 1. \quad (12)$$

For the purpose of illustration, we present the structure functions for the single-component states of the $^3P_2$-pairing problem for the projection M equal to 0, 1, and 2 in absolute value.

The structure function corresponding to zero value of M,

$$d^2_{M=0}(\theta, \varphi) = \frac{1}{2}(1 + 3\cos^2\theta), \quad (13)$$

is positive everywhere, while the remaining two structure functions,

$$d^2_{M=1}(\theta, \varphi) = \frac{3}{2}(1 - \sin^2\theta\sin^2\varphi),$$
$$d^2_{M=2}(\theta, \varphi) = \frac{3}{2}\sin^2\theta, \quad (14)$$

have zeros.

If we introduce the harmonic variables $z = \cos\theta$, $x = \sin\theta\cos\varphi$, and $y = \sin\theta\sin\varphi$, each of the structure functions in (13) and (14) will obviously depend only on one of these harmonic variables—the first and the third on z and the second on y:

$$d^2_{M=0}(x, y, z) = \frac{1}{2}(1 + 3z^2),$$
$$d^2_{M=1}(x, y, z) = \frac{3}{2}(1 - y^2), \quad (15)$$
$$d^2_{M=2}(x, y, z) = \frac{3}{2}(1 - z^2).$$

Below, we will see that, in the $^3P_2$-pairing problem, all multicomponent solutions have the same structure functions.

By substituting relations (2)–(8) into (1), we arrive at a set of an infinite number of coupled equations for the components $\Delta_L^{JM}(p)$:

$$\Delta_L^{JM}(p) = \sum_{L'L_1J_1M_1} (-1)^{1+(L-L')/2} \times \int\int \mathcal{V}^J_{LL'}(p, p_1) S^{JMJ_1M_1}_{L'L_1}(\mathbf{n}_1) \frac{\tanh\frac{E(\mathbf{p}_1)}{2T}}{2E(\mathbf{p}_1)} \times \Delta^{J_1M_1}_{L_1}(p_1) \frac{p_1^2 dp_1 d\mathbf{n}_1}{2\pi^2}. \quad (16)$$

Our objective is to simplify this set of equations and to reveal the structure of its solutions and of its energy spectrum. In order to tackle this problem, it is necessary to know the matrix function $S^{JMJ_1M_1}_{L'L_1}(\mathbf{n})$. It is more straightforward to calculate its elements if, in (8), we go over to $3j$ coefficients, which are more convenient in such calculations,

$$S^{JMJ_1M_1}_{LL_1}(\mathbf{n}) = \sum_{M_S, m, m_1} (-1)^{M-L+M_1-L_1} \times \sqrt{(2J+1)(2J_1+1)} \begin{pmatrix} 1 & L & J \\ M_S & m & -M \end{pmatrix} \times \begin{pmatrix} 1 & L_1 & J_1 \\ M_S & m_1 & -M_1 \end{pmatrix} Y^*_{Lm}(\mathbf{n}) Y_{L_1m_1}(\mathbf{n}), \quad (17)$$

and if, in performing summation over m and m_1, we make use of the formula [30]

$$Y^*_{Lm}(\mathbf{n}) Y_{L_1m_1}(\mathbf{n}) = \sum_{K\kappa} i^{-L+L_1+K} (-1)^m \times \sqrt{\frac{(2L+1)(2L_1+1)(2K+1)}{4\pi}} \times \begin{pmatrix} L & L_1 & K \\ -m & m_1 & \kappa \end{pmatrix} \begin{pmatrix} L & L_1 & K \\ 0 & 0 & 0 \end{pmatrix} Y^*_{K\kappa}(\mathbf{n}). \quad (18)$$

As a result, we obtain

$$S^{JMJ_1M_1}_{LL_1}(\mathbf{n}) = \sum_{M_S, m, m_1, K, \kappa} (-1)^{(L-L_1+K)/2+m+M+M_1} \times \sqrt{\frac{(2L+1)(2L_1+1)(2J+1)(2J_1+1)(2K+1)}{4\pi}} \times \begin{pmatrix} L & L_1 & K \\ 0 & 0 & 0 \end{pmatrix} \begin{pmatrix} L & L_1 & K \\ -m & m_1 & \kappa \end{pmatrix} \begin{pmatrix} 1 & L & J \\ M_S & m & -M \end{pmatrix} \times \begin{pmatrix} 1 & L_1 & J_1 \\ M_S & m_1 & -M_1 \end{pmatrix} Y^*_{K\kappa}(\mathbf{n}). \quad (19)$$

Here, summation over magnetic quantum numbers is performed with the aid of the formula [30]

$$\sum_{m_4m_5m_6} (-1)^{j_4+j_5+j_6+m_4+m_5+m_6} \begin{pmatrix} j_1 & j_5 & j_6 \\ m_1 & -m_5 & m_6 \end{pmatrix}$$

$$\times \begin{pmatrix} j_4 & j_2 & j_6 \\ m_4 & m_2 & -m_6 \end{pmatrix} \begin{pmatrix} j_4 & j_5 & j_3 \\ -m_4 & m_5 & m_3 \end{pmatrix} \tag{20}$$

$$= \begin{pmatrix} j_1 & j_2 & j_3 \\ m_1 & m_2 & m_3 \end{pmatrix} \begin{Bmatrix} j_1 & j_2 & j_3 \\ j_4 & j_5 & j_6 \end{Bmatrix}.$$

As a result, we arrive at

$$S_{LL_1}^{JMJ_1M_1}(\mathbf{n}) = -\sum_{K,\kappa}(-1)^{(L-L_1+K)/2+M} \times \sqrt{\frac{(2L+1)(2L_1+1)(2J+1)(2J_1+1)(2K+1)}{4\pi}} \tag{21}$$

$$\times \begin{pmatrix} K & L & L_1 \\ 0 & 0 & 0 \end{pmatrix} \begin{pmatrix} K & J_1 & J \\ \kappa & M_1 & -M \end{pmatrix} \begin{Bmatrix} K & J_1 & J \\ 1 & L & L_1 \end{Bmatrix} Y_{K\kappa}^*(\mathbf{n}).$$

The phases of the spherical functions appearing in this expression are chosen according to [30]:

$$Y_{lm}^* = (-1)^{l-m} Y_{l,-m}.$$

With the aid of these relations, we can show that, in the triplet case, the matrix $S_{LL_1}^{JMJ_1M_1}(\mathbf{n})$ possesses the symmetry properties

$$\begin{aligned} \mathrm{Re}\, S_{LL_1}^{JMJ_1M_1}(\mathbf{n}) &= \mathrm{Re}\, S_{LL_1}^{JM_1J_1M}(\mathbf{n}), \\ \mathrm{Im}\, S_{LL_1}^{JMJ_1M_1}(\mathbf{n}) &= -\mathrm{Im}\, S_{LL_1}^{JM_1J_1M}(\mathbf{n}), \end{aligned} \tag{22}$$

which make it possible to halve the volume of the calculations. To complete the presentation of the general formulas, it only remains to add one more (see [30]),

$$Y_{lm}(\theta,\varphi) = i^l(-1)^{(m+|m|)/2} \times \sqrt{\frac{(2l+1)(l-m)!!}{4\pi(l+m)!!}} P_l^{|m|}(\cos\theta) e^{im\varphi}, \tag{23}$$

where P_l^m are associated Legendre polynomials.

3. TRANSFORMED BCS SET OF EQUATIONS FOR DESCRIBING TRIPLET PAIRING

We begin our analysis of the phase diagram of superfluid dense neutron matter by simplifying—more precisely, by truncating—the set of Eqs. (16). Specifically, we discard all terms that are off-diagonal in the orbital angular and in the total angular momentum. There are a few factors justifying this step. The first one is the smallness of the contributions of the $L_1 \neq L$ off-diagonal elements of the functions $S_{LL_1}^{JMJ_1M_1}(\mathbf{n})$ (this fact was indicated in [5]). The second one is the relative smallness of the off-diagonal components of tensor forces, which are responsible for the mixing of channels characterized by different values of the orbital angular momentum. The final one is the smallness of corrections associated with the mixing of channels having different values of the total angular momentum. These corrections are of paramount importance in describing the A phase of superfluid ^{3}He, but they are immaterial in neutron matter because the matrix elements $\mathcal{V}_{11}^{J\neq 2}$ are small in relation to the elements $\mathcal{V}_{11}^{J=2}$. In Section 4, the most important of these contributions, which are omitted for the time being, are analyzed in detail and are taken into account.

Upon all simplifications, the set of Eqs. (16) breaks down into blocks. On its right-hand sides, there remains only one summation over the projections M of the total angular momentum J; therefore, there are $(2J+1)$ equations for the component of the vector $\Delta_L^{JM}(p)$ in each individual sector:

$$\Delta_L^{JM}(p) = -\sum_{M_1}\int\!\!\int \mathcal{V}_{LL}^J(p,p_1) S_{LL}^{JMJM_1}(\mathbf{n}_1) \times \frac{\tanh\dfrac{E(\mathbf{p}_1)}{2T}}{2E(\mathbf{p}_1)} \Delta_L^{JM_1}(p_1) \frac{p_1^2 dp_1 d\mathbf{n}_1}{2\pi^2}. \tag{24}$$

We now proceed to transform this set of equations, following a procedure similar to that used in the case of S pairing [1, 2]. A generalization to the case of triplet pairing is quite straightforward [28]. We break down the diagonal matrix element $\mathcal{V}_{LL}^J(p,p_1)$ of the interaction according to the same scheme as in [1, 2]:

$$\mathcal{V}_{LL}^J(p,p_1) = \mathcal{V}_\mathrm{F}\phi(p)\phi(p_1) + W(p,p_1). \tag{25}$$

Here, the first term representing a separable part in which $\phi(p) = \mathcal{V}_{LL}^J(p,p_\mathrm{F})/\mathcal{V}_\mathrm{F}$, where $\mathcal{V}_\mathrm{F} = \mathcal{V}_{LL}^J(p_\mathrm{F},p_\mathrm{F})$, was singled out in such a way that the residual part $W(p,p_1)$ vanishes identically when one of the arguments p and p_1 occurs at the Fermi surface. Owing to this, the main contributions to the integrals featuring the block W come from the region far off the Fermi surface, where we can make the substitutions $E \longrightarrow |\xi|$ and $\tanh(E/2T) \longrightarrow 1$. The discarded terms are of order $\Delta_\mathrm{F}^2/(\varepsilon_\mathrm{F}^0)^2$, where $\varepsilon_\mathrm{F}^0 = p_\mathrm{F}^2/2M$ is the energy of a perfect Fermi gas and M is the neutron mass. In dense neutron matter with $\varepsilon_\mathrm{F}^0 \sim 100$ MeV, these terms manifest themselves in the fifth to the sixth decimal place, so that we will ignore them below. The substitution of (25) into (24) yields

$$\Delta_L^{JM}(p) + \int \frac{W(p,p_1)}{2|\xi(p_1)|}\Delta_L^{JM}(p_1)\frac{p_1^2 dp_1}{2\pi^2} = D_L^{JM}\phi_{LJ}(p), \tag{26}$$

where

$$D_L^{JM} = -\mathcal{V}_F \sum_{M_1} \iint \phi(p) S_{LL}^{JMJM_1}(\mathbf{n}) \times \frac{\tanh\frac{E(\mathbf{p})}{2T}}{2E(\mathbf{p})} \Delta_L^{JM_1}(p) \frac{p^2 dp d\mathbf{n}}{2\pi^2}. \quad (27)$$

By examining the first of these equations, it is easy to establish that the dependence of the components $\Delta_L^{JM}(p)$ on the absolute value of the momentum is entirely contained in the numbers D_L^{JM}. By introducing the shape factor $\chi(p)$ via the relation

$$\Delta_L^{JM}(p) = D_L^{JM}\chi(p) \quad (28)$$

and substituting this equality into Eq. (26), we arrive at the integral equation

$$\chi(p) + \int W(p, p_1) \frac{\chi(p_1)}{2|\xi(p_1)|} \frac{p_1^2 dp_1}{2\pi^2} = \phi(p), \quad (29)$$

which is essentially identical to the equation for the shape factor in the *S*-pairing problem [1, 2], since the orbital angular momentum *L* and the total angular momentum *J* do not appear in (29) explicitly.

Thus, we conclude that, apart from corrections of order $\Delta_F^2/(\varepsilon_F^0)^2$, all components $\Delta_L^{JM}(p)$ have the same *p* dependence and that the shape factor $\chi(p)$ is independent of temperature *T*. Generally, only $(2J + 1)$ complex coefficients D_L^{JM}, which determine the structure of the multicomponent solutions near the Fermi surface are temperature-dependent. According to the property in Eq. (3), the real and the imaginary parts of these coefficients are related as

$$(D_L^{JM})^* = (-1)^{J-M} D_L^{J,-M}. \quad (30)$$

The equation for them can be obtained by substituting (28) into the expression on the right-hand side of (27). The result is

$$D_L^{JM} = -\mathcal{V}_F \sum_{M_1} D_L^{JM_1} \times \iint \phi(p) S_{LL}^{JMJM_1}(\mathbf{n}) \frac{\tanh\frac{E(\mathbf{p})}{2T}}{2E(\mathbf{p})} \chi(p) \frac{p^2 dp d\mathbf{n}}{2\pi^2}, \quad (31)$$

$$M = 0, \pm 1, \pm 2, \ldots, \pm J.$$

The set of Eqs. (29) and (31) is much more convenient for numerical calculations than the original set of Eqs. (16) because the problem in question has been broken down into two independent problems. On the basis of the nonsingular integral Eq. (29), one first calculates the shape factor $\chi(p)$ and then substitutes the resulting solution into Eqs. (31), thereby reducing them to a set of nonlinear algebraic equations.

Yet another useful relation for the gap Δ_F is derived by multiplying each of Eqs. (31) by $(D_L^{JM})^*$ and by performing summation over *M*. By considering that $D^2(\mathbf{p}) = \sum_{M_1 M_2} (D_L^{JM_1})^* D_L^{JM_2} S_{LL}^{JMJM_1}(\mathbf{n}) \chi^2(p) \equiv \Delta_F^2 d^2(\mathbf{n}) \chi^2(p)$, we then obtain

$$1 = -\mathcal{V}_F \iint \phi(p) d^2(\mathbf{n}) \frac{\tanh\frac{E(\mathbf{p})}{2T}}{2E(\mathbf{p})} \chi(p) \frac{p^2 dp d\mathbf{n}}{(2\pi)^3}. \quad (32)$$

This formula can be simplified by using the fact that it also determines the critical temperature T_c if we set Δ_F to zero in it:

$$1 = -\mathcal{V}_F \int \phi(p) \frac{\tanh\frac{\xi(p)}{2T_c}}{2\xi(p)} \chi(p) \frac{d^3 p}{(2\pi)^3}. \quad (33)$$

Equation (32) can then be recast into the form

$$\iint \phi(p) \left[\frac{\tanh\frac{\xi(p)}{2T_c}}{\xi(p)} - d^2(\mathbf{n}) \frac{\tanh\frac{E(\mathbf{p})}{2T}}{E(\mathbf{p})} \right] \times \chi(p) p^2(\xi) \frac{dp}{d\xi} d\xi d\mathbf{n} = 0. \quad (34)$$

Here, the integrand decreases fast with increasing $|\xi(p)|$; therefore, the dominant contribution to the integral comes from the region $|\xi(p)| \le \Delta_F$, where we can replace the functions $\chi(p)$ and $\phi(p)$ by unity and $p^2(dp/d\xi)$ by $p_F M^*$. As a result, we arrive at

$$\iint \left[\frac{\tanh\frac{\xi}{2T_c}}{\xi} - d^2(\mathbf{n}) \frac{\tanh\frac{E(\xi, \mathbf{n})}{2T}}{E(\xi, \mathbf{n})} \right] d\xi d\mathbf{n} = 0, \quad (35)$$

where $E(\mathbf{p}) = \sqrt{\xi^2(p) + \Delta_F^2 d^2(\mathbf{n})}$.

We see that, if the structure function is preset, the gap Δ_F is a universal function of $\tau = T/T_c$. From the analysis of the case of pure $^3P_2$ pairing in the next section, it can be deduced that the structure of solutions to the set of Eqs. (31) that describe various superfluid phases is such that it admits structure functions of only two types. This means that, in the problem being discussed, the structure of superfluid phases is degenerate and is independent either of density, or of temperature, or of other input parameters.

4. $^3P_2$ PAIRING IN DENSE NEUTRON MATTER

4.1. Formulation of the Problem

A nontrivial solution to the BCS equations exists, provided that the particles involved are attracted in the

channel being considered. The prevalent opinion, which is based on an analysis of experimental data on *nn* scattering in a vacuum, is that, in dense neutron matter, where characteristic momenta are such that the vacuum $^1S_0$ phase shift has already changed sign, the most favorable channel for pairing is that where the spin and the total angular momentum of Cooper pairs are $S = 1$ and $J = 2$, respectively. This conclusion is drawn on the basis of the fact that the vacuum phase shift $\delta(^3P_2)$ exceeds all the remaining ones in the energy region under consideration.

In general, this argument is insufficient because the interaction between particles in nuclear matter differs from that in a vacuum, so that vacuum attraction can easily give way to repulsion in a medium. However, $^3P_2$ scattering is dominated by spin–orbit interaction, which is followed, in order of importance, by tensor forces. In the case of $S = L = 1$ triplet pairing in neutron matter, spin–orbit forces ensure attraction only for Cooper pair states whose spin is parallel to the orbital angular momentum—that is, precisely in the $^3P_2$ channel. Since the spin–orbit component of $\hat{V}$ is of a relativistic origin, it is local in the coordinate representation and its renormalization is weak in nuclear matter. To make sure that this is indeed the case, it is sufficient to examine data on the spin–orbit splitting of single-particle levels of nuclei. As to tensor forces, whose amplitude in a vacuum is less than the amplitude of spin–orbit forces, their contribution is maximal in zero-helicity states [31] (vol. 1)—that is, in the $^3P_0$ channel. In the $J = 2$ channel, their role is insignificant precisely because, in the $^3P_2$ state, pairs do not possess specific helicity values; as a result, tensor forces only lead to the mixing of the $L = 1$ and $L = 3$ channels.

We postpone a discussion on these problems for the time being and focus our attention on solving the problem of pure $^3P_2$ pairing, the most popular one indeed in the physics of superfluid neutron liquid. On one hand, rich experience of numerical calculations has been accumulated here [18, 19, 24, 26]; on the other hand, the relevant analytic solution was obtained in [28]. The objective of this section is to give an account of an analytic method and to compare the results that it produces with the numerical results.

In the system featuring $^3P_2$ correlations, the set of Eqs. (31) often is rewritten as that for five real numbers δ_0, δ_1, δ_2, n_1, and n_2 that characterize the order parameter $D_o^2(p_\mathrm{F}, \mathbf{n})$ and which are related to D_1^{2M} as [24]

$$D_1^{20} = \delta_0, \quad D_1^{2M} = \delta_M + in_M, \quad M = \pm 1, \pm 2; \quad (36)$$

additionally, we have $\delta_{-2} = \delta_2$, $\delta_{-1} = \delta_1$, $n_{-2} = -n_2$, $n_{-1} = n_1$, and $n_0 = 0$. The last equality is equivalent to the well-known option $\alpha = 0$ for the phase α of the gap Δ in the theory of *S* pairing.

In terms of the new variables, the function $D_o^2(\mathbf{p})$ has the form

$$\begin{aligned} D_o^2(p, \theta, \varphi) = \frac{\chi^2(p)}{8\pi}\Big(&3[\delta_2^2 + n_2^2]\sin^2\theta \\ &+ 3[\delta_1^2 + n_1^2]\Big(1 - \frac{1}{2}\sin^2\theta\Big) + \frac{1}{2}\delta_0^2(1 + 3\cos^2\theta) \\ &+ \sqrt{6}[\delta_0 n_1 + \sqrt{6}\delta_1 n_2 - \sqrt{6}\delta_2 n_1]\sin\theta\cos\theta\sin\varphi \\ &- \sqrt{6}[\delta_0\delta_1 + \sqrt{6}\delta_1\delta_2 + \sqrt{6}n_1 n_2]\sin\theta\cos\theta\cos\varphi \\ &+ \frac{1}{2}[3\delta_1^2 - 3n_1^2 - 2\sqrt{6}\delta_0\delta_2]\sin^2\theta\cos 2\varphi \\ &+ \frac{1}{2}[2\sqrt{6}\delta_0 n_2 - 6\delta_1 n_1]\sin^2\theta\sin 2\varphi\Big), \end{aligned} \quad (37)$$

where the shape factor $\chi(p)$ is determined by Eq. (29). In relation to the conventional formula for $D_o^2(\mathbf{p})$ from [24], the *p* dependence of the order parameter is factorized in (37).

In order to write explicitly the transformed set of BCS equations for the parameters δ_M and n_M, we must know the matrix function $S_{11}^{2M2M_1}(\theta, \varphi)$. Its nonvanishing elements calculated on the basis of Eq. (21) are

$$\begin{aligned} S_{11}^{2020}(\theta, \varphi) &= \frac{3}{8\pi}\Big(\frac{1}{3} + \cos^2\theta\Big), \\ S_{11}^{2121}(\theta, \varphi) &= \frac{3}{8\pi}\Big(1 - \frac{1}{2}\sin^2\theta\Big), \\ S_{11}^{2222}(\theta, \varphi) &= \frac{3}{8\pi}\sin^2\theta, \\ S_{11}^{2221}(\theta, \varphi) &= -\frac{3}{8\pi}\sin\theta\cos\theta e^{-i\varphi}, \\ S_{11}^{2220}(\theta, \varphi) &= -\frac{3}{8\pi\sqrt{6}}\sin^2\theta e^{-2i\varphi}, \\ S_{11}^{2120}(\theta, \varphi) &= -\frac{3}{8\pi\sqrt{6}}\sin\theta\cos\theta e^{-i\varphi}, \\ S_{11}^{212,-1}(\theta, \varphi) &= \frac{3}{16\pi}\sin^2\theta e^{-2i\varphi}. \end{aligned} \quad (38)$$

By substituting these results into the set of Eqs. (31) and introducing the notation $\nu_\mathrm{F} = 2\mathcal{V}_\mathrm{F}/\pi$ and

$$K(\mathbf{n}) = \int \phi(p)\frac{\tanh\dfrac{E(\mathbf{p})}{2T}}{2E(\mathbf{p})}\chi(p)p^2 dp, \quad (39)$$

we find, after some simple algebra, that

$$\begin{aligned} \delta_2 = -\frac{3}{2}\nu_\mathrm{F}\int\Big[&\delta_2\sin^2\theta - \delta_1\sin\theta\cos\theta\cos\varphi \\ &- n_1\sin\theta\cos\theta\sin\varphi - \frac{\delta_0}{\sqrt{6}}\sin^2\theta\cos 2\varphi\Big]K(\mathbf{n})\frac{d\mathbf{n}}{4\pi}, \end{aligned}$$

$$n_2 = -\frac{3}{2}v_F\int\Big[n_2\sin^2\theta + \delta_1\sin\theta\cos\theta\sin\varphi$$
$$- n_1\sin\theta\cos\theta\cos\varphi + \frac{\delta_0}{\sqrt{6}}\sin^2\theta\sin 2\varphi\Big]K(\mathbf{n})\frac{d\mathbf{n}}{4\pi},$$

$$\delta_1 = -\frac{3}{2}v_F\int\Big[-\delta_2\sin\theta\cos\theta\cos\varphi + n_2\sin\theta\cos\theta\sin\varphi$$
$$+ \delta_1\Big(1 - \frac{(1-\cos 2\varphi)}{2}\sin^2\theta\Big) - \frac{1}{2}n_1\sin^2\theta\sin 2\varphi$$
$$- \frac{\delta_0}{\sqrt{6}}\sin\theta\cos\theta\cos\varphi\Big]K(\mathbf{n})\frac{d\mathbf{n}}{4\pi}, \qquad (40)$$

$$n_1 = -\frac{3}{2}v_F\int\Big[-\delta_2\sin\theta\cos\theta\sin\varphi - n_2\sin\theta\cos\theta\cos\varphi$$
$$-\frac{1}{2}\delta_1\sin^2\theta\sin 2\varphi + n_1\Big(1 - \frac{(1+\cos 2\varphi)}{2}\sin^2\theta\Big)$$
$$+ \frac{\delta_0}{\sqrt{6}}\sin\theta\cos\theta\cos\varphi\Big]K(\mathbf{n})\frac{d\mathbf{n}}{4\pi},$$

$$\delta_0 = -\frac{3}{2}v_F\int\Big[-\sqrt{\frac{2}{3}}\delta_2\sin^2\theta\cos 2\varphi$$
$$+ \sqrt{\frac{2}{3}}n_2\sin^2\theta\sin 2\varphi - \sqrt{\frac{2}{3}}\delta_1\sin\theta\cos\theta\cos\varphi$$
$$+ \sqrt{\frac{2}{3}}n_1\sin\theta\cos\theta\sin\varphi + \delta_0\Big(\frac{1}{3} + \cos^2\theta\Big)\Big]K(\mathbf{n})\frac{d\mathbf{n}}{4\pi}.$$

This set of equations has three obvious single-component solutions corresponding to the projections of the total angular momentum of a pair that are equal to $M = 0, 1, 2$. It should be emphasized that, for the last of these, the spatial dependence of the order parameter, $\Delta \sim (x + iy)$, is identical in form to that in the A phase of superfluid ^{3}He. This solution corresponds to the set of the values $\delta_2 \neq 0$ and $\delta_1 = \delta_0 = 0$. The two others are obtained from here by means of a permutation of the indices 0, 1, 2.

We begin a pursuit of multicomponent solutions to the set of Eqs. (40) by assuming that $\delta_0 \neq 0$. Our search is simplified considerably upon introducing, instead of the coefficients δ_M and n_M, the ratios of these coefficients to the scale factor $\delta = \delta_0/\sqrt{6}$,

$$\delta_M = (\lambda_M + i\kappa_M)\delta, \quad M = 1, 2. \qquad (41)$$

Owing to this choice of δ, the irrational number $\sqrt{6}$ is eliminated from all relevant relations. The structure function $d^2(\theta, \varphi)$ calculated on the basis of Eqs. (11) and (37) can be represented as

$$d^2(\theta,\varphi) = d^2\Big[1 + 3\cos^2\theta + (\lambda_2^2 + \kappa_2^2)\sin^2\theta$$
$$+ \frac{(\lambda_1^2 + \kappa_1^2)}{2}(1 + \cos^2\theta)$$
$$+ 2(\kappa_1 + \lambda_1\kappa_2 - \lambda_2\kappa_1)\sin\theta\cos\theta\sin\varphi$$
$$- 2(\lambda_1 + \lambda_1\lambda_2 + \kappa_1\kappa_2)\sin\theta\cos\theta\cos\varphi \qquad (42)$$
$$+ \frac{1}{2}(\lambda_1^2 - \kappa_1^2 - 4\lambda_2)\sin^2\theta\cos 2\varphi$$
$$+ (2\kappa_2 - \lambda_1\kappa_1)\sin^2\theta\sin 2\varphi\Big],$$

while the numerical factor d^2 is determined by the normalization condition (12),

$$d^2 = \frac{1}{2\Big[1 + \frac{1}{3}(\lambda_2^2 + \kappa_2^2 + \lambda_1^2 + \kappa_1^2)\Big]}. \qquad (43)$$

The analysis is further simplified by the circumstance that seven functions in (38) can be written as linear combinations of the smaller number of the basis functions f_i, where

$$f_0 = 1 - 3\cos^2\theta, \quad f_1 = \frac{3}{2}\cos\theta\sin\theta\cos\varphi,$$
$$f_2 = \frac{3}{2}\cos\theta\sin\theta\sin\varphi, \quad f_3 = \frac{3}{2}\sin^2\theta\cos 2\varphi, \qquad (44)$$
$$f_4 = \frac{3}{2}\sin^2\theta\sin 2\varphi, \quad f_5 = \frac{1}{2}(1 + 3\cos^2\theta).$$

Substituting $4\pi\sigma_{11}^{2M2M_1}$ for $S_{11}^{2M2M_1}$, we obtain

$$\sigma_{11}^{2020} = f_5, \quad \sigma_{11}^{2121} = \frac{1}{4}f_0 + f_5,$$
$$\sigma_{11}^{2222} = f_0 + f_5, \quad \sigma_{11}^{2221} = -f_1 + if_2,$$
$$\sigma_{11}^{2220} = -\frac{f_3 - if_4}{\sqrt{6}}, \quad \sigma_{11}^{2120} = -\frac{f_1 - if_2}{\sqrt{6}}, \qquad (45)$$
$$\sigma_{11}^{212,-1} = -\frac{1}{2}(f_3 - if_4).$$

In the set of Eqs. (40), we further go over to λ_i and κ_i, taking into account relations (45); after some simple algebra, we then find that the parameters λ_1, λ_2, κ_1, κ_2, and δ satisfy the set of five nonlinear equations [28]

$$\lambda_2 = -v_F[\lambda_2(J_0 + J_5) - \lambda_1 J_1 - \kappa_1 J_2 - J_3],$$
$$\kappa_2 = -v_F[\kappa_2(J_0 + J_5) + \lambda_1 J_2 - \kappa_1 J_1 + J_4],$$
$$\lambda_1 = -v_F\Big[-\lambda_2 J_1 + \kappa_2 J_2$$
$$+ \frac{\lambda_1}{4}(J_0 + 4J_5 + 2J_3) - \frac{\kappa_1}{2}J_4 - J_1\Big], \qquad (46)$$

$$\kappa_1 = -\nu_F\Big[-\lambda_2 J_2 - \kappa_2 J_1 - \frac{\lambda_1}{2}J_4 + \frac{\kappa_1}{4}(J_0 + 4J_5 - 2J_3) + J_2\Big],$$

$$1 = -\nu_F\Big[-\frac{1}{3}(\lambda_2 J_3 - \kappa_2 J_4 + \lambda_1 J_1 - \kappa_1 J_2) + J_5\Big],$$

where the integrals J_i, $i = 1, \ldots, 5$ are given by

$$J_i = \iint f_i(\theta, \varphi)K(\theta, \varphi)\frac{\sin\theta d\theta d\varphi}{4\pi}. \quad (47)$$

It should be noted that, if we had disregarded the angular dependence of $E(\mathbf{p})$, all integrals in (47), with the exception of the last one (J_5), would have vanished. It is the integral J_5 that controls the averaged value of the gap Δ_F in the spectrum of single-particle excitations at the Fermi surface, while all the remaining integrals are responsible for the gap structure.

We note that the first four integrals are not independent. In order to prove this, we introduce an additional integral of the type in (47) with an integrand that involves the partial derivative $f = \partial d^2(\theta, \varphi)/\partial\varphi$ of the structure function $d^2(\theta, \varphi)$ with respect to the angle φ. Integration with respect to this angle obviously yields zero result. On the other hand, the derivative $\partial d^2(\theta, \varphi)/\partial\varphi$ can easily be expressed in terms of the functions f_i ($i = 1, \ldots, 5$); taking this into account, we find, after some simple algebra, that

$$\sum_{i=1}^{4} c_i J_i = 0, \quad (48)$$

where $c_1 = \kappa_1 + \lambda_1\kappa_2 - \lambda_2\kappa_1$, $c_2 = \lambda_1 + \lambda_1\lambda_2 + \kappa_1\kappa_2$, $c_3 = 2\kappa_2 - \kappa_1\lambda_1$, and $c_4 = 2\lambda_2 - (\lambda_1^2 - \kappa_1^2)/2$. Relation (48) plays a key role in seeking multicomponent solutions to the set of Eqs. (46). This becomes obvious upon multiplying the second, the third, and the fourth equation in (46) by λ_2, $2\kappa_1$, and $2\lambda_1$, respectively, and then subtracting the sum of the results obtained by applying these three operations from the first equation multiplied by κ_2; indeed, this yields (48). Thus, only four of the five equations in (46) are independent. Since the number of independent equations is less than the number of the parameters to be determined by solving these equations, one of the parameters λ_i and κ_i can be chosen arbitrarily. In just the same way as in [28], we set $\kappa_1 = 0$ and eliminate the penultimate equation in (46) as that which follows from the remaining four and relation (48). As a result, we are left with four equations

$$\lambda_2 = -\nu_F[\lambda_2(J_0 + J_5) - \lambda_1 J_1 - J_3],$$
$$\kappa_2 = -\nu_F[\lambda_1 J_2 + \kappa_2(J_0 + J_5) + J_4],$$
$$\lambda_1 = -\nu_F\Big[-\lambda_2 J_1 + \frac{\lambda_1}{4}(J_0 + 4J_5 + 2J_3) + \kappa_2 J_2 - J_1\Big], \quad (49)$$
$$1 = -\nu_F\Big[-\frac{1}{3}(\lambda_2 J_3 + \lambda_1 J_1 - \kappa_2 J_4) + J_5\Big].$$

Their solutions are real-valued at $\kappa_2 = 0$ and complex-valued at $\kappa_2 \neq 0$.

4.2. Real-Valued Solutions

This section is devoted to seeking real-valued solutions to the set of Eqs. (49) (those for which $\kappa_1 = \kappa_2 = 0$). In this case, the number of equations in (49) reduces again because the second equation is satisfied automatically. Indeed, it follows from (42) that, at $\kappa_1 = \kappa_2 = 0$, the structure function assumes the form

$$d^2(\theta, \varphi) = \frac{1}{2\Big[1 + \frac{1}{3}(\lambda_1^2 + \lambda_2^2)\Big]}\Big[1 + 3\cos^2\theta + \lambda_2^2\sin^2\theta + \frac{\lambda_1^2}{2}(1 + \cos^2\theta) - 2\lambda_1(1 + \lambda_2)\sin\theta\cos\theta\cos\varphi + \frac{1}{2}(\lambda_1^2 - 4\lambda_2)\sin^2\theta\cos 2\varphi\Big]. \quad (50)$$

It is invariant under the substitution $\varphi \longrightarrow -\varphi$, and so is the function $K(\theta, \varphi)$ given by (39). At the same time, the functions $f_2(\theta, \varphi)$ and $f_4(\theta, \varphi)$, which enter into the integrals J_2 and J_4 and which are proportional to $\sin\varphi$ [see Eqs. (44) and (47)], change sign under this substitution. Upon integration with respect to the angle φ, both integrals then vanish:

$$J_2(\lambda_1, \lambda_2) = J_4(\lambda_1, \lambda_2) = 0. \quad (51)$$

As a result, there remain only three equations in (49):

$$\lambda_2 = -\nu_F[\lambda_2(J_0 + J_5) - \lambda_1 J_1 - J_3],$$
$$\lambda_1 = -\nu_F\Big[-\lambda_2 J_1 + \frac{\lambda_1}{4}(J_0 + 4J_5 + 2J_3) - J_1\Big], \quad (52)$$
$$1 = -\nu_F\Big[-\frac{1}{3}(\lambda_2 J_3 + \lambda_1 J_1) + J_5\Big].$$

One of these equations can be reserved for determining Δ_F; therefore, it is sufficient to analyze only two of them in order to clarify the structure of real-valued solutions characterized by the numbers λ_1 and λ_2. It is natural to expect that solutions are represented by some points on the (λ_1, λ_2) plane. We will see below that the majority of solutions to the $^3P_2$-pairing problem are multiply degenerate, forming a family of second-order curves on the (λ_1, λ_2) plane.

As was indicated above, the equation that determines the gap Δ_F must involve the integral J_5, which governs the magnitude of the gap in the spectrum of single-particle excitations. Therefore, the best way to derive two equations appropriate for analyzing the structure of solutions to the set of Eqs. (52) is to eliminate this integral. The simplest method for implementing this consists in multiplying the last equation first by λ_2 and then by λ_1 and in successively subtracting the

resulting equations from the first and the second equation in (52). Prior to doing this, however, we will investigate the case where one of the parameters λ_1 or λ_2 vanishes—only in this case will no solution to the original set of Eqs. (52) be lost. We do not need to investigate the case of $\lambda_1 = \lambda_2 = 0$, because λ_1 and λ_2 cannot vanish simultaneously in multicomponent real-valued solutions.

First, we assume that $\lambda_2 = 0$ and $\lambda_1 \neq 0$. In this case, two parameters, λ_1 and Δ_F, must satisfy all three equations in (52). From rather a tedious analysis, it can then be deduced that this set of equations has no nontrivial solutions.

In the other case ($\lambda_1 = 0$, $\lambda_2 \neq 0$), the situation is totally different. The second equation in (52) is now satisfied automatically; hence, the number of remaining equations is equal to the number of unknown parameters. This statement must be further clarified. The point is that, at $\lambda_1 = 0$, the φ-dependent part of the structure function (50) involves $\cos 2\varphi$; therefore, it is invariant under the substitution $\varphi \longrightarrow \pi + \varphi$, while $f_1 \sim \cos\varphi$ changes sign. At any value of λ_2, we therefore have

$$J_1(0, \lambda_2) = 0, \tag{53}$$

which proves the above statement that the left-hand side of the second equation in (52) vanishes identically. The simplest way to draw this conclusion, as well as the majority of others that are based on the symmetry properties of the integrals involved, is to use the harmonic coordinates x, y, and z rather than spherical coordinates. In terms of the harmonic coordinates, the set of the basis functions f_i (44) is given by

$$f_0 = 1 - 3z^2, \quad f_1 = \frac{3}{2}xz, \quad f_2 = \frac{3}{2}yz,$$
$$f_3 = \frac{3}{2}(2x^2 + z^2 - 1), \quad f_4 = 3xy, \quad f_5 = \frac{1}{2}(1 + 3z^2), \tag{54}$$

while the structure function (50) can be written as

$$d^2(x, y, z) = d^2[(1 + \lambda_2)^2 + (\lambda_1^2 - 4\lambda_2)x^2 - 2\lambda_1(1 + \lambda_2)xz + (\lambda_1^2 - \lambda_2^2 - 2\lambda_2 + 3)z^2] \tag{55}$$

with the normalization factor (43). The integrals with respect to the angles are calculated with the aid of the formula

$$\iint F(\theta, \varphi)\sin\theta d\theta d\varphi = 2\iiint F(x, y, z)\delta(1 - x^2 - y^2 - z^2)dxdydz. \tag{56}$$

As a result, we obtain

$$J_i = \iiint f_i(x, y, z)K(x, y, z) \times \delta(1 - x^2 - y^2 - z^2)\frac{dxdydz}{2\pi}. \tag{57}$$

In terms of these variables, the vanishing of $J_1(0, \lambda_2)$ follows from the fact that the integrand is odd because the function $f_1 = 3xz/2$ changes sign upon the substitution $x \longrightarrow -x$, while the structure function (55) at $\lambda_1 = 0$ and, hence, the function $K(x, y, z)$ do not change sign. We then have

$$J_1 \sim \iiint xzK(x, y, z) \times \delta(1 - x^2 - y^2 - z^2)dxdydz = 0. \tag{58}$$

Upon this digression, we now return to the remaining two equations (52). Upon eliminating the integral J_5 from these two equations, we find that λ_2 satisfies the equation

$$3\lambda_2 J_0(0, \lambda_2) + (\lambda_2^2 - 3)J_3(0, \lambda_2) = 0. \tag{59}$$

It has two solutions

$$|\lambda_2| = 3, \quad |\lambda_2| = 1, \tag{60}$$

which correspond to different energies.

In order to prove this, we check the vanishing of the left-hand side of Eq. (59) by successively substituting all numbers λ_2 from (60) into it. It can easily be verified that, at $\lambda_2 = 3$, the left-hand side of (59) takes the form

$$9J_0 + 6J_3 = 18\iiint(x^2 - z^2)K(x, y, z) \times \delta(1 - x^2 - y^2 - z^2)\frac{dxdydz}{2\pi}, \tag{61}$$

which involves the difference $(x^2 - z^2)$. Hence, its sign is reversed upon the interchange of x and z because, according to (55), the structure function for this phase,

$$d^2(x, y, z; \lambda_1 = 0, \lambda_2 = 3) = \frac{1}{2}(4 - 3(x^2 + z^2)) = \frac{1}{2}(1 + 3y^2), \tag{62}$$

and the function $K(x, y, z)$, together with it, do not change sign upon the above interchange. As a result, the integral in (59) vanishes because the integrand is odd under the interchange of x and z.

The situation is similar for the solution $\lambda_2 = -1$: the structure function

$$d^2(x, y, z; \lambda_1 = 0, \lambda_2 = -1) = \frac{3}{2}(x^2 + z^2) = \frac{3}{2}(1 - y^2) \tag{63}$$

and the function K, together with it, depend only on y and remain invariant under the interchange of x and z, while the left-hand side of Eq. (59),

$$-(3J_0 + 2J_3) = 6\iiint(z^2 - x^2)K(y)\delta(1 - x^2 - y^2 - z^2)\frac{dxdydz}{2\pi},$$

changes sign again. Therefore, the integral with respect to the angles in (59)—it is identical to the above integral—vanishes again.

As to the remaining two solutions—$\lambda_2 = 1$ and $\lambda_2 = -3$—the integrand in (59) is proportional to $3f_0 - 2f_3 = -6(2z^2 + x^2 - 1)$ in either case, while the structure function depends only on x. We also have

$$d^2(x, y, z;\ \lambda_1 = 0, \lambda_2 = 1) = \frac{3}{2}(1 - x^2), \qquad (64)$$

$$d^2(x, y, z;\ \lambda_1 = 0, \lambda_2 = -3) = \frac{1}{2}(1 + 3x^2). \qquad (65)$$

Since the structure function and the function K, together with it, actually depend only on x in either case, we can perform integration in (59) with respect to z and y and obtain the required zero result,

$$\iiint K(x)(2z^2 + x^2 - 1)\delta(1 - x^2 - y^2 - z^2)dxdydz = \int_{-1}^{1} K(x)dx \int_{-\sqrt{1-x^2}}^{\sqrt{1-x^2}} \frac{2z^2 + x^2 - 1}{\sqrt{1 - x^2 - z^2}}dz = 0, \qquad (66)$$

since

$$\int_{-\sqrt{1-x^2}}^{\sqrt{1-x^2}} \frac{2z^2 + x^2 - 1}{\sqrt{1 - x^2 - z^2}}dz = 0.$$

Finally, we must substitute each of the numbers in (60) into the last equation in (52) and find the corresponding expressions for Δ_F. As can easily be seen, the gap Δ_F and the pairing energy, together with it, are independent of the sign of λ_2. Postponing the analysis of the energy spectrum to a special section, we will now summarize some of the above results. We have found two two-component solutions to the ${}^3P_2$-pairing problem at $\delta_1 = 0$ (and not one as in [24]). Their order parameters are different: the order parameter for the $\lambda_2 = \pm 3$ phases is positive everywhere, while the order parameter for the $\lambda_2 = \pm 1$ phases vanishes on the equator.

We now proceed to consider the main version, where λ_1 and λ_2 are both nonzero. Let us multiply the last equation in (52) by λ_2 and subtract the result from the first equation. We further multiply the last equation in (52) by λ_1 and subtract the result from the second equation. In this way, we recast the first two equation in (52) into the form

$$\begin{aligned} 3\lambda_2 J_0 + \lambda_1(\lambda_2 - 3)J_1 + (\lambda_2^2 - 3)J_3 &= 0, \\ 3\lambda_1 J_0 + 4(\lambda_1^2 - 3\lambda_2 - 3)J_1 + 2\lambda_1(2\lambda_2 + 3)J_3 &= 0. \end{aligned} \qquad (67)$$

It can easily be verified that, if we set here $\lambda_2 = -1$, the left-hand sides of Eqs. (67) will coincide. This is because the integral J_1 then vanishes, which follows from the invariance of the structure function (55),

$$d^2(x, y, z;\ \lambda_1, \lambda_2 = -1) = \frac{3}{2}(x^2 + z^2), \qquad (68)$$

and, hence, of the function K under the interchange of x and z. Therefore, the integrand in the integral in (58), which determines J_1, is antisymmetric; therefore, we have $J_1(\lambda_1, \lambda_2 = -1) = 0$ at any value of λ_1. As a result, the two equations in (67) appear to be identical:

$$3J_0(\lambda_1, \lambda_2 = -1) + 2J_3(\lambda_1, \lambda_2 = -1) = 0.$$

From (61), it follows that the last equality is valid irrespective of λ_1 values. Thus, we have found yet another solution to the ${}^3P_2$-pairing problem:

$$\lambda_2 = -1. \qquad (69)$$

On the (λ_1, λ_2) plane, this is a straight line parallel to the abscissa. Thus, we have obtained a line instead of the expected point—the solution proved to be degenerate. We will now see that the result in (69) is not the only degenerate solution to the problem under consideration.

Let us now assume that $\lambda_2 \neq -1$. By successively eliminating first J_3 and then J_0 from the two equations in (67), we rewrite them in the more compact equivalent form

$$\begin{aligned} 3\lambda_1(\lambda_2 + 1)J_0 - 2(\lambda_1^2 - 2\lambda_2^2 + 6)J_1 &= 0, \\ (\lambda_1^2 - 4\lambda_2)J_1 + \lambda_1(\lambda_2 + 1)J_3 &= 0. \end{aligned} \qquad (70)$$

Further, we rotate the axes of the coordinate frame (x, z) through some angle β, which will be specified below. We then have

$$z = t\cos\beta + u\sin\beta, \quad x = -t\sin\beta + u\cos\beta. \qquad (71)$$

In terms of the new variables, the structure function (55) takes the form

$$\begin{aligned} d^2(t, u) = d^2((1 + \lambda_2)^2 + [(\lambda_1^2 - \lambda_2^2 - 2\lambda_2 + 3)\cos^2\beta \\ + (\lambda_1^2 - 4\lambda_2)\sin^2\beta + 2\lambda_1(1 + \lambda_2)\sin\beta\cos\beta]t^2 \\ + [(\lambda_1^2 - \lambda_2^2 - 2\lambda_2 + 3)\sin^2\beta + (\lambda_1^2 - 4\lambda_2)\cos^2\beta \\ - 2\lambda_1(1 + \lambda_2)\sin\beta\cos\beta]u^2 \\ - 2(\lambda_2 + 1)[\lambda_1(\cos^2\beta - \sin^2\beta) + (\lambda_2 - 3)\sin\beta\cos\beta]tu). \end{aligned} \qquad (72)$$

We choose the angle β in such a way as to annihilate the coefficient of the term involving the product tu, whereby the expression for $d^2(t, u)$ is reduced to the form

$$\begin{aligned} d^2(t, u) = d^2((1 + \lambda_2)^2 + [(\lambda_1^2 - \lambda_2^2 - 2\lambda_2 + 3)\cos^2\beta \\ + (\lambda_1^2 - 4\lambda_2)\sin^2\beta + 2\lambda_1(1 + \lambda_2)\sin\beta\cos\beta]t^2 \\ + [(\lambda_1^2 - \lambda_2^2 - 2\lambda_2 + 3)\sin^2\beta + (\lambda_1^2 - 4\lambda_2)\cos^2\beta \\ - 2\lambda_1(1 + \lambda_2)\sin\beta\cos\beta]u^2). \end{aligned} \qquad (73)$$

We then arrive at the condition

$$\zeta^2 - \frac{\lambda_2 - 3}{\lambda_1}\zeta - 1 = 0, \tag{74}$$

where $\zeta = \tan\beta$. This equation has two solutions

$$\zeta_{1,2}(\lambda_1, \lambda_2) = \frac{\lambda_2 - 3}{2\lambda_1} \pm \sqrt{\frac{(3-\lambda_2)^2}{4\lambda_1^2} + 1}. \tag{75}$$

They exist at all values of the parameters λ_1 and λ_2, their product being –1. Thus, the angles β_1 and β_2 corresponding to these solutions are related by the simple equation $\beta_1 = \pi/2 + \beta_2$.

Let us now find out how the integrals J_i change upon this rotation. We begin by considering the relevant integrands:

$$f_0 = 1 - 3z^2 \longrightarrow (1 - 3t^2)\left(\cos^2\beta - \frac{1}{2}\sin^2\beta\right)$$
$$-\frac{3}{2}(2u^2 + t^2 - 1)\sin^2\beta,$$
$$f_3 = \frac{3}{2}(2x^2 + z^2 - 1) \longrightarrow -\frac{3}{4}(1 - 3u^2)\sin^2\beta \tag{76}$$
$$+\frac{3}{4}(2\cos^2\beta + \sin^2\beta)(2t^2 + u^2 - 1),$$
$$f_1 = \frac{3}{2}xz \longrightarrow \left[\frac{3}{4}(2u^2 + t^2 - 1) + \frac{3}{4}(1 - 3t^2)\right]\sin\beta\cos\beta.$$

On the right-hand sides, we have already discarded here the terms involving *tu*, which are insignificant for the ensuing analysis because, in calculating the integrals J_i, they drop out of the final results for the same symmetry reasons as above—that part of the integrand which involves *tu* changes sign upon the substitution $t \longrightarrow -t$ (or $u \longrightarrow -u$). As a result, we obtain

$$J_0 \longrightarrow \left(\cos^2\beta - \frac{1}{2}\sin^2\beta\right)J_0 - \sin^2\beta J_3,$$
$$J_3 \longrightarrow -\frac{3}{4}\sin^2\beta J_0 + \frac{1}{2}(2\cos^2\beta + \sin^2\beta)J_3, \tag{77}$$
$$J_1 \longrightarrow \left[\frac{3}{4}J_0 + \frac{1}{2}J_3\right]\sin\beta\cos\beta.$$

By substituting these expressions into (70), we arrive at two equations involving only the integrals J_0 and J_3; these equations have the form of a linear set of equations for the unknown J_0 and J_3:

$$A_{11}J_0 + A_{12}J_3 = 0,$$
$$A_{21}J_0 + A_{22}J_3 = 0. \tag{78}$$

Simple calculations based on relations (77) lead to the following formulas for the coefficients:

$$A_{11}(\lambda_1, \lambda_2) = \frac{3}{2}\lambda_1(1 + \lambda_2)(2 - \zeta^2(\lambda_1, \lambda_2))$$
$$-\frac{3}{2}(\lambda_1^2 - 2\lambda_2^2 + 6)\zeta(\lambda_1, \lambda_2),$$
$$A_{12}(\lambda_1, \lambda_2) = -3\lambda_1(1 + \lambda_2)\zeta^2(\lambda_1, \lambda_2)$$
$$-(\lambda_1^2 - 2\lambda_2^2 + 6)\zeta(\lambda_1, \lambda_2),$$
$$A_{21}(\lambda_1, \lambda_2) = -\frac{3}{4}\lambda_1(1 + \lambda_2)\zeta^2(\lambda_1, \lambda_2) \tag{79}$$
$$+\frac{3}{4}(\lambda_1^2 - 4\lambda_2)\zeta(\lambda_1, \lambda_2),$$
$$A_{22}(\lambda_1, \lambda_2) = \frac{1}{2}\lambda_1(1 + \lambda_2)(2 + \zeta^2(\lambda_1, \lambda_2))$$
$$+\frac{1}{2}(\lambda_1^2 - 4\lambda_2)\zeta(\lambda_1, \lambda_2).$$

A straightforward calculation of the determinant for this set of equations, $\mathcal{D} = A_{11}A_{22} - A_{12}A_{21}$, yields

$$\mathcal{D} = 3\lambda_1(\lambda_2 + 1)^2[-\lambda_1\zeta^4 - (\lambda_2 - 3)\zeta^3$$
$$-(\lambda_2 - 3)\zeta + \lambda_1] \tag{80}$$
$$\equiv -3(\lambda_2 + 1)^2(\zeta^2 + 1)[\lambda_1\zeta^2 - (\lambda_2 - 3)\zeta - \lambda_1].$$

Recalling condition (74), we conclude that

$$\mathcal{D} = 0 \tag{81}$$

at any values of λ_1 and λ_2. This is possible only if the coefficients in the first equation in (78) are in the same proportion as the coefficients in the second equation, so that the latter replicates the former, carrying no new information.

Thus, it only remains to solve the single equation

$$A_{21}(\lambda_1, \lambda_2)J_0(\lambda_1, \lambda_2)$$
$$+ A_{22}(\lambda_1, \lambda_2)J_3(\lambda_1, \lambda_2) = 0. \tag{82}$$

Its solution—some curve on the (λ_1, λ_2) plane—can also be found by analytic methods. In order to demonstrate how this is done, we return to the structure function (72). It can easily be seen that, for a specific relation between the sought parameters λ_2 and λ_1, we can find a rotation such that the structure function becomes a function of only one variable, say, *t*. From (73), it does indeed follows that this is so under the condition

$$(\lambda_1^2 - \lambda_2^2 - 2\lambda_2 + 3)\zeta^2$$
$$-2\lambda_1(1 + \lambda_2)\zeta + \lambda_1^2 - 4\lambda_2 = 0. \tag{83}$$

We then have

$$d^2(t) = d^2((1+\lambda_2)^2 + [(\lambda_1^2 - \lambda_2^2 - 2\lambda_2 + 3)\cos^2\beta + (\lambda_1^2 - 4\lambda_2)\sin^2\beta + 2\lambda_1(1+\lambda_2)\sin\beta\cos\beta]t^2). \quad (84)$$

The set of Eqs. (74) and (83) is solved analytically, its solution,

$$\zeta_0(\lambda_1, \lambda_2) = \frac{\lambda_1^2 - 4\lambda_2}{\lambda_1(1+\lambda_2)}, \quad (85)$$

being defined not on the entire (λ_1, λ_2) plane but on the curves representing solutions to the equation

$$\lambda_1^4 - 2\lambda_1^2\lambda_2^2 + 4\lambda_2^3 - 8\lambda_2\lambda_1^2 + 8\lambda_2^2 + 2\lambda_1^2 - 12\lambda_2 = 0,$$

which can be simplified to become

$$(\lambda_1^2 - 2\lambda_2 + 2)(\lambda_1^2 - 2\lambda_2^2 - 6\lambda_2) = 0. \quad (86)$$

That, under condition (86), expression (85) is a solution to the set of Eqs. (74) and (83) can be verified by a direct substitution.

Let us now show that, the constraint in (86), owing to which the structure function d^2 and the function K, together with it, become functions of the single variable t upon the rotation of the axes, makes it possible to satisfy Eq. (82). Indeed, the integral J_3 vanishes upon this rotation because the u dependence in the integrand is entirely concentrated in $f_3(u, t) = 3(2u^2 + t^2 - 1)/2$; in accordance with formula (57), integration with respect to u in J_3 can be performed irrespective of the form of the function $K(t)$, whereby we find, as before [see Eq. (66)], that $J_3 = 0$. Hence, it is sufficient to verify that the coefficient A_{21} vanishes if Eq. (85) holds—Eq. (82) is then satisfied automatically. The substitution of (85) into the expression for the coefficient A_{21} written in (79) immediately proves this.

Thus, we see that, if Eq. (85) holds, the rotation R specified by condition (74) makes it possible to achieve simultaneously two goals—the structure function becomes a function of one variable, and, additionally, the two equation in (78) are satisfied. As a result, we find the missing solutions to the $^3P_2$-pairing problem, and the spectrum of these solutions appears to be degenerate.

This proves that the iterative procedure for numerically solving the original set of equations is inadequate here since it is impossible, even with the aid of the most elaborate numerical methods, to find out whether we are dealing with states whose energies are close or with states that are strictly degenerate.

Relation (86) generates three branches $\lambda_2(\lambda_1)$ (see Fig. 1). One of these, the parabola $\lambda_2 = \lambda_1^2/2 + 1$ issues from the point $\lambda_2(0) = 1$. Its structure function is calculated by using Eq. (72) and by considering that the value of ζ_0 on the parabola is $-2/\lambda_1$. After some simple algebra, we obtain

$$d^2(t) = \frac{3}{2}(1 - t^2). \quad (87)$$

This result is analogous to those in Eqs. (63) and (64)—the structure function vanishes as before, but this time at $t = 1$.

On two other branches, where $\lambda_1^2 = 2\lambda_2^2 + 6\lambda_2$, we have $\zeta_0 = 2\lambda_2/\lambda_1$ and the structure function calculated with the aid of (72) has no zeros,

$$d^2(t) = \frac{1}{2}(1 + 3t^2), \quad (88)$$

in just the same way as the corresponding expressions in (62) and (65).

So far, our consideration has been performed under the assumption that $\delta_0 \neq 0$. In order to find out whether there exist two-component solutions for $\delta_0 = 0$, we must investigate the asymptotic behavior of solution (69) and of the relevant solution to Eq. (86). The first of these ($|\lambda_1| \longrightarrow \infty$) corresponds to the situation where $\delta_1 =$ const and $\delta_0, \delta_2 \longrightarrow 0$. In the limit, we arrive at the $|M| = 1$ one-component solution. The asymptotic behavior of the parabola $\lambda_2 = \lambda_1^2/2 + 1$ specifies the solution for $\delta_2 =$ const and $\delta_0, \delta_1 \longrightarrow 0$. This is the one-component $|M| = 2$ solution. For the remaining pair of curves that correspond to Eq. (86) and which are given by $\lambda_1^2 = 2\lambda_2^2 + 6\lambda_2$, we have $|\lambda_1|/|\lambda_2| \longrightarrow \sqrt{2}$ for $|\lambda_1| \longrightarrow \infty$. In this way, there arises the solution for $|\delta_1| = \sqrt{2}\,|\delta_2|$ and $\delta_0 = 0$. Thus, we have found the answer to the above question—in the problem of $^3P_2$ pairing, superfluid phases characterized by $\delta_0 = 0$ and $\delta_1, \delta_2 \neq 0$ do indeed exist.

An analysis of numerical calculations shows that, in the $^3P_2$-pairing problem, there are no degenerate real-valued solutions other than those described by Eqs. (69) and (86). Thus, the full spectrum of the real-valued solutions to this problem consists of (i) three one-component states characterized by the total-angular-momentum projections $|M| = 0, 1, 2$; (ii) the points whose coordinates are $(\lambda_1 = 0, |\lambda_2| = 3)$ and $(\lambda_1 = 0, |\lambda_2| = 1)$; (iii) the straight line $\lambda_2 = -1$; and (iv) three second-order curves specified by Eq. (86).

The structure of any of the above multicomponent solutions depends neither on density, nor on the temperature, nor on other input parameters. The entire set of structure functions for the phases found here can be partitioned into two groups—one including those that vanish at some point and the other comprising those that preserve sign. Upon a rotation of the coordinate axes that reduces the structure function to a function of one variable, we always obtain $d^2(t) = 3(1 - t^2)/2$ and $d^2(t) = (1 + 3t^2)/2$ in the first and in the second case, respectively.

As to the results of the numerical calculations from [18, 19, 24, 26], the number of the phases found there is much less than the number of the phases obtained analytically here, although all numerical solutions also form two groups according to energy. The distinctions

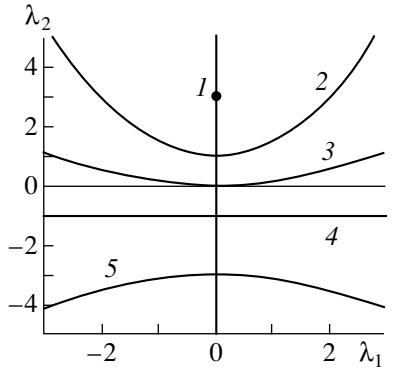

Fig. 1. Real-valued solutions to the $^3P_2$-pairing problem: (*1*) $\lambda_1 = 0, \lambda_2 = 3$ two-component state; (*2*) $\lambda_2 = \lambda_1^2/2 + 1$ state; (*3*) $\lambda_2 = (-3 + \sqrt{9 + 2\lambda_1^2})/2$ state; (*4*) $\lambda_2 = -1$ state; and (*5*) $\lambda_2 = (-3 - \sqrt{9 + 2\lambda_1^2})/2$ state.

between the predictions of the two approaches will be quantified in the following section.

4.3. Energy Spectrum of Real-Valued Solutions

Physical considerations and Eq. (35) indicate that the energies of the phases characterized by the same structure functions are degenerate and that the phases whose structure functions have no zeros lie lower on the energy scale than the phases whose structure functions have zeros. First, the difference F_S of the pairing contributions to the free energy F due to the difference of the phase structure functions will be related to the difference of the corresponding gaps Δ_F. To do this, use will be made of the method based on integration of the expectation value $\langle H_{int}\rangle$ with respect to the coupling constant g, since we can write [32]

$$\frac{\partial F}{\partial g} = \left\langle \frac{\partial H_{int}}{\partial g} \right\rangle. \tag{89}$$

Replacing, as usual, the partial derivative on the right-hand side of (89) by H_{int}/g and substituting, for the expectation value, the expression (see, for example, [24])

$$\langle H_{int}\rangle = -\frac{1}{2}\int D^2(\mathbf{p}) \frac{\tanh\frac{\sqrt{\xi^2(p) + D^2(\mathbf{p})}}{2T}}{\sqrt{\xi^2(p) + D^2(\mathbf{p})}} \frac{d^3p}{(2\pi)^3} V, \tag{90}$$

we arrive at

$$F_S = -\frac{1}{2}\int\int D^2(\mathbf{p}) \frac{\tanh\frac{\sqrt{\xi^2(p) + D^2(\mathbf{p})}}{2T}}{\sqrt{\xi^2(p) + D^2(\mathbf{p})}} \frac{d^3p}{(2\pi)^3}\frac{dg}{g} V, \tag{91}$$

where V is the volume of the system. Recalling that

$$D^2(\mathbf{p}) = \Delta_F^2 d^2(\mathbf{n})\chi^2(p) \equiv \Delta_F^2 d^2(\mathbf{n})\phi(p)\chi(p) + \Delta_F^2 d^2(\mathbf{n})(\chi(p) - \phi(p))\chi(p),$$

we substitute this sum into (91).

It should be noted that, in the expression

$$F_S^{(2)} = \frac{1}{2}\int\int \Delta_F^2(\mathscr{V}_F) d^2(\mathbf{n})(\chi(p) - \phi(p)) \times \chi(p) \frac{\tanh\frac{\sqrt{\xi^2(p) + D^2(\mathbf{p})}}{2T}}{\sqrt{\xi^2(p) + D^2(\mathbf{p})}} \frac{d^3p}{(2\pi)^3}\frac{dg}{g} V, \tag{92}$$

the integration domain adjacent to the Fermi surface does not make an appreciable contribution because the difference $[\chi(p) - \phi(p)]$ vanishes there. Furthermore, this difference vanishes for $g \longrightarrow 0$ as well. Consequently, the ratio of the second term in the expression for $D^2(\mathbf{p})$ to the first one appears to be proportional to the square of the dimensionless pairing constant $\mathscr{V}_F/\varepsilon_F^0$ and is therefore disregarded in the following.

With the aid of relation (32), the first term on the right-hand side of (92) can be recast into the form

$$F_S = \int \Delta_F^2(\mathscr{V}_F) \frac{d\mathscr{V}_F}{\mathscr{V}_F^2} V, \tag{93}$$

where we have used the equality $dg/g = d\mathscr{V}_F/\mathscr{V}_F$, since g differs from $\mathscr{V}_F$ insignificantly. It follows from formula (93) that the hierarchy of the pairing energies of the phases coincides with the hierarchy of the gaps Δ_F in the case of triplet pairing as well—the greater the gaps, the greater the corresponding pairing energies.

For the pairing energies, we can derive explicit formulas with the aid of (93), which are analogous to those in the case of S pairing. For this, we differentiate (32) with respect to $\mathscr{V}_F$. In calculating the resulting integral, it is convenient to go over to integration with respect to ξ. An overwhelming contribution to this integral comes from the domain $|\xi| \le \Delta_F$, where it is legitimate to make the substitutions $\phi, \chi \longrightarrow 1$ and $p^2dp/d\xi \longrightarrow p_F M^*$ (M^* is the effective mass). We then have

$$\frac{1}{\mathscr{V}_F^2} \simeq -2p_F M^* \Delta_F \frac{d\Delta_F}{d\mathscr{V}_F} \times \int\int (d^2(\mathbf{n}))^2 \left[\frac{\tanh\frac{(\xi^2 + \Delta_F^2 d^2(\mathbf{n}))^{1/2}}{2T}}{2(\xi^2 + \Delta_F^2 d^2(\mathbf{n}))^{3/2}} - \frac{\cosh^{-2}\frac{(\xi^2 + \Delta_F^2 d^2(\mathbf{n}))^{1/2}}{2T}}{2T(\xi^2 + \Delta_F^2 d^2(\mathbf{n}))^{1/2}} \right] \frac{d\xi d\mathbf{n}}{(2\pi)^3}. \tag{94}$$

By using relation (91), we can now calculate the energy splitting of the phases characterized by different structure functions. The subscripts 0 and 1 will label quantities corresponding to the phases associated with $d_0^2(t) = (1 + 3t^2)/2$ and $d_1^2(t) = 3(1 - t^2)/2$, respectively. At $T = 0$, we can easily find from (94) that

$$\frac{F_0 - F_1}{N} = -\frac{3(\Delta_0^2 - \Delta_1^2)}{8\varepsilon_F} \simeq \frac{F_0}{N}(1 - \eta^2), \qquad (95)$$

where N is the total number of particles in the system, $\varepsilon_F = p_F^2/2M^*$, and $\eta = \Delta_1/\Delta_0$. This result coincides with the analogous result obtained in [24] by a different method. The difference of the quantities Δ_i, which appears in Eq. (95), can be found with the aid of relation (35). The result has the form

$$\iint\left[\frac{1 + 3\cos^2\theta}{E_0(\xi, \theta)} - \frac{3\sin^2\theta}{E_1(\xi, \theta)}\right]d\xi \sin\theta d\theta = 0, \qquad (96)$$

where $E_0(\xi, \theta) = \sqrt{\xi^2 + \Delta_0^2 d_0^2(\theta)}$ and $E_1(\xi, \theta) = \sqrt{\xi^2 + \Delta_1^2 d_1^2(\theta)}$. Integration with respect to ξ is performed analytically, and expression (96) can be reduced to the form

$$\ln\eta^2(T = 0) = \int_0^1\left[\frac{1}{2}(1 + 3z^2)\ln\left(\frac{1}{2}(1 + 3z^2)\right) - \frac{3}{2}(1 - z^2)\ln\left(\frac{3}{2}(1 - z^2)\right)\right]dz. \qquad (97)$$

The integrals in (97) can be also calculated analytically. As a result, we obtain [28]

$$\ln\eta^2(T = 0) = \frac{2\pi}{9\sqrt{3}} + \frac{2}{3} - \ln 3 \simeq -0.028, \qquad (98)$$

which is in accord with the result of the numerical calculations from [24, 26].

Thus, we can see that, at $T = 0$, the phases where the gap in the spectrum of single-particle excitations has no zeros at the Fermi surface lie 3% lower on the energy scale than the phases whose gap in this spectrum has zeros. Mathematically, this can easily be understood by analyzing relation (96). Each of the integrals in (96), with the exception of the conventional logarithmic term $\ln(1/\Delta_F)$, involves an additional (positive!) term proportional to the logarithm of the structure function. The greater this contribution, the less the corresponding gap Δ_F—it would have been maximal had such a contribution been absent, as this occurs in the B phase in superfluid ^{3}He, where the total angular momentum of Cooper pairs is $J = 0$ and where the structure function is equal to unity.

Analytic calculations can be performed for $T \longrightarrow T_c$ as well. In this region, the ratio $\tanh x/x$ can be expanded in the series [32]

$$\frac{1}{2y}\tanh\frac{y}{2} = \sum_{-\infty}^{\infty}\frac{1}{(2s + 1)^2 + y^2}, \qquad (99)$$

and each term of this series is integrated with respect to ξ. Retaining, for $T \longrightarrow T_c$, only the leading terms proportional to Δ_F^2, we find from (35) that

$$\left(\frac{\Delta_i(T \longrightarrow T_c)}{T_c}\right)^2 = \frac{8\pi^2}{7\zeta(3)}\left(1 - \frac{T}{T_c}\right)\left[\int_0^1 (d_i^2(z))^2 dz\right]^{-1}. \qquad (100)$$

This formula differs from the corresponding standard BCS formula in the theory of S pairing by an additional factor that stems from the angular dependence of the gap due to the structure function $d^2(z)$.

Integration with respect to angles yields the same factor, irrespective of the phase being considered. As a result, we arrive at

$$\Delta_i^2(T \longrightarrow T_c) = \frac{5}{6}\Delta_{BCS}^2(T \longrightarrow T_c). \qquad (101)$$

A similar integral with respect to angles arises in the expression for the free energy in the limit $T \longrightarrow T_c$:

$$\frac{F_i}{N} = -\frac{21\zeta(3)}{64\pi^2 T_c^2 \varepsilon_F}\Delta_i^4\int_0^1 (d_i^2(z))^2 dz. \qquad (102)$$

Thus, we can see that, in the vicinity of T_c, the energies of all phases in the $^3P_2$-pairing problem prove to be identical and that the jump in the heat capacity $C = -T\frac{dS}{dT}$ for any phase at the critical point differs from the analogous jump in the S-pairing problem by the same factor of 5/6 as in the A phase of superfluid ^{3}He.

4.4. Complex-Valued Solutions

As was mentioned above, complex-valued solutions to the set of Eqs. (49) are characterized by a nonvanishing value of κ_2, whereby the second equation in this set is revived. In the S-pairing problem, these solutions arise upon the phase transformation $\Delta \longrightarrow \Delta e^{i\alpha}$ of the order parameter, the pairing energy remaining unchanged under this transformation. There are such solutions in the $^3P_2$-pairing problem as well. One of these can be obtained from the solution ($\lambda_1 = 0$, $\lambda_2 = 3$) by means of the substitution $\lambda_2 \longrightarrow (\lambda_2^2 + \kappa_2^2)^{1/2}$.

In seeking $\kappa_2 \neq 0$ solutions, we can again make use of the procedure relying on the diagonalization of the

structure function with the aid of rotations of the coordinate frame (x, y, z). We now have to deal with two rotation angles, so that the procedure becomes much more complicated. Its implementation initiated in [28] has yet to be completed. For this reason, we restrict ourselves here to the most general arguments that make it possible to determine the features of phases characterized by a complex-valued order parameter for $\kappa_2 \neq 0$. We return to the structure function (42), setting $\kappa_1 = 0$ in it, and rewrite its part that is odd under the substitution $\varphi \longrightarrow -\varphi$,

$$d^2_{\text{odd}}(\theta, \varphi) = -2\lambda_1[(1 + \lambda_2)\cos\varphi - \kappa_2\sin\varphi]\sin\theta\cos\theta,$$

in the form

$$d^2_{\text{odd}}(\theta, \varphi) = -2\lambda_1\sqrt{(1 + \lambda_2)^2 + \kappa_2^2}\cos(\varphi - \alpha_{\text{odd}})\sin\theta\cos\theta,$$

where $\tan\alpha_{\text{odd}} = -\kappa_2/(1 + \lambda_2)$.

In the structure function, we can similarly transform the part that is even under the substitution $\varphi \longrightarrow -\varphi$,

$$d^2_{\text{ev}}(\theta, \varphi) = \frac{\lambda_1^2 - 4\lambda_2}{2}\cos 2\varphi + 2\kappa_2\sin 2\varphi.$$

As a result, we arrive at

$$d^2_{\text{ev}}(\theta, \varphi) = \frac{1}{2}\sqrt{(\lambda_1^2 - 4\lambda_2)^2 + 16\kappa_2^2}\cos(2\varphi - \alpha_{\text{ev}})\sin^2\theta,$$

where $\tan\alpha_{\text{ev}} = 4\kappa_2/(\lambda_1^2 - 4\lambda_2)$.

In general, the angles α_{odd} and α_{ev} are independent. If, however, the relations between λ_1, λ_2, and κ_2 are such that

$$\alpha_{\text{ev}} = 2\alpha_{\text{odd}} + \pi, \tag{103}$$

the structure function $d^2(\mathbf{n})$ assumes the same form (50) as in the $\kappa_2 = 0$ case considered above. We can verify that, for condition (103) to be satisfied, the relation between the parameters κ_2, λ_1, and λ_2 must have the form

$$\kappa_2^2 = (1 + \lambda_2)(\lambda_1^2/2 - \lambda_2 + 1). \tag{104}$$

It can be shown that, if this condition holds, all the equations in (46) are satisfied automatically.

Relation (104) determines two branches of solutions $\kappa_2(\lambda_1, \lambda_2)$. On the plane $\kappa_2 = 0$, the first branch coincides with the straight line $\lambda_2 = -1$, while the second coincides with the parabola $\lambda_1^2/2 = \lambda_2 - 1$. Thus, all solutions (104), which are characterized by a complex-valued order parameter are degenerate. Their structure functions have zeros; therefore, their energies coincide, as can easily be verified, with the energy of the group of phases whose order parameter can vanish.

In summary, an analytic treatment of the model of pure $^3P_2$ pairing has revealed that, if the sought parameters of the problem satisfy relations (86), a rotation of the coordinate frame exists such that the structure function $d^2(\mathbf{n})$ reduces to a function of one variable t. In this case, all equations are satisfied, and the problem is thus completely solved along these lines. We have found that, irrespective of temperature, density, and any parameters characterizing nn interaction, the set of all phases can be partitioned into two groups containing phases whose structure functions reduce either to the form $d^2(t) = (1 + 3t^2)/2$ (first group) or to the form $d^2(t) = 3(1 - t^2)/2$ (second group). That the structure functions of the phases coincide entails the degeneracy of the energy spectrum of the problem, the energies of the phases belonging to the first group being lower than the energies of the phases belonging to the second group. Their relative splitting, which is a universal function of T/T_c, can be calculated in a closed form.

5. $^3P_2$–$^3F_2$ PAIRING

5.1. Removal of Degeneracy: Perturbation Theory

In this subsection, we analyze the effects of the mixing of the $L = 1$ and $L = 3$ channels that is due to tensor forces. The structure of tensor interaction undergoes no changes in a medium—in just the same way as in a vacuum, the amplitude of the tensor component of the irreducible block $\mathcal{V}(\mathbf{p}, \mathbf{p}_1)$ is proportional to the factor $(\boldsymbol{\sigma}_1(\mathbf{p} - \mathbf{p}_1))(\boldsymbol{\sigma}_2(\mathbf{p} - \mathbf{p}_1))$. In contrast to central forces, this interaction conserves only the total angular momentum $\mathbf{J} = \mathbf{L} + \mathbf{S}$ (it does not conserve the orbital angular momentum $\mathbf{L}$). Because of the mixing of channels characterized by different values of L, the resulting formulas will be much more complex than those obtained in the preceding sections. But what is more important is that this mixing removes degeneracy peculiar to the $^3P_2$-pairing problem. In this subsection, we therefore investigate in detail this aspect of the problem. We assume that the contribution of the tensor component, which is responsible for the mixing of the $^3P_2$ and $^3F_2$ channels, can be calculated within perturbation theory. There is every reason for this in a vacuum, but it is not obvious whether this assumption is adequate to what occurs in dense neutron matter. Its verification requires a dedicated analysis, which is beyond the scope of the present study.

Application of the formalism from [1] to systems featuring tensor forces, which mix the orbital angular momenta of Cooper pairs, does not present serious difficulties, apart from those of a purely technical character. Technical difficulties stem from the fact that we must also extract separable components in matrix elements of the block $\mathcal{V}$ that are off-diagonal in the orbital angular moment L. Because of this, our procedure becomes much more cumbersome. In describing it, we

will follow [33]. The generalization of formula (25) now takes the form

$$\mathcal{V}^J_{LL'}(p, p_1) = \mathcal{V}^J_{LL'}\phi^J_{LL'}(p)\phi^J_{LL'}(p_1) + W^J_{LL'}(p, p_1), \tag{105}$$

where $\phi^J_{LL'}(p) = \mathcal{V}^J_{LL'}(p, p_F)/\mathcal{V}^J_{LL'}$ and $\mathcal{V}^J_{LL'} = \mathcal{V}^J_{LL'}(p_F, p_F)$. The residual (second) term on the right-hand side of (105), $W^J_{LL'}(p, p_1)$, again vanishes identically when one of the arguments, p or p_1, occurs at the Fermi surface; therefore, the main contribution to the integrals involving the block $W^J_{LL'}$ comes from the domain that is sufficiently far off the Fermi surface, where we can make the substitutions $E \longrightarrow |\xi|$ and $\tanh(E/2T) \longrightarrow 1$. Inserting (105) into (16), we obtain

$$\Delta^{JM}_L(p) + \sum_{L'}(-1)^{(L-L')/2}\int\frac{W^J_{LL'}(p, p_1)}{2|\xi(p_1)|}\Delta^{JM}_{L'}(p_1)d\tau_1 = \sum_{L'}D^{JM}_{LL'}\phi^J_{LL'}(p), \tag{106}$$

where

$$D^{JM}_{LL'} = \mathcal{V}^J_{LL'}(-1)^{(L-L')/2+1} \times \sum_{L_1J_1M_1}\iint\phi^J_{LL'}(p)S^{JMJ_1M_1}_{L'L_1}(\mathbf{n})\frac{\tanh\dfrac{E(\mathbf{p})}{2T}}{2E(\mathbf{p})}\Delta^{J_1M_1}_{L_1}(p)d\tau d\mathbf{n}. \tag{107}$$

Here, we have used the notation $d\tau = p^2dp/2\pi^2$. In contrast to (26), the right-hand side of (106) is a superposition of a few independent terms. This significantly modifies the resulting formulas. In particular, relation (28) is replaced by

$$\Delta^{JM}_L(p) = \sum_{L_1L_2}D^{JM}_{L_1L_2}\chi^{L_1L_2}_{LJ}(p). \tag{108}$$

Substituting this equality into (106), we find that the components of the shape factor satisfy the set of integral equations

$$\chi^{L_1L_2}_{LJ}(p) + \sum_{L'}(-1)^{(L-L')/2} \times\int W^J_{LL'}(p, p_1)\frac{\chi^{L_1L_2}_{L'J}(p_1)}{2|\xi(p_1)|}d\tau_1 = \delta_{LL_1}\phi^J_{L_1L_2}(p). \tag{109}$$

Setting $p = p_F$ in (109), we find that

$$\chi^{L_1L_2}_{LJ}(p_F) = \delta_{LL_1} \tag{110}$$

for any L_2 since any block $W^J_{LL'}(p, p')$ vanishes at the Fermi surface, while $\phi^J_{L_1L_2}(p_F) = 1$ at any values of L_1 and L_2.

Equations for the coefficients $D^{JM}_{LL'}$ are derived by substituting (108) into the expression on the right-hand side of (107). This yields

$$D^{JM}_{LL'} = (-1)^{(L-L')/2+1}\mathcal{V}^J_{LL'}\sum_{L_1J_1M_1L_2L_3}D^{J_1M_1}_{L_2L_3} \times\iint\phi^J_{LL'}(p)S^{JMJ_1M_1}_{L'L_1}(\mathbf{n})\frac{\tanh\dfrac{E(\mathbf{p})}{2T}}{2E(\mathbf{p})}\chi^{L_2L_3}_{L_1J_1}(p)d\tau d\mathbf{n}. \tag{111}$$

As was mentioned above, all coefficients $D^{JM}_{LL'}$, with the exception of the leading set D^{2M}_1, will be calculated within perturbation theory. This makes it possible to replace $E(\mathbf{p})$ by $E_o(\mathbf{p}) = \sqrt{\xi^2(p) + D^2_o(\mathbf{p})}$; in addition, the coefficient $D^2_o(p_F, \mathbf{n}) \equiv \Delta^2_F d^2_o(\mathbf{n})$ is given by (37). From (111), we then obtain

$$\begin{aligned}
D^{J_1\neq 2, M_1}_{11} &= -\mathcal{V}^{J_1\neq 2}_{11}\sum_{M_2}D^{2M_2}_1 \times\iint\phi^{J_1}_{11}(p)\frac{\tanh\dfrac{E_o(\mathbf{p})}{2T}}{2E_o(\mathbf{p})}S^{J_1\neq 2, M_1 2M_2}_{11}(\mathbf{n})\chi(p)d\tau d\mathbf{n},\\
D^{J_1M_1}_{13} &= \mathcal{V}^J_{13}\sum_{M_2}D^{2M_2}_1 \times\iint\phi^{J_1}_{13}(p)\frac{\tanh\dfrac{E_o(\mathbf{p})}{2T}}{2E_o(\mathbf{p})}S^{J_1M_1 2M_2}_{31}(\mathbf{n})\chi(p)d\tau d\mathbf{n},\\
D^{J_1M_1}_{31} &= \mathcal{V}^J_{31}\sum_{M_2}D^{2M_2}_1 \times\iint\phi^{J_1}_{31}(p)\frac{\tanh\dfrac{E_o(\mathbf{p})}{2T}}{2E_o(\mathbf{p})}S^{J_1M_1 2M_2}_{11}(\mathbf{n})\chi(p)d\tau d\mathbf{n},\\
D^{JM_1}_{33} &= -\mathcal{V}^J_{33}\sum_{M_2}D^{2M_2}_1 \times\iint\phi^{J_1}_{33}(p)\frac{\tanh\dfrac{E_o(\mathbf{p})}{2T}}{2E_o(\mathbf{p})}S^{J_1M_1 2M_2}_{31}(\mathbf{n})\chi(p)d\tau d\mathbf{n}.
\end{aligned} \tag{112}$$

At the same time, the equations for the leading coefficients $D^{2M}_{11} \equiv D^{2M}_1$ now have the form

$$D^{2M}_1 + \mathcal{V}_F\sum_{M'}D^{2M'}_1\iint\phi(p)\frac{\tanh\dfrac{E(\mathbf{p})}{2T}}{2E(\mathbf{p})}S^{2M2M'}_{11}(\mathbf{n})\chi(p)d\tau d\mathbf{n}$$

$$= -\mathcal{V}_F \iint \phi(p) \frac{\tanh \frac{E_o(\mathbf{p})}{2T}}{2E^{(0)}(\mathbf{p})}$$

$$\times \sum_{J_1 M_1} [S_{11}^{2MJ_1 \neq 2M_1}(\mathbf{n}) \chi_{1J_1 \neq 2}^{11}(p) D_{11}^{J_1 \neq 2M_1}$$

$$+ S_{11}^{2MJ_1M_1}(\mathbf{n}) \chi_{1J_1}^{13}(p) D_{13}^{J_1M_1}$$

$$+ S_{11}^{2MJ_1M_1}(\mathbf{n}) D_{31}^{J_1M_1} \chi_{1J_1}^{31}(p) \quad (113)$$

$$+ S_{11}^{2MJ_1M_1}(\mathbf{n}) D_{33}^{J_1M_1} \chi_{1J_1}^{33}(p) + S_{13}^{2MJ_1M_1}(\mathbf{n}) D_{11}^{J_1M_1} \chi_{3J_1}^{11}(p)$$

$$+ S_{13}^{2MJ_1M_1}(\mathbf{n}) \chi_{3J_1}^{13}(p) D_{13}^{J_1M_1} + S_{13}^{2MJ_1M_1}(\mathbf{n}) \chi_{3J_1}^{31}(p) D_{31}^{J_1M_1}$$

$$+ S_{13}^{2MJ_1M_1}(\mathbf{n}) \chi_{3J_1}^{33}(p) D_{33}^{J_1M_1}] d\tau d\mathbf{n},$$

where we have used the notation $\phi = \phi_{11}^{J=2}$ and $\mathcal{V}_F = \mathcal{V}_{11}^{J=2}$, which was introduced in the preceding section for the quantities involved in the ${}^3P_2$-pairing problem. In order to simplify these formulas, we first expand the energy factor in spherical harmonics,

$$\frac{\tanh \frac{E_o(\mathbf{p})}{2T}}{2E_o(\mathbf{p})} = \sqrt{4\pi} \sum_{K\kappa} T_{K\kappa}(p) Y_{K\kappa}(\mathbf{n}). \quad (114)$$

Retaining only the first term in this expansion, as was proposed in [34], we obtain quite accurate results in calculating the gap $\Delta_F(T)$—approximately, it can be calculated on the basis of the equation

$$1 = -\mathcal{V}_F \int \phi(p) T_{00}(p) \chi(p) d\tau. \quad (115)$$

If we substitute the first term of the expansion in (114) into Eqs. (112), all coefficients $D_{LL'}^{2M}$ vanish, with the exception of the single one

$$D_{31}^{2M} = -\frac{\mathcal{V}_{13}^{J=2}}{\mathcal{V}_F} D_1^{2M} \equiv -\eta D_1^{2M}. \quad (116)$$

In deriving this relation, use has been made of Eq. (115). If we substitute the first term of the expansion in (114) into Eqs. (113), only one term survives in this case as well, that which is proportional to the coefficient D_{13}^{2M}. The contributions involving D_{13}^{2M} and D_{31}^{2M} remain dominant when we include the energy factor completely instead of retaining only its zero-order harmonic. Taking into account only these terms and making some simplifications, we arrive at the set of equations

$$D_1^{2M} + \mathcal{V}_F \sum_{M'} D_1^{2M'} \iint \phi(p) \frac{\tanh \frac{E(\mathbf{p})}{2T}}{2E(\mathbf{p})} S_{11}^{2M2M'}(\mathbf{n}) \chi(p) d\tau d\mathbf{n}$$

$$= \eta \mathcal{V}_F \sum_{M_1} D_1^{2M_1} \iint \frac{\tanh \frac{E_o(\mathbf{p})}{2T}}{2E_o(\mathbf{p})} [S_{31}^{2M2M_1}(\mathbf{n}) \quad (117)$$

$$+ S_{13}^{2M2M_1}(\mathbf{n})] d\tau d\mathbf{n},$$

$$M = 0, \pm 1, \pm 2,$$

where all quantities $\phi(p)$ and $\chi(p)$ have already been replaced by unity on the right-hand sides, because all integrals converge near the Fermi surface.

From this set of equations, we can derive a useful relation for Δ_F by multiplying each of these equations by $(D_1^{2M})^*$ and performing summation over M. Dividing the result by the sum $\sum_M |D_1^{JM}|^2 = 2\delta^2(3 + \lambda_1^2 + \lambda_2^2 + \kappa_1^2 + \kappa_2^2)$, we obtain

$$1 + \mathcal{V}_F \iint \phi(p) d_o^2(\mathbf{n}) \frac{\tanh \frac{E(\mathbf{p})}{2T}}{2E(\mathbf{p})} \chi^{-1}(p) d\tau \frac{d\mathbf{n}}{4\pi} \quad (118)$$

$$= \eta \mathcal{V}_F \iint K_{13}(\mathbf{n}) \frac{\tanh \frac{E_o(\mathbf{p})}{2T}}{2E_o(\mathbf{p})} d\tau d\mathbf{n},$$

where

$$K_{13}(\mathbf{n})$$

$$= \sum_{MM_1} \frac{(D_1^{2M})^* D_2^{2M_1}}{\sum_M |D_1^{2M}|^2} [S_{31}^{2M2M_1}(\mathbf{n}) + S_{13}^{2M2M_1}(\mathbf{n})]. \quad (119)$$

It should be noted that, for single-component phases, the structure function $d_o^2(\mathbf{n})$ is given by (13) and (14), while the function $K_{13}(\mathbf{n})$ has the form

$$K_{13}(\mathbf{n})$$

$$= \begin{cases} [S_{31}^{2020}(\mathbf{n}) + S_{13}^{2020}(\mathbf{n})] & \text{for } M = 0 \\ [S_{31}^{2121}(\mathbf{n}) + S_{13}^{2121}(\mathbf{n}) + S_{31}^{212,-1}(\mathbf{n}) + S_{13}^{212,-1}(\mathbf{n})] & \text{for } M = 1 \\ [S_{31}^{2222}(\mathbf{n}) + S_{13}^{2222}(\mathbf{n}) + S_{31}^{222,-2}(\mathbf{n}) + S_{13}^{222,-2}(\mathbf{n})] & \text{for } M = 2. \end{cases} \quad (120)$$

For multicomponent solutions, the function $d_o^2(\mathbf{n})$ can be calculated on the basis of (42). For the function

$K_{13}(\mathbf{n})$, similar calculations yield

$$K_{13}(\mathbf{n}) = 2d^2\Bigg[(S_{31}^{2020}(\mathbf{n}) + S_{13}^{2020}(\mathbf{n})) + \frac{1}{\sqrt{6}}\sum_{M_1\neq 0}\lambda_{M_1}(S_{31}^{2M_120}(\mathbf{n}) + S_{13}^{2M_120}(\mathbf{n})) + \frac{1}{3}\sum_{M_1>0,\,M_2\neq 0}\lambda_{M_1}\lambda_{M_2}(S_{31}^{2M_12M_2}(\mathbf{n}) + S_{13}^{2M_12M_2}(\mathbf{n}))\Bigg]. \quad (121)$$

In computing the normalization factor d^2 by formula (43), we can use the relations between the parameters λ_i and κ_i from the preceding section.

Let us now return to Eq. (118). In order to eliminate the functions ϕ and χ from it completely, we introduce the critical temperature T_c in (118) with the aid of formula (33). This enables us to replace $\chi(p)$ and $\phi(p)$ by unity because the resulting integral now converges near the Fermi surface:

$$\iint d_o^2(\mathbf{n})\left[\frac{\tanh\frac{E(\mathbf{p})}{2T}}{2E(\mathbf{p})} - \frac{\tanh\frac{\xi(p)}{2T}}{2\xi(p)}\right]d\tau\frac{d\mathbf{n}}{4\pi} = \eta\iint K_{13}(\mathbf{n})\frac{\tanh\frac{E_o(\mathbf{p})}{2T}}{2E_o(\mathbf{p})}d\tau d\mathbf{n}. \quad (122)$$

A further simplification of the calculations is achieved by simplifying the expression for the quasiparticle energy on the left-hand side of (122). First of all, we note that, owing to a fast convergence of this integral, we can use the approximate formula $E(\mathbf{p}) = \sqrt{\xi^2(p) + D^2(p_F, \mathbf{n})}$ in it. In formula (7), which determines the gap, we retain only the leading contributions of tensor forces. With the aid of (108), we then arrive at

$$\begin{aligned} D^2(p_F,\mathbf{n}) &\simeq \frac{1}{2}\sum_{M_1M_2}[(\Delta_1^{2M_1}(p_F))^*\Delta_1^{2M_2}(p_F)S_{11}^{2M_12M_2}(\mathbf{n}) \\ &+ (\Delta_1^{2M_1}(p_F))^*\Delta_3^{2M_2}(p_F)S_{13}^{2M_12M_2}(\mathbf{n}) \\ &+ (\Delta_3^{2M_1}(p_F))^*\Delta_1^{2M_2}(p_F)S_{31}^{2M_12M_2}(\mathbf{n}) \\ &+ (\Delta_3^{2M_1}(p_F))^*\Delta_3^{2M_2}(p_F)S_{33}^{2M_12M_2}(\mathbf{n})] \quad (123) \\ &= \Delta_F^2 d_o^2(\mathbf{n}) + \frac{1}{2}\sum_{M_1M_2}[(D_1^{2M_1})^*D_{31}^{2M_2}S_{13}^{2M_12M_2}(\mathbf{n}) \\ &+ (D_{31}^{2M_1})^*D_1^{2M_2}S_{31}^{2M_12M_2}(\mathbf{n}) \\ &+ (D_{31}^{2M_1})^*D_{31}^{2M_2}S_{33}^{2M_12M_2}(\mathbf{n})]. \end{aligned}$$

In this formula, the coefficient D_{31}^{2M} is calculated on the basis of (116). As a result, we obtain

$$D^2(p_F,\mathbf{n}) = \Delta_F^2[d_o^2(\mathbf{n}) - \eta K_{13}(\mathbf{n}) + \eta^2 K_{33}(\mathbf{n})], \quad (124)$$

where

$$K_{33}(\mathbf{n}) = \sum_{M_1M_2}\frac{(D_1^{2M_1})^*D_1^{2M_2}}{\sum_M\left|D_1^{2M}\right|^2}S_{33}^{2M_12M_2}(\mathbf{n}). \quad (125)$$

The substitution of the above results into (122) yields

$$\iint d_o^2(\mathbf{p})\left[\frac{\tanh\frac{E_o(\mathbf{p})}{2T}}{2E_o(\mathbf{p})} - \frac{\tanh\frac{\xi(p)}{2T_c}}{2\xi(p)}\right]d\tau\frac{d\mathbf{n}}{4\pi} \simeq \eta\iint\Bigg[K_{13}(\mathbf{n})\frac{\tanh\frac{E_o(\mathbf{p})}{2T}}{2E_o(\mathbf{p})} + \left(\frac{\tanh\frac{y}{2T}}{2y}\right)'\Bigg|_{y=E_o(\mathbf{p})} \times\frac{\Delta_F^2K_{13}(\mathbf{n})}{2E_o(\mathbf{p})}\Bigg]d\tau d\mathbf{n}, \quad (126)$$

where we discarded the second-order terms in η. For one-component states, the above equation is closed and can be directly used to calculate the variation in the quantity Δ_F in response to the inclusion of tensor forces. For multicomponent states, the situation is more complicated because we must also take into account the variations in the parameters λ_i and κ_i on the left-hand side of (126).

In order to determine these variations, we must perform similar transformations in the set of Eqs. (117). We then obtain five new equations for the same five numbers characterizing the order parameter in the $^3P_2$-pairing problem. The new set of equations,

$$\begin{aligned} &D_1^{2M} + \mathcal{V}_F\sum_{M'}D_1^{2M'}\iint\phi(p)\frac{\tanh\frac{E_o(\mathbf{p})}{2T}}{2E_o(\mathbf{p})}S_{11}^{2M2M'}(\mathbf{n})\chi(p)d\tau d\mathbf{n} \\ &= \eta\mathcal{V}_F\sum_{M_1}D_1^{2M_1}\iint\Bigg[\frac{\tanh\frac{E_o(\mathbf{p})}{2T}}{2E_o(\mathbf{p})}[S_{31}^{2M2M_1}(\mathbf{n}) + S_{13}^{2M2M_1}(\mathbf{n})] \\ &+ \left(\frac{\tanh\frac{y}{2T}}{2y}\right)'\Bigg|_{y=E_o(\mathbf{p})}S_{11}^{2M2M_1}(\mathbf{n}) \\ &\times\frac{\Delta_F^2K_{13}(\mathbf{n})}{2E_o(\mathbf{p})}\Bigg]d\tau d\mathbf{n}, \end{aligned} \quad (127)$$

differs from the old one by the presence of right-hand sides that are proportional to the coupling constant associated with tensor forces since, in deriving these equations, we have written them in such a way as to retain the original form of the left-hand sides. It should be emphasized that, on the right-hand sides of the set of

equations displayed immediately above, the parameters λ_i and κ_i can be taken to be equal to their values found in the problem of pure $^3P_2$ pairing.

In order to avoid encumbering the presentation, we restrict our analysis to real-valued solutions. For this, it is sufficient to investigate only a set of three equations that are similar to Eqs. (52). It is convenient preserve the original form of the left-hand side by including all corrections induced by tensor forces on the right-hand side. The set of Eqs. (52) then becomes

$$\begin{aligned}\lambda_2 + \nu_F[\lambda_2(J_0 + J_5) - \lambda_1 J_1 - J_3] &= \eta\mathcal{V}_F r_2,\\ \lambda_1 + \nu_F[-(\lambda_2 + 1)J_1 &\\ + \lambda_1(J_0 + 4J_5 + 2J_3)/4] &= \eta\mathcal{V}_F r_1,\\ 1 + \nu_F[-(\lambda_2 J_3 + \lambda_1 J_1)/3 + J_5] &= \eta\mathcal{V}_F r_0.\end{aligned} \tag{128}$$

The explicit expressions for the right-hand sides can be written on the basis of (127) and are given by

$$\begin{aligned}r_2 &= \lambda_2(s_{22} + q_{22}) + \lambda_1(s_{21} + q_{21}) + \lambda_0\sqrt{6}(s_{20} + q_{20}),\\ r_1 &= \lambda_2(s_{12} + q_{12}) + \lambda_1(s_{11} + q_{11}) + \lambda_0\sqrt{6}(s_{10} + q_{10}),\\ r_0 &= \lambda_2(s_{02} + q_{02}) + \lambda_1(s_{01} + q_{01}) + \lambda_0(s_{00} + q_{00}),\end{aligned} \tag{129}$$

where

$$s_{MM_1} = \iint \frac{\tanh\dfrac{E_o(\mathbf{p})}{2T}}{2E_o(\mathbf{p})}[S_{13}^{2M2M_1}(\mathbf{n}) + S_{31}^{2M2M_1}(\mathbf{n})]d\tau d\mathbf{n}, \tag{130}$$

$$q_{MM_1} = \iint K_{13}(\mathbf{n})S_{11}^{2M2M_1}(\mathbf{n})\left(\frac{\tanh\dfrac{y}{2T}}{2y}\right)'\Bigg|_{y = E_o(\mathbf{p})}\frac{1}{2E_o(\mathbf{p})}d\tau d\mathbf{n}. \tag{131}$$

In order to find a solution, we again multiply the first and the last equation in (128) by –3 and $3\lambda_2$, respectively, and sum the results. Further, we multiply the last and the second equation by $12\lambda_1$ and –12, respectively, and again sum the results. This yields

$$\begin{aligned}3\lambda_2 J_0 + \lambda_1(\lambda_2 - 3)J_1 + (\lambda_2^2 - 3)J_3 &= -3\eta(\lambda_2 r_0 - r_2),\\ 3\lambda_1 J_0 + 4(\lambda_1^2 - 3\lambda_2 - 3)J_1 + 2\lambda_1(2\lambda_2 + 3)J_3 &= -12\eta(\lambda_1 r_0 - r_1).\end{aligned} \tag{132}$$

We now begin by analyzing the specific solution $\lambda_2 = -1$, which existed in the absence of tensor forces. We set $\lambda_2 = -1 + l$. If the right-hand sides are small, l is also small. Dividing one equation of the set in (132) by the other, we find that the left-hand side of the resulting equality is close to –1 and that its right-hand side is some fraction. For this fraction to be –1 in the limit $\eta \longrightarrow 0$, the condition

$$\frac{4[\lambda_1 r_0(\lambda_1, \lambda_2 = -1) - r_1(\lambda_1, \lambda_2 = -1)]}{r_2(\lambda_1, \lambda_2 = -1) + r_0(\lambda_1, \lambda_2 = -1)} = 1 \tag{133}$$

must be satisfied. Numerical calculations show that this equation does not have nontrivial solutions. Taking this into account, we transform Eqs. (132) by successively eliminating J_3 and J_0. As a result, we arrive at

$$\begin{aligned}A_{11}J_0 + A_{12}J_3 &= \eta B_1,\\ A_{21}J_0 + A_{22}J_3 &= \eta B_2,\end{aligned} \tag{134}$$

where

$$\begin{aligned}B_1 &= 2\frac{\lambda_1(2\lambda_2 + 3)r_2 - 2(\lambda_2^2 - 3)r_1 - 3\lambda_1(\lambda_2 + 2)r_0}{(\lambda_2 + 1)},\\ B_2 &= -\frac{\lambda_1 r_2 - 4\lambda_2 r_1 + 3\lambda_1\lambda_2 r_0}{(\lambda_2 + 1)}.\end{aligned} \tag{135}$$

For the ensuing analysis, it is important that the integrals J_i have the same form as in the preceding section. If the unknown quantities J_0 and J_3 are calculated on the basis of Eqs. (134), the determinant $\mathcal{D}$ of the set of Eqs. (132) remains, in accordance with (80), equal to zero. In this case, the right-hand sides of (132) must obey specific relations; otherwise, the set of Eqs. (128) will not have solutions. We obtain

$$J_0 = \frac{\mathcal{D}_0}{\mathcal{D}}, \quad J_3 = \frac{\mathcal{D}_3}{\mathcal{D}}, \tag{136}$$

where $\mathcal{D}_0 = B_1A_{22} - B_2A_{12}$ and $\mathcal{D}_3 = -B_1A_{21} + A_{11}B_2$. Since $\mathcal{D} = 0$ at any values of λ_1 and λ_2, it is necessary that $\mathcal{D}_0 = \mathcal{D}_3 = 0$. From here, we find that the parameters λ_1 and λ_2 satisfy the equation

$$\frac{A_{22}(\lambda_1, \lambda_2)}{A_{12}(\lambda_1, \lambda_2)} = \frac{B_2(\lambda_1, \lambda_2)}{B_1(\lambda_1, \lambda_2)}. \tag{137}$$

If the strength of tensor forces is small (only this case is analyzed here), the right- and the left-hand side of Eq. (137) are computed for a specific branch of solutions to the $^3P_2$-pairing problem; hence, each of them actually depends only on λ_1. Upon the substitution of (86), we find that the final equation for obtaining solutions to the problem of $^3P_2$–$^3F_2$ pairing has the form

$$\begin{aligned}&-2\frac{\lambda_1(1 + \lambda_2)(2 + \zeta_0^2) + (\lambda_1^2 - 4\lambda_2)\zeta_0}{3\lambda_1(1 + \lambda_2)\zeta_0^2 + (\lambda_1^2 - 2\lambda_2^2 + 6)\zeta_0}\\ &= -\frac{\lambda_1 r_2 - 4\lambda_2 r_1 + 3\lambda_1\lambda_2 r_0}{2[\lambda_1(2\lambda_2 + 3)r_2 - 2(\lambda_2^2 - 3)r_1 - 3\lambda_1(\lambda_2 + 2)r_0]},\end{aligned} \tag{138}$$

where ζ_0 is calculated with the aid of (85).

The situation is further simplified owing to the fact that, on all branches of (86), the left-hand side of Eq. (138) takes the single value of –1/2, as can easily be

verified. Thus, the final equation for determining λ_1 takes the form

$$\mathcal{L} = \frac{-\lambda_1 r_2 + 4\lambda_2 r_1 - 3\lambda_1\lambda_2 r_0}{[\lambda_1(2\lambda_2+3)r_2 - 2(\lambda_2^2-3)r_1 - 3\lambda_1(\lambda_2+2)r_0]} = -1. \quad (139)$$

5.2. Basic Results

Equations (126) and (139) were solved numerically, and the results were presented in [35]. Let us briefly describe them in this subsection. First of all, we note that degeneracy peculiar to the $^3P_2$-pairing problem is entirely removed—the number of different superfluid phases and all structure coefficients characterizing these phases are fixed, while the energies of the various phases no longer coincide.

At low temperatures, the phase diagram of superfluid neutron matter is determined by the competition between the energies of the phases whose structure functions are nodeless, since formidable renormalizations of the parameters of *nn* interaction are required for overcoming a 3% barrier [see Eq. (98)] separating the energies of the phases characterized by the structure functions with and without zeros. Moreover, tensor forces have the coupling constant whose sign is such that this barrier only grows when we take them into account [24]. Calculations show [35] that, at low temperatures, only five phases can survive as candidates for forming the phase diagram. These are the $M = 0$ one-component solution, the $|\lambda_2| \simeq 3$ two-component solution, and three three-component solutions. One of the competitors is represented by the quasiparabola that is given by Eq. (86) and which has the vertex at the point $\lambda_2 = -3$, while the remaining pair is associated with the quasiparabola having the vertex at the origin of coordinates.

It turns out that, irrespective of T, the set of the solutions found here is broken down into a few groups degenerate in energy. For $T \longrightarrow 0$, the lowest group is formed by $\lambda_1 = 3\sqrt{2(17 \pm 3\sqrt{21})}/5$ nodeless states (see Fig. 2). The next group in the order of increase in energy consists of the $M = 0$ one-component state and the $|\lambda_2| = 3$ two-component state, which are also nodeless. The most important conclusion that follows from the calculations presented in [35] is that, in the region of T around $0.7T_c$, the situation is inverted—the second group proves to be lower than the first one on the energy scale. The last nodeless solution, that for which $\lambda_1 = 6$, comes into play, as all solutions characterized by structure functions having zeros do (see Fig. 3), in the temperature region $T \sim 0.8$–$0.9T_c$, where the phase diagram can undergo drastic changes since the energy barrier separating the two groups of phases in the problem of pure $^3P_2$ pairing decreases very fast with increasing temperature.

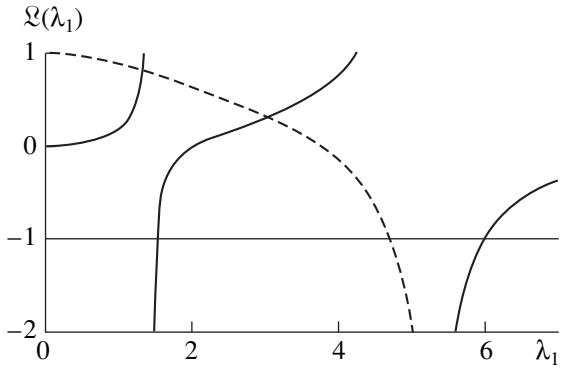

Fig. 2. Left-hand side $\mathcal{L}(\lambda_1)$ of the dispersion Eq. (139) as calculated for the branches (solid line) $\lambda_2 = (-3 + \sqrt{9 + 2\lambda_1^2})/2$ and (dashed line) $\lambda_2 = (-3 - \sqrt{9 + 2\lambda_1^2})/2$.

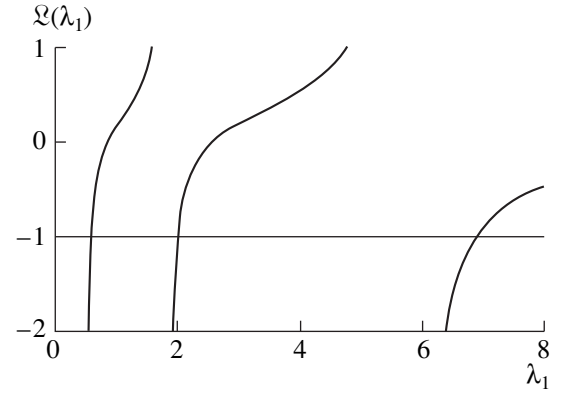

Fig. 3. As in Fig. 2, but for (solid line) the parabola $\lambda_2 = \lambda_1^2/2 + 1$ and the straight line $\lambda_2 = -1$ [in this case, $\mathcal{L}(\lambda_1) \equiv -1$].

6. CONCLUSION

In 1959, A.B. Migdal put forth the idea of superfluidity in neutron stars [8]. This idea was explained in only a few lines of his article, but it proved to be so fruitful that an enormous number of articles and a few tens of books have been written on the subject over the past 40 years and that, even now, the present study has been devoted to discussing the phase diagram of superfluid neutron matter.

The phrase "the phase diagram of superfluid matter" has been repeated a few times throughout this review article. But in this connection, there is the question of whether it is worthwhile to investigate it when we know that the manifestations of neutron-star superfluidity are very scanty. A point in favor of such investigations is that the rearrangement of the neutron-matter state in a response to a superfluid transition is accompanied by phenomena that are observable in principle.

One of these phenomena is associated with the irregularities in the period of pulsar rotation, which are observed in many pulsars. Above T_c, a star rotates as a

rigid body. When some part of its volume goes over to a superfluid state upon the lowering of temperature, a fraction of the total angular momentum of the rotating star is transferred to vortices. In order to find out how this total angular momentum is distributed between the vortices and the core of the star, it is necessary to solve a complicated set of equations. Phase transitions lead to a change in the moment of inertia in the superfluid subsystem and, hence, in the moment of inertia of the whole star; as a result, the angular velocity Ω of the star changes abruptly. In this way, one could explain giant glitches whose amplitude exceeds conventional amplitudes by two orders of magnitude. They were discovered for many pulsars. That these variations of the angular velocity are peculiar precisely to a superfluid phase is confirmed by data on relaxation processes. Yet another argument in favor of the above explanation of giant glitches is that they disappear with the aging (cooling) of a star [16]. For some pulsars, however, the number of such abrupt changes in Ω is quite large, whence it follows that, if one wants to explain giant glitches in terms of the phase diagram of a superfluid neutron liquid, this phase diagram must be rather complicated. Of course, we have three different fluids at our disposal in a neutron star—a proton one and two neutron ones (an external neutron fluid, which has a density on the order of the equilibrium nuclear density and which undergoes S pairing, and an internal neutron fluid, which is characterized by P pairing in the superfluid phase). If, in addition, a dense neutron fluid can undergo phase transitions similar to the transition between the A and B phases in superfluid ^{3}He, the system of vortices must also rearrange in response to this change in the scenery; as a result, some part of the angular momentum can again be transferred to the core, with the result that the period of star rotation exhibits an irregularity. The number of the phase transitions is completely determined by the phase diagram.

We have studied in detail one scheme, which is characterized by neutron pairing in the channel where the total angular momentum is $J = 2$ (many researchers believe that this scheme is the most probable one). This version is favored by the fact that spin–orbit forces, which single it out, considerably exceed tensor forces in vacuum neutron–neutron interactions. For this reason, we have proceeded from pure $^3P_2$ pairing, in which case we have been able to calculate the structure of the superfluid phases and their spectra analytically. That pairing energies of the phases whose structure functions belong to the same type has proved to be degenerate is a feature peculiar to this problem. It is this fact that underlies speculations on the possibility of phase transitions within the superfluid phase of a neutron liquid owing to the removal of the strong degeneracy of the energies of different phases in the problem of pure $^3P_2$ pairing upon the inclusion of tensor forces.

We have considered the simplest possibility for the removal of the above degeneracy, restricting our analysis to perturbation theory in the strength of tensor forces. Strictly speaking, this assumption does not seem realistic: in his pioneering studies [36, 37], Migdal showed that one-pion exchange in nuclear matter is strongly enhanced with increasing density, so that one cannot rule out the possibility that, in the region preceding the emergence of a pion condensate, the amplitude of tensor forces becomes commensurate with the amplitude of spin–orbit forces. Not only does the enhancement of tensor interactions intensify the mixing of the channels characterized by the orbital angular momenta of $L = 1$ and $L = 3$ and lead to significant mixing between the channels where the total angular momenta are $J = 2$ and $J = 0$, 1, but it also can generate a significant dependence of the structure of the phase diagram of superfluid neutron matter on the strength of the tensor forces and, hence, on the density of neutron matter. If this is indeed the case, different neutron stars can have different phase diagrams and, hence, different numbers of giant glitches. Unfortunately, it is hardly possible at present to calculate reliably the phase diagram of superfluid neutron matter. A further investigation of this problem requires knowing all features of effective neutron–neutron interaction in greater detail; therefore, it can be performed only in the future.

ACKNOWLEDGMENTS

I am grateful to G.E. Volovik, D.N. Voskresensky, M.V. Zverev, J.W. Clark, and E.E. Saperstein for stimulating discussions on the problems considered here. I am indebted to Washington University (St. Louis) and to J.W. Clark for warm hospitality.

This work was supported in part by NSF (grant no. 9900713) and by the McDonnel Center for the Space Sciences.

REFERENCES

1. V. A. Khodel, V. V. Khodel, and J. W. Clark, Nucl. Phys. A **598**, 390 (1996).
2. V. A. Khodel, Yad. Fiz. **60**, 1157 (1997) [Phys. At. Nucl. **60**, 1033 (1997)].
3. D. D. Osheroff, R. C. Richardson, and D. M. Lee, Phys. Rev. Lett. **28**, 885 (1972).
4. J. C. Wheatley, Rev. Mod. Phys. **47**, 415 (1975).
5. P. W. Anderson and P. Morel, Phys. Rev. **123**, 1911 (1961).
6. A. J. Leggett, Rev. Mod. Phys. **47**, 331 (1975).
7. Z.-X. Shen and D. Dessau, Phys. Rep. **253**, 1 (1995).
8. A. B. Migdal, Zh. Éksp. Teor. Fiz. **37**, 249 (1959) [Sov. Phys. JETP **10**, 176 (1960)].
9. P. E. Boynton *et al.*, Astrophys. J. **175**, 217 (1972).
10. E. Lohsen, Astron. Astrophys., Suppl. Ser. **44**, 1 (1981).
11. G. S. Downs, Astrophys. J. **249**, 687 (1981).
12. P. M. McCulloch, P. A. Hamilton, G. W. R. Royle, and R. N. Manchester, Nature **302**, 319 (1983).
13. P. R. Backus, J. H. Taylor, and M. Damashek, Astrophys. J. Lett. **255**, L63 (1982).

14. D. Pines and J. Shaham, Nature (London), Phys. Sci. **55**, 42 (1972).
15. P. W. Anderson and M. Itoh, Nature **256**, 25 (1975).
16. D. Pines and M. A. Alpar, Nature **316**, 27 (1985).
17. M. Hoffberg, A. E. Glassgold, R. W. Richardson, and M. Ruderman, Phys. Rev. Lett. **24**, 775 (1970).
18. T. Takatsuka and R. Tamagaki, Prog. Theor. Phys. **46**, 114 (1971).
19. T. Takatsuka, Prog. Theor. Phys. **48**, 1517 (1972).
20. D. Page and J. H. Applegate, Astrophys. J. Lett. **394**, L17 (1992).
21. J. A. Sauls, D. L. Stein, and J. W. Serene, Phys. Rev. D **25**, 967 (1982).
22. D. Vollhardt and P. Wölfle, *The Superfluid Phases of Helium 3* (Taylor & Francis, London, 1990).
23. G. E. Volovik, in *Helium Three*, Ed. by W. P. Halperin and L. P. Pitaevskii (North-Holland, Amsterdam, 1990).
24. L. Amundsen and E. Østgaard, Nucl. Phys. A **442**, 163 (1985).
25. M. Baldo, J. Gugnon, A. Lejeune, and U. Lombardo, Nucl. Phys. A **515**, 409 (1990).
26. T. Takatsuka and R. Tamagaki, Prog. Theor. Phys. Suppl. **112**, 27 (1993).
27. Ø. Elgarøy, L. Engvik, M. Hjorth-Jensen, and E. Osnes, Nucl. Phys. A **607**, 425 (1996).
28. V. A. Khodel, V. V. Khodel, and J. W. Clark, Phys. Rev. Lett. **81**, 3828 (1998).
29. A. A. Abrikosov, L. P. Gor'kov, and I. E. Dzyaloshinskiĭ, *Methods of Quantum Field Theory in Statistical Physics* (Fizmatgiz, Moscow, 1962; Prentice-Hall, Englewood Cliffs, 1963).
30. L. D. Landau and E. M. Lifshitz, *Quantum Mechanics: Non-Relativistic Theory* (Nauka, Moscow, 1974; Pergamon, New York, 1977).
31. A. Bohr and B. M. Mottelson, *Nuclear Structure* (Benjamin, New York, 1969, 1974; Mir, Moscow, 1981), Vols. 1, 2.
32. E. M. Lifshitz and L. P. Pitaevskiĭ, *Statistical Physics* (Nauka, Moscow, 1978; Pergamon, New York, 1980).
33. V. V. Khodel, V. A. Khodel, and J. W. Clark, Nucl. Phys. (in press).
34. M. Baldo, J. Cugnon, A. Lejeune, and U. Lombardo, Nucl. Phys. A **536**, 349 (1992).
35. V. A. Khodel, M. V. Zverev, and J. W. Clark, Nucl. Phys. (in press).
36. A. B. Migdal, Rev. Mod. Phys. **50**, 107 (1978).
37. A. B. Migdal, E. E. Saperstein, M. A. Troitsky, and D. N. Voskresensky, Phys. Rep. **192**, 179 (1990).

Translated by A. Isaakyan

Physics of Atomic Nuclei, Vol. 64, No. 3, 2001, pp. 416–422. From Yadernaya Fizika, Vol. 64, No. 3, 2001, pp. 471–477.

90th ANNIVERSARY OF A.B. MIGDAL'S BIRTHDAY
NUCLEI

Theory of Doorway States for One-Nucleon Transfer Reactions: Model-Independent Study of Nuclear Correlation Effects*

B. L. Birbrair and V. I. Ryazanov**

Petersburg Nuclear Physics Institute, Russian Academy of Sciences, Gatchina, 188350 Russia

Received March 29, 2000; in final form, July 27, 2000

Abstract—Nuclear correlation effects owing to which nuclear wave functions are different from Slater determinants are studied within the theory developed in our previous study. The calculated numbers of nucleons off the nuclear Fermi surface are in reasonable agreement with the finding from the high-momentum components of the momentum distributions of nucleons in nuclei. Problems concerning the nuclear binding energy are also discussed. © *2001 MAIK "Nauka/Interperiodica".*

1. INTRODUCTION

Nucleon–nucleon interaction still remains one of the central problems in nuclear structure theory. It seems natural to use free-space forces, but the majority of nuclear-structure theorists prefer effective ones instead. The basic motivations are as follows:

(a) Historically, the first one arose from the widespread belief in the 1960s that the free-space *NN* potential has a hard repulsive core. Clearly, such an interaction does not apply directly because of the divergence of finite-order Feynman diagrams. The most popular way to overcome this difficulty is to calculate the Brueckner *G* matrix and to use it as an effective interaction in the Hartree–Fock problem. This is the Hartree–Fock–Brueckner approximation (for details, see [1] and references therein). But soon, it became clear that the description of the two-nucleon system—that is, the properties of the deuteron and phase shifts for elastic *NN* scattering below the pion-production threshold—does not require a hard repulsive core. As a result, all contemporary *NN* potentials are of soft-core character, so that the above difficulty is actually nonexistent. Under such conditions, the calculation of the Brueckner *G* matrix is not compulsory.

(b) The second factor is associated with the renormalization of the free-space interaction due to medium-polarization effects. Such effects are treated by conventional methods of quantum many-body theory; therefore, the above reason is not an argument in favor of effective forces.

(c) There is medium QCD renormalization due to the fact that the quark composition of the QCD vacuum changes in nuclear medium, thus leading to changes in both mesons and meson–nucleon vertices [2–5]. Such processes can hardly be described in all details since an exact theory has not yet been constructed for the nonperturbative region. Nevertheless, there is at least one exact statement. The QCD-renormalized interaction is a functional of the nuclear density, and this functional possesses the following obvious property: it reduces to the free-space one in the zero-density limit. For this reason, it can be represented as the functional expansion

$$f_{\text{QCD-}r}(\mathbf{r}_1, \mathbf{r}_2; \{\rho\}) = f_2(|\mathbf{r}_1 - \mathbf{r}_2|) + \int f_3(|\mathbf{r}_1 - \mathbf{r}_2|, |\mathbf{r}_1 - \mathbf{r}'|)\rho(r')d\mathbf{r}' + \iint f_4(|\mathbf{r}_1 - \mathbf{r}_2|, |\mathbf{r}_1 - \mathbf{r}'|, |\mathbf{r}_1 - \mathbf{r}''|)\rho(r')\rho(r'')d\mathbf{r}'d\mathbf{r}'' + \ldots. \quad (1)$$

In this way, we conclude that the medium QCD renormalization is equivalent to the existence of many-particle *NN* forces in addition to the two-particle ones. This conclusion is confirmed by the fact that the physics of strong interaction is essentially nonlinear. But nonlinearity automatically leads to many-particle forces.

The above reasons are grounds for our starting point: both two-particle and many-particle *NN* forces must be taken into account for the treatment of nuclear structure.

Three-particle *NN* forces were indeed included in the calculations of few-nucleon systems [6]. But there arises the question of whether this is sufficient for complex nuclei. This point, as well as a number of those concerning the nuclear structure, can be clarified by studying model-independent nuclear objects obeying exactly solvable equations.

As was discussed in our previous study [7], such objects are exemplified by doorway states for one-nucleon-transfer reactions. As follows from the theorem of Baranger [8], such states are eigenstates of a nucleon in the static field of a nucleus. According to this theorem, the behavior of the single-particle propagator

$$S(x, x'; \tau) = -i\langle A_0|T\psi(x, \tau)\psi^+(x', 0)|A_0\rangle \quad (2)$$

* This article was submitted by the authors in English.

** e-mail: birbrair@thd.pnpi.spb.ru

1063-7788/01/6403-0416$21.00 © 2001 MAIK "Nauka/Interperiodica"

at the initial instant $t = 0$ is determined by the high-energy asymptotic behavior of the mass operator. Let us explain this. The quantity in (2) describes the evolution of the state that arises from one-nucleon transfer at the initial instant. Its Fourier transform

$$G(x, x'; \varepsilon) = \int_{-\infty}^{+\infty} S(x, x'; \tau) e^{i\varepsilon\tau} d\tau, \tag{3}$$

which is referred to as a single-particle Green's function, obeys the Dyson equation

$$\begin{aligned} \varepsilon G(x, x'; \varepsilon) &= \delta(x - x') + \hat{k}_x G(x, x'; \varepsilon) \\ &+ \int M(x, x_1; \varepsilon) G(x_1, x'; \varepsilon) dx_1, \end{aligned} \tag{4}$$

where the $\hat{k}_x$ is the kinetic energy and $M(x, x'; \varepsilon)$ is the mass operator.

The main content of the Baranger theorem is the identity

$$\begin{aligned} &-[\dot{S}(x, x'; +0) - \dot{S}(x, x'; -0)] \\ &= h_{\text{st}}(x, x') = \hat{k}_x \delta(x - x') + \lim_{\varepsilon \to \infty} M(x, x'; \varepsilon), \end{aligned} \tag{5}$$

where the above limit is just the static nuclear field and where $\dot{S} = \partial S / \partial \tau$. As can be seen from the left-hand side of (5), the Hamiltonian h_{st} describes the very beginning of the evolution under consideration. But it can be seen from the right-hand side that it describes the motion of a nucleon in the static nuclear field, the eigenstates of h_{st} thus being doorway states for one-nucleon-transfer processes. A detailed demonstration of the Baranger theorem is discussed in [7]. We showed the following:

(i) At least three-particle repulsion and four-particle attraction must be taken into account in addition to two-particle forces.

(ii) Nuclear relativity is an actually existing phenomenon rather than the hypothesis of Walecka [9].

(iii) A dominant contribution to the isovector nuclear potential comes from many-particle forces.

(iv) The observed spectra of doorway states can be used to specify the neutron-density distributions in nuclei; the densities specified in this way were indeed obtained for the closed-shell nuclei ^{40}Ca, ^{90}Zr, and ^{208}Pb.

In the present article, our approach is applied to "empirical" studies of nuclear correlation effects owing to which nuclear wave functions are different from Slater determinants. Such effects are treated by a variety of approximate methods since exact ones do not exist. For this reason, it is very important to obtain model-independent quantitative information about the above effects. The possibility provided by our approach is based on the fact that the wave functions of the above doorway states [7] describe the correlation-free single-particle states of nucleons rather than Landau–Migdal quasiparticles [10] (which include the correlations by definition) or single-particle states in nuclear Hartree–Fock calculations with effective forces (where the correlations are implicitly included in phenomenological effective force parameters). Calculating correlation-free quantities and comparing them with the observed ones, we therefore derive a quantitative measure of correlation effects. In Section 2, this procedure is applied to the nucleon density distributions. Problems concerning the nuclear binding energy are discussed in Section 3.

2. DENSITY DISTRIBUTIONS

The nucleon density distribution in the ground state of nucleus A is (see [7] for the notation)

$$\begin{aligned} \rho(r) &= \langle A_0 | \psi^+(x) \psi(x) | A_0 \rangle \\ &= \sum_j^{(A-1)} \langle A_0 | \psi^+(x) | (A-1)_j \rangle \langle (A-1)_j | \psi(x) | A_0 \rangle \\ &= \sum_j^{(A-1)} \Psi_j^+(x) \Psi_j(x) = \int_C \frac{d\varepsilon}{2\pi i} G(x, x; \varepsilon). \end{aligned} \tag{6}$$

The integration contour C includes the real axis and an infinite-radius semicircle in the upper half of the complex ε plane. As can be seen from (6), the density is expressed in terms of single-particle amplitudes of $(A-1)$ nuclear states. Expanding them in a complete set of doorway states,

$$\Psi_j(x) = \sum_\lambda C_j^{(\lambda)} \psi_\lambda(x), \tag{7}$$

and substituting (7) into (6), we obtain

$$\rho(r) = \sum_\lambda n_\lambda |\psi_\lambda(x)|^2 + 2 \sum_{\substack{\lambda\nu \\ \nu > \lambda}} \rho_{\lambda\nu} \psi_\lambda^+(x) \psi_\nu(x), \tag{8}$$

where

$$\begin{aligned} n_\lambda = \rho_{\lambda\lambda} &= \sum_j^{(A-1)} \left| C_j^{(\lambda)} \right|^2 = \sum_j^{(A-1)} s_j^{(\lambda)}, \\ \rho_{\lambda\nu} &= \sum_j^{(A-1)} C_j^{(\lambda)*} C_j^{(\nu)} \end{aligned} \tag{9}$$

(actually, the coefficients $C_j^{(\lambda)}$ are real-valued quantities if parity violation due to weak interaction is disregarded). The diagonal elements $\rho_{\lambda\lambda} = n_\lambda$ are the doorway-state occupation numbers. Indeed, the particle number is

$$N = \int \rho(r) d\mathbf{r} = \sum_\lambda n_\lambda, \tag{10}$$

since the off-diagonal elements do not contribute because of the orthogonality of ψ_λ and ψ_ν. The quantities n_λ and $\rho_{\lambda\nu}$ obey the constraints

$$0 < n_\lambda < 1, \quad |\rho_{\lambda\nu}| < \frac{1}{2}(n_\lambda + n_\nu). \tag{11}$$

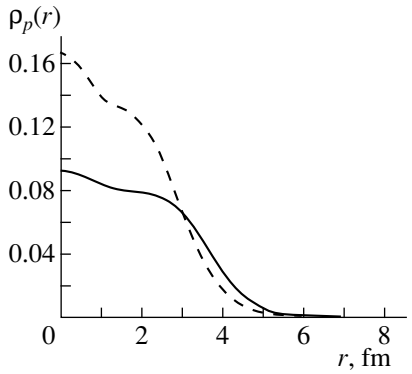

Observed (solid curve) and correlation-free (dashed curve) proton-density distributions in ^{40}Ca.

The first follows from the fact that doorway states are distributed over the actual states of both the $(A-1)$ and the $(A+1)$ nucleus {see (13c) in [7]}, whereas the second is a consequence of the Cauchy–Buniakowski inequality.

The relations $n_\lambda < 1$ and $\rho_{\lambda\nu} \neq 0$ reflect the Fermi surface smearing due to correlation effects. The quantities n_λ and $\rho_{\lambda\nu}$ carrying quantitative information about these effects can be found "empirically" by considering relation (8) together with constraints (11) as equations for n_λ and $\rho_{\lambda\nu}$. The results will be published elsewhere.

Owing to correlations, part of the nucleons are off the nuclear Fermi surface. The number N_{out} of such nucleons is calculated by comparing the observed density distribution with the correlation-free density distribution

$$\rho_{\text{cf}}(r) = \sum_\lambda \Theta(\varepsilon_{\text{F}} - \varepsilon_\lambda)|\psi_\lambda(x)|^2, \tag{12}$$

where ε_{F} is the Fermi level energy. This comparison is illustrated in the figure for the proton density distribution in ^{40}Ca. As can be seen from the figure, the correlation-free density contains more nucleons in the inner region $0 < r < r_i$ than the observed one; here, r_i is the intersection point at which $\rho_{\text{cf}}(r_i) = \rho(r_i)$. The situation in the outer region $r_i < r < \infty$ is clearly opposite since both densities correspond to the same number of nucleons. The number of redistributed nucleons is

$$\begin{aligned} N_{\text{out}} &= 4\pi\int_0^{r_i}[\rho_{\text{cf}}(r) - \rho(r)]r^2 dr \\ &= 4\pi\int_{r_i}^{\infty}[\rho(r) - \rho_{\text{cf}}(r)]r^2 dr. \end{aligned} \tag{13}$$

This is just N_{out} because the only reason for the redistribution is the Fermi surface smearing due to correlations.

The numbers N_{out} in doubly closed-shell nuclei are quoted in Table 1, which shows that these nucleons constitute an appreciable part of the total mass number. To the best of our knowledge, this fact was first mentioned by Frankfurt and Strikman [11] on the basis of the analysis of high-momentum components (i.e., those with $k > 300$ MeV/c) of the momentum distributions of nucleons in nuclei. According to their most recent results for these data [12], the ratio A_{out}/A is $(20 \pm 3)\%$ for heavy nuclei. This is in reasonable agreement with our results.

It is worth mentioning that our calculations furnish no information about the nature of the underlying correlations; at the same time, the high-momentum tails of the momentum distributions arise from the *NN* interactions at short distances [11, 12]. Therefore, the reasonable agreement between the two results gives rise to the conclusion that the main reason for the Fermi surface smearing in doubly closed-shell nuclei is due to short-range correlations.

3. BINDING ENERGY

We can also calculate that part of the nuclear binding energy which is caused by the motion of nucleons in the static nuclear field. This static energy partly includes correlation effects since it is expressed in terms the observed nucleon density distributions. A comparison of the observed binding energy $\mathscr{E}_b$ and the static binding energy $\mathscr{E}_{\text{st}}$ provides a measure of the proper correlation energy of the nucleus.

To clarify this point, we derive an exact expression for the binding energy. Following the procedure proposed in [10], we obtain

$$\begin{aligned} \mathscr{E}_b &= \int dx \int_C \frac{d\varepsilon}{2\pi i}\operatorname{tr}\hat{k}_x G(x, x; \varepsilon) + \frac{1}{2}\iint dx dx_1 \\ &\times \iint_C \frac{d\varepsilon d\varepsilon_1}{(2\pi i)^2} f_2(|\mathbf{r} - \mathbf{r}_1|; \omega) K_2(x, x_1; x, x_1; \varepsilon, \varepsilon_1) \\ &+ \frac{1}{3}\iiint dx dx_1 dx_2 \iiint_\chi \frac{d\varepsilon d\varepsilon_1 d\varepsilon_2}{(2\pi i)^3} \\ &\times f_3(|\mathbf{r} - \mathbf{r}_1|, |\mathbf{r} - \mathbf{r}_2|; \omega, \omega_1) \\ &\times K_3(x, x_1, x_2; x, x_1, x_2; \varepsilon, \varepsilon_1, \varepsilon_2) \\ &+ \frac{1}{4}\iiint dx dx_1 dx_2 dx_3 \iiint_C \frac{d\varepsilon d\varepsilon_1 d\varepsilon_2 d\varepsilon_3}{(2\pi i)^4} \\ &\times f_4(|\mathbf{r} - \mathbf{r}_1|, |\mathbf{r} - \mathbf{r}_2|, |\mathbf{r} - \mathbf{r}_3|; \omega, \omega_1, \omega_2) \\ &\times K_4(x, x_1, x_2, x_3; x, x_1, x_2, x_3; \varepsilon, \varepsilon_1, \varepsilon_2, \varepsilon_3), \end{aligned} \tag{14}$$

where $K(x_1, \ldots, x_n; x_1', \ldots, x_n'; \varepsilon_1, \ldots, \varepsilon_n)$ stands for the n-particle Green's functions. We take into account three- and four-particle forces in addition to two-particle ones, as well as the possible dependence of the interactions on the appropriate energy transfers ω_i. In these terms, the single-particle Green's function is

$$(\varepsilon - \hat{k}_x)G(x, x'; \varepsilon) = \delta(x - x')$$

$$+\int dx_1 \int_C \frac{d\varepsilon_1}{2\pi i} f_2(|\mathbf{r}-\mathbf{r}_1|;\,\omega) K_2(x, x_1;\, x', x_1;\, \varepsilon, \varepsilon_1)$$

$$+\iint dx_1 dx_2 \int_C\int \frac{d\varepsilon_1 d\varepsilon_2}{(2\pi i)^2} f_3(|\mathbf{r}-\mathbf{r}_1|, |\mathbf{r}-\mathbf{r}_2|;\, \omega, \omega_1)$$

$$\times K_3(x, x_1, x_2;\, x', x_1, x_2;\, \varepsilon, \varepsilon_1, \varepsilon_2) \qquad (15)$$

$$+\iiint dx_1 dx_2 dx_3 \int_C\int\int \frac{d\varepsilon_1 d\varepsilon_2 d\varepsilon_3}{(2\pi i)^3}$$

$$\times f_4(|\mathbf{r}-\mathbf{r}_1|, |\mathbf{r}-\mathbf{r}_2|, |\mathbf{r}-\mathbf{r}_3|;\, \omega, \omega_1, \omega_2)$$

$$\times K_4(x, x_1, x_2, x_3;\, x', x_1, x_2, x_3;\, \varepsilon, \varepsilon_1, \varepsilon_2, \varepsilon_3).$$

Comparing this with the Dyson equation (4), we see that

$$\int M(x, x_1;\, \varepsilon) G(x_1, x';\, \varepsilon) dx_1$$

$$= \int dx_1 \int_C \frac{d\varepsilon_1}{2\pi i} f_2(|\mathbf{r}-\mathbf{r}_1|;\, \omega) K_2(x, x_1;\, x', x_1;\, \varepsilon, \varepsilon_1)$$

$$+\iint dx_1 dx_2 \int_C\int \frac{d\varepsilon_1 d\varepsilon_2}{(2\pi i)^2} f_3(|\mathbf{r}-\mathbf{r}_1|, |\mathbf{r}-\mathbf{r}_2|;\, \omega, \omega_1)$$

$$\times K_3(x, x_1, x_2;\, x', x_1, x_2;\, \varepsilon, \varepsilon_1, \varepsilon_2) \qquad (16)$$

$$+\iiint dx_1 dx_2 dx_3 \int_C\int\int \frac{d\varepsilon_1 d\varepsilon_2 d\varepsilon_3}{(2\pi i)^3}$$

$$\times f_4(|\mathbf{r}-\mathbf{r}_1|, |\mathbf{r}-\mathbf{r}_2|, |\mathbf{r}-\mathbf{r}_3|;\, \omega, \omega_1, \omega_2)$$

$$\times K_4(x, x_1, x_2, x_3;\, x', x_1, x_2, x_3;\, \varepsilon, \varepsilon_1, \varepsilon_2, \varepsilon_3).$$

As can be seen from (14) and (16), the binding energy can be written as

$$\mathscr{E}_b = \iint dx dx' \int_C \frac{d\varepsilon}{2\pi i} (\mathrm{Tr}\,\hat{k}_x \delta(x-x')$$

$$+ M(x, x';\, \varepsilon)) G(x', x;\, \varepsilon) - \frac{1}{2}\iint dx dx_1$$

$$\times \int_C\int \frac{d\varepsilon d\varepsilon_1}{(2\pi i)^2} f_2(|\mathbf{r}-\mathbf{r}_1|;\, \omega) K_2(x, x_1;\, x, x_1;\, \varepsilon, \varepsilon_1)$$

$$-\frac{2}{3}\iiint dx dx_1 dx_2 \int_C\int\int \frac{d\varepsilon d\varepsilon_1 d\varepsilon_2}{(2\pi i)^3}$$

$$\times f_3(|\mathbf{r}-\mathbf{r}_1|, |\mathbf{r}-\mathbf{r}_2|;\, \omega, \omega_1) \qquad (17)$$

Table 1. N_{out} in doubly closed-shell nuclei

	^{16}O	^{40}Ca	^{90}Zr	^{208}Pb
N_{out}	1.10	3.15	7.34	13.15
Z_{out}	1.15	3.53	6.46	13.22
A_{out}	2.25	6.68	13.80	26.37
A_{out}/A, %	14	16.7	15.3	12.7

$$\times K_3(x, x_1, x_2;\, x, x_1, x_2;\, \varepsilon, \varepsilon_1, \varepsilon_2)$$

$$-\frac{3}{4}\iiint dx dx_1 dx_2 dx_3 \int_C\int\int\int \frac{d\varepsilon d\varepsilon_1 d\varepsilon_2 d\varepsilon_3}{(2\pi i)^4}$$

$$\times f_4(|\mathbf{r}-\mathbf{r}_1|, |\mathbf{r}-\mathbf{r}_2|, |\mathbf{r}-\mathbf{r}_3|, \omega, \omega_1, \omega_2)$$

$$\times K_4(x, x_1, x_2, x_3;\, x, x_1, x_2, x_3;\, \varepsilon, \varepsilon_1, \varepsilon_2, \varepsilon_3).$$

Taking into account the spectral representation of $G(x, x';\, \varepsilon)$ {see Eq. (5) in [7]} and performing the integration with respect to ε, we reduce the first term in (17) to the form

$$\mathscr{E}_b^{(1)} = \sum_j^{(A-1)} \int dx \Psi_j^+(x) (\hat{k}_x \Psi_j(x) + \int M(x, x';\, E_j) \Psi_j(x') dx'). \qquad (18)$$

As follows from the Dyson equation (4) and from the above spectral representation, the amplitudes $\Psi_j(x)$ obey the equation

$$\hat{k}_x \Psi_j(x) + \int M(x, x';\, E_j) \Psi_j(x') dx' = E_j \Psi_j(x); \quad (19)$$

therefore, we have

$$\mathscr{E}_b^{(1)} = \sum_j^{(A-1)} E_j \int |\Psi_j(x)|^2 dx = \sum_\lambda \sum_j^{(A-1)} E_j s_j^{(\lambda)}, \quad (20)$$

where we have used expansion (7).

In general, the many-particle Green's functions $K_n(x_1, \ldots, x_n;\, x_1', \ldots, x_n';\, \varepsilon_1, \ldots, \varepsilon_n)$ obey an infinite set of integro-differential equations, Eq. (15) being the first one. As was mentioned above, there do not exist exact methods for solving it. It should also be mentioned that approximate methods (see [13, 14] and references therein) were developed only for instantaneous two-particle forces. For these reasons, an exact calculation of the nuclear binding energy is impossible at present. Therefore, it is important to calculate the static energy.

Both the static nuclear field and the static energy are obtained from the above relations by setting

$$K_n(x_1, \ldots, x_n; x_1', \ldots, x_n'; \varepsilon_1, \ldots, \varepsilon_n) = \prod_{i=1}^{n} G(x_i, x_i'; \varepsilon_i). \quad (21)$$

This means that we neglect the difference between the many-particle Green's functions and the unsymmetrized products of the single-particle ones. This difference arises from both antisymmetrization and from higher order terms of perturbation theory—that is, from effects leading to the proper correlation energy. Substituting (21) into (16) and (17), we obtain (all energy transfers ω_i vanish in this case)

$$U_{\rm st}(r) = \int f_2(|\mathbf{r}-\mathbf{r}_1|)\rho(r_1)d\mathbf{r}_1 + \iint f_3(|\mathbf{r}-\mathbf{r}_1|, |\mathbf{r}-\mathbf{r}_2|)\rho(r_1)\rho(r_2)d\mathbf{r}_1 d\mathbf{r}_2 + \iiint f_4(|\mathbf{r}-\mathbf{r}_1|, |\mathbf{r}-\mathbf{r}_2|, |\mathbf{r}-\mathbf{r}_3|) \times \rho(r_1)\rho(r_2)\rho(r_3)d\mathbf{r}_1 d\mathbf{r}_2 d\mathbf{r}_3; \quad (22)$$

$$\mathscr{E}_{\rm st} = \sum_{j}^{(A-1)} \int \Psi_j^+(x)(\hat{k}_x + U_{\rm st}(r))\Psi_j(x)dx - \frac{1}{2}\iint f_2(|\mathbf{r}-\mathbf{r}_1|)\rho(r)\rho(r_1)d\mathbf{r}d\mathbf{r}_1 - \frac{2}{3}\iiint f_3(|\mathbf{r}-\mathbf{r}_1|, |\mathbf{r}-\mathbf{r}_2|)\rho(r)\rho(r_1)\rho(r_2)d\mathbf{r}d\mathbf{r}_1 d\mathbf{r}_2 - \frac{3}{4}\iiint\int f_4(|\mathbf{r}-\mathbf{r}_1|, |\mathbf{r}-\mathbf{r}_2|, |\mathbf{r}-\mathbf{r}_3|) \times \rho(r)\rho(r_1)\rho(r_2)\rho(r_3)d\mathbf{r}d\mathbf{r}_1 d\mathbf{r}_2 d\mathbf{r}_3. \quad (23)$$

As follows from relations (7) and (9), the first term in (23) is

$$\mathscr{E}_{\rm st}^{(1)} = \sum_{\lambda} n_\lambda \varepsilon_\lambda. \quad (24)$$

But it can be seen from (20) and from the sum rule

$$\varepsilon_\lambda = \sum_{j}^{(A-1)} E_j s_j^{(\lambda)} + \sum_{k}^{(A+1)} E_k s_k^{(\lambda)} \quad (25)$$

for the doorway-state energies {see (14c) in [7]} that the quantity $\mathscr{E}_{\rm st}^{(1)}$ contains unphysical contributions from the energies of $(A+1)$ nuclear states. To eliminate them, we represent $\mathscr{E}_{\rm st}^{(1)}$ as the sum of two parts,

$$\mathscr{E}_{\rm st}^{(1)} = \mathscr{E}_{\rm st}^{<} + \mathscr{E}_{\rm st}^{>}, \quad \mathscr{E}_{\rm st}^{<} = \sum_{\lambda \le F} n_\lambda \varepsilon_\lambda, \quad \mathscr{E}_{\rm st}^{>} = \sum_{\lambda > F} n_\lambda \varepsilon_\lambda, \quad (26)$$

those including summations over $\varepsilon_\lambda \le \varepsilon_{\rm F}$ and $\varepsilon_\lambda > \varepsilon_{\rm F}$ states. The doorway states contributing to $\mathscr{E}_{\rm st}^{<}$ are mainly distributed over the states of the $(A-1)$ nucleus, the first term in (25) thus giving a dominant contribution to ε_λ in this case. A small unphysical contribution from the second term in (25) arises from the states of the $(A+1)$ nucleus that have the same quantum numbers as the low-lying states of the $(A-1)$ nucleus. Such states lie either in the continuum or near its boundary. Therefore, a reasonable estimate for their energies is $E_k \approx 0$, the unphysical contribution thus being negligible for this case.

The situation is opposite for $\mathscr{E}_{\rm st}^{>}$, because $\varepsilon_\lambda > \varepsilon_{\rm F}$ doorway states are mainly distributed over the states of the $(A+1)$ nucleus, a dominant contribution to ε_λ thus being unphysical from the viewpoint of the binding energy. Under such conditions, it is reasonable to use a more appropriate relation for $\mathscr{E}_{\rm st}^{>}$,

$$\tilde{\mathscr{E}}_{\rm st}^{>} = \sum_{\lambda > F} \sum_{j}^{(A-1)} E_j s_j^{(\lambda)}. \quad (27)$$

It follows that the $(A-1)$ nuclear states whose quantum numbers are identical to those of the low-lying states of the $(A+1)$ nucleus contribute in this case. There are no such states among the low-lying states of the $(A-1)$ nucleus; therefore, we have

$$E_j < E_{\rm F} = \mathscr{E}_0(A) - \mathscr{E}_g(A-1) \quad (28)$$

(see [7] for details). Nevertheless, it is reasonable to use the estimate

$$E_j = E_{\rm F}, \quad (29)$$

which provides the least absolute value for $\tilde{\mathscr{E}}_{\rm st}^{>}$. In this way, we obtain

$$\tilde{\mathscr{E}}_{\rm st}^{>} = E_{\rm F}\sum_{\lambda > F}\sum_{j}^{(A-1)} s_j^{(\lambda)} = E_{\rm F}\sum_{\lambda > F} n_\lambda = E_{\rm F}\tilde{N}_{\rm out}, \quad (30)$$

so that

$$\mathscr{E}_{\rm st} = \sum_{i=n}^{p}\left(\sum_{\lambda \le F} n_\lambda \varepsilon_\lambda + \tilde{N}_{\rm out}E_{\rm F}\right)_i - \frac{1}{2}\int (S(r)\rho_s(r) + V_\omega(r)\rho(r) + S^-(r)\rho_s^-(r) + V_\rho(r)\tilde{\rho}^-(r) + C(r)\rho_{\rm ch}(r))d\mathbf{r} - \int\left(\frac{2}{3}a_3\rho^3(r) + \frac{3}{4}a_4\rho^4(r) + \frac{1}{2}[a_3^-\rho(r) + a_4^-\rho^2(r)](\rho^-(r))^2\right)d\mathbf{r}. \quad (31)$$

We have taken into account the Lorentz and the isospin structure of two-particle forces and the resulting

Table 2. Static and observed binding energies (in MeV), together with the dominant contributions to $\mathscr{E}_{\rm st}$ [those from the Coulomb and the isovector terms are not shown, but they are included in $\mathscr{E}_{\rm st}$; the notation corresponds to the terms in (31)]

	$\mathscr{E}_{\rm st}^{(1)}$	$-\frac{1}{2}S$	$-\frac{1}{2}V_\omega$	$-\frac{2}{3}a_3$	$-\frac{3}{4}a_4$	$\mathscr{E}_{\rm st}$	$\mathscr{E}_b$
^{16}O	–345.6	+1528.4	–1224.0	–451.2	+461.8	–47.0	–127.6
^{40}Ca	–991.7	+4456.0	–3570.8	–1346.0	+1411.3	–120.7	–342.0
^{90}Zr	–2251.6	+10699.0	–8565.6	–3236.5	+3386.0	–234.2	–783.9
^{208}Pb	–4998.2	+26463.4	–21255.6	–8190.9	+8694.0	–233.3	–1636.5

expressions of scalar and vector fields (see [7] for details). We have also considered that only the total strength parameters of the many-particle forces,

$$a_3 = \iint f_3(\xi,\eta)d\boldsymbol{\xi}d\boldsymbol{\eta},$$
$$a_4 = \iiint f_4(\xi,\eta,\zeta)d\boldsymbol{\xi}d\boldsymbol{\eta}d\boldsymbol{\zeta}, \tag{32}$$

can be introduced in a model-independent way; therefore, we are constrained to the contact forces

$$f_3(|\mathbf{r}-\mathbf{r}_1|,|\mathbf{r}-\mathbf{r}_2|) = a_3\delta(\mathbf{r}-\mathbf{r}_1)\delta(\mathbf{r}-\mathbf{r}_2),$$
$$f_4(|\mathbf{r}-\mathbf{r}_1|,|\mathbf{r}-\mathbf{r}_2|,|\mathbf{r}-\mathbf{r}_3|) \tag{33}$$
$$= a_4\delta(\mathbf{r}-\mathbf{r}_1)\delta(\mathbf{r}-\mathbf{r}_2)\delta(\mathbf{r}-\mathbf{r}_3).$$

To calculate the first term, we used the following ansatz for the occupation numbers, setting $\tilde{N}_{\rm out} = N_{\rm out}$ (see Section 2):

$$n_\lambda = \frac{1}{2}\left[1-\frac{\varepsilon_\lambda-\mu}{\sqrt{(\varepsilon_\lambda-\mu)^2+C^2}}\right],$$
$$\sum_\lambda n_\lambda = N, \quad \sum_{\lambda>F} n_\lambda = \tilde{N}_{\rm out}. \tag{34}$$

This is incorrect because the sum $\sum_{\lambda>F} n_\lambda$ is different from $N_{\rm out}$ given by (13). Indeed, both diagonal and off-diagonal elements of the density matrix [see Eq. (8)] contribute to $N_{\rm out}$. This shortcoming will be corrected in future by calculating n_λ and $\rho_{\lambda\nu}$ (see the discussion in Section 2). Of course, the ansatz in (34) will then become unnecessary.

The results of the calculations are given in Table 2, which shows that the static energy is the sum of a number of contributions with different sign, the dominant ones greatly exceeding the total static energy as well as the observed binding one. This is a source of ambiguities because all disregarded effects can be of importance in such a situation.

One such effect is associated with a finite range of many-particle forces. A possible way of estimation is illustrated for three-particle forces. As can be seen from (14), the original contribution is

$$\mathscr{E}_3 = \frac{1}{3}\iiint f_3(|\mathbf{r}-\mathbf{r}_1|,|\mathbf{r}-\mathbf{r}_2|)\rho(r)\rho(r_1)\rho(r_2)d\mathbf{r}d\mathbf{r}_1d\mathbf{r}_2$$
$$= \frac{1}{3}\iiint \rho(r)f_3(\xi,\eta)\rho(|\mathbf{r}+\boldsymbol{\xi}|)\rho(|\mathbf{r}+\boldsymbol{\eta}|)d\mathbf{r}d\boldsymbol{\xi}d\boldsymbol{\eta}$$
$$\cong \frac{1}{3}\iiint \rho(r)f_3(\xi,\eta)\Big[\rho(r)+\boldsymbol{\xi}\cdot\boldsymbol{\nabla}\rho(r)$$
$$+\frac{1}{2}\xi_i\xi_k\partial_i\partial_k\rho(r)+\ldots\Big]\Big[\rho(r)+\boldsymbol{\eta}\cdot\boldsymbol{\nabla}\rho(r)$$
$$+\frac{1}{2}\eta_j\eta_l\partial_j\partial_l\rho(r)+\ldots\Big]d\mathbf{r}d\boldsymbol{\xi}d\boldsymbol{\eta} \tag{35}$$
$$= \frac{1}{3}\iiint \rho(r)f_3(\xi,\eta)\Big[\rho(r)+\frac{1}{6}\xi^2\Delta\rho(r)+\ldots\Big]$$
$$\times\Big[\rho(r)+\frac{1}{6}\eta^2\Delta\rho(r)+\ldots\Big]d\mathbf{r}d\boldsymbol{\xi}d\boldsymbol{\eta}$$
$$= \frac{1}{3}a_3\int\rho(r)[\rho(r)+r_0^2\Delta\rho(r)+\ldots]^2d\mathbf{r}$$
$$\cong \frac{1}{3}a_3\int\rho^3(r)d\mathbf{r}+\frac{2}{3}a_3r_0^2\int\rho^2(r)\Delta\rho(r)d\mathbf{r},$$

where

$$a_3r_0^2 = \frac{1}{6}\iint\xi^2f_3(\xi,\eta)d\boldsymbol{\xi}d\boldsymbol{\eta}$$
$$= \frac{1}{6}\iint\eta^2f_3(\xi,\eta)d\boldsymbol{\xi}d\boldsymbol{\eta}. \tag{36}$$

In this way, we obtain

$$\delta_{r_0^2}\mathscr{E}_{\rm st} = r_0^2\int\Big(\frac{2}{3}a_3\rho^2(r)+\frac{3}{4}a_4\rho^3(r)\Big)\Delta\rho(r)d\mathbf{r} = -Dr_0^2,$$
$$D = \int\Big(\frac{4}{3}a_3\rho(r)+\frac{9}{4}a_4\rho^2(r)\Big)(\rho'(r))^2d\mathbf{r}. \tag{37}$$

The calculated D values are shown in Table 3. A reasonable value of the range parameter is the ω-meson Compton wavelength—that is, a typical scale of strong interaction. Hence, we have $r_0^2 = m_\omega^{-2} = 0.1$ fm^2, the effect thus being negligibly small.

A second source of possible ambiguity can be seen from the results (Table 4) presented in [7] for the con-

Table 3. Many-particle finite-range effect

	^{16}O	^{40}Ca	^{90}Zr	^{208}Pb
D, MeV fm^{-2}	–12.12	–3.29	22.02	34.08

Table 4. Contributions to the static field

	U_2	U_3	U_4
Bonn B	–83	+96.5	–104
OSBEP	–82	+97	–107

tributions of two-, three-, and four-particle forces to the static nuclear field {Eqs. (44) and (45) in [7]}.

As follows from the table, this sequence does not seem to converge. This observation suggests the possible existence of contributions from higher many-particle forces; therefore, the whole sequence should be summed up. But this can be done only within some reasonable model for many-particle forces that includes those of all higher orders, as well as the finite range and the mechanism for the saturation of the nuclear density. The corresponding investigation is in progress.

REFERENCES

1. R. Machleidt, nucl-th/9911059.
2. F. Klingl and W. Weise, hep-ph/9802211.
3. G. E. Brown *et al.*, nucl-th/9806026.
4. S. Leopold and U. Mosel, nucl-th/9805024.
5. A. M. Rakhimov *et al.*, nucl-th/9806062.
6. J. L. Friar, nucl-th/9911075.
7. B. L. Birbrair and V. I. Ryazanov, nucl-th/9907058; Yad. Fiz. **63**, 1842 (2000) [Phys. At. Nucl. **63**, 1753 (2000)].
8. M. Baranger, Nucl. Phys. A **149**, 225 (1970).
9. J. D. Walecka, Ann. Phys. (N.Y.) **83**, 491 (1974).
10. A. B. Migdal, *Theory of Finite Fermi Systems and Applications to Atomic Nuclei* (Nauka, Moscow, 1983).
11. L. L. Frankfurt and M. I. Strikman, Phys. Rep. **76**, 215 (1981).
12. L. L. Frankfurt, M. I. Strikman, D. B. Day, and M. Sargsyan, Phys. Rev. C **48**, 2451 (1993).
13. V. A. Khodel and V. R. Shaginyan, Fiz. Élem. Chastits At. Yadra **22**, 436 (1991) [Sov. J. Part. Nucl. **22**, 210 (1991)].
14. H. Müther and A. Polls, nucl-th/0001007.

Physics of Atomic Nuclei, Vol. 64, No. 3, 2001, pp. 423–439. Translated from Yadernaya Fizika, Vol. 64, No. 3, 2001, pp. 478–494.

90th ANNIVERSARY OF A.B. MIGDAL'S BIRTHDAY
NUCLEI

Theory of Nuclear Reactions and Decays with Allowance for Antisymmetrization Effects

S. G. Kadmensky

Voronezh State University, Universitetskaya pl. 1, Voronezh, 394693 Russia

Received March 27, 2000; in final form, July 17, 2000

Abstract—On the basis of an explicit implementation of the projection-operator method and with due regard to antisymmetrization effects, formulas are constructed for the amplitudes of elastic and inelastic nuclear reactions induced by nucleons and composite particles and for the widths with respect to the nucleonic, alpha-particle, and cluster decays of nuclei. It is shown that equations governing the behavior of elastic-scattering form factors represent generalizations of the equations of the resonating-group model and coincide, provided that ground-state correlations are taken into account, with the analogous equations in the theory of open Fermi systems. It is demonstrated that the nonretarded part of the effective potential of nucleus–nucleus interaction coincides with the Hartree–Fock potential, which has a deep attractive character in accordance with the Levinson theorem, and that the retarded part of the effective potential is determined by the fragmentation of the initial states of colliding nuclei into compound states. It is revealed that the use of different elastic-form-factor representations associated with taking into account antisymmetrization effects leads to the same results for the amplitudes of elastic and inelastic nuclear reactions. The formulas obtained here for the amplitudes of direct inelastic nuclear reactions are found to differ significantly from the corresponding formulas of the distorted-wave method in the Born approximation. Problems that are concerned with the emergence of potential optical resonances for elastic form factors and with their relation to the shell-model wave functions for a compound system are investigated. A new regime of interpolation for the amplitudes of cluster form factors from the shell to the asymptotic region of a decaying nucleus is found. Implications of this interpolation for the calculated alpha-particle and cluster widths and for understanding the nature of superfluid correlations in nuclei are analyzed.

1. INTRODUCTION

Albeit leading to rigorous formulas, the theory of nuclear reactions and decays involving composite particles that was developed in [1] on the basis of the wave-packet representation and the *T*-matrix formalism and which takes into account antisymmetrization effects is hardly appropriate for a quantitative treatment of specific problems because this theory employs exact many-body wave functions.

The unified theory of the nucleus [2]—it considers the structure of a nucleus and nuclear reactions on the basis of the nonorthogonal-variation method—develops an approach that is more detailed than that in [1] and which makes it possible to extend the resonating-group method [3, 4] (which was successfully used in describing nuclear reactions involving light nuclei—see, for example, [5]) to the case where colliding nuclei have arbitrary masses. Even in this theory, however, there nevertheless remain some unclear questions of fundamental importance that are associated with consistently taking into account antisymmetrization effects. On this basis, it was concluded in [6–8] that antisymmetrization effects substantially renormalize, in relation to conventional computational schemes, spectroscopic shell factors in the theory of alpha-particle and cluster decays of nuclei and amplitudes for inelastic nuclear reactions involving composite particles. A theory of nuclear reactions was developed in [9, 10] that relies on the projection-operator method and which made it possible to relate nuclear reactions featuring nucleons to the multiparticle shell model of the nucleus. Unfortunately, no specific definition of projection operators was actually given in those studies, so that the results presented there could not be generalized to the case of nuclear reactions involving composite particles. Finally, mention should also be made of yet another approach to the theory of nuclear reactions, that [11] which is based on the method of *K* harmonics and which appears to be one of the implementations of the nonorthogonal-variation method [2]. Within this approach, it was deduced in [12] that, because of the effect of the Pauli exclusion principle, there is a strong repulsion in the effective nucleus–nucleus potential. Within the theory of open Fermi system and the projection-operator method, equations were derived in [13, 14] that describe elastic and inelastic nuclear reactions featuring nucleons and composite particles and which imply the use of various regimes of averaging. The objective of the present study is to develop further, within the same conceptual framework as in [13, 14], the theory of nuclear reactions and decays involving composite particles toward a consistent inclusion of antisymmetrization effects.

1063-7788/01/6403-0423$21.00

2. DESCRIPTION OF NUCLEAR REACTIONS WITHIN THE *T*-MATRIX FORMALISM

By using the methods developed in [1], we will study nuclear reactions of the type

$$a + A \longrightarrow b + B, \tag{1}$$

where a, A, b, and B are nucleons or nuclei that have mass numbers A_a, A_A, A_b, and A_B ($A_a \le A_A$) and the internal energies $\bar{E}_a$, $\bar{E}_A$, $\bar{E}_b$, and $\bar{E}_B$ and which are described by antisymmetrized intrinsic wave functions χ_a, χ_A, χ_b, and χ_B. We denote by the generic index b (a) the reaction channel including particles b and B (a and A). In the c.m. frame, the wave function $|\Psi_a^+\rangle$ describing the system of particles under study and corresponding to the incident wave in the input reaction channel a and to diverging waves in all open final reaction channels c satisfies the Schrödinger equation

$$(E - H)|\Psi_a^+\rangle = 0, \tag{2}$$

where the total Hamiltonian of the system, H, can be represented as

$$H = H_c + H_C + T_c + V_c = H_c^0 + V_c. \tag{3}$$

Here, c is any channel of reactions of the type in (1); H_c and H_C are the intrinsic Hamiltonians of particles c and C, respectively; V_c is the relevant interaction potential; $T_c = \hbar^2\hat{\mathbf{k}}_c^2/2m_c$ is the kinetic-energy operator; $\hat{\mathbf{k}}_c = -i\dfrac{\partial}{\partial \mathbf{R}_c}$ is the wave-vector operator; $\mathbf{R}_c$ is the coordinate of the relative motion of particles c and C; and $m_c = \dfrac{A_cA_C}{A_c + A_C}m$ is the reduced mass as expressed in terms of the nucleon mass m. Since particles a and A (c and C) consist of nucleons, which can be treated as identical particles differing only by spatial, spin, and isospin coordinates, the wave functions of the system being considered that are defined in the configuration space of all nucleon coordinates must be antisymmetric under any permutation of the nucleon coordinates. We introduce the antisymmetrized function $|\Phi_a\rangle$ corresponding to the unperturbed state of particles in the channel a:

$$|\Phi_a\rangle = |\hat{A}_a\{\chi_a\chi_A e^{i\mathbf{k}_a\cdot\mathbf{R}_a}\}\rangle$$
$$= \int |\hat{A}_a\{\chi_a\chi_A\delta(\mathbf{R}_a - \mathbf{R}_a')\}\rangle e^{i\mathbf{k}_a\cdot\mathbf{R}_a'}d\mathbf{R}_a' = |a_0\rangle e^{i\mathbf{k}_a\cdot\mathbf{R}_a}. \tag{4}$$

Here, $\mathbf{k}_a$ is the wave vector whose absolute value is determined in terms of the energy E_a of the relative motion of the particles in the channel a ($E_a = E - \bar{E}_a - \bar{E}_A$) from the relation $\hbar^2\mathbf{k}_a^2/2m_a = E_a$, while the antisymmetrization operator $\hat{A}_a$ has the form

$$\hat{A}_a = C_a\sum_P \delta_p P, \tag{5}$$

where there appear all permutation operators P between particles a and A, the quantity δ_p is equal to a plus (minus) unity for an even (odd) permutation P, and the normalization constant is $C_a = \left(\dfrac{A_a!A_A!}{(A_a + A_A)!}\right)^{1/2}$. We note that the function $P\{\chi_a\chi_A e^{i\mathbf{k}_a\cdot\mathbf{R}_a}\}$ is an eigenfunction of the Hamiltonian PH_a^0P for the same permutation P, but that there is not, in principle, a Hamiltonian for which the function $|\Phi_a\rangle$ (4) would be an eigenfunction. This circumstance has far-reaching consequences for the use of the functions $|\Phi_a\rangle$ in the theory of nuclear reactions. In Eq. (4), we have introduced the vector $|a_0\rangle$ with which we associated the operator-valued function $|\hat{A}_a\{\chi_a\chi_A\delta(\mathbf{R}_a - \mathbf{R}_a')\}\rangle$ corresponding to the channel a and acting as a nonlocal operator on functions depending on the relative coordinate $\mathbf{R}_a$. Upon introducing the function $|\Phi_c\rangle$ by substituting the subscript c for a in Eq. (4) and considering the corresponding state vector $|c_0\rangle$ for an arbitrary channel c of reactions of the type in (1), we can obtain the condition

$$\langle\Phi_c|\Phi_a\rangle = \langle e^{i\mathbf{k}_c\cdot\mathbf{R}_c}|W_{ca}|e^{i\mathbf{k}_a\cdot\mathbf{R}_a}\rangle, \tag{6}$$

where the nonlocal operator W_{ca}, which is a generalization of the operator W_{aa} used in the resonating-group method [3, 4], is defined as

$$W_{ca}(\mathbf{R}_c, \mathbf{R}_a) = \langle c_0|a_0\rangle$$
$$= \langle\hat{A}_c\{\chi_c\chi_C\delta(\mathbf{R}_c - \mathbf{R}_c')\}|\hat{A}_a\{\chi_a\chi_A\delta(\mathbf{R}_a - \mathbf{R}_a')\}\rangle. \tag{7}$$

Integration in Eq. (7) is performed with respect to all coordinates of the system, including the coordinate $\mathbf{R}_a'$ related by a linear equation to the coordinate $\mathbf{R}_c'$ for all permutations. By using the methods developed in [1], we can represent a solution to Eq. (2) as

$$|\Psi_a^\pm\rangle = |\Phi_a\rangle + \frac{1}{E - H \pm i\delta}|V_a\Phi_a\rangle, \tag{8}$$

where the form $|V_a\Phi_a\rangle$ means that the potential V_a must be introduced under the sign of the antisymmetrization operator $\hat{A}_a$ in Eq. (4). With the aid of the formalism constructed in [1], we can express the differential cross section for reactions (1) in terms of the amplitude A_{ba} for reactions (1) as

$$\frac{d\sigma_{ba}}{d\Omega_{\mathbf{k}_b}} = \frac{k_bm_a}{k_am_b}|A_{ba}(\Omega_{\mathbf{k}_b})|^2, \tag{9}$$

where

$$A_{ba} = -\frac{m_b}{2\pi\hbar^2}T_{ba}. \quad (10)$$

Here, T_{ba} is the relevant T-matrix element given by

$$T_{ba} = \langle\Phi_b V_b|\Psi_a^+\rangle = \langle\Psi_b^-|V_a\Phi_a\rangle. \quad (11)$$

After the substitution of the subscript a for the subscript b and the wave vector $\mathbf{k}_a'$, which differs only in direction from the asymptotic wave vector $\mathbf{k}_a$ for the input channel of reactions (1), for the wave vector $\mathbf{k}_b$ in (9), expressions (9)–(11) describe the differential cross section for elastic scattering.

Although expressions (9)–(11) are quite rigorous, it is difficult in general to perform specific calculations on their basis, because they involve the wave functions $|\Psi_a^+\rangle$ and $|\Psi_b^-\rangle$, which appear to be solutions to the exact multiparticle Schrödinger equation (2).

3. DESCRIPTION OF NUCLEAR REACTIONS WITHIN THE FORMALISM OF THE PROJECTION-OPERATOR METHOD

We will now make use of the projection-operator method, which was developed previously in [9–11]. We represent the wave function $|\Psi_a^+\rangle$ of the system in the form

$$|\Psi_a^+\rangle = \sum_c |P_c\Psi_a^+\rangle + |Q\Psi_a^+\rangle, \quad (12)$$

where the sum over c is taken over all open channels of reactions (1), while the operators P_c and Q possess all the properties of projection operators: $\sum_c P_c + Q = 1$, $P_cQ = QP_c = 0$, $P_cP_{c'} = P_{c'}P_c = P_c\delta_{cc'}$, and $Q^2 = Q$. The operator P_c projects the wave function of the system of $(A_a + A_A)$ nucleons onto the intrinsic states of particles c and C for the open channel c, while the operator Q projects the wave function of the system onto those states that do not have open decay channels and which therefore possess discrete energies and are finite in configuration space. Multiplying Eq. (2) from the left by the operators P_c and Q, we can obtain the set of coupled equations

$$P_c(E-H)|\Psi_a^+\rangle = 0, \quad (13)$$

$$Q(E-H)|\Psi_a^+\rangle = 0. \quad (14)$$

We further represent Eq. (14) in the form

$$Q(E-H)|Q\Psi_a^+\rangle = -Q(E-H)\sum_c |P_c\Psi_a^+\rangle \quad (15)$$

and introduce a complete orthonormalized basis in the subspace of eigenfunctions $|\varphi_p\rangle$ that is singled out by the operator Q for the Schrödinger equation

$$(E_p - QHQ)|\varphi_p\rangle = 0. \quad (16)$$

In this case, the projection operator Q can be represented in the form $Q = \sum_p |\varphi_p\rangle\langle\varphi_p|$. By using the Green's function $G_Q^\pm$ corresponding to this equation,

$$G_Q^\pm = \sum_p \frac{|\varphi_p\rangle\langle\varphi_p|}{E - E_p \pm i\delta}, \quad (17)$$

we can write a solution to Eq. (15) as

$$|Q\Psi_a^+\rangle = -G_Q^+(E-H)\sum_c |P_c\Psi_a^+\rangle = \sum_p |\varphi_p\rangle a_p, \quad (18)$$

where

$$a_p = -\frac{\langle\varphi_p|(E-H)\sum_c |P_c\Psi_a^+\rangle}{E - E_p + i\delta} = -\frac{\langle\varphi_p|\sum_c V_cP_c\Psi_a^+\rangle}{E - E_p + i\delta}. \quad (19)$$

Substituting solution (18) into Eq. (12) and using Eqs. (2) and (13), we find that, for a specific channel c, the equations for the function $|P_c\Psi_a^+\rangle$ are given by

$$P_c(E - H_Q^+)\sum_{c'} |P_{c'}\Psi_a^+\rangle = 0. \quad (20)$$

The last of these can be represented as

$$P_c(E - H_Q^+)|P_c\Psi_a^+\rangle = -P_c(E - H_Q^+)\sum_{c'\neq c} |P_{c'}\Psi_a^+\rangle, \quad (21)$$

where

$$H_Q^+ = H + \Delta H_Q^+ = H + (E-H)G_Q^+(E-H). \quad (22)$$

For a channel $c \neq a$, we now introduce the Green's function G_c^+ corresponding to the Schrödinger equation (21) with zero right-hand side. This makes it possible to find the function $|P_c\Psi_a^+\rangle$ in terms of the functions $|P_{c'}\Psi_a^+\rangle$, $c \neq c'$. Continuing this process iteratively, we can close up the set of equations in question and arrive at the following equation for the input reaction channel a:

$$P_a(E - H_{Q_a}^+)|P_a\Psi_a^+\rangle = 0. \quad (23)$$

Here, the Hamiltonian $H^+_{Q_a}$ is determined by Eq. (22), where the projection operator Q is replaced by $Q_a = \sum_{c \neq a} P_c + Q = 1 - P_a$ and where the Green's function G^+_Q is replaced by the Green's function $G^+_{Q_a}$ defined by formulas of types in (16) and (17). Similarly, we can construct an equation for the function $|P_b\Psi^+_a\rangle$ for an inelastic open channel $b \neq a$. It has the form

$$P_b(E - H_{Q_{ba}})^+|P_b\Psi^+_a\rangle = -P_b(E - H_{Q_{ba}})^+|P_a\Psi^+_a\rangle, \quad (24)$$

where the Hamiltonian $H^+_{Q_{ba}}$ is determined by Eq. (22) with the substitution of the operator $Q_{ba} = \sum_{c \neq a,\, b} P_c + Q$ for the operator Q. The set of Eqs. (21) and Eqs. (23) and (24), which follow from it, include both the direct coupling of open reaction channels c to the input channel a and to one another and their coupling through the Green's function G_Q and discrete compound states $|\varphi_p\rangle$. This means that, in contrast to what occurs in the R-matrix theory of nuclear reactions [15], the set of equations in question describes not only multistep direct and multistep statistical nuclear reactions but also situations of an intermediate type associated with transitions between states that are singled out by the operators P_c and states that are singled out by the operator Q.

4. CONSTRUCTING PROJECTION OPERATORS

We will make use of the properties of the nonlocal operators $\sqrt{W_{aa}}$ and $\frac{1}{\sqrt{W_{aa}}}$, which are extensively used in the resonating-group method [4] and which are related to the operator W_{aa} specified by Eq. (7) at $c = a$. For the input channel a of reactions (1), we define the nonlocal projection operator P_a as

$$\begin{aligned} P_a &= P_a(\mathbf{R}_a, \mathbf{R}'_a) \\ &= \int d\mathbf{R}_1 d\mathbf{R}_2 d\mathbf{R}_3 |\hat{A}_a\{\chi_a\chi_A\delta(\mathbf{R}_a - \mathbf{R}_1)\}\rangle \\ &\quad \times \frac{1}{\sqrt{W_{aa}(\mathbf{R}_1, \mathbf{R}_2)}} \frac{1}{\sqrt{W_{aa}(\mathbf{R}_2, \mathbf{R}_3)}} \\ &\quad \times \langle \hat{A}_a\{\chi_a\chi_A\delta(\mathbf{R}_3 - \mathbf{R}'_a)\}| = |a\rangle\langle a|, \end{aligned} \quad (25)$$

where the symbol $|a\rangle$ stands for the vector related to the vector $|a_0\rangle$ in (4) by the equation

$$|a\rangle = |a_0\rangle \frac{1}{\sqrt{W_{aa}}}. \quad (26)$$

From the definition in (26), it follows that $|a\rangle$ is a unit vector since its norm is equal to unity. For this reason, the operator P_a possesses the basic property of the projection operator; that is, $P^2_a = P_a$. The action of the operator P_a on the wave function $|\Psi^+_a\rangle$ of the system can be represented in the form

$$|P_a\Psi^+_a\rangle = |a\rangle\langle a|\Psi^+_a\rangle = |a\rangle \tilde{f}^+_a(\mathbf{R}_a), \quad (27)$$

where the form factor $\tilde{f}^+_a(\mathbf{R}_a)$ is related to the cluster form factor of the system,

$$f^+_a(\mathbf{R}_a) = \langle \hat{A}_a\{\chi_A\chi_a\delta(\mathbf{R}_a - \mathbf{R}'_a)\}|\Psi^+_a\rangle = \langle a_0|\Psi^+_a\rangle, \quad (28)$$

which is extensively used in describing clustering effects in nuclei [5], by the equation

$$\tilde{f}^+_a(\mathbf{R}_a) = \frac{1}{\sqrt{W_{aa}}} f^+_a(\mathbf{R}_a). \quad (29)$$

For a specific inelastic channel b, the projection operator P_b satisfying the conditions $P_aP_b = P_bP_a = 0$ and $P^2_b = P_b$ can be represented in the form

$$P_b = |b_1\rangle\langle b_1|, \quad (30)$$

where the state vector $|b_1\rangle$ is defined as

$$|b_1\rangle = |b - \overline{W}_{ab}a\rangle \frac{1}{\sqrt{1 - \overline{W}^2_{ba}}}. \quad (31)$$

Here,

$$\overline{W}_{ab} = \frac{1}{\sqrt{W_{aa}}} W_{ab} \frac{1}{\sqrt{W_{bb}}}, \quad (32)$$

$|b\rangle$ is a unit vector similar to the vector $|a\rangle$ (26), and the operator W_{ab} is defined by (7). From expression (31), it can be seen that $|b_1\rangle$ is a unit vector that lies in the plane spanned by the vectors $|a\rangle$ and $|b\rangle$ and which is orthogonal to the vector $|a\rangle$. By using an iterative scheme based on the orthogonalization recipe proposed above, we can construct mutually orthogonal projection operators P_c for all open reaction channels.

The ensuing analysis can be substantially simplified for the case where the nucleus A in the input channels of reactions of the type in (1) is sufficiently heavy. The operator W_{ca}, which determines the scale of nonorthogonality of the vectors $|c_0\rangle$ and $|a_0\rangle$, is then equal to zero in the asymptotic region of large values of R_c or R_a and takes a very small value in the region where the densities of the reaction fragments c and C strongly overlap and so do the densities of particles a and A. For the projection operators P_c, we can therefore use formulas of the type in (25) with the substitution of the subscript a for c. In this approximation, noticeable deviations for the operators P_c $(c \neq a)$ can in principle arise in not very frequent cases of light colliding nuclei of pronounced cluster structure. It will be shown below that this choice of the operators P_c corresponds to the ideas of the theory of open Fermi systems [13] and leads to the important property $\langle c|\varphi_p\rangle = 0$ of the functions $|\varphi_p\rangle$ defined in the configuration space that is singled out by the oper-

ator Q. This property implies that the functions $|\varphi_p\rangle$ are expressed in terms of multiparticle shell functions of a compound system, provided that the components corresponding to open reaction channels are eliminated from them.

5. COMPARISON OF THE PROJECTION-OPERATOR AND THE NONORTHOGONAL-VARIATION METHOD

The nonorthogonal-variation method was developed in [2] for describing nuclear reactions and decays with allowance for antisymmetrization effects. Within this method, a solution to Eq. (2) is sought in the form

$$|\Psi_a^+\rangle = \sum_c |c_0\rangle f_c^+(\mathbf{R}_c) + \sum_p a_p|\varphi_p\rangle, \quad (33)$$

where the sum over c is taken over all open reaction channels, the state vector $|c_0\rangle$ is given by (4), and the sum over p covers some states of the system that are characterized by discrete energies and which are finite in configuration space. Let us consider a variation of the function $|\Psi_a^+\rangle$,

$$\delta|\Psi_a^+\rangle = \sum_c |c_0\rangle \delta f_c^+(\mathbf{R}_c) + \sum_p \delta a_p|\varphi_p\rangle, \quad (34)$$

where $\delta f_c^+(\mathbf{R}_c)$ and δa_p are independent variations of the form factors $f_c^+(\mathbf{R}_c)$ and of the coefficients a_p. By successively multiplying Eq. (2) from the left by terms of the sums appearing on the right-hand side of Eq. (34) and considering that the variations $\delta f_c^+(\mathbf{R}_c)$ and δa_p are independent, we then arrive at the set of coupled equations

$$\begin{aligned} \langle c_0|(E-H)|\Psi_a^+\rangle &= 0, \\ \langle \varphi_p|(E-H)|\Psi_a^+\rangle &= 0, \end{aligned} \quad (35)$$

whose number is equal to the sum of the number of open channels and the number of states $|\varphi_p\rangle$ used in Eq. (33). The nonorthogonal-variation method is convenient in that it is not necessary, in implementing it, to require mutual orthogonality of the vectors $|c_0\rangle$ and the functions $|\varphi_p\rangle$—it is sufficient to choose a sufficiently full and physically reasonable set of states $|\varphi_p\rangle$ in Eq. (33). For the function $|\Psi_a^+\rangle$, the projection-operator method, which was developed in the preceding sections, employs expression (12), which can be formally recast into the form (33) by using the definitions of the projection operators P_c (25) and relations (18), (27), and (29). At the same time, the set of Eqs. (13) and (14) can also be formally reduced to the set of Eqs. (35) if we use the required number of terms in the expansion in (33). But this brings about the question of why the projection-operator method should be preferred to the nonorthogonal-variation method. The answer to this question is the following. First, the projection-operator method is exact in the general theoretical sense, since it employs, from the outset, the complete basis of states in the configuration space of all coordinates of the system. Second, the projection-operator method makes it possible to simplify the resulting formulas in relation to those in the nonorthogonal-variation method because of orthogonality of the projection operators P_c for different channels c to each other and to the operator Q. Finally, the projection-operator method, in contrast to the nonorthogonal-variation method, permits imparting clear physical meaning to the form factors $f_c^+(\mathbf{R}_c)$ and the functions $|\varphi_p\rangle$ and relating them to the properties of the exact wave function $|\Psi_a^+\rangle$ of the system. At the same time, the results obtained in [2] within the nonorthogonal-variation method can easily be extended to the case of the projection-operator method owing to a formal coincidence of the two representations in question.

6. DESCRIPTION OF ELASTIC SCATTERING IN THE PROJECTION-OPERATOR FORMALISM

Multiplying Eq. (23) from the left by the vector $\langle a|$, performing integration with respect to all coordinates of the system, and using expression (27), we find that the form factor $\tilde{f}_a^+(\mathbf{R}_a)$ satisfies the equation

$$\langle a|E - H_{Q_a}^+|a\rangle \tilde{f}_a^+(\mathbf{R}_a) = 0. \quad (36)$$

Since the operator $H_{Q_a}^+$ commutes with the operator of permutation of the nucleon coordinates, we can introduce the expression $(E - H_{Q_a}^+)$ under the sign of the antisymmetrization operator $\hat{A}_a$ appearing in the definition of the vector $|a_0\rangle$ in formula (26). By further representing the Hamiltonian H of the system in the form (3) at $c = a$, we can then recast Eq. (36) into the form

$$(E_a - T_a - \tilde{V}_a^+)\tilde{f}_a^+(\mathbf{R}_a) = 0, \quad (37)$$

where the nonlocal potential $\tilde{V}_a^+$ is defined as

$$\tilde{V}_a^+ = \frac{1}{\sqrt{W_{aa}}}\langle a_0|(T_a + V_a + \Delta H_{Q_a}^+)a_0\rangle\frac{1}{\sqrt{W_{aa}}} - T_a. \quad (38)$$

Equation (37) differs from the analogous resonating-group-method equation reduced to the Hermitian form [4] by the addition of the term $\Delta H_{Q_a}^+$ to the potential V_a. This term is of paramount physical importance, because it ensures the conservation of the total probability flux in the system under consideration upon taking into account antisymmetrization effects. Indeed, a

decrease in the values of the operator W_{aa} in the region of a strong overlap of the densities of particles a and A due to the antisymmetrization effect is accompanied in Eq. (37) by transitions from the input reaction channel to all states singled out by the operator $Q_a = 1 - P_a$, but this is taken into account precisely by the term $\Delta H^+_{Q_a}$. It should be emphasized that states of the compound system that are characterized by the wave functions $|\varphi_p\rangle$ and which enter into the definition of the operator $\Delta H^+_{Q_a}$ can be treated as intruder states of discrete energies in the continuous spectrum of excitations of this system. In the asymptotic region of large values of R_a, the form factor $\tilde{f}^+_a(\mathbf{R}_a)$ can be represented, apart from a constant factor associated with its normalization, as

$$\tilde{f}^+_a(\mathbf{R}_a) \longrightarrow e^{i\mathbf{k}_a\cdot\mathbf{R}_a} + A_{aa}(\Omega_{\mathbf{k}'_a})\frac{e^{ik_aR_a}}{R_a}, \qquad (39)$$

where the elastic-scattering amplitude $A_{aa}(\Omega_{\mathbf{k}'_a})$ is given by expression (10), in which the T-matrix element (11) is replaced by the matrix element

$$\tilde{T}_{aa} = \langle e^{i\mathbf{k}'_a\cdot\mathbf{R}_a}|\tilde{V}^+_a|\tilde{f}^+_a(\mathbf{R}_a)\rangle. \qquad (40)$$

By using Eq. (37), this matrix element can be recast into the equivalent form

$$\tilde{T}_{aa} = \langle e^{i\mathbf{k}'_a\cdot\mathbf{R}_a}|E_a - T_a|\tilde{f}^+_a(\mathbf{R}_a)\rangle. \qquad (41)$$

Considering that the function $e^{i\mathbf{k}'_a\cdot\mathbf{R}_a}$ is a solution to the equation $(E_a - T_a)e^{i\mathbf{k}'_a\cdot\mathbf{R}_a} = 0$, we can represent expression (41) as

$$\tilde{T}_{aa} = \int\Big\{\tilde{f}^+_a(\mathbf{R}_a)T_a e^{-i\mathbf{k}'_a\cdot\mathbf{R}_a} - e^{-i\mathbf{k}'_a\cdot\mathbf{R}_a}T_a\tilde{f}^+_a(\mathbf{R}_a)\Big\}d\mathbf{R}_a. \qquad (42)$$

The explicit form of the operator T_a is $T_a = -\frac{\hbar^2}{2m_a}\frac{\partial^2}{\partial\mathbf{R}_a^2}$. Using this and the Gauss theorem, we can reduce the volume integral on the right-hand side of Eq. (42) to an integral over the surface S of a sphere of large radius R_a; that is,

$$\tilde{T}_{aa} = -\frac{\hbar^2}{2m_a}\oint_S d\Omega_{\mathbf{R}_a}\Big\{(\tilde{f}^+_a(\mathbf{R}_a)R_a)\frac{\partial}{\partial R_a}(e^{-i\mathbf{k}'_a\cdot\mathbf{R}_a}R_a) - (e^{-i\mathbf{k}'_a\cdot\mathbf{R}_a}R_a)\frac{\partial}{\partial R_a}(\tilde{f}^+_a(\mathbf{R}_a)R_a)\Big\}. \qquad (43)$$

Since the operator W_{aa} is equal to unity in the region of sufficiently large values of R_a, the matrix element (41) reduced to the form (43) is invariant under multiplication of the form factor $\tilde{f}^+_a(\mathbf{R}_a)$ by arbitrary positive or negative powers of the operator $\frac{1}{\sqrt{W_{aa}}}$ and by arbitrary functions of R_a that are equal to unity in the region of large R_a. This implies that the matrix element (41) can be represented in the equivalent forms

$$\tilde{T}_{aa} = \langle e^{i\mathbf{k}'_a\cdot\mathbf{R}_a}|E_a - T_a|f^+_a(\mathbf{R}_a)\rangle = \langle e^{i\mathbf{k}'_a\cdot\mathbf{R}_a}|V^+_a|f^+_a(\mathbf{R}_a)\rangle, \qquad (44)$$

where the form factor $f^+_a(\mathbf{R}_a)$ is given by (28) and, by virtue of relation (29), satisfies the Schrödinger equation (37) with the potential $V^+_a = \langle a_0|(V_a + \Delta H^+_{Q_a})|a_0\rangle\frac{1}{W_{aa}}$ substituted for the effective potential $\tilde{V}^+_a$ (38). It follows that the matrix element T_{aa} [1], which is given by expression (11) at $b = a$ and which is reduced, with the aid of relations (3) and (28), to expression (44) for the form factor $f^+_a(\mathbf{R}_a)$, coincides with the matrix element (41).

Thus, the potentials $\tilde{V}^+_a$ and V^+_a in Schrödinger equations of the form (37) for the form factors $\tilde{f}^+_a(\mathbf{R}_a)$ and $f^+_a(\mathbf{R}_a)$ are phase-equivalent from the viewpoint of describing elastic scattering, albeit their structures differ substantially. In processing experimental data on the elastic scattering of nucleons and composite particles on nuclei, use is made of phenomenological potentials that do not include the kinetic-energy operator T_a—that is, those that correspond to the potential V^+_a. This means that the Schrödinger equation for the form factor $\tilde{f}^+_a(\mathbf{R}_a)$ should be preferred to that for the form factor $f^+_a(\mathbf{R}_a)$, which, in the resonating-group method [4, 6], stands out among other form factors. This conclusion can be confirmed by contrasting the results obtained above against the ideas of the theory of open Fermi systems [13].

7. ELASTIC SCATTERING AND THEORY OF OPEN FERMI SYSTEMS

We begin by considering the simplest case where a nucleon plays the role of particle a in the channel a. We denote by $\mathbf{R}_a$ its total coordinate, which includes the aforementioned coordinate of the relative motion of the nucleon and particle A and the projections of the

nucleon spin and isospin onto the z axis. For the case of a sufficiently heavy nucleus A, the vector $|a_0\rangle$ given by (4) can be written in the second-quantization representation as

$$|a_0\rangle = \psi^+(\mathbf{R}_a)|A\rangle, \tag{45}$$

where $|A\rangle \equiv |\chi_A\rangle$ and $\psi^+(\mathbf{R}_a)$ is the nucleon creation operator in the coordinate representation. The quantities that appear in an equation of the type in (37) for the form factor $f_a^+(\mathbf{R}_a)$ are given by

$$f_a^+(\mathbf{R}_a) = \langle A|\psi(\mathbf{R}_a)|\Psi_a^+\rangle, \tag{46}$$

$$\begin{aligned} W_{aa}(\mathbf{R}_a, \mathbf{R}'_a) &= \langle A|\psi(\mathbf{R}_a)\psi^+(\mathbf{R}'_a)|A\rangle \\ &= \delta(\mathbf{R}_a - \mathbf{R}'_a) - \rho^{(1)}(\mathbf{R}'_a, \mathbf{R}_a), \end{aligned} \tag{47}$$

$$\begin{aligned} \langle a_0|V_a a_0\rangle \frac{1}{W_{aa}} &= V_a^{\mathrm{HF}}(\mathbf{R}_a, \mathbf{R}'_a) \\ &- \int V(\mathbf{R}_a - \mathbf{r}_1)[\rho_A^{(2)}(\mathbf{r}_1, \mathbf{R}'_a; \mathbf{r}_1, \mathbf{R}_a) \\ &- \rho^{(1)}(\mathbf{r}_1, \mathbf{r}_1)\rho^{(1)}(\mathbf{R}'_a, \mathbf{R}_a) \\ &+ \rho^{(1)}(\mathbf{r}_1, \mathbf{R}_a)\rho^{(1)}(\mathbf{R}'_a, \mathbf{r}_1)]\frac{1}{W_{aa}} d\mathbf{r}_1, \end{aligned} \tag{48}$$

where $V(\mathbf{r}_1 - \mathbf{r}_2)$ is the pair potential of the interaction between nucleons having the coordinates $\mathbf{r}_1$ and $\mathbf{r}_2$;

$$\begin{aligned} V_a^{\mathrm{HF}}(\mathbf{R}_a, \mathbf{R}'_a) &= \int V(\mathbf{R}_a - \mathbf{r}_1)\rho_A^{(1)}(\mathbf{r}_1, \mathbf{r}'_1) d\mathbf{r}_1 \\ &\times \delta(\mathbf{R}_a - \mathbf{R}'_a) - V(\mathbf{R}_a - \mathbf{R}'_a)\rho_A^{(1)}(\mathbf{R}'_a, \mathbf{R}_a) \end{aligned} \tag{49}$$

is the nonlocal Hartree–Fock potential; and

$$\rho_A^{(1)}(\mathbf{r}_1, \mathbf{r}'_1) \equiv \langle A|\psi^+(\mathbf{r}_1)\psi(\mathbf{r}'_1)|A\rangle$$

and

$$\rho_A^{(2)}(\mathbf{r}_1, \mathbf{r}_2; \mathbf{r}'_1, \mathbf{r}'_2) \equiv \langle A|\psi^+(\mathbf{r}_1)\psi^+(\mathbf{r}_2)\psi(\mathbf{r}'_2)\psi(\mathbf{r}'_1)|A\rangle$$

are, respectively, the single- and the two-particle density matrices for nucleus A.

From the above formulas, it follows, quite unexpectedly, that, in the rigorous resonating-group-method equation, which is obtained from Eq. (37) by eliminating the operator $\Delta H_{Q_a}^+$ from it, expression (48) involves, in addition to the Hartree–Fock potential V_a^{HF}, a term that is determined by the difference of the two-particle density matrix and the product of single-particle density matrices for nucleus A and which can be related to the retarded part of the nucleon self-energy operator (see below).

Within the theory of open Fermi systems, it was shown [13] that the form factor $f_a^+(\mathbf{R}_a)$ (46) coincides with the amplitude of the residue of the exact one-nucleon Green's function $G_a(\mathbf{r}, \mathbf{r}', \varepsilon)$ for nucleus A at its pole occurring at the energy value $\varepsilon = E_a$ and corresponding to the state $|\Psi_a^+\rangle$ of the system of $(A + 1)$ nucleons. In this case, the equation for $f_a^+(\mathbf{R}_a)$ has the form [13, 16]

$$\{(E_a - T_a - M_a(\mathbf{R}_a, \mathbf{R}'_a, E_a))\} f_a^+(\mathbf{R}_a) = 0, \tag{50}$$

where $M_a(\mathbf{R}_a, \mathbf{R}'_a, E_a)$ is the nonlocal nucleon self-energy operator, whose Lehmann's expansion is written in the form

$$M_a(\mathbf{R}_a, \mathbf{R}'_a, E_a) = V_a^{\mathrm{HF}}(\mathbf{R}_a, \mathbf{R}'_a) + \tilde{M}_a(\mathbf{R}_a, \mathbf{R}'_a, E_a). \tag{51}$$

By using the method of variational derivatives of the S matrix, the retarded part $\tilde{M}_a$ of the above self-energy operator can be represented as [13]

$$\begin{aligned} &\tilde{M}_a(\mathbf{R}_a, \mathbf{R}'_a, \varepsilon) \\ &= \sum_t \frac{X_t(\mathbf{R}_a)X_t^*(\mathbf{R}'_a)}{\varepsilon - \varepsilon_t + i\delta} + \sum_{t'} \frac{X_{t'}(\mathbf{R}_a)X_{t'}^*(\mathbf{R}'_a)}{\varepsilon - \varepsilon_{t'} - i\delta}, \end{aligned} \tag{52}$$

where

$$\begin{aligned} X_t(\mathbf{R}_a) &= \left\langle t\left|\frac{\delta H_{\mathrm{int}}}{\delta\psi(\mathbf{R}_a)}\right|A\right\rangle, \\ X_{t'}(\mathbf{R}_a) &= \left\langle t'\left|\frac{\delta H_{\mathrm{int}}}{\delta\psi^+(\mathbf{R}_a)}\right|A\right\rangle, \end{aligned} \tag{53}$$

H_{int} being the second-quantized Hamiltonian for nucleon interaction. Comparing Eqs. (37) and (50), we can see that they coincide if the Green's function G_Q^+ appearing in the definition (21) of the operator $\Delta H_{Q_a}^+$ is supplemented with the sum of pole terms corresponding to a complete set of states of the $(A - 1)$-nucleon system that are described by the reduced Hamiltonian $Q'_a H Q'_a$, where the projection operator Q'_a differs from the projection operator $Q_a = 1 - P_a$ by the substitution of the operator $|a_0^+\rangle \equiv \psi(\mathbf{R}_a)|A\rangle$ for the operator $|a_0\rangle$. The addition of the above terms to the operator $\Delta H_{Q_a}^+$ corresponds to taking into account a correlation between a nucleon and the ground state of the system of A nucleons.

It follows that, apart from ground-state correlations, the potential V_a^+ for the form factor $f_a^+(\mathbf{R}_a)$ coincides with the nucleon self-energy, the energy-independent (nonretarded) part of the potential V_a^+ and its retarded part, which takes into account the coupling of the form factor $f_a^+(\mathbf{R}_a)$ to inelastic channels and compound states, being determined by, respectively, the Hartree–Fock potential and the retarded part of the self-energy operator. This means that the operator $1/W_{aa}$ appearing in the definition of the potential V_a^+ plays a very impor-

tant role, because it is this operator that makes it possible to separate, in this potential, the term that coincides with the Hartree–Fock potential from correlation terms that are associated with the difference of the two-particle density matrix for nucleus A and the sum of the products of its single-particle density matrices.

By using the technique of multiparticle Green's functions that was developed in [16, 17] for describing elastic scattering and nuclear reactions involving nucleons and composite particles, the cluster form factor $f_a^+(\mathbf{R}_a)$ (28) for the channel a can be expressed in terms of the amplitude of the residue of the A_a-particle two-time Green's function G_{A_a} for nucleus A at its pole corresponding to the state in which the $(A_a + A_A)$-nucleon system is characterized by the energy value E and the wave function $|\Psi_a^+\rangle$. An equation of the type in (37) with the potential V_a^+ for the form factor $f_a^+(\mathbf{R}_a)$ reduces to an equation of the form (50), where the effective self-energy operator for the particles in the channel a has the same structure as expression (51). The generalized Hartree–Fock potential $V_a^{\mathrm{HF}}(\mathbf{R}_a, \mathbf{R}_a')$ is then given by [18, 19]

$$
\begin{aligned}
&V_a^{\mathrm{HF}}(\mathbf{R}_a, \mathbf{R}_a') \\
&= \int V(\mathbf{s})\rho_a^{(1)}(\mathbf{y}_1, \mathbf{y}_1)\rho_A^{(1)}(\mathbf{y}_2, \mathbf{y}_2)d\mathbf{y}_1 d\mathbf{y}_2 \delta(\mathbf{R}_a - \mathbf{R}_a') \\
&\quad - \int V(\mathbf{s})\rho_A^{(1)}\left(\mathbf{y}_1, \mathbf{y}_1 + \frac{A_A - 1}{A_A}\mathbf{s}\right) \\
&\quad \times \rho_a^{(1)}\left(\mathbf{y}_2, \mathbf{y}_2 - \frac{A_a - 1}{A_a}\mathbf{s}\right)d\mathbf{y}_1 d\mathbf{y}_2 \delta(\mathbf{R}_a - \mathbf{R}_a' - \mu\mathbf{s}),
\end{aligned}
\tag{54}
$$

where $\mathbf{s} = \mathbf{R}_a + \mathbf{y}_2 - \mathbf{y}_1$ and $\mu = \dfrac{A_a + A_A}{A_a A_a}$. At $A_a = 1$ and $\rho_a^{(1)}(\mathbf{y}_1, \mathbf{y}_1) = \delta(\mathbf{y}_1)$, this potential reduces to the one-nucleon Hartree–Fock potential (49). The retarded part $\tilde{M}_a$ of the effective self-energy operator includes, in addition to the term corresponding to the operator $\Delta H_{Q_a}^+$ in the potential V_a^+, terms corresponding to transitions to states of the systems of $(A_a + A_A - 1)$, $(A_a + A_A - 2)$, …, $(A_A - A_a)$ nucleons and taking into account correlations between particle a and the ground state of nucleus A. In just the way as in the case of elastic nucleon scattering on nucleus A, the operator $1/W_{aa}$ appearing in the definition of the potential V_a^+ plays an extremely important role in describing the elastic scattering of a composite particle a on nucleus A, because it is this operator that makes it possible to eliminate, from the matrix element $\langle a_0|V_a|a_0\rangle$, the exchange terms that are associated with the permutations of those nucleons between particles a and A that do not interact with one another and which do not therefore contribute to the Hartree–Fock potential (54). Thus, the T-matrix element T_{aa} in the form (44), which is directly related to the standard cluster form factor $f_a^+(\mathbf{R}_a)$ (28) obeying the Schrödinger equation (50) with an effective potential that has the form (51) and which takes into account ground-state correlations, conforms best of all to the ideas of open Fermi systems.

The calculations of the Hartree–Fock potentials (54) within various approximations in [18, 19] showed that these potentials are also attractive and have a large deepness that corresponds to the Levinson theorem [20]. No effective repulsion associated with the inclusion of antisymmetrization effects arises in these potentials.

Let us now consider the form factor $f_{a0}^+(\mathbf{R}_a)$ obeying the equation

$$
\{(E_a - T_a - V_a^{\mathrm{HF}})\} f_{a0}^+(\mathbf{R}_a) = 0, \tag{55}
$$

which is obtained from Eq. (50) if only the first term is retained in the effective potential (51).

Because of a large depth of the Hartree–Fock potential, a potential resonance state arises in this equation at a certain energy value E_{a0}. The form factor for this state can be normalized to unity in the internal region of the compound system. If the energy-dependent potential $\tilde{M}_a(\mathbf{R}_a, \mathbf{R}_a', E_a)$ is included in Eq. (55), the resonance state $f_{a0}^+(\mathbf{R}_a)$ will fragment into the multiparticle states $|\varphi_p\rangle$ of the compound system. Owing to this fragmentation, the elastic-scattering amplitude $A_{aa}(\Omega_{\mathbf{k}_a'})$ develops, in addition to potential resonances, multiparticle resonances associated with the functions $|\varphi_p\rangle$. In order to describe the regime of this fragmentation, the concept of a strength function introduced previously for nucleons (see [13, 21]) can be generalized to the case of arbitrary particles a. The strength function $S_{a0}(E_a)$ for the state $f_{a0}^+(\mathbf{R}_a)$—it coincides with the energy distribution of the weight of this state among the exact states of the system—has the form of the Breit–Wigner distribution that is peaked at energy E_{a0} and which has an effective width Γ_{a0} determined by the imaginary part of retarded component (52) of the self-energy operator. An analysis of the strength function $\bar{S}_{a0}(E_a)$ averaged over a sufficiently broad energy interval ΔE shows that its effective width, which is close to the effective width of the exact strength function $S_{a0}(E_a)$, is determined by the imaginary part of the optical potential of interaction between particles a and A. In turn, an analysis of the imaginary parts of phenomenological optical potentials for arbitrary composite particles a and sufficiently heavy particles A [21, 22] leads to the conclusion that the width Γ_{a0}, in contrast to the analogous width for the case where particle a is a nucleon, is commensurate

with or greater than the energy spacings between the neighboring resonance states at E_{a0} that are characterized by fixed integrals of the motion (this situation corresponds to the black-nucleus model). The form factor $f_a^+(\mathbf{R}_a)$ for arbitrary composite particles a that is determined as a solution to Eq. (52) with allowance for the retarded part of the self-energy operator will then involve, at any energy E_a, including the energy E_{a0}, only a small admixture of the resonance state $f_{a0}^+(\mathbf{R}_a)$.

8. DESCRIPTION OF INELASTIC NUCLEAR REACTIONS WITHIN THE PROJECTION-OPERATOR FORMALISM

In order to describe transitions from the input reaction channel a into an inelastic channel $b \neq a$, we multiply Eq. (13) for $c = b$ from the left by the vector $\langle b_0|$ and perform integration with respect to all nucleon coordinates. As a result, we arrive at

$$\langle (E_b - T_b) b_0 | \Psi_a^+ \rangle = \langle b_0 V_b | \Psi_a^+ \rangle. \quad (56)$$

Further, we make use of the notation $\langle b_0|\Psi_a^+\rangle \equiv f_b^+(\mathbf{R}_b)$, where the form factor $f_b^+(\mathbf{R}_b)$ is similar to the above form factor $f_a^+(\mathbf{R}_a)$ (28) for the elastic-scattering channel. Introducing the Green's function $G_b(\mathbf{R}_b, \mathbf{R}_b')$ obeying the equation that is obtained from Eq. (56) by replacing its right-hand side by $\delta(\mathbf{R}_b - \mathbf{R}_b')$ and considering its asymptotic behavior at large values of R_b, we can derive the formula obtained in [1] for the amplitude A_{ba} of reactions (1), which is related by Eq. (9) to the differential cross section for reactions (1) and by Eq. (10) to the T-matrix element T_{ba} (11). This matrix element in turn can be represented as

$$T_{ba} = \langle e^{i\mathbf{k}_b \cdot \mathbf{R}_b} | (E_b - T_b) | f_b^+(\mathbf{R}_b) \rangle. \quad (57)$$

By using the method for going over from Eq. (41) to Eq. (43), we can recast expression (57) into the form (43) with the substitution of the subscript b for the subscript a, the form factor f_b^+ for the form factor $\tilde{f}_a^+$, and the wave vector $\mathbf{k}_b$ for the wave vector $\mathbf{k}_a'$. It follows that the matrix element T_{ba} (57) is invariant under the multiplication of the form factor f_b^+ by an arbitrary positive or negative power of the operator $\sqrt{W_{bb}}$ and under the multiplication by arbitrary functions of R_a that are equal to unity in the region of large values of R_a. The matrix element T_{ba} (57) can then be recast into the equivalent form

$$T_{ba} = \langle e^{i\mathbf{k}_b \cdot \mathbf{R}_b} | (E_b - T_b) | \tilde{f}_b^+(\mathbf{R}_b) \rangle, \quad (58)$$

where $\tilde{f}_b^+(\mathbf{R}_b) = \frac{1}{\sqrt{W_{bb}}} f_b^+(\mathbf{R}_b)$. Multiplying Eq. (24) from the left by the vector $\langle b_0|$ and performing integration with respect to the nucleon coordinates, we find that the form factor f_b^+ satisfies the equation

$$\begin{aligned} &(E_b - T_b - V_b^+) f_b^+(\mathbf{R}_b) \\ &= \langle b_0 | (V_b + \Delta H_{Q_{ab}}^+) | a_0 \rangle \frac{1}{W_{aa}} f_a^+(\mathbf{R}_a), \end{aligned} \quad (59)$$

where the nonlocal potential V_b^+ coincides, upon substituting the subscript b for the subscript a and the operator Q_{ab} for the operator Q_a, with the potential V_a^+, which was introduced above. By using the Green's function $G_b^+(\mathbf{R}_b, \mathbf{R}')$ for Eq. (59) [that is, the Green's function that satisfies the equation obtained from Eq. (59) by replacing its right-hand side by $\delta(\mathbf{R}_b - \mathbf{R}_b')$], we can represent the form factor $f_b^+(\mathbf{R}_b)$ as

$$f_b^+(\mathbf{R}_b) = G_b^+ \left\langle b_0 (V_b + \Delta H_{Q_{ab}}^+) | a_0 \rangle \frac{1}{W_{aa}} f_a^+(\mathbf{R}_a) \right\rangle. \quad (60)$$

Substituting (60) into (57) and transforming the plane wave $e^{i\mathbf{k}_b \cdot \mathbf{R}_b}$ into the distorted wave $f_b^-(\mathbf{R}_b)$ that is found as a solution to Eq. (59), where the right-hand side and a plus sign in the superscript are replaced, respectively, by zero and by a minus sign, we arrive at

$$T_{ba} = \langle f_b^-(\mathbf{R}_b) | \langle b_0 (V_b + \Delta H_{Q_{ab}}^+) | a_0 \rangle \left| \frac{1}{W_{aa}} f_a^+(\mathbf{R}_a) \right\rangle. \quad (61)$$

With the aid of formula (58), the matrix element T_{ba} can be represented in the equivalent form

$$\begin{aligned} &T_{ba} \\ &= \left\langle f_b^-(\mathbf{R}_b) \frac{1}{W_{bb}} \left| \langle b_0 (V_b + \Delta H_{Q_{ab}}^+) | a_0 \rangle \right| \frac{1}{W_{aa}} f_a^+(\mathbf{R}_a) \right\rangle. \end{aligned} \quad (62)$$

A comparison of Eqs. (61) and (62) reveals that the matrix element T_{ba} remains unchanged upon the addition of arbitrary powers of the operator $\sqrt{W_{bb}}$ to the extreme left bra vector on the right-hand side of Eq. (61). At the same time, the operator $\frac{1}{W_{aa}}$ in the extreme right ket vector in expressions (61) and (62) plays the same role as in the case of the elastic-scattering amplitude, correcting the structure of exchange terms in Eq. (61). It should be noted that, although expression (61) for the matrix element T_{ba} is exact, it is close in structure to the similar expression for T_{ba} within the popular distorted-wave method in the Borne approximation.

9. OPTICAL MODEL AND DISTORTED-WAVE METHOD FOR AMPLITUDES OF NUCLEAR REACTIONS

Let us introduce the T-matrix elements $\bar{T}_{aa}$ (44) and $\bar{T}_{ba}$ (61) averaged over a certain energy interval ΔE and associated with the direct mechanism of elastic and inelastic nuclear reactions. The averaged form factor $\bar{f}_a^+$, which determines the amplitude $\bar{T}_{aa}$, satisfies the Schrödinger equation (37) with the substitution of the nonlocal optical potential V_a^{opt} for the potential V_a^+. For the case of nonoverlapping resonances, it was shown in [2] that, in the amplitudes describing nuclear reactions of the type in (1) and arising from the bare states $|\varphi_p\rangle$ that appear in the definition of the Green's function G_Q, the optical potential V_a^{opt} coincides with the potential V_a^+ upon the substitution of the complex energy $E + i\Delta E$ for the energy E in (18). In this case, the real and the imaginary part of the potential V_a^{opt} are given by

$$\operatorname{Re} V_a^{\text{opt}} = V_a^{\text{HF}} + \sum_p \frac{|\langle a_0|E - H|\varphi_p\rangle|^2 (E - E_p)}{(E - E_p)^2 + \Delta E^2} \frac{1}{W_{aa}}, \tag{63}$$

$$\operatorname{Im} V_a^{\text{opt}} = -\sum_p \frac{|\langle a_0|E - H|\varphi_p\rangle|^2 \Delta E}{(E - E_p)^2 + \Delta E^2} \frac{1}{W_{aa}}, \tag{64}$$

where the basis of functions $|\varphi_p\rangle$ must be constructed with allowance for ground-state correlations.

If we employ the nucleon-coordinate-displacement operators, which are expressed in terms of the nucleon-wave-vector operators, and the methods developed in [18], the nonlocal optical potential V_a^{opt} as given by Eqs. (63) and (64) can be reduced to the equivalent local momentum-dependent optical potential $V_a^{\text{opt}}(\mathbf{R}_a, \hat{\mathbf{k}}_a)$. Considering that a gradient term proportional to the wave-vector operator $\hat{\mathbf{k}}_a$ appears in the potential $V_a^{\text{opt}}(\mathbf{R}_a, \hat{\mathbf{k}}_a)$ [18], we can represent the form factor $\bar{f}_a^+(\mathbf{R}_a)$ as

$$\bar{f}_a^+(\mathbf{R}_a) = F_a(\mathbf{R}_a)\varphi_a^+(\mathbf{R}_a), \tag{65}$$

where the function $\varphi_a^+(\mathbf{R}_a)$ satisfies the Schrödinger equation

$$(E_a - T_a - V_a^{\text{opt}}(\mathbf{R}_a, E_a))\varphi_a^+(\mathbf{R}_a) = 0 \tag{66}$$

with the local energy-dependent complex optical potential $V_a^{\text{opt}}(\mathbf{R}_a, E_a)$, while the form factor $F_a(\mathbf{R}_a)$, which was first introduced by Perey [23], is given by

$$F_a(\mathbf{R}_a) = \left(\frac{m_a^*(\mathbf{R}_a, E_a)}{m_a}\right)^{1/2} = \left(1 - \frac{dV_a^{\text{opt}}(\mathbf{R}_a, E_a)}{dE_a}\right)^{1/2}, \tag{67}$$

$m_a^*(\mathbf{R}_a, E_a)$ being the effective reduced mass of particles a and A [18]. Since the form factor $F_a(\mathbf{R}_a)$ tends to unity at large R_a, Eq. (66) for the function $\varphi_a^+(\mathbf{R}_a)$ is phase-equivalent to the analogous equation with $V_a^{\text{opt}}(\mathbf{R}_a, E_a)$ for the function $\bar{f}_a^+(\mathbf{R}_a)$, so that the matrix element $\bar{T}_{aa}$ that is averaged over the interval ΔE and which describes the direct component of elastic scattering can be represented as

$$\bar{T}_{aa} = \langle e^{i\mathbf{k}_a' \cdot \mathbf{R}_a} | V^{\text{opt}}(\mathbf{R}_a, E_a) | \varphi_a^+(\mathbf{R}_a)\rangle. \tag{68}$$

It should be emphasized that phenomenological optical potentials describing the direct component of the elastic scattering of particles a on particles A are always constructed in the form of local energy-dependent complex potentials $V^{\text{opt}}(\mathbf{R}_a, E_a)$ [21]; therefore, phenomenological optical wave functions correspond to the wave functions $\varphi_a^+(\mathbf{R}_a)$. For a global regime of averaging [14], in which case the contribution of the second term can be disregarded in Eq. (63), the real part of the optical potential $V_a^{\text{opt}}(\mathbf{R}_a, E_a)$ coincides with the Hartree–Fock potential (54), which, as was indicated above, has an attractive character and a depth satisfying the Levinson theorem [20]. For the inclusion of input-state fragmentation into compound states in going over to the internal region of the system, it is not necessary, in this case, to introduce the effective repulsion in the real part of the optical potential $V_a^{\text{opt}}(\mathbf{R}_a, E_a)$; this fragmentation is completely determined by the effect of its imaginary part, which leads to an exponential suppression of the absolute value of the function $\varphi_a^+(\mathbf{R}_a)$ in the internal region of the system.

If we disregard, upon averaging over the interval ΔE, the contribution of the operator $\Delta H_{Q_{ab}}^+$, which has an oscillatory character, the averaged T-matrix element $\bar{T}_{ba}$ (61) takes the form

$$\bar{T}_{ba} = \langle \varphi_b^- F_b | \left\langle b_0 V_b \middle| a_0 \middle| \frac{1}{W_{aa}} \right\rangle | F_a \varphi_a^+ \rangle, \tag{69}$$

where the optical wave functions φ_a^- and φ_b^- obey optical-model equations of the type in (66). By using the

properties of antisymmetrized functions of the type specified by Eqs. (4) and (5), expression (69) can be recast into the equivalent form

$$\bar{T}_{ba} = \frac{C_a}{C_b}\langle\chi_b\chi_B\varphi_b^- F_b V_b|\frac{1}{W_{aa}}\sum_P \delta_p P\{\chi_a\chi_A\varphi_a^+ F_a\rangle. \quad (70)$$

Expression (70) differs from the analogous expression corresponding to the popular distorted-wave method in the Born approximation [23] not only by the presence of Perey factors in the former but also by a consistent inclusion of antisymmetrization effects that lead to the emergence of the operator $\frac{1}{W_{aa}}$ in (70).

10. NUCLEONIC AND CLUSTER DECAYS OF NUCLEI WITHIN THE PROJECTION-OPERATOR METHOD

The *R*-matrix theory of nuclear reactions [1, 15] is usually used to analyze resonances observed in cross sections for nuclear reactions and the properties of long-lived nuclear states that decay via the emission of nucleons, alpha particles, and other composite particles. However, one has yet to find out conclusively how the wave functions X_λ that are employed in this theory to describe the internal region of a compound system and which correspond to resonances observed in nuclear reactions are related to the finite wave functions of the multiparticle shell model that are often invoked in describing the structural properties of nuclei. The projection-operator method, which was developed above, introduces the basis of eigenfunctions $|\varphi_p\rangle$ of the reduced Hamiltonian *QHQ* that are orthogonal by definition to the channels functions $|c_0\rangle$; therefore, they correspond neither to the *R*-matrix functions X_λ nor to multiparticle shell functions. It follows that, in order to solve the problems in question with due regard to antisymmetrization effects, the projection-operator method developed above must be recast into a form that would be in line with the ideas of *R*-matrix theory, on one hand, and make it possible to use, in the calculations, multiparticle shell wave functions for nuclei, on the other hand.

Let us examine the general case where, in the problem of particle scattering, the system occurs in the state that is described by the wave function $|\Psi_a^+\rangle$ introduced above and which is characterized by a specific angular momentum J_i, its projection M_i, and a parity π_i. We further go over from the vector $|a_0\rangle$ that is given by (4) and which is dependent on the three-dimensional vectors $\mathbf{R}_a$ and $\mathbf{R}_a'$ to the analogous radial vector

$$|a_0\rangle = \left|A_a\left\{\frac{U_a}{R_a}\delta(R_a - R_a')\right\}\right\rangle, \quad (71)$$

where the channel function U_a has the form

$$U_a\{\chi_a\chi_A Y_{l_a m_a}(\Omega_{\mathbf{R}_a})\}_{J_i M_i \pi_i}. \quad (72)$$

Here, $Y_{l_a m_a}$ is a spherical harmonic associated with the orbital angular momentum l_a of the relative motion of particles *a* and *A* in the channel *a* and its projection m_a, while the braces denote the vector composition of the orbital angular momentum l_a and the spins of particles *a* and *A* into the total angular momentum J_i of the system. We can then introduce the radial vector $|a\rangle = \frac{1}{\sqrt{W_{aa}}}|a_0\rangle$ and the radial projection operator $P_a = |a\rangle\langle a|$, where the radial operator W_{aa} is defined by analogy with the three-dimensional operator W_{aa} (7) for the radial vectors $|a_0\rangle$. In order that finite multiparticle shell wave functions of the compound system with quantum numbers J_i, M_i, and π_i could be used for the eigenfunctions $|\varphi_p\rangle$ of the reduced Hamiltonian *QHQ*, we generalize the projection-operator method, following the lines of reasoning of Wildermuth and Tang [2]. Specifically, we represent the operator *Q* in the form

$$Q = \sum_p |\varphi_p\rangle\langle\varphi_p|, \quad (73)$$

where the sum over *p* covers the shell states $|\varphi_p\rangle$ of the compound nucleus that form a set over which a complete fragmentation of potential resonances occurs in all open channels *c*. In this case, the radial projection operators P_c must be redefined in such a way as to ensure fulfillment of the conditions $P_c Q = Q P_c = 0$ and $P_c P_{c'} = P_{c'} P_c = \delta_{cc'} P_c$—this means that these operators are defined in the subspace singled out by the projection operator $1 - Q$; that is,

$$P_c = |c_1\rangle\langle c_1|, \quad (74)$$

where

$$|c_1\rangle = (1 - Q)|c\rangle\frac{1}{\sqrt{\bar{W}_{cc}}}. \quad (75)$$

Symbolically, the operator $\bar{W}_{cc}$ appearing in Eq. (75) can be written as

$$\bar{W}_{cc} = 1 - \sum_p \langle c|\varphi_p\rangle\langle\varphi_p|c\rangle. \quad (76)$$

We note that, as a matter of fact, our method for choosing the projection operators *Q* (73) and P_c (74) conforms to the conceptual framework of the study of Baz' *et al.* [11], with the only difference that the more traditional basis of multiparticle shell functions is used here instead of the basis of *K*-harmonic functions.

By using the above radial operator (74) instead of the operator P_c (27), we can recast the set of Eqs. (21)

into the form

$$P_c(E-H_Q^{\prime+})\sum_{c'}|P_{c'}\Psi_a^+\rangle$$
$$(E-H)|\varphi_0\rangle\langle\varphi_0|(E-H)\sum_{c'}|P_{c'}\Psi_a^+\rangle \quad (77)$$
$$= P_c\frac{}{E-E_0},$$

where the operator $H_Q^{\prime+}$ is given by expression (22) with the Green's function G_Q^+ (18), where the $p = 0$ term corresponding to the energy E_0, which is close to the energy E of the system under study, is discarded. Ignoring the coupling of open channels that is due to the action of the operator $H_Q^{\prime+}$ on the right-hand side of Eq. (77), multiplying this equation from the left by the vector $\langle c_1|$, and performing integration with respect to all coordinates of the system, we find that the radial form factor $\tilde{f}_c^+(R_c) = \langle c_1|\Psi_a^+\rangle$ satisfies the equation

$$\langle c_1|E-H_Q^{\prime+}|c_1\rangle\tilde{f}_c^+(R_c)$$
$$\langle c_1|E-H|\varphi_0\rangle\langle\varphi_0|\sum_{c'}(E-H)\,|c_1'\rangle|\tilde{f}_{c'}^+(R_c)\rangle \quad (78)$$
$$= \frac{}{E-E_0} = D_c(R_c).$$

Imposing the condition that the channel a is the input reaction channel, we seek the relevant solution to this equation in the form

$$\tilde{f}_c^+(R_c) = \delta_{ca}\tilde{f}_c^{\prime+} + G_c^{\prime+}D_c, \quad (79)$$

where the form factor $\tilde{f}_c^{\prime+}(R_c)$ obeys the equation

$$\{E_c - T_c - \tilde{V}_c^+\}\tilde{f}_c^{\prime+}(R_c) = 0. \quad (80)$$

Here, the operators T_c and $\tilde{V}_c^+$ are defined as

$$T_c = -\frac{\hbar^2 d^2}{2m_c dR_c^2} + \frac{\hbar^2 l(l+1)}{2m_c R_c^2}, \quad (81)$$

$$\tilde{V}_c^+ = \langle c_1|H_Q'|c_1\rangle - T_c, \quad (82)$$

while the radial Green's function $G_c^{\prime+}$ satisfies the equation obtained from Eq. (80) by substituting $\delta(R_c - R_c')$ for its right-hand side. Multiplying the function in (79) from the left by the operator $\langle\varphi_0|E-H|c_1\rangle$ and summing the resulting expression over c, we obtain

$$\sum_c\langle\varphi_0|E-H|c_1\rangle|\tilde{f}_c^+\rangle = K_a^{-1}\langle\varphi_0|E-H|a_1\rangle|\tilde{f}_a^{\prime+}\rangle, \quad (83)$$

where

$$K_a = E - E_0 + \sum_c\langle\varphi_0|E-H|c_1\rangle G_c'\langle c_1|E-H|\varphi_0\rangle. \quad (84)$$

Substituting (83) into (79), we represent the form factor $\tilde{f}_c^+(R_c)$ as

$$\tilde{f}_c^+(R_c) = \delta_{ca}\tilde{f}_c^{\prime+}$$
$$+ G_c'K_a^{-1}\langle c_1|E-H|\varphi_0\rangle\langle\varphi_0|E-H|a_1\rangle|\tilde{f}_a^{\prime+}\rangle. \quad (85)$$

For the radial Green's function G_c', we further use the expression

$$G_c' = \pi\{\tilde{g}_c^{\prime+}(R_>) + i\tilde{f}_c^{\prime+}(R_>)\}\tilde{f}_c^{\prime+}(R_<), \quad (86)$$

where $R_<$ ($R_>$) is the smaller (larger) value of R_c and $R_{c'}$, while $\tilde{g}_c^{\prime+}$ and $\tilde{f}_c^{\prime+}$ are, respectively, the irregular and the regular solution to Eq. (80) that are normalized to the delta function of energy. Considering the asymptotic behavior of the form factor (85), we can then reduce the S-matrix element S_{ca} to the form

$$S_{ca} = e^{i(\delta_c' + \delta_a')}\left[\delta_{ca} - \frac{i\sqrt{\Gamma_{0c}}\sqrt{\Gamma_{0a}}}{E - E_0 + \Delta_0(E) + \dfrac{i\Gamma_0}{2}}\right], \quad (87)$$

where δ_c' is the phase shift associated with the function $\tilde{f}_c^{\prime+}(R_c)$; Γ_{0c} and $\Gamma_0 = \sum_c\Gamma_{0c}$ are, respectively, the partial and the total decay width of the resonance state of the system; and $\Delta_0(E)$ is the energy shift. Specifically, we have

$$\sqrt{\Gamma_{0c}} = \sqrt{2\pi}\langle\tilde{f}_c^{\prime+}c_1|(E-H)|\varphi_0\rangle, \quad (88)$$

$$\Delta_0(E) = \sum_c\langle\varphi_0|(E-H)|c_1\rangle G_c^{\prime+R}\langle c_1|(E-H)|\varphi_0\rangle. \quad (89)$$

In Eq. (89), $G_c^{\prime+R}$ is the real part of the Green's function G_c', while, in Eq. (88), the form factor $\tilde{f}_c^{\prime+}(R_c)$ is normalized to the delta function of energy.

In contrast to the form factor $\tilde{f}_c^+(R_c)$, which is a solution to Eq. (78) with the vector $|c\rangle$ substituted for the vectors $|c_1\rangle$, the form factor $\tilde{f}_c^{\prime+}(R_c)$ does not involve potential resonance states associated with the deep Hartree–Fock potential, since the projection operator $1 - Q$ appearing in the definition of the vector $|c_1\rangle$ and including a sufficiently vast basis of shell wave functions $|\varphi_p\rangle$ leads to the elimination of these states from the form factor $\tilde{f}_c^{\prime+}(R_c)$ and to their inclusion, as

components, in the multiparticle shell functions $|\varphi_p\rangle$. In this case, the phase shift as a function of the energy E_c shows a rather smooth behavior. Therefore, the S-matrix element S_{ca} in the form (87) corresponds to the analogous matrix element in R-matrix theory, so that the width Γ_{0c} (88) can be treated as the decay width of the true resonance state of the system of $(A_a + A_A)$ nucleons.

11. DECAY WIDTHS OF NUCLEAR STATES FOR THE DEEP-SUBBARRIER CASE

Let us now consider the decay of an $A_0 = (A_c + A_C)$ nucleus through all open channels c, including the channel a. A decaying nucleus in the quasystationery state characterized by a spin J_i, its projection M_i, and a parity π_i will be described by the Gamow function $|\Psi^{J_iM_i\pi_i}\rangle$ that is normalized in the internal region to unity and which satisfies the Schrödinger equation (2) with a complex-valued energy $E_i = E_i^0 - \dfrac{i\Gamma_i}{2}$ $(\Gamma_i \ll E_i^0)$ and the asymptotic boundary condition corresponding to the emergence of diverging spherical waves in all open decay channels c [22, 24]; that is,

$$|\Psi^{J_iM_i\pi_i}\rangle \longrightarrow \sum_c \sqrt{\frac{\Gamma_{ic}k_{ic}}{2E_{ic}}}\left|A_c\left\{U_c\frac{G_c + iF_c}{R_c}\right\}\right\rangle, \qquad (90)$$

where $E_{ic} = E_i - \bar{E}_C - \bar{E}_c$, $k_{ic} = \sqrt{\dfrac{2m_cE_{ic}}{\hbar^2}}$, and Γ_{ic} is the partial width of the A_0 nucleus with respect to its decay through the channel c (it is related to the total width Γ_i by the relation $\Gamma_i = \sum_c \Gamma_{ic}$). Relation (90) is valid in the case where the decaying state of the A_0 nucleus is an isolated resonance such that the energy spacings $D^{J_iM_i\pi_i}$ between the neighboring (on the energy scale) decaying states characterized by the quantum numbers J_i, M_i, and π_i are much greater than the total decay widths Γ_i of the resonances in question.

Let us consider the problem inverse to that of the decay of the A_0 nucleus—that is, the problem where particle a is incident on a daughter nucleus A, so that nuclear reactions of the type in (1) occur. In the asymptotic region of large R_c values, the above function $|\Psi_a^+\rangle$, which corresponds to the scattering problem and which possesses the integrals of the motion J_i, M_i, and π_i, can be represented as [22]

$$|\Psi_a^+\rangle \longrightarrow \sum_c A_c\left\{\frac{B_c}{R_c}U_c[(G_c - iF_c)\delta_{ca} - \tilde{S}_{ca}(G_c + iF_c)]\right., \qquad (91)$$

where F_c and G_c are, respectively, the regular and the irregular radial Coulomb function. Their asymptotic forms are

$$F_c(R_c) \longrightarrow \sin\left(k_cR_c - \frac{l_c\pi}{2} + \delta_{l_c}^{\mathrm{C}}\right),$$
$$G_c(R_c) \longrightarrow \cos\left(k_cR_c - \frac{l_c\pi}{2} + \delta_{l_c}^{\mathrm{C}}\right), \qquad (92)$$

$\delta_{l_c}^{\mathrm{C}}$ being the Coulomb phase shift. In (91), the constant $B_c = \dfrac{i}{2}\sqrt{\dfrac{k_c}{2E_c}}$ is chosen from the condition requiring that the function $|\Psi_a^+\rangle$ be normalized to the delta function of energy; U_c is the channel function (74); and $\tilde{S}_{ca} = e^{-i(\delta_c^{\mathrm{C}} + \delta_a^{\mathrm{C}})}S_{ca}$, where S_{ca} is the S-matrix element (87).

The protonic, alpha-particle, and cluster decays of the ground state and low-lying excited states of A_0 nuclei are of a deep-subbarrier character, since the outer Coulomb turning point R_{c0}^{Coul} determined from the condition $E_{ic}^0 = V_0^{\mathrm{Coul}}(R_{c0}^{\mathrm{Coul}})$ is far off the point R_{cB} corresponding to the peak of the potential barrier. In this case, there exists the region $R_{cB} \le R_{c1} < R_{c0}^{\mathrm{Coul}}$, where $G_c(R_c) \gg F_c(R_c)$. Since the channel radius R_{c0}, off which one can disregard short-range nuclear forces, belongs to this region, it follows from Eq. (86) that the potential nuclear phase shift $\delta_c^{\mathrm{pot}} = \delta_c' - \delta_c^{\mathrm{Coul}}$ is much less than unity. In the region $R_{cB} \le R_c \le R_{c1}$, the complex asymptotic condition (90) reduces to the real condition

$$|\Psi_0^{I_iM_i\pi_i}\rangle \longrightarrow \sum_c \sqrt{\frac{\Gamma_{ic}k_{ic}}{2E_{ic}}}\left|A_c\left\{\frac{U_c}{R_c}G_c\right\}\right\rangle. \qquad (93)$$

This makes it possible to replace, over the entire region $R_c \le R_{c1}$, the quasistationary function $|\Psi^{I_iM_i\pi_i}\rangle$ corresponding to a complex-valued energy E_i by the time-independent function $|\Psi_0^{I_iM_i\pi_i}\rangle$ that is characterized by a real-valued energy virtually indistinguishable from the energy E_i^0 and by the asymptotic behavior as given by Eq. (93). If Eq. (86) is used, the asymptotic condition (91) can be recast, apart from a constant, into the asymptotic condition (93), whence it follows that, over the entire region $R_{cB} \le R_c \le R_{c1}$, the function $|\Psi_a^+\rangle$ can be represented in the form

$$|\Psi_a^+\rangle = -\sqrt{\frac{\Gamma_{ia}}{2\pi}}\frac{1}{E - E_i^0 + \dfrac{i\Gamma_i}{2}}|\Psi_0^{I_iM_i\pi_i}\rangle. \qquad (94)$$

The S-matrix element S_{aa} for the case of elastic scattering can be expressed in terms of the T-matrix element T_{aa} as

$$S_{aa} = 1 - 2\pi i T_{aa}, \tag{95}$$

where the explicit form of the matrix element T_{aa} can be obtained [22] from Eq. (11) by going over to a representation where the wave function $|\Psi_a^+\rangle$ possesses fixed quantum numbers I_i, M_i, and π_i and obeys the asymptotic boundary condition (94). The result is

$$T_{aa} = \left\langle \frac{\tilde{j}_a(R_a)}{R_a} \middle| \langle a_0 V_a | \Psi_a^+ \rangle e^{i\delta_a^C}, \right. \tag{96}$$

where $\tilde{j}_a(R_a)$ is a spherical Bessel function normalized to the delta function of energy. By using the theorem of the redistribution of potentials [1] and taking into account Eqs. (95) and (96), one can recast the matrix element $\tilde{S}_{aa}$ into the form [22]

$$\tilde{S}_{aa} = 1 - 2\pi i \left\langle \frac{\tilde{F}_a}{R_a} \middle| \langle a_0 (V_a - V_{a0}^{\mathrm{Coul}}) | \Psi_a^+ \rangle, \right. \tag{97}$$

where V_{a0}^{Coul} is a pointlike Coulomb potential and $\tilde{F}_a$ is a regular Coulomb radial function normalized to the delta function of energy. Substituting (94) into (97) and comparing the resulting expression with the expression for $\tilde{S}_{aa}$ corresponding to representation (87), we can find that the amplitude $\sqrt{\Gamma_{ia}}$ of the partial decay width can be represented as

$$\sqrt{\Gamma_{ia}} = \sqrt{2\pi} \left\langle \frac{\tilde{F}_a}{R_a} \middle| \langle a_0 (V_a - V_{a0}^{\mathrm{C}}) | \Psi_0^{I_i M_i \pi_i} \rangle. \right. \tag{98}$$

Considering that, in the region $R_c \le R_{c1}$, the function $|\Psi_0^{I_i M_i \pi_i}\rangle$ satisfies the Schrödinger equation

$$(E_i^0 - H)|\Psi_0^{I_i M_i \pi_i}\rangle = (E_i^0 - H_a - H_A - T_a - V_a)|\Psi_0^{I_i M_i \pi_i}\rangle,$$

we can reduce expression (98) to the form

$$\sqrt{\Gamma_{ia}} = \sqrt{2\pi} \left\langle \frac{\tilde{F}_a}{R_a} \middle| \langle a_0 (E_{ia} - T_a - V_{a0}^{\mathrm{C}}) | \Psi_0^{I_i M_i \pi_i} \rangle. \right. \tag{99}$$

By using the method developed above in going over from Eq. (41) to Eq. (43), we can recast expression (99) into the form

$$\sqrt{\Gamma_{ia}} = \sqrt{2\pi} \left(-\frac{\hbar^2}{2m_a} \right) \times \left[\tilde{F}_a(R_a) \frac{d f_{0a}(R_a)}{dR_a} - f_{0a}(R_a) \frac{d\tilde{F}_a(R_a)}{dR_a} \right], \tag{100}$$

where the standard cluster form factor $f_{0a}(R_a)$ is defined as $f_{0a}(R_a) = \langle a_0 | \Psi_0^{J_i M_i \pi_i} \rangle$ and where the radius R_a is taken in the region $R_{aB} < R_a \le R_{a1}$. Considering that, in this region, the channel functions $|a_0\rangle$ and $|c_0\rangle$ are strictly orthogonal for $c \ne a$ and using the asymptotic formula (93), we represent the form factor $f_{0a}(R_a)$ as $f_{0a}(R_a) = \sqrt{\frac{\Gamma_{ia} k_{ia}}{2E_{ia}}} G_c(R_a)$. Having substituted this representation of the form factor $f_{0a}(R_a)$ into the expression on the right-hand side of Eq. (100) and having used the theorem $\frac{dF_a}{dR_a} G_a - F_a \frac{dG_a}{dR_a} = k_{ia}$, which is valid for radial Coulomb functions, we reduce the right-hand side of Eq. (100) to $\sqrt{\Gamma_{ia}}$, which coincides with its left-hand side. This additionally confirms the correctness of Eq. (98). We note that the structure of expressions (98) and (100) conforms fully to the ideas of the R-matrix theory of nuclear reactions [15], provided that time-independent functions of the type $|\Psi_0^{I_i M_i \pi_i}\rangle$ are used for the R-matrix functions X_λ in the internal region of the decaying nucleus.

Since the operator W_{aa} is equal to unity in the asymptotic region of large R_a values, expression (100) can be reduced to the equivalent form

$$\sqrt{\Gamma_{ia}} = \sqrt{2\pi} \left(-\frac{\hbar^2}{2m_a} \right) \times \left[\tilde{F}_a(R_a) \frac{d\tilde{f}_{0a}(R_a)}{dR_a} - \tilde{f}_{0a}(R_a) \frac{d\tilde{F}_a(R_a)}{dR_a} \right], \tag{101}$$

where $\tilde{f}_{0a}(R_a) = \frac{1}{\sqrt{W_{aa}}} f_{0a}(R_a)$. This means that, in expression (100), the replacement of the cluster form factor $f_{0a}(R_a)$ by the new form factor $\tilde{f}_{0a}(R_a)$, according to the terminology adopted in [6–8], does not change the decay width Γ_{ia}. Previously, this conclusion was drawn in [25]. In [6–8], the radius R_a in a formula similar to that in (101) was continued to the internal region of the A_0 nucleus, where the operator W_{aa} differs substantially from unity. There, the multiparticle shell function $|\varphi_0\rangle$ for the A_0 nucleus was used for the function $|\Psi_0^{I_i M_i \pi_i}\rangle$, while the Coulomb function F_a was replaced by a function that satisfies a resonating-group-method equation of the type in (37) not allowing for polarization terms. Since the amplitude of the form factor $\tilde{f}_{0a}(R_a)$ considerably exceeds, in the internal region, that of the conventional cluster form factor $f_{0a}(R_a)$, it was conjectured in [6–8] that antisymmetrization effects enhance the widths with respect to the alpha-particle and cluster decays of nuclei. It should be emphasized that the method used there to continue

expression (101) to the internal region of the nucleus was not substantiated consistently. Therefore, it would be reasonable to investigate this problem on a sounder basis.

For the system in question, we consider the wave function $|\Psi_a^+\rangle$ that is given by Eqs. (12) and (18) and which corresponds to the scattering problem. By using Eqs. (79) and (89), this wave function taken at an energy E close to the resonance energy in the S-matrix element (87) can be reduced to the form

$$\begin{aligned}|\Psi_a^+\rangle &= |a_1\rangle\tilde{f}_a'^+(R_a)\\ &+ K_a^{-1}\sum_c |c_1\rangle G_c'\langle c_1|E-H|\varphi_0\rangle\langle\varphi_0|E-H|a_1\rangle|\tilde{f}_a'^+\rangle\\ &- K_a^{-1}|\varphi_0\rangle\langle\varphi_0|E-H|a_1\rangle|\tilde{f}_a'^+\rangle\\ &- \sum_{p\neq 0}\frac{|\varphi_p\rangle\langle\varphi_p|(E-H)\sum_c|c_1\rangle|\tilde{f}_c^+\rangle}{E-E_p}.\end{aligned} \tag{102}$$

If we make use of the approximation where the S-matrix resonances are isolated in the energy region under study and consider that all open channels correspond to the deep-subbarrier region, we can disregard the first and the last term in expression (102) and reduce it to the form

$$\begin{aligned}|\Psi_a^+\rangle &= \Bigg[\sum_c |c_1\rangle G_c'\langle c_1|E-H|\varphi_0\rangle\\ &- |\varphi_0\rangle\Bigg]\sqrt{\frac{\Gamma_{a0}}{2\pi}}\frac{1}{E-E_0+\Delta_0(E)+\dfrac{i\Gamma_0}{2}}.\end{aligned} \tag{103}$$

A comparison of this formula with that in (94) reveals that they fully coincide. For the function $|\Psi_0^{I_iM_i\pi_i}\rangle$ in (93)—it describes a decaying state in the internal region of the system—we have the expression

$$|\Psi_0^{I_iM_i\pi_i}\rangle = -|\varphi_0\rangle + \sum_c |c_1\rangle G_c'\langle c_1|E-H|\varphi_0\rangle, \tag{104}$$

which correctly reproduces the asymptotic condition (93) for the function $|\Psi_0^{I_iM_i\pi_i}\rangle$ if we consider that, in the region $R_{cB}\le R_c$, the function $\tilde{g}_c'^+$ coincides with the irregular Coulomb function normalized to a delta function of energy.

With the aid of expressions (104) and (75), we can now calculate the form factor $f_{0a}(R_a)$ appearing in the definition (100) of the width of the A_0 nucleus with respect to its decay through the channel a. The result is

$$f_{0a}(R_a) = -f_{0a}^{\rm sh} + \sqrt{W_{aa}}\sqrt{\overline{W}_{aa}}G_a'\langle a_1|E-H|\varphi_0\rangle, \tag{105}$$

where $f_{0a}^{\rm sh} = \langle a_0|\varphi_0\rangle$ is the cluster form factor for the shell state $|\varphi_0\rangle$. As was indicated above, the operator $\overline{W}_{aa}$ vanishes in the internal region of the decaying nucleus, whence it follows that, in this region, the form factor $f_{0a}(R_a)$ coincides with the form factor $f_{0a}^{\rm sh}$ in absolute value, their signs being opposite. In the asymptotic region of large R_a values, the operators $\overline{W}_{aa}$ and W_{aa} are equal to unity each, so that the form factor $f_{0a}(R_a)$ is then determined by the second term in expression (105), but this term reduces, in this region, to an expression corresponding to formula (93). On this basis, we conclude that it is the operator $\sqrt{\overline{W}_{aa}W_{aa}}$—rather than the operator $\sqrt{W_{aa}}$, which conforms to the ideas presented in [6–8]—that controls a transition of the form factor $f_{0a}(R_a)$ from the internal to the asymptotic region of a decaying nucleus. We note that, when we go over to the internal region of a decaying nucleus, the operator $\sqrt{\overline{W}_{aa}W_{aa}}$ decreases faster than the operator $\sqrt{W_{aa}}$.

The above investigation makes it possible to answer the question that was posed in [22] and which appears to be one of the key points in evaluating the alpha-particle-decay and cluster-decay widths of nuclei. In order to find these widths, it is necessary to know the regime of interpolation of the form factor $f_{0a}(R_a)$ from the internal (shell) region of a decaying nucleus, where the form factor $f_{0a}(R_a)$ coincides with the shell-model form factor $f_{0a}^{\rm sh}(R_a)$, to the external (cluster) region, where decay fragments have already been formed. In [22, 24], use was made of the interpolation regime where the amplitude of the form factor $f_{0a}(R_a)$ in the cluster region was set to the amplitude of the shell-model form factor $f_{0a}^{\rm sh}$ at the external maximum. The ideas developed in [6–8] actually imply a different interpolation regime, that in which the amplitude of the form factor $f_{0a}(R_a)$ in the cluster region is set to the amplitude of the "new" shell-model form factor $\dfrac{1}{\sqrt{W_{aa}}}f_{0a}^{\rm sh}(R_a)$ at its external maximum. Finally, the above expression (105) corresponds to the interpolation regime where the amplitude of the form factor $f_{0a}(R_a)$ in the cluster region coincides with the amplitude of the reduced shell-model form factor $\dfrac{1}{\sqrt{\overline{W}_{aa}W_{aa}}}f_{0a}^{\rm sh}(R_a)$ at its external maximum. This means that, qualitatively, the results presented in [6–8] remain in force upon the replacement of the operator $\dfrac{1}{\sqrt{W_{aa}}}$ by the operator $\dfrac{1}{\sqrt{\overline{W}_{aa}W_{aa}}}$.

It was shown in [22, 24] that the inclusion of superfluid correlations in evaluating the shell-model form factors f_{0a}^{sh} for alpha-particle and cluster decays of nuclei leads to a considerable increase in the amplitudes of these form factors; as a result, the interpolation regime used in those studies leads to theoretical alpha- and cluster-decay widths close to the corresponding experimental values. Provided that the same shell-model form factors f_{0a}^{sh} are used with allowance for the superfluid enhancement coefficients as obtained in [22, 24], a transition to the interpolation regime that follows from expression (105) leads to theoretical alpha- and cluster-decay widths that exceed the corresponding experimental values by one order of magnitude for alpha decay or by many orders of magnitude for cluster decay. This suggests that, for the widths being studied, the superfluid enhancement coefficients as obtained in [22, 24] are exaggerated and that it is necessary to find a physical motivation for reducing them considerably. It was shown in [22] that, for alpha decay, the superfluid enhancement coefficient is determined by the effective number N of those shell states of two-identical nucleons that are coherently summed when these nucleons form a Cooper pair. The quantity N in turn is determined by the range r_0 of effective nucleon interaction in the particle–particle channel. In the studies quoted in [22], the superfluid enhancement coefficients for alpha- and cluster-decay widths were computed under the assumption that the range r_0 is close to the range of short-range vacuum nucleon–nucleon interactions ($r_0 = 1.7$ fm). It was shown in [26], however, that the effective nucleon–nucleon interaction in the particle–particle channel receives a significant contribution from nucleon–nucleon interaction associated with collective-phonon exchange. The effective range of this interaction is about the nuclear range R_{A_0}. Obviously, the inclusion of this interaction must substantially reduce N and, hence, the scale of the superfluid enhancement of alpha- and cluster-decay widths. Of course, it is necessary to continue investigations along these lines.

12. CONCLUSION

By developing, on the basis of explicit expressions for projection operators, the theory of nuclear reactions induced by nucleon–nucleus and nucleus–nucleus collisions and the theory of the decay of nuclei emitting not only nucleons but also various clusters, it has become possible to obtain a number of new results for reaction amplitudes and decay widths with due regard to antisymmetrization effects and to establish relationships between different theoretical approaches in these realms. In particular, a relationship between the wave functions used in R-matrix theory and multiparticle shell-model wave functions for nuclei has been derived, which has made it possible to describe the regime of interpolation from the internal to the asymptotic region of a nucleus (knowledge of this regime is necessary for theoretically calculating the width of nuclear states with respect to their nucleonic and cluster decays). Here, the application of the ideas of the theory of open Fermi systems, which is in fact an extension of the theory of finite Fermi systems [27] and which employs the formalism of multiparticle Green's functions to describe the structural properties of nuclei and nuclear reactions within the same conceptual framework, has proved to be very fruitful in analyzing the structure of form factors in elastic-scattering channels.

REFERENCES

1. M. L. Goldberger and K. M. Watson, *Collision Theory* (Wiley, New York, 1964; Mir, Moscow, 1967).
2. K. Wildermuth and Y. C. Tang, *A Unified Theory of the Nucleus* (Academic, New York, 1977; Mir, Moscow, 1980).
3. S. Saito, Prog. Theor. Phys. (Suppl.) **62**, 11 (1977).
4. H. Horiuchi, in *Proceedings of the 4th International Conference on Clustering Aspects of Nuclear Structure, Chester, 1984.*
5. O. F. Nemets, V. G. Neudatchin, A. T. Rudchik, *et al.*, *Nucleon Clusters in Nuclei and Multinucleon-Transfer Nuclear Reactions* (Naukova Dumka, Kiev, 1988).
6. T. Fliessbach, Z. Phys. A **272**, 39 (1975).
7. T. Fliessbach and H. I. Mang, Nucl. Phys. A **263**, 75 (1976).
8. R. Blendowske, T. Fliessbach, and A. Wallizer, Nucl. Phys. A **464**, 1930 (1987).
9. H. Feshbach, Ann. Phys. (N.Y.) **5**, 357 (1958).
10. C. Mahaux and H. A. Weidenmuller, *Shell Model Approach to Nuclear Reactions* (North-Holland, Amsterdam, 1977).
11. A. I. Baz' *et al.*, Fiz. Élem. Chastits At. Yadra **3**, 2 (1972) [Sov. J. Part. Nucl. **3**, 1 (1972)].
12. A. I. Baz' and M. K. Zhukov, Yad. Fiz. **16**, 60 (1972) [Sov. J. Nucl. Phys. **16**, 31 (1972)].
13. S. G. Kadmensky, Yad. Fiz. **62**, 236 (1999) [Phys. At. Nucl. **62**, 201 (1999)].
14. S. G. Kadmensky, Yad. Fiz. **62**, 639 (1999) [Phys. At. Nucl. **62**, 592 (1999)].
15. A. M. Lane and R. G. Thomas, Rev. Mod. Phys. **30**, 257 (1958).
16. S. G. Kadmenskiĭ, Izv. Akad. Nauk SSSR, Ser. Fiz. **26**, 1194 (1962).
17. S. G. Kadmenskiĭ, Izv. Akad. Nauk SSSR, Ser. Fiz. **30**, 1349 (1966).
18. S. G. Kadmensky, Yad. Fiz. **60**, 28 (1997) [Phys. At. Nucl. **60**, 24 (1997)].
19. D. T. Khoa and O. M. Knjazkov, Z. Phys. A **328**, 67 (1987).
20. N. Levinson, K. Dan. Vidensk. Selsk. Mat. Fys. Medd. **45** (9) (1949).

21. A. Bohr and B. Mottelson, *Nuclear Structure* (Benjamin, New York, 1977).
22. S. G. Kadmensky and W. I. Furman, *Alpha Decay and Allied Nuclear Reactions* (Énergoatomizdat, Moscow, 1985).
23. F. G. Perey, *Direct Interactions and Nuclear Reaction Mechanisms* (Gordon and Breach, New York, 1963).
24. S. G. Kadmenskiĭ, S. D. Kurgalin, V. I. Furman, and Yu. M. Chuvil'skiĭ, Yad. Fiz. **56** (8), 80 (1993) [Phys. At. Nucl. **56**, 1038 (1993)].
25. I. Tonozuka and A. Arima, Nucl. Phys. A **323**, 45 (1970).
26. S. G. Kadmenskiĭ and P. A. Luk'yanovich, Yad. Fiz. **49**, 384 (1989) [Sov. J. Nucl. Phys. **49**, 238 (1989)].
27. A. B. Migdal, *Theory of Finite Fermi Systems and Applications to Atomic Nuclei* (Nauka, Moscow, 1983).

Translated by A. Isaakyan

Physics of Atomic Nuclei, Vol. 64, No. 3, 2001, pp. 440–447. Translated from Yadernaya Fizika, Vol. 64, No. 3, 2001, pp. 495–502.

90th ANNIVERSARY OF A.B. MIGDAL'S BIRTHDAY
NUCLEI

Behavior of Solutions to the Pion Dispersion Equation in the Complex Frequency Plane

V. A. Sadovnikova and M. G. Ryskin

Petersburg Nuclear Physics Institute, Russian Academy of Sciences, Gatchina, 188350 Russia

Received June 16, 2000

Abstract—Solutions to the pion dispersion equation in the complex plane of the pion frequency ω are obtained for symmetric nuclear matter. Three well-known solution branches—a sound, a pion, and an isobar one—exist on the physical sheet at the medium density below its critical value ($\rho < \rho_c$). For $\rho > \rho_c$, the fourth branch ω_c appears on the physical sheet. The condition $\omega_c^2 \le 0$ is valid for this branch (in general, $\mathrm{Re}\,\omega_c^2 \le 0$). This suggests ground-state instability, possibly associated with pion condensation. The behavior of these solutions is analyzed for various medium densities. The appearance of each solution on the physical sheet of the complex frequency plane and its disappearance are also studied. © *2001 MAIK "Nauka/Interperiodica".*

1. INTRODUCTION

Some time ago, much attention was given to the interesting pion-condensation phenomenon predicted in [1] (see [2–4]). This prediction was based on the observation that, with increasing density, one solution (we denote it by ω_c) to the pion dispersion equation begins to satisfy the condition $\omega_c^2(k) \le 0$ (at a nonzero momentum k). The emergence of such excitations in a medium requires a rearrangement of the ground state—there occurs a phase transition.

One version of this rearrangement consisted in that a pion condensate, specified in one way or another, was included in the ground state, and this resulted in the prediction of pion condensation. A great number of studies were devoted to searches for this phenomenon. The eventual opinion as expressed in the monograph [2] was that pion condensation reveals itself weakly and that it is unlikely to exist (at least, it is not observed) at normal nuclear densities. Nevertheless, this phenomenon can substantially affect the equation of state of matter at higher densities that can be realized in heavy-ion collisions and in neutron stars.

In this study, we consider in detail solutions to the pion dispersion equation in the complex plane of frequency ω. This will make it possible to obtain additional information about solutions to the dispersion equation. The pion dispersion equation has the form [1]

$$\omega^2 - k^2 - m_\pi^2 - \Pi(\omega, k, p_F) = 0, \qquad (1)$$

where Π is the pion self-energy in a medium. Solutions to this equation will be constructed on the physical sheet and on unphysical sheets of the complex plane of ω. The path from the physical sheet to unphysical sheets intersects the logarithmic cut that is determined by the form of the self-energy Π.

Our basic results are the following. We consider 0^- excitations in symmetric nuclear matter. At the equilibrium density, there are three solutions to the dispersion equation (1): the solution $\omega_s(k)$ describing the propagation of spin–isospin zero sound, the isobar solution $\omega_\Delta(k)$, and the pion solution $\omega_\pi(k)$.

On the physical sheet of the complex plane of ω, Eq. (1) has logarithmic cuts determined by the form of the self-energy Π. For the sake of clarity, we assume that the width of the $\Delta_{33}(1232)$ isobar with respect to its decay into a pion and a nucleon is equal to its vacuum value of $\Gamma_\Delta = 115$ MeV. In this case, all solutions to the dispersion equation are shifted from the real (or imaginary) axis to the complex plane. Owing to this, it is easier to trace the behavior of the solutions as functions of k. In cases of importance, we will consider the effect of Γ_Δ on the solutions $\omega_i(k)$.

The branches $\omega_s(k)$, $\omega_\pi(k)$, and $\omega_\Delta(k)$ lie on the physical sheet at the momenta k within the intervals $0 \le k \le k_f$, where k_f is dependent on the branch type, the medium density, and the coupling constants. For $k \ge k_f$, the solutions go through the cut to unphysical sheets. Everywhere on the physical sheet, the aforementioned solutions are such that $\omega_i^2 > 0$ for $\Gamma_\Delta = 0$ and $\mathrm{Re}\,\omega_i^2 > 0$ for $\Gamma_\Delta \ne 0$.

Our investigation shows that there are sets of solutions on unphysical sheets. With increasing density, some branches go over to the physical sheet. By way of example, we indicate that, for $p_F \ge 283$ MeV (for our choice of parameter values), a fourth solution branch $\omega_c(k)$ appears on the physical sheet. It issues from the same point as $\omega_\pi(k)$, moving in an unphysical sheet. It goes over to the physical sheet at $k = k_1$ and returns to the same unphysical sheet at $k = k_2$. The momenta k_1 and k_2 are dependent on the density: at the Fermi

momentum corresponding to the critical density, we have $k_1 = k_2 \simeq 1.8m_\pi$. It is precisely for $\omega_c(k)$ that the condition $\mathrm{Re}\,\omega_c^2(k) \leq 0$ is satisfied. The solutions depend on the isobar width: at $\Gamma_\Delta = 0$, the values of ω_c on the physical sheet are purely imaginary and $\omega_c^2 \leq 0$.

We denote by ρ_c the critical density at which the branch ω_c first appears on the physical sheet. We have obtained $\rho_c = 1.2\rho_0$, with $\rho_0 = 2p_{F0}^3/3\pi^2$, where $p_{F0} = 268$ MeV, being the equilibrium nuclear density. The critical density ρ_c is determined by the parameters of the theory, by the choice of models for the πNN and $\pi N\Delta$ vertices, by the effective charges in these vertices, and by the choice of the self-energy operators (characterized by the degree to which relativistic effects are taken into account). In the present study, we do not aim at calculating anew ρ_c—our objective is to demonstrate qualitatively how the solution branch that is responsible for the rearrangement of the ground state appears on the physical sheet. For this reason, we decided on the customary nonrelativistic expressions for all self-energy operators [1, 5, 6], with the exception of the scalar part of the self-energy operator (Subsection 2.1).

Our investigation reveals that $\omega_c(k)$ has a negative imaginary part on the physical sheet. This is indicative of extremely strong damping with time rather than of the accumulation of the corresponding excitations. However, the fact that, at the critical density $\rho = \rho_c$, there appears a solution such that $\omega_c^2(k) = 0$ for $k \neq 0$ means that, in the system being considered, the ground state, which was used to derive the dispersion Eq. (1), must rearrange, whereupon (at $\rho > \rho_c$) the sign of the imaginary part of $\omega_c(k)$ becomes immaterial.

If, in addition, we consider physical processes like that in Fig. 1, where an external field interacts with a pion in a medium, the emergence of $\omega_c(k)$ generates an irremovable singularity in the integral with respect to the intermediate energy in the loop in Fig. 1 (see below). The divergence of such a diagram can have various physical consequences depending on the type of external field. By way of example, we indicate that, in calculating a scalar quark condensate in a medium, a closed circle in Fig. 1 stands for the interaction of the quark current with the pion [7]; here, the divergence in the integral is due to the restoration of chiral symmetry in nuclear matter at near-critical densities—in our case, the densities in question slightly exceed nuclear densities since $\rho_c = 1.2\rho_0$.

The ensuing exposition is organized as follows. First, we consider expressions for the particle–hole self-energy operator Π. Next, we present solutions to the pion dispersion equation on the physical sheet and on unphysical sheets of the complex plane of ω: we show how the solution branches go to unphysical sheets across the logarithmic cuts of the self-energy operator. We discuss in detail the behavior of the condensate solution ω_c at various values of the density ρ and of the isobar width Γ_Δ.

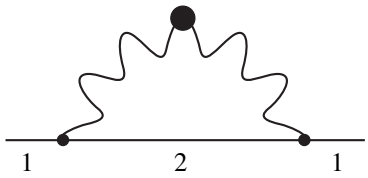

Fig. 1. Diagram representing the interaction of an external field with pions in a medium.

2. SELF-ENERGY OPERATOR AND ITS SINGULARITIES

In this section, we consider the expression that we use for the self-energy operator Π, because it differs somewhat from the conventional expressions from [1, 8]. The total self-energy operator Π is represented as the sum of the scalar (Π_S) and the vector (Π_P) term:

$$\Pi(\omega, k) = \Pi_S(\omega, k) + \Pi_P(\omega, k). \tag{2}$$

2.1. Scalar Self-Energy Operator

The scalar self-energy operator Π_S is constructed on the basis of the Gell-Mann–Oakes–Renner (GMOR) relation [9] for the pion mass in matter:

$$m_\pi^{*2} = -\frac{\langle NM|\bar{q}q|NM\rangle(m_u + m_d)}{2f_\pi^{*2}}. \tag{3}$$

Here, $\kappa = \langle NM|\bar{q}q|NM\rangle$ is the scalar quark condensate calculated in nuclear matter; m_u and m_d are the masses of the u and d quarks, respectively; and f_π^* is the pion decay constant in nuclear matter.

The quantity κ can be expanded into a power series in the density ρ as [7, 10]

$$\kappa = \kappa_0 + \rho\langle N|\bar{q}q|N\rangle + \text{higher order terms}, \tag{4}$$

where $\kappa_0 = -0.03$ GeV^3 is the vacuum value of the scalar quark condensate and $\langle N|\bar{q}q|N\rangle \simeq 8$ is the matrix element of the scalar quark condensate between the nucleon states. In this problem, it is sufficient to retain the first two terms in expansion (4) (this corresponds to the gas approximation for κ [10]). From (3), we then obtain (here, we assume that $f_\pi^* = f_\pi = 92$ MeV)

$$m_\pi^{*2} = m_\pi^2 - \rho\frac{\langle N|\bar{q}q|N\rangle(m_u + m_d)}{2f_\pi^2}. \tag{5}$$

On the other hand, we can define m_π^{*2} in the dispersion Eq. (1) as

$$m_\pi^{*2} = m_\pi^2 + \Pi(\omega, k = 0). \tag{6}$$

Considering that $\Pi_P(k = 0) = 0$ and comparing (5) and (6), we arrive at

$$\Pi_S = -\rho\frac{\langle N|\bar{q}q|N\rangle(m_u + m_d)}{2f_\pi^2}. \quad (7)$$

We note that m_π^* decreases with increasing medium density. This reflects the tendency toward the restoration of chiral symmetry in a dense medium. When the mass m_π^* becomes small, it is necessary to take into account the next terms in expansion (4).

Expression (7) differs significantly from the expression constructed on the basis of the vacuum *S*-wave amplitudes for pion–nucleon scattering [8]. First, the signs of Π_S are different. A positive value of Π_S assumes an increase in the pion mass with increasing density. In terms of the GMOR relation (3), the pion can become heavier in a medium in the following case. The constant f_π^* in (3) can depend on κ. Within the Nambu–Jona-Lasinio model [11], f_π^* is proportional to κ, while the pion mass is in inverse proportion to κ (in the case of $f_\pi^* = f_\pi = \text{const}$, we would have $m_\pi^{*2} \propto \kappa$). At extremely low densities, we accordingly have

$$\Pi_S = \rho\frac{\langle N|\bar{q}q|N\rangle(m_u + m_d)}{2f_\pi^2}. \quad (8)$$

However, this approximation is valid only as long as, at very low densities, the pion remains the lightest particle and its radius $r_\pi \sim 1/f_\pi$ is less than the confinement radius.

2.2. P-Wave Self-Energy Π_P

Following [1, 2, 6, 8], we represent Π_P as the sum of the nucleon and the isobar self-energy operator; that is,

$$\Pi_P = \Pi_N + \Pi_\Delta,$$

where Π_N (Π_Δ) is the sum of the nucleon–hole (isobar–hole) loops without a pion in the intermediate state. Let us now consider the known expressions [1, 2, 8] for Π_N and rewrite them in a form that is more convenient for our purposes. We will also analyze the analytic properties of Π_N and Π_Δ in the complex plane of frequency:

$$\Pi_N = \Pi_N^0\frac{1 + (\gamma_\Delta - \gamma_{\Delta\Delta})\Pi_\Delta^0/k^2}{E},$$

$$\Pi_\Delta = \Pi_\Delta^0\frac{1 + (\gamma_\Delta - \gamma_{NN})\Pi_N^0/k^2}{E}, \quad (9)$$

$$E = 1 - \gamma_{NN}\frac{\Pi_N^0}{k^2} - \gamma_{\Delta\Delta}\frac{\Pi_\Delta^0}{k^2} + (\gamma_{NN}\gamma_{\Delta\Delta} - \gamma_\Delta^2)\frac{\Pi_N^0\Pi_\Delta^0}{k^4}.$$

The contribution of nucleon–hole loops is given by

$$\Pi_N^0(\omega, k) = \mathrm{tr}\int\frac{d^3p}{(2\pi)^3}\Gamma_{\pi NN}^2 \times\left[\frac{\theta(p - p_F)\theta(p_F - |\mathbf{p} + \mathbf{k}|)}{E_{\mathbf{p}+\mathbf{k}} - E_p - \omega} + \frac{\theta(p_F - p)\theta(|\mathbf{p} + \mathbf{k}| - p_F)}{E_p - E_{\mathbf{p}+\mathbf{k}} + \omega}\right], \quad (10)$$

where $E_p = p^2/2m$. A similar expression can be written for Π_Δ^0.

The vertex of pion production by a baryon, $\Gamma_{\pi NB}$, is taken in the conventional form

$$\Gamma_{\pi NB} = \Gamma_{\pi NB}^0 d_B(k),$$
$$\Gamma_{\pi NN}^0 = i\frac{g_A}{\sqrt{2}f_\pi}\chi^*(\boldsymbol{\sigma}\cdot\mathbf{k})\chi, \quad (11)$$
$$\Gamma_{\pi N\Delta}^0 = f_{\Delta/N}i\frac{g_A}{\sqrt{2}f_\pi}\chi^*(\mathbf{S}_\alpha^+\cdot\mathbf{k})\chi^\alpha,$$

where χ are the nucleon Pauli 2-spinors, $\boldsymbol{\sigma}$ is the nucleon spin operator; $\mathbf{S}^+$ is the operator transforming the spin of 3/2 into the spin of 1/2, and $f_{\Delta/N} \simeq 2$ [8]. A nonzero baryon size is taken into account through the form factor $d_B(k) = (1 - m_\pi^2/\Lambda_B^2)/(1 + k^2/\Lambda_B^2)$.

The constants γ_{NN}, γ_Δ, and $\gamma_{\Delta\Delta}$ in (9) are expressed in terms of the effective coupling constants for quasiparticles as [1, 5]

$$\gamma_{NN} = C_0 g'_{NN}\left(\frac{\sqrt{2}f_\pi}{g_A}\right)^2,$$

$$\gamma_\Delta = \frac{C_0 g'_{N\Delta}}{f_{\Delta/N}}\left(\frac{\sqrt{2}f_\pi}{g_A}\right)^2, \quad \gamma_{\Delta\Delta} = \frac{C_0 g'_{\Delta\Delta}}{f_{\Delta/N}^2}\left(\frac{\sqrt{2}f_\pi}{g_A}\right)^2,$$

where $C_0 = \pi^2/(p_F m)$ is the density of states at the Fermi surface [1, 2].

We present our results for the following parameter values: $\Lambda_N = 0.667$ GeV, $\Lambda_\Delta = 1$ GeV; $g'_{NN} = 1.0$, $g'_{N\Delta} = 0.2$, $g'_{\Delta\Delta} = 0.8$, and $g_A = 1$.

We can perform integration in (10) by two methods.

(i) We can integrate the first and the second term separately. For Π_N^0, we then obtain

$$\Pi_N^0(\omega, k) = -4\left(\frac{g_A}{\sqrt{2}f_\pi}\right)^2 k^2[\Phi_N(\omega, k) + \Phi_N(-\omega, k)]d_N^2(k). \quad (12)$$

For $0 \le k \le 2p_F$, the function $\Phi_N(\omega, k)$ appearing in (12) has the form

$$\Phi_N(\omega, k) = \frac{m}{k}\frac{1}{4\pi^2}\left(\frac{-\omega m + kp_F}{2} - \omega m \ln\left(\frac{\omega m}{\omega m - kp_F + k^2/2}\right)\right. \quad (13)$$
$$\left. + \frac{(kp_F)^2 - (\omega m - k^2/2)^2}{2k^2}\ln\left(\frac{\omega m - kp_F - k^2/2}{\omega m - kp_F + k^2/2}\right)\right),$$

while, for $k \ge 2p_F$, it reduces to the Migdal function

$$\Phi_N(\omega, k) = \frac{1}{4\pi^2}\frac{m^{*3}}{k^3}\left[\frac{a^2 - b^2}{2}\ln\left(\frac{a+b}{a-b}\right) - ab\right], \quad (14)$$

where $a = \omega - (k^2/2m)$ and $b = kp_F/m$.

Let us consider the cuts of $\Pi_N^0(\omega, k)$ (12)–(14) in the complex plane of ω. It is clear that, for $k \le 2p_F$, there are two cuts (we denote them by I and II). The cuts stem from the first and the second logarithm in (13) and occur in the intervals

$$\text{(I)}\ 0 \le \omega \le \frac{kp_F}{m} - \frac{k^2}{2m};$$
$$\text{(II)}\ \frac{kp_F}{m} - \frac{k^2}{2m} \le \omega \le \frac{kp_F}{m} + \frac{k^2}{2m}. \quad (15)$$

The cuts of the function $\Phi_N(-\omega, k)$ lie on the negative semiaxis symmetrically with respect to the cuts in (15), and Π_N^0 is symmetric with respect to the transformation $\omega \longleftrightarrow -\omega$. Therefore, Π_N^0 has four cuts in the complex plane of ω, which are shown in Fig. 2.

When the momentum k grows, approaching $2p_F$, cut I becomes shorter and degenerates into a point at $k = 2p_F$; for $k > 2p_F$, there is only one cut, as follows from (14).

(ii) The other method for performing integration in (10) is based on a more compact expression obtained for Π_N^0 upon the substitution $\theta(p - p_F) = 1 - \theta(p_F - p) = 1 - n(p)$ in (10). For Π_N^0, we then arrive at the well-known expression in terms of the Migdal function [1, 2, 8]. This expression has the same form for all values of the momentum k. Of course, the same expression (12) is obtained for the two versions of integration. In the case being considered, however, Π_N^0 has two overlapping cuts in the complex plane ω instead of four. The cuts cease to overlap for $k > 2p_F$. It can easily be shown [12] that cut I is merely the sum of two overlapping cuts. The reason for which so much attention has been given to the well-known [13] analytic properties of the self-energy operator is the following. In constructing solutions to the dispersion Eq. (1), it is much more convenient to deal with one cut than with two overlapping cuts. When a solution goes to an unphysical sheet under cut I, we can explicitly indicate (display), in the first version, that sheet of the Riemann surface where the solution resides. In the second version, we obtain the same solution, but it simultaneously resides on the upper sheet of one cut and on the lower sheet of the other cut, which overlaps the first one. Since this encumbers a graphical presentation, we use the expressions (12)–(14) for Π_N^0.

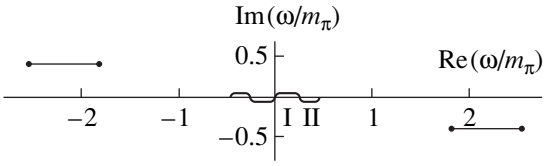

Fig. 2. Cuts (15) and (16) of the self-energy operators Π_N^0 and Π_Δ^0 on the physical sheet of the complex plane of ω at p_F = 290 MeV and $k = m_\pi$.

For $\Pi_\Delta^0(\omega, k)$, we have a conventional expression in terms of the Migdal function (14) with $a = \omega - (k^2/2m) - \Delta m$ and $b = kp_F/m$. Figure 2 shows the cuts of the function $\Phi_\Delta^0(\omega, k)$. For $\omega \ge 0$, the cut lies in the interval

$$\frac{k^2}{2m} + \Delta m - \frac{kp_F}{m} \le \omega \le \frac{k^2}{2m} + \Delta m + \frac{kp_F}{m}. \quad (16)$$

We recall that the cut is shifted to the complex plane by $-i\Gamma_\Delta/2$.

In this study, we use the Landau expression for the effective mass of the nucleon [14]:

$$m = \frac{m_0}{1 + (2mp_F/\pi^2)f_1}. \quad (17)$$

The parameter f_1 is fixed by the condition $m(p_F = p_{F0}) = 0.8m_0$, where m_0 = 940 MeV. We assume that the mass difference between the isobar and the nucleon does not change in the medium: $\mathrm{Re}(\Delta m)$ = 292 MeV.

3. SOLUTIONS TO THE DISPERSION EQUATION

In this section, we present solutions to the dispersion Eq. (1). Using the same parameter values as in the preceding section, we have found that ω_c appears on the physical sheet of the complex plane of ω at p_F = 283 MeV. The results of our calculations for the zero-sound $\omega_s(k)$, the pion $\omega_\pi(k)$, and the isobar $\omega_\Delta(k)$ branch are given for Γ_Δ = 115 MeV at p_F = 268 MeV and p_F = 290 MeV. For cases of interest, we also consider other values of p_F and Γ_Δ. We now proceed to discuss specific results.

Branch $\omega_s(k)$. Figure 3*a* displays the solutions $\omega_s(k)$. This branch begins at the point $\omega_s(k = 0) = 0$; with

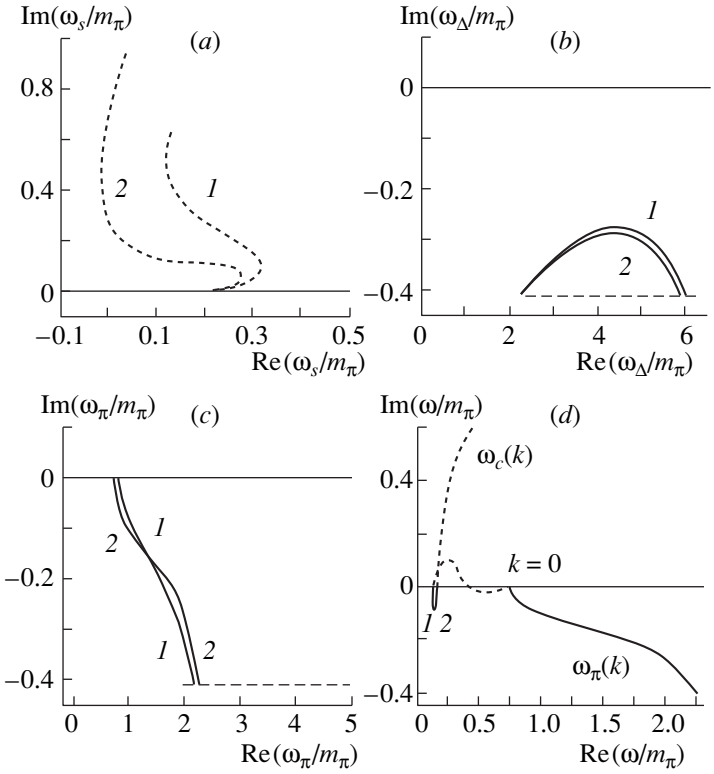

Fig. 3. Branches of solutions to Eq. (1) in the complex plane of ω: (*a*) zero-sound wave $\omega_s(k)$, (*b*) isobar branch $\omega_\Delta(k)$ [the horizontal dashed line depicts cut (16) at $p_F = 290$ MeV for the momentum value at which ω_Δ goes under the cut], (*c*) pion branch $\omega_\pi(k)$ (the horizontal dashed line has the same meaning as in Fig. 3*b*), and (*d*) pion [$\omega_\pi(k)$] and condensate [$\omega_c(k)$] branches at $p_F = 290$ MeV. The solid curves *1* (*2*) correspond to $p_F = 280$ (290) MeV. The dashed curves *1* and *2* lie on unphysical sheets.

increasing k, it moves nearly along the real axis and, at $k_f = 0.436m_\pi$ for $p_F = 268$ MeV ($k_f = 0.430m_\pi$ for $p_F = 290$ MeV), goes over under cut II (15) to an unphysical sheet of the second logarithm in (13). In Fig. 3*a*, the solution in question is presented up to $k = 1.6m_\pi$ for both values of p_F. It can be continued still further.

We note that the point where ω_s goes over to another sheet [k_f and $\omega_s(k_f)$] depends on g'_{NN}. With decreasing g'_{NN}, k_f and $\omega_s(k_f)$ also decrease (see Appendix).

Branch $\omega_\Delta(k)$. The isobar branch $\omega_\Delta(k)$ (see Fig. 3*b*) issues from the point $\omega = \Delta m$ at $k = 0$ and terminates under the isobar cut (16) at $k = 5.1m_\pi$ for $p_F = 268$ MeV ($k = 4.8m_\pi$ for $p_F = 290$ MeV).

Branch $\omega_\pi(k)$. The pion branch (Fig. 3*c*) starts at the point m_π^* (5):

$$\omega_\pi^2 = m_\pi^{*2} = m_\pi^2 + \Pi_S = m_\pi^2 - \rho\frac{\langle N|\bar{q}q|N\rangle(m_u + m_d)}{2f_\pi^2}. \quad (18)$$

As was mentioned in Subsection 2.1, the point $\omega_\pi(k = 0)$ at which this branch emerges is shifted to the lower values if we use the GMOR relation for m_π^* [9]. The pion is lighter in nuclear matter than in a vacuum: $m_\pi^*(k = 0) = 0.8m_\pi$ ($0.74m_\pi$) at $p_F = 268$ (290) MeV. The pion branch terminates under the isobar cut—this corresponds to the picture of pion decay into a nucleon hole and an isobar. This occurs at $k = 3.5m_\pi$ for $p_F = 268$ MeV ($k = 3.8m_\pi$ for $p_F = 290$ MeV).

Branch $\omega_c(k)$. With increasing matter density, there arises yet another solution $\omega_c(k)$ on the physical sheet. Figure 3*d* shows the pion branch, $\omega_\pi(k)$, and the condensate branch $\omega_c(k)$ at $p_F = 290$ MeV. That section of $\omega_c(k)$ which is shown by the dashed curve lies on the upper unphysical sheet of the logarithmic cut I (Fig. 2). The branch $\omega_c(k)$ issues from $k = 0$ at the same point as $\omega_\pi(k)$ and moves over the unphysical sheet. The branch appears on the physical sheet at $k = k_1 = 1.3m_\pi$ and returns on the same unphysical sheet at $k = k_2 = 2.3m_\pi$.

We can trace the position of the other solutions in the momentum interval (k_1, k_2) and confirm that ω_c does not coincide with any known branch (ω_s, ω_π, and ω_Δ).

At $k = 0$, all logarithmic cuts of the first and the second logarithm in (13) degenerate into a point, and the dispersion Eq. (1) can have a solution that issues from this point on the physical sheet and on other sheets as well. The branch $\omega_c(k)$ moves over the upper (with respect to the physical sheet) sheet and appears on the physical sheet in the region of the momenta k and p_F considered here. A solution that moves over the lower

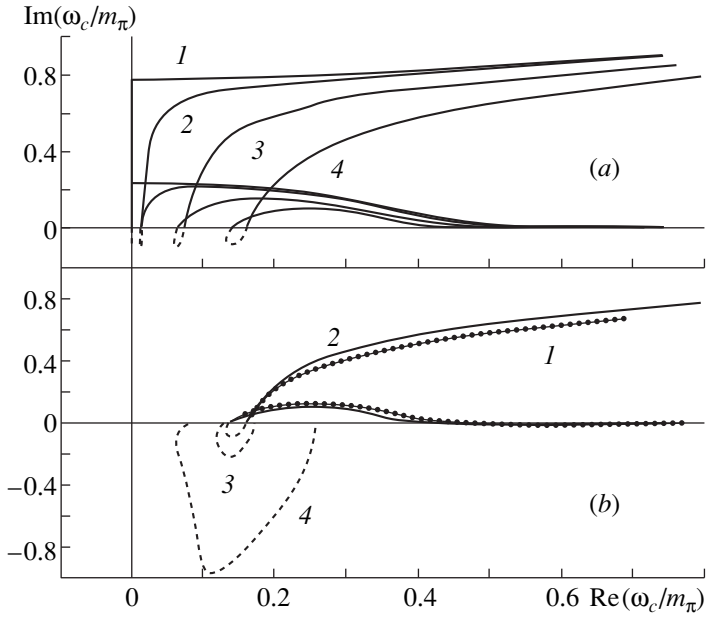

Fig. 4. Condensate branch $\omega_c(k)$ in the complex plane of ω [the dashed (solid) curves represent those parts of the solution branches that lie on the physical (unphysical) sheet]: (*a*) branch $\omega_c(k)$ at $p_F = 290$ MeV for the isobar-width values of $\Gamma_\Delta =$ (*1*) 0, (*2*) 10, (*3*) 50, and (*4*) 115 MeV and (*b*) branch $\omega_c(k)$ at $\Gamma_\Delta = 115$ MeV for the Fermi momentum values of $p_F =$ (*1*) 280, (*2*) 290, (*3*) 300, and (*4*) 360 MeV. Only the parts occurring on the physical sheet are displayed for the curves *3* and *4*. Curve *1* for $p_F = 280$ MeV completely lies on an unphysical sheet.

sheet, not appearing on the physical sheet (this solution is of no interest for this reason, but it supplements the pattern of solutions), was presented in [12].

In just the same way as other branches, the branch ω_c greatly depends on the isobar width Γ_Δ. As the isobar width decreases, the isobar cut comes closer to the real axis; as a result, the branches ω_s, ω_π, and ω_Δ will then have imaginary parts that are accordingly reduced. At $\Gamma_\Delta = 0$, the branches ω_s, ω_π, and ω_Δ become real. At the same time, the branch $\omega_c(k)$ approaches the imaginary axis with decreasing Γ_Δ (Fig. 4*a*); at $\Gamma_\Delta = 0$, we arrive at a pure imaginary solution on the physical sheet: $\omega_c^2 \leq 0$.

Figure 4*b* displays the branch $\omega_c(k)$ for various densities ($p_F = 280$, 290, 300, 360 MeV). At $p_F = 280$ MeV (that is, at $\rho < \rho_c$), the solution (curve *1*) has not yet appeared on the physical sheet.

It was mentioned above that, owing to the invariance of expression (1) under the substitution $\omega \longleftrightarrow -\omega$, both $\omega_i(k)$ and $-\omega_i(k)$ are solutions to the dispersion equation. Let us examine Fig. 1, which was discussed in the Introduction. The integral with respect to the energy of the internal loop corresponds to integration along the real axis in Fig. 4. At the critical density ρ_c, the branch $\omega_c(k)$ is tangent to the real axis at one point. At $\rho = \rho_c$ and $\Gamma_\Delta = 0$, $\omega_c(k)^2 = 0$, and the branch $\omega_c(k)$ is tangent to the real axis at the origin. The symmetric branches $\omega_c(k)$ and $-\omega_c(k)$ then grasp the integration contour at $k = k_1 = k_2$. As a result, there arises an irremovable singularity leading to the divergence of the relevant integral [7]. If $\Gamma_\Delta \neq 0$, the integration leads to a result depending on Γ_Δ and having a characteristic density dependence near ρ_c [7, 15].

It would be of interest to discuss the physical content of $\omega_c(k)$, but this solution occurs on an unphysical sheet; its very emergence on the physical sheet implies a phase transition in nuclear matter. Nevertheless, it is possible to consider in more detail that cut of the self-energy operator through which this solution appears on the physical sheet. Let us return (15) and rewrite cut II in the form

$$\frac{k^2 + 2kp_F(1 - k/p_F) + p_F^2}{2m} - \frac{p_F^2}{2m} \leq \omega \leq \frac{k^2 + 2kp_F + p_F^2}{2m} - \frac{p_F^2}{2m}. \quad (19)$$

We can interpret this cut as the excitation of a hole with momentum p_F and a particle with momentum $\mathbf{k} + \mathbf{p}_F$, the angle between the vectors $\mathbf{k}$ and $\mathbf{p}_F$ changing in the interval $1 - k/p_F \leq \cos\theta \leq 1$.

Cut I as specified by (15) corresponds to the excitation of a particle with momentum p_F and a hole with momentum $\mathbf{p}_F - \mathbf{k}$, the angle between the vectors $\mathbf{p}_F$ and $\mathbf{k}$ changing in the interval $k/p_F \leq \cos\theta \leq 1$. Since ω_c appears through cut I, the instability of the ground state is realized owing to the transition of nucleons from occupied states below the Fermi surface to the Fermi surface. This result is supplemented with the result of an analysis of the Pomeranchuk stability conditions in

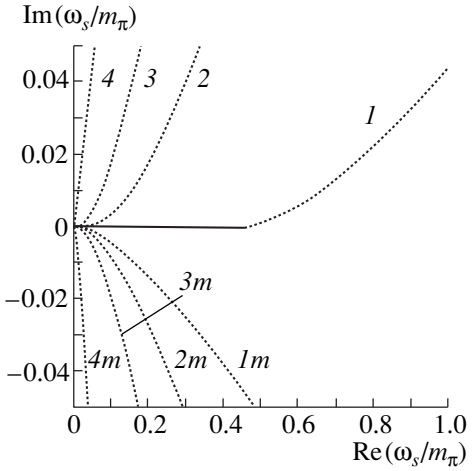

Fig. 5. Zero sound in nucleon matter (p_F = 268 MeV) in the complex plane of ω for g' = (*1*) 1.0, (*2*) 0.3, (*3*) 0.1, and (*4*) 0.0001 and g' = (*1m*) –1.0, (*2m*) –0.3, (*3m*) –0.1, and (*4m*) –0.0001.

the Appendix. There, we exhibit the solution branch ω_P that ensures instability of the ground state when the values of the strength constants do not satisfy the stability condition. It turns out that ω_P comes on the physical sheet through cut I as well.

4. CONCLUSION

We have considered in detail solutions to the pion dispersion equation. We have shown that, in addition to known 0^- solution branches (a zero-sound, a pion, and an isobar one), there is a fourth branch $\omega_c(k)$ satisfying the condition $\omega_c^2 \le 0$. Therefore, it is the solution that is responsible for the instability of the matter ground state. This instability can be treated, for example, as the onset of pion condensation. We have demonstrated that, at densities below the critical value, $\rho < \rho_c$, the branch $\omega_c(k)$ lies on an unphysical sheet; it appears on the physical sheet at $\rho \ge \rho_c$.

ACKNOWLEDGMENTS

We are grateful to E.G. Drukarev and E.E. Saperstein for stimulating discussions.

This work was supported by the Russian Foundation for Basic Research (project no. 00-02-16853).

APPENDIX

The method the we have used to analyze the above solutions can be applied to a well-known case. Let us consider zero-sound waves in symmetric nuclear matter that consists of nucleons.

The stability condition for such waves in matter was obtained by Pomeranchuk in 1958 [16]. The meaning of this condition is that the frequencies of excitations in the system must be positive. In symmetric nuclear matter governed by effective interaction between quasiparticles (in absence of tensor forces [17]), the stability condition takes the same form for all effective-interaction constants [5]:

$$1 + \frac{2g'}{2l+1} > 0. \qquad \text{(A.1)}$$

We consider the zeroth harmonics of the interaction (l = 0). The stability condition then assumes the form

$$1 + 2g' > 0, \quad g' > -1/2. \qquad \text{(A.2)}$$

Saperstein proposed checking the validity of condition (A.2) in our case. In terms of the solutions to the dispersion equation for the zero-sound wave, we have

$$1 + 4C_0 g'[\Phi_N(\omega, k) + \Phi_N(-\omega, k)] = 0. \qquad \text{(A.3)}$$

The breakdown of condition (A.2) would then be associated with the emergence of a divergent solution at $g' < -1/2$. The function Φ_N is defined by Eqs. (13) and (14). If, for a Fermi liquid consisting of a single particle species, we consider the limit $k, \omega \longrightarrow 0$ and denote $s = \omega m/p_F k$, Eq. (A.3) reduces to the well-known equation for sound frequencies,

$$\frac{1}{f_0} = \frac{s}{2}\ln\frac{s+1}{s-1} - 1,$$

where f_0 is the coupling constant for the scalar or the spin–spin interaction of quasiparticles. We will solve Eq. (A.3) by varying g'. It is clear from Fig. 5 that, as g' is reduced from unity to zero, the branches go over to an unphysical sheet at lower momenta k_f and lower values of $\omega_s(k_f)$. The dotted curves in Fig. 5 show those segments of the branches that lie on the unphysical sheet. We emphasize once again that the branch ω_s goes to the unphysical sheet through cut II (15). For negative values of g', we obtain solution branches lying in the lower half-plane of the same unphysical sheet.

We define $v = 1/g'$. The results of the calculations then show (see Fig. 5) that, when v decreases smoothly from large values of 10^4 to zero and further to -10^4 (v = 10^4, 10, 10/3, 1, –1, –10/3, –10, -10^4), the solution branches successively transform into one another ($4 \longrightarrow 3 \longrightarrow 2 \longrightarrow 1$; upon the reversal of the sign of v, we move to the branch 1*m* and further have the sequence $2m \longrightarrow 3m \longrightarrow 4m$). The branch $\omega_s(k)$ does not exhibit any singularity that could result in a phase transition.

There is, however, yet another set of solution branches for (A.3); we denoted it by $\omega_P(k)$. These are pure imaginary solutions [$\mathrm{Re}(\omega_P(k)) = 0$], which lead to instability. They lie on an unphysical sheet for $g' > -1/2$ and appear on the positive imaginary semiaxis of the physical sheet for $g' < -1/2$ (Fig. 6). These branches come to the physical sheet from under cut I—that is, from the lower sheet of the Riemann surface of the first logarithm in (13). From Fig. 6, it can be seen that, for $g' > -1/2$, these solutions are under the cut (on the lower

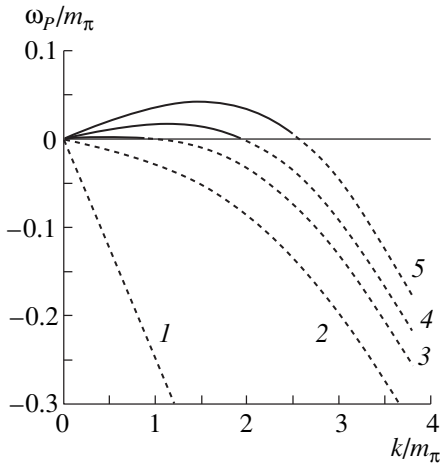

Fig. 6. Solution branches $\omega_P(k)$ at g' = (*1*) –0.2, (*2*) –0.45, (*3*) –0.51, (*4*) –0.55, and (*5*) –0.6.

unphysical sheet) and that, for $g' < -1/2$ $\omega_P(k)$, they appear on the physical sheet in the upper half-plane. Thus, we have demonstrated that divergent solutions appear among solutions to Eq. (A.3) for $g' < -1/2$; that is, the matter ground state is unstable at those values of the constants g' that do not satisfy condition (A.2).

REFERENCES

1. A. B. Migdal, Rev. Mod. Phys. **50**, 107 (1978); Zh. Éksp. Teor. Fiz. **63**, 1993 (1972) [Sov. Phys. JETP **34**, 1184 (1972)].
2. A. B. Migdal, D. N. Voskresensky, E. E. Saperstein, and M. A. Troitsky, *Pionic Degrees of Freedom of Nuclear Matter* (Nauka, Moscow, 1991); Phys. Rep. **192**, 179 (1990).
3. D.-O. Backman, G. E. Brown, and J. A. Niskanen, Phys. Rep. **124**, 1 (1985).
4. G. E. Brown and W. Weise, Phys. Rep. **27**, 1 (1976).
5. A. B. Migdal, *Theory of Finite Fermi Systems and Applictions to Atomic Nuclei* (Nauka, Moscow, 1983).
6. W. H. Dickhoff, A. Faessler, J. Meyer-ter-Vehn, and H. Muthner, Phys. Rev. C **23**, 1154 (1981).
7. E. G. Drukarev, M. G. Ryskin, and V. A. Sadovnikova, Eur. Phys. J. A **4**, 171 (1999).
8. T. E. O. Ericson and W. Weise, *Pions and Nuclei* (Clarendon, Oxford, 1988; Nauka, Moscow, 1991).
9. M. Gell-Mann, R. Oakes, and B. Renner, Phys. Rev. **175**, 2195 (1968).
10. E. G. Drukarev and E. M. Levin, Pis'ma Zh. Éksp. Teor. Fiz. **48**, 374 (1988) [JETP Lett. **48**, 338 (1988)].
11. Y. Nambu and G. Jona-Lasinio, Phys. Rev. **122**, 345 (1961); Phys. Rev. **124**, 246 (1961).
12. V. A. Sadovnikova, in *Proceedings of the 33rd PNPI Winter School, St. Petersburg, 1999*, p. 109.
13. J. Meyer-ter-Vehn, Phys. Rep. **74**, 323 (1981).
14. L. D. Landau, Zh. Éksp. Teor. Fiz. **30**, 1058 (1956) [Sov. Phys. JETP **3**, 920 (1956)].
15. E. G. Drukarev, M. G. Ryskin, and V. A. Sadovnikova, in *Proceedings of the 33rd PNPI Winter School, St. Petersburg, 1999*, p. 140.
16. I. Ya. Pomeranchuk, Zh. Éksp. Teor. Fiz. **35**, 524 (1958) [Sov. Phys. JETP **8**, 361 (1958)].
17. S.-O. Backman, O. Sjoberg, and A. D. Jackson, Nucl. Phys. A **321**, 10 (1979).

Translated by M. Kobrinsky

Physics of Atomic Nuclei, Vol. 64, No. 3, 2001, pp. 448–453. From Yadernaya Fizika, Vol. 64, No. 3, 2001, pp. 503–508.

90th ANNIVERSARY OF A.B. MIGDAL'S BIRTHDAY
NUCLEI

Nuclear Anapole Moment and Axial Neutral Current in Nuclei*

V. F. Dmitriev**

Budker Institute of Nuclear Physics, Siberian Division, Russian Academy of Sciences, pr. Akademika Lavrentieva 11, Novosibirsk, 630090 Russia

Received July 11, 2000

Abstract—Nuclear anapole moments and axial neutral currents are calculated for a set of nuclei. The accuracy of the leading approximation is studied in detail. The core polarization renormalizing both the anapole moment and the axial current is treated in the random-phase approximation with effective forces. Parameters of parity-violating nuclear forces are discussed. The experimental value of the anapole moment of the ^{133}Cs nucleus as extracted from data with allowance for axial-current renormalization is found to be $\kappa = 0.39 \pm 0.06$. © *2001 MAIK "Nauka/Interperiodica".*

1. INTRODUCTION

The existence of parity nonconservation in atoms has been firmly established at present (see, for example, [1]). To be precise, it is nuclear-spin-independent parity-nonconservation effects in heavy atoms that have received the most detailed study. These effects are enhanced in proportion to Z^2Q. The last enhancement factor, the so-called weak nuclear charge Q, which is numerically close to the number of neutron, $N = A - Z$, is due to the fact that, in nuclear-spin-independent phenomena, all nucleons act coherently.

As to the atomic parity-nonconservation effects dependent on the nuclear spin, they obviously do not have this coherent enhancement and are therefore much smaller. There are strong reasons to expect that these effects are dominated by the contact electromagnetic interaction of electrons with the nuclear anapole moment [2, 3].

An anapole is a new electromagnetic moment arising in a system that has no center of inversion [4]. It exists even in such a common object as a chiral molecule in a state with a nonzero angular momentum [5]. A nuclear anapole moment is induced by parity-nonconservation nuclear forces.

The first measurement of the anapole moment of cesium was reported in [6]. An immediate application of this measurement was an attempt at deducing the pion–nucleon weak parity-nonconserving coupling constant f_π [7, 8]. A comparison of the measured anapole moment with that calculated by using a purely single-particle model leads to an f_π value that is four times as great as that deduced from a measurement of parity-violation in ^{18}F [9]. A more sophisticated comparison was performed in [10], where the results for ^{18}F, the anapole moment of ^{133}Cs, and the upper bound on the anapole moment of ^{205}Tl [11] were used to deduce the parity-nonconserving coupling constants f_π and f_ρ. A combination of the coupling constants was found that satisfies both the ^{18}F and the ^{133}Cs experiment and which is consistent with theory. However, these values are inconsistent with the constraint obtained from a measurement for ^{205}Tl. This situation, even independently of ^{18}F experiments, raises the question of how accurate the theory of nuclear anapole moments is.

Although the anapole moment makes the largest contribution to spin-dependent parity-nonconserving interaction of atomic electrons with a nucleus, other contributions must be calculated in order to determine accurately the anapole moment. The interaction of the vector electron current with the nuclear axial current is the largest of these [12]. The nuclear axial current is proportional to the isovector component of the nuclear spin. It is determined predominantly by the spin of a valence nucleon. However, the core polarization changes this value, and this effect must also be taken into consideration. Here, we present a calculation of the nuclear anapole moment and the nuclear axial current using the random-phase approximation with effective short-range nuclear forces.

2. LEADING APPROXIMATION FOR THE NUCLEAR ANAPOLE MOMENT AND ITS ACCURACY

Parity-nonconserving interaction in a system mixes opposite-parity states of the same total angular momentum and creates a spin helical structure in it [1, 4]. In this way, such a system with a nonzero magnetic moment acquires a specific magnetic-field configuration of the type created by a toroidal winding. This is what is referred to as an anapole [4].

The anapole-moment vector can be conveniently defined as [1–3]

$$\mathbf{a} = -\pi\int d^3 r r^2 \mathbf{j}(\mathbf{r}), \qquad (1)$$

* This article was submitted by the author in English.

** e-mail: dmitriev@inp.nsk.su

where $\mathbf{j}(\mathbf{r})$ is the current-density operator. The vector potential produced by the anapole moment is

$$\mathbf{A}(\mathbf{r}) = \mathbf{a}\delta(\mathbf{r}). \quad (2)$$

In calculating the anapole moment of a heavy nucleus, we begin with the shell model and the single-particle approximation. We assume that the nuclear spin $\mathbf{I}$ coincides with the total angular momentum of an odd valence nucleon and that the other nucleons form a core with zero angular momentum. The effective P-odd potential for an external nucleon can be represented as

$$W_a = \frac{G_F}{\sqrt{2}}\frac{g_a}{2m}\boldsymbol{\sigma}[\mathbf{p}\rho(r) + \rho(r)\mathbf{p}], \quad (3)$$

where $\boldsymbol{\sigma}$ and $\mathbf{p}$ are, respectively, the spin and the momentum operator of the valence nucleon, while $\rho(r)$ is the density of core nucleons that is normalized by the condition $\int d^3r\rho(r) = A$ (the atomic number is assumed to be large, $A \gg 1$). In the case of an external proton, the numerical value of the dimensionless constant g_p is likely to be about 4 to 5 (see below). For an external neutron, the corresponding constant g_n is smaller, most probably $g_n \ll 1$.

The leading approximation for the anapole moment of a heavy nucleus corresponds to the disregard of the spin–orbit component of the single-particle nuclear potential and to the assumption that the density $\rho(r)$ is constant in space and that it coincides with the mean nuclear density ρ_0. This approximation, first used in [13], is reasonable if the wave function of the external nucleon is basically localized in the core region. The Schrödinger equation for the external nucleon,

$$\left[-\frac{1}{2m}\Delta + U(r) + W(\mathbf{r})\right]\psi(\mathbf{r}) = E\psi(\mathbf{r}), \quad (4)$$

has, to first order in W, the elementary solution (recall that we assume here that $\rho(r) = \rho_0 = \text{const}$)

$$\psi(\mathbf{r}) = \left(1 - i\frac{G_F}{\sqrt{2}}g_a\rho_0(\boldsymbol{\sigma}\cdot\mathbf{r})\right)\psi_0(\mathbf{r}), \quad (5)$$

where $\psi_0(\mathbf{r})$ is the unperturbed wave function of the external nucleon. Simple calculations using Eqs. (1) and (5) yield the anapole moment for the spin current density in the form

$$\mathbf{a} = \frac{G_F g_a \rho_0}{\sqrt{2}}\frac{2\pi e\mu}{m}\langle r^2\rangle\frac{K\mathbf{I}}{I(I+1)}, \quad (6)$$
$$K = (l-I)(2I+1),$$

where l is the orbital angular momentum of the external nucleon. Its mean-squared radius $\langle r^2\rangle$ is very close to the squared charge radius of the nucleus:

$$r_q^2 = (3/5)R^2 = (3/5)r_0^2A^{2/3}, \quad r_0 = 1.2 \text{ fm}. \quad (7)$$

Setting $\rho_0 = (4\pi r_0^3/3)^{-1}$ and using (6), we finally obtain

$$\mathbf{a} = \frac{G_F}{\sqrt{2}}\frac{9}{10}g_a\frac{e\mu}{mr_0}A^{2/3}\frac{K\mathbf{I}}{I(I+1)}. \quad (8)$$

The A dependence of the anapole moment is very natural. Since the anapole corresponds to the magnetic-field configuration induced by a toroidal winding, the anapole-moment value must indeed be proportional to the magnetic flux—that is, to the cross-sectional area of the torus. This is the origin of $\langle r^2\rangle$ in Eq. (6) and of $A^{2/3}$ in Eq. (8). The Fermi constant G_F serves as a natural unit for the anapole moment, which arises in the first order in weak interaction, and has dimensions of cm^2. In terms of this unit, a convenient characteristic of the nuclear anapole moment for the atomic-parity-nonconservation problem is the dimensionless constant κ defined as

$$e\mathbf{a} = \frac{G_F}{\sqrt{2}}\frac{K\mathbf{I}}{I(I+1)}\kappa, \quad (9)$$

where e is an elementary charge. According to (8), this constant is [3]

$$\kappa = \frac{9}{10}g_a\frac{\alpha\mu}{mr_0}A^{2/3}. \quad (10)$$

The enhancement in proportion to $A^{2/3}$ compensates, to a large degree, the small fine-structure constant $\alpha = 1/137$. That is why the nuclear anapole moment is perhaps the main source of nuclear-spin-dependent parity-nonconservation effects in heavy atoms [2, 3].

To estimate the accuracy of the leading approximation, we have calculated the admixture of opposite-parity states $\delta\psi(\mathbf{r})$ using the total single-particle potential and a realistic nuclear density. The correction $\delta\psi(\mathbf{r})$ can be represented in the form

$$\delta\psi(\mathbf{r}) = -i\frac{G_F}{\sqrt{2}}g_a\rho_0(\boldsymbol{\sigma}\cdot\mathbf{n})\delta R(r)\Omega_{Ilm}(\mathbf{n}) \quad (11)$$

[which is similar to that in (5)], where $\Omega_{Ilm}(\mathbf{n})$ is the spherical spinor and $\mathbf{n} = \mathbf{r}/r$. The results are different for two components of the spin–orbit doublet. For the upper level of the spin–orbit doublet, a typical difference between exact $\delta R(r)$ and $rR(r)$, which is $\delta R(r)$ in the leading approximation, is shown in Fig. 1*a*. The difference is insignificant. The main contribution to the difference comes from the spin–orbit component of the potential. For the lower state of the doublet, the difference in the peak heights can reach a factor of two, as can be seen from Fig. 1*b*. In all cases, the exact correction and the leading approximation peak near the surface. However, the ratio of the peak heights differs considerably for the upper and the lower states of spin–orbit doublets. In calculating the contribution of core nucleons to the anapole moment, we therefore use exact $\delta R(r)$ instead of that in the leading approximation.

3. MANY-BODY CONTRIBUTION TO THE ANAPOLE MOMENT

The effect of core nucleons on the nuclear anapole moment is twofold. First, core polarization reduces the single-particle anapole moment. The reduction is due to

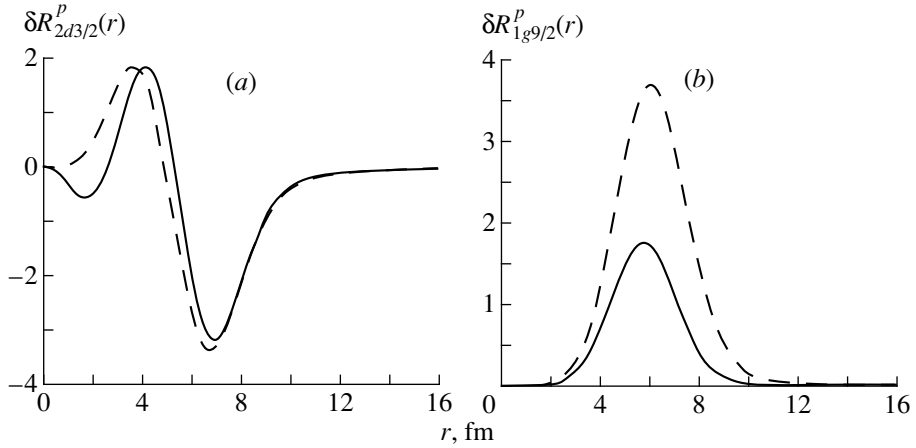

Fig. 1. Admixture of an opposite parity, $\delta R(r)$ for various components of the spin–orbit doublet: (*a*) results for the $2d_{3/2}$ level and (*b*) results for the $1g_{9/2}$ level. The solid curves were computed in the leading approximation. The dashed curves represent an exact solution.

the repulsive nature of the residual spin–spin interaction. Second, core nucleons produce an additional contribution to the anapole moment owing to parity violation in the single-particle orbitals occupied by core nucleons. This contribution compensates partly for the reduction due to core polarization.

A convenient way to describe core polarization is to use the effective renormalized operators or effective fields in terms of the theory of finite Fermi systems [14]. In the random-phase approximation, effective fields are solutions to a set of integral equations describing the particle–hole renormalization of the bare vertex.

The anapole moment is a *T*-odd operator. Thus, the effective two-particle interaction involved in anapole-moment renormalization must change sign under *T* inversion of one of the two particles:

$$T_a F(ab) T_a^{-1} = T_b F(ab) T_b^{-1} = -F(ab).$$

The simplest interaction satisfying this condition is the same spin–spin interaction that changes nuclear magnetic moments:

$$F_s(ab) = C(g_0 + g_0' \boldsymbol{\tau}_a \cdot \boldsymbol{\tau}_b)\boldsymbol{\sigma}_a \cdot \boldsymbol{\sigma}_b \delta(\mathbf{r}_a - \mathbf{r}_b). \quad (12)$$

Here, C is the normalization constant that we set, according to [14], C = 300 MeV fm^3; we choose g_0' = 1.01 and g_0 = 0.63.

The effective interaction between the valence and the core nucleons changes the interaction of the valence nucleon with an external field, producing an additional core field. In the theory of finite Fermi systems, this effect is taken into account by introducing a dressed effective vertex V that satisfies the equation [14]

$$V = V_0 + FAV, \quad (13)$$

where V_0 is the bare anapole-moment operator

$$V_0^a = \frac{\pi e \mu_a}{m} \mathbf{r} \times \boldsymbol{\sigma} \quad (14)$$

and A is the static polarization loop of a particle–hole pair,

$$A_{\nu_1\nu_1';\,\nu_2\nu_2'} = \int \frac{d\epsilon}{2\pi i} G_{\nu_1\nu_2}(\epsilon) G_{\nu_2'\nu_1'}(\epsilon). \quad (15)$$

Here $G_{\nu_1\nu_2}(\epsilon)$ is the single-particle nucleon propagator. In (13), F is the sum of spin–spin interaction (12) and the effective weak interaction:

$$F_w = \frac{G_F}{\sqrt{2}} \frac{1}{4m} \sum_{a,b} (\{(g_{ab}\boldsymbol{\sigma}_a - g_{ba}\boldsymbol{\sigma}_b) \cdot (\mathbf{p}_a - \mathbf{p}_b), \delta(\mathbf{r}_a - \mathbf{r}_b)\} + g_{ab}'[\boldsymbol{\sigma}_a \times \boldsymbol{\sigma}_b] \cdot \nabla \delta(\mathbf{r}_a - \mathbf{r}_b)). \quad (16)$$

Interaction (16) generates a mean-field weak potential (3) with the interaction constants

$$g_a = g_{ap}\frac{Z}{A} + g_{an}\frac{N}{A}. \quad (17)$$

The propagator $G_{\nu_1\nu_2}(\epsilon)$ must be calculated in the total mean-field potential, including the weak potential (3). Strictly speaking, the effective interaction constants g_{ab}, g_{ba}, and g_{ab}' must be found from experimental data. On the other hand, they can be estimated by using the initial finite-range parity-nonconserving interaction [15] in the zero-range limit with allowance for short-range particle–particle repulsion [3, 16]. These "best"-value estimates lead to $g_n \ll 1$, while the constant g_p is approximately 4.5.

It is convenient to disentangle weak-interaction effects treating them explicitly in the first order of perturbation theory. Let δV be a correction to the vertex from weak forces. For the unperturbed vertex V and the correction δV, we have the equations

$$V = V_0 + F_s A V, \quad (18)$$

$$\delta V = F_w A V + F_s \delta A V + F_s A \delta V, \quad (19)$$

where F_w is the weak nucleon–nucleon interaction (16). The anapole-moment value is given by

$$a = \langle \delta\psi | V | \psi \rangle + \langle \psi | V | \delta\psi \rangle + \langle \psi | \delta V | \psi \rangle. \quad (20)$$

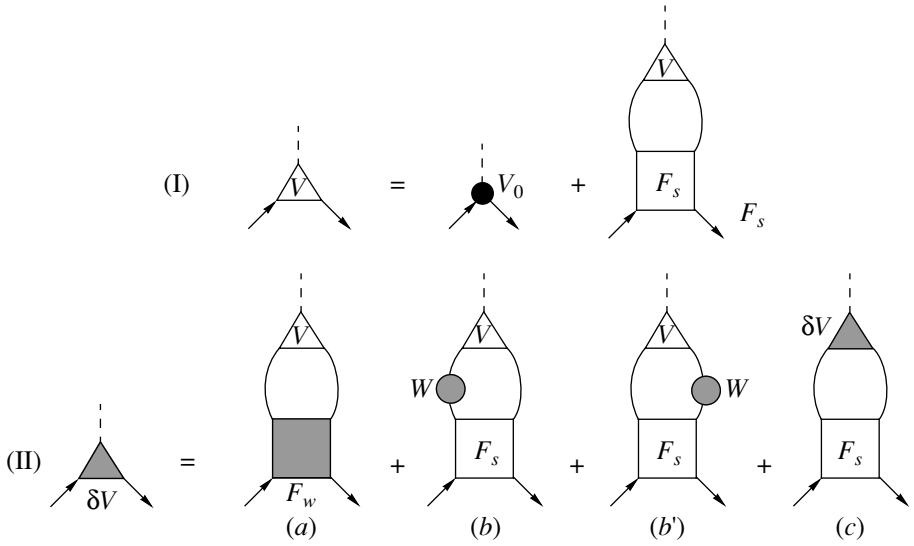

Fig. 2. Feynman diagrams corresponding to equations (18) and (19). (I) The anapole moment renormalization diagram describing the core polarization effects. The closed circle is the bare anapole operator, and the open triangle is the dressed one. The open square is the spin–spin residual strong interaction. (II) Additional contribution to the anapole moment due to the parity violation in the core states: (*a*) direct contribution of the two-particle effective PNC interaction, (*b* and *b*') effective contribution due to parity violation in the core states, and (*c*) renormalization diagram. A shaded circle is the single-particle PNC interaction. The shaded square is the two-particle effective PNC interaction. The shaded triangle is the additional contribution δV.

The Feynman diagrams corresponding to (18) and (19) are shown in Fig. 2. Equation (18), which is illustrated in the upper part of Fig. 2 (diagrams I), describes the conventional renormalization of the bare operator V_0 in the random-phase approximation. The next Eq. (19), which is illustrated in the lower part of Fig. 2 (diagrams II), describes an additional contribution from core nucleons that arises both from the direct *P*-odd nucleon–nucleon interaction F_w [see Fig. 2 (II*a*)] and from the *P*-even residual interaction via the admixture of opposite-parity states to the wave functions of core nucleons [see Fig. 2 (II*b* and II*b*')]. The last term in Eq. (19) [see Fig. 2 (II*c*)] is responsible for the renormalization of these contributions.

The values of the anapole moment that result from solving Eqs. (18) and (19) are compiled in Table 1. For the sake of comparison, the single-particle values $\kappa_{\text{s.p.}}$ are listed in the second column of this table. The results of the present calculations are listed in the last column. One can see that the core-polarization contribution is about half of the single-particle one and that its sign is opposite to sign of the single-particle contribution. This is in accord with the repulsive nature of the residual spin–spin interaction [see Eq. (12)]. In this case, the core is responsible for the screening of the valence-nucleon spin. The terms proportional to the weak-interaction constants g_{ab} come from δV. They compensate partly for the reduction induced by core polarization.

The anapole moment of the ^{133}Cs nucleus is $\kappa_{\text{theor}} = 0.16$ for the "best" values of the weak-interaction constants. This value is to be compared with the experimental value κ_{expt}. To extract this value from data, it is necessary to estimate other spin-dependent parity-nonconservation effects.

4. NUCLEAR AXIAL CURRENT

The nuclear neutral axial current is proportional to the isovector-spin operator:

$$\mathbf{A} \sim \sum_{j=1}^{A} \boldsymbol{\sigma}_j \tau_j^3. \tag{21}$$

The main contribution to the expectation value of the isovector spin comes from the valence odd nucleon since the spin of the core is zero. This single-particle value analogous to the Schmidt values of nuclear magnetic moment is

$$\langle \boldsymbol{\sigma} \rangle = \pm \frac{I(I+1) - l(l+1) + 3/4}{I(I+1)} \mathbf{I}, \tag{22}$$

where the plus and the minus sign correspond to the proton and the neutron, respectively. The core polarization changes this value in the same way as it changes the anapole and the magnetic moments. Moreover, the

Table 1. Anapole moments calculated for the listed nuclei

Nuclei	$\kappa_{\text{s.p.}} \times 10^2$	$\kappa \times 10^2$
Odd proton nuclei		
^{133}Cs	$4.9g_p + 0.65g_{pn}$	$2.9g_p + 0.18g_n + 0.36g_{pn} - 0.02g_{np}$
^{205}Tl	$7.8g_p + 0.85g_{pn}$	$4.3g_p + 0.1g_n + 0.64g_{pn} - 0.06g_{np}$
^{209}Bi	$5.4g_p + 0.96g_{pn}$	$2.5g_p + 0.3g_n + 0.57g_{pn} - 0.04g_{np}$
Odd neutron nuclei		
^{135}Ba	$-6.5g_n - 0.25g_{np}$	$-0.1g_p - 4.6g_n + 0.01g_{pn} - 0.19g_{np}$
^{137}Ba	$-6.5g_n - 0.25g_{np}$	$-0.2g_p - 5.7g_n + 0.01g_{pn} - 0.23g_{np}$
^{207}Pb	$-9.6g_n - 0.16g_{np}$	$-0.1g_p - 6.7g_n + 0.01g_{pn} - 0.14g_{np}$

Table 2. Isovector spin calculated for the listed nuclei

Nuclei	μ_{exp}	$\mu_{s.p}$	$(\sigma\tau_3)_{s.p}$	$(\sigma\tau_3)_{exp}$	$(\sigma\tau_3)_{theor}$
Odd proton nuclei					
^{133}Cs	2.58	1.72	−0.78	−0.43	−0.46
^{205}Tl	1.63	2.79	1	0.44	0.57
^{209}Bi	4.11	2.62	−0.82	−0.20	−0.43
Odd neutron nuclei					
^{135}Ba	0.84	1.15	0.6	0.48	0.41
^{137}Ba	0.94	1.15	0.6	0.53	0.51
^{207}Pb	0.59	0.64	0.33	0.32	0.25

equations for isovector-spin renormalization are identical to those for the renormalization of the spin component of the magnetic moment. They correspond to the diagrams in Fig 2 (I).

Although no direct isovector-spin data exist, we can use the analogy between the magnetic moment and the isovector spin to extract some information about the isovector-spin expectation value. The idea is that the spin part of the magnetic moment is an almost pure isovector. The isoscalar contribution is less than 20%. On the other hand, the orbital part of the magnetic moment is much less affected by the core polarization, and pure single-particle values can be used for it. On the basis of these considerations, we can extract, just from magnetic-moment data, the expectation value of the isovector spin to within 20%. The results of this procedure, together with the results of theoretical calculations, are summarized in Table 2. The second and the third column of this table display the magnetic moment and its single-particle or Schmidt values. The fourth and the fifth column present the single-particle values of the isovector spin and the values extracted from the magnetic moments. The last column gives the results of our calculations.

The agreement between the calculated values of the isovector spin and those extracted from the magnetic moment is satisfactory within the accuracy of the extraction procedure. The only case that shows significant deviations is that of ^{209}Bi. The reason can be found in the large orbital angular momentum of the valence proton. Although it is not renormalized itself by the core polarization, it can produce, owing to the spin–orbit potential, an additional contribution to the spin part of the magnetic moment in higher orders in the residual interaction [see Eq. (12)].

The total spin-dependent κ value extracted from the data in [6] is $\kappa = 0.44 \pm 0.06$ [17]. The contribution of the nuclear axial current based on the single-particle value of –0.78 was found in [17] to be 0.06. Therefore, the anapole-moment contribution was 0.37 ± 0.06 if we take into account other small spin-dependent effects. Our renormalized value for the axial nuclear current leads to a slightly larger value of $\kappa = 0.39 \pm 0.006$ for the anapole moment of the ^{133}Cs nucleus.

5. PARITY-NONCONSERVING INTERACTION CONSTANTS

As was mentioned above, the constants g_{ab} and g'_{ab} of the parity-nonconserving interaction (16) must be treated as phenomenological ones and must be found from experimental data. However, we can try to relate them to the parameters of the free nucleon–nucleon interaction [15]. The relevant relations are [16]

$$\begin{aligned} g_{pp} &= -(\mu + 2) W_\rho A_\rho h^0_\rho, \\ g'_{pp} &= g_{nn} = g'_{nn} = g_{pp}, \\ g_{pn} &= -(2\mu + 1) W_\rho A_\rho h^0_\rho + W_\pi A_\pi f_\pi, \\ g_{np} &= -(2\mu + 1) W_\rho A_\rho h^0_\rho - W_\pi A_\pi f_\pi, \\ g'_{pn} &= g'_{np} = (\mu - 1) W_\rho A_\rho h^0_\rho, \end{aligned} \tag{23}$$

where

$$A_\rho = \frac{\sqrt{2} g_\rho}{G_F m_\rho^2}, \quad A_\pi = \frac{g_\pi}{G_F m_\pi^2}$$

are the dimensional constants, μ is the isovector nucleon magnetic moment, and h^0_ρ and f_π are the parity-nonconserving rho–nucleon and pion–nucleon couplings. The dimensionless factors W_ρ and W_π were introduced to normalize the matrix elements of the interaction in (16) to the matrix elements of the original finite-range interaction [15].

Following [10], we plot, in Fig. 3, the extracted values of coupling constants H^1_π and H^0_ρ in the notation of Adelberger and Haxton [9]. They are related to f_π and h^0_ρ as

$$H^1_\pi = \frac{g_\pi f_\pi}{\sqrt{32}}, \quad H^0_\rho = -\frac{g_\rho h^0_\rho}{2},$$

where g_π and g_ρ are the strong-coupling constants. The bands corresponding to the ^{205}Tl and ^{133}Cs data are slightly different from those extracted in [10], where our previous results from [18] were used to determine the coupling constants from the anapole-moment data.

Our improved calculations did not change the general situation. The coupling constants extracted from the ^{133}Cs and ^{205}Tl data are still inconsistent independently of the ^{19}F data. This situation eventually raises the question of how reliable the theory of the nuclear anapole moment is. Our calculation has been performed in the random-phase approximation. There are two more calculations including many-body effects [19, 20] within the shell-model approach. In [20], the shell-model basis used to calculate the anapole moment of ^{205}Tl was sufficiently large to take into account simultaneously the single-particle anapole moment and core-polarization effects. The value obtained in [20] for the spin component of the anapole moment of ^{205}Tl is

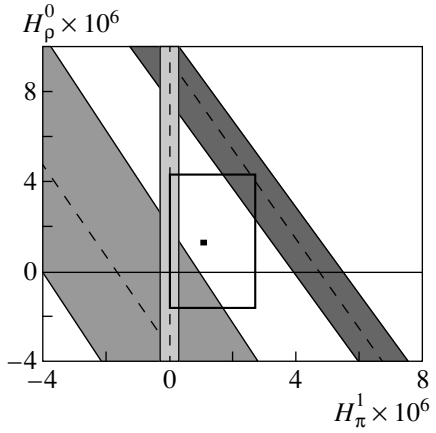

Fig. 3. Regions allowed for the weak-coupling constants H_π^1 and H_ρ^0 extracted from (light shading) ^{18}F, (medium shading) ^{205}Tl, and (dark shading) ^{133}Cs experiments. Also shown are the Desplanques–Donoghue–Holstein [15] (small closed square) best values and (large open rectangle) "reasonable range."

$\kappa_s = 0.35$. Our calculation, where we have used the completely different quasiparticle interaction and the random-phase interaction, yields $\kappa_s = 0.37$ for the best values of the coupling constants. Such close values obtained within the completely different approaches give sufficient grounds to hope for a weak model dependence of the anapole moment, although we cannot rule out the possibility that this is merely a coincidence.

The relation between the effective parity-nonconserving-interaction constants and the meson–nucleon coupling constants given by Eq. (23) is less reliable. The normalization factors W_π and W_ρ were determined by comparing the matrix elements of the interaction (16) and the finite-range Desplanques–Donoghue–Holstein interaction [15] for low-energy N^4He scattering. Therefore, we can hardly expect them to be constant in a broad range of all bound single-particle states. There is an additional reason why Eq. (23) can be become invalid. As was shown in [21, 22], the parity-nonconserving nucleon–nucleon interaction can be strongly renormalized in nuclear media. As a result, the neutron parity-nonconserving-potential constant g_n, which is small according to estimates based on Eq. (23), can be comparable with the proton constant g_p (see also discussion in [23]). From this point of view, measurements sensitive to g_n would be extremely interesting. These could be measurements of the anapole moment of a nucleus with an odd neutron or, another possibility, measurement of neutron spin rotation in helium [24].

In order to obtain the measured value of the anapole moment of ^{133}Cs, the parity-nonconserving-interaction constants [see Eq. (16)] should be increased approximately by a factor of 2 in relation to their best values [see Eq. (23)]. It is interesting to note that a similar conclusion was drawn from a statistical analysis of parity-nonconservation effects in compound nuclei [25].

ACKNOWLEDGMENTS

The discussions with I.B. Khriplovich are greatly appreciated. The contribution of the late V.B. Teterin was invaluable in this field.

This work was supported by the Russian Foundation for Basic Research (project no. 98-02-17797).

REFERENCES

1. I. B. Khriplovich, *Parity Nonconservation in Atomic Phenomena* (Gordon and Breach, London, 1991).
2. V. V. Flambaum and I. B. Khriplovich, Zh. Éksp. Teor. Fiz. **79**, 1656 (1980) [Sov. Phys. JETP **52**, 835 (1980)].
3. V. V. Flambaum, I. B. Khriplovich, and O. P. Sushkov, Phys. Lett. B **146B**, 367 (1984).
4. Ya. B. Zel'dovich, Zh. Éksp. Teor. Fiz. **33**, 1531 (1957) [Sov. Phys. JETP **6**, 1184 (1957)].
5. I. B. Khriplovich and M. E. Pospelov, Z. Phys. D **17**, 81 (1990).
6. C. S. Wood *et al.*, Science **275**, 1759 (1997).
7. W. C. Haxton, Science **275**, 1753 (1997).
8. V. V. Flambaum and D. W. Murray, Phys. Rev. C **56**, 1641 (1997).
9. E. G. Adelberger and W. C. Haxton, Annu. Rev. Nucl. Part. Sci. **35**, 501 (1985).
10. W. S. Wilburn and J. D. Bowman, Phys. Rev. C **57**, 3425 (1998).
11. P. A. Vetter *et al.*, Phys. Rev. Lett. **74**, 2658 (1995).
12. I. B. Khriplovich, Yad. Fiz. **31**, 1529 (1980) [Sov. J. Nucl. Phys. **31**, 793 (1980)].
13. Curtis F. Michel, Phys. Rev. **133B**, 329 (1964).
14. A. B. Migdal, *Theory of Finite Fermi Systems and Applications to Atomic Nuclei* (Nauka, Moscow, 1982).
15. B. Desplanques, J. F. Donoghue, and B. R. Holstein, Ann. Phys. (N.Y.) **124**, 449 (1980).
16. O. P. Sushkov and V. B. Telitsin, Phys. Rev. C **48**, 1069 (1993).
17. I. B. Khriplovich, Usp. Fiz. Nauk **167**, 1213 (1997) [Phys. Usp. **40**, 1161 (1997)].
18. V. F. Dmitriev and V. B. Telitsin, Nucl. Phys. A **613**, 237 (1997).
19. W. C. Haxton, E. M. Henley, and M. J. Musolf, Phys. Rev. Lett. **63**, 949 (1989).
20. N. Auerbach and B. A. Brown, Phys. Rev. C **60**, 025501 (1999).
21. V. V. Flambaum and O. K. Vorov, Phys. Rev. C **49**, 1827 (1994).
22. V. V. Flambaum and G. F. Gribakin, Prog. Part. Nucl. Phys. **35**, 423 (1995).
23. B. Desplanques, Phys. Rep. **297**, 1 (1998).
24. V. F. Dmitriev, V. V. Flambaum, O. P. Sushkov, and V. B. Telitsin, Phys. Lett. B **125B**, 1 (1983).
25. S. Tomsovich, Mikkel B. Johnson, A. Hayes, and J.D. Bowman, Phys. Rev. C **62**, 054607 (2000).

Physics of Atomic Nuclei, Vol. 64, No. 3, 2001, pp. 454–464. Translated from Yadernaya Fizika, Vol. 64, No. 3, 2001, pp. 509–519.

90th ANNIVERSARY OF A.B. MIGDAL'S BIRTHDAY
NUCLEI

Simple Microscopic Model for the Scalar–Isoscalar Component of the Landau–Migdal Amplitude

M. Baldo[1)], U. Lombardo[1)], E. E. Saperstein, and M. V. Zverev[2)]

Russian Research Centre Kurchatov Institute, pl. Kurchatova 1, Moscow, 123182 Russia

Received July 12, 2000

Abstract—A simple microscopic model is proposed that describes the coordinate dependence of the zeroth harmonic $f_0(r)$ of the scalar–isoscalar component of the Landau–Migdal amplitude. In the theory of finite Fermi systems due to Migdal, such a dependence was introduced phenomenologically. The model presented in this study is based on a previous analysis of the Brueckner G matrix for a planar slab of nuclear matter; it expresses the function $f_0(r)$ in terms of the off-mass-shell T matrix for free nucleon–nucleon scattering. The result involves the T matrix taken at the negative energy value equal to the doubled chemical potential μ of the nucleus being considered. The amplitude $f_0(r)$ found in this way is substituted into the condition that, in the theory of finite Fermi systems, ensures consistency of the self-energy operator, effective quasiparticle interaction, and the density distribution. The calculated isoscalar component of the mean nuclear field $V(r)$ agrees fairly well with a phenomenological nuclear potential. Owing to a strong E dependence of the T matrix at low energies, the potential-well depth $V(0)$ depends sharply on μ, increasing as $|\mu|$ is reduced. This effect must additionally stabilize nuclei near the nucleon drip line, where μ vanishes. © *2001 MAIK "Nauka/Interperiodica".*

1. INTRODUCTION

The theory of finite Fermi systems, which was developed by A.B. Migdal in the early 1960s and which was set forth in the monograph [1], still appears to be the most consistent many-body approach to the theory of the nucleus. Conceptually, it is close to Fermi liquid theory due to Landau [2], where the amplitude for quasiparticle scattering at zero angle near the Fermi surface, the so-called Landau amplitude, plays the role of effective quasiparticle interaction. For liquid ^{3}He—the main object to which Landau theory is applied—the Landau amplitude is the sum of two invariant components, a scalar and a spin one (f and g, respectively). Each of these depends only on one variable, the angle θ between the momenta of scattered particles. In Landau theory, the invariant amplitudes are expanded in series in Legendre polynomials $P_l(\cos\theta)$, the expansion coefficients, so-called harmonics, being treated as phenomenological parameters of the theory. The first terms are unambiguously related to physical observables. For example, the zeroth harmonic f_0 of the scalar amplitude determines the compressibility of a Fermi liquid, while its first harmonic f_1 controls the effective mass, by virtue of the so-called Pitaevskiĭ identity [3]. In liquid helium, the effective mass differs strongly from the bare mass, whence it follows that the harmonic f_1 is great. Higher harmonics of the Landau amplitude decrease slowly with increasing l. This is due to special physical reasons, which will not be discussed here.

In nuclei, there are also isospin variables, in addition to spin variables, so that the structure of effective quasiparticle interaction is more complicated. The relevant analog of the Landau amplitude is referred to as, by convention, the Landau–Migdal amplitude. In the standard notation adopted in the theory of finite Fermi systems, its central component has the form

$$F = C_0[f + f'\boldsymbol{\tau}_1\cdot\boldsymbol{\tau}_2 + (g + g'\boldsymbol{\tau}_1\cdot\boldsymbol{\tau}_2)\boldsymbol{\sigma}_1\cdot\boldsymbol{\sigma}_2], \quad (1)$$

where $\boldsymbol{\sigma}$ and $\boldsymbol{\tau}$ are the spin and isospin Pauli matrices. The normalization factor C_0 in (1) is equal to the inverse density of states near the Fermi surface: $C_0 = (dn/d\varepsilon_F)^{-1}$. Following the prescription from [4], we will use the value of $C_0 = 300$ MeV fm^3. It can be seen that there are now four invariant amplitudes: a scalar–isoscalar, a scalar–isovector, a spin–isoscalar, and a spin–isovector one.

Of course, expression (1) is a very rough approximation of the Landau–Migdal amplitude for actual nuclei. In order to describe phenomena associated with spin variables—especially at high momentum transfers—this expression must be supplemented with spin–orbit and tensor terms. The general tensor structure of the full Landau–Migdal is rather complicated [5], but there are many nuclear-physics problems that are virtually independent of spin–orbit and tensor amplitudes. These include the problems of calculating the total energy of a nucleus, the central part of the mean field, and the distribution of the nucleon density in a nucleus—that is, problems that are considered within

[1)] Istituto Nazionale di Fisica Nucleare, Sezione di Catania, Corso Italia 57, I-95129 Catania, Italy.
[2)] Moscow State Engineering Physics Institute (Technical University), Kashirskoe sh. 31, Moscow, 115409 Russia.

self-consistent theory of finite Fermi systems [4, 5]. For these, it is sufficient to use the central amplitude in (1)—more precisely, its first two terms, f and f'. Only the zeroth and the first harmonics of these amplitudes are usually retained in the theory of finite Fermi systems. Even the first harmonics f_1 and f_1' are small, which follows from the fact that the effective masses of neutrons and protons in nuclei are close to their vacuum values (and, hence, to each other). There is also experimental evidence for the smallness of higher harmonics. By way of example, we indicate that the presence of the second harmonic f_2 leads to the dependence of the mean nuclear field on the nucleon orbital angular momentum l, but this dependence has not been observed experimentally.

We can see that, in one aspect, the Landau–Migdal amplitude for intranuclear nucleons is even simpler than the Landau amplitude for liquid helium, but there is another aspect, that which is associated with finite dimensions of nuclei and which generates additional complications due to a strong dependence of the zeroth harmonic f_0 of the scalar–isoscalar amplitude f on the observation point $\mathbf{r}$. Within the theory of finite Fermi systems [1], such a dependence was introduced on the basis of an analysis of experimental data for various quantities. In particular, it is necessary for simultaneously describing isotopic and isomeric shifts of levels in conventional atoms and in mesic atoms and the quadrupole moments of odd nuclei [6]. In [1], it was proposed to use the simplest form of such a dependence,

$$f_0(\mathbf{r}) = f_0^{\mathrm{ex}} + (f_0^{\mathrm{in}} - f_0^{\mathrm{ex}})\frac{\rho(\mathbf{r})}{\rho_0}, \qquad (2)$$

where $\rho(\mathbf{r})$ is the nuclear density at the point $\mathbf{r}$ and $\rho_0 = \rho(r = 0)$. It should be emphasized that expression (2) was considered in [1] as a simple interpolation ansatz for describing a transition from the internal value f_0^{in} of the scalar–isoscalar amplitude to the value f_0^{ex} outside the nucleus rather than the actual density dependence. What is of fundamental importance here is that the parameters f_0^{in} and f_0^{ex} differ greatly: the dimensionless constant f_0^{ex} is approximately equal to –3, while f_0^{in} is close to zero. If these constants were on the same order of magnitude, the dependence of the type in (2) could be of importance only for a precise description of a vast array of experimental data because the contribution of f_0^{ex} is proportional to the small surface-to-volume ratio; therefore, it must be retained in the matrix elements of effective interaction only owing to a large numerical value of the constant itself.

Phenomenological Skyrme forces, which have remained popular so far and which are used within the Hartree–Fock method relying on effective interactions [7], yield results that are equivalent to those produced by the ansatz in (2). There also exist alternative versions of an interpolation formula of the type in (2), for example,

$$f_0(\mathbf{r}) = f_0^{\mathrm{ex}} + (f_0^{\mathrm{in}} - f_0^{\mathrm{ex}})\left(\frac{\rho(\mathbf{r})}{\rho_0}\right)^{\alpha}, \qquad (3)$$

where the exponent α is not equal to unity. But in each case, the parameters f_0^{in} and f_0^{ex} differ considerably. Modified Skyrme forces, which are often used at present, correspond to a density dependence of the form (3) with $\alpha = 2/3$ or $1/3$.

We note that a density dependence of a somewhat more general form was introduced in [8, 9] for the isovector–scalar amplitude f' in order to obtain a detailed description of the masses and radii of some long isotope families (Pb, Ba, Sn, etc.). There, the parameters $(f_0')^{\mathrm{in}}$ and $(f_0')^{\mathrm{ex}}$ are of the same sign and differ in magnitude by a factor of about 2. It goes without saying that, at the precision to which the properties of nuclei were described theoretically within the period when the monograph of Migdal [1] was written, this distinction could not be noticed.

The problem of microscopically calculating the constants of the theory of finite Fermi systems (that is, the parameters that determine the Landau–Migdal amplitude) was formulated even in the pioneering monograph of Migdal [1]. The majority of attempts along these lines have been based on the Brueckner theory of nuclear matter (see, for example, [10, 11]) and have been aimed at calculating exclusively the internal values of the invariant amplitudes in terms of the Brueckner G matrix. Brueckner theory describes reasonably most of the constants of the theory of finite Fermi systems, but it fails to reproduce an f_0^{in} value close to zero. The inclusion of polarization corrections to Brueckner theory cannot improve this situation substantially [12].

On the other hand, an analysis of expression (2) in [13, 14] on the basis of Brueckner theory was performed for the surface region of nuclei. The external constant values f_0^{ex} and $(f_0')^{\mathrm{ex}}$ and the analogous parameters of the spin amplitudes g and g' were calculated there by considering that the conditions for the applicability of Brueckner theory are improved in the surface region. Indeed, it can easily be shown that, with increasing distance from the nucleus, the polarization corrections die out faster than the correlation term in the equation for the G matrix. Owing to this, Brueckner theory becomes asymptotically exact. At the same time, the G matrix tends asymptotically to the free T matrix. As a result, the surface values of the Landau–Migdal amplitude are expressed in terms of the off-mass-shell T matrix for free nucleon–nucleon scattering at the negative energy $E = 2\mu$, where μ is the chemical potential

of the nucleus being considered [13, 14]. If we treat the constant f_0^{ex} in relation (2) as the asymptotic value of $f_0(r)$ for $r \longrightarrow \infty$ and if we use the same conjecture for other invariant amplitudes, then such a calculation of these parameters in terms of the free T matrix can formally be considered to be exact. Obviously, such calculations cannot provide the answer to the question of how fast the asymptotic regime is reached. That the constants found in [13, 14] proved to be very close to their phenomenological values suggests that this occurs immediately beyond the nuclear boundary.

In order to obtain a more detailed description of the behavior of the function $f_0(r)$ in the surface region, it is necessary to calculate precisely the G matrix for a nucleus. A method was developed in [15] for solving the Bethe–Goldstone equation for the G matrix characteristic of a planar slab of nuclear matter. However, it proved to be very difficult to construct a full solution to the problem, so that this equation was solved only for some particular cases. Here, we will make use of the results presented in [15] to develop a simple microscopically motivated model for $f_0(r)$. This model is formulated in Section 2. In Section 3, the proposed model for $f_0(r)$ is used to calculate the central component of the mean nuclear field $V(r)$ on the basis of the condition of self-consistency of the theory of finite Fermi systems [5, 16]. In the same section, the Landau–Migdal amplitude and the mean field induced by it are analyzed as functions of the chemical potential of the nucleus being considered. The main conclusions are presented in Section 4.

2. MOTIVATION OF A SIMPLE MICROSCOPIC MODEL FOR $f_0(r)$

We proceed from the simplest version of Brueckner theory, where the Landau–Migdal amplitude is determined in terms of the G matrix as

$$F(\mathbf{r}_1, \mathbf{r}_2, \mathbf{r}_3, \mathbf{r}_4) = \sqrt{Z(\mathbf{r}_1)Z(\mathbf{r}_2)Z(\mathbf{r}_3)Z(\mathbf{r}_4)}\,G(\mathbf{r}_1, \mathbf{r}_2, \mathbf{r}_3, \mathbf{r}_4; E = 2\mu), \quad (4)$$

where $Z(\mathbf{r})$ is the renormalization factor in the single-particle Green's function $\mathcal{G}$ (Z factor). This G matrix obeys the Bethe–Goldstone equation, which takes consistently into account two-particle correlations in a nuclear medium. Symbolically, it has the form

$$G(E) = \mathcal{V} + \mathcal{V}A(E)G(E), \quad (5)$$

where $\mathcal{V}$ is the potential of pair interaction of free nucleons, while A is the two-particle propagator, an integral of the product $(\mathcal{G}^p\mathcal{G}^p)$ of two-particle components of the single-particle Green's function with respect to the relative energy. We note that the propagator for the Bethe–Goldstone equation does not involve the two-hole contribution $(\mathcal{G}^h\mathcal{G}^h)$.

It is convenient to renormalize Eq. (5) with the aid of the off-mass-shell T matrix describing the scattering of free nucleons at the negative energy $E = 2\mu$ and obeying the Lippmann–Schwinger equation

$$T(E) = \mathcal{V} + \mathcal{V}A^{fr}(E)T(E), \quad (6)$$

where $A^{fr}(E)$ is the propagator for two free nucleons whose total energy is E.

The renormalized Bethe–Goldstone equation has the form

$$G = T + T(A - A^{fr})G. \quad (7)$$

Let us analyze qualitatively Eq. (7) as applied to the surface region of a sufficiently heavy nucleus. It is obvious that, at large distances from the nucleus, $(A - A^{fr}) \longrightarrow 0$, so that the G matrix asymptotically tends to the T matrix. At the same time, the constant f_0^{ex} in relation (2) is also the asymptotic value of the amplitude $f_0(r)$ for $r \longrightarrow \infty$. This circumstance was used in [13, 14] to calculate f_0^{ex} and the analogous external values of other invariant components of the Landau–Migdal amplitude (1) in terms of the free T matrix in the singlet and in the triplet S-wave channel. As was indicated in the Introduction, such a calculation is formally exact, but there remains the problem of assessing the rate of convergence to this asymptotic regime. In order to resolve this problem and to reproduce the Landau–Migdal amplitude in the surface region more precisely, it is necessary to solve directly Eq. (5) or (7) for the G matrix.

A method was developed in [15] for solving the Bethe–Goldstone equation for a planar slab of nuclear matter placed in a well created by an external potential $V(x)$ in the one-dimensional Woods–Saxon form with realistic nuclear parameters. This system makes it possible to reproduce the surface properties of nuclei reasonably well. In this formulation, the problem can be considerably simplified by using the coordinate representation only in the direction of the x axis and the momentum representation in the plane orthogonal to it (that is, in the slab plane, denoted as the **s** plane).

A further simplification is associated with the use of a separable version [17, 18] of the Paris nucleon–nucleon potential [19]. Previously, this version was tested in calculations based on the Brueckner method that were performed for infinite and semi-infinite nuclear matter (see [20, 21] and [22, 23], respectively). The last two studies were devoted to the problem of singlet pairing, where it is legitimate to consider only zero value of the total momentum $\mathbf{P}_\perp$ of two nucleons in the **s** plane.

The quantity $P_\perp$ appears as a free parameter in the Bethe–Goldstone equation, but it should be noted that, in calculating the Landau–Migdal amplitude on the basis of Eq. (4), there arises an integral over all possible values of $P_\perp$. Because of this, the relevant numerical calculations are extremely cumbersome and have yet to be fully performed. As a matter of fact, the calculation

of the G matrix in [15] was performed precisely at $P_\perp = 0$ and approximately at one specific nonzero value of $P_\perp$, whose choice will be discussed below. Here, we will use these results to substantiate microscopically a simple model for the scalar–isoscalar amplitude $f_0(r)$.

Presented immediately below are those basic points of the calculation from [15] that are necessary for understanding the ensuing analysis. For the simpler case of the $^1S_0$ singlet channel, the potential from [17, 18] has the 3×3 separable form

$$\mathcal{V}(\mathbf{k}, \mathbf{k}') = \sum_{ij} \lambda_{ij} g_i(k^2) g_j(k'^2). \tag{8}$$

The $^3S_1$ triplet channel is known to be strongly coupled to the $^3D_1$ channel; therefore, a separable expansion of the type in (8) for $S = 1$ must be generalized with allowance for channel coupling [17]. As a result, the form factors $g_i(k^2)$ are replaced by the two-component columns

$$\hat{g}_i(k^2) = \begin{pmatrix} g_i^{L=0}(k^2) \\ g_i^{L=2}(k^2) \end{pmatrix}, \tag{9}$$

where L is the orbital angular momentum of relative motion in the c.m. frame. In the $^3S_1$–$^3D_1$ channel, use was made here of the 4×4 PEST4 potential from [17]. For the sake of brevity, we present explicit expressions only for the singlet channel, suppressing, as a rule, the index $S = 0$. A formal transition to the $S = 1$ triplet channel is accomplished by making the substitution $g_i \longrightarrow \hat{g}_i$ in all the relations involved.

The G matrix was sought [15] in the mixed coordinate-momentum representation by using the ansatz

$$G(k_\perp^2, k_\perp'^2, \mathbf{P}_\perp; x_1, x_2, x_3, x_4; E) = \sum_{ij} G_{ij}(X, X'; E, \mathbf{P}_\perp) g_i(k_\perp^2, x) g_j(k_\perp'^2, x'), \tag{10}$$

where the form factors $g_i(k_\perp^2, x)$ in the mixed representation are determined as the inverse Fourier transforms of the quantities $g_i(k_\perp^2 + k_x^2)$ in the variable k_x. In the direction of the x axis, we have introduced the obvious notation X and X' for the c.m. coordinates and x and x' for the relative coordinates prior to and after the scattering event, respectively.

A similar expansion is valid for the T matrix as well; that is,

$$T(k_\perp^2, k_\perp'^2, \mathbf{P}_\perp; x_1, x_2, x_3, x_4; E) = \sum_{ij} T_{ij}(X - X'; E, \mathbf{P}_\perp) g_i(k_\perp^2, x) g_j(k_\perp'^2, x'), \tag{11}$$

the coefficients T_{ij} being of course dependent only on the difference $t = X - X'$ of the c.m. coordinates. Substituting Eqs. (10) and (11) into (7), we arrive at the set of one-dimensional integral equations

$$G_{ij}(X, X'; E, \mathbf{P}_\perp) = T_{ij}(X - X'; E, \mathbf{P}_\perp) + \sum_{lm} \int dX_1 dX_2 T_{il}(X - X_1; E, \mathbf{P}_\perp) \times \delta B_{lm}(X_1, X_2; E, \mathbf{P}_\perp) G_{mj}(X_2, X'; E, \mathbf{P}_\perp), \tag{12}$$

where

$$\delta B_{lm} = B_{lm} - B_{lm}^{\mathrm{fr}} \tag{13}$$

is the difference of the convolution B_{lm} of the two-particle propagator A with the form factors g_l and g_m and the analogous convolution B_{lm}^{fr} for the free propagator A^{fr}. The explicit expressions for the integrals B_{lm} and B_{lm}^{fr} can be found in [15].

In analyzing the Landau–Migdal amplitude near the nuclear surface, we make use of the circumstance that, in the region being discussed, all the momenta are small, so that we can restrict our consideration to S-wave scattering. In the same approximation, we can retain only the zeroth harmonics of the Landau–Migdal amplitude,

$$F(\mathbf{r}, \mathbf{r}', \mathbf{r}_1, \mathbf{r}_1') = F_0(\mathbf{r}) \delta(\mathbf{r} - \mathbf{r}') \delta(\mathbf{r} - \mathbf{r}_1) \delta(\mathbf{r}_1 - \mathbf{r}_1'), \tag{14}$$

in which case relation (4) takes the form

$$F_0(\mathbf{r}) = Z^2(\mathbf{r}) G_0(\mathbf{r}), \tag{15}$$

where

$$G_0(\mathbf{r}) = \int d\mathbf{r}' d\mathbf{r}_1 d\mathbf{r}_1' G(\mathbf{r}, \mathbf{r}', \mathbf{r}_1, \mathbf{r}_1'). \tag{16}$$

Recalling the physical meaning of the Landau–Migdal amplitude, which describes the interaction of nucleons near the Fermi surface, we conclude that the quantity $G(\mathbf{r}_i)$ appearing in the integrand in (16) should be interpreted in some indirect way—namely, the use of the mixed coordinate–momentum representation [15] dictates that the absolute values of the momenta must be fixed at the local Fermi momentum $k_{\mathrm{F}}(r) = \sqrt{2m(\mu - V(r))}$ in the classically allowed region specified by the inequality $\mu - V(r) > 0$. We note that we must set $k_{\mathrm{F}}(r) = 0$ in the classically forbidden region [23].

A localized representation of the G matrix in the planar-slab model is especially simple at $P_\perp = 0$. In the singlet channel, it has the form [15]

$$\langle G_{\mathrm{F}}^{S=0} \rangle(X) = \sum_{ij} \langle G_{ij}^{S=0} \rangle(X) g_i(k_{\mathrm{F}}^2(X)) g_j(k_{\mathrm{F}}^2(X)), \tag{17}$$

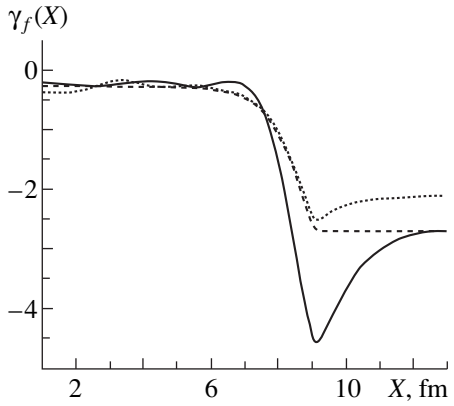

Fig. 1. Scalar–isoscalar combinations of the components of the G matrix, $\gamma_f(X)$ (solid curve), and the T matrix, $t_f(X)$ (dashed curve), at $P_\perp = 0$. The dotted curve represents the combinations $\gamma_f(X)$ calculated at $P_\perp^2 = 0.656$ fm^{-2}.

where

$$\langle G_{ij}^{S=0}\rangle(X) = \int_{-t_c}^{t_c} dt G_{ij}^{S=0}(X, X+t) \tag{18}$$

is a cutoff zeroth moment. For details associated with the need for introducing a cutoff in the integral in Eq. (18) and with the choice of value for the parameter t_c, the reader is referred to [15].

For the triplet channel, the quantity similar to that in Eq. (17) for the average of the G matrix becomes a 2×2 matrix in angular-momentum space; that is,

$$\langle G_{\rm F}^{S=1}\rangle_{LL'}(X) = \sum_{ij} \langle G_{ij}^{S=1}\rangle(X) g_i^{(L)}(k_{\rm F}^2(X)) g_j^{(L')}(k_{\rm F}^2(X)). \tag{19}$$

It was shown in [15], however, that terms involving $L = 2$ or $L' = 2$ are small within the slab; at the surface, they are negligibly small. For this reason, we will retain only the leading term $\langle G_{\rm F}^{S=1}\rangle(X) \equiv \langle G_{\rm F}^{S=1}\rangle_{00}(X)$.

The analogs of the averages (17) and (19) of the T matrix are given by

$$\langle T_{\rm F}^{S=0,1}\rangle(X; E) = \sum_{ij} \bar{T}_{ij}^{S=0,1}(E) g_i(k_{\rm F}^2(X)) g_j(k_{\rm F}^2(X)), \tag{20}$$

where the zeroth moments of the T matrix are introduced in the conventional way (without cutoff):

$$\bar{T}_{ij}^{S=0,1}(E) = \int dt T_{ij}^{S=0,1}(t; E) = T_{ij}^{S=0,1}(E, P_x = 0). \tag{21}$$

By g_i for $S = 1$ in Eq. (20), we mean the form-factor components $g_i^{L=0}$. Recall that we consider here the case of $P_\perp = 0$. Since we will subsequently have to differentiate relations (20) and (21) with respect to the energy E, it is written down explicitly as the argument in these relations. Needless to say, the variable $E = 2\mu$ is implied in all the relations (15)–(19).

Let us introduce the dimensionless averaged components of the G matrix in the singlet and in the triplet channel as

$$\gamma_{0,1}(X, E) = \frac{1}{C_0}\langle G_{\rm F}^{S=0,1}\rangle(X, E). \tag{22}$$

The analogous quantities for the T matrix are given by

$$t_{0,1}(X, E) = \frac{1}{C_0}\langle T_{\rm F}^{S=0,1}\rangle(X, E). \tag{23}$$

A detailed comparison of the G matrix and the T matrix was drawn in [15] for the singlet and the triplet channel individually. Here, we make use of the results presented in [15] in order to perform a direct comparison of those combinations of these components that correspond to zero spin and zero isospin in the particle–hole channel:

$$\gamma_f(X, E) = \frac{3}{16}(\gamma_0(X, E) + \gamma_1(X, E)), \tag{24}$$

$$t_f(X, E) = \frac{3}{16}(t_0(X, E) + t_1(X, E)). \tag{25}$$

Obviously, these are the combinations that enter into the scalar–isoscalar amplitude f_0 (this is indicated by the subscript f).

The quantities obtained by averaging, near the Fermi surface, the combinations (24) and (25) of the G matrix and the T matrix are compared in Fig. 1 for a planar slab at $P_\perp = 0$. It can be seen that the two curves are close to each other everywhere, with the exception of the region adjacent to the surface, where the quantity $\gamma_f(X)$ exceeds $t_f(X)$ in absolute value by a factor of about 2. Also shown in Fig. 1 is the quantity $\gamma_f(X)$ at the value of $P_\perp^2 = 0.656$ fm^{-2}, for which the calculations were performed in [15]. This value was chosen on the basis of the following considerations. An accurate method for averaging over $P_\perp$ in calculating $f_0(X)$ for a slab [or $f_0(r)$ for spherical nuclei] on the basis of Eq. (4) has yet to be developed. It is only obvious how we can do this in the asymptotic region off the slab (nucleus), where we can set $P_\perp = 0$, and within the slab, where we can use a method that is virtually identical to that within infinite nuclear matter and which involves integration with respect to $P_\perp$ from 0 to $2k_{\rm F}$. In dealing with the surface region, it must be considered that, for actual spherical nuclei, the orthogonal momentum in planar-slab geometry corresponds to the angular momentum. The result for $f_0(r)$ will then involve a sum over all possible

values of the total two-particle orbital angular momentum $\mathscr{L}$. Strictly speaking, the definition introduced above for the local Fermi momentum $k_F(r)$ is valid only for $\mathscr{L} = 0$. For $\mathscr{L} \neq 0$, the classical turning point beyond which we set $k_F(r) = 0$ is displaced toward smaller values of r. Obviously, this is of importance only for points such that $r \simeq R$, where R is the radius of the nucleus being considered. At a fixed value of $\mathscr{L}$, we then have $P_\perp^2 = \mathscr{L}(\mathscr{L}+1)/R^2$. In heavy nuclei from the region around ^{208}Pb, the maximal values of the single-particle orbital angular momentum, l_{max}, are 6 to 7. Accordingly, we have $\mathscr{L}_{max} = 12$–14. In order to assess the role of nonzero values of $P_\perp$, it is therefore reasonable to take the intermediate value of $\mathscr{L} = 6$, as was done in [15]. Setting $R = 8$ fm (the half-width of the slab in [15]), we obtain the $P_\perp^2$ value quoted above.

From Fig. 1, it can be seen that a nonzero $P_\perp$ value affects insignificantly the value of $f_0(X)$, but that it levels out the distinction between the $f_0(X)$ values at the surface that were calculated in terms of the G matrix and in terms of the T matrix corresponding to $P_\perp = 0$. The shape of the curve for nonzero $P_\perp$ beyond the slab boundary is of no concern because only zero value of $\mathscr{L}$ and, hence, zero value of $P_\perp$ survive in the classically forbidden region. It follows that, upon a correct averaging over $P_\perp$, the result of the calculation for $f_0(X)$ on the basis of Eq. (4) must be very close to the result obtained by applying the simplest recipe relying on the substitution $G \longrightarrow T(P_\perp = 0)$.

Obviously, the definitions in (17) and (19) and those that follow can be applied to a sufficiently heavy spherical nucleus upon the substitution $X \longrightarrow r$.

In the approximation of S-wave scattering, the zeroth harmonics of the invariant components of the Landau–Migdal amplitude can easily be found from (15) in terms of the functions $\gamma_0(r)$ and $\gamma_1(r)$. As a result, we obtain

$$f_0(r, E) = \frac{3}{16}Z^2(r)(\gamma_0(r, E) + \gamma_1(r, E)), \quad (26)$$

$$f_0'(r, E) = \frac{1}{16}Z^2(r)(\gamma_0(r, E) - 3\gamma_1(r, E)), \quad (27)$$

$$g_0(r, E) = -\frac{1}{16}Z^2(r)(3\gamma_0(r, E) - \gamma_1(r, E)), \quad (28)$$

$$g_0'(r, E) = -\frac{1}{16}Z^2(r)(\gamma_0(r, E) + \gamma_1(r, E)). \quad (29)$$

Strictly speaking, relations (26)–(29) are valid only far off the nucleus being studied, where we have $f_0(r) \longrightarrow f_0^{ex}$ [$f_0'(r) \longrightarrow (f_0')^{ex}$, etc.], on one hand, and where the quantities $\gamma_{0,1}$ go over to $t_{0,1}$, on the other hand. In Eq. (20), we must set $k_F = 0$ and $g_i = 1$, so that the functions t_0 and t_1 reduce to mere numbers at a fixed value of μ, Moreover, it is legitimate to assume that $Z = 1$ in this region. It is the way in which the above relations were used in [13, 14] to determine the parameters f_0^{ex} and so on. At $\mu = -8$ MeV, we have $t_0 = -4.60$ and $t_1 = -9.38$ [13, 14]. The substitution of these values into the expressions on the right-hand sides of (26)–(29) yields

$$f_0^{ex} = -2.62, \quad (f_0')^{ex} = 1.47,$$
$$g_0^{ex} = 0.27, \quad (g_0')^{ex} = 0.87. \quad (30)$$

These values, found in [13, 14], reproduce extremely well the empirical constants of the theory of finite Fermi systems (see the relevant discussion in [13, 14]). This suggests that the asymptotic relation $G = T$ becomes valid sufficiently fast. Another argument in support of this is provided by the results in Fig. 1, which were computed in [15]. On the basis of the above discussion of the data in this figure, we can replace $\gamma_{0,1}(r)$ by $t_{0,1}(r)$ on the right-hand side of Eq. (26).

Thus, we conclude that, to a high precision, the scalar–isoscalar amplitude $f_0(r)$ can be approximated by the expression

$$f_0(r) = \frac{3}{16}Z^2(r)(t_0(r) + t_1(r)), \quad (31)$$

which is fully determined by the potential of free-nucleon interaction and which is microscopic in this sense.

In support of the model specified by Eq. (31), we can also adduce the following simple consideration. Within the self-consistent theory of finite Fermi systems [4, 5], the scalar–isoscalar component $f_0(r)$ of the Landau–Migdal amplitude determines the central part of the mean nuclear potential, and the accuracy to which it is reproduced is the main criterion for correctly choosing the form of the function $f_0(r)$. In calculating the mean field $V(r)$ in the next section, we will rely on the exact many-body condition of the self-consistency of the theory of finite Fermi systems [5, 16]. The simplest form of this condition for spherical nuclei is

$$\frac{dV(r)}{dr} = C_0 f_0(r)\frac{d\rho(r)}{dr}, \quad (32)$$

where $\rho(\mathbf{r})$ is the isoscalar nuclear density. We can easily integrate Eq. (32) with $f_0(r)$ in the form (2) [or in the more general form (3)]. The result is

$$V(r) = C_0\left(f_0^{ex}\rho(r) + \frac{f_0^{in} - f_0^{ex}}{1+\alpha}\left(\frac{\rho(r)}{\rho_0}\right)^{1+\alpha}\right). \quad (33)$$

At $r = 0$, this yields

$$V(0) = \frac{C_0\rho_0}{1+\alpha}(\alpha f_0^{ex} + f_0^{in}). \quad (34)$$

It follows, in particular, that a soft density dependence corresponding, for example, to $\alpha = 2/3$ should be preferred to the harder linear interpolation (2). Let us dwell on this point at some length. By taking the realistic nuclear values of $V(0) = -50$ MeV and $\rho_0 = 0.16$ fm^{-3} and setting $f_0^{ex} = -2.62$ [see Eq. (30)], we arrive at $f_0^{in} \simeq 0.6$ at $\alpha = 1$ and $f_0^{in} \simeq 0$ at $\alpha = 2/3$. However, the first value of the constant f_0^{in} can be rejected since it leads to an overly great value of $K \simeq 400$ MeV for nuclear-matter compressibility, a value that is approximately twice as large as experimental values of $K = 150$–200 MeV, which were extracted from data on giant resonances [24]. The above compressibility factor is related to the constant f_0^{in} by the well-known Migdal formula

$$K = 9\frac{k_F^2}{3m}(1 + 2f_0^{in}), \tag{35}$$

where the extra factor of 9, which is absent from the corresponding formula in [1], was introduced in order to reduce the normalization of K to that which is used most often in the current literature and which was adopted in [24]. From Eq. (35), it follows that the constant f_0^{in} can take either a value close to zero or a small negative value.

In accordance with the aforesaid, expression (31) guarantees a correct value of the external constant f_0^{ex}, but it can lead to an error in f_0^{in}. Since the contribution of $|f_0^{ex}|$ in relation (34) is one order of magnitude greater than the contribution of $|f_0^{in}|$, even a 100% error in the quantity f_0^{in} would lead to only a 10% error in the well depth $V(0)$.

3. DEPENDENCE OF THE MEAN NUCLEAR FIELD OF THE CHEMICAL POTENTIAL

In this section, the proposed model expression (31) for the scalar–isoscalar Landau–Migdal amplitude is used to calculate the central part of the mean nuclear potential. Our consideration is based here on the exact many-body condition that, for a finite Fermi system that is bound in the absence of external fields, ensures consistency of the self-energy operator Σ, the effective interaction, and the single-particle Green's function $\mathcal{G}$. This condition is a corollary of a spontaneous breakdown of translation invariance and has the form

$$\frac{\partial\Sigma(\mathbf{r}, \mathbf{r}'; \varepsilon)}{\partial\mathbf{R}} = \int\frac{d\varepsilon'}{2\pi i}d\mathbf{r}_1 d\mathbf{r}_1' \mathcal{U}(\mathbf{r}, \mathbf{r}', \mathbf{r}_1, \mathbf{r}_1'; \varepsilon, \varepsilon')\frac{\partial\mathcal{G}(\mathbf{r}_1, \mathbf{r}_1'; \varepsilon')}{\partial\mathbf{R}_1}, \tag{36}$$

where $\mathbf{R} = (\mathbf{r} + \mathbf{r}')/2$, $\mathbf{R}_1 = (\mathbf{r}_1 + \mathbf{r}_1')/2$, and $\mathcal{U}$ is the NN-interaction block irreducible in the particle–hole channel.

Within Brueckner theory, we can set $\mathcal{U} = G$, and the approximation specified by Eq. (31) is equivalent to the condition

$$\mathcal{U}(\mathbf{r}, \mathbf{r}', \mathbf{r}_1, \mathbf{r}_1'; \varepsilon, \varepsilon') = C_0 t_f(\mathbf{r}; \varepsilon, \varepsilon')\delta(\mathbf{r} - \mathbf{r}')\delta(\mathbf{r} - \mathbf{r}_1)\delta(\mathbf{r}_1 - \mathbf{r}_1'). \tag{37}$$

From the above equations, it is obvious that the quantity t_f actually depends on the total energy $E = \varepsilon + \varepsilon'$. In the same approximation, we have $\Sigma(\mathbf{r}, \mathbf{r}'; \varepsilon) = \Sigma(\mathbf{r}; \varepsilon)\delta(\mathbf{r} - \mathbf{r}')$; in a spherical system, the mean field then has the form

$$V(r) = Z(r)\Sigma(r; \varepsilon = \mu). \tag{38}$$

By taking into account (37), we can approximately recast Eq. (36) into the form [5]

$$\frac{d\Sigma(r; \varepsilon)}{dr} = Z(r)C_0 t_f(r; \varepsilon, \mu)\frac{d\rho(r)}{dr}. \tag{39}$$

If the normalization factor $Z(r)$ in the Green's function is known, we find from (38) and (39) that the central part of the nuclear potential can be represented as

$$V(r) = -C_0 Z(r)\int_r^\infty ds Z(s)t_f(s; \mu, \mu)\frac{d\rho(s)}{ds}. \tag{40}$$

In principle, the consistency condition (36) can also be used to compute the Z factor $Z(r)$. However, estimates show that this quantity, which involves the derivative of the effective interaction with respect to energy, is more sensitive to details than the mean potential, so that the substitution $G \longrightarrow T$ is questionable in this case. For the Z factor, we will therefore use, for the time being, the phenomenological expression [5]

$$Z(r) = \frac{2}{1 + \sqrt{1 - 4C_0\alpha_2\rho(r)/\varepsilon_F^0}}, \tag{41}$$

where $\varepsilon_F^0 = (k_F^0)^2/2m$ [the normalization value is $k_F^0 = \pi^2/(mC_0)$] and the dimensionless constant α_2 is equal to -0.25.

The ensuing calculations are performed as follows. For the nucleus being considered, we first take an input mean field in the Woods–Saxon form

$$V(r) = -\frac{V_0}{1 + \exp((r - R)/d)} \tag{42}$$

with realistic nuclear-parameter values of $V_0 = 50$ MeV and $d = 0.65$ fm and with the potential radius of $R = r_0 A^{1/3}$ (here, $r_0 = 1.1$ fm and A is the mass number). By way of example, we consider the value of $A = 200$. For a preset potential well and a fixed value of the chemical potential μ, we determine the local Fermi momentum $k_F(r)$ at each point and the function in (25).

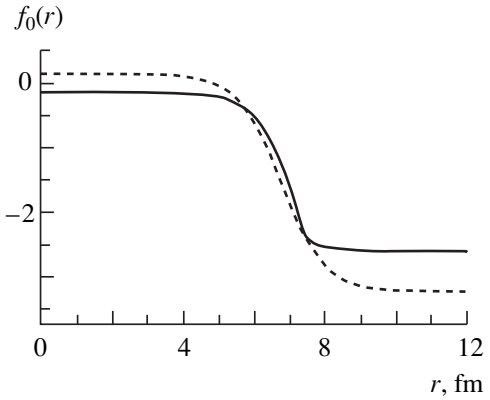

Fig. 2. Scalar–isoscalar component $f_0(r)$ of the Landau–Migdal amplitude: (solid curve) results of the calculation within the microscopic model proposed in the present study and (dashed curve) phenomenological amplitude in the self-consistent theory of finite Fermi systems [5].

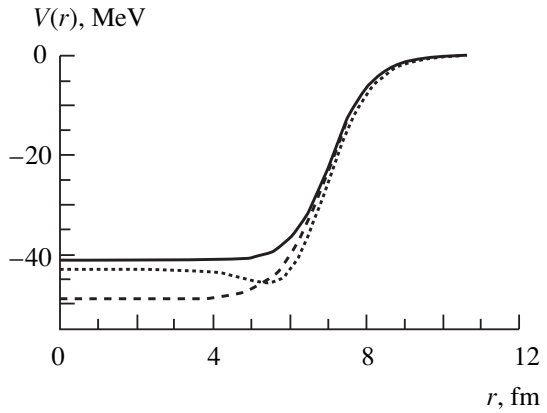

Fig. 3. Mean field $V(r)$ as calculated (solid curve) by formula (40), (dashed curve) by means of integration of Eq. (32) with the amplitude given by (31), and (dotted curve) by formula (44).

The density $\rho(r)$ is also taken in the simplest Fermi form

$$\rho(r) = \frac{\rho_0}{1 + \exp((r - \tilde{R})/d)}, \tag{43}$$

where the density radius $\tilde{R} = R - \Delta$ is less than the potential radius by the value of $\Delta = 0.5$ fm. The constant ρ_0 is determined by the normalization to the total number of particles.

Figure 2 shows the scalar–isoscalar component $f_0(r)$ of the Landau–Migdal amplitude according to Eqs. (31) and (41). For the sake of comparison, we also present the phenomenological amplitude (2) as calculated in [5, 25]. This amplitude can be determined by doubly differentiating the effective quasiparticle Hamiltonian of the self-consistent theory of finite Fermi systems. Referring the interested reader to [25] for the explicit form of this Hamiltonian, we only present here the eventual expressions for the first derivative, which is nothing but the mean field $V(r)$, and the second derivative, which represents the amplitude $f_0(r)$; that is,

$$V(r) = \frac{C_0 Z(\rho)}{1 - 4C_0\alpha_2\rho/\varepsilon_F^0} \times \left[\frac{3}{5}\frac{k_F^2(\rho)}{(k_F^0)^2}\rho\left(Z(\rho)\alpha_1 + \frac{m}{m^*(\rho)}\alpha_2\right) + \alpha_0 Z\rho + \frac{\gamma}{2\rho_0}Z^2\rho^2\right], \tag{44}$$

$$f_0(r) = \frac{k_F(\rho)m^*(\rho)}{\pi^2}\frac{C_0}{1 - 4C_0\alpha_2\rho/\varepsilon_F^0} \times \left[\alpha_0 + \frac{\gamma}{\rho_0}Z(\rho)\rho + 2\alpha_1\frac{k_F^2(\rho)}{(k_F^0)^2} + 2\alpha_2\frac{\mu(\rho)}{\varepsilon_F^0}\right], \tag{45}$$

where

$$\mu(\rho) = \frac{k_F^2(\rho)}{2m^*(\rho)}\frac{C_0(\alpha_0 Z(\rho)\rho + \gamma Z^2(\rho)\rho^2/(2\rho^0))}{\sqrt{1 - 4C_0\alpha_2\rho/\varepsilon_F^0}}, \tag{46}$$

$$\frac{m}{m^*(\rho)} = Z(\rho)(1 + C_0\alpha_1 Z(\rho)\rho/\varepsilon_F^0). \tag{47}$$

We note that the normalization density ρ^0 appearing in (46) is determined by the normalization Fermi momentum k_F^0 introduced in (41) and can be somewhat different from the density ρ_0 in (43). For the sake of simplicity, we have omitted here gradient terms: their inclusion would have been meaningful if we had addressed the problem of comparing the detailed behavior of the phenomenological amplitude and the detailed behavior of the microscopic amplitude, but we do not pursue this goal here. Moreover, we discarded terms that vanish upon the substitution of the phenomenological parameter values adopted in [5] ($\alpha_0 = -3.25$, $\alpha_1 = -\alpha_2 = 0.25$, $\gamma = 3.21$). Returning to the data in Fig. 2, we notice that, in the internal region, the two amplitudes are close to zero and that they behave similarly in the surface region, revealing distinctions of about 15% in the external region.

Figure 3 shows the mean field $V(r)$ calculated by three methods: (i) on the basis of relations (40) and (41); (ii) by integrating Eq. (32) with the Landau–Migdal amplitude $f_0(r)$ as given by (31) (solid curve in Fig. 2); and (iii) by formula (44) [we recall that this mean field corresponds to the amplitude $f_0(r)$ (45) depicted by the dashed curve in Fig. 2]. The distinctions between the results represented by the three curves (of about 15%) can be treated as a rough estimate of the accuracy of the proposed simple model.

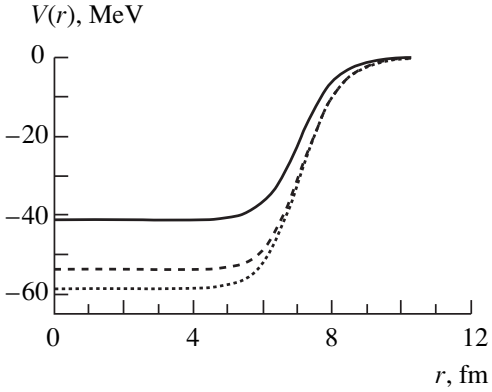

Fig. 4. Mean field $V(r)$ calculated by formula (40): (solid curve) results of the calculation at $|\mu| = 8$ MeV and results of the calculation at $|\mu| = 4$ MeV for $V_0 =$ (dashed curve) 50 and (dotted curve) 46 MeV.

All the interaction amplitudes considered here (the constant $f_0^{\rm ex}$ above all) depend on energy; therefore, the mean nuclear field must depend on the chemical potential μ of the nucleus under study. Let us analyze this dependence in some detail. For various values of μ, the table presents values of $f_0^{\rm ex}$ and of some other quantities that characterize $f_0(r)$. The constants t_0 and t_1 both grow in absolute value with decreasing $|\mu|$ because of the approach to the T-matrix pole in energy (a virtual pole at $S = 0$ and a real, deuteron, pole at $S = 1$). It is natural that the effect is stronger in the second case. The constant $f_0^{\rm ex}$, which is proportional to the sum of t_0 and t_1, also grows fast. On the basis of relation (34), which is of course approximate, we can state that, with decreasing $|\mu|$, the nuclear potential well must become deeper. Instead of the constant $f_0^{\rm in}$, the combination (25) of the $S = 0$, 1 components of the T matrix that is taken at the point $r = 0$ and which is proportional to this constant is presented in the fourth column. Actually, the constant $f_0^{\rm in}$, differing from it by the factor $Z(r = 0)^2$, is quoted only for the chemical-potential value of $\mu = 8$ MeV, at which the Z factor is known. At present, we are unable to indicate a reliable method for establishing the μ dependence of the Z factor. Estimates show that, with decreasing $|\mu|$, it decreases in magnitude, so that the values of $f_0^{\rm in}$ in the lower part of the table are expected to be less than $|t_f(r = 0)|$ by approximately one order of magnitude. Anyway, it is clear that, in estimating the well depth on the basis of relation (34), the term $f_0^{\rm in}$ can be disregarded against the term $f_0^{\rm ex}$.

Parameters determining the Landau–Migdal amplitude $f_0(r)$ versus the chemical potential μ

μ, MeV	t_0	t_1	$t_f(r = 0)$	$f_0^{\rm in}$	$f_0^{\rm ex}$
−10	−4.40	−8.21	−0.26		−2.36
−9	−4.49	−8.72	−0.26		−2.48
−8	−4.60	−9.38	−0.25	−0.14	−2.62
−7	−4.74	−10.24	−0.25		−2.81
−6	−4.91	−11.43	−0.26		−3.06
−5	−5.13	−13.23	−0.27		−3.44
−4	−5.44	−16.30	−0.30		−4.08
−3	−5.90	−22.91	−0.37		−5.40
−2	−6.66	−49.02	−0.67		−10.44

Figure 4 illustrates variations in the potential well for the nucleus in response to the reduction of the absolute value of the chemical potential down to $|\mu| = 4$ MeV. In order to avoid encumbering the picture, we present here the results obtained by only one method, that which is based on relation (40). When $|\mu|$ is reduced within the computational procedure used, which fixes the depth V_0 of the well of the input Woods–Saxon potential (42), we can see two effects. The first is the growth of the absolute values of the constants t_0 and t_1. The second is an increase in the local Fermi momentum $k_{\rm F}(r)$, the form factors in Eq. (20) changing accordingly. In order to eliminate the second effect, we have performed an alternative calculation where, changing μ, we varied accordingly the well depth V_0 (from 50 to 46 MeV) in such a way as to ensure invariability of the difference $V(r) - \mu$, which appears in $k_{\rm F}(r)$. The result of this calculation is represented by the dotted curve in Fig. 4. We can see that, with decreasing $|\mu|$, the potential well becomes much deeper, the effect from the variation in $k_{\rm F}(r)$ being much weaker than the direct energy dependence of the T matrix. In this connection, it should be noted that the present calculation is not fully self-consistent since the resulting potential differs from the input one (especially at small values of $|\mu|$). A procedure that would ensure full self-consistency is very complicated and must include a recipe for calculating densities for a preset potential. In the present study, we did not aim at developing such a procedure. On the basis of the analysis illustrated in Fig. 4, we can expect, however, that rendering the procedure self-consistent would not induce any qualitative changes in the result because the effect that we found is due primarily to the direct energy dependence of the constant $f_0^{\rm ex}$. The results of a more systematic analysis of the amplitude $f_0(r)$ and the mean nuclear potential as functions of μ are illustrated in Fig. 5. It can be seen that the effect being considered is very large at extremely small values of $|\mu|$. Estimates show that it is somewhat exaggerated in the present rough calculation and that the inclusion of the energy dependence of the Z factor must weaken the chemical-potential dependence of the potential. However, the result does not change qualitatively, and

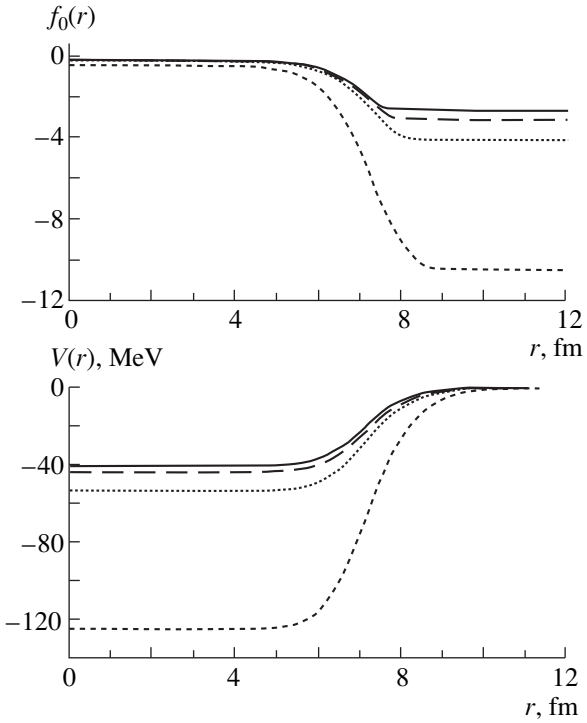

Fig. 5. Scalar–isoscalar component $f_0(r)$ of the Landau–Migdal amplitude (upper panel) and mean nuclear potential $V(r)$ (lower panel) according to the calculation at various values of the chemical potential: $|\mu|$ = (solid curve) 8, (long dashes) 6, (dotted curve) 4, and (short dashes) 2 MeV.

it is necessary to take this result into account in analyzing nuclei far off the beta-stability valley.

4. CONCLUSION

A simple microscopic model has been proposed for the zeroth harmonic of the scalar–isoscalar component $f_0(r)$ of the Landau–Migdal amplitude, which is usually introduced phenomenologically in Migdal's theory of finite Fermi systems. In constructing the model, we relied on Brueckner theory, where the Landau–Migdal amplitude is expressed in terms of the G matrix. In the surface region of nuclei, which determines, to a great extent, the form of the function $f_0(r)$, the conditions of applicability of Brueckner theory are better satisfied than in the interior of nuclear matter. We can therefore hope that the accuracy of the present approach is higher than the accuracy of Brueckner theory for nuclear matter. On the basis of the analysis performed previously [15] for the Brueckner G matrix in a planar slab of nuclear matter, we have investigated the combination of the G matrices for spin values of $S = 0$ and 1 that corresponds to zero spin and zero isospin in the particle–hole channel. It has been shown that this quantity, which determines the scalar–isoscalar component $f_0(r)$ of the Landau–Migdal amplitude, is approximately equal to the analogous combination of the off-mass-shell T matrices for free nucleon–nucleon scattering at the negative energy of $E = 2\mu$. The resulting amplitude $f_0(r)$ induces the mean nuclear field $V(r)$, which, at μ = –8 MeV, agrees reasonably well with the phenomenological nuclear potential. Since the T matrix depends sharply on E at small energies, the depth $V(0)$ of the computed potential well increases greatly with decreasing $|\mu|$. This effect is of importance for analysis of stability of nuclei near the nucleon drip line, where μ vanishes.

ACKNOWLEDGMENTS

This work was supported by in part by the Ministry for Higher Education of the Russian Federation (grant no. 97-0-6.1-7) and by the Russian Foundation for Basic Research (project nos. 00-02-17319 and 00-15-96590).

REFERENCES

1. A. B. Migdal, *Theory of Finite Fermi Systems and Applications to Atomic Nuclei* (Nauka, Moscow, 1965; Interscience, New York, 1967).
2. L. D. Landau, Zh. Éksp. Teor. Fiz. **35**, 97 (1958) [Sov. Phys. JETP **8**, 70 (1959)].
3. A. A. Abrikosov, L. P. Gor'kov, and I. E. Dzyaloshinskiĭ, *Methods of Quantum Field Theory in Statistical Physics* (Fizmatgiz, Moscow, 1962; Prentice-Hall, Englewood Cliffs, 1963).
4. A. B. Migdal, *Theory of Finite Fermi Systems and Applications to Atomic Nuclei* (Nauka, Moscow, 1983, 2nd ed.).
5. V. A. Khodel and E. E. Saperstein, Phys. Rep. **92**, 183 (1982).
6. G. G. Bunatyan and M. A. Mikulinskiĭ, Yad. Fiz. **1**, 38 (1965) [Sov. J. Nucl. Phys. **1**, 26 (1965)].
7. D. Vautherin and D. Brink, Phys. Rev. C **5**, 626 (1972).
8. S. A. Fayans and D. Zawischa, Phys. Lett. B **363**, 12 (1995).
9. S. A. Fayans and D. Zawischa, Phys. Lett. B **383**, 19 (1996).
10. H. A. Bethe, Annu. Rev. Nucl. Sci. **21**, 93 (1971).
11. P. Ring and P. Schuck, *The Nuclear Many-Body Problem* (Springer-Verlag, Berlin, 1980).
12. M. Baldo and L. S. Ferreira, Phys. Rev. C **50**, 1887 (1994).
13. M. Baldo, U. Lombardo, E. E. Saperstein, and M. V. Zverev, Yad. Fiz. **60**, 2170 (1997) [Phys. At. Nucl. **60**, 1988 (1997)].
14. M. Baldo, U. Lombardo, E. E. Saperstein, and M. V. Zverev, Phys. Lett. B **421**, 8 (1998).
15. M. Baldo, U. Lombardo, E. E. Saperstein, and M. V. Zverev, Yad. Fiz. **64**, 247 (2001) [Phys. At. Nucl. **64**, 203 (2001)].
16. S. A. Fayans and V. A. Khodel', Pis'ma Zh. Éksp. Teor. Fiz. **17**, 633 (1973) [JETP Lett. **17**, 444 (1973)].
17. J. Haidenbauer and W. Plessas, Phys. Rev. C **30**, 1822 (1984).
18. J. Haidenbauer and W. Plessas, Phys. Rev. C **32**, 1424 (1985).

19. M. Lacombe, B. Loiseaux, J. M. Richard, *et al.*, Phys. Rev. C **21**, 861 (1980).

20. M. Baldo, J. Cugnon, A. Lejeune, and U. Lombardo, Nucl. Phys. A **515**, 409 (1990).

21. M. Baldo, I. Bombaci, G. Giansiracusa, and U. Lombardo, Nucl. Phys. A **545**, 741 (1992).

22. M. Baldo, U. Lombardo, E. E. Saperstein, and M. V. Zverev, Yad. Fiz. **60**, 1206 (1997) [Phys. At. Nucl. **60**, 1081 (1997)].

23. M. Baldo, U. Lombardo, E. E. Saperstein, and M. V. Zverev, Nucl. Phys. A **628**, 503 (1998).

24. A. Bohr and B. Mottelson, *Nuclear Structure* Vol. 2: *Nuclear Deformations* (Benjamin, New York, 1974; Mir, Moscow, 1977).

25. V. A. Khodel, E. E. Saperstein, and M. V. Zverev, Nucl. Phys. A **465**, 397 (1987).

Translated by A. Isaakyan

Physics of Atomic Nuclei, Vol. 64, No. 3, 2001, pp. 465–470. From Yadernaya Fizika, Vol. 64, No. 3, 2001, pp. 520–524.

90th ANNIVERSARY OF A.B. MIGDAL'S BIRTHDAY
NUCLEI

Q-Phonon Scheme in the Collective Nuclear Model*

R. V. Jolos**

Joint Institute for Nuclear Research, Dubna, Moscow oblast, 141980 Russia

Received July 17, 2000

Abstract—The *Q*-phonon scheme developed on the basis of the algebraic collective nuclear model is discussed. It is shown that, within this scheme, low-lying collective states of even–even nuclei can be described to a precision higher than 90% of the norm by using one or, at maximum, two components of the *Q*-phonon basis constructed by applying a fixed number of the quadrupole operators *Q* to the exact ground state of the system. Various applications of this approximate scheme are discussed. It is shown that, by using this scheme, the relations between several *E*2-transition probabilities or between the energies of the collective states can be derived. It is also shown that the *Q*-phonon scheme can be used to extract information about the equilibrium shapes of nuclei and their fluctuations from data on the *E*2-transition probabilities. *© 2001 MAIK "Nauka/Interperiodica".*

This article is dedicated to the 90th anniversary of the birthday of Professor A.B. Migdal, who made an enormous contribution to nuclear physics. It was characteristic of his scientific work to develop quantitatively new nonperturbative methods and to use phenomenological approaches. The structure of nuclei is an interesting field of investigations, which requires both phenomenological approaches to select the most important degrees of freedom for describing phenomena and nonperturbative methods since the interaction is strong.

The nuclear ground states have a very complicated structure. For their description, they require a huge configuration space. Thus, a complete description of the ground-state wave functions is beyond the possibilities of the existing theoretical approaches. However, excited states can be produced by applying one-body operators to ground-state wave functions. This is just the way realized within the *Q*-phonon approach to describing collective nuclear states [1–4]. In this approach, an attempt was made to describe low-lying collective states of even–even nuclei in terms of multiple *Q*-phonon excitations of the ground state,

$$|L^+, n\rangle = \mathcal{N}^{(L,n)}(\underbrace{Q\ldots Q}_{n})_L|0_1^+\rangle, \quad (1)$$

where $|0_1^+\rangle$ is the ground-state wave vector.

Within the interacting-boson model (IBM), the quadrupole-moment operator *Q* is expressed in terms of the monopole *s*-boson and the quadrupole *d*-boson operators as

$$Q = s^+\tilde{d} + d^+s + \chi(d^+\tilde{d})_2. \quad (2)$$

In general, the *Q* configurations (1) form a basis, which can be used to expand the eigenstates of the IBM Hamiltonian. There arises the question of how many basis states of the type in (1) are required for describing eigenstates to a sufficient precision. It was shown that the wave vectors of yrast states can be described to a high precision (better than 90% of the norm) over the whole parameter space of the consistent *Q* Hamiltonian *H* [1, 2],

$$H = \epsilon_d\sum_\mu d_\mu^+ d_\mu - \kappa Q(\chi)Q(\chi), \quad (3)$$

by simple universal expressions containing only one multiple *Q*-phonon configuration

$$|L^+, 1\rangle = \mathcal{N}^{(L,1)}(\underbrace{Q\ldots Q}_{L/2})_L|0_1^+\rangle. \quad (4)$$

Later, it was shown [3] that the second 2^+ state, which is a two-phonon state in the case of a harmonic vibrator and a $K = 2$ one-phonon gamma-vibrational state in the rotor limit, can be described to a precision higher than 90% over the whole parameter space of Hamiltonian (3) as a two-*Q*-phonon configuration

$$|2_{QQ}^+\rangle = \mathcal{N}^{(2,2)}\left[(QQ)_{(2)} - \frac{\langle 0_1^+|(QQQ)_{(0)}|0_1^+\rangle}{\langle 0_1^+|(QQ)_{(0)}|0_1^+\rangle}Q\right]|0_1^+\rangle. \quad (5)$$

The state vector (5) is orthogonal to the one-*Q*-phonon configuration. To describe a weak decay of the 2_2^+ state to the ground state, it is necessary to take into account a small admixture of the one-*Q*-phonon configuration

$$|2_Q^+\rangle = \mathcal{N}^{(2,1)}Q|0_1^+\rangle \quad (6)$$

to the state vector (5). In this case, the 2_2^+-state vector is described to a precision of about 98% of the norm [3].

* This article was submitted by the author in English.

** e-mail: jolos@thsun1.jinr.ru

The 0_2^+ state, which is interpreted as a two-phonon state in the case of vibrator nuclei and as a β-vibrational state in the case of strongly deformed nuclei, was considered in [4]. It was shown that the 0_2^+ state can be described to a precision higher than 90% of the norm over the whole parameter space of Hamiltonian (3) as a linear combination of only two components

$$|0^+_{QQ}\rangle = \frac{((QQ)_0 - \langle 0^+_1|(QQ)_0|0^+_1\rangle)}{\sqrt{\langle 0^+_1|(QQ)_0(QQ)_0|0^+_1\rangle - \langle 0^+_1|(QQ)_0|0^+_1\rangle^2}}|0^+_1\rangle \quad (7)$$

and

$$|0^+_{QQQ}\rangle = \frac{((QQQ)_0 - \langle 0^+_1|(QQQ)_0|0^+_1\rangle)}{\sqrt{\langle 0^+_1|(QQQ)_0(QQQ)_0|0^+_1\rangle - \langle 0^+_1|(QQQ)_0|0^+_1\rangle^2}}|0^+_1\rangle. \quad (8)$$

The wave vectors (7) and (8) are linearly independent, but they are not orthogonal. In view of this, it is convenient to subtract, from (8), its projection on (7), whereby the state vector $|\widetilde{0^+_{QQQ}}\rangle$ is introduced, which is orthogonal to $|0^+_{QQ}\rangle$,

$$|\widetilde{0^+_{QQQ}}\rangle = \frac{|0^+_{QQQ}\rangle - \langle 0^+_{QQ}|0^+_{QQQ}\rangle|0^+_{QQ}\rangle}{\sqrt{1 - \langle 0^+_{QQ}|0^+_{QQQ}\rangle^2}}. \quad (9)$$

Now, the 0_2^+ state can be approximately represented as

$$|0^+_2\rangle = \cos\phi \cdot |0^+_{QQ}\rangle + \sin\phi \cdot |\widetilde{0^+_{QQQ}}\rangle. \quad (10)$$

In vibrator nuclei or in the isotopes of Sm and Gd belonging to the beginning of the deformed region, the first component in (10) is the main one. In the region of γ-unstable nuclei like heavy Pt isotopes, the second component becomes the main one.

Summarizing the results described above, we can write the following approximate expressions for several low-lying collective states:

$$|2^+_1\rangle = \mathcal{N}^{(2,1)}Q|0^+_1\rangle = |2^+_Q\rangle, \quad (11)$$

$$|4^+_1\rangle = \mathcal{N}^{(4,1)}(QQ)_4|0^+_1\rangle, \quad (12)$$

$$|6^+_1\rangle = \mathcal{N}^{(6,1)}(QQQ)_6|0^+_1\rangle, \quad (13)$$

$$|2^+_2\rangle = |2^+_{QQ}\rangle, \quad (14)$$

$$|0^+_2\rangle = \cos\phi \cdot |0^+_{QQ}\rangle + \sin\phi \cdot |\widetilde{0^+_{QQQ}}\rangle. \quad (15)$$

As a matter of fact, relations (11)–(15) give us the expressions for the wave vectors belonging to the three main bands of even–even nuclei: the ground-state band, the (quasi)β band, and the (quasi)γ band.

Although the consideration above was based on the IBM, it was shown in [5, 6] that the calculations are correct for some other models as well. Therefore, we hope that the results formulated above have a more general applicability. It is also useful to emphasize that, in expressions (11)–(15), the properties of the ground state, as well as the properties of the quadrupole operator, change with the Hamiltonian parameters and with the number of valence nucleons. Therefore, the properties of the states represented by the *Q*-phonon configurations also change. However, the relations between them undergo virtually no changes. These results cannot be obtained by perturbation theory near one of the dynamical symmetry limits. In terms of bosons, the wave functions of the states considered above seem complicated. However, the expressions for the wave vectors of excited states take a much more compact form since we use the exact ground-state wave function in (11)–(15).

Having universal expressions for the eigenvectors, we can derive various relations between the matrix elements of the quadrupole operator—that is, between *B*(*E*2) and the spectroscopic quadrupole moments. The accuracy of these relations can be improved if we take into account a small admixture of the $|2^+_{QQ}\rangle$ component in the wave function of the 2_1^+ state and, correspondingly, a small admixture of the $|2^+_Q\rangle$ component in the wave function of the 2_2^+ state.

Using the expressions for the wave vectors of the low-lying states described above, we can calculate directly the reduced matrix elements of the quadrupole operator *Q* between the ground and the low-lying collective states. As can be seen from the structure of the wave vectors (11)–(15), these reduced matrix elements will be determined by the ground-state expectation values of the scalars constructed from the various numbers of *Q* operators like $\langle 0^+_1|(QQ)_0|0^+_1\rangle$, $\langle 0^+_1|(QQQ)_0|0^+_1\rangle$, $\langle 0^+_1|(QQ)_0(QQ)_0|0^+_1\rangle$, and so on up to the scalar of highest order. The highest order is determined by the angular momentum of the wave vector under consideration. However, it was shown in [7] that, in the physically interesting region, this highest order scalar can be approximately expressed in terms of the lower order scalars with a sufficient accuracy. Expressing observables in terms of the smaller number of scalars, we can eliminate these scalars from the expressions and obtain relations between the observables.

The first of the relations obtained in this way is the relation expressing the absolute value of the spectroscopic quadrupole moment of the 2_1^+ state in terms of some *B*(*E*2) [8],

$$q(2^+_1) = \frac{|Q(2^+_1)|}{\sqrt{B(E2;\, 2^+_1 \longrightarrow 0^+_1)}} = \frac{8}{7}\sqrt{\pi G(1 + R_1 - W)}, \quad (16)$$

where

$$G = \frac{7}{10}\frac{B(E2; 4_1^+ \longrightarrow 2_1^+)}{B(E2; 2_1^+ \longrightarrow 0_1^+)}, \quad (17)$$

$$R_1 = \frac{B(E2; 2_2^+ \longrightarrow 0_1^+)}{B(E2; 2_1^+ \longrightarrow 0_1^+)}, \quad (18)$$

$$W = \frac{B(E2; 2_2^+ \longrightarrow 2_1^+)}{B(E2; 4_1^+ \longrightarrow 2_1^+)}. \quad (19)$$

We have checked the accuracy of relation (16) by exact calculations within the IBM in the full parameter space of Hamiltonian (3). We compared the exact values of the $Q(2_1^+)$ found in the calculations with those obtained by substituting the exact values of G, R_1, W, and $B(E2; 2_1^+ \longrightarrow 0_1^+)$ into (16). For the total number N of bosons equal to 12, the deviations are less than 2.2%. For $N = 6$, the deviations are less than 8%. The largest deviations are obtained near the limit of the vibrator nuclei [$U(5)$ dynamical symmetry limit]. However, the quadrupole moment tends to zero in this limit.

We used relation (16) to calculate $q(2_1^+)$ for a set of nuclei taking, as an input, the experimental data on the ratios of $B(E2)$ and their errors. There is satisfactory agreement between the calculated values and the data; for instance, for ^{106}Pd, we have $q_{\text{calc}}(2_1^+) = 1.51 \pm 0.32$ and $q_{\text{expt}}(2_1^+) = 1.54 \pm 0.22$; for ^{108}Pd, $q_{\text{calc}}(2_1^+) = 1.17 \pm 0.30$ and $q_{\text{expt}}(2_1^+) = 1.58 \pm 0.34$; for ^{188}Os, $q_{\text{calc}}(2_1^+) = 1.92 \pm 0.03$ and $q_{\text{expt}}(2_1^+) = 1.95 \pm 0.05$; and, for ^{196}Pt, $q_{\text{calc}}(2_1^+) = 0.91 \pm 0.08$ and $q_{\text{expt}}(2_1^+) = 1.26 \pm 0.23$.

The ground-state decay of the 2_2^+ state is due to the admixture of the one Q-phonon configuration $|2_Q^+\rangle$. The relative $E2$ strength for the transition from the ground state to the 2_1^+ state is much larger and is also determined by the square of the amplitude of the $|2_Q^+\rangle$ configuration. Thus, the ratio $B(E2; 0_1^+ \longrightarrow 2_2^+)/B(E2; 0_1^+ \longrightarrow 2_1^+)$ is determined by the ratio of the squares of these amplitudes. An alternative measure of this ratio is the branching ratio for the $E2$ decay of the 3_1^+ state, which can be approximated by the 3-Q-phonon configuration $|3_1^+\rangle \approx \mathcal{N}^{(3,1)}(QQQ)_3|0_1^+\rangle$, to the lower 2^+ states. It is possible to deduce a formula that makes it possible to estimate the absolute value of $B(E2)$ for the decay of the 2_2^+ state from the $E2$ branching ratio for the 3_1^+ state and $B(E2; 2_1^+ \longrightarrow 0_1^+)$, which are often known. This formula is [3]

$$B(E2; 2_2^+ \longrightarrow 0_1^+) \approx \frac{B(E2; 3_1^+ \longrightarrow 2_1^+)}{B(E2; 3_1^+ \longrightarrow 2_2^+)} B(E2; 2_1^+ \longrightarrow 0_1^+). \quad (20)$$

This relation allows one to predict the $E2$ excitation strength of the 2_2^+ state from the knowledge of the following two observables: the $E2$ branching ratio for the 3_1^+ state and the lifetime of the first excited 2_1^+ state. It is interesting to compare Eq. (20) with experimental data. A comparison shows that, while the branching ratio for the decay of the 3_1^+ state and the ratio of the $E2$ excitation strengths for the ground state vary within an order of magnitude in the nuclei being considered, Eq. (20) is valid within a factor of about 2. Equation (20) describes data for all collective nuclei: vibrators, rotors, γ-soft nuclei, and various types of transitional nuclei. In rotor nuclei, the relative decay intensity for the $3_1^+ \longrightarrow 2_2^+$ transition is rarely known experimentally because of low transition energies, but data for ^{168}Er, which is one of the best-studied rotors, support the validity of (20) for rotors.

The multi-Q-phonon representation of collective states helps us establish new selection rules for $E2$ transitions. It was shown in [2] that, for the yrast states that can be described approximately as the pure multi-Q-phonon configurations, there exists a simple selection rule for the $E2$-transition probabilities—namely, the $E2$ transitions between states differing by more than one unit of Q are weak in relation to the $E2$ transitions between states differing by one unit of Q. For instance, it was shown that the branching ratios $B(E2; 3_{QQQ}^+ \longrightarrow 2_Q^+)/B(E2; 3_{QQQ}^+ \longrightarrow 2_{QQ}^+)$ and $B(E2; 5_{QQQQ}^+ \longrightarrow 4_{QQ}^+)/B(E2; 5_{QQQQ}^+ \longrightarrow 4_{QQQ}^+)$ are very small for all collective nuclei. Because of this selection rule, the ratio $B(E2; 0_{QQQ}^+ \longrightarrow 2_{QQ}^+)/B(E2; 0_{QQQ}^+ \longrightarrow 2_Q^+)$ is expected to be much larger than the ratio $B(E2; 0_{QQ}^+ \longrightarrow 2_{QQ}^+)/B(E2; 0_{QQ}^+ \longrightarrow 2_Q^+)$. This means that, at least for γ-soft or nearly γ-soft nuclei, where the 0_2^+ state is approximated by the $|0_{QQQ}^+\rangle$ configuration, $B(E2; 0_2^+ \longrightarrow 2_2^+)/B(E2; 0_2^+ \longrightarrow 2_1^+)$ must be large. Since, for large γ rigidity, the 0_2^+ state is described mainly by the $|0_{QQ}^+\rangle$ configuration, the ratio $B(E2; 0_2^+ \longrightarrow 2_2^+)/B(E2; 0_2^+ \longrightarrow 2_1^+)$ is expected to decrease with increasing γ rigidity. The γ rigidity must increase when nuclei approach the region of static deformations—that is, when, for instance, the ratio $B(E2; 4_1^+ \longrightarrow 2_1^+)/B(E2; 2_1^+ \longrightarrow 0_1^+)$ decreases.

From the results obtained in [4] for the description of the γ-soft nuclei, it follows that the two lowest excited collective 0^+ states can be described as approximately pure three-Q-phonon and two-Q-phonon configurations. These two multi-Q-phonon configurations are characterized by different $E2$ decay properties: the three-Q-phonon configuration decays mainly to the 2_2^+ state, but the two-Q-phonon configuration decays mainly to the 2_1^+ state. A nice example is provided by the ^{196}Pt nucleus [9]. In this case, $B(E2; 0_2^+ \longrightarrow 2_2^+)/B(E2; 0_2^+ \longrightarrow 2_1^+) = 6.32$ and $B(E2; 0_3^+ \longrightarrow 2_2^+)/B(E2; 0_3^+ \longrightarrow 2_1^+) = 0.16$. A similar situation is realized in ^{194}Pt for 0_2^+ and 0_4^+ states produced in the Coulomb excitation experiments [10]. In this case, $B(E2; 0_2^+ \longrightarrow 2_2^+)/B(E2; 0_2^+ \longrightarrow 2_1^+) = 10.9$ and $B(E2; 0_4^+ \longrightarrow 2_2^+)/B(E2; 0_4^+ \longrightarrow 2_1^+) = 0.97$.

As was indicated above, the Q-phonon representation of the collective states gives the possibility of expressing the reduced matrix elements of the $E2$-transition operator in terms of the ground-state expectation values of the scalars constructed by the various numbers of Q operators. These scalars are also known as shape invariants in nuclear-structure physics [11, 12]. In the geometric collective model [13], they are functions of the variables β and γ, which describe the nuclear shape. By definition, these functions are invariant under the rotation of the coordinate frame.

The lowest order shape invariants are defined as

$$K_2 \equiv 5\langle 0_1^+|(QQ)_0|0_1^+\rangle, \tag{21}$$

$$K_3 \equiv \frac{\left|\langle 0_1^+|(QQQ)_0|0_1^+\rangle\right|}{\langle 0_1^+|(QQ)_0|0_1^+\rangle^{3/2}}\sqrt{5\sqrt{5}}, \tag{22}$$

$$K_4 \equiv \langle 0_1^+|(QQ)_0^2|0_1^+\rangle/\langle 0_1^+|(QQ)_0|0_1^+\rangle^2, \tag{23}$$

$$K_5 \equiv \langle 0_1^+|(QQQ)_0(QQ)_0|0_1^+\rangle/(\langle 0_1^+|(QQQ)_0|0_1^+\rangle \times \langle 0_1^+|(QQ)_0|0_1^+\rangle), \tag{24}$$

$$K_6 \equiv \langle 0_1^+|(QQQ)_0(QQQ)_0|0_1^+\rangle/\langle 0_1^+|(QQQ)_0|0_1^+\rangle^2. \tag{25}$$

In the geometric model, we have

$$K_2 \sim \langle 0_1^+|\beta^2|0_1^+\rangle, \tag{26}$$

$$K_3 = \sqrt{\frac{2}{35}}\,\frac{\langle 0_1^+|\beta^3\cos 3\gamma|0_1^+\rangle}{\langle 0_1^+|\beta^2|0_1^+\rangle^{3/2}}, \tag{27}$$

$$K_4 = \frac{\langle 0_1^+|\beta^4|0_1^+\rangle}{\langle 0_1^+|\beta^2|0_1^+\rangle^2}, \tag{28}$$

$$K_5 = \frac{\langle 0_1^+|\beta^5\cos 3\gamma|0_1^+\rangle}{\langle 0_1^+|\beta^3\cos 3\gamma|0_1^+\rangle\langle 0_1^+|\beta^2|0_1^+\rangle}, \tag{29}$$

$$K_6 = \frac{\langle 0_1^+|\beta^6\cos^2 3\gamma|0_1^+\rangle}{\langle 0_1^+|\beta^3\cos 3\gamma|0_1^+\rangle^2}. \tag{30}$$

The first invariant K_2 is almost useless in the Q-phonon formalism, because, in order to extract the average value of β^2 in the ground state, we must know the effective charge for the quadrupole transitions. The second invariant K_3 can be used to obtain the average value of γ in the ground state. The invariants K_4, K_5, and K_6 furnish important information about the fluctuations of β and γ.

To obtain the values of these invariants directly from experimental data by using only the definitions of the invariants, we need a huge number of experimental matrix elements of the quadrupole-moment operator connecting high-lying collective states as well. In practice, they can be extracted from the Coulomb excitation data, but with large errors in many cases. Only for low-lying collective states that are well known or can be measured to a sufficient precision does the Q-phonon scheme provide the possibility of deriving analytic expressions for the shape invariants in terms of the $E2$-transition probabilities. These expressions are [7]

$$K_3 = \sqrt{\frac{2G}{35}}\left[\left(\frac{1-R_1}{1+R_1}\right)\sqrt{1-\frac{W}{1+R_1}} - \frac{2}{1+R_1}\sqrt{\frac{R_1 W}{1+R_1}}\right], \tag{31}$$

$$K_4 = \frac{7}{10}\,\frac{B(E2; 4_1^+ \longrightarrow 2_1^+)}{B(E2; 2_1^+ \longrightarrow 0_1^+)}. \tag{32}$$

A comparison with the results of exact IBM calculations shows that, in general, expressions (31) and (32) are correct to a precision higher than 85%. In the entire region of interest in the full parameter space of Hamiltonian (3), the accuracy is still higher. These expressions were used to determine the shape invariants for several nuclei characterized by different collective properties [7].

The expressions for the K_5 and K_6 invariants are more complicated. They can be more easily expressed in terms of the $E2$-transition probabilities if we assume that the lowest two collective 0^+ excited states are described as the pure $|0_{QQQ}^+\rangle$ and $|0_{QQ}^+\rangle$ configurations. This is true in the region of heavy Pt and Os isotopes. However, this region of the nuclide chart is the most interesting for determining the K_5 and K_6 invariants, since these invariants characterize the γ softness of the

nuclei and since the heavy Pt and Os isotopes belong to the region of γ-soft nuclei. These expressions are [4]

$$\frac{B(E2;\,0^+_{QQQ}\longrightarrow 2^+_{QQ})}{B(E2;\,0^+_{QQQ}\longrightarrow 2^+_{Q})} = \frac{1}{5\sqrt{5}}\,\frac{z}{1-z}\left(\frac{K_6-K_5}{K_5-1}\right)^2, \quad (33)$$

$$\frac{B(E2;\,0^+_{QQ}\longrightarrow 2^+_{QQ})}{B(E2;\,0^+_{QQ}\longrightarrow 2^+_{Q})} = \frac{1}{5\sqrt{5}}\,\frac{z}{1-z}\left(\frac{K_5-K_4}{K_4-1}\right)^2, \quad (34)$$

where $z = (35/2)K_3^2/K_4$. They can be used to determine K_6 and K_5 if K_3, K_4, and the branching ratios are known. Let us consider the ^{196}Pt nucleus as an example. The values of K_3 and K_4 can be extracted from $B(E2)$ values. They are $\sqrt{35/2}\,K_3 = 0.446$ and $K_4 = 1.06$. Substituting these values into (33) and (34) and using experimental data on the branching ratios, we find for ^{196}Pt that $K_5 = 1.11$ and $K_6 = 1.69$. The deviations of K_4, K_5, and K_6 from unity characterize the amplitudes of fluctuations of the corresponding dynamical quantities. It can be seen from the results obtained that, in ^{196}Pt, fluctuations of γ are much greater than fluctuations of β.

The *Q*-phonon representation of collective states is mainly useful for deducing relations between *E*2-transition probabilities. As is shown below, this formalism can also be used to obtain relations between the energies of collective states.

It was shown in [14, 15] that nearly universal empirical behavior characterizes nuclei between the vibrator and rotor limits. Specifically, $E(4^+_1)$ is empirically linear in $E(2^+_1)$ with a slope of 2.0 for all $Z = 38$–82 nuclei with

$$2.05 \le E(4^+_1)/E(2^+_1) \le 3.15. \quad (35)$$

Such behavior is described be the equation

$$E(4^+_1) = 2.0E(2^+_1) + \epsilon_4, \quad (36)$$

where ϵ_4 is a constant for nuclei whose underlying structure exhibits such variations. To approach this problem, we consider an yrast (stretched) state (with $I = 2n$) in the *Q*-phonon basis

$$|I, M = I\rangle \equiv |n\rangle = \mathcal{N}^{-1/2}(Q_{22})^n|0^+_1\rangle. \quad (37)$$

In order to avoid encumbering the presentation, we suppress the subscript on Q_{22} in the following. Let us consider a Hamiltonian H and evaluate $H|n\rangle \equiv \mathcal{N}_n^{-1/2}HQ^n|0^+_1\rangle$. The simple relation

$$HQ = QH + [H, Q] \quad (38)$$

is an example of the general relation

$$\begin{aligned} HQ^n &= Q^nH + nQ^{n-1}[H, Q] \\ &+ \frac{n(n-1)}{2}Q^{n-2}[[H, Q], Q] \\ &+ \frac{n(n-1)(n-2)}{6}Q^{n-3}[[[H, Q], Q], Q] + \ldots. \end{aligned} \quad (39)$$

Equation (39) terminates after $(n + 1)$ terms. This means that, for the 4^+_1 state ($n = 2$), Eq. (39) resembles the form of Eq. (36) with terms up to ϵ_4. Of course, one has not yet shown that ϵ_4 in (36) is a constant. Applying relation (39) to the 0^+_1 state (which is assigned zero energy) and using the *Q*-phonon approximation for yrast states, we obtain

$$\begin{aligned} H|n\rangle = \mathcal{N}_n^{-1/2}\Big(& nQ^{n-1}\mathcal{N}_1^{-1/2}Q|0^+_1\rangle\langle 2^+_1|[H, Q]|0^+_1\rangle \\ &+ \frac{n(n-1)}{2}Q^{n-2}\mathcal{N}_2^{-1/2}Q^2|0^+_1\rangle\langle 4^+_1|[[H, Q], Q]|0^+_1\rangle \\ &+ \frac{n(n-1)(n-2)}{6}Q^{n-3}\mathcal{N}_3^{-1/2}Q^3|0^+_1\rangle \\ &\times\langle 6^+_1|[[[H, Q], Q], Q]|0^+_1\rangle + \ldots\Big). \end{aligned} \quad (40)$$

Using (37) to replace $\mathcal{N}_n^{-1/2}$ factors and the relation $H|n\rangle = E(n)|n\rangle$, we arrive at

$$\begin{aligned} E(n) = nE(2^+_1) &+ \frac{n(n-1)}{2}\,\frac{\langle 4^+_1|[[H, Q], Q]|0^+_1\rangle}{\langle 4^+_1|QQ|0^+_1\rangle} \\ &+ \frac{n(n-1)(n-2)}{6}\,\frac{\langle 6^+_1|[[[H, Q], Q], Q]|0^+_1\rangle}{\langle 6^+_1|QQQ|0^+_1\rangle} + \ldots. \end{aligned} \quad (41)$$

For $n = 2$, we arrive at

$$E(4^+_1) = 2E(2^+_1) + \frac{\langle 4^+_1|[[H, Q], Q]|0^+_1\rangle}{\langle 4^+_1|QQ|0^+_1\rangle}. \quad (42)$$

The analysis performed in [16] revealed that $\epsilon_4 \equiv \langle 4^+_1|[[H, Q], Q]|0^+_1\rangle/\langle 4^+_1|QQ|0^+_1\rangle$ takes the values of 0.12 ± 0.04 MeV for a wide range of the parameters of Hamiltonian (3). This result is close to the experimental ϵ_4 value of 0.16 ± 0.01.

REFERENCES

1. N. Pietralla, P. von Brentano, R. F. Casten, *et al.*, Phys. Rev. Lett. **73**, 2962 (1994).
2. N. Pietralla, P. von Brentano, T. Otsuka, and R. F. Casten, Phys. Lett. B **349**, 1 (1995).
3. N. Pietralla, T. Mizusaki, P. von Brentano, *et al.*, Phys. Rev. C **57**, 150 (1998).
4. Yu. P. Palchikov, P. von Brentano, and R. V. Jolos, Phys. Rev. C **57**, 3026 (1998).

5. R. V. Jolos, P. von Brentano, and A. Gelberg, Phys. Rev. C **53**, 168 (1996).
6. K.-H. Kim and T. Otsuka, Phys. Rev. C **52**, 2792 (1995).
7. R. V. Jolos, P. von Brentano, N. Pietralla, and I. Schneider, Nucl. Phys. A **618**, 126 (1997).
8. R. V. Jolos and P. von Brentano, Phys. Lett. B **381**, 1 (1996).
9. R. F. Casten and J. A. Cizewski, Phys. Lett. B **185**, 293 (1987).
10. C. Y. Wu *et al.*, Nucl. Phys. A **607**, 178 (1996).
11. K. Kumar, Phys. Rev. Lett. **28**, 249 (1972).
12. D. Cline, Annu. Rev. Nucl. Part. Sci. **36**, 683 (1986).
13. A. Bohr and B. Mottelson, *Nuclear Structure*, Vol. 2: *Nuclear Deformations* (Benjamin, New York, 1974; Mir, Moscow, 1977).
14. R. F. Casten, N. V. Zamfir, and D. S. Brenner, Phys. Rev. Lett. **71**, 227 (1993).
15. N. V. Zamfir and R. F. Casten, Phys. Lett. B **341**, 1 (1994).
16. R. V. Jolos, P. von Brentano, R. F. Casten, and N. V. Zamfir, Phys. Rev. C **51**, R2298 (1995).

Physics of Atomic Nuclei, Vol. 64, No. 3, 2001, pp. 471–476. Translated from Yadernaya Fizika, Vol. 64, No. 3, 2001, pp. 525–530.

90th ANNIVERSARY OF A.B. MIGDAL'S BIRTHDAY
NUCLEI

Coulomb Energy of Nuclei

V. R. Shaginyan

Petersburg Nuclear Physics Institute, Russian Academy of Sciences, Gatchina, 188350 Russia

Received July 17, 2000

Abstract—The density functional determining the Coulomb energy of nuclei is calculated to the first order in e^2. It is shown that the Coulomb energy includes three terms: the Hartree energy; the Fock energy; and the correlation Coulomb energy (CCE), which contributes considerably to the surface energy, the mass difference between mirror nuclei, and the single-particle spectrum. A CCE-based mechanism of a systematic shift of the single-particle spectrum is proposed. A dominant contribution to the CCE is shown to come from the surface region of nuclei. The CCE effect on the calculated proton drip line is examined, and the maximum charge Z of nuclei near this line is found to decrease by 2 or 3 units. The effect of Coulomb interaction on the effective proton mass is analyzed. © *2001 MAIK "Nauka/Interperiodica".*

1. INTRODUCTION

Relatively weak Coulomb interaction substantially affects the properties of nuclei owing to its long-range character. It is reliably established that the electrostatic Coulomb energy of the distributed charge is the dominant term in the Coulomb energy of nuclei. This term, also known as the Hartree energy, is proportional to Z^2e^2/R, where Z is the number of intranuclear protons, R is the nuclear radius, and e is the proton charge; at large values of Z, it induces the breakup of nuclei. At the same time, there are a few less significant contributions to the Coulomb energy. These include the Fock exchange contribution and a number of terms associated with the correlated motion of nucleons. It will be shown below that, in constructing the density functional determining the Coulomb energy of a nucleus, it is sufficient to calculate all these terms to the first order in e^2. The presence of these terms is clearly illustrated by the well-known Nolen–Schiffer anomaly [1], which was discovered more than 30 years ago. This anomaly was deduced from a comparison of the calculated mass difference between two mirror nuclei with its experimental value. The comparison revealed that, on average, the results of the calculations performed without taking consistently into account the correlation Coulomb energy (CCE) fall short of relevant experimental values by 10% [2, 3]. This discrepancy can be removed by introducing charge-dependent forces [4] whose strength is assumed to be preset by this discrepancy. However, this is possible if we are sure that nuclear dynamics is taken properly into account and that all the Coulomb contributions are consistently included. A new mechanism that enhances the contribution of Coulomb interaction to the energy of the nuclear ground state and which is caused by the presence of a surface (a general property of equilibrium finite Fermi systems) was found in [5, 6]. This contribution, which is proportional to the nuclear surface ($Z^{2/3}$), made it possible to explain a dominant part of the above anomaly.

The main objective of this study is to calculate consistently the density functional determining the Coulomb energy. As the result of this calculation, which will be performed to the first order in e^2 and which will take into account the mechanism enhancing the CCE contribution, we will be able to clarify the effect of this mechanism on the single-particle spectrum of nuclei, on the effective nucleon mass, and on the position of the proton drip line. In what follows, we do not highlight the difference between this functional and the Coulomb energy unless this leads to confusion.

The ensuing exposition is organized as follows. A general formulation of our approach to calculating the Coulomb energy is given in Section 2. Section 3 is devoted to calculating the systematic CCE-induced shifts of the single-particle spectrum and the proton drip line. The effect of Coulomb interaction on the effective proton mass is considered in Section 4. Section 5 summarizes the basic results.

2. COULOMB CORRELATION ENERGY

In order to formulate the aforementioned mechanism and to consider its effect, we will make use of the Hartree–Fock method employing effective forces, which was substantiated within density-functional theory [7]. In this case, the energy E of the nuclear ground state has the form

$$E = F_0[\rho_p, \rho_n] + F_c[\rho_p, \rho_n], \quad (1)$$

where F_0 is that part of the functional which is due to nuclear forces. Since we assume that the charge symmetry of nuclear forces, F_0 depends identically on the single-particle densities ρ_p and ρ_n of protons and neutrons (these densities are determined by minimizing E). The term F_c is due to other interactions, which are

weaker than nuclear forces. The smallness of these interactions can be characterized by the ratio α of the potential energy of these interactions between two nucleons to the Fermi energy $\varepsilon_F \simeq 40$ MeV. For the Coulomb interaction, this ratio is $\alpha \simeq e^2/(r_0\varepsilon_F) \simeq 0.03$, where r_0 is the mean spacing between nucleons in equilibrium nuclear matter. Therefore, it is sufficient to calculate the functional F_c in the first order in the relevant coupling constant. In the case of Coulomb interaction, which is the main subject of the present study, the functional F_c will be calculated to the first order in e^2. This functional could be approximated by some simple expression, as was done, for example, for the functional F_0. However, experience gained in calculating the mass differences between mirror nuclei (these mass differences are directly determined by the functional F_c) proves the inefficiency of such attempts. Moreover, this oversimplified approximation does not reveal the physics behind the functional F_c. Therefore, it is preferable to calculate the functional F_c. In doing this, it is assumed that the functional F_0 is known. It can be taken in the form specified by the Skyrme interaction [8] or in the form proposed in [9]. The latter is advantageous in that it is characterized by a high precision, is simple in use, and involves the bare nucleon mass. By construction, the functional F_0 must contain the unnrenormalized mass M of the proton (neutron) rather than its effective mass M^* because the effective mass, as well as the nuclear spectrum, cannot be directly included in it [10].

The single-particle distributions of the proton and neutron densities (ρ_p and ρ_n, respectively) are specified as

$$\rho_p(\mathbf{r}) = \sum_l n_p^l \left|\phi_p^l(\mathbf{r})\right|^2, \quad \rho_n(\mathbf{r}) = \sum_l n_n^l \left|\phi_n^l(\mathbf{r})\right|^2, \quad (2)$$

where n_p^l and n_n^l are the occupation numbers for single-particle proton and neutron levels, respectively, while ϕ_p^l and ϕ_n^l are, respectively, the proton and neutron single-particle wave functions determined from the Hartree–Fock equation [8]. The term $F_c[\rho_p]$ is usually taken in the first order in the Coulomb interaction in the Hartree–Fock approximation [7, 8]:

$$F_c = \frac{e^2}{2}\left[\int \frac{\rho_p(\mathbf{r}_1)\rho_p(\mathbf{r}_2)}{|\mathbf{r}_1-\mathbf{r}_2|}d\mathbf{r}_1 d\mathbf{r}_2 - \int\left[\frac{\chi_p^0(\mathbf{r}_1,\mathbf{r}_2,i\omega)+2\pi\rho_p(\mathbf{r}_1)\delta(\mathbf{r}_1-\mathbf{r}_2)\delta(\omega)}{|\mathbf{r}_1-\mathbf{r}_2|}\right] \times \frac{d\mathbf{r}_1 d\mathbf{r}_2 d\omega}{2\pi}\right]. \quad (3)$$

Here, $\chi_p^0(\mathbf{r}_1, \mathbf{r}_2, \omega)$ is the linear-response function for noninteracting protons moving in the self-consistent single-particle field V_p. The first and the second term on the right-hand side of Eq. (3) are, respectively, the Hartree and the Fock density functional (F_c^{H} and F_c^{F}). The exchange term F_c^{F} is usually approximated by the expression [8]

$$F_c^{\mathrm{F}} = -\frac{3e^2}{4}\left(\frac{3}{\pi}\right)^{1/3}\int \rho_p^{4/3}(\mathbf{r})d\mathbf{r}. \quad (4)$$

However, the equality in (3) is not exact even in the first order in the Coulomb interaction (e^2 order) because it does not include the functional $F_c^{\mathrm{corr}}[\rho_p(\mathbf{r})]$ taking into account the contribution to the Coulomb energy from the correlated motion of protons under the effect of the effective (residual) nuclear interaction $R_{\alpha\beta}(\mathbf{r}_1, \mathbf{r}_2)$. In the first order in e^2, the CCE functional F_c^{corr} has the form [6]

$$F_c^{\mathrm{corr}}[\rho_p] = -\frac{e^2}{2}\int\left[\frac{\chi_{pp}(\mathbf{r}_1,\mathbf{r}_2,i\omega)-\chi_p^0(\mathbf{r}_1,\mathbf{r}_2,i\omega)}{|\mathbf{r}_1-\mathbf{r}_2|}\right] \times \frac{d\mathbf{r}_1 d\mathbf{r}_2 d\omega}{2\pi}, \quad (5)$$

where $\chi_{pp}(\mathbf{r}_1, \mathbf{r}_2, \omega)$ is the exact function representing the linear response of intranuclear protons to an external electric field. It should be noted that the function χ_{pp} is completely determined by the functional F_0 [6] and that it involves no smallness associated with the Coulomb interaction. The total response function contains three independent components—χ_{pp}, χ_{nn}, and χ_{np}—and satisfies the equation

$$\chi_{\alpha\beta} = \chi_\alpha^0\delta_{\alpha\beta} + \sum_\gamma \chi_\alpha^0 R_{\alpha\gamma}\chi_{\gamma\beta}, \quad (6)$$

where integration signs are omitted for the sake of simplicity. The response function χ_p^0 for noninteracting nucleons (protons) moving in the self-consistent field V_p has the form

$$\chi_p^0(\mathbf{r}_1,\mathbf{r}_2,\omega) = \sum_{i,k} n_p^i(1-n_p^k)\phi_p^{i*}(\mathbf{r}_1)\phi_p^i(\mathbf{r}_2) \times \phi_p^{k*}(\mathbf{r}_2)\phi_p^k(\mathbf{r}_1)\left[\frac{1}{\omega-\omega_p^{ik}-i\eta}-\frac{1}{\omega+\omega_p^{ik}-i\eta}\right]. \quad (7)$$

The single-particle eigenvalues ε_p^i, the frequencies $\omega_p^{ik} = \varepsilon_p^k - \varepsilon_p^i$, the single-particle wave functions $\phi_p^i(\mathbf{r})$, and the corresponding densities ρ_p and ρ_n are determined by solving the single-particle Hartree–Fock equations

$$\left(-\frac{\nabla^2}{2M}+V_p(\mathbf{r})\right)\phi_p^i(\mathbf{r}) = \varepsilon_p^i\phi_p^i(\mathbf{r}), \quad (8)$$

which are derived by means of a conventional procedure that amounts to varying Eq. (1) with respect to the single-particle functions $\phi_{n,p}^l$ [7, 8]. The self-consistent

potential V_p and the effective interaction $R_{\alpha\beta}$ are given by

$$V_p(\mathbf{r}) = \frac{\delta(F_0[\rho_p, \rho_n] - T_0[\rho_p, \rho_n])}{\delta\rho_p(\mathbf{r})},$$
$$R_{\alpha\beta}(\mathbf{r}_1, \mathbf{r}_2) = \frac{\delta^2(F_0[\rho_p, \rho_n] - T_0[\rho_p, \rho_n])}{\delta\rho_\alpha(\mathbf{r}_1)\delta\rho_\beta(\mathrm{r}_2)}, \quad (9)$$

where $T_0[\rho_p, \rho_n]$ is the kinetic-energy functional for noninteracting nucleons. Thus, we conclude that, to the first order in e^2, the eventual form of the functional F_c is

$$F_c = F_c^{\mathrm{H}} + F_c^{\mathrm{F}} + F_c^{\mathrm{corr}}. \quad (10)$$

Equations (1), (3), (5), and (10) provide a basis for consistently calculating the Coulomb energy and for taking into account the Coulomb interaction effect on the properties of nuclei. The poles of the response function χ_{pp} determine the collective spectrum of nuclei, while the residues at these poles govern the relevant transition probabilities. As can be seen from Eq. (5), a dominant contribution to F_c^{corr} comes from collective isoscalar surface vibrations whose excitation energies are much lower than those of corresponding isovector modes. Thus, the functional F_c^{corr} is controlled by the isoscalar components of the effective interaction.

It is instructive to consider the CCE for symmetric infinite nuclear matter [5, 6], in which case the relevant equations are considerably simplified. The function χ_{pp} assumes the form

$$\chi_{pp}(q, \omega) = \frac{1}{2}\left[\frac{\chi^0(q, \omega)}{1 - R_+(q, \omega, \rho)\chi^0(q, \omega)} + \frac{\chi^0(q, \omega)}{1 - R_-(q, \omega, \rho)\chi^0(q, \omega)}\right] \quad (11)$$

and determines the functional F_c^{corr}:

$$F_c^{\mathrm{corr}}[\rho_p] = -2\pi e^2 \int\left[\frac{\chi_{pp}(q, i\omega) - \chi_p^0(q, i\omega)}{q^2}\right]\frac{d\mathbf{q}\,d\omega}{(2\pi)^4}. \quad (12)$$

For symmetric matter, we have $\chi_p^0 = \chi_n^0 = \chi^0/2$; the effective interaction $R(\rho)$ is similar to the local interaction $f(\rho)$ between nucleons that was introduced by Migdal [11]:

$$\frac{p_{\mathrm{F}}M}{\pi^2}R_+(\rho) = f(\rho), \quad \frac{p_{\mathrm{F}}M}{\pi^2}R_-(\rho) = f'(\rho). \quad (13)$$

Considering that the isoscalar amplitude $f(\rho \longrightarrow 0)$ is approximately equal to –2.5 and that $p_{\mathrm{F}}M/\pi^2 = \chi^0(0, i0)$, one can see from Eq. (11) that, at relatively low densities corresponding to the surface region of nuclei, the denominator $1 - R_+\chi^0$ vanishes at small values of q and ω. Therefore, the function χ_{pp} develops poles on the imaginary axis. These poles, which evince instability of low-density nuclear matter [11], lead to the divergence of the integral in Eq. (12), and this prevents a calculation of the CCE at these nuclear-matter densities. We can conclude that the main contribution to this integral comes from the isoscalar response function. From the above, it also follows that the conventional procedure based on calculating various quantities in the local-density approximation (LDA) in infinite uniform matter fails in this case. In this connection, it is worth noting that, although an attempt was made in [12] to construct the functional F_0 within the LDA, this is impossible for the same reason.

It is convenient to calculate the CCE in semi-infinite nuclear matter, where there is a region of low-density nuclear matter near the surface. In the generalized LDA, we then obtain [5, 6]

$$F_c^{\mathrm{corr}}[\rho_p] = \int\rho_p(\mathbf{r})e_c(\rho_p(\mathbf{r}))d\mathbf{r}, \quad (14)$$

where $e_c(\rho_p)$ is the CCE per proton and ρ_p is the single-particle proton density. The calculation of the energy $e_c(\rho_p)$ for semi-infinite nuclear matter revealed that, at the surface, this energy has a pronounced positive peak, which corresponds to smoothing the divergence in (12) for uniform nuclear matter [6]. It is convenient to approximate the energy e_c by the simple expression

$$e_c(\rho_p(r)) = D\left[\frac{\rho_p(r)}{\rho_0}\left(1 - \frac{\rho_p(r)}{\rho_0}\right)\right]^{4/3}, \quad (15)$$

where $2\rho_0 = 0.16$ fm^{-3} is the equilibrium nuclear density and $D \simeq 6$ MeV. In contrast to the terms F_c^{H} and F_c^{F}, the energy $e_c(\rho_p)$, which has a pronounced peak at the nuclear surface, makes a noticeable contribution (σ_c) to the surface tension:

$$\sigma_c = \int_{-\infty}^{\infty}\rho_p(z)[e_c(\rho_p(z)) - e_c(\rho_p(-\infty))]dz. \quad (16)$$

Hence, the Weizsäcker mass formula must be supplemented with the term ΔE whose contribution to the total binding energy of a nucleus can be represented as

$$\Delta E = a_1'Z + a_2'Z^{2/3}, \quad (17)$$

where $a_1' \simeq -0.1$ MeV and $a_2' \simeq 1.0$ MeV. Thus, we can see from Eq. (17) that the surface tension has an isovector component. It will be shown below that this is so for the effective mass as well. It follows from Eq. (17) that the surface tension of the proton nuclear Fermi liquid is effectively greater than that of neutron matter. This means that, when protons are added to a nucleus, their binding energy becomes somewhat smaller because of an increase in the surface of the proton liquid component. It will also be proven below that this decrease in the proton binding energy is sufficient for explaining the mass difference between mirror nuclei. Further, the additional surface tension σ_c and the addition of extra

neutrons are expected to induce opposite modifications in the root-mean-square radius $\langle r_p \rangle$ of the intranuclear-proton distribution: the former would moderate an increase associated with the latter. The preliminary calculations reveal that this could explain the anomalously small increase in the radius $\langle r_p \rangle$ in going over from the ^{40}Ca to the ^{48}Ca nucleus. The contribution σ_c must also be taken into account in considering fission barriers for heavy nuclei.

3. SINGLE-PARTICLE SPECTRUM AND THE PROTON DRIP LINE

Let us calculate the CCE-induced shift of the single-particle proton excitation spectrum ε_p^l. For this, we will use the well-known Landau equation [13]

$$\frac{\delta E}{\delta n_p^l} = \varepsilon_p^l. \tag{18}$$

It follows from Eqs. (5) and (18) that this shift $\Delta\varepsilon_p^l$ can be represented as

$$\Delta\varepsilon_p^l = \frac{\delta F_c^{\rm corr}}{\delta n_p^l} = -\frac{e^2}{2}\frac{\delta}{\delta n_p^l} \times \int\left[\frac{\chi_{pp}(\mathbf{r}_1, \mathbf{r}_2, i\omega) - \chi_p^0(\mathbf{r}_1, \mathbf{r}_2, i\omega)}{|\mathbf{r}_1 - \mathbf{r}_2|}\right]\frac{d\mathbf{r}_1 d\mathbf{r}_2 d\omega}{2\pi}. \tag{19}$$

The variational derivative $\delta\chi_p^0/\delta n_p^l$ has the simple functional form

$$\frac{\delta\chi_p^0(\mathbf{r}_1, \mathbf{r}_2, \omega)}{\delta n_p^l} = [G^p(\mathbf{r}_1, \mathbf{r}_2, \omega + \varepsilon_p^l) + G^p(\mathbf{r}_1, \mathbf{r}_2, -\omega + \varepsilon_p^l)]\phi_p^{l*}(\mathbf{r}_1)\phi_p^l(\mathbf{r}_2), \tag{20}$$

where $G^p(\mathbf{r}_1, \mathbf{r}_2, \omega)$ is the single-particle Green's function for the system of Z noninteracting protons moving in a self-consistent single-particle nuclear potential. The functional derivative $\delta\chi_{pp}/\delta n_p^l$ is determined by the matrix equation

$$\frac{\delta\chi_{\alpha\beta}}{\delta n_p^l} = \frac{\delta\chi_\alpha^0}{\delta n_p^l}\delta_{\alpha\beta} + \sum_\gamma\left[\frac{\delta\chi_\alpha^0}{\delta n_p^l}R_{\alpha\gamma}\chi_{\gamma\beta} + \chi_\alpha^0\frac{\delta R_{\alpha\gamma}}{\delta n_p^l}\chi_{\gamma\beta} + \chi_\alpha^0 R_{\alpha\gamma}\frac{\delta\chi_{\gamma\beta}}{\delta n_p^l}\right], \tag{21}$$

which can be derived by directly varying Eq. (6). Integration with respect to spatial coordinates is implied in Eq. (21) in just the same way as in Eq. (6). As can be seen from Eq. (9), the effective interaction $R_{\alpha\beta}$ is determined by the form of the functional F_0. In order to simplify the calculations, we took, however, the interaction $R_{\alpha\beta}$ in the separable representation [14]

$$R_{\alpha\beta}(\mathbf{r}_1, \mathbf{r}_2) = \lambda\frac{dV_\alpha(r_1)}{dr_1}\frac{dV_\beta(r_2)}{dr_2}\delta(\Omega_1 - \Omega_2), \tag{22}$$

where $V_{\alpha,\beta}(r)$ is the self-consistent single-particle proton (neutron) potential. The value of the parameter λ is chosen in such a way that the dipole response has a pole at $\omega = 0$. The above separable form of the effective (residual) interaction is extensively used and, as was shown in [7, 15], provides a good description of collective nuclear excitations. The value calculated here for the shift $\Delta\varepsilon_p^l$ of single-particle proton levels located near the Fermi level is 0.2–0.4 MeV both for medium-mass and heavy nuclei, in overall agreement with the value of the Nolen–Schiffer anomaly. It is worthwhile to verify these results by using the simple LDA expressions (14) and (15) for $F_c^{\rm corr}[\rho_p]$. The shift $\Delta\varepsilon_p^l$ then assumes the form

$$\Delta\varepsilon_p^l = \int\frac{\delta F_c^{\rm corr}[\rho_p]}{\delta\rho_p}\left|\phi_p^l(\mathbf{r})\right|^2 d\mathbf{r}. \tag{23}$$

It is convenient to approximate the single-particle density $\rho_p(r)$ by the Fermi distribution

$$\rho_p(r, R) = \frac{\rho_0}{1 + \exp((r - R)/a)}, \tag{24}$$

where R is the nuclear radius and the diffuseness parameter a is taken to be 0.6 fm. In this case, the functional $F_c^{\rm corr}[\rho_p]$ given by Eq. (14) reduces to a function $F_c^{\rm corr}(R)$ of the nuclear radius. An addition of a proton increases the radius R by the quantity ΔR that is determined from the normalization condition

$$\int[\rho_p(r, R + \Delta R) - \rho_p(r, R)]d\mathbf{r} = 1.$$

The CCE-induced shift of a proton level occurring near the Fermi surface is given by

$$\Delta\varepsilon_p = F_c^{\rm corr}(R + \Delta R) - F_c^{\rm corr}(R).$$

After simple transformations of the relevant integrals of the Fermi functions, we find that, for medium-mass and heavy nuclei, the sought shift of a proton level near the Fermi level is

$$\Delta\varepsilon_p \simeq \frac{Da}{2R} \simeq 0.3\text{–}0.4\ \text{MeV}. \tag{25}$$

Since corrections of order $D(a/R)^3$ were discarded, the result in (25) slightly overestimates the shift.

The calculated mass differences between mirror nuclei are quoted in the table. In this calculation, the functional F_0 was constructed on the basis of the SIII interaction [8], while the functionals F_c and $F_c^{\rm corr}$ were, respectively, taken in the form (10) and specified by Eqs. (14) and (15). The table demonstrates that the mass differences between mirror nuclei are closely reproduced. The remaining disagreement can be used to determine the coupling constants for forces violating the charge symmetry of nuclear interaction. Thus, tradi-

Mass differences between mirror nuclei (in MeV)

Nuclei	^{15}O–^{15}N	^{17}F–^{17}O	^{39}Ca–^{39}K	^{41}Sc–^{41}Ca	^{48}Ni–^{48}Ca
Theory	3.48	3.56	7.23	7.24	66.70
Experiment [2, 16]	3.54	3.54	7.30	7.28	67.06

tional nuclear physics can be advantageous in calculating the constants concerning elementary-particle physics.

Equation (25) shows that the shift $\Delta\varepsilon_p$ of a single-particle level approximately compensates for the level shift caused by exchange Coulomb interaction. It should be recalled that the exchange Coulomb interaction reduces the energy of a single-particle level, as can be seen from Eq. (4). Therefore, the total shift of a single-particle level due to Coulomb interaction can be derived by taking into account solely the direct Coulomb interaction—that is, by retaining only the term F_c^{H} in Eq. (10). A similar procedure was postulated in [9, 16]. It should be noted that the recipe assuming mutual cancellation of the exchange Coulomb interaction and the CCE does not lead to a noticeable value of the coefficient a_2' in Eq. (17) (recall this coefficient determines the isovector component of the surface tension) because the contribution from F_c^{H} and F_c^{F} [see Eq. (4)] to the surface tension is small. On the contrary, our calculations indicate that the coefficient a_2' is not small. It also follows from Eq. (25) that, upon taking the CCE into account, the last filled single-particle proton level is shifted upward by 0.3 to 0.4 MeV. As a result, the maximal charge Z of a nucleus occurring near the proton drip line decreases by 2 or 3 units, as follows from [17]. Therefore, we conclude that, in calculating the proton drip line, it is important to take the CCE into account.

4. EFFECTIVE MASS

Let us consider the change ΔM that Coulomb interaction induces in the effective proton mass M^*. In the case of uniform nuclear matter, the single-particle spectrum depends on the momentum p, while the effective mass, as follows from Eq. (18), is determined by the expression

$$\frac{1}{M^*} = \frac{1}{p_{\mathrm{F}}}\frac{d\varepsilon_p(p)}{dp}\bigg|_{p=p_{\mathrm{F}}}, \tag{26}$$

where p_{F} is the Fermi momentum. In order to calculate ΔM, we use Eq. (26), replacing $\varepsilon_p(p)$ by the shift of the single-particle spectrum due to Coulomb interaction. We have

$$\frac{\Delta M}{M^*(M^*+\Delta M)} = \frac{e^2}{p_{\mathrm{F}}}\frac{d}{dp}\frac{\delta}{\delta n_p} \times \int\left[\frac{\chi_{pp}(q,i\omega)+2\pi\rho_p\delta(\omega)}{q^2}\right]\frac{d\mathbf{q}\,d\omega}{(2\pi)^3}. \tag{27}$$

Evaluating variations in Eq. (27) and considering that, in the case of uniform matter, Eqs. (6) and (21) reduce to algebraic equations, we obtain [14, 18]

$$\frac{\Delta M}{M^*(M^*+\Delta M)} = \frac{e^2}{p_{\mathrm{F}}}\frac{d}{dp}\int\frac{\delta\chi^0(q,i\omega)}{\delta n_p} \times \frac{1}{(1-R_+(q,i\omega)\chi^0(q,i\omega))^2}\frac{d\mathbf{q}\,d\omega}{q^2(2\pi)^3}, \tag{28}$$

where M^* is the effective proton mass in the absence of Coulomb interaction and $R_+ = (R_{pp}+R_{pn})/2$ is the effective interaction. The derivative d/dp was taken at the point $p = p_{\mathrm{F}}$. Let us consider the effective-mass variation ΔM for the case where the system under consideration is characterized by the compressibility parameter κ, $1/\kappa = \rho^2 d^2E/d\rho^2$, tending to infinity. This state is similar to states existing in the surface region of nuclei. This consideration will enable us to draw qualitative conclusions on the behavior of the effective mass in a nucleus. It can be shown that [18]

$$\frac{d}{dp}\frac{\delta}{\delta n_p}\chi^0(q,\omega)\big|_{p\to p_{\mathrm{F}}} = -\frac{4\pi}{p_{\mathrm{F}}^2}\delta(p_{\mathrm{F}}-|\mathbf{p}+\mathbf{q}|)\delta(\omega)\mathbf{p}\cdot(\mathbf{p}+\mathbf{q}). \tag{29}$$

Substituting (29) into (28) and retaining only the leading term, we obtain

$$\frac{1}{M^*+\Delta M} = \frac{1}{M^*}+\frac{e^2}{2\pi p_{\mathrm{F}}} \times \int_{-1}^{1}\frac{x\,dx}{(1-x)[1-R_+(q(x),0)\chi^0(q(x),0)]^2}, \tag{30}$$

where $q(x) = p_{\mathrm{F}}\sqrt{2(1-x)}$. At the point where the compressibility diverges, the denominator $(1-R_+\chi^0)^2$ of the integrand in Eq. (30) vanishes at $x = 1$ ($q = 0$). The relevant integral, which is positive, diverges, which results in the vanishing of the effective mass—that is, $M^* + \Delta M \longrightarrow 0$. This result demonstrates that, in equilibrium nuclear systems, the CCE noticeably affects the effective mass, the decrease ΔM in the effective proton mass being dependent on the degree to which the density of the system, ρ, deviates from its equilibrium value ρ_0. In a nucleus, the divergence of the integral in Eq. (30)—it could be due to the decrease in the density near the surface of the nucleus—gives way to a finite value. As a result, the effective proton mass decreases in relation to M^* and becomes smaller than the effective neutron

mass. It can be said that the effective nucleon mass acquires an isovector component. This possibility was discussed in [16]. A theoretical validation of this effect has been given here.

5. CONCLUSION

The basic results of the present study can be summarized as follows. A consistent scheme for constructing the density functional determining the Coulomb energy of a nucleus has been developed to the first order in e^2. Using this functional, we have calculated the single-particle spectra of nuclei and the systematic shift of these spectra that is induced by the CCE. It has been shown that the Nolen–Schiffer anomaly is removed to a considerable extent by this systematic shift of the single-particle spectrum. Owing to the same mechanism, the proton drip line undergoes a shift of 2 or 3 units toward smaller values of the charge Z of a nucleus occurring near this line. It has been shown that the CCE must be taken into account in calculating the effective nucleon mass. This opens the possibility of estimating the coupling constants for forces violating charge symmetry. The contribution of these forces must be treated in the same manner as this has been done for the Coulomb interaction. It can be expected that the proposed procedure will make it possible to construct a density functional applicable to describing various properties of nuclei occurring both in the valley of stability and beyond it.

ACKNOWLEDGMENTS

I am grateful to A. Bulgac for stimulating discussions on the problems analyzed in this study.

This work was supported in part by the International Association for the Promotion of Cooperation with Scientists from the Independent States of the Former Soviet Union (grant no. INTAS-OPEN-97-603).

REFERENCES

1. J. A. Nolen and J. P. Schiffer, Annu. Rev. Nucl. Sci. **19**, 471 (1964).
2. S. Shlomo, Rep. Prog. Phys. **41**, 957 (1978); S. Shlomo and M. G. Love, Phys. Scr. **26**, 280 (1982).
3. N. Auerbach, Phys. Rep. **98**, 273 (1983).
4. G. A. Miller, B. M. K. Nefkens, and I. Slaus, Phys. Rep. **194**, 1 (1990).
5. V. R. Shaginyan, Yad. Fiz. **39**, 346 (1984) [Sov. J. Nucl. Phys. **39**, 218 (1984)]; **40**, 1144 (1984) [**40**, 728 (1984)].
6. A. Bulgak and V. R. Shaginyan, Pis'ma Zh. Éksp. Teor. Fiz. **62**, 833 (1995) [JETP Lett. **62**, 843 (1995)]; A. Bulgac and V. R. Shaginyan, Nucl. Phys. A **601**, 103 (1996).
7. P. Ring and P. Schuck, *Nuclear Many-Body Problem* (Springer-Verlag, New York. 1980).
8. D. Vautherin and D. M. Brink, Phys. Rev. C **5**, 626 (1972); M. Beiner, H. Flocard, Ngueyn van Giai, and P. Quentin, Nucl. Phys. A **238**, 29 (1975).
9. S. A. Fayans, Pis'ma Zh. Éksp. Teor. Fiz. **68**, 161 (1998) [JETP Lett. **68**, 169 (1998)].
10. P. Hohenberg and W. Kohn, Phys. Rev. B **136**, 864 (1964); W. Kohn and L. J. Sham, Phys. Rev. A **140**, 1133 (1965).
11. A. B. Migdal, *Theory of Finite Fermi Systems and Applications to Atomic Nuclei* (Nauka, Moscow, 1965; Interscience, New York, 1967).
12. H. A. Bethe, Annu. Rev. Nucl. Sci. **23**, 93 (1971).
13. L. D. Landau, Zh. Éksp. Teor. Fiz. **30**, 1058 (1956) [Sov. Phys. JETP **3**, 920 (1956)].
14. A. Bulgac and V. R. Shaginyan, Eur. Phys. J. A **5**, 247 (1999); Phys. Lett. B **469**, 1 (1999).
15. A. Bohr and B. R. Mottelson, *Nuclear Structure* Vol. 2: *Nuclear Deformations* (Benjamin, New York, 1975; Mir, Moscow, 1977).
16. B. A. Brown, Phys. Rev. C **58**, 220 (1998).
17. A. Bohr and B. R. Mottelson, *Nuclear Structure*, Vol. 1: *Single-Particle Motion* (Benjamin, New York, 1969; Mir, Moscow, 1971), Fig. 2.30.
18. V. A. Khodel', V. R. Shaginyan, and M. V. Zverev, Pis'ma Zh. Éksp. Teor. Fiz. **65**, 242 (1997) [JETP Lett. **65**, 253 (1997)].

Translated by R. Tyapaev

Physics of Atomic Nuclei, Vol. 64, No. 3, 2001, pp. 477–481. From Yadernaya Fizika, Vol. 64, No. 3, 2001, pp. 531–535.

90th ANNIVERSARY OF A.B. MIGDAL'S BIRTHDAY
NUCLEI

On the Solution of the Number-Projected Hartree–Fock–Bogolyubov Equations*

J. A. Sheikh, E. Lopes, and P. Ring**
Physik-Department, Technische Universität München, Germany
Received July 20, 2000

Abstract—The numerical solution of the recently formulated number-projected Hartree–Fock–Bogolyubov (HFB) equations is studied in an exactly solvable cranked-deformed shell-model Hamiltonian. It is found that the solution of these number-projected equations involves similar numerical effort as that of bare HFB. We consider that this is significant progress in the mean-field studies of quantum many-body systems. The results of the projected calculations are shown to be in almost complete agreement with the exact solutions of the model Hamiltonian. The phase transition obtained in the HFB theory as a function of the rotational frequency is shown to be smeared out with the projection. *© 2001 MAIK "Nauka/Interperiodica".*

The mean-field models with effective forces have been quite successful in describing the gross features of quantum many-body systems. Although the mean-field approaches are appropriate for systems with a very large number of particles, they have also been quite useful to describe the properties of finite quantum systems, for instance, the atomic nucleus. The ground-state properties of atomic nuclei have been well described using the Hartree–Fock (HF) and Hartree–Fock–Bogolyubov (HFB) mean-field approaches with various effective interactions [1]. However, the mean-field application to a finite system suffers from a fundamental problem that it leads to sharp phase transitions. The phase transition is an artifact of the mean-field approach and is not observed in the experimental data. The phase transition obtained is due to the neglect of the quantal fluctuations, which become quite strong for finite systems.

There are various methods in the literature to consider the quantal fluctuations on the mean-field solution for the finite system. One very powerful method is through the restoration of the broken symmetries by employing projection methods [1]. In the present work, we shall consider the restoration of the gauge symmetry associated with the particle number. It is known in the HFB studies that one often obtains a phase transition from the superfluid paired phase to the normal unpaired phase. This phase transition is due to the fluctuations in the particle number, since the HFB wave function does not have a well-defined particle number. In most of the analyses, the particle-number fluctuations are treated in an approximate way by employing the Lipkin–Nogami prescription [2–4]. However, it has been shown that this approach also breaks down at high rotational frequencies and as a matter of fact violates the variational principle [5].

The exact particle-number projection can be performed by using gradient methods [1]. But this approach is numerically quite involved and has been applied only to separable interactions with restricted model spaces [6, 7]. There has been an unresolved issue whether HFB-like equations can be obtained with the projected-energy functional. This problem has been recently solved [8], and it has been shown that it is possible to obtain the HFB equations from an arbitrary real-energy functional which is completely expressible in terms of the density matrix and the pairing tensor. The projected-energy functional can be expressed in terms of the density matrix and the pairing tensor, and one obtains the HFB equations with modified expressions for the pair-gap and the Hartree–Fock potential. The expressions for these quantities acquire a relatively simple form for the case of particle-number projection [8].

To check the applicability of the number-projected HFB (PHFB) formalism, detailed numerical analysis is carried out in a simple cranked-deformed shell model Hamiltonian [9]. Although this model cannot be used directly to study the experimental data, it contains all the basic ingredients of a more realistic model. The advantage of this model is that it can be solved exactly and it is possible to check the accuracy of an approximate method. We consider that it is quite instructive to test the number-projection method in a cranking model as the Coriolis forces destroy the pair correlations and the results become quite sensitive to the treatment of the pairing interaction. As we shall demonstrate, the present projection method reproduces almost exactly the results of the shell model calculations for all the cases studied.

The model Hamiltonian consists of a cranked-deformed one-body term h' and a scalar two-body delta

* This article was submitted by the authors in English.
** e-mail: ring@ph.tum.de

interaction [9]. The one-body term is the familiar cranked Nilsson mean-field potential which takes into account the long-range part of the nucleon–nucleon interaction. The residual short-range interaction is specified by the delta interaction. The deformed shell model Hamiltonian employed is given by

$$H = h'_{\rm def} + V_2, \tag{1}$$

$$H = h_{\rm def} - \omega J_x + V_2, \tag{2}$$

where

$$h_{\rm def} = -4\kappa\sqrt{\frac{4\pi}{5}}\sum_m \langle jm|Y_{20}|jm\rangle c^\dagger_{jm}c_{jm}, \tag{3}$$

and

$$V_2 = \frac{1}{2}\sum_{LM} E_L A^\dagger_{LM}A_{LM}, \tag{4}$$

with $A^\dagger_{LM} = (c^\dagger_j c^\dagger_j)_{LM}$ and $A_{LM} = (A^\dagger_{LM})^\dagger$. For the antisymmetric normalized two-body matrix element (E_J), we use the delta interaction which for a single-j shell is given by [10]

$$E_L = -G\frac{(2j+1)^2}{2(2L+1)}\begin{bmatrix} j & j & L \\ \frac{1}{2} & -\frac{1}{2} & 0\end{bmatrix}^2, \tag{5}$$

where the symbol [ ] denotes the Clebsch–Gordan coefficient. We use $G = g\int R^4_{nl}\, r^2 dr$ as our energy unit, and the deformation energy κ is related to the deformation parameter β. For the case of $h_{11/2}$ shell, $\kappa = 2.4$ approximately corresponds to $\beta = 0.23$.

It has been shown in [8] that the variation of the number-projected energy functional results in the HFB matrix equation

$$\mathscr{H}'\begin{pmatrix} U \\ V\end{pmatrix} = E'_i\begin{pmatrix} U \\ V\end{pmatrix}, \tag{6}$$

where

$$\mathscr{H}' = \begin{pmatrix} \varepsilon'_{n_1n_2} + \Gamma_{n_1n_2} + \Lambda_{n_1n_2} - \lambda\delta_{n_1n_2} & \Delta_{n_1n_2} \\ -\Delta^*_{n_1n_2} & -\varepsilon'^*_{n_1n_2} - \Gamma^*_{n_1n_2} - \Lambda^*_{n_1n_2} + \lambda\delta_{n_1n_2}\end{pmatrix}. \tag{7}$$

The number-projected expressions for $\varepsilon'_{n_1n_2}$, $\Gamma_{n_1n_2}$, $\Lambda_{n_1n_2}$, and $\Delta_{n_1n_2}$ are given by

$$\varepsilon' = \frac{1}{2}\int d\phi y(\phi)(Y(\phi){\rm tr}[e'\rho(\phi)] + [1 - 2ie^{-i\phi}\sin\phi\rho(\phi)]e'C(\phi)) + {\rm h.c.}, \tag{8}$$

$$\Gamma = \frac{1}{2}\int d\phi y(\phi)\Big(Y(\phi)\frac{1}{2}{\rm tr}[\Gamma(\phi)\rho(\phi)] + \frac{1}{2}[1 - 2ie^{-i\phi}\sin\phi\rho(\phi)]\Gamma(\phi)C(\phi)\Big) + {\rm h.c.}, \tag{9}$$

$$\Lambda = -\frac{1}{2}\int d\phi y(\phi)\Big(Y(\phi)\frac{1}{2}{\rm tr}[\Delta(\phi)\bar\kappa^*(\phi)] - 2ie^{-i\phi}\sin\phi C(\phi)\Delta(\phi)\bar\kappa^*(\phi)\Big) + {\rm h.c.}, \tag{10}$$

$$\Delta = \frac{1}{2}\int d\phi y(\phi)e^{-2i\phi}C(\phi)\Delta(\phi) - (\ldots)^T, \tag{11}$$

with

$$\Gamma_{n_1n_3}(\phi) = \sum_{n_2n_4}\bar V_{n_1n_2n_3n_4}\rho_{n_4n_2}(\phi), \tag{12}$$

$$\Delta_{n_1n_2}(\phi) = \frac{1}{2}\sum_{n_3n_4}\bar V_{n_1n_2n_3n_4}\kappa_{n_3n_4}(\phi), \tag{13}$$

$$\bar\Delta^*_{n_3n_4}(\phi) = \frac{1}{2}\sum_{n_1n_2}\bar\kappa^*_{n_1n_2}(\phi)\bar V_{n_1n_2n_3n_4}, \tag{14}$$

$$\rho(\phi) = C(\phi)\rho, \tag{15}$$

$$\kappa(\phi) = C(\phi)\kappa = \kappa C^T(\phi), \tag{16}$$

$$\bar\kappa(\phi) = e^{2i\phi}\kappa C^*(\phi) = e^{2i\phi}C^\dagger(\phi)\kappa, \tag{17}$$

$$C(\phi) = e^{2i\phi}(1 + \rho(e^{2i\phi} - 1))^{-1}, \tag{18}$$

$$x(\phi) = \frac{1}{2\pi}\frac{e^{i\phi}\det(e^{i\phi})}{\sqrt{\det C(\phi)}}, \tag{19}$$

$$y(\phi) = \frac{x(\phi)}{\int dg x(\phi)}, \quad \int dg y(\phi) = 1, \tag{20}$$

and

$$Y(\phi) = ie^{-i\phi}\sin\phi C(\phi) - i\int d\phi' y(\phi')e^{-i\phi'}\sin\phi' C(\phi'). \tag{21}$$

The quantities ρ and κ in the above equations are the HFB density matrix and the pairing tensor. e' in (8) are the single-particle energies of the cranked-deformed Hamiltonian (1), and $\bar V$ in (12)–(14) is the uncoupled antisymmetric matrix element of the two-body delta interaction (5).

The term designated by Λ in (10) does not appear in the ordinary HFB formalism and it can be immediately shown that it vanishes for the gauge angle $\phi = 0$. This term originates from the variation of the pairing energy with respect to the density matrix. In normal HFB, the pairing energy depends only on the pairing tensor, but the PHFB pairing energy also depends on the density matrix through the norm overlap. Actually, in general the norm overlap depends on both the density matrix and the pairing tensor [8]. But for the special case of number projection, the term in the overlap matrix which depends on the pairing tensor can be rewritten in terms of the density matrix by using the HFB relation ($\rho - \rho^2 = \kappa\kappa^\dagger$). Due to this transformation, the expression for Δ in (11) has a very simple appearance and reduces to the familiar form in the canonical representation [8, 11].

The integration in (8)–(11) over the gauge angle has been performed using the Gauss–Chebyshev quadrature method [12]. In this method, the integration over the gauge angle is replaced by a summation. It can be shown [12] that the optimal number of mesh points in the summation which eliminates all the components having undesired particle numbers is given by

$$M = \max\left(\frac{1}{2}N, \Omega - \frac{1}{2}\right) + 1, \tag{22}$$

where N is the number of particles and Ω is the degeneracy of the single-j shell. In the present study with $N = 6$ and $\Omega = 6$, the optimal number of points required is $M = 4$.

In the present analysis of a single-j shell, the basis in which the HFB matrix is constructed is formed by the magnetic substates of $j = 11/2$ with $m = (11/2, 9/2, \ldots, -9/2, -11/2)$. The summation indices n_1, n_2, n_3, and n_4 in all the expressions given above run over these magnetic states. In order to check the dependence of the HFB and PHFB results on the pairing interaction, the calculations have been performed with monopole ($L = 0$), monopole plus quadrupole ($L = 0$ and 2), and with full delta interaction. The results of the HFB and PHFB will be compared with the exact results for the three pairing interactions.

The results of the cranking calculations with monopole-pairing force are compared in Fig. 1. In the figure, we compare the total energy ($E_{\rm tot}$); the pairing energy ($E_{\rm pair}$); and the alignment ($\langle J_x \rangle$), which is the expectation value of the angular momentum along the rotational x axis, as functions of the rotational frequency. The expression for the total energy is given by

$$E_{\rm tot} = \int d\phi y(\phi)(H_{\rm sp}(\phi) + H_{ph}(\phi) + H_{pp}(\phi)), \tag{23}$$

where

$$H_{\rm sp}(\phi) = {\rm tr}(e\rho(\phi)), \tag{24}$$

$$H_{ph}(\phi) = \frac{1}{2}{\rm tr}(\Gamma(\phi)\rho(\phi)), \tag{25}$$

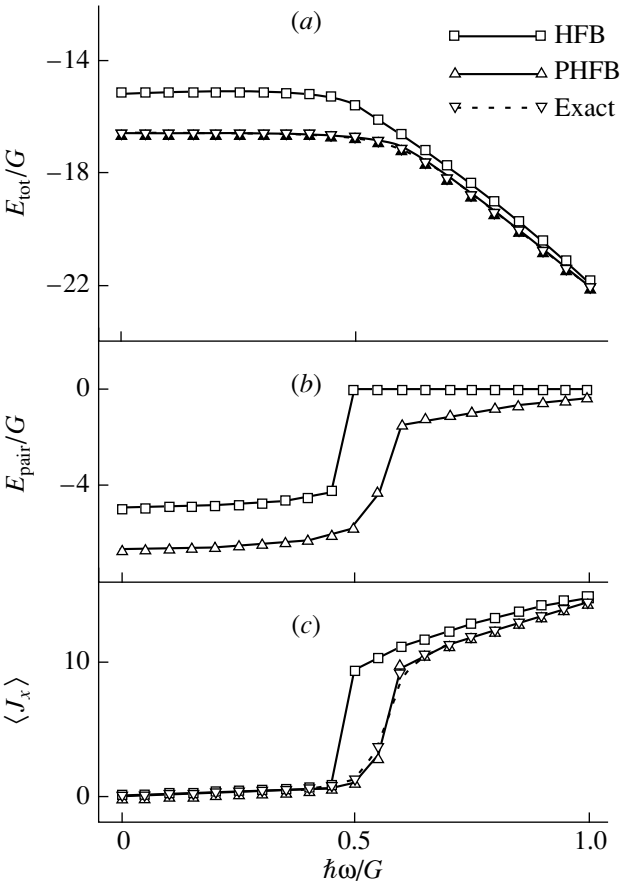

Fig. 1. The results of (*a*) the total energy $E_{\rm tot}$, (*b*) the pairing energy $E_{\rm pair}$, and (*c*) the alignment $\langle J_x \rangle$ for six particles in a deformed $j = 11/2$ orbital using the monopole interaction. The PHFB results are indistinguishable from the exact shell model results.

$$H_{pp}(\phi) = -\frac{1}{2}{\rm tr}(\Delta(\phi)\bar{\kappa}^*(\phi)). \tag{26}$$

The expressions for the pairing energy and the alignment are given by

$$E_{\rm pair} = \int d\phi H_{pp}(\phi), \tag{27}$$

$$\langle J_x \rangle = \int d\phi\, {\rm tr}(J_x \rho(\phi)). \tag{28}$$

It can be easily shown that for the gauge angle $\phi = 0$, the normal HFB expressions for these quantities are recovered.

It is apparent from Fig. 1*a* that the results of the exact shell model and the PHFB are very similar; the two curves are almost indistinguishable for all the frequency points. The results of HFB, on the other hand, deviate considerably from the exact results at lower frequencies. However, it can be seen from Fig. 1 that the HFB results converge towards the exact results with increasing rotational frequency. The HFB energy before the bandcrossing at $\hbar\omega = 0.5G$ is shifted from the exact energy by a constant amount and can be

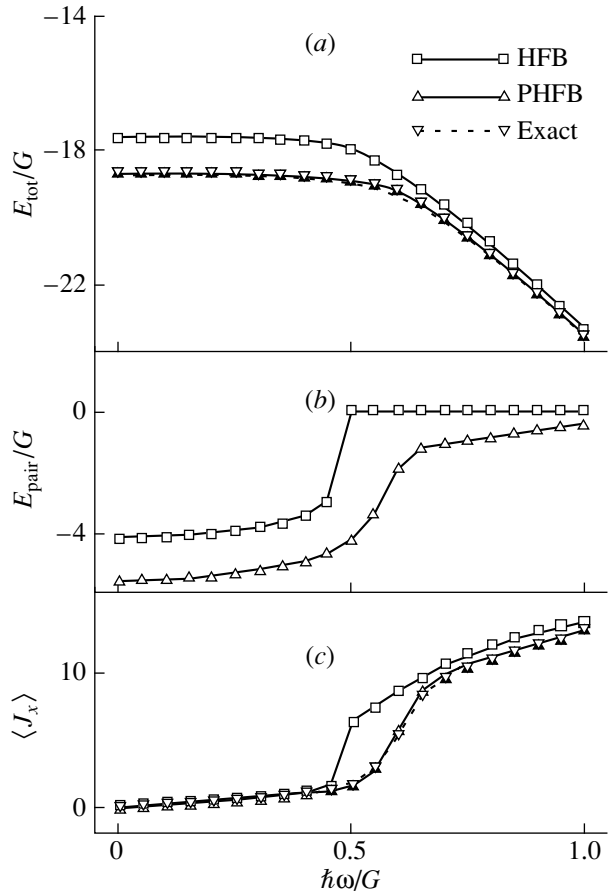

Fig. 2. The results of (*a*) the total energy E_{tot}, (*b*) the pairing energy E_{pair}, and (*c*) the alignment $\langle J_x \rangle$ for six particles in a deformed $j = 11/2$ orbital using the monopole-plus-quadrupole interaction.

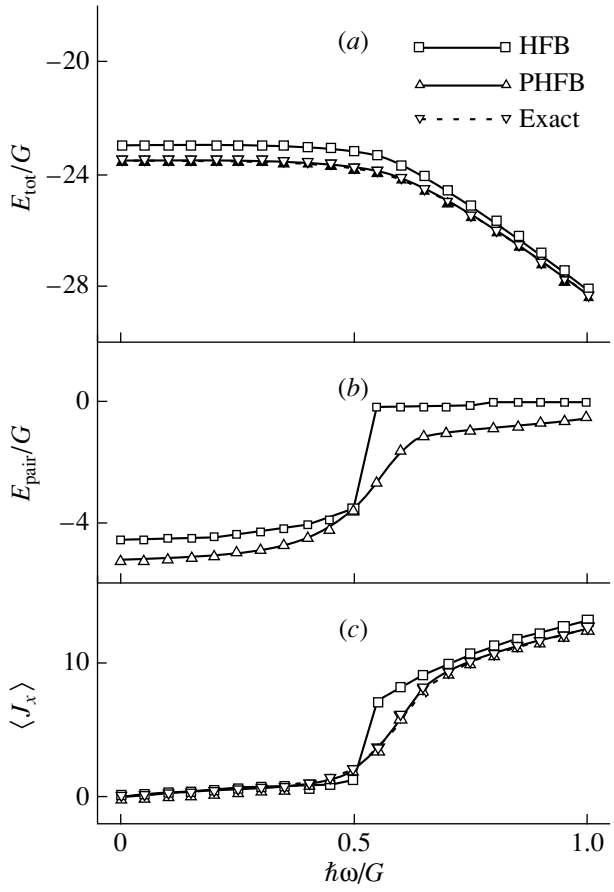

Fig. 3. The results of (*a*) the total energy E_{tot}, (*b*) the pairing energy E_{pair}, and (*c*) the alignment $\langle J_x \rangle$ for six particles in a deformed $j = 11/2$ orbital using the full delta interaction.

improved by renormalizing the strength of the pairing interaction. Therefore, for the total energy, the HFB approach is not a poor approximation. The actual problem in HFB lies in the analysis of the pairing energy and the alignment, which are shown in Figs. 1*b* and 1*c*. The HFB pairing energy has a finite value until $\hbar\omega = 0.45G$ and then suddenly goes to zero at $\hbar\omega = 0.5G$. This transition is an artifact of the HFB approach, as is clearly evident from Fig. 1. The PHFB pairing energy does drop at the bandcrossing but has a finite value at all the rotational frequencies. This feature of the pairing energy is also reflected in the alignment, which is determined by the competition between the Coriolis forces and the pairing correlations. The alignment until $\hbar\omega = 0.45G$ is very similar in all three cases, but then HFB value suddenly jumps to $\langle J_x \rangle = 10$; the exact and the PHFB values, on the other hand, do not show this sharp transition. The gain in alignment at the first crossing, referred to as the *AB* crossing, is quite similar in all the cases; however, the crossing occurs somewhat earlier in HFB.

The results of pairing interaction with monopole-plus-quadrupole terms are shown in Fig. 2. The comparison among HFB, PHFB, and the exact results is quite similar to Fig. 1. The total HFB energy is shifted by a constant factor from exact and PHFB energies before the bandcrossing. After the crossing, the HFB results become closer to the exact ones. The HFB pairing energy depicts a transition, and the PHFB pairing energy, on the other hand, drops smoothly at the bandcrossing. However, the HFB gain in alignment at the *AB* crossing is much lower than 10 and has a clearly wrong behavior after the crossing.

The results with the full delta interaction are presented in Fig. 3. The HFB total energy is now in better agreement with the exact results and PHFB as compared to the results shown in Figs. 1 and 2. In fact, it is evident by comparing the three figures that the total energy improves by including higher multipoles in the pairing interaction; the maximum deviation is noted for the monopole case. This appears to be in contradiction to our basic understanding of the mean-field approach, in which one normally expects that HFB or BCS is a better approximation for the pure monopole pairing. However, it should be mentioned that, in our HFB and PHFB analysis, we have included all the terms in the

Hamiltonian. In particular, the particle-hole contribution (Γ) amounts to about $6G$ in the total energy and is at a maximum with the full delta interaction. If one excludes this contribution, the discrepancy would be the largest for the delta interaction.

The pairing energy in Fig. 3 again depicts a phase transition at $\hbar\omega = 0.55G$, which is slightly higher than with monopole interaction. The HFB *AB* crossing with full delta interaction is now close to the exact result and PHFB. The gain in alignment at the *AB* crossing is lower than 10, as in the case of monopole and quadrupole pairing forces. The overall agreement with full delta interaction appears to be better for HFB. The good agreement between PHFB and exact result, on the other hand, is independent of the interaction used.

To conclude, in the present work, the recently developed number-projected HFB approach has been applied to an exactly solvable cranked-deformed shell Hamiltonian. The main motivation has been to check the numerical applicability of the projection method. It is clear from the present study that the projected HFB approach gives an accurate description of the yrast states of the model Hamiltonian. The transition from a superfluid to the normal phase obtained in the HFB theory is shown to be smeared out with the projection.

We would like to stress that the main advantage of the present projection method is that it has the same structure as that of normal HFB equations. Therefore, one can use the existing HFB computer codes, and only the expressions for the HF potential and the pairing field need to be redefined. Instead of the normal HFB fields, in the projection method one needs to calculate the projected quantities as given by (8)–(11). In the present model study, we find that the numerical work involved in the projection is similar to performing the bare HFB calculations. For each rotational frequency, the average CPU time on a Pentium (166 MHz) was 6.14 s with projection as compared to 5.97 s for normal HFB. The present projection method, therefore, preserves all the mathematical and computational simplicity of the HFB mean-field approach.

REFERENCES

1. P. Ring and P. Schuck, *The Nuclear Many-Body Problem* (Springer-Verlag, New York, 1980).
2. P. Magierski, S. Cwiok, J. Dobaczewski, and W. Nazarewicz, Phys. Rev. C **48**, 1686 (1993).
3. G. Gall, B. Bonche, J. Dobaczewski, and P.-H. Heenen, Z. Phys. A **348**, 183 (1994).
4. A. Valor, J. L. Egido, and R. Robledo, Phys. Rev. C **53**, 172 (1996).
5. H. Flocard and N. Onishi, Ann. Phys. (N.Y.) **254**, 275 (1997).
6. J. L. Egido and P. Ring, Nucl. Phys. A **383**, 189 (1982).
7. J. L. Egido and P. Ring, Nucl. Phys. A **388**, 19 (1982).
8. J. A. Sheikh and P. Ring, Nucl. Phys. A **665**, 71 (2000).
9. J. A. Sheikh, N. A. Nagarajan, N. Rowley, and K. F. Pal, Phys. Lett. B **223**, 1 (1989).
10. J. P. Brussaard and P. W. M. Glaudemans, *Shell Model Applications in Nuclear Spectroscopy* (North-Holland, Amsterdam, 1977).
11. K. Dietrich, H. J. Mang, and J. H. Pradal, Phys. Rev. B **135**, 22 (1964).
12. K. Hara, S. Iwasaki, and K. Tanabe, Nucl. Phys. A **332**, 69 (1979).

Physics of Atomic Nuclei, Vol. 64, No. 3, 2001, pp. 482–493. From Yadernaya Fizika, Vol. 64, No. 3, 2001, pp. 536–547.

90th ANNIVERSARY OF A.B. MIGDAL'S BIRTHDAY
NUCLEI

Electromagnetic Response Functions of Few-Nucleon Systems*

V. D. Efros, W. Leidemann[1)], and G. Orlandini[1)]**

Russian Research Centre, Kurchatov Institute, pl. Kurchatova 1, Moscow, 123182 Russia

Received July 25, 2000

Abstract—Inclusive electromagnetic reactions in few-nucleon systems are studied based on accurate three- and four-body calculations. The longitudinal ^{4}He(e, e') response function in the q range of 300–600 MeV/c; the ^{4}He spectral function; the corresponding quasielastic ^{4}He(e, e') response; and the total photoabsorption cross sections of ^{3}H, ^{3}He, and ^{4}He are considered. Descriptions of the continuum, the role of final-state interactions, sensitivity to nuclear dynamics, and effects of *NNN* forces are discussed. © *2001 MAIK "Nauka/Interperiodica".*

1. INTRODUCTION: FORMULATION OF THE METHOD

Our recent theoretical results on electromagnetic processes in three- and four-nucleon systems are presented in the paper. In Sections 2–4, the results on four-nucleon response functions are reviewed. A considerable part of the present discussion is not contained in work published previously. In Section 2, the issue of accuracy of the conventional 4*N* formulation for the ^{4}He(e, e') reaction is addressed. In Section 3, we present the exact spectral function (SF) of the ^{4}He nucleus and study the accuracy of the description of the ^{4}He(e, e') process in the framework of the SF approximation. The interest in this approximation rests in part on the fact that, unlike a complete few-body formulation, both the spectral function and its distorted-wave generalizations may be readily obtained in the framework of relativistic kinematics. In Section 4, the total ^{4}He photodisintegration cross section is studied, and a sizable disagreement with recent experimental data on the strength of the giant resonance peak is revealed. In Section 5, the total photodisintegration cross sections of ^{3}H and ^{3}He are studied using realistic *NN* and *NNN* forces. Sensitivity of the results to nuclear dynamics and, in particular, the effect which an *NNN* force has on the cross section are considered.

We calculate response functions having the form

$$R(\epsilon) = \overline{\sum_{M_0}}\left\{\sum_{n=0}^{N}\sum_{M_n}\left|\langle\Psi_n|\hat{O}|\Psi_0\rangle\right|^2\delta[(E_n-E_0)-\epsilon] + \int df\left|\langle\Psi_f|\hat{O}|\Psi_0\rangle\right|^2\delta[(E_f-E_0)-\epsilon]\right\}. \quad (1)$$

Here, M_n and M_0 are projections of the total spin, Ψ_n are bound states (in particular, Ψ_0 is the ground state), and Ψ_f are continuum states satisfying

$$(H-E_n)\Psi_n = 0, \quad (H-E_f)\Psi_f = 0,$$

where H is the few-nucleon nonrelativistic Hamiltonian, and all the quantities are "intrinsic" ones, i.e., refer to the subspace spanning Jacobi coordinates or momenta. States Ψ_n plus Ψ_f form a complete set. Below, we consider ^{3}H, ^{3}He, and ^{4}He nuclei; hence, there is only one bound state in Eq. (1). In the (e, e') case, the excitation energy ϵ is equal to $\omega - q^2/(2AM)$, where q and ω are momentum and energy transferred to the nucleus. In the photodisintegration case, we have $q = \omega$. We neglect the very small nuclear recoil energy, so that $\epsilon = \omega = E_\gamma$.

We obtain the response (1) with the method of integral transforms. This method eliminates the need to compute a complete set of final-state continuum wave functions and to perform summation over their contributions in Eq. (1). At the first step, the Lorentz transform of the response (1)

$$\Phi(\sigma_R, \sigma_I) = \sum_{n=0}^{N}\frac{R_n}{(\sigma_R-\epsilon_n)^2+\sigma_I^2} + \int_{\epsilon_{\min}}^{\infty} d\epsilon\frac{R(\epsilon)}{(\sigma_R-\epsilon)^2+\sigma_I^2}, \quad (2)$$

$$R_n = \overline{\sum_{M_0}}\sum_{M_n}\left|\langle\Psi_n|\hat{O}|\Psi_0\rangle\right|^2 \quad (3)$$

is calculated. Denoting $\sigma = -\sigma_R + i\sigma_I$ and writing the kernel of the transform as

$$K \equiv \frac{1}{(\sigma_R-\epsilon_n)^2+\sigma_I^2} = \frac{1}{(\sigma^*+\epsilon)(\sigma+\epsilon)},$$

one can see that, if $\hat{O}$ is independent of ϵ, the transform is expressed as the norm of the state $\tilde{\Psi}$:

$$\Phi(\sigma_R, \sigma_I) = \langle\tilde{\Psi}|\tilde{\Psi}\rangle, \quad (4)$$

* Thus article was submitted by the authors in English.

** e-mail: efros@mbslab.kiae.ru

1) Dipartimento di Fisica, Università di Trento, and Instituto Nazionale di Fisica Nucleare, Gruppo collegato di Trento, Italy.

which satisfies the Schrödinger-like equation with the source

$$(H - E_0 + \sigma)\tilde{\Psi} = \hat{O}\Psi_0. \quad (5)$$

Since the transform (2) is finite, the norm (4) exists and the solution $\tilde{\Psi}$ to Eq. (5) is localized. Therefore, $\tilde{\Psi}$ can be found with bound-state-type methods, which is a substantial point of the present approach. Finally, the response (1) is obtained by inverting the transform (2).

In general, the operator $\hat{O}$ in (1) depends on both **q** and ϵ as parameters, while the method for calculating the response listed above is applicable directly when $\hat{O}$ is independent of ϵ. To avoid this problem in the most general case, one could replace the operator $\hat{O}(\mathbf{q}, \epsilon)$ with $\hat{O}(\mathbf{q}, \bar{\epsilon})$, where $\bar{\epsilon}$ is independent of ϵ; calculate the extended response $R(q, \bar{\epsilon}, \epsilon)$; and consider it at $\bar{\epsilon} = \epsilon$. A simpler way to remove the ϵ dependence of the operator of the type listed below usually exists. The photon case, when retardation corrections are taken into account, can be obtained from the transverse response $R_t(q, \epsilon)$ of the electron cross section by setting $q = \epsilon$.

If, as in our case, an expansion

$$\tilde{\Psi} = \sum_{j=0}^{J} c_i \phi_i \quad (6)$$

over a complete set of localized functions is used to solve Eq. (5), then the method allows the following simple interpretation. Use of expansion (6) is equivalent to expressing $\tilde{\Psi}$ in terms of $J + 1$ discrete states $\Psi_j^{(J)}$ obtained upon the diagonalization of H in the subspace spanning the $J + 1$ states ϕ_j. Let $E_j^{(J)}$ be the eigenenergies pertaining to $\Psi_j^{(J)}$, and let $\epsilon_j^{(J)} = E_j^{(J)} - E_0^{(J)}$ be the corresponding excitation energies. The first $N + 1$ $E_j^{(J)}$ values are approximations to the energies of discrete levels in a system. With the aid of Eq. (4), the corresponding approximate transform (2) may be written as

$$\Phi(\sigma_R, \sigma_I) = \sum_{j=0}^{J} \frac{R_j^{(J)}}{(\sigma_R - \epsilon_j^{(J)})^2 + \sigma_I^2},$$
$$R_j^{(J)} = \overline{\sum_{M_0}} \sum_{M_j} \left| \langle \Psi_j^{(J)} | \hat{O} | \Psi_0^{(J)} \rangle \right|^2, \quad (7)$$

which corresponds to a substitution of the pseudoresponse

$$\overline{\sum_{M_0}} \sum_{j=N+1}^{J} \sum_{M_j} \left| \langle \Psi_j^{(J)} | \hat{O} | \Psi_0^{(J)} \rangle \right|^2 \delta[(E_j^{(J)} - E_0^{(J)}) - \epsilon] \quad (8)$$

into the continuum part on the right-hand side of Eq. (2). Thus, the transform provides smoothing of the pseudoresponse (8). When J becomes sufficiently high, this smoothed pseudoresponse approaches the transform of the true response. Then, imposing the requirement in the course of the inversion procedure that the result of the inversion be a smooth function, one obtains a good approximation to the true response.

An approach similar to that outlined above can be applied for calculating other observables. For example, the cross section $d^2\sigma/d\epsilon d\Omega$ for scattering of a particle off a few-body system in the Glauber approximation is obtained if the profile function (expressed in the usual way in terms of elementary scattering amplitudes) is substituted for the operator $\hat{O}$ in Eq. (1).

The Lorentz transform (2) was proposed in [1]. In [2], it was suggested to study response functions at the transform level with bound-state techniques using the transforms with the Stieltjes-type kernels $K = 1/(\sigma + \epsilon)^n$, where $n = 1, 2, \ldots$, and σ is real. In [3], the general method for perturbation-induced inclusive and exclusive reactions and strong-interaction-induced $2 \longrightarrow N$ reactions was formulated. The kernels $K = 1/(\sigma + \epsilon)$ and $1/(\sigma + \epsilon)^2$, where σ is real, were employed to produce specific transforms. In [4], the exclusive $d(e, e'p)$ reaction was studied using the Lorentz transform. In [5], a procedure for inclusive reactions was given which eliminates summation over final states in Eq. (1) as above but has a nonlocalized object as a solution to the inhomogeneous equation of Eq. (5) type. No inversion is required in this case. Additional information on the approach can be found in [6–8].

Independently, a procedure based on the Laplace transform for calculating inclusive quantities was developed in condensed-matter physics (see, e.g., [9]). In this approach, no dynamical equation like Eq. (5) is solved, and the transform is calculated with path-integral techniques. An attempt to obtain a few-body response in this way was made in [10], and in [11] a comparison of a response with experiment was performed at the transform level. Unlike the Laplace or Stieltjes transform, the inversion of the Lorentz transform is facilitated by the fact that the kernel of the transform looks like a smoothed δ function up to a normalization, so that, at a proper choice of the σ_I value, the transform considered as a function of σ_R is already similar to the response to be obtained. This should be a practical advantage of the Lorentz transform.

We also want to comment on the description of special features of a system like resonances in the framework of the present approach. If the width of a resonance is larger than σ_I, then the resonance shows up in $\tilde{\Psi}$ and will "automatically" be reproduced in the final response. If the width is narrower than σ_I, then the resonance is smoothed or smeared out in $\tilde{\Psi}$. In this case, in order to reproduce the width of the resonance in the

final response correctly, either the input transform $\tilde{\Psi}$ of enhanced accuracy is required or the width found separately in advance should be used in the inversion process. The same applies to peculiarities of breakup-reaction amplitudes corresponding to long-living subsystems.

In our calculations, we solved Eq. (5) with the help of expansion (6) over the correlated hyperspherical and hyperradial bases. A selection of the basis states has been applied. In the three-nucleon case, the Euler angles were eliminated and the remaining three-dimensional integration was done with Gauss-type quadratures, while in the four-nucleon case the matrix elements were calculated with the Monte Carlo method. The convergence of the final results with respect to the number of terms retained in the expansion, as well as the stability of the inversion, was checked. Various sum rules were used as additional checks. Realistic *NN* plus *NNN* forces were employed in the three-nucleon case, and semirealistic *NN* forces in the four-nucleon case. Within the adopted formulations of the problems, the results below, except those in Section 4, are accurate at the percent level. While in the three-nucleon case the calculations are fast, in the four-nucleon case they are lengthy and to deal with realistic forces an improvement of our techniques for solving Eq. (5) is required. Along with trying to apply expansion techniques, other bound-state-type methods should be sought for solving Eq. (5) for larger systems.

2. LONGITUDINAL ^{4}He(e, e') RESPONSE FUNCTION

The longitudinal ^{4}He(e, e') response in the q range of 300–600 MeV/c has been calculated [12, 13, 7]. A nonrelativistic 4N Hamiltonian with central even local *NN* potentials reproducing the $^1S_0$ and $^3S_1$ *NN* phase shifts up to high energy was used as a dynamical input. This Trento (TN) potential is listed in [7]. It leads to correct values of binding energy and radius of ^{4}He. The conventional single-particle transition operator

$$\hat{O} = (1/2)[\tilde{G}_E^p(Q^2) + \tilde{G}_E^n(Q^2)]\sum_{i=1}^{A} e^{i\mathbf{q}\cdot(\mathbf{r}_i - \mathbf{R}_{\text{c.m.}})} + (1/2)[\tilde{G}_E^p(Q^2) - \tilde{G}_E^n(Q^2)]\sum_{i=1}^{A} e^{i\mathbf{q}\cdot(\mathbf{r}_i - \mathbf{R}_{\text{c.m.}})}\tau_{zi} \quad (9)$$

has been adopted. Here, τ_{zi} is the isospin operator, $Q^2 = q^2 - \omega^2$, and $\tilde{G}_E^{p,n}$ denote the Sachs form factors $G_E^{p,n}$ times the usual relativistic correction [14]. The spin–orbit relativistic correction is disregarded in Eq. (9). As the sum-rule estimates show, its contribution is very small in our case. In the ^{4}He case, the first and second term in Eq. (9) lead to $T = 0$ and $T = 1$ final states, respectively. Therefore, there is no interference between their contributions to the response (1) in this case. These contributions were calculated separately with the ω-dependent factors $[\tilde{G}_E^p(Q^2) \pm \tilde{G}_E^n(Q^2)]^2$ separated out from the calculation.[2)]

No further approximations have been made, and the final-state interaction (FSI) is thus fully taken into account. In Fig. 1, the calculated inelastic longitudinal response function $R_L(q, \omega)$ is shown with solid curves for four values of the transferred momentum q (in MeV/c) along with the Bates [15] and Saclay [16] data. One observes a very good agreement with experiment in the whole range of q values. The drop in the Saclay data at $q = 500$ MeV/c in the vicinity of $\omega = 250$ MeV is at variance with the corresponding sum-rule systematics.

To comment on this agreement with experiment, let us estimate the initial-state momenta contributing substantially to the response. Let us consider, e.g., the processes where only one nucleon is ejected with high momentum. Let $\mathbf{k}_{\text{rel}}$ be the relative momentum of the fast nucleon and the remaining $A - 1$ subsystem,

$$\mathbf{k}_{\text{rel}} = [(A-1)/A][\mathbf{k}_N - (A-1)^{-1}\mathbf{K}_{A-1}] = \mathbf{k}_N - A^{-1}\mathbf{K}_A,$$

where $\mathbf{k}_N$, $\mathbf{K}_{A-1}$, and $\mathbf{K}_A = \mathbf{q}$ are the momentum of the fast nucleon, that of the residual $A - 1$ subsystem, and the total momentum, respectively.

The ground-state single-particle momentum probed in the electrodisintegration process is $\mathbf{q}(A-1)/A - \mathbf{k}_{\text{rel}} = \mathbf{q} - \mathbf{k}_N \equiv \mathbf{k}_{\text{miss}}$. The predominant contribution comes from the states with $\mathbf{k}_{\text{rel}}$ directed along $\mathbf{q}$. Adopting the approximation $k_{\text{miss}} \simeq |q(A-1)/A - k_{\text{rel}}|$, using the energy conservation in the form $\omega = k_{\text{rel}}^2 A/[2(A-1)m] + q^2/(2Am) - E_0$, and setting $\omega + E_0 = q^2/(2m) + \Delta$, one obtains

$$k_{\text{miss}} \simeq [(A-1)/A]\left|\{q^2 + [A/(A-1)]2m\Delta\}^{1/2} - q\right|.$$

Let us consider the response on the right-hand side of the peak. Setting, for example, $q = 600$ MeV/c, $\Delta \le 100$ MeV (cf. Fig. 1), one gets $k_{\text{miss}} \le 0.7$ fm^{-1}. Further, let us consider the left-hand side of the peak at $q = 600$ MeV/c and set $\omega \ge \omega_{\min} + 50$ MeV. Then, one gets $k_{\text{miss}} \le 0.9$ fm^{-1}. The FSI admixes, to $\mathbf{k}_{\text{rel}}$, the momenta lying in the range $\Delta\mathbf{k}$. The momenta $\Delta\mathbf{k}$ are determined by the nuclear force, and for large enough momentum transfer they will be much lower than $\mathbf{k}_{\text{rel}}$, thus affecting the previous estimates of k_{miss} very little. The reaction mechanism described above is plausible in the mentioned kinematical regions, so that, even if higher

[2)]When the ground-state isospin is different from zero, the response includes a cross term between the isoscalar and isovector components of the operator (9) in addition. The calculation can be done in a similar way if one, e.g., splits the response into the isoscalar–isoscalar, isovector–isovector, and cross components and separates out the corresponding ω-dependent factors.

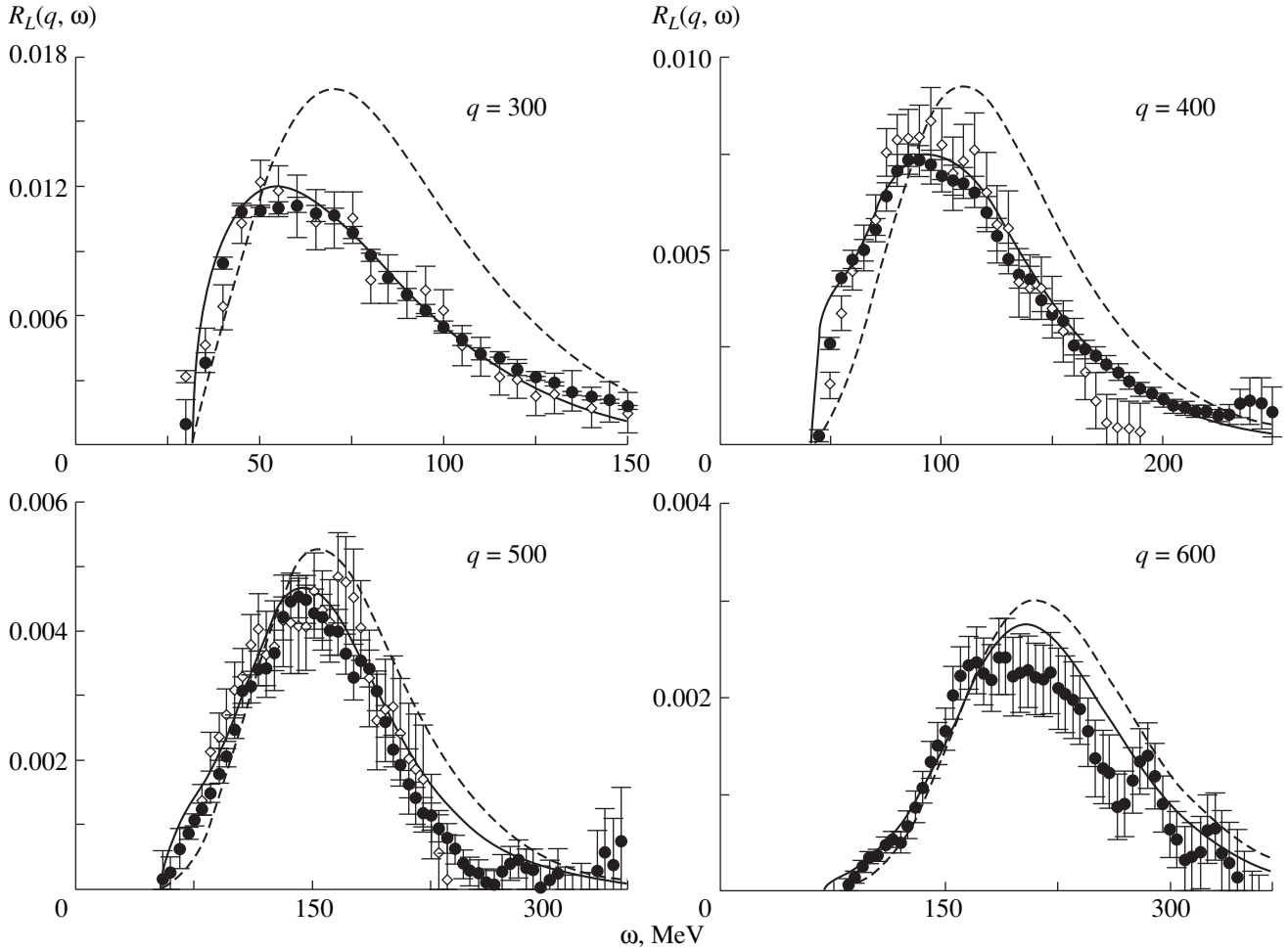

Fig. 1. Longitudinal response of ^{4}He (in MeV^{-1}): full results (solid curves) and PWIA calculation (dashed curves). Bates [15] and Saclay [16] data are represented with open diamonds and closed circles, respectively; q in units of MeV/c.

ground-state momenta are probed with other reaction mechanisms, the contributions of those momenta would be suppressed because of a smaller weight of higher momenta in the ground state.

From what has been said above, one may conclude that low ground-state single-nucleon momenta play a major role in the above kinematical regions for all the q values we consider. But the semirealistic *NN* potentials of the type we used probably lead to the low-momentum content of wave functions close to that for a fully realistic nuclear force. This is illustrated in Fig. 2, where the single-particle momentum distribution of ^{4}He for our *NN* potential is compared with that obtained from a realistic nuclear force [17]. The probabilities of higher momenta in the realistic case are considerably larger due to correlations generated by the tensor force missing in our potential. As a result, one may suggest that the agreement above with experiment testifies to a correct description of the corresponding low-momentum content of wave functions within the adopted 4*N* formulation. It also shows that the nonrelativistic framework and the use of the conventional single-particle electromagnetic operator are justified. However, at high q values and ω values close to the threshold, rather high nucleon momenta in the ground state $k_{\text{miss}} \simeq [(A-1)/A]q$ are probed at the left wing of the response. We plan to consider this region in more detail in the future.

3. SPECTRAL FUNCTION AND QUASIELASTIC RESPONSE OF ^{4}He

The SF of ^{4}He and the corresponding quasielastic (QE) response have been calculated exactly with the same *NN* potential [13, 7]. The SF $S_{t_z}(k, E)$ represents the joint probability of finding a nucleon with momentum $\mathbf{k}$ and a residual $A-1$ system with energy $E + E_0^A$ in a ground state at rest:

$$S_{t_z}(k, E) = \overline{\sum_{M_0}} \sum_{s_z = \pm 1/2} \left\{ \sum_{n=0}^{N} \sum_{M_n} \left| \langle \Psi_{n,-\mathbf{k}}^{A-1}; \mathbf{k}, s_z, t_z | \Psi_0^A \rangle \right|^2 \times \delta[E - (E_n^{A-1} - E_0^A)] + \int df \left| \langle \Psi_{f,-\mathbf{k}}^{A-1}; \mathbf{k}, s_z, t_z | \Psi_0^A \rangle \right|^2 \delta[E - (E_f^{A-1} - E_0^A)] \right\}. \quad (10)$$

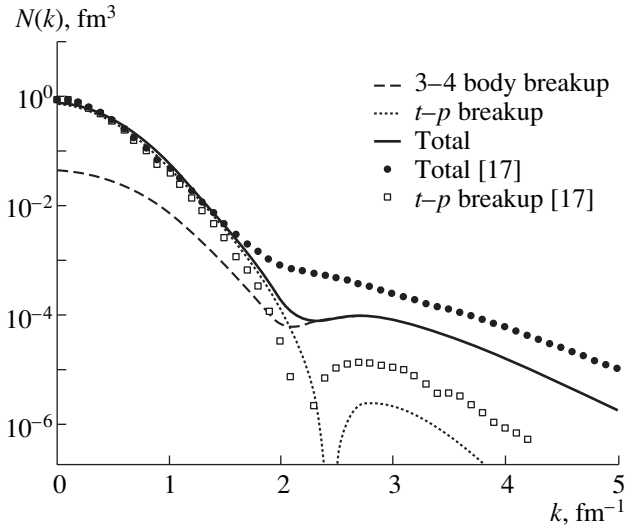

Fig. 2. Total and partial momentum distributions of ^{4}He with the TN potential and with AV18-plus-UrbanaIX interaction [17].

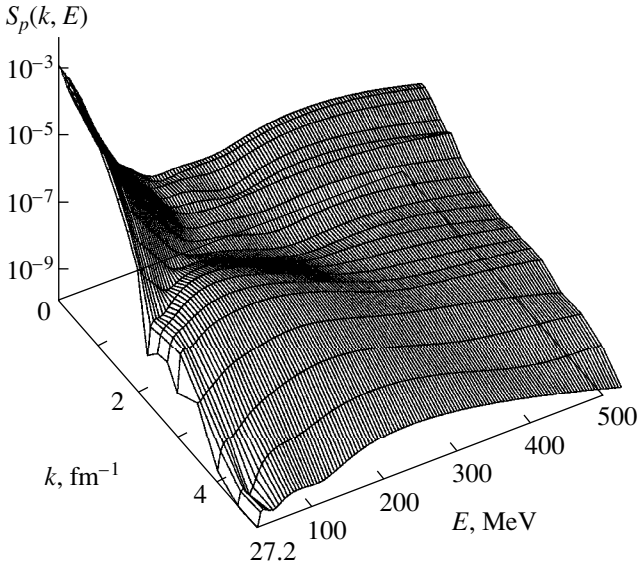

Fig. 3. SF $S_p(k, E)$ of ^{4}He with the TN potential in units of fm^3 MeV^{-1}.

Unlike the formulas above, the matrix element is taken here in the center-of-mass system in the total space, and not in the subspace of intrinsic variables. In Eq. (10), the ground state is

$$\Psi_0^A = \int f(\mathbf{P})d\mathbf{P}\int d\mathbf{k}_1\ldots d\mathbf{k}_A\varphi_0^A(\mathbf{k}_1\ldots\mathbf{k}_A) \times\delta\left(\sum_{i=1}^{A}\mathbf{k}_i-\mathbf{P}\right)|\mathbf{k}_1\ldots\mathbf{k}_A\rangle, \quad (11)$$

where φ_0^A is the corresponding wave function, $f(\mathbf{P})$ represents a narrow peak concentrated in the vicinity of $\mathbf{P} = 0$, and $\int|f(\mathbf{P})|^2d\mathbf{P} = 1$. In Eq. (11), we omitted spin and isospin variables. Further, $\Psi_{n,-\mathbf{k}}^{A-1}$ and $\Psi_{f,-\mathbf{k}}^{A-1}$ are discrete and continuum states of the Hamiltonian of the $A-1$ subsystem having total momenta $-\mathbf{k}$, the quantities $E_0^A = M_0^A - Am$ and $E_{n,f}^{A-1} = M_{n,f}^{A-1} - (A-1)m$ are the corresponding intrinsic energies of the system and subsystem, and s_z and t_z are the spin and isospin quantum numbers of the nucleon.[3)] The energy E can be viewed as the removal energy of the nucleon. The calculation of the SF from its definition requires obtaining the complete set of states of the residual $A-1$ subsystem. Previously, the SF has been calculated in the $A = 3$ case, which is essentially the two-body problem, and, approximately, for nuclear matter (see [18] for the references). We avoided calculating the complete set of $A = 3$ continuum states with the help of the method of the type outlined in Section 1. The proton SF $S_p(k, E)$, Eq. (10), obtained in this way includes two contributions: one from the $A = 3$ rest subsystem being in the ground state and the other from the continuum. The second of these contributions is shown in Fig. 3. The values of $S_p(k, E) \geq E_{\text{thr}}^{A-1} + 1$ MeV are plotted. [We note that $S_p(k, E_{\text{thr}}^{A-1}) = 0$; thus, $S_p(k, E)$ exhibits a strong slope at low energy.] For momenta below 2 fm^{-1}, one finds a sharp maximum at about 2 MeV above E_{thr}^{A-1}. In Fig. 4, the cut of the calculated spectral function at $k = 0.25$ fm^{-1} is shown.

Our SF compares fairly well with experiments performed at k values about 0.5–0.75 fm^{-1} [19]. For $k >$ 2 fm^{-1}, the calculated spectral function exhibits a ridge where the peak position shifts to higher E for increasing k. This ridge should presumably correspond to a proton struck from the region of a strong two-nucleon correlation, see [18, 20].

The (e, $e'N$) cross section can be expressed in terms of the SF if the following approximations are adopted. The single-particle transition operator is used, as in Eq. (9). The factorized form for the final-state wave functions is used: a plane wave describing the knocked-out nucleon times a final-state wave function of the

[3)] In the nonrelativistic case, when the calculation is reduced to the center-of-mass subspace in the configuration representation, the exponent pertaining to the free motion with the momentum $\mathbf{k}$ in (10) has the form $\exp(-i\mathbf{k}_{\text{rel}}\cdot\mathbf{r}_{\text{rel}}) = \exp\{-i[A/(A-1)]\mathbf{k}\cdot(\mathbf{r}_A - \mathbf{R}_{\text{c.m.}})\}$. See also [8], Eqs. (11)–(17), in connection with the definitions used. (Note the following misprints in [8]: in Eq. (11), the integral sign was dropped; in Eq. (16), $d\boldsymbol{\pi}_1\ldots d\boldsymbol{\pi}_{A-1}$ should be replaced by $d\boldsymbol{\pi}_1\ldots d\boldsymbol{\pi}_{A-2}$; in Eq. (17), $e^{-i\boldsymbol{\pi}_{A-1}\boldsymbol{\xi}_{A-2}}$ should be replaced by $e^{-i\boldsymbol{\pi}_{A-1}\boldsymbol{\xi}_{A-1}}$.)

$A-1$ subsystem, i.e., the plane-wave impulse approximation (PWIA). Only the component of the single-particle transition operator acting upon the knocked out nucleon is retained. The QE longitudinal response R_L^{QE} can be calculated within the same approximations via summation over the corresponding (e, $e'p$) contributions. This gives

$$R_L^{\mathrm{QE}}(q,\omega) = A[\tilde{G}_E^p(Q)]^2 \int d\mathbf{k}_N dE S_p(|\mathbf{k}_N - \mathbf{q}|, E) \times \delta[\omega - E - (\mathbf{k}_N^2/(2m) - \mathbf{K}_{A-1}^2/[2(A-1)m]]. \quad (12)$$

The approximate response (12) is shown in Fig. 1 with the dashed curve. At q = 600 MeV/c, the height of the peak is overestimated by about 9% in the framework of the QE approximation. The rate of convergence at the peak of the QE response towards the true one slows down when q reaches about 0.5 GeV/c. Within our dynamical framework, this probably happens due to strong short-range components of nuclear force. From these results, one can extrapolate that for q exceeding 1 GeV/c the relative error of the QE response approximation at the peak becomes less than 5%. For energies far from the peak value, the relative contribution to the cross section of disregarded nonplane wave components of the final-state wave function increases. At low ω, the PWIA assumption inherent to R_L^{QE} obviously breaks down. As is shown in [8], the generalized SF that corresponds to a replacement of the PWIA for the fast knocked-out nucleon with the distorted-wave impulse approximation can also be calculated with an approach similar to that used above. A relativistic Glauber-type ansatz may be used for the distorted wave at high q in some cases.

It is seen from Fig. 1 that the QE peak is shifted to higher energies with respect to the true one. The shift of the peak can be qualitatively understood considering a nucleon at rest in a potential well: ω_{peak} can be estimated as $q^2/(2m) + V_f(q) - V_i$, where V_i and V_f are the potential energies before and after interaction with the virtual photon, respectively. While V_f is negative, it becomes zero in PWIA, leading to an increase in ω_{peak}.

It is advantageous to have a simple and good approximation for the QE response. The continuum part of the SF depicted in Fig. 3 is to be simplified in the integrand in Eq. (12). It is seen from Fig. 3 that for low k values relevant to us almost all the strength in this part is concentrated close to the threshold $E = E_{\mathrm{min}}$. This suggests the approximation [to be substituted into (12)]

$$S(k,E) \simeq n_{tp}(k)\delta[E - E_0(^3\mathrm{H}) + E_0(^4\mathrm{He})] + n_{t^*p}(k)\delta[E - E_{t^*p} + E_0(^4\mathrm{He})], \quad (13)$$

where E_{t^*p} is the threshold breakup energy of the residual $A = 3$ nucleus, and $n_{tp}(n_{t^*p})$ is the proton momentum distribution in the channel where the residual nucleus is bound (unbound). The continuum part of SF is represented by the second term in (13). Using (13), one does not need continuum-state calculations since $n_{t^*p}(k) = n(k) - n_{tp}(k)$, $n(k)$ being the total momentum distribution. One obtains an even simpler approximation considering that $E_{t^*p} \simeq E_0(^3\mathrm{H})$:

$$S(k,E) \simeq n(k)\delta[E - E_0(^3\mathrm{H}) + E_0(^4\mathrm{He})]. \quad (14)$$

Equation (14) was used in the literature (see, e.g., [10]). At small k values of interest, the second term in (13) is comparatively small (e.g., the integrated values of n_{tp} and n_{t^*p} are equal to 0.89 and 0.11, respectively), which improves the quality of the approximations (13) and (14). In Fig. 5, we show the responses obtained from Eq. (12) with these approximations relative to that of Eq. (12) with the full spectral function. Except for small ω, where the wrong threshold behavior in

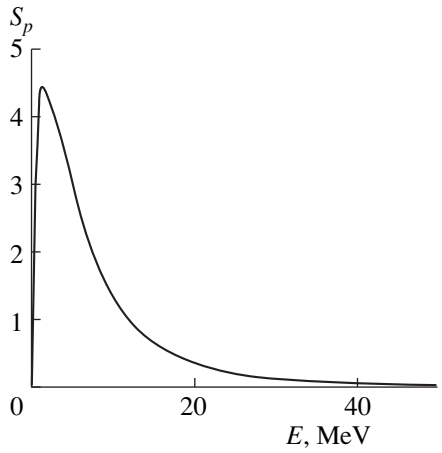

Fig. 4. The cut of the ^{4}He SF at $k = 0.25$ fm^{-1}. The values of SF are in 10^{-3} fm^3 MeV^{-1}.

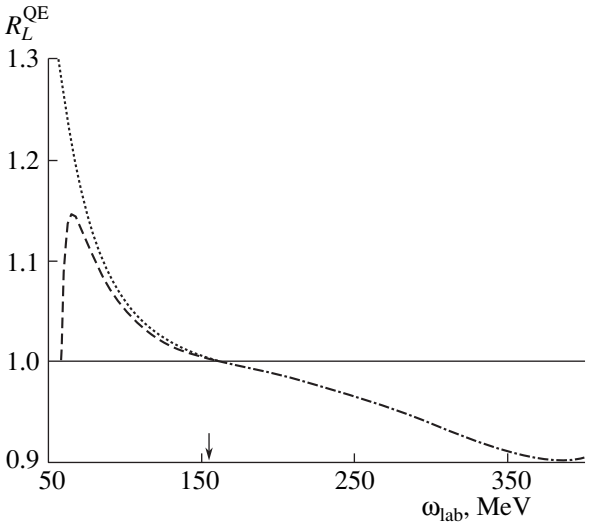

Fig. 5. QE response (12) at q = 500 MeV/c with the SF of Eq. (13) (dashed curve) and of Eq. (14) (dotted curve) relative to that with the full SF (the QE peak is marked by an arrow).

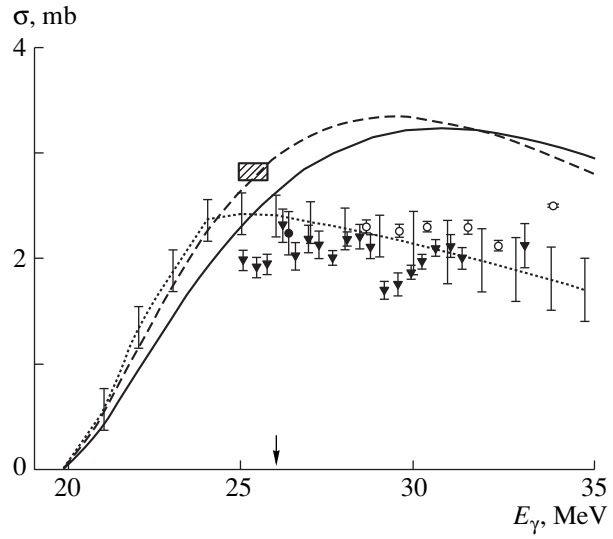

Fig. 6. Theoretical results for the total ^{4}He photoabsorption cross section at low energy with the MT (dashed curve) and TN (solid curve) potentials. Also shown is the cross section based on the experimental results of [25, 26] (dotted curve with typical size of the experimental error) as well as doubled experimental cross sections for $(\gamma, p)^3$H (open circles) [29] and $(\gamma, n)^3$He (triangles) [28] and (closed circle) [30]. The cross section [33] estimated from the experimental data on photon scattering off ^{4}He is shown with a rectangular.

Eq. (14) may play a role, the three responses are very similar, particularly in the peak region. At q = 300, 400, and 1000 MeV/c, one has very similar results.

4. PHOTODISINTEGRATION OF ^{4}He: STRENGTH OF THE GIANT DIPOLE RESONANCE

We have calculated for the first time the total cross section of the α-particle photodisintegration in the framework of four-nucleon dynamics with FSI taken into account [21]. The whole energy range below the pion threshold was considered. We confined ourselves to the unretarded $E1$ approximation for the transition operator, which is known to be a very good one, at least for not overly high energies. It is especially accurate for the total cross section since there is no multipole interference in this case. According to the Siegert theorem, the transition current operator may be rewritten exactly within this approximation as the dipole momentum operator,

$$\mathbf{D} = \sum_{i=1}^{Z} (\mathbf{r}_i - \mathbf{R}_{\text{c.m.}}), \qquad (15)$$

while MEC are taken into account automatically. The $E2$ contributions to the total cross section are small even at high photon energy [22], and they tend to cancel with the $E1$ retardation contributions [23].

We can write down the cross section as

$$\sigma_{\text{tot}}(E_\gamma) = 4\pi^2(e^2/\hbar c)E_\gamma R(E_\gamma),$$

where R is the dipole response function (1) with $\hat{O} = D_z$. The problem was solved with two central even local NN potentials reproducing the $^1S_0$ and $^3S_1$ NN phase shifts up to high energy: the TN potential used above and the Malfliet–Tjon (MT) potential [24].

Our final total cross sections are shown in Fig. 6 along with experimental data. The three-body breakup threshold at 26.1 MeV is marked with an arrow. The data include the sum of the $(\gamma, n)X$ [25] and $(\gamma, p)^3$H [26] cross sections, which is shown with the dotted curve. This sum represents the total cross section if one disregards the $(\gamma, d)d$ cross section. Within the framework of the unretarded $E1$ approximation, the latter cross section vanishes, and it can safely be neglected (see, e.g., [27]). We also show the doubled cross sections of other low-energy $(\gamma, p)^3$H and $(\gamma, n)^3$He experiments [28–30]. Below the three-body breakup threshold, these cross sections represent the total cross section, provided that the $(\gamma, p)^3$H cross section is equal to the $(\gamma, n)^3$He cross section, which is true with good accuracy. Above the threshold, they may be considered as representing the total cross section if one assumes in addition that the cross sections for three- and four-body breakups may be disregarded. This seems plausible at least for small energies above the threshold. According to the experimental results of [25, 31, 32], the three- and four-body breakup cross sections are quite small in the peak region.

Below the three-body breakup threshold, one observes a rather good agreement of the obtained cross section with the experimental data. Beyond the threshold, the data show a flattening, while our cross sections reveal a further increase and become markedly different from the experimental ones. On the other hand, in older experiments [31, 32], a more pronounced giant-resonance peak has been found, which is in qualitative agreement with our theoretical cross sections. Our cross sections agree better with that estimated in [33] from the data on photon scattering off ^{4}He. The latter cross section is shown with a rectangle in Fig. 6.

Our results are shown in Fig. 7 on an extended energy range. The dotted curve represents the same experimental data as in Fig. 6. Additional two-fragment disintegration data are also shown. They include the sum of the $(\gamma, p)^3$H and $(\gamma, n)^3$He cross sections from [31] and the doubled $(\gamma, p)^3$H cross sections from [29, 34].

Commenting on the results presented in Figs. 6 and 7, one should mention that supplementing the experimental two-body breakup cross sections in these figures with the corresponding three- and four-body breakup cross sections does not lead to significant changes in the peak region. We also indicate that our calculated cross sections agree nicely with the inverse-energy-weighted sum rule, which, up to quite small

corrections, is model independent and is expressed in terms of the square of the ^{4}He radius. To achieve an agreement at the peak with the experimental data presented in Fig. 7 preserving the agreement with this sum rule, one would need to put additional strength at high energy. This strength should be considerable due to the inverse energy factor, even in presence of retardation corrections and contributions from other multipoles omitted in the calculation. Though such an enhancement of the tail cross section does not seem to be plausible, it cannot be totally excluded.

Recently, a calculation of the cross section has been performed taking into account more terms in the Eq. (6)–type expansion. It has shown an unexpected slower convergence pattern for the higher terms. The calculation has also been performed in a somewhat different approach where an effective interaction in the hyperspherical formalism was introduced [35], leading to much faster convergence. The resulting cross section shifts to some extent to lower energy. However, the height of the maximum becomes even a few percent larger, so that our conclusions above remain valid. A detailed comparison between the two calculations will be published elsewhere [36]. In principle, use of simplified nuclear forces in our calculation might lead to the above disagreement with experiment. Indeed, in the three-nucleon case, realistic *NN* + *NNN* forces lead to somewhat lower peaks than the above-used semirealistic *NN* forces (see the next section). However, due to the above-mentioned sum rule, the cross section in the peak region is mainly governed by the size of the system, while details of the nuclear force are less important. In fact, the ratio of the heights of the peaks obtained in our calculation and in the above-listed experiments is 1.3–1.5, while the ratio of the heights of the peaks obtained with the above-used semirealistic *NN* forces and with realistic *NN* + *NNN* forces in the three-nucleon case is around 1.1. Therefore, the problem remains open, and more experimental and theoretical work is required.

5. PHOTODISINTEGRATION OF THREE-BODY NUCLEI WITH REALISTIC *NN* AND *NNN* FORCES

In this section, the total photoabsorption cross sections of the trinucleons are studied using realistic *NN* and *NNN* interactions, and sensitivity to nuclear forces is explored.[4)] Effects of *NNN* forces on the cross section are found, in particular. The only other calculations of trinucleon photodisintegration covering a larger range of energies and employing realistic *NN* forces are, to our knowledge, those of [38, 39]. However, these calculations are for the exclusive process of two-body breakup, while we compute the inclusive (two-body + three-body breakup) cross sections over a larger energy range. It is because we are looking for effects of *NN* and *NNN* forces that energies in the tail region, $E_\gamma >$ 70 MeV, are included here.

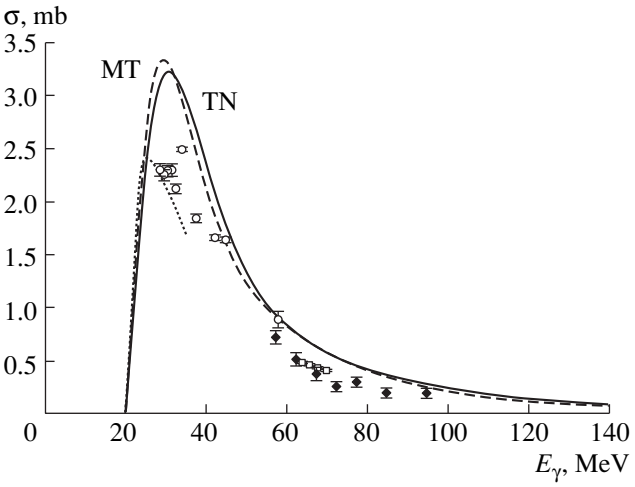

Fig. 7. As in Fig. 6, but for an extended energy range up to 140 MeV. Additional two-fragment data from [31] (diamonds), [29] (open circles), and [34] (open boxes) are also shown (for further explanations see text).

We use the Argonne AV14 *NN* interaction [40] that includes central, tensor, *ls*, l^2, and $(ls)^2$ components and the Bonn-A *r*-space potential [41] that includes central, tensor, *ls*, and p^2 components. As *NNN* potentials, the Urbana-VIII (UrbVIII) [42] and Tucson–Melbourne (TM) [43, 44] models are used.

The table gives our results for the ground-state properties of ^{3}H using the various potential models described above. In order to obtain the correct binding energy with the TM *NNN* potential, we have adjusted the cutoff mass Λ in the monopole form factor. This requires $\Lambda = 4.67\mu$ and $\Lambda = 4.07\mu$, in the notation of [44], for use with the AV14 and Bonn-A (*r*-space) cases, respectively. Previously published ground-state properties are available [45, 17] for the AV14 and AV14 + UrbVIII potentials. The corresponding results in the table are in agreement with these. The last two columns contain the results obtained for the inverse-energy-weighted sum $\sigma_{-1} = \int_{E_{\min}}^{\infty} E_\gamma^{-1}\sigma_{\rm tot}(E_\gamma)dE_\gamma$. This sum was calculated in two ways: (i) by direct integration of the response giving $\sigma_{-1}^{\rm int}$, and (ii) with the help of the sum rule, i.e., by use of the ground-state wave function giving $\sigma_{-1}^{\rm g.s}$, which is related to the triton point proton radius:

$$\sigma_{-1}^{\rm g.s}(^3{\rm H}) = \frac{4\pi^2}{3}\frac{e^2}{\hbar c}\langle r_p^2(^3{\rm H})\rangle.$$

As seen in the table, agreement is obtained to better than 0.5%.

The value of the cross section at the peak depends on the ground-state details, especially the radius. This

[4)]The results of this section are obtained in collaboration with Tomusiak [37].

^{3}H ground-state properties for AV14, Bonn-A, AV14 + UrbVIII, AV14 + TM, and Bonn-A + TM potential models

Potential	E_B, MeV	$\sqrt{\langle r_p^2 \rangle}$, fm	$P(D)$, %	σ_{-1}^{int}, mb	$\sigma_{-1}^{\text{g.s.}}$, mb
AV14	7.69	1.66	8.94	2.636	2.645
Bonn-A	8.15	1.61	6.88	2.481	2.486
AV14 + UrbVIII	8.49	1.60	9.67	2.442	2.453
AV14 + TM	8.48	1.60	9.67	2.448	2.459
Bonn-A + TM	8.47	1.59	7.25	2.411	2.415

Note: E_B is the binding energy, $\sqrt{\langle r_p^2 \rangle}$ is the proton root-mean-square radius, and $P(D)$ is the D-wave probability.

is evident from the remarks above on the inverse-energy-weighted sum rule. Figure 8 shows the results [46] obtained using the MT and TN potentials together with results obtained for the AV14 and AV14 + UrbVIII potentials. Ground-state point proton radii computed from these potentials are 1.61, 1.59, 1.66, and 1.60 fm, respectively. The similar peak heights for these rather different potentials are due largely to the similarity of these radii. However, some sensitivity to a force model still remains, and while the semirealistic TN and MT potentials and the realistic AV14 + UrbVIII model give nearly the same radii, the latter one leads to roughly 10% lower peak height. In this connection, one may note that, while components of the ground-state wave function with single-nucleon momenta close to zero are probed in the peak in the above-considered case of the (e, e') reaction, components of the ground-state wave function with higher momenta are probed in the peak region in the present case. The corresponding single-nucleon momenta are much higher in the tail region. Two of the four potentials, AV14 and AV14 + UrbVIII, produce cross sections with significantly larger high-energy tails than the semirealistic MT and TN models. Part of the difference must be attributed to the tensor force contained in the realistic potential models.

Figure 9 shows the peak region of the $T = 1/2$ contribution to the absorption cross section as computed from the five potential models of the table. The addition of *NNN* forces lowers the peak height since it increases the binding energy and decreases the radius in all cases. The results in the $T = 3/2$ case are similar.

Figures 10 and 11 show the tail regions of the $T = 1/2$ and 3/2 contributions to the cross section, respectively. In the $T = 1/2$ case, despite the increase in the cross section in the tail region due to *NNN* forces, no clear separation between the cross section with and without *NNN* forces is seen. We note the importance of binding in this channel by observing in the tail region the rather disparate curves for the pure NN cases of AV14 and Bonn-A. According to the table, these *NN*

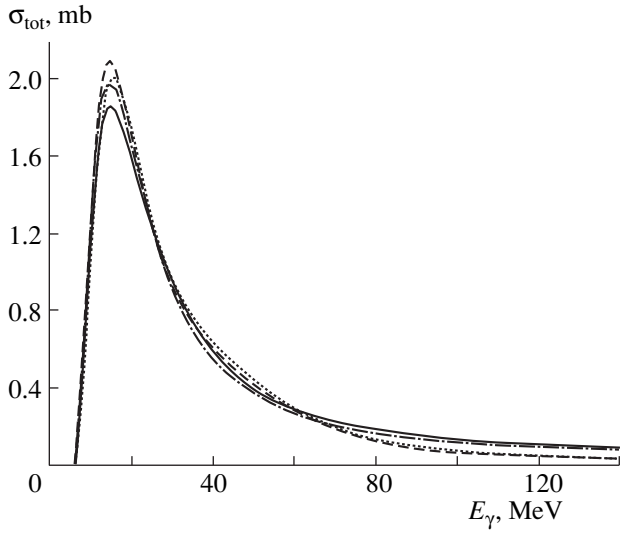

Fig. 8. Total ^{3}H photoabsorption cross sections predicted by the TN (dotted curve), MT (dashed curve), AV14 (dash-dotted curve), and the AV14 + UrbVIII (solid curve) potential models.

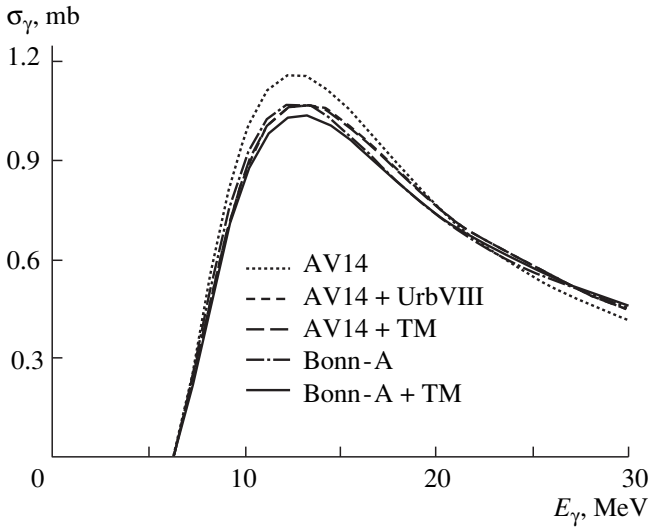

Fig. 9. $T = 1/2$ part of the ^{3}H total photoabsorption cross sections in the peak region. The AV14 + UrbVIII and AV14 + TM results are indistinguishable in the figure.

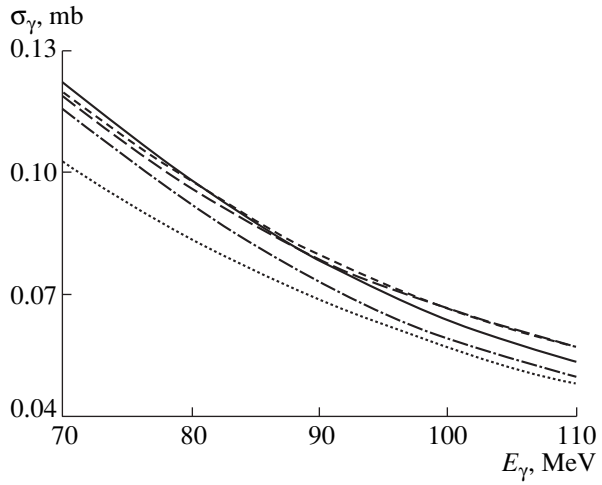

Fig. 10. $T = 1/2$ part of the ^{3}H total photoabsorption cross sections in the tail region. The notation for the curves is the same as in Fig. 9.

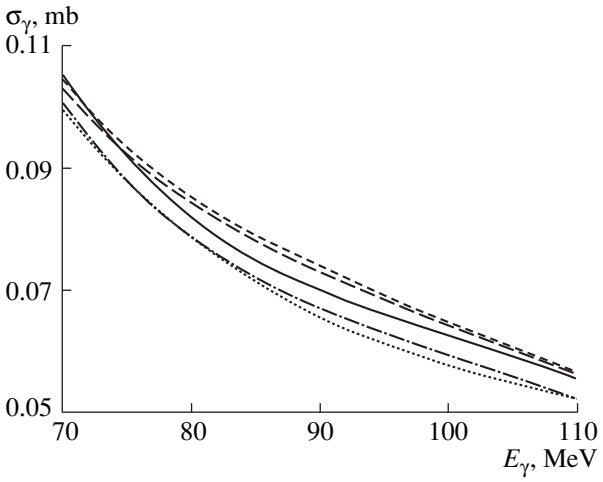

Fig. 11. As in Fig. 10, but for $T = 3/2$.

potentials correspond to ^{3}H binding energies of 7.69 and 8.15 MeV, respectively. In addition, the three curves corresponding to the inclusion of *NNN* forces are rather close and difficult to distinguish, reinforcing the argument that effects here are mainly due to binding.

Figure 11 shows that the $T = 3/2$ channel clearly separates all models containing an *NNN* force from those with purely *NN* forces. This is a 5–10% effect in the energy range 70–110 MeV. However, contrary to the $T = 1/2$ case, binding effects here do not play an important role, as evidenced by the nearly overlapping *NN* curves in the tail region. As a result, the separation between the curves in Fig. 11 is dominantly an effect due to *NNN* forces; i.e., the $T = 3/2$ channel is more sensitive to *NNN* forces in the tail region. The import of this observation is that it is the three-body breakup channels which might show more evidence of an *NNN* force since they carry all of the $T = 3/2$ strength. In fact, the analysis of our theoretical results and the experimental *nd* and *ppn* data from [47] lead us to conclude that, in this energy region, the $T = 1/2$ content of the *ppn* channel is about 1/3.

At this point, one may question the reliability of our total cross section results, since only the unretarded dipole operator is used in the calculation. For the total cross section in deuteron photodisintegration, it is known that corrections to the unretarded dipole operator are small in the energy range studied here. In fact, it is shown in [48] that the combined contributions of $E1$ retardation and one-body current effects for other multipoles lead to an enhancement of about 10% for the total deuteron photoabsorption cross section at E_γ = 80 MeV. Further contributions due to meson exchange and isobar currents are cancelled by relativistic contributions in the whole energy range from 5 to 100 MeV [49]. For the photodisintegration of three-body nuclei, the exact size of these corrections is not known, but we

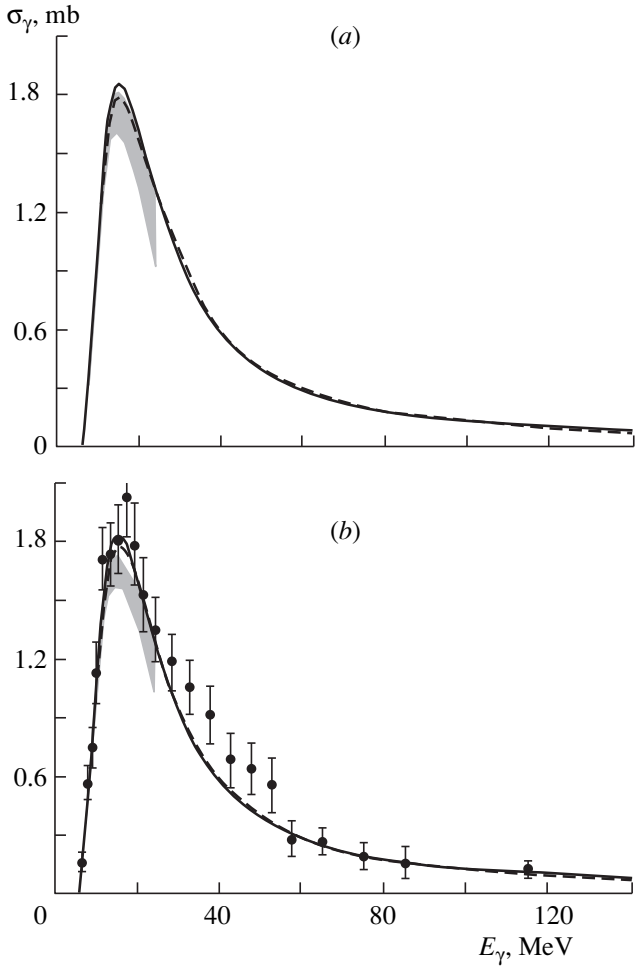

Fig. 12. Total photoabsorption cross sections for ^{3}H (*a*) and ^{3}He (*b*) computed from the AV14 + UrbVIII (solid curve) and *r*-space Bonn-A + TM (dashed curve) models. The shaded area represents the data from [50], while the dots are the data of [47].

believe that the picture is not too different from the deuteron case. It seems plausible that the main effect of the above corrections would consist in a relatively small shift of our curves, while the relative contribution of the *NNN* force to the cross section would not change sizably.

Figures 12*a* and 12*b* compare to the available data [47, 50] the total cross sections for ^{3}H and ^{3}He as computed with two of our more complete potential models, AV14 + UrbVIII and Bonn-A + TM. The ^{3}He calculations include the full Coulomb interaction between the protons. Our calculations agree rather closely with the available data. We note by reference to Fig. 8 that the semirealistic models do not yield the same level of agreement with the data.

Thus, the results obtained show clear sensitivity to the underlying nuclear dynamics. In particular, the tail region of the $T = 3/2$ channel appears to be sensitive to the presence of the *NNN* forces. Therefore, further theoretical and experimental effort should be devoted to this promising kinematical region. On the theoretical side, several corrections, expected to be minor, will be investigated in the future. These are the effects of higher multipoles, retardation in the one-body operators, and the inclusion of explicit two-body currents beyond the Siegert theorem. The most recent *NN* force models such as AV18 and Nijmegen will also be employed. The rather large effect of the *NNN* force found in the tail region could imply a much larger effect in some selected kinematics of the exclusive three-body breakup reaction.

ACKNOWLEDGMENTS

V. D. Efros thanks B.V. Danilin and Yu.E. Pokrovsky for enlightening comments.

This work was supported by the Russian Foundation for Basic Research, project 00-15-96590.

REFERENCES

1. V. D. Efros, W. Leidemann, and G. Orlandini, Phys. Lett. B **338**, 130 (1994).
2. V. D. Efros, Ukr. Fiz. Zh. (Russ. Ed.) **25**, 907 (1980).
3. V. D. Efros, Yad. Fiz. **41**, 1498 (1985) [Sov. J. Nucl. Phys. **41**, 949 (1985)].
4. A. La Piana and W. Leidemann, Nucl. Phys. A **677**, 493 (2000).
5. S. Ishikawa *et al.*, Phys. Lett. B **339**, 293 (1994).
6. V. D. Efros, W. Leidemann, and G. Orlandini, Nucl. Phys. A **631**, 658 (1998).
7. V. D. Efros, W. Leidemann, and G. Orlandini, Few-Body Syst. **26**, 251 (1999).
8. V. D. Efros, Yad. Fiz. **62**, 1975 (1999) [Phys. At. Nucl. **62**, 1833 (1999)].
9. J. E. Gubernatis, M. Jarell, R. N. Silver, and D. S. Silva, Phys. Rev. B **44**, 6011 (1991), and references therein.
10. J. Carlson and R. Schiavilla, Phys. Rev. Lett. **68**, 3682 (1992).
11. J. Carlson and R. Schiavilla, Phys. Rev. C **49**, R2880 (1994); V. R. Pandharipande *et al.*, Phys. Rev. C **49**, 789 (1994).
12. V. D. Efros, W. Leidemann, and G. Orlandini, Phys. Rev. Lett. **78**, 432 (1997).
13. V. D. Efros, W. Leidemann, and G. Orlandini, Phys. Rev. C **58**, 582 (1998).
14. T. De Forest, Jr., Nucl. Phys. A **414**, 347 (1984).
15. S. A. Dytman *et al.*, Phys. Rev. C **38**, 800 (1988).
16. A. Zghiche *et al.*, Nucl. Phys. A **572**, 513 (1994).
17. A. Arriaga, V. R. Pandharipande, and R. B. Wiringa, Phys. Rev. C **52**, 2362 (1995).
18. C. Ciofi degli Atti and S. Simula, Phys. Rev. C **53**, 1689 (1996).
19. A. Kozlov *et al.*, nucl-ex/9911005.
20. L. L. Frankfurt and M. I. Strikman, Phys. Rep. **76**, 215 (1981); **160**, 235 (1988).
21. V. D. Efros, W. Leidemann, and G. Orlandini, Phys. Rev. Lett. **78**, 4015 (1997).
22. G. Elkermann, W. Sandhas, S. A. Sofianos, and H. Fideldey, Phys. Rev. C **53**, 2638 (1996).
23. S. B. Gerasimov, Phys. Lett. **13**, 240 (1964).
24. R. A. Malfliet and J. Tjon, Nucl. Phys. A **127**, 161 (1969).
25. B. L. Berman, D. D. Faul, P. Meyer, and D. Olson, Phys. Rev. C **22**, 2273 (1980).
26. G. Feldman *et al.*, Phys. Rev. C **42**, R1167 (1990).
27. E. L. Tomusiak, W. Leidemann, and H. M. Hoffmann, Phys. Rev. C **52**, 1963 (1995).
28. L. Ward *et al.*, Phys. Rev. C **24**, 317 (1981).
29. R. Bernabei *et al.*, Phys. Rev. C **38**, 1990 (1988).
30. J. Asai *et al.*, Few-Body Syst., Suppl. **7**, 136 (1994).
31. A. N. Gorbunov, Tr. Fiz. Inst. Akad. Nauk SSSR **71**, 1 (1976).
32. Yu. M. Arkatov *et al.*, Ukr. Fiz. Zh. (Russ. Ed.) **23**, 1818 (1978).
33. D. R. Wells, D. S. Dale, R. A. Eisenstein, *et al.*, Phys. Rev. C **46**, 449 (1992).
34. R. T. Jones *et al.*, Phys. Rev. C **43**, 2052 (1991).
35. N. Barnea, W. Leidemann, and G. Orlandini, Phys. Rev. C **61**, 054001 (2000).
36. N. Barnea, V. D. Efros, W. Leidemann, and G. Orlandini (submitted to Phys. Rev. C).
37. V. D. Efros, W. Leidemann, G. Orlandini, and E. L. Tomusiak, Phys. Lett. B **484**, 223 (2000).
38. W. Schadow and W. Sandhas, Phys. Rev. C **55**, 1074 (1997); W. Sandhas, W. Schadow, G. Ellerkmann, *et al.*, Nucl. Phys. A **631**, 210 (1998); W. Schadow and W. Sandhas, Nucl. Phys. A **631**, 588 (1998).
39. W. Glöckle, J. Golak, H. Witala, and H. Kamada, in *Proceedings of Workshop on Electron Nucleus Scattering*, Ed. by O. Benhar, A. Fabrocini, and R. Schiavilla (ETS, Pisa, 1999), p. 261.
40. R. B. Wiringa, R. A. Smith, and T. L. Ainsworth, Phys. Rev. C **29**, 1207 (1984).
41. R. Machleidt, Adv. Nucl. Phys. **19**, 189 (1989).
42. R. B. Wiringa, Phys. Rev. C **43**, 1585 (1991).

43. S. A. Coon, M. D. Scadron, P. C. McNamee, *et al.*, Nucl. Phys. A **317**, 242 (1979).

44. S. A. Coon and W. Glöckle, Phys. Rev. C **23**, 1790 (1981); S. A. Coon, private communication, giving the most recent parameters as $a' = -1.35\mu^{-1}$, $b = -2.86\mu^{-3}$, and $d = -0.64\mu^{-3}$.

45. C. R. Chen, G. L. Payne, J. L. Friar, and B. F. Gibson, Phys. Rev. C **31**, 2266 (1985).

46. V. D. Efros, W. Leidemann, and G. Orlandini, Phys. Lett. B **408**, 1 (1997).

47. V. N. Fetisov, A. N. Gorbunov, and A. T. Varfolomeev, Nucl. Phys. **71**, 305 (1965).

48. F. Partovi, Ann. Phys. (N.Y.) **27**, 79 (1964).

49. H. Arenhövel and M. Sanzone, Few-Body Syst. Suppl. **3**, 1 (1991).

50. D. D. Faul, B. L. Berman, P. Meyer, and D. Olson, Phys. Rev. C **24**, 849 (1981).

Physics of Atomic Nuclei, Vol. 64, No. 3, 2001, pp. 494–505. Translated from Yadernaya Fizika, Vol. 64, No. 3, 2001, pp. 548–559.

90th ANNIVERSARY OF A.B. MIGDAL'S BIRTHDAY
NUCLEI

Applicability of Kinetic Approaches to Heavy-Ion Reactions

V. E. Bunakov*

Petersburg Nuclear Physics Institute, Russian Academy of Sciences, Gatchina, 188350 Russia

Received July 26, 2000

Abstract—The Boltzmann (or Vlasov–Uehling–Uhlenbeck) equation for heavy-ion collisions is derived on the basis of the Dyson equation. Special attention is given to correctly choosing a statistical ensemble. This makes it possible to determine physically small parameters in the gradient expansion; to establish the range of applicability of kinetic approaches to heavy-ion reactions; to write, in a simple form, generalized Boltzmann equations consistently taking into account all corrections for medium effects; and to analyze the role of these corrections. *© 2001 MAIK "Nauka/Interperiodica".*

1. INTRODUCTION

Nowadays, kinetic approaches to heavy-ion collisions are among the most popular methods for physically describing the dynamics of this process. The discussion between the supporters of approaches relying on Vlasov–Uehling–Uhlenbeck equations (see, for example, [1]), which represent a semiclassical form of Boltzmann equations, and those who advocate the method of quantum molecular dynamics (see, for example, [2, 3]) and who state that they solve multiparticle dynamical equations in the semiclassical approximation has not yet led to definitive conclusions.

Attempts at finding out which of the aforementioned approaches makes it possible to obtain deeper insights into the physics of the process immediately run into two challenging problems.

The first stems from the fact that researchers following the different lines employ different Monte Carlo codes, making no attempt at relating these codes either to equations of the Boltzmann type or to dynamical equations of motion. Some twenty years ago, a similar situation was discussed in studying the applicability of various Monte Carlo codes (algorithms for the intranuclear-cascade model) to describing nucleon–nucleus collisions. It turned out (see, for example, [4, 5]) that a comparison of different intranuclear-cascade codes is meaningless as long as it is not clear which equations are solved numerically on the basis of these codes. The analysis performed in [5, 6] revealed that these are master kinetic equations for multiparticle distribution functions rather than Boltzmann equations since the latter, which are equations for single-particle functions, cannot in principle describe the results of correlation experiments for reactions products. At the same time, the intranuclear-cascade model describes such experiments quite successfully (see, for example, [7]).

The second problem is associated with the fact that nuclear physics borrows all kinds of kinetic equations from other (predominantly, classical) realms of physics. Therefore, it is necessary to make an attempt at finding out why these equations describe reasonably well quantum processes in nuclear physics and whether we must modify them by taking into account its multiparticle quantum aspects. An attempt was made in [5] (see also references quoted in that article) to perform such an analysis for the case of nucleon–nucleus collisions. Independently, this problem for nucleus–nucleus collisions was considered by some other authors (see, for example, [8, 9] and the detailed review article by Botermans and Malfliet [10]). However, Botermans and Malfliet [10] only aimed at formally deriving quantum kinetic equations of the Vlasov–Uehling–Uhlenbeck type rather than at analyzing physical applicability of mathematical approximations used in this derivation. Therefore, the physics behind the derivation of the equations was lost almost completely. In particular, those authors paid no attention to the fact that the technique of nonequilibrium Green's functions [11–13] that was used in their derivation was developed for macroscopic quantum ensembles in a heat bath. At the same time, the choice of a statistical ensemble for describing two colliding finite ground-state nuclei is a problem in itself [5]. They indicated that, in all practical calculations performed by that time, use had been made of the approximation $\Gamma = 0$ (Γ is the decay width of a quasiparticle—that is, the imaginary part of the self-energy operator, $\mathrm{Im}\Sigma$) and erroneously concluded that this approximation (and the kinetic approach in general) ceases to be valid at projectile-ion energies exceeding a value of about 100 MeV per nucleon. Those authors were the first who were able to write, in a closed form, the set of the generalized Boltzmann equations, which was introduced by Kadanoff and Baym [12] and which takes into account first-order corrections to the $\Gamma = 0$ approximation. However, the form obtained in [10] included four coupled equations involving the commutators of rather complicated functions [see Eqs. (38)–(41) below]. That set of equations must be solved self-consistently, but its complexity far exceeds the com-

* e-mail: vadim.bunakov@pobox.spbu.ru

plexity of conventional Boltzmann equations. For this reason, no attempts have been made so far to find self-consistent solutions to those equations.

The objective of the present study is to analyze physical small parameters behind the aforementioned formal derivation and to check the applicability of relevant approximations in the realistic case of heavy-ion collisions. The procedure basically consist in introducing a statistical ensemble that can be used in the case of two colliding nuclei and in estimating the small parameters of the so-called gradient (or semiclassical) expansion that are averaged over this ensemble in order to determine the region where the kinetic approach can be applied to heavy-ion reactions.

In particular, it will be proven that it is not $\Gamma/\mathrm{Re}\Sigma$ ($\mathrm{Re}\Sigma$ is the real part of the self-energy operator), as was advocated in [10], but Γ/E (E is the kinetic energy per projectile nucleon) that plays the role of the expansion parameter. This removes almost completely the restriction that Botermans and Malfliet [10] imposed on energies at which the kinetic approach is applicable. It will also be shown that the choice of an appropriate ensemble (this involves averaging over an interval ΔE of projectile-beam energies, with the result that all fine features of observables are smoothed) makes it possible to simplify the form of generalized Boltzmann equations and to represent them as conventional Boltzmann (or Vlasov–Uehling–Uhlenbeck) equations with some modifications, which are obviously due to the nuclear-matter effect on the propagation and collisions of particles. We will further try to find out how each such modification affects solutions to the generalized Boltzmann equations.

The ensuing exposition is organized as follows. In Section 2, we recall the derivation of quantum kinetic equations in macroscopic systems in order to highlight small physical parameters in the gradient expansion. This is necessary since these parameters were analyzed very rarely (see [5, 11, 12]). In Section 3, we consider the model case of uniform nuclear matter and investigate corrections for nonzero values of Γ in that case. It is the effect of the self-stabilization of matter transparency due to the reduction of the collision integral with increasing Γ that is the most interesting and the most general here. The point is that the width Γ itself is approximately in direct proportion to the collision integral, whereby there arises a negative feedback, which, in particular, reduces the dependence of the free path of a particle on the cross section for collisions of this particle with medium particles. In Section 4, we analyze the parameters of the gradient expansion for realistic collisions of heavy ions and present a generalized Boltzmann equation that takes into account all gradient corrections and which has the form of a simple modification of the conventional Boltzmann equation.

2. DERIVATION OF KINETIC EQUATIONS FOR AN INFINITE MACROSCOPIC SYSTEM

This derivation is usually performed for a nearly ideal Fermi gas of temperature Θ about the Fermi energy E_F [11–13]. The method employed to do this relies on nonequilibrium Green's functions [10, 13] expressed in terms of the second-quantized operators $\hat{\Psi}^\dagger(x)$ and $\hat{\Psi}(x)$, where $x = (\mathbf{r}, t)$ is a 4-vector; that is,

$$G^c(1,2) = \frac{1}{i\hbar}\langle T^c[\hat{\Psi}(1)\hat{\Psi}^\dagger(2)]\rangle, \tag{1}$$

where the superscript c labels the causal function, T^c is the chronological-ordering operator, and angular brackets denote averaging over an ensemble. In the same way, we introduce the antichronological Green's function

$$G^a(1,2) = \frac{1}{i\hbar}\langle T^a[\hat{\Psi}(1)\hat{\Psi}^\dagger(2)]\rangle \tag{2}$$

and two functions featuring no chronological ordering,

$$G^>(1,2) = \frac{1}{i\hbar}\langle\hat{\Psi}(1)\hat{\Psi}^\dagger(2)\rangle, \tag{3}$$

$$G^<(1,2) = -\frac{1}{i\hbar}\langle\hat{\Psi}(1)\hat{\Psi}^\dagger(2)\rangle. \tag{4}$$

These four Green's functions are related by the equation

$$G^c + G^a = G^< + G^>. \tag{5}$$

Use is sometimes made of the advanced (G^+) and retarded (G^-) Green's functions

$$\begin{aligned} G^\pm(1,2) &= G^c(1,2) - G^\lessgtr(1,2) \\ &= G^\gtrless(1,2) - G^a(1,2). \end{aligned} \tag{6}$$

In terms of these functions, we can develop the diagram technique [10, 11, 13] and introduce the corresponding self-energy functions $\Sigma^\gtrless$, $\Sigma^{c,a}$, and $\Sigma^\pm$ satisfying the equation

$$\Sigma^a + \Sigma^c = \Sigma^< - \Sigma^>. \tag{7}$$

For a uniform ideal Fermi gas, the corresponding Green's function can be expressed in terms of the occupation numbers $n_\mathbf{p}$ as

$$G^{0<}(t,\mathbf{r}) = \frac{i}{\hbar}\int n_\mathbf{p}\exp[i(\mathbf{p}\cdot\mathbf{r} - \epsilon(\mathbf{p})t)]\frac{d^3p}{(2\pi\hbar)^3}, \tag{8}$$

where $t = t_1 - t_2$, $\mathbf{r} = \mathbf{r}_1 - \mathbf{r}_2$, and $\epsilon(p) = p^2/2m$. Applying the Fourier transformation to (8), we obtain

$$G^{0<}(\omega,\mathbf{p}) = 2\pi i n_\mathbf{p}\delta(\omega - \epsilon(\mathbf{p})). \tag{9}$$

The analogous expression for $G^{0>}$ has the form

$$G^{0>}(\omega,\mathbf{p}) = -2\pi i(1 - n_\mathbf{p})\delta(\omega - \epsilon). \tag{10}$$

The conventional Dyson equation

$$\begin{aligned} G(1,2) &= G^0(1,2) \\ &= \int G^0(1,4)\Sigma(4,3)G(3,2)dx_3dx_4 \end{aligned} \tag{11}$$

now takes the matrix form, where

$$G = \begin{pmatrix} G^c & G^< \\ G^> & G^a \end{pmatrix}, \quad \Sigma = \begin{pmatrix} \Sigma^c & \Sigma^< \\ \Sigma^> & \Sigma^a \end{pmatrix}.$$

In addition to the difference variables t and $\mathbf{r}$, we introduce the conventional summary variables forming the 4-vector X,

$$T = \frac{1}{2}(t_1 + t_2), \quad \mathbf{R} = \frac{1}{2}(\mathbf{r}_1 + \mathbf{r}_2).$$

These variables are local coordinates of the distribution function, and we further perform a gradient expansion near these coordinates.

By using Eq. (11), we can derive a kinetic equation for the Wigner distribution function $f(\mathbf{p}, \mathbf{R}, T)$, which is expressed in terms of $G^<$ in the same way as $n_\mathbf{p}$ is expressed in terms of $G^{0<}$ [see Eqs. (8), (9)]; that is,

$$f(\mathbf{p}, \mathbf{R}, T) = -i\int\frac{d\omega}{2\pi\hbar}\exp[i(\mathbf{p}\cdot\mathbf{r} + \omega t)]$$
$$\times G^<(\mathbf{R} + \mathbf{r}/2, T + t/2; \mathbf{R} - \mathbf{r}/2, T - t/2)d^3r dt \quad (12)$$
$$\equiv \int\frac{d\omega}{2\pi\hbar}G^<(\mathbf{p}, \omega; \mathbf{R}, T).$$

In order to accomplish this derivation, we must take the components $G^<$ from the Dyson equation (11), apply the operators $S_2^\dagger = (-i\hbar\partial/\partial t_2 + \hbar^2/2m\nabla_2^2)$ and $S_1 = (i\hbar\partial/\partial t_1 + \hbar^2/2m\nabla_1^2)$ to it, and subtract the second result from the first one (for details, see [13]). In this way, we obtain

$$(S_2^\dagger - S_1)G^<(1, 2) = -\int[\Sigma^c(1, 3)G^<(3, 2)$$
$$+ \Sigma^<(1, 3)G^a(3, 2) + G^<(1, 3)\Sigma^a(3, 2) \quad (13)$$
$$+ G^c(1, 3)\Sigma^<(3, 2)]dx_3.$$

Upon replacing the variables x_1 and x_2 by $\mathbf{r}$, $\mathbf{R}$, t, and T, we further recast the left-hand side of (13) into the form

$$-\left(i\hbar\frac{\partial}{\partial T} + \frac{\hbar^2}{2m}\nabla_r\nabla_R\right)G^<(\mathbf{r}, t; \mathbf{R}, T). \quad (14)$$

The integrand on the right-hand side of (13) involves the sum of terms of the form $\Sigma(1, 3)G(3, 2)$, which can be written by using the summary and the difference coordinates as

$$\Sigma\left(x_1 - x_3, \frac{x_1 + x_3}{2}\right)G\left(x_3 - x_2, \frac{x_3 + x_2}{2}\right). \quad (15)$$

We now go over to the basic approximation often referred to as the semiclassical approximation. Assuming that the functions $G(\mathbf{r}, t; \mathbf{R}, T)$ and $\Sigma(\mathbf{r}, t; \mathbf{R}, T)$ change slowly as functions of $\mathbf{R}$ and T and that they have a sharp maximum in the vicinity of the point $(\mathbf{r}, t)$, we expand expression (15) in a Taylor series in the vicinity of the point $X = (x_1 + x_2)/2$ (usually, this expansion is referred to as a gradient one),

$$G\left(x_3 - x_2, \frac{x_3 + x_2}{2}\right)$$
$$= G(x_3 - x_2, X) + \frac{x_1 - x_3}{2}\frac{\partial G}{\partial X} + \ldots,$$
$$\Sigma\left(x_1 - x_3, \frac{x_1 + x_3}{2}\right) \quad (16)$$
$$= \Sigma(x_1 - x_3, X) + \frac{x_3 - x_2}{2}\frac{\partial\Sigma}{\partial X} + \ldots,$$

and retain only the first term in each of the integrands. In conjunction with expression (5), this approximation makes possible it to represent the right-hand side of (13) in the form

$$\int d\mathbf{r}'dt'[G^>(\mathbf{r}', t'; \mathbf{R}, T)\Sigma^>(\mathbf{r} - \mathbf{r}', t - t'; \mathbf{R}, T)$$
$$- G^<(\mathbf{r}', t'; \mathbf{R}, T)\Sigma^<(\mathbf{r} - \mathbf{r}', t - t'; \mathbf{R}, T)]. \quad (17)$$

Taking the Fourier transformation of expressions (14) and (15), we go over from (13) to (below, we will use the system of units where $\hbar = 1$)

$$\left(\frac{\partial}{\partial T} + \frac{\mathbf{p}}{m}\nabla_R\right)G^<(\mathbf{p}, \omega; \mathbf{R}, T)$$
$$= -G^<(\mathbf{p}, \omega; \mathbf{R}, T)\Sigma^>(\mathbf{p}, \omega; \mathbf{R}, T) \quad (18)$$
$$+ G^>(\mathbf{p}, \omega; \mathbf{R}, T)\Sigma^<(\mathbf{p}, \omega; \mathbf{R}, T).$$

In the first Born approximation in the two-particle interaction $V(\mathbf{R}_1 - \mathbf{R}_2)$, the expression for $\Sigma^{\gtrless}$ assumes the form

$$\Sigma^{\gtrless}(\mathbf{p}, \omega; \mathbf{R}, T)$$
$$= \int\frac{d^3p_1}{(2\pi)^3}\frac{d\omega_1}{2\pi}\frac{d^3p_2}{(2\pi)^3}\frac{d\omega_2}{2\pi}\frac{d^3p_3}{(2\pi)^3}\frac{d\omega_3}{2\pi}(2\pi)^4$$
$$\times\delta(\mathbf{p} + \mathbf{p}_1 - \mathbf{p}_2 - \mathbf{p}_3)\frac{1}{2}[V(\mathbf{p} - \mathbf{p}_2) - V(\mathbf{p} - \mathbf{p}_3)]^2 \quad (19)$$
$$\times\delta(\omega + \omega_1 - \omega_2 - \omega_3)G^{\lessgtr}(\mathbf{p}_1, \omega_1; \mathbf{R}, T)$$
$$\times G^{\gtrless}(\mathbf{p}_2, \omega; \mathbf{R}, T)G^{\gtrless}(\mathbf{p}_3, \omega; \mathbf{r}, T).$$

Following the same procedure as that employed to derive Eq. (18), we can obtain an equation for $G^>(\mathbf{p}, \omega; \mathbf{R}, T)$. The result is

$$\left(\frac{\partial}{\partial T} + \frac{\mathbf{p}}{m}\nabla_R\right)G^> = -G^<\Sigma^> + G^>\Sigma^<. \quad (20)$$

The relevant spectral function

$$a(\mathbf{p}, \omega; \mathbf{R}, T) = i(G^> - G^<) \quad (21)$$

satisfies the equation

$$\left(\frac{\partial}{\partial T} + \frac{\mathbf{p}}{m}\nabla_R\right)a = 0. \tag{22}$$

For an ideal gas [see Eqs. (9), (10)], we have

$$a(\omega, \mathbf{p}) = -2\pi i\delta(\omega - \varepsilon(\mathbf{p})), \tag{23}$$

so that

$$\begin{aligned} G^<(\omega, \mathbf{p}) &= a(\omega, \mathbf{p})n_\mathbf{p}, \\ G^>(\omega, \mathbf{p}) &= a(\omega, \mathbf{p})(1 - n_\mathbf{p}). \end{aligned} \tag{24}$$

Let us assume that, for a slightly nonideal gas, the spectral function has the delta-function form (23), as previously. From expressions (12) and (24), we then obtain

$$\begin{aligned} G^<(\mathbf{p}, \omega; \mathbf{R}, T) &= a(\mathbf{p}, \omega; \mathbf{R}, T)f(\mathbf{p}, \mathbf{R}, T), \\ G^>(\mathbf{p}, \omega; \mathbf{R}, T) &= a(\mathbf{p}, \omega; \mathbf{R}, T)(1 - f(\mathbf{p}, \mathbf{R}, T)). \end{aligned} \tag{25}$$

Substituting these expressions into Eqs. (18) and (19), we arrive at the Boltzmann equation.

Let us consider in greater detail the gradient expansion (16) because the disregard of all terms in it but the first one was the key point in deriving the Boltzmann equation. First, we restrict our analysis to the time components t and T of the 4-vectors. In this case, the disregard of the second term in (16) means that

$$\begin{aligned} \Sigma(t, T)\frac{t}{2}\frac{\partial G}{\partial t} &< \Sigma(t, T)G(t, T), \\ G(t, T)\frac{t}{2}\frac{\partial \Sigma}{\partial T} &< G(t, T)\Sigma(t, T). \end{aligned} \tag{26}$$

These inequalities can be valid if

$$\frac{\langle t\rangle}{\langle T\rangle} < 1, \tag{27}$$

where $\langle T\rangle$ is the ensemble-averaged characteristic interval of G and Σ variations with time T, while $\langle t\rangle$ is determined by the width of the distribution of the functions G and Σ with respect to the difference variable t.

For the function G, the quantity $\langle T\rangle$ is determined by the free-path time—that is, it is approximately in inverse proportion to the quantity

$$\Gamma = \Sigma^> - \Sigma^< = 2\,\mathrm{Im}\,\Sigma^+. \tag{28}$$

It can be directly seen from Eq. (8) that, for $n_\mathbf{p}$ specified by the Fermi distribution at temperature $\Theta \approx E_\mathrm{F}$, the characteristic interval $\langle t\rangle$ can be estimated as

$$\langle t\rangle \sim \frac{1}{E_\mathrm{F}} \sim \frac{1}{E}, \tag{29}$$

where E is the mean energy of the particle in the system. Since the interaction of particles is local in time $V(t_1, t_2) \sim \delta(t_1 - t_2)$, the dependence of Σ on T and t is of the same character as the corresponding dependence of G. Therefore, the gradient expansion is valid if

$$\frac{\langle t\rangle}{\langle T\rangle} \sim \frac{\Gamma}{E} < 1. \tag{30}$$

The disregard of the second term in the gradient expansion is equivalent to the $\Gamma \longrightarrow 0$ approximation often referred to as the quasiparticle approximation (it seems more correct to call it the free-particle approximation). Keldysh [11] was the first who indicated that this condition is of prime importance for deriving kinetic equations. As will be seen below, another approximation that is used in deriving kinetic equations—that in which the spectral function has a delta-like form—also follows from the condition $\Gamma \longrightarrow 0$.

So far, we have considered a uniform medium; as long as we do this, all derivatives $\partial/\partial R$ in the gradient expansion vanish. Following [11–13], we can analyze the case of a weakly changing external potential. By using the same arguments as before, we can demonstrate that, in this case,

$$\frac{1}{pU}\frac{\partial U}{\partial R} < 1 \tag{31}$$

is the small parameter in the gradient expansion for this system. This is an ordinary condition under which the semiclassical approximation is valid (here, p is the mean momentum of a particle in the system).

If we retain two spatial-coordinate-dependent terms of the gradient expansion (16) on the left-hand side of Eq. (13) and only one such term on its right-hand side, we obtain the kinetic equation [12]

$$\begin{aligned} &\left[\frac{\partial}{\partial T} + \frac{\mathbf{p}}{m}\nabla_R - \nabla U_\mathrm{eff}\nabla_p\right]f(\mathbf{p}, \mathbf{R}, T) \\ &= -f(\mathbf{p}, \mathbf{R}, T)\Sigma^>(\mathbf{p}, \omega = E(\mathbf{p}, \mathbf{R}, T); \mathbf{R}, T) \\ &+ [1 - f(\mathbf{p}, \mathbf{R}, T)]\Sigma^<(\mathbf{p}, \omega = E(\mathbf{p}, \mathbf{R}, T); \mathbf{R}, T), \end{aligned} \tag{32}$$

where

$$E(\mathbf{p}, \mathbf{R}, T) = \frac{p^2}{2m} + U_\mathrm{eff}(\mathbf{R}, T) \tag{33}$$

$$\begin{aligned} &U_\mathrm{eff}(\mathbf{R}, T) \\ &= U(\mathbf{R}) + i\int d^3\mathbf{R}'V(\mathbf{R} - \mathbf{R}')G^<(\mathbf{R}', T; \mathbf{R}', T). \end{aligned} \tag{34}$$

The second term on the right-hand side of Eq. (34) is the ordinary self-consistent Hartree potential.

Kadanoff and Baym [12] were the first to indicate that the derivation of Eq. (32) is inconsistent. Retaining two terms of the gradient expansion on the left- and on the right-hand side of the relevant equations, they obtained the so-called generalized Boltzmann equation,

$$\left[\omega - \frac{p^2}{2m} - U(\mathbf{R}, T)\right.$$

$$- \operatorname{Re}\Sigma^+(\mathbf{p}, \omega; \mathbf{R}, T), G^<(\mathbf{p}, \omega; \mathbf{R}, T)\Big]$$

$$+ [\operatorname{Re}G^+(\mathbf{p}, \omega; \mathbf{R}, T), \Sigma^<(\mathbf{p}, \omega; \mathbf{R}, T)] \quad (35)$$

$$= -\Sigma^>(\mathbf{p}, \omega; \mathbf{R}, T)G^<(\mathbf{p}, \omega; \mathbf{R}, T)$$

$$+ \Sigma^<(\mathbf{p}, \omega; \mathbf{R}, T)G^>(\mathbf{p}, \omega; \mathbf{R}, T),$$

and the corresponding equation for the spectral function,

$$\left[\omega - \frac{p^2}{2m} - U(\mathbf{R}, T) - \operatorname{Re}\Sigma^+, a(\mathbf{p}, \omega; \mathbf{R}, T)\right] \quad (36)$$

$$+ [\operatorname{Re}G^+, \Gamma(\mathbf{p}, \omega; \mathbf{R}, T)] = 0.$$

Here, [,] is the quantum Poisson bracket defined as

$$[A, B] = \frac{\partial A}{\partial \omega}\frac{\partial B}{\partial T} - \frac{\partial A}{\partial T}\frac{\partial B}{\partial \omega} + \nabla_R A \nabla_p B - \nabla_p A \nabla_R B.$$

Solving Eq. (36), we can find the spectral function in the form

$$a(\mathbf{p}, \omega; \mathbf{R}, T) = \frac{\Gamma(\mathbf{p}, \omega; \mathbf{R}, T)}{\left(\omega - \frac{p^2}{2m} - \operatorname{Re}\Sigma^+\right)^2 + (\Gamma/2)^2}. \quad (37)$$

It follows that the true form of the spectral function for interacting particles is given by Eq. (37)—only in the limit $\Gamma \longrightarrow 0$ does this expression reduce to the delta-like form (23).

Botermans and Malfliet [10] were able to write the generalized Boltzmann equation (35) in the simpler closed form [trivial terms associated with the external field $U(\mathbf{r})$, which are immaterial for our problem of heavy-ion collisions, are discarded here]

$$a\left[\left(\omega - \frac{p^2}{2m} - \operatorname{Re}\Sigma^+\right), F\right](1 - \operatorname{Re}\alpha) \quad (38)$$

$$- [\operatorname{Im}\Sigma^+, F]\operatorname{Im}\alpha = -ia[\Sigma^> F + \Sigma^<(1 - F)],$$

where a is a function that has the form (37) and which satisfies the equation (we recall that $\Gamma = 2\operatorname{Im}\Sigma^+$)

$$\left(\frac{\partial}{\partial T} + \frac{\mathbf{p}}{m}\nabla_{\mathbf{R}}\right)a - [\operatorname{Re}\Sigma^+(\mathbf{p}, \omega; \mathbf{R}, T), a] \quad (39)$$

$$+ 2[\operatorname{Im}\Sigma^+(\mathbf{p}, \omega; \mathbf{R}, T), \operatorname{Re}G^+(\mathbf{p}, \omega; \mathbf{R}, T)] = 0.$$

The relevant Green's functions are now given by

$$G^< = ia(\mathbf{p}, \omega; \mathbf{R}, T)F(\mathbf{p}, \omega; \mathbf{R}, T),$$
$$G^> = -ia(\mathbf{p}, \omega; \mathbf{R}, T)(1 - F(\mathbf{p}, \omega; \mathbf{R}, T)), \quad (40)$$

where the function $F(\mathbf{p}, \omega; \mathbf{R}, T)$ plays the role of the old distribution function $f(\mathbf{p}, \mathbf{R}, T)$ [see Eqs. (12), (22), and (24)]. The function α in (38) is determined by the equations

$$1 - \operatorname{Re}\alpha = \frac{2\operatorname{Im}\Sigma^+}{\left(\omega - \frac{p^2}{2m} - \operatorname{Re}\Sigma^+\right)^2 + (\operatorname{Im}\Sigma^+)^2},$$
$$\operatorname{Im}\alpha = \frac{2\operatorname{Im}\Sigma^+ - \left(\omega - \frac{p^2}{2m} - \operatorname{Re}\Sigma^+\right)}{\left(\omega - \frac{p^2}{2m} - \operatorname{Re}\Sigma^+\right)^2 + (\operatorname{Im}\Sigma^+)^2}. \quad (41)$$

3. HEAVY-ION COLLISIONS (UNIFORM MODEL)

The set of generalized Boltzmann equations, together with the equations for Σ [see Eqs. (37)–(41)], which was obtained in [10], is closed in contrast to the Kadanoff–Baym equations, and one can in principle try to solve it. However, these equations are much more complicated than the standard Boltzmann equations. For a possible simplification, Botermans and Malfliet [10] considered only the semiclassical approximation, going over to the limit $\Gamma \longrightarrow 0$ and choosing the strength function a in the delta-function form

$$a(\mathbf{p}, \omega; \mathbf{R}, T) = 2\pi\delta\left(\omega - \frac{p^2}{2m} - \operatorname{Re}\Sigma^+(\mathbf{p}, \omega; \mathbf{R}, T)\right).$$

They state that this approximation is valid only if

$$\frac{\operatorname{Im}\Sigma^+}{\operatorname{Re}\Sigma^+} \ll 1. \quad (42)$$

By comparing the real and the imaginary part of the nucleon optical potential at various energies per nucleon, E_{HI}/A, in heavy-ion collisions, those authors arrived at the conclusion that the semiclassical approximation ceases to be valid at energies higher than $E_{\mathrm{HI}}/A \sim 100$ MeV, since the ratio in (42) is approximately equal to 0.2 in this region and exceeds unity at energies E_{HI}/A higher than 300 MeV.

Since Eqs. (37)–(41) were derived by retaining the first two terms of the gradient expansion, any estimate of their applicability can be obtained only by analyzing the small parameters in this expansion. For the sake of simplicity, we first perform such an analysis for the model in which two semi-infinite walls of nuclear matter collide. In the initial state, we then have, in momentum space, two Fermi spheres whose centers are separated by the momentum $\mathbf{p}_b$ of the beam incident on the target. This momentum corresponds to the beam energy per particle, $E_b = E_{\mathrm{HI}}/A$.

In our case, the statistical ensemble over which the averaging of G is performed can be obtained (see, for example, [4, 5]) by averaging over the beam-particle momenta $\mathbf{p}_b$ (or over beam energies E_b). This averaging

slightly smears the initial Fermi surfaces over the intervals Δp_b or $\Delta E = (p_b \Delta p_b/m)$. Such roughening makes it possible to smooth all possible fine structures in the behavior of the functions $\Gamma(\omega, \mathbf{p})$ and $F(\omega)$ and to treat Γ as a constant (at least, within the energy interval of width about Γ itself).

We can now assume that the spectral function has a Lorentzian form with constant Γ and neglect the remaining ω dependence of the function F in Eqs. (40). In this case, the function $G^<$ takes the form

$$G^<(\mathbf{p}, t; \mathbf{R}, T) = F(\mathbf{p}, \mathbf{R}, T)\int \frac{e^{i\omega t}}{2\pi} a(\mathbf{p}, \omega) d\omega = f(\mathbf{p}, \mathbf{R}, T)\exp(-iE(\mathbf{p})t - \Gamma t), \quad (43)$$

where the quantity

$$E(\mathbf{p}) = \frac{p^2}{2m} + \mathrm{Re}\,\Sigma^+(\mathbf{p}, E(\mathbf{p}))$$

determines the position of the pole of the function $a(\mathbf{p}, \omega)$ on the real axis of energy.

By applying the Fourier transformation to (43), we obtain

$$G^<(\mathbf{r}, t; \mathbf{R}, T) = \int \frac{d^3p}{(2\pi)^3} e^{i(\mathbf{p}\cdot\mathbf{r} - E(\mathbf{p})t) - \Gamma t} f(\mathbf{p}, \mathbf{R}, T). \quad (44)$$

In order to estimate the scale of localization of this function in the variables $\mathbf{r}$ and t, we consider, for the sake of simplicity, the one-dimensional integral in (44) (for example, in the incident-beam direction, $\mathbf{r} \parallel \mathbf{p}$). For the case of $E_b > E_\mathrm{F}$, the integral

$$\int_{p_b - p_\mathrm{F}/2}^{p_b + p_\mathrm{F}/2} dp e^{i[pr - (p^2/2m)t]} \quad (45)$$

provides a fairly accurate approximation for the initial distribution $f(\mathbf{p}, T = 0)$ in momentum space. By using the expansion

$$E(p) \approx \frac{p^2}{2m} = E(p_b) + (p - p_b)\left.\frac{\partial E}{\partial p}\right|_{p = p_b},$$

we reduce the integral (45) to

$$G(r, t, T = 0) = e^{-iE(p)t - \Gamma t}\frac{2}{(r - v_b t)}\sin\left[\frac{(r - v_b t)p_\mathrm{F}}{2}\right], \quad (46)$$

where $v_b = p_b/m$ is the nucleon velocity in the incident beam.

It is obvious that the characteristic width $\langle r \rangle$ of the maximum of G in the vicinity of the point $r = 0$ is

$$\langle r \rangle \sim \frac{1}{p_\mathrm{F}}. \quad (47)$$

The localization of the function in the variable $\langle t \rangle$ is determined by the competition between the quantity $1/\Gamma$ arising in the exponential function in (46) and the quantity $\langle t_1 \rangle$ associated with the sinusoidal dependence in this equation:

$$\langle t_1 \rangle \approx \frac{1}{m v_\mathrm{F} v_b} = \frac{1}{\sqrt{E_\mathrm{F} E_b}}. \quad (48)$$

For energies $E_b > E_\mathrm{F}$, this quantity is much less than $1/\Gamma$. This can easily be confirmed by using experimental data (see [14]) or estimates obtained within theories of the Brueckner type [15, 16]. Hence, the characteristic value of $\langle t \rangle$ is

$$\langle t \rangle \sim \frac{1}{\sqrt{E_b E_\mathrm{F}}}. \quad (49)$$

However, even the first nucleon–nucleon collisions strongly wash out the Fermi surface. If we do not aim at precisely describing the initial stages of the process, we can therefore assume that this parameter can be estimated as

$$\langle t \rangle \sim \frac{1}{E_b} \sim \frac{1}{E}. \quad (50)$$

Here—in just the same way as in (29)—E is the mean energy of a particle in the system of colliding ions.

Addressing once again the problem of estimating small parameters in the gradient expansion (16), we obtain either the inequality

$$\frac{\Gamma}{\sqrt{E_b E_\mathrm{F}}} < 1, \quad (51)$$

which enables one to obtain a kinetic description of the earliest stages of heavy-ion collisions, or the weaker inequality

$$\frac{\Gamma}{E} < 1, \quad (52)$$

which coincides with the Keldysh estimate (30).

Let us now consider the generalized Boltzmann equation (38), which is valid to the first order in Γ/E (see above). In order to take into account ω dependence of the optical potential $\mathrm{Re}\,\Sigma^+(\omega, \mathbf{p})$, we expand it in the vicinity of the zeros $\omega_p = \varepsilon_p$ of the expression

$$\left(\omega - \frac{p^2}{2m} - \mathrm{Re}\,\Sigma^+(\omega, \mathbf{p})\right).$$

As a result, we obtain

$$\omega - \frac{p^2}{2m} - \mathrm{Re}\,\Sigma^+(\omega, \mathbf{p}) \approx (\omega - \omega_p)\left(1 - \left.\frac{\partial\,\mathrm{Re}\,\Sigma^+}{\partial\omega}\right|_{\omega = \omega_p}\right) \equiv (\omega - \omega_p)Z_p^{-1}. \quad (53)$$

The quantity Z is given by [15]

$$Z = \frac{m}{\bar{m}}, \quad (54)$$

where $\bar{m}$ is the effective E mass of the nucleon in nuclear matter.

By integrating Eq. (38) with respect to ω, we find within our uniform-matter model that

$$\frac{\partial}{\partial T}F(\mathbf{p}, T) = Z_p[\Sigma^> F + \Sigma^<(1-F)]\big|_{\omega=\omega_p}. \quad (55)$$

It should be noted that the second Poisson bracket in Eq. (38) merely vanishes for our constant Γ smoothed (roughened) in energy. In the Born approximation, the relevant collision integrals in (55) have the form

$$\Sigma^>(\mathbf{p}, \omega = \omega_p; T)$$
$$= \int d^3p_1 d^3p_2 d^3p_3 d\omega_1 d\omega_2 d\omega_3 (2\pi)^4$$
$$\times \delta(\mathbf{p}+\mathbf{p}_1-\mathbf{p}_2-\mathbf{p}_3)\delta(\omega_p+\omega_1-\omega_2-\omega_3) \quad (56)$$
$$\times \frac{1}{2}[V(\mathbf{p}-\mathbf{p}_2)-V(\mathbf{p}-\mathbf{p}_3)]^2 a(\omega_1, \mathbf{p}_1)a(\omega_2, \mathbf{p}_2)$$
$$\times a(\omega_3, \mathbf{p}_3)F(\omega_1, \mathbf{p}_1)[1-F(\omega_2, \mathbf{p}_2)][1-F(\omega_3, \mathbf{p}_3)].$$

Similar expressions hold for $\Sigma^<$.

Performing integration with respect to ω_1, ω_2, and ω_3 in (56), we arrive at

$$\Sigma^> = \int d^3p_1 d^3p_2 d^3p_3 (2\pi)^4$$
$$\times \delta(\mathbf{p}+\mathbf{p}_1-\mathbf{p}_2-\mathbf{p}_3)\delta^\Gamma(\epsilon(p)+\epsilon(p_1)-\epsilon(p_2)-\epsilon(p_3))$$
$$\times Z_{p_1}Z_{p_2}Z_{p_3}\frac{1}{2}[V(\mathbf{p}-\mathbf{p}_2)-V(\mathbf{p}-\mathbf{p}_3)]^2 \quad (57)$$
$$\times F(\mathbf{p}_1)(1-F(\mathbf{p}_2))(1-F(\mathbf{p}_3)),$$

where δ^Γ is a Lorentzian function of width $\Gamma = \Gamma_1 + \Gamma_2 + \Gamma_3$. Since Eqs. (38) and (55) were derived by retaining the gradient terms of order Γ/E, it is quite natural that Lorentzian functions appear instead of delta functions in the collision integrals. Physically, their emergence means that, in the propagation of particles in a medium, we take into account off-mass-shell effects. The quasiparticle energies $\epsilon(p)$ appearing in (57) were introduced above as

$$\epsilon(p) = \frac{p^2}{2m} + \mathrm{Re}\,\Sigma(p, \epsilon(p)) \equiv \frac{p^2}{2m} + U(p), \quad (58)$$

where $U(p)$ is the real part of the optical-model potential (see [15]). Expanding $U(p)$ in the vicinity of the point $p = 0$, we arrive at

$$U(p) \approx U(0) + p\frac{dU}{dp}. \quad (59)$$

The second term in this expression can be related to the effective mass m^* [15] as

$$\frac{dU}{dp} = \frac{p}{m}\frac{(m-m^*)}{m^*}. \quad (60)$$

By substituting (58)–(60) into (57) and using the relation $\delta^\Gamma(ax) = \delta^\Gamma(x)/a$, we obtain

$$\Sigma^> = \int d^3p_1 d^3p_2 d^3p_3 (2\pi)^4 \delta(\mathbf{p}+\mathbf{p}_1-\mathbf{p}_2-\mathbf{p}_3)$$
$$\times \delta^\Gamma\left(\frac{p^2}{2m}+\frac{p_1^2}{2m}-\frac{p_2^2}{2m}-\frac{p_3^2}{2m}\right)\frac{m^*}{2m-m^*}Z_{p_1}Z_{p_2}Z_{p_3} \quad (61)$$
$$\times \frac{1}{2}[V(\mathbf{p}-\mathbf{p}_2)-V(\mathbf{p}-\mathbf{p}_3)]^2$$
$$\times F(\mathbf{p}_1)(1-F(\mathbf{p}_2))(1-F(\mathbf{p}_3)).$$

It can be seen that, apart from the smearing of the delta function in the collision term, we have obtained two more deviations from what we have in the quasiparticle approximation $\Gamma \longrightarrow 0$—the quantity Z that is dependent on the E mass and the quantity b that contains the effective mass m^*,

$$b = \frac{m^*}{2m-m^*}. \quad (62)$$

These effects are direct consequences of particle interaction with nuclear matter, thereby representing part of the off-shell-mass effects in our kinetic approach. In the majority of calculations for nuclear matter (see [15, 16]), the quantities Z prove to be slightly below unity. Therefore, their product in Eqs. (55)–(57) can reduce the collision integrals by a factor of about 2. For energies on the order of 100 MeV, the mean values of the ratio m^*/m are close to 0.7 [15]. Therefore, $b \approx 0.5$, which reduces the collision integrals by yet another factor of about 2.

We will now try to analyze off-mass-shell effects associated with the smearing of the delta functions in the collision integrals (57) and (61). As a matter of fact, this is a challenging problem involving ninefold integration of the distribution functions F, which are solutions to the generalized kinetic Eqs. (55). These effects must be assessed self-consistently: since the generalized kinetic equations are applicable only to the first order in the parameter Γ/E, the corrections to the collision integral must also be taken into account only to the first order in this parameter. In order to achieve a qualitative understanding of the effects in question, the corrections to $\Sigma^>$ that are associated with nonvanishing values of Γ will be estimated analytically without taking into account blocking due to the Pauli exclusion principle. This can be a reasonable approximation for the initial stages of nucleus–nucleus collisions at energies per nucleon E much greater than E_F. We will also neglect exchange terms in Eq. (61) and consider potentials (more precisely, Born amplitudes) of the form

$$V = V_0 \exp(-\alpha q^2),$$

where $\mathbf{q} = \mathbf{p} - \mathbf{p}_2$ is the momentum transfer. The results obtained by estimating the collision integrals and their derivation are presented in the Appendix.

From these results, we can see that a nonvanishing value of Γ reduces the collision integrals. This reduction is proportional to the parameter

$$\alpha\Gamma m \approx \frac{\Gamma m}{\langle q^2\rangle} \approx \frac{\Gamma}{E_{\rm tr}}, \tag{63}$$

where $\langle q^2\rangle$ is the mean square of the momentum transfer and $E_{\rm tr}$ is the mean energy transfer in binary nucleon–nucleon collisions.

The physical meaning of this effect is quite understandable. At nonzero values of Γ, the phase space of particles breaks down into energy cells of finite size Γ (since the quasiparticle energy can be specified only to within this accuracy) and into the corresponding finite-size momentum cells. If a typical energy transfer in a collision, $E_{\rm tr}$, is less than Γ, the colliding particles remain in their initial cells—the collision event appears to be overly soft for changing the distribution of quasiparticles. Because of this, only hard collision events characterized by energy transfers $E_{\rm tr} > \Gamma$ contribute to the collision integral, and this contribution decreases with increasing $\Gamma/E_{\rm tr}$.

As long as Γ is less than $\langle q^2\rangle/m$, these corrections are of purely academic interest since they are expected to be be beyond the accuracy of the theory (that is, less than Γ/E). If, however, Γ approaches $\langle q^2\rangle/m$, they can pronouncedly reduce the collision integrals. Typical estimated values of $\langle q^2\rangle/m$ fall within range 50–70 MeV. Experimental and theoretical estimates (see [14–16]) show that, as E grows up to $E \approx 300$ MeV, the width Γ increases linearly up to 20–30 MeV. These values were obtained, however, for nuclear matter characterized by a normal density and zero temperature. Calculations of the Brueckner type (see, for example, [16]) reveal that, at the density twice as large as the normal one, Γ can become 50 MeV at $E \approx 300$ MeV. This increases the parameter $\Gamma m/\langle q^2\rangle$ up to unity and can lead to the reduction of the collision integrals.

Here, it is worth mentioning the results of Danielewicz [9], who performed a numerical model comparison of precise solutions to the Dyson equation and solutions to the ordinary Boltzmann equations obtained in the zero-order approximation in Γ/E. In the collision integrals, use was made there of the Born approximation for Gaussian potentials for $\langle q^2\rangle/m \approx 60$ MeV. By varying the coupling constant in the potential V_0, that author noticed that the Dyson equation led to a lower collision frequency than the Boltzmann equation at Γ values exceeding approximately 50 MeV. It is possible that this is a manifestation of the off-mass-shell effect considered here.

We should recall Eq. (28), which relates the width Γ to the collision integrals $\Sigma^>$ and $\Sigma^<$ and which, in conjunction with the aforementioned off-mass shell effect, can lead to the negative feedback moderating the growth of Γ with increasing density or cross sections for pair interactions. This new mechanism of self-stabilization of matter transparency can appear to be of importance in studying transport phenomena in dense media. It has long been known that, in the expression for the free path in a rarefied gas,

$$l_{\rm mf} = \frac{1}{\langle\sigma\rangle\rho},$$

it is necessary to take into account corrections for blocking associated with the Pauli exclusion principle in Fermi systems (this is the main reason for the self-transparency of nuclear matter for nucleons). The medium effects discussed in this section may generate new corrections, especially in studying extremal states of nuclear matter and dense media governed by the long-range interparticle interaction potentials leading to low energy transfers in binary collisions.

To summarize the discussion in the present section, the following comment is in order. Any attempt at improving the accuracy of the kinetic approach by including, for example, second-order terms in Γ/E in the gradient expansion would result in that the second derivatives $\partial^2/\partial t^2$ and $\partial^2/\partial\omega^2$ would appear in kinetic equations, whereupon solving them would not be easier than solving the original Dyson equations.

4. REALISTIC CASE OF HEAVY-ION COLLISIONS

We begin this section by presenting a brief analysis of the spatial small parameters in the gradient expansion for realistic heavy-ion collisions. In perfect analogy with Eq. (26), the smallness of the second term in the gradient expansion (16) means that

$$\Sigma(r, R)\frac{r}{2}\frac{\partial G}{\partial R} < \Sigma(r, R)G(r, R), \tag{64}$$

$$G(r, R)\frac{r}{2}\frac{\partial \Sigma}{\partial R} < \Sigma(r, R)G(r, R). \tag{65}$$

The characteristic width $\langle r\rangle_G$ of the maximum of the function G in the vicinity of the point $r = 0$ was determined by Eq. (47) as $1/p_{\rm F}$ at the instant preceding collisions between nucleons. If we do not aim at achieving a high accuracy in describing the very first collisions, this estimate changes to become

$$\langle r\rangle_G \sim \frac{1}{p_b} \sim \frac{1}{p}, \tag{66}$$

where p is the mean nucleon momentum in the system of two colliding ions. However, the localization in the variable r of three Green's functions in the integrals Σ is smeared over the characteristic interval of width $1/\langle q\rangle$, where $\langle q\rangle$ is the mean momentum transfer in a nucleon–nucleon collision. Therefore, the localization of Σ in the variable r differs from the localization of G, the corresponding radius being given by

$$\langle r\rangle_\Sigma \sim \frac{1}{\langle q\rangle}. \tag{67}$$

The behavior of the quantities Σ and G in R space is determined by the gradients of the nuclear density; that is,

$$\frac{1}{G}\frac{\partial G}{\partial R} \approx \frac{1}{\Sigma}\frac{\partial \Sigma}{\partial R} \approx \frac{1}{\langle L\rangle}, \tag{68}$$

where $\langle L\rangle$ is the characteristic interval of nuclear-density variations; therefore, inequalities (64) and (65) imply

$$\begin{aligned} \langle L\rangle p &> 1, \\ \langle L\rangle \langle q\rangle &> 1. \end{aligned} \tag{69}$$

The first of these inequalities involves a conventional small parameter of any semiclassical approximation. It remains sufficiently small even at energies as low as a few MeV per nucleon (see, for example, [17], where the validity of the semiclassical approximation was demonstrated in numerically constructing semiclassical solutions to the time-dependent Hartree–Fock equations at an energy of 3.5 MeV per nucleon).

The second inequality may be the weakest point in using the gradient expansion. Typical values of $\langle q\rangle$ are 1.5–1.7 fm^{-1}. An estimate of $\langle L\rangle$ for an uncompressed stable nuclear system can be obtained from the diffuseness of the nuclear surface ($\langle L\rangle \sim$ 2–3 fm). In this case, we have $\langle L\rangle\langle q\rangle \sim$ 3–5, and corrections from the discarded second-order terms are 0.1–0.04. In phenomena of the shock-wave type, however, $\langle L\rangle$ can be on the order of the internucleon spacing, in which case the above product decreases to about 2, while the disregarded corrections increase approximately to 0.25. It should be noted that the same parameter $\langle L\rangle\langle q\rangle$ determines the validity of the so-called T approximation (see [10]), in which the collision integrals involve the exact amplitudes for nucleon–nucleon scattering rather than the Born amplitudes.

We will now try to reduce the generalized kinetic Eqs. (38) to the simpler and more familiar form. In order to do this, we make use of the fact that all partial derivatives with respect to any variable y in the first Poisson bracket of Eq. (38) can be represented as

$$\frac{\partial(\omega-\varepsilon)}{\partial y} = -\frac{\partial\varepsilon}{\partial y}\left(1-\frac{\partial \operatorname{Re}\Sigma^+}{\partial\omega}\right) = -\frac{\partial\varepsilon}{\partial y}Z^{-1},$$

where

$$\varepsilon = \frac{p^2}{2m} + \operatorname{Re}\Sigma^+.$$

By expanding the denominators of the functions $a(\omega, \mathbf{p}; \mathbf{R}, T)$ [see Eq. (37)] in the vicinity of their zeros ε_p [see Eq. (53)] and by integrating both parts of (38) with respect to ω, we obtain

$$\begin{aligned} &\left(\frac{\partial}{\partial t} + \frac{\mathbf{p}}{\tilde m}\nabla_R - \nabla_R \operatorname{Re}\Sigma^+\cdot\nabla_p\right)F \\ &\quad = Z_p(\Sigma^< F + \Sigma^> F)\big|_{\omega=\varepsilon_p}, \end{aligned} \tag{70}$$

where $\tilde m$ is the effective K mass, which is determined by the relation (see [15])

$$\frac{\tilde m}{m} = \left[1 + \frac{m}{p}\frac{\partial\Sigma^+}{\partial p}\bigg|_{\omega=\omega_p}\right]^{-1}.$$

In the Born approximation, the collision terms are given by

$$\begin{aligned} \Sigma^> &= \int d^3p_1 d^3p_2 d^3p_3 d\omega_1 d\omega_2 d\omega_3 \frac{1}{(2\pi)^5} \\ &\times \delta(\mathbf{p}+\mathbf{p}_1-\mathbf{p}_2-\mathbf{p}_3)\delta(\varepsilon_p+\omega_1-\omega_2-\omega_3) \\ &\times \frac{1}{2}[V(\mathbf{p}-\mathbf{p}_2)-V(\mathbf{p}-\mathbf{p}_3)]^2 \frac{\Gamma_1}{(\omega_1-\varepsilon_1)^2+(\Gamma_1)^2/4} \\ &\times \frac{\Gamma_2}{(\omega_2-\varepsilon_2)^2+(\Gamma_2)^2/4}\,\frac{\Gamma_3}{(\omega_3-\varepsilon_3)^2+(\Gamma_3)^2/4} \\ &\times F(\omega_1,\mathbf{p}_1)[1-F(\omega_2,\mathbf{p}_2)][1-F(\omega_3,\mathbf{p}_3)] \\ &= \int d^3p_1 d^3p_2 d^3p_3 \frac{1}{(2\pi)^5}\delta(\mathbf{p}+\mathbf{p}_1-\mathbf{p}_2-\mathbf{p}_3) \\ &\times \delta^\Gamma(\varepsilon_p+\varepsilon_{p_1}-\varepsilon_{p_2}-\varepsilon_{p_3})\frac{1}{2}[V(\mathbf{p}-\mathbf{p}_2)-V(\mathbf{p}-\mathbf{p}_3)]^2 \\ &\times Z_1Z_2Z_3F(\varepsilon_{p_1},\mathbf{p}_1)[1-F(\varepsilon_{p_2},\mathbf{p}_2)][1-F(\varepsilon_{p_3},\mathbf{p}_3)]. \end{aligned} \tag{71}$$

The expressions for $\Sigma^<$ have a similar form.

The first-order terms in the expression for $\operatorname{Re}\Sigma^+$ represent the ordinary self-consistent Hartree–Fock potential (the expressions for higher order terms can be found in [10]).

Thus, we have obtained equations that are very similar in form to the ordinary Boltzmann equations, but which include all first-order corrections in the gradient expansion. In Eqs. (70) and (71), all these corrections take into account the medium effect on the propagation and collisions of particles. The meaning of the off-mass-shell corrections associated with δ^Γ and of the quantities Z and b was discussed in the preceding section. As was indicated above, they all lead to a reduction of the collision terms (that is, to an increase in free paths). The effective K mass $\tilde m$, which was introduced in this section, is less than m, whereby the free path increases at fixed collision integrals. Therefore, all corrections that have been taken into account here lead to an increase in the transparency of nuclear matter for nucleons.

5. CONCLUSION

Numerous mathematical transformations that are necessary for going from the Dyson to kinetic equations conceal physical approximations that make it possible to accomplish a transition from quantum equations that are dynamically reversible in time to simpler kinetic equations, which are, however, irreversible in

time. The gradient expansion (16) in small parameters determined by the characteristics of the system that are averaged over the statistical ensemble is one of the key points in this transition. This is precisely the reason why the present analysis of the applicability of kinetic equations to our problem has been begun from the choice of the statistical ensemble for the system of two colliding nuclei that originally occurred in the ground states. Following [5, 18], we have introduced the statistical averaging over a small interval ΔE of incident-beam energies. This interval was chosen in such a way as to smooth entirely the fine structure of the ω dependences of the functions G and Σ that is associated with the complex multiparticle excitations of our system. Such smoothing is completely analogous to the smoothing that is introduced in constructing the ordinary optical model of the nucleus. Performing such roughening, we deliberately refuse to take into account the fine structure of cross sections for various processes, but we can instead describe, in a simplified way, the evolution of our system on the basis of kinetic equations. Such roughening is a quantum analog of the roughening of the phase space in classical mechanics, whereupon (see, for example, [19, 20]) the memory is lost in the system and a chaotic system becomes irreversible.

By choosing the statistical ensemble, we have been able to find small parameters of the gradient expansion and to determine the region where kinetic equations can be applied to nucleus–nucleus collisions. The analysis of the small parameters for the spatial part of the gradient expansion has led to relations (51) and (69), which are satisfied fairly well for heavy-ion collisions. A similar analysis of the time variables of the expansion has made it possible to obtain relations (51) and (52) and has demonstrated the incorrectness of the statements from [10] that kinetic approaches are inapplicable at energies exceeding 100 MeV per nucleon.

The above smoothing of the fine structure of the ω and p dependences of the functions G and Σ has enabled us to write the generalized Boltzmann equations in the simple form of the conventional Boltzmann equation [see Eqs. (70) and (71)] with modifications that take consistently into account all first-order corrections in the gradient expansion. An analysis of these modifications have revealed that they reduce to taking into account the effect of a medium on the propagation and collisions of particles in it. The majority of these modifications are expressed in terms of effective masses.

Of particular interest is the effect induced by a finite quasiparticle width Γ. Since the energy (momentum) of a quasiparticle can be determined only to within this width, soft binary collisions characterized by low energy transfers ($E_{tr} < \Gamma$) do not contribute to the collision integral Σ. That Γ is proportional to the collision integral can induce a negative feedback and a stabilization of dense-matter transparency. It is obvious that this phenomenon is quite general and can be especially pronounced in dense media characterized by pair-interaction potentials that lead to low energy transfers in collisions. Since the generalized Boltzmann equations obtained in this study are very similar in form to ordinary Boltzmann equations, it is worthwhile to investigate their solutions numerically and to analyze in greater detail the role of the aforementioned modifications. According to rough estimates, all of these lead to the growth of nuclear-matter transparency to nucleons.

ACKNOWLEDGMENTS

I am grateful to Prof. J. Huefner and to Deutsche Forschungs Gemeinschaft for support of this research.

APPENDIX

Let us estimate the effect of a finite-width Γ of the spectral function on the collision integrals in Eq. (61).

For the sake of simplicity, we consider the situation at the very beginning of the nuclear-collision event at an energy per nucleon greater than E_F. In this case, we can neglect the effect of blocking due to the Pauli exclusion principle. We also restrict our consideration to the direct term in the Born amplitude in Eq. (61). In this case, the collision integral of interest takes the form

$$\Sigma^{>}(\mathbf{p}_0) = bZ'V_0^2\int d^3p_1F(\mathbf{p}_1) \times \int d^3p_2d^3p_3e^{-\alpha(\mathbf{p}_0-\mathbf{p}_2)^2}\delta^\Gamma\left(\frac{1}{2m}(p_0^2+p_1^2-p_2^2-p_3^2)\right), \tag{A.1}$$

where quantity Z' stands for the product of all Z_i in Eq. (61). Going over to the variables

$$\mathbf{p}_0-\mathbf{p}_2 = \mathbf{q}, \quad \mathbf{p}_1-\mathbf{p}_3 = -\mathbf{q}, \quad \mathbf{p}_0-\mathbf{p}_1 = \mathbf{p},$$

we obtain

$$\Sigma^{>}(\mathbf{p}_0) = bZ'V_0^2\int d^3pF(\mathbf{p})g_\Gamma(\mathbf{p}), \tag{A.2}$$

where

$$g_\Gamma(\mathbf{p}) = 2m\int d^3qe^{-\alpha q^2}\delta^\Gamma(\mathbf{q}\cdot\mathbf{p}-q^2). \tag{A.3}$$

Introducing the components $q_\parallel$ and $q_\perp$ that are parallel and perpendicular to the vector $\mathbf{p}$, we arrive at

$$\begin{aligned} g_\Gamma &= 4m\pi\int dq_\parallel\int q_\perp dq_\perp e^{-\alpha(q_\perp^2+q_\parallel^2)}\delta^\Gamma(q_\parallel p-q_\parallel^2-q_\perp^2) \\ &\equiv 2m\pi\int_{-\infty}^{\infty}dq_\parallel\int_0^\infty dQe^{-\alpha(Q+q_\parallel^2)}\delta^\Gamma(Q_0-Q), \end{aligned} \tag{A.4}$$

where $Q = q_\perp^2$ and $Q_0 = q_\parallel p - q_\parallel^2$.

In order to simplify the calculations further, we will use, instead of the Lorentzian function $\delta^\Gamma(x)$, the step function having a width Γ and the center at the point $x = 0$.

In this case, the integral in (A.4) can be broken down into three parts

$$I_1 = \frac{\pi}{\Gamma}\int_{q_1}^{q_{01}} dq e^{-\alpha q^2} \int_0^{Q_0 + m\Gamma} dQ e^{-\alpha Q}, \quad (A.5)$$

$$I_2 = \frac{\pi}{\Gamma}\int_{q_{01}}^{q_{02}} dq e^{-\alpha q^2} \int_{Q_0 - m\Gamma}^{Q_0 + m\Gamma} dQ e^{-\alpha Q}, \quad (A.6)$$

$$I_3 = \frac{\pi}{\Gamma}\int_{q_{02}}^{q_2} dq e^{-\alpha q^2} \int_0^{q_0 + m\Gamma} dQ e^{-\alpha Q}, \quad (A.7)$$

where

$$\begin{aligned} q_1 &= p/2(1 - \sqrt{1 + m\Gamma/p^2}), \\ q_{01} &= p/2(1 - \sqrt{1 - m\Gamma/p^2}), \\ q_{02} &= p/2(1 + \sqrt{1 - m\Gamma/p^2}), \\ q_2 &= p/2(1 + \sqrt{1 + m\Gamma/p^2}). \end{aligned} \quad (A.8)$$

It is important to recall that the generalized Boltzmann equations (55) with the collision integrals (57) were obtained by consistently retaining, in the gradient expansion, only the zero- and the first-order terms in the small parameter Γ/E. Therefore, we must further take into account only the zero- and the first-order corrections in this parameter. The inclusion of higher order terms (for example, terms of second order in Γ/E) is meaningless because this is beyond the accuracy of Eq. (55). Taking into account this important circumstance, we can approximately set the integration limits in (A.8) to

$$q_1 \approx -p\epsilon/2, \quad q_{01} \approx p\epsilon/2,$$
$$q_{02} \approx p - p\epsilon/2, \quad q_2 \approx p + p\epsilon/2,$$

where $\epsilon = m\Gamma/p^2$.

Thus, the above three integrals determining g_Γ become

$$I_1 = \frac{\pi}{\alpha\Gamma}\left[\int_{q_1}^{q_{01}} e^{-\alpha q^2} dq + \frac{(e^{-\alpha\Gamma m} - 1)}{p\alpha} e^{-\alpha\Gamma m\epsilon}\right], \quad (A.9)$$

$$I_2 = \frac{\pi}{\alpha\Gamma}[e^{-\alpha p^2}(1 - e^{\alpha\Gamma m})e^{\alpha\Gamma m\epsilon} - (e^{-\alpha\Gamma m} - 1)e^{-\alpha\Gamma m\epsilon/2}], \quad (A.10)$$

$$I_3 = \frac{\pi}{\alpha\Gamma}\left[\int_{q_{02}}^{q_2} e^{-\alpha q^2} dq + e^{-\alpha p^2}\frac{(e^{-\alpha\Gamma m} - 1)}{\alpha p} e^{\alpha\Gamma m\epsilon}\right]. \quad (A.11)$$

In order to estimate the bracketed integral in expression (A.9) for I_1, we use the expansion of the error function erf(z) at small values of z. The integral in expression (A.11) for I_3 can be estimated by expanding the relevant exponential in the vicinity of the point $q = p$. In this way, we obtain

$$g_\Gamma(p) \approx \frac{\pi}{\alpha\Gamma\alpha p}\left[\alpha\Gamma m - \frac{\alpha^2\Gamma^2 m^2\epsilon}{12} + e^{-\alpha p^2}(1 - e^{-\alpha\Gamma m})e^{\alpha\Gamma m\epsilon/4} - e^{-\alpha p^2}\left[\frac{(e^{\alpha\Gamma m} - e^{-\alpha\Gamma m})}{2} e^{\alpha\Gamma m\epsilon/2} - (1 - e^{\alpha\Gamma m})e^{\alpha\Gamma m\epsilon/4}\right]\right]. \quad (A.12)$$

It is worthwhile to compare $g_\Gamma(p)$ with the quantity

$$g_0(p) = \frac{m\pi}{\alpha p}(1 - e^{-\alpha p^2}), \quad (A.13)$$

which is obtained from (A.3) in the quasiparticle approximation $\Gamma \longrightarrow 0$.

It can be seen that the difference $\Delta(p) = g_\Gamma(p) - g_0(p)$ of expressions (A.12) and (A.13), which arises owing to a nonzero value of Γ, is given by

$$\Delta(p) = \frac{m\pi}{\alpha p}\left[-\frac{\alpha\Gamma m\epsilon}{12} - \frac{e^{-\alpha p^2}}{\alpha\Gamma m}\left[\frac{(e^{\alpha\Gamma m} - e^{-\alpha\Gamma m})}{2} e^{\alpha\Gamma m\epsilon/2} - (2 - e^{-\alpha\Gamma m} - e^{\alpha\Gamma m})e^{\alpha\Gamma m\epsilon/4} + \alpha\Gamma m\right]\right]. \quad (A.14)$$

We note that, for any value of $\alpha\Gamma m$, the result in (A.14) is negative, which means the reduction of the collision integral.

Let us integrate the function $g_0(p)$ in (A.2) with the distribution function describing the initial stage of the process (two Fermi spheres in momentum space, its centers being separated by the incident-beam momentum $p = \sqrt{2mE}$). In the case being considered, we have $p \gg p_F$, and integration yields

$$I_0 \approx \frac{3m\pi p}{2\alpha p_F^2}. \quad (A.15)$$

Performing a similar integration (within the same approximations) of the difference $\Delta(p)$ given by (A.14), we obtain

$$\Delta \approx -\frac{3m^3\pi\Gamma^2}{2 \times 12 p p_F^2}. \quad (A.16)$$

Thus, the relative reduction of the collision integral due to a nonzero value of Γ is given by

$$R = \frac{\Delta}{I_0} \approx -\frac{\alpha\Gamma m}{12}\frac{\Gamma}{E} + O\left(\frac{\Gamma^2}{E^2}\right). \quad (A.17)$$

A similar calculation performed for the distribution $\delta_\Gamma(x) = \frac{1}{\Gamma} e^{-2|x|/\Gamma}$, whose boundaries are smeared to a greater extent than those of the step function, leads to a still sharper dependence of the ratio in (A.17) on the parameter $\alpha\Gamma m$. In this case, the relative reduction of the collision integrals for $\alpha\Gamma m \le 1$ is

$$R' \approx -\frac{(\alpha\Gamma m)^2}{4-(\alpha\Gamma m)^2} + O\left(\frac{\Gamma^2}{E^2}\right). \qquad (A.18)$$

Since the Lorentzian distribution used in this study is even more smeared, one would expect a still more pronounced dependence of the relative reduction of the collision integrals on the parameter $\alpha\Gamma m$.

REFERENCES

1. G. F. Bertsch and S. Das Gupta, Phys. Rep. **160**, 189 (1988); C. Gregoire, B. Remaud, F. Sebille, *et al.*, Nucl. Phys. A **465**, 315 (1987).
2. J. Aichelin, Phys. Rep. **202**, 233 (1991).
3. G. Peilert, H. Stoeker, W. Greiner, *et al.*, Phys. Rev. C **39**, 1402 (1989).
4. V. E. Bunakov, Yad. Fiz. **25**, 505 (1977) [Sov. J. Nucl. Phys. **25**, 271 (1977)]; Fiz. Élem. Chastits At. Yadra **11**, 1285 (1980) [Sov. J. Part. Nucl. **11**, 507 (1980)].
5. V. Bunakov and G. Matvejev, Z. Phys. A **322**, 511 (1985).
6. A. S. Iljinov, M. V. Kazarnovsky, and E. Ya. Paryev, *Intermediate Energy Nuclear Physics* (CRC, Boca Raton. 1993).
7. V. E. Bunakov, E. N. Vol'nin, and G. V. Matveev, Izv. Akad. Nauk SSSR, Ser. Fiz. **50**, 171 (1986).
8. P. Danielewicz, Ann. Phys. (N.Y.) **152**, 239 (1984).
9. P. Danielewicz, Ann. Phys. (N.Y.) **152**, 305 (1984).
10. W. Botermans and R. Malfliet, Phys. Rep. **198**, 116 (1990).
11. L. V. Keldysh, Zh. Éksp. Teor. Fiz. **47**, 1515 (1964) [Sov. Phys. JETP **20**, 1018 (1964)].
12. L. Kadanoff and G. Baym, *Quantum Statistical Mechanics* (Benjamin, New York, 1962).
13. E. M. Lifshitz and L. P. Pitaevskiĭ, *Physical Kinetics* (Nauka, Moscow, 1979; Pergamon, Oxford, 1981).
14. A. Bohr and B. R. Mottelson, *Nuclear Structure* Vol. 1: *Single-Particle Motion* (Benjamin, New York, 1969; Mir, Moscow, 1971).
15. J. P. Jeukenne, A. Lejeune, and C. Mahaux, Phys. Rep. **25**, 83 (1976).
16. B. ter Haar and R. Malfliet, Phys. Rep. **149**, 3 (1987).
17. C. J. Wong, Phys. Rev. C **25**, 1460 (1982).
18. V. Bunakov, Z. Phys. A **297**, 323 (1980).
19. G. M. Zaslavsky, *Chaos in Dynamical Systems* (Nauka, Moscow, 1984; Harwood, Chur, 1985).
20. G. M. Zaslavsky and R. Z. Sagdeev, *Introduction to Nonlinear Physics* (Nauka, Moscow, 1988).

Translated by A. Isaakyan

Physics of Atomic Nuclei, Vol. 64, No. 3, 2001, pp. 506–515. Translated from Yadernaya Fizika, Vol. 64, No. 3, 2001, pp. 560–569.

90th ANNIVERSARY OF A.B. MIGDAL'S BIRTHDAY
NUCLEI

Structure and Direct Protonic Decay of Isobaric Analogous and Isovector Monopole Giant Resonances

M. L. Gorelik and M. H. Urin

Moscow State Engineering Physics Institute (Technical University), Kashirskoe sh. 31, Moscow, 115409 Russia

Received July 27, 2000

Abstract—A description of the partial protonic widths of isobaric analogous resonances is proposed on the basis of the continuum random-phase approximation and a partly self-consistent phenomenological version of the theory of finite Fermi systems. The results of the calculations performed for spherical nuclei over a wide interval of atomic-mass values are in satisfactory agreement with the corresponding experimental widths. The probability of the direct protonic decay of an isovector monopole giant resonance in the β^- channel is estimated in connection with some recent experiments. © *2001 MAIK "Nauka/Interperiodica".*

On one of the copies of his monograph [1], A.B. Migdal wrote, "Nuclear reactions are missing here …." We hope that the present study conforms to the desire of the Teacher, at least to some extent.

1. INTRODUCTION

A vast body of experimental data on the partial protonic widths of isobaric analogous resonances has been obtained over the past period of more than 30 years. These data come primarily from an analysis of resonance reactions involving protons. In the 1970s and 1980s, a serious effort was mounted to obtain a quantitative description of the protonic widths of isobaric analogous resonances (see, for example, [2, 3] and references therein). Those investigations were motivated by the quest for obtaining deeper insights into the structure of isobaric analogous resonances and the mechanism of their decays, which is directly related to violation of isospin symmetry in nuclei. There was also the hope for implementing an alternative method for determining single-particle spectroscopic factors by comparing the experimental and the calculated single-particle protonic widths of isobaric analogous resonances (the single-particle protonic widths of isobaric analogous resonances are calculated under the assumption that the relevant states of a parent or a product nucleus are of a single-particle character). In order to accomplish this goal, it is necessary to have, among other things, a sufficiently precise method for calculating single-particle partial widths of isobaric analogous resonances that is stable against variations in model parameters within reasonable limits. As applied to reduced single-particle protonic widths of isobaric analogous resonances (that is, widths divided by the penetrability of the potential barrier for protons), these requirements are met in self-consistent approaches developed over the past decade and based on the random-phase approximation (RPA) or the Tamm–Dankov approximation (TDA) that take exactly into account a single-particle continuum (CRPA or CTDA, respectively). A CTDA description of the relative intensities of the direct protonic decay of an analog of the ^{208}Pb ground state was proposed in [4], where use was made of the Hartree–Fock mean field and Skyrme forces. In [5], the partial protonic widths of this isobaric analogous resonance were calculated on the basis of the CTDA as well.

In [6], the partial protonic widths of isobaric analogous resonances were calculated within the CRPA. Those calculations, actually based on the phenomenological version of the theory of finite Fermi systems, employed (i) the phenomenological nuclear mean field and the isovector (spinless) component of the Landau–Migdal amplitude, (ii) the condition that ensures partial self-consistency in isospin [7] and which makes it possible to avoid a unphysical violation of isospin symmetry in the phenomenological shell model, (iii) a CRPA calculation of the S matrix for nucleon–nucleus scattering [8], and (iv) experimental values of the spectroscopic factors for the relevant states of neutron-odd nuclei. The partial protonic widths of isobaric analogous resonances in spherical nuclei as calculated in [6] on this basis are in satisfactory agreement with experimental data over a wide range of nuclear masses. There are, however, some flaws in the approach implemented in [6]. These include (a) a non-self-consistent calculation of the mean Coulomb field of a nucleus, (b) the use of some version of perturbation theory in the formulation of the theory of isobaric analogous resonances in terms of the variable part of the mean Coulomb field of a nucleus, and (c) inability of the approach to describe direct protonic decays of isobaric analogous resonances in nuclei featuring well-developed neutron pairing.

The properties of an analogous resonance treated as that which corresponds to a compound-nucleus state characterized by an anomalous isospin are often asso-

1063-7788/01/6403-0506$21.00

ciated with the properties of an isovector giant monopole resonance (see, for example, [2]). In fact, the latter resonance, which corresponds to a compound-nucleus state having a "normal" isospin value, can be considered as an overtone of the corresponding isobaric analogous resonance. It should be noted that attempts were made to detect experimentally isovector giant monopole resonances in cross sections for charge-exchange reactions involving pions [9] or light ions [10].

In order to improve the accuracy in calculating single-particle protonic widths of isobaric analogous resonances and to simplify the computational scheme, we modify here the approach from [6] along the following lines:

(i) Instead of the S matrix for proton–nucleus scattering, we calculate here, within the CRPA, the proton-emission amplitude for the relevant reactions [11] (the two methods for computing the partial nucleonic widths of giant resonances are equivalent, but the implementation of the latter is simpler in practice).

(ii) The mean Coulomb field of a nucleus is calculated self-consistently.

(iii) The single-particle protonic widths of isobaric analogous resonances are exactly expressed within the CRPA in terms of the variable part of the mean Coulomb field of a nucleus.

(iv) The approach is extended to nuclei featuring well-developed neutron pairing.

We also aim here at assessing the branching ratio for the direct protonic decay of isovector giant monopole resonances in medium-mass and heavy nuclei. This part of the study was motivated by a recent attempt at experimentally detecting an isovector giant monopole resonance in the cross section for the reaction ^{208}Pb(^{3}He, tp) [10] and by the results of the aforementioned study of Erell *et al.* [9].

The ensuing exposition is organized as follows. In Section 2, we present basic relations of our approach to calculating the single-particle protonic widths of isobaric analogous resonances. In Section 3, we discuss the choice of values for model parameters and describe the results of our calculations for the partial protonic widths of isobaric analogous resonances in nuclei from a wide atomic-mass interval. In Section 4, we propose a theory of isobaric analogous and isovector giant monopole resonances in terms of a variable part of the mean Coulomb field of a nucleus and assess the branching ratio for the direct protonic decay of an isovector giant monopole resonance. The basic results of the present study are summarized in Section 5.

Previously, a brief account of some of these results was given in [12, 13].

2. BASIC RELATIONS

Because of approximate isospin conservation, the decay properties of isobaric analogous resonances in medium-mass and heavy nuclei can be described in terms of the mean Coulomb field of a nucleus, $U_C(r)$. In order to implement this possibility within a phenomenological version of the theory of finite Fermi systems, it is necessary to satisfy the isovector condition of partial self-consistency. In just the same way as in [6, 11], the CRPA will be developed in terms of the following phenomenological quantities: isoscalar part of the mean nuclear field (including the spin–orbit term), $U_o(x)$, and the isovector component of the Landau–Migdal amplitude, $F(x_1, x_2) \longrightarrow F'\boldsymbol{\tau}_1 \cdot \boldsymbol{\tau}_2\delta(\mathbf{r}_1 - \mathbf{r}_2)$. The Coulomb field $U_C(r)$ is calculated self-consistently (in the Hartree approximation) in terms of the proton density $n^p(r)$. The isovector part of the mean field, $U_1(x) = \tau^{(3)}V(r)/2$ [$V(r)$ is a symmetry potential], is also calculated self-consistently. Within the RPA, the self-consistency condition that relates $V(r)$ and F' can be obtained with the aid of the relation [14]

$$[\hat{H}, \hat{\mathrm{T}}^{(-)}] = -\sum_a (V(r_a) - 2F'n^{(-)}(r_a))\tau_a^{(-)} + \sum_a U_C(r_a)\tau_a^{(-)} = \Delta_C\hat{\mathrm{T}}^{(-)} + \hat{V}_C^{(-)}, \quad (1)$$

where $\hat{H} = \sum_a H_o(\mathbf{r}_a) + \hat{F}$ is the nuclear Hamiltonian in the interacting-quasiparticle approximation, $\hat{\mathrm{T}}^{(-)} = \sum_a \tau_a^{(-)}$ is the single-particle Fermi operator, $n^{(-)} = n^n - n^p$ is the neutron-excess density, Δ_C is the so-called Coulomb shift energy (it is defined below), and $\hat{V}_C^{(-)} = \sum_a (U_C(r_a) - \Delta_C)\tau_a^{(-)}$. Taking into account approximate isospin conservation and using Eq. (1), we obtain the isovector self-consistency equation $V(r) = 2F'n^{(-)}(r)$ and the Coulomb operator $\hat{V}_C^{(-)}$ in a representation that is convenient for describing the decays of isobaric analogous and isovector monopole giant resonances.

The general properties of fermion excitations in nuclei are characterized by the model-independent non-energy-weighted sum rule $(\mathrm{NEWSR})_F$,

$$(\mathrm{NEWSR})_F = \sum_s |\langle s|\hat{\mathrm{T}}^{(-)}|o\rangle|^2 - \sum_{s'} |\langle s'|\hat{\mathrm{T}}^{(+)}|o\rangle|^2 = N - Z, \quad (2)$$

or by the model-dependent energy-weighted sum rule $(\mathrm{EWSR})_F$,

$$(\mathrm{EWSR})_F = \sum_s (E_s - E_o)|\langle s|\hat{\mathrm{T}}^{(-)}|o\rangle|^2 + \sum_{s'} (E_{s'} - E_o)|\langle s'|\hat{\mathrm{T}}^{(+)}|o\rangle|^2 = \langle o|[\hat{\mathrm{T}}^{(+)}[\hat{H}, \hat{\mathrm{T}}^{(-)}]]|o\rangle. \quad (3)$$

Here, $E_{s,s'}$ and E_o are, respectively, the energies of states of isobaric nuclei and the energy of the ground state of the parent nucleus. Within the model being considered, we find on the basis of Eqs. (1) and (3) that $(\mathrm{EWSR})_\mathrm{F} = \int U_\mathrm{C}(r) n^{(-)}(r) d\mathbf{r}$. From Eqs. (1)–(3), it follows that, if an isobaric analogous resonance had saturated 100% of the sum rule in (2) (exact isospin conservation), its wave function and energy would have been

$$|IAS\rangle = \frac{1}{\sqrt{N-Z}}\hat{\mathrm{T}}^{(-)}|o\rangle;$$
$$\omega_A = E_A - E_o = \frac{1}{N-Z}\int U_\mathrm{C}(r) n^{(-)}(r) d\mathbf{r}. \quad (4)$$

But in fact, these relations are satisfied only approximately.

Owing to the isovector self-consistency condition, an isobaric analogous resonance can be treated, within the phenomenological version of the theory of finite Fermi systems, as a conventional giant resonance. Here, we proceed to develop such a description. In order to find the partial protonic width of an isobaric analogous resonance, we will calculate two functions of the excitation energy—namely, the Fermi strength function and the amplitude for proton emission under the effect of an external Fermi field. By definition, the Fermi strength function is given by

$$S_\mathrm{F}(\omega) = \sum_s \left|\langle s|\hat{\mathrm{T}}^{(-)}|o\rangle\right|^2 \delta(E_s - E_o - \omega), \quad (5)$$

where ω is the isobaric-nucleus excitation energy reckoned from E_o. Within the CRPA, $S_\mathrm{F}(\omega)$ is determined by relations that are well known in the theory of finite Fermi systems [1] and which can be represented as

$$S_\mathrm{F}(\omega) = -\frac{1}{\pi}\mathrm{Im}\,P_\mathrm{F}(\omega),$$
$$P_\mathrm{F}(\omega) = \int V_\mathrm{F}^*(r) A(r, r', \omega) \tilde{V}_\mathrm{F}(r', \omega) dr dr', \quad (6)$$

where $P_\mathrm{F}(\omega)$ is the Fermi polarizability; $(r^2 r'^2)^{-1} A(r, r', \omega)$ is the monopole component of the free response function in the corresponding charge-exchange channel; $V_\mathrm{F}(r) = 1$; and $\tilde{V}_\mathrm{F}(r, \omega)$ is the effective Fermi field, which satisfies the equation

$$\tilde{V}_\mathrm{F}(r, \omega) = V_\mathrm{F}(r) + \frac{2F'}{4\pi r^2}\int A(r, r', \omega)\tilde{V}_\mathrm{F}(r', \omega) dr'. \quad (7)$$

For nuclei where there is no nucleon pairing, the function $A(r, r', \omega)$ can be represented in a form that takes exactly into account the contribution of the single-particle continuum; that is,

$$A(r, r', \omega)$$
$$= \sum_\nu n_\nu (2j_\nu + 1)\chi_\nu(r)\chi_\nu(r') g_{(\pi)}(r, r', \varepsilon_\nu + \omega)$$
$$+ \sum_\pi n_\pi (2j_\pi + 1)\chi_\pi(r)\chi_\pi(r') g_{(\nu)}(r, r', \varepsilon_\pi - \omega), \quad (8)$$

where $\lambda = \nu, \pi$ is the set of the quantum numbers n_r, j, l $[(\lambda) = j, l]$, which determine single-particle quantum states in the mean nuclear field for neutrons $(\lambda = \nu)$ and for protons $(\lambda = \pi)$ with $(\nu) = (\pi)$; $N_\lambda = n_\lambda(2j_\lambda + 1)$ is the number of nucleons on the level λ, n_λ being the occupation factor; $r^{-1}\chi_\lambda$ stands for bound-state radial wave functions; and $(rr')^{-1} g_{(\lambda)}(r, r', \varepsilon)$ are the Green's functions for the radial Schrödinger equation

$$(H_{(\lambda)}(r) - \varepsilon_\lambda)\chi_\lambda = 0,$$
$$(H_{(\lambda)}(r) - \varepsilon) g_{(\lambda)}(r, r', \varepsilon) = -\delta(r - r'). \quad (9)$$

Here, the radial part of the single-particle Hamiltonian,

$$H_{(\lambda)}(r) = H_{o(\lambda)}(r) + \frac{1}{2}\tau^{(3)} v(r) + \frac{1}{2}(1 - \tau^{(3)}) U_\mathrm{C}(r), \quad (10)$$

involves an isoscalar, an isovector, and a Coulomb component. The neutron and the proton density, which are used in the implementation of the conditions of partial self-consistency, are given by

$$n(r) = \frac{1}{4\pi r^2}\sum_\lambda n_\lambda (2j_\lambda + 1)\chi_\lambda^2(r),$$
$$N = \sum_\lambda n_\lambda (2j_\lambda + 1). \quad (11)$$

In continuous-spectrum problems, where the excitation energy of the nucleus being considered exceeds the nucleon binding energy, it is convenient to use an alternative representation for the strength function [15]. On the basis of relations (6)–(8), we obtain

$$S_\mathrm{F}(\omega) = -\frac{1}{\pi}\mathrm{Im}\int \tilde{V}_\mathrm{F}^*(r, \omega) A(r, r', \omega)\tilde{V}_\mathrm{F}(r', \omega) dr dr'$$
$$= \sum_\nu \left|M_\nu^\mathrm{F}(\omega)\right|^2, \quad (12)$$

where

$$M_\nu^\mathrm{F}(\omega) = N_\nu^{1/2}\int \chi_{\varepsilon,(\pi)}(r)\tilde{V}_\mathrm{F}(r, \omega)\chi_\nu(r) dr. \quad (13)$$

Here, $r^{-1}\chi_{\varepsilon,(\pi)}(r)$ is the continuum radial wave function for protons that corresponds to the energy of $\varepsilon = \varepsilon_\nu + \omega$ and which is normalized to a delta function of energy; in addition, we have $(\pi) = (\nu)$. The quantity $M_\nu^\mathrm{F}(\omega)$ has the meaning of the amplitude for a reaction that is induced by an external Fermi field and which results in that the nucleus goes over into a ν^{-1} neutron-hole state upon the emission of a proton with energy ε. The strength function $S_\mathrm{F}(\omega)$ (6) or (12) and the reaction amplitude $M_\nu^\mathrm{F}(\omega)$ (13) calculated within the CRPA show a narrow maximum corresponding to the excita-

tion of an isobaric analogous resonance. The Breit–Wigner parametrization of these quantities,

$$S_{\rm F}(\omega) = -\frac{1}{\pi}{\rm Im}\frac{S_A}{\omega-\omega_A+\frac{i}{2}\Gamma},$$
$$\left|M^{\rm F}_{\nu}(\omega)\right| = \frac{1}{\sqrt{2\pi}}\left|\frac{S_A^{1/2}\Gamma_{\nu}^{1/2}}{\omega-\omega_A+\frac{i}{2}\Gamma}\right|, \quad (14)$$

makes it possible to find the excitation energy ω_A, the Fermi strength S_A, and the partial (Γ_ν) and the total (Γ) protonic widths of an isobaric analogous resonance ($\Gamma = \sum_\nu \Gamma_\nu$). Prior to comparing the calculated widths Γ_ν with corresponding experimental widths $\Gamma_\nu^{\rm expt}$, it is necessary to note the following:

(i) The proton energies $\varepsilon_A = \varepsilon_\nu + \omega_A$ calculated within the phenomenological interacting-quasiparticle model may differ from the experimental energies $\varepsilon^{\rm expt}$.

(ii) Occupation numbers for neutron levels, N_ν, in nuclei featuring no nucleon pairing differ from the corresponding spectroscopic factors $s_\nu^{\rm expt} = S_\nu^{\rm expt}(2j_\nu + 1)$ ($S_\nu^{\rm expt}$ is the reduced spectroscopic factor) owing primarily to coupling to low-lying collective states. For the reasons indicated above, the calculated quantities that will be compared with the experimental partial protonic widths of isobaric analogous resonances, $\Gamma_\nu^{\rm expt}$, are

$$\Gamma_\nu^{\rm calc} = s_\nu^{\rm expt}\Gamma_\nu^{\rm calc}({\rm s.p.}),$$
$$\Gamma_\nu^{\rm calc}({\rm s.p.}) = \frac{\Gamma_\nu(\varepsilon_A)}{N_\nu}\frac{P_l(\varepsilon^{\rm expt})}{P_l(\varepsilon_A)}, \quad (15)$$

where $P_l(\varepsilon)$ is the penetrability of the potential barrier for protons, while the ratio $\Gamma_\nu(\varepsilon_A)/N_\nu P_l(\varepsilon_A)$ is the reduced single-particle protonic width of an isobaric analogous resonance as calculated within the CRPA by using the partly self-consistent phenomenological model of interacting quasiparticles. It is the reduced width that appears to be stable to variations of the model parameters within reasonable limits.

In just the same way as in the case of other giant resonances, coupling to multiparticle configurations leads to the broadening of isobaric analogous resonances owing to the emergence of a spreading width in expressions of the type in (14) for energy-averaged reaction amplitudes, but the widths with respect to direct nucleonic decays remain unchanged [8, 11]. In contrast to other giant resonances, the fragmentation width of isobaric analogous resonances is strongly suppressed because of approximate isospin conservation in nuclei (see, for example, [2, 3]). A theoretical interpretation of this width is beyond the scope of the present study.

A vast body of experimental data on partial protonic widths of isobaric analogous resonances has been accumulated for nuclei with well-developed nucleon pairing. A self-consistent version of the CRPA for such nuclei has yet to be developed. However, the above method for calculating single-particle partial protonic widths $\Gamma_\nu^{\rm calc}$(s.p.) of isobaric analogous resonances provides a satisfactory accuracy for these nuclei as well. In view of a high excitation energy of isobaric analogous resonances, we can disregard, to a precision of order $(2\Delta/\omega_A)^2$ (Δ is the energy gap), pairing in the equation for the effective Fermi field $\tilde{V}_{\rm F}(r, \omega)$. For this reason, the algorithm for calculating the widths $\Gamma_\nu^{\rm calc}$(s.p.) remains unchanged for parent nuclei featuring the magic number N_m of neutrons or $N_m + 1$ neutrons. As a matter of fact, this circumstance was used in [6]. Pairing in the neutron subsystem changes the calculated energy ε_A of a proton in the continuum and the occupation number n_ν for neutron levels. Since the energies ε_A cannot be calculated to a satisfactory precision even in the presence of pairing, it is preferable to find the widths $\Gamma_\nu^{\rm calc}$(s.p.) (15) by using the experimental proton energies $\varepsilon^{\rm expt}$. A modification to the occupation numbers because of pairing is only one part of the effect—the second is due to the coupling of quasiparticles to low-lying collective states. In just the same way as in the case of magic and near-magic parent nuclei, we therefore either use the experimental values of spectroscopic factors, $s_\nu^{\rm expt}$, in the first of relations (15) or determine the spectroscopic factors with the aid of the ratio of the widths $\Gamma_\nu^{\rm expt}$ and $\Gamma_\nu^{\rm calc}$(s.p.).

The conjecture that it is possible to avoid a direct consideration of pairing in calculating the single-particle partial widths of isobaric analogous resonances, $\Gamma_\nu^{\rm calc}$(s.p.), is additionally supported by results obtained with the aid of a method (see below) for approximately taking into account pairing in the neutron subsystem [12]. With the aim of preserving the isovector self-consistency condition, we will allow for pairing {within the Bardeen–Cooper–Schrieffer (BCS) model [16]} only by modifying the occupation numbers in the CRPA equation without changing the energy of quasiparticles. It can easily be verified that, in the case of such a modification (affecting the neutron-excess density as well), an isobaric analogous state remains an exact state of the system with the wave function (4) even in the limit $\hat{V}_{\rm C}^{(-)} \longrightarrow 0$. Our further analysis will be performed only for an odd-neutron parent nucleus having a quasiparticle on a level ν (a case of importance for practical applications indeed). The pairing gap is found here by fitting the observed neutron-separation energy in the parent nucleus. In this case, it is necessary to solve only one BCS equation for determining the chemical poten-

tial. With allowance for the blocking effect, this equation has the form [16]

$$N = \sum_{\nu' \neq \nu} v_{\nu'}^2 (2j_{\nu'} + 1) + (v_\nu^2 2j_\nu + u_\nu^2), \qquad (16)$$

where v_ν and u_ν are the well-known coefficients in the Bogolyubov canonical transformation. Expressions (11), (12), and (13) for the neutron density, the Fermi strength function, and the reaction amplitude M_ν^F [12], respectively, change appropriately. We note that the amplitude of the reaction populating the ground state of the even-neutron product nucleus is given by an expression of the form (13) where the factor u_ν is substituted for the quantity $N_\nu^{1/2}$. This is the same factor that appears in the amplitude of the β^- decay of an odd-neutron parent nucleus [16, 17]. The widths Γ_ν^{calc} (s.p.) (15) where the aforementioned substitution has been made is then contrasted against the relevant experimental widths Γ_ν^{expt}. Provided that the corresponding conditions of partial self-consistency are satisfied, the difference of the widths Γ_ν^{calc} (s.p.) as calculated with and without allowance for pairing is due to the effect of the pairing-induced smearing of the Fermi boundary on the effective field $\tilde{V}_F(r, \omega)$. In accordance with the above estimate of this effect, the distinction between the above widths is expected to be modest.

3. CHOICE OF MODEL PARAMETERS: RESULTS OF THE CALCULATIONS FOR THE PARTIAL PROTONIC WIDTH OF ISOBARIC ANALOGOUS RESONANCES

As was indicated above, the isoscalar part of the mean nuclear field and the isovector part of the Landau–Migdal amplitude are phenomenological quantities used in implementing the CRPA. The isoscalar part of the mean field is chosen to be (see, for example, [8])

$$U(r) = -U_o f(r, R, a) + U_{so} \frac{\Lambda_\pi^2}{r} \frac{df}{dr} \mathbf{l} \cdot \mathbf{s}, \qquad (17)$$

where $f(r, R, a) = \left(1 + \exp\left(\frac{r-R}{a}\right)\right)^{-1}$ is the Woods–Saxon function, $R = r_o A^{1/3}$ and a being, respectively, the nuclear radius and diffuseness. The parameters are set to the following values: $U_o = 54$ MeV, $r_o = 1.24$ fm, $U_{so} = 14.02\left(1 + 2\frac{N-Z}{A}\right)$ MeV, and $\Lambda_\pi = 1.41$ fm.

The mean energy of Coulomb interaction between a proton and a nucleus was calculated self-consistently in the Hartree approximation:

$$U_C(r) = e^2 \int \frac{n^p(r')}{|\mathbf{r} - \mathbf{r}'|} d\mathbf{r}'. \qquad (18)$$

The strength of the isovector component of the Landau–Migdal amplitude was chosen in the form $F' = Cf'$ with $C = 300$ MeV fm^3 and $f' = 1.0$.

The single-particle radial wave functions and the Green's functions were calculated on the basis of Eqs. (9) and (10), while the nucleon densities were evaluated according to Eq. (11). We recall that, in addition to the self-consistent method for calculating the mean Coulomb field of a nucleus, we also made use of the isovector self-consistency condition, which relates the symmetry potential to the neutron-excess density through the constant f'. With due regard to this comment, the above set of model parameters makes it possible to reproduce satisfactorily, in the calculations, the nucleon binding energy in *mag + one nucleon* subsystems and the single-quasiparticle spectrum near the ground state for *mag ± one nucleon* subsystems in nuclei from Zr to Pb. The experimental value of the neutron binding energy was used to calculate the single-quasiparticle spectrum and occupation numbers for odd nuclei featuring neutron pairing.

A CRPA calculation of the Fermi strength function $S_F(\omega)$ and the Fermi reaction amplitude $M_\nu^F(\omega)$ was performed according to Eqs. (6)–(8) and (13), respectively, at ω values in the vicinity of ω_A. The partial protonic widths $\Gamma_\nu(\varepsilon_A)$, the Fermi strength S_A, and the isobaric-analogous-resonance energy ω_A were computed on the basis of Eqs. (14). The single-particle protonic widths of isobaric analogous resonances, Γ_ν^{calc} (s.p.), were evaluated according to Eq. (15) with the aid of the expression for the potential-barrier penetrability $P_l(\varepsilon)$ from the monograph [18]. For the nuclei considered here, the calculated Fermi strength S_A for isobaric analogous resonances changes between 92 and 98% of $(\text{NEWSR})_F$ (2), while the calculated isobaric-analogous-resonance energy ω_A is approximately 4% less than the value given by relation (4).

Now, we proceed to present the results of our calculations for the partial protonic widths of isobaric analogous resonances. For a direct protonic decay leading to the population of the single-hole states of the ^{207}Pb nucleus, Table 1 displays the calculated partial widths of the 0^+ isobaric analogous resonance in the ^{208}Bi nucleus (analog of the ^{208}Pb ground state). The calculations relied on rather old values of the reduced spectroscopic factors, S_ν^{expt} [19], as determined from the cross sections for the relevant (p, d) reaction. In this connection, we have also calculated the factors S_ν^{expt} (IAR) as the partial-width ratio $\Gamma_\nu^{expt}/\Gamma_\nu^{calc}$ (s.p.). The width values Γ_ν^{expt} were borrowed from the article of van der Werf *et al.* [20], who analyzed the entire body of experimental data on the direct protonic decay of the isobaric analogous resonance being considered.

For protonic decays into the ground state of the product nucleus, the calculated partial widths of the analogs of the ground state and some excited states of nuclei containing $N_m + 1$ neutrons are quoted in Table 2 for nuclei from ^{49}Ca to ^{209}Pb. No account was taken here of pairing in the even-proton (nonmagic) subsystem. The values s_ν^{expt} found for the spectroscopic factors from the (d, p) cross sections were borrowed from the compilation presented in [3]. The results of the calculations are compared with experimental data taken predominantly from the same compilation.

The tables that follow give the calculated partial protonic widths of isobaric analogous resonances in nuclei featuring well-developed neutron pairing. The analysis covers isobaric analogous resonances studied in detail by Guzhovskiĭ's group over the 1960s and 1970s in resonance-proton-scattering reactions. For decays into the ground states of the Sn and Te nuclei, Table 3 displays the calculated partial widths of the $1/2^+$ isobaric analogous resonances in the nuclei of Sb and I isotopes. The spectroscopic-factor and partial-width values (s_ν^{expt} and Γ_ν^{expt}) were borrowed from [23] and [25, 26], respectively. The calculated single-particle partial widths Γ_ν^{calc} (s.p.) of the $3/2^+$ isobaric analogous resonances in the nuclei of the Sb and I isotopes are quoted in Table 4 for decays into the ground states of the Sn and Te nuclei, respectively. The width values Γ_ν^{expt} were taken from [25, 26]. For want of experimental data on the spectroscopic factors (s_ν^{expt}), we present the results of the calculations for s_ν^{expt}(IAR).

The calculations of the single-particle protonic widths of isobaric analogous resonances—the results are given in Tables 3 and 4—were performed according to the scheme where pairing is taken into account approximately (see Section 2). The same widths were also calculated without allowance for pairing. In that case, it was assumed that an odd neutron populates a single-particle level ν and that the filling of the core corresponds to its ground state. If the conditions of self-consistency are satisfied, the widths Γ_ν^{calc} (s.p.) as calculated with and without allowance for pairing differ by not more than 3%. For decays into the ground states of the Cd and Pd nuclei, the single-particle protonic widths of isobaric analogous resonances in the nuclei of the In and Ag isotopes, respectively, were calculated without allowing for pairing. The results of these calculations are given in Tables 5 and 6, along with the values s_ν^{expt}(IAR). The relevant experimental data were borrowed from [25, 27].

On the basis of the data presented in Tables 1–6, we can draw the following conclusions:

(i) The calculated partial protonic widths of isobaric analogous resonances in nuclei are in satisfactory agreement with available experimental data over a wide range of atomic masses.

Table 1. Partial protonic-decay widths of the 0^+ isobaric analogous resonances in ^{208}Bi

ν	S_ν^{expt} [19]	$\varepsilon^{\text{expt}}$, MeV [3]	Γ_ν^{expt}, keV [20]	Γ_ν^{calc}, keV	S_ν^{expt} (IAR)
$3p_{1/2}$	1.0	11.46	51.9 ± 1.6	72	0.72
$2f_{5/2}$	0.98	10.91	26.4 ± 2	25	1.03
$3p_{3/2}$	1.00	10.59	64.7 ± 3.4	88	0.73
$1i_{13/2}$	0.91	9.74		0.2	
$2f_{7/2}$	0.70	9.15	4.2 ± 0.6	4.8	0.61

Table 2. Partial protonic-decay widths of the analogs of odd-neutron parent nuclei

Parent nucleus	ν	s_ν^{expt} [3, 21]	$\varepsilon^{\text{expt}}$, MeV [3]	Γ_ν^{expt}, keV [3]	Γ_ν^{calc}, keV
^{49}Ca	$p_{3/2}$	0.93	1.93	1.9 ± 0.2	2.3
^{91}Zr	$d_{5/2}$	0.89	4.67	4.0 ± 0.5	3.3
	$s_{1/2}$	0.72*	5.88*	38 ± 6*	42
	$d_{3/2}$	0.45	6.78	15 ± 3	18
^{139}Ba	$f_{7/2}$	0.7	9.93	16 ± 2	24
	$p_{3/2}$	0.32	10.56	26 ± 3	35
	$p_{1/2}$	0.27	11.01	22 ± 2	28
^{141}Ce	$f_{7/2}$	0.8	9.68	11 ± 1	20
	$p_{3/2}$	0.4	10.33	24 ± 2	40
	$p_{1/2}$	0.4	10.81	19 ± 2	40
	$h_{9/2}$	1.0	11.06	1.2	1.5
^{209}Pb	$g_{9/2}$	0.78	14.83	22.7 ± 0.6	27
	$i_{11/2}$	0.96	15.58	1.6 ± 0.4	1.3
	$j_{15/2}$	0.53	16.30	0.9 ± 0.8	0.75
	$d_{5/2}$	0.88	16.39	50.2 ± 1.0	89
	$s_{1/2}$	0.88	16.87	56.6 ± 3.4	79
	$g_{7/2}$	0.78	17.32	42.9 ± 3.6	42
	$d_{3/2}$	0.88	17.37	62.8 ± 5.4	69

* Data from [22].

Table 3. Partial protonic-decay widths of the $(1/2)^+$ isobaric analogous resonances in the nuclei of the Sb and I isotopes

Parent nucleus	s_ν^{expt} [23]	$\varepsilon^{\text{expt}}$, MeV*	Γ_ν^{expt}, keV [25]	Γ_ν^{expt}, keV [26]	Γ_ν^{calc}, keV
^{113}Sn	0.491	6.20		10.3 ± 2.1	12.4
^{115}Sn	0.430	6.35		8.0 ± 1.6	11.8
^{117}Sn	0.375	6.87	17.0 ± 0.5	16.5 ± 3.3	15.5
^{119}Sn	0.327	7.26		17.0 ± 3.4	17.0
^{121}Sn	0.285	7.57	17.0 ± 0.6	24.0 ± 4.8	17.2
^{123}Sn	0.249	7.82	18.4 ± 0.7	17.0 ± 3.4	16.4
^{125}Sn	0.220	8.07	11.7 ± 0.4	14.0 ± 2.8	15.7
^{125}Te	0.249	7.49		12.2 ± 2.4	11.6
^{127}Te	0.220	7.80		13.7 ± 2.7	11.8
^{129}Te	0.197	8.06		9.9 ± 2.0	11.7
^{131}Te	0.181	8.38		10.2 ± 2.0	12.0

* Results calculated on the basis of the compilation from [24].

Table 4. Partial protonic-decay widths of the $(3/2)^+$ isobaric analogous resonances in the nuclei of the Sb and I isotopes

Parent nucleus	ε^{expt}, MeV*	Γ_p^{expt}, keV [25]	Γ_p^{expt}, keV [26]	Γ_p^{calc} (s.p.), keV	s_p^{expt} (IAR)
^{117}Sn	7.02	7.5 ± 0.3		12.0	0.63
^{121}Sn	7.50	10.5 ± 0.7	7.5 ± 1.5	15.9	0.66/0.47
^{123}Sn	7.69	8.0 ± 0.5	7.0 ± 1.4	17.5	0.46/0.40
^{125}Sn	7.87	7.6 ± 0.3	9.0 ± 1.8	18.9	0.40/0.48
^{125}Te	7.52		4.8 ± 1.0	12.7	0.38
^{127}Te	7.73		5.7 ± 1.1	14.2	0.40
^{129}Te	7.87		6.2 ± 1.2	15.0	0.41
^{131}Te	8.07		8.5 ± 1.7	16.6	0.51

* Results calculated on the basis of the compilation from [24].

Table 5. Single-particle partial protonic-decay widths of the J^π isobaric analogous resonances in the nuclei of the In isotopes

Parent nucleus	J^π	ε^{expt}, MeV [25]	Γ_p^{expt}, keV [25]	Γ_p^{calc} (s.p.), keV	s_p^{expt} (IAR)	Parent nucleus	J^π	ε^{expt}, MeV [25]	Γ_p^{expt}, keV [25]	Γ_p^{calc} (s.p.), keV	s_p^{expt} (IAR)
^{111}Cd	$1/2^+$	6.44	15.5 ± 0.5	38.4	0.40	^{115}Cd	$1/2^+$	7.14	19.2 ± 0.5	58.5	0.33
	$5/2^+$	6.70	1.6 ± 0.2	10.8	0.15		$3/2^+$	7.36	9.8 ± 0.3	19.2	0.51
	$3/2^+$	6.80	5.0 ± 0.4	13.7	0.36	^{117}Cd	$1/2^+$	7.43	21 ± 1.0	67.6	0.31
^{113}Cd	$1/2^+$	6.80	19.0 ± 0.5	48.6	0.39		$3/2^+$	7.56	10.2 ± 0.5	21.2	0.48
	$3/2^+$	7.10	9.5 ± 0.5	17.0	0.56						

Table 6. Single-particle partial protonic-decay widths of the J^π isobaric analogous resonances in the nuclei of the Ag isotopes

Parent nucleus	J^π	ε^{expt}, MeV [27]	Γ_p^{expt}, keV [27]	Γ_p^{calc} (s.p.), keV	s_p^{expt} (IAR)
^{105}Pd	$5/2^+$	5.97	1.2 ± 0.2	7.5	0.16
	$1/2^+$	6.29	18 ± 0.1	45.4	0.40
	$3/2^+$	6.63	4.0 ± 0.4	16.7	0.24
	$1/2^+$	6.97	3.9 ± 0.5	77.0	0.05
^{107}Pd	$5/2^+$	6.42	2.0 ± 0.2	11.1	0.18
	$1/2^+$	6.51	19 ± 0.6	51.0	0.37
	$3/2^+$	6.81	4.0 ± 0.3	18.2	0.22
	$1/2^+$	6.86	1.6 ± 0.5	66.4	0.02
	$3/2^+$	6.91	1.9 ± 0.3	19.9	0.10
	$5/2^+$	7.01	1.0 ± 0.5	19.7	0.05
^{109}Pd	$5/2^+$	6.76	2.8 ± 0.3	13.7	0.20
	$1/2^+$	6.85	19 ± 0.4	62.4	0.30
	$1/2^+$	7.02	2 ± 0.5	70.0	0.03
	$3/2^+$	7.04	5.7 ± 0.5	20.8	0.27
^{111}Pd	$3/2^+$	7.07	3.6 ± 0.3	7.24	0.18
	$1/2^+$	7.11	15 ± 0.7	70.2	0.21
	$5/2^+$	7.25	4.8 ± 0.3	20.3	0.24
	$1/2^+$	7.26	5.4 ± 0.5	77.0	0.07
	$1/2^+$	7.53	24 ± 0.3	89.4	0.27
	$5/2^+$	7.78	3.9 ± 0.2	30.2	0.13

(ii) For the reason indicated above, estimating single-particle spectroscopic factors by comparing the experimental and the calculated values of the single-particle protonic widths of isobaric analogous resonances leads to results that also seem satisfactory.

(iii) Within the proposed method, the calculated single-particle protonic widths of isobaric analogous resonances show but a weak dependence on pairing.

The last circumstance has made it possible to include, in our analysis, a vast body of experimental data on partial protonic widths of isobaric analogous resonances.

4. "COULOMB DESCRIPTION" OF ISOBARIC ANALOGOUS AND ISOVECTOR GIANT MONOPOLE RESONANCES

Within the phenomenological version of the theory of finite Fermi systems, Eq. (1) makes it possible to formulate the theory of isobaric analogous resonances in medium-mass and heavy nuclei in terms of the mean Coulomb field of a nucleus. Proceeding from the definition of the Fermi strength function as given in (5) and using Eq. (1), we can represent $S_F(\omega)$ as

$$S_F(\omega) = \frac{S_C(\omega)}{|\omega - \Delta_C|^2},$$
$$S_C(\omega) = \sum_s |\langle s|\hat{V}_C^{(-)}|o\rangle|^2 \delta(E_s - E_o - \omega), \quad (19)$$

where $S_C(\omega)$ is the Coulomb strength function corresponding to the external field $\hat{V}_C^{(-)} = \sum_a V_C(r_a)\tau_a^{(-)}$. Within the CRPA, the Coulomb strength function $S_C(\omega) = \sum_\nu |M_\nu^C(\omega)|^2$ and the Coulomb reaction amplitude are determined by relations (6), (7), (12), and (13), where the operator $V_F = 1$ is replaced by the Coulomb operator $V_C(r) = U_C(r) - \Delta_C$. Comparing relations (19) at an energy ω close to ω_A with the first equation in (14), we arrive at

$$\Delta_C = \omega_A - \frac{i}{2}\Gamma, \quad \Gamma_\nu = 2\pi S_A^{-1}\left|M_\nu^C(\omega = \omega_A)\right|^2. \quad (20)$$

From (20), it follows that the Coulomb shift energy Δ_C has an imaginary part proportional to the total (protonic) width of the relevant isobaric analogous resonance, $\Gamma = \sum_\nu \Gamma_\nu$. This conclusion is the result of an accurate CRPA description in terms of the mean Coulomb field of a nucleus. That there is no resonance in the energy dependence of the Coulomb strength function $S_C(\omega)$ and the Coulomb effective field $\tilde{V}_C(r, \omega)$ and, hence, in the Coulomb reaction amplitude $M_\nu^C(\omega)$ at ω values in the vicinity of ω_A is an important point in this description. The absence of such resonances—in other words, the vanishing of the isobaric-analogous-resonance strength corresponding to the operator $\hat{V}_C^{(-)}$—follows from the first equation in (14) and from relations (19) and (20). We note that, apart from the term $\mathrm{Im}\Delta_C$, expression (20) for the width Γ_ν coincides in form with the corresponding expression from [6], since the Fermi strength of isobaric analogous resonances is close to $N - Z$.

The partial protonic widths Γ_ν of isobaric analogous resonances as calculated according to Eqs. (14) and (20) coincide, provided that the isovector self-consistency condition is satisfied. However, the description of processes forbidden in isospin in terms of the variable part of the mean Coulomb field $V_C(r)$ of a nucleus is preferable (in this connection, see [2, 3]).

The Coulomb strength function $S_C^{(-)}(\omega)$ calculated within the CRPA for a sufficiently wide energy interval shows a broad isovector giant monopole resonance associated with the β^- charge-exchange channel (IVGMR$^{(-)}$), its mean energy $\omega^{(-)}$ being about 40 MeV. Naturally, there also exists a similar resonance associated with the inverse (β^+) charge-exchange channel (IVGMR$^{(+)}$). The latter manifests itself as a maximum in the energy dependence of the strength function $S_C^{(+)}(\omega')$ corresponding to the operator $\hat{V}_C^{(+)} = \sum_a V_C(r_a)\tau_a^{(+)}$. We note that the CRPA equations (6)–(8) are invariant under the simultaneous substitutions $n \rightleftarrows p$ and $\omega \longrightarrow -\omega$, so that $\omega' = -\omega$ is the excitation energy in the β^+ channel of the isobaric nucleus. This energy is also reckoned from the ground state of the parent nucleus. In general, the model-dependent non-energy-weighted sum rule of the form (2),

$$(\mathrm{NEWSR})_V = \sum_s \left|\langle s|\hat{V}^{(-)}|o\rangle\right|^2 - \sum_{s'} \left|\langle s'|\hat{V}^{(+)}|o\rangle\right|^2 = \int V^2(r) n^{(-)} d\mathbf{r}, \quad (21)$$

is satisfied for charge-exchange excitations.

In order to describe the properties of IVGMR$^{(\mp)}$, one usually studies the energy dependence of the monopole strength functions $S_M^{(\mp)}$ corresponding to the operators $r^2\tau^{(\mp)}$. The strength of a charge-exchange giant resonance is characterized by the ratio $x_V^{(\mp)} = \int S_V^{(\mp)}(\omega)d\omega/(\mathrm{NEWSR})_V$, where the integral is taken over a rather broad vicinity of the resonance maximum. The quantity $x_M^{(-)}$ is small, since the isobaric analogous resonance saturates a major part of the monopole strength. At the same time, the relative Coulomb strength $x_C^{(-)}$ of IVGMR$^{(-)}$ is maximal, since the Coulomb strength of isobaric analogous resonances is equal to zero. Within the CRPA, we have calculated not only the Coulomb strength functions $S_C^{(\mp)}(\omega)$ but also the mean energies $\omega^{(\mp)} = \int \omega S_C^{(\mp)}(\omega)d\omega / \int S_C^{(\mp)}(\omega)d\omega$ and the relative Coulomb strengths of IVGMR$^{(\mp)}$ for some parent nuclei where IVGMR$^{(\mp)}$ excitation was studied experimentally [9, 10]. The results of the calculations performed by using the model-parameter values quoted in Section 3 are compiled in Table 7. Also presented in this table for the sake of comparison are the results obtained for the same IVGMR$^{(\mp)}$ parameters from a CRPA analysis of the monopole strength functions $S_M^{(\mp)}$ that was performed by using the Hartree–Fock mean field and Skyrme forces [28]. The experimental values of the IVGMR$^{(\mp)}$ energies, $\omega_{\mathrm{expt}}^{(\mp)}$, were borrowed from [9]. From the quoted data, it follows that, by and large, the results of our calculations satisfactorily reproduce the resonance energies. As might have been expected, the relative Coulomb strength of IVGMR$^{(\mp)}$ proved to be much greater than the corresponding monopole strength.

The IVGMR$^{(-)}$ width obtained within the CRPA proved to be somewhat less than the experimental width. Since the excitation energy of IVGMR$^{(-)}$ is high, the last result is not unexpected, implying that, in contrast to what occurs for known giant resonances, the probability of a direct protonic decay of IVGMR$^{(-)}$ is

Table 7. Energies and relative strengths calculated for isovector monopole giant resonances associated with the β^- and β^+ charge-exchange channels

Nucleus	$x_C^{(-)}$	$x_M^{(-)}$ [28]	$\omega^{(-)}$	$\omega^{(-)}$ [28]	$\omega_{expt}^{(-)}$ [9]	$x_C^{(+)}$	$x_M^{(+)}$ [28]	$\omega^{(+)}$	$\omega^{(+)}$ [28]	$\omega_{expt}^{(+)}$ [9]
	%		MeV			%		MeV		
^{90}Zr	228	51	42.1	42.3	34.6 ± 2.9	123	54	22.3	22.9	22.0 ± 2.0
^{120}Sn	166	33	38.2	39.6	30.0 ± 3.0	72	17	23.4	22.4	21.4 ± 2.2
^{140}Ce	138	–	40.2	–	35.4 ± 3.5	36	–	20.3	–	19.9 ± 2.4
^{208}Pb	121	18	40.3	43.5	37.2 ± 3.5	20	9	14.7	16.3	12.0 ± 2.8

rather high. In order to evaluate this probability, it is necessary to take into account the contribution to the total resonance width from the effect of coupling to multiparticle configurations. Following [8, 11], we take into account this coupling in terms of a phenomenological quantity I defined as the mean fragmentation widths of 0^+ doorway states of the *proton + neutron hole* type that form IVGMR$^{(-)}$. The energy-averaged Coulomb strength function $\bar{S}_C(\omega)$ and the energy-averaged Coulomb reaction amplitude $\overline{M}_\nu^C(\omega)$ can be found with the aid of CRPA equations of the form (6)–(8), (12), and (13), where the substitution $\omega \longrightarrow \omega + \frac{i}{2}I$ is made. The quantity I is found by comparing, for each nucleus, the total resonance width in the energy dependence $\bar{S}_C(\omega)$ with the experimental width Γ^{expt}. The I values found in this way proved to be relatively small (see Table 8), which results in a large probability of the direct protonic decay of IVGMR$^{(-)}$. The relevant partial and the total branching ratio were calculated by the formulas [11]

$$b_\nu = \frac{\int \left|\overline{M}_\nu^C(\omega)\right|^2 d\omega}{\int \bar{S}_C(\omega) d\omega}, \quad b = \sum_\nu b_\nu. \qquad (22)$$

The calculated b values are quoted in Table 8. In these calculations, the reduced spectroscopic factors S_ν were taken to be unity for all neutron-hole states of product nuclei. For the isovector spin-monopole resonance in the parent nucleus ^{208}Pb, a similar result for b was obtained in [29].

Table 8. Calculated total probability of the direct protonic decay of isovector giant monopole resonances associated with the β^- charge-exchange channel

Nucleus	Γ^{expt}, MeV [9]	I, MeV	b, %
^{90}Zr	18.9 ± 4.1	1.8	89
^{120}Sn	16.0 ± 4.1	3.0	76
^{140}Ce	16.6 ± 4.2	3.2	76
^{208}Pb	15.0 ± 6.0	4.0	70

5. CONCLUSION

On the basis of the continuum random-phase approximation and the phenomenological partly self-consistent version of the theory of finite Fermi systems, we have proposed a description of a direct protonic decay of isobaric analogous and isovector giant monopole resonances in medium-mass and heavy nuclei.

The partial protonic widths of isobaric analogous resonances have been computed by using the experimental values of decay-channel energies and of single-particle spectroscopic factors (the latter being found from the cross sections for relevant one-nucleon-transfer reactions). For nuclei in a wide range of atomic masses, the results are in satisfactory agreement with experimental widths. In this connection, an attempt made here to determine single-particle spectroscopic factors by comparing the calculated partial protonic widths of isobaric analogous resonance with the corresponding experimental widths seems viable. In our opinion, a practical implementation of this possibility also requires estimating relevant experimental data.

The use of the isovector self-consistency condition has enabled us to formulate a method for describing isobaric analogous and isovector giant monopole resonances in terms of the mean Coulomb field of a nucleus. On the basis of this method, we have shown, among other things, that, in contrast to other giant resonances in the β^- channel (for example, Gamow–Teller and spin–dipole resonances), IVGMR$^{(-)}$ are strongly coupled to a single-particle continuum. Estimates of the probability of direct protonic decay confirm the above conclusion and make it possible to understand why IVGMR$^{(-)}$ (as well as the corresponding spin-monopole resonances [29]) can be observed in the protonic channel of a reaction involving the excitation of this resonance [10].

ACKNOWLEDGMENTS

We are grateful to M. Fujiwara, M.N. Harakeh, V.A. Rodin, O.A. Rumyantsev, and A.G. Zvenigorod-

skiĭ for stimulating discussions and enlightening comments.

REFERENCES

1. A. B. Migdal, *Theory of Finite Fermi Systems and Applications to Atomic Nuclei* (Nauka, Moscow, 1983).
2. N. Auerbach, Phys. Rep. **98**, 273 (1983).
3. V. G. Guba and M. G. Urin, Nucl. Phys. A **460**, 222 (1986).
4. G. Colo *et al.*, Phys. Rev. C **50**, 1496 (1994).
5. D. P. Knobles, S. A. Stotts, and T. Udagawa, Phys. Rev. C **52**, 2257 (1995).
6. O. A. Rumyantsev and M. G. Urin, Yad. Fiz. **56** (2), 99 (1993) [Phys. At. Nucl. **56**, 203 (1993)]; O. A. Rumyantsev and M. H. Urin, Phys. Rev. C **49**, 537 (1994).
7. B. L. Birbrair and V. A. Sadovnikova, Yad. Fiz. **20**, 645 (1974) [Sov. J. Nucl. Phys. **20**, 347 (1975)].
8. S. E. Murav'ev and M. G. Urin, Yad. Fiz. **55**, 2688 (1992) [Sov. J. Nucl. Phys. **55**, 1501 (1992)]; S. E. Muraviev and M. H. Urin, Nucl. Phys. A **572**, 267 (1994).
9. A. Erell *et al.*, Phys. Rev. C **34**, 1822 (1986).
10. R. G. T. Zegers *et al.*, Phys. Rev. Lett. **84**, 3779 (2000).
11. E. A. Moukhai, V. A. Rodin, and M. H. Urin, Phys. Lett. B **447**, 8 (1999).
12. M. L. Gorelik *et al.*, Izv. Akad. Nauk, Ser. Fiz. **63**, 883 (1999).
13. M. L. Gorelik and M. H. Urin, submitted to Phys. Rev. C.
14. O. A. Rumyantsev and M. H. Urin, Phys. Lett. B **443**, 51 (1998).
15. M. G. Urin, *Relaxation of Nuclear Excitations* (Énergoatomizdat, Moscow, 1991).
16. V. G. Solov'ev, *Theory of the Nucleus: Nuclear Models* (Énergoizdat, Moscow, 1981).
17. M. G. Urin, Zh. Éksp. Teor. Fiz. **38**, 1852 (1960) [Sov. Phys. JETP **11**, 1331 (1960)].
18. A. Bohr and B. R. Mottelson, *Nuclear Structure*, Vol. 1: *Single-Particle Motion* (Benjamin, New York, 1969; Mir, Moscow, 1971).
19. C. A. Whitten, Phys. Rev. **188**, 1941 (1969).
20. S. Y. van der Werf, M. N. Harakeh, and E. N. M. Quint, Phys. Lett. B **216**, 15 (1989).
21. A. Likar and T. Vidmar, Nucl. Phys. A **615**, 18 (1997).
22. K. P. Lieb *et al.*, Phys. Lett. B **32B**, 273 (1970).
23. J. Janecke *et al.*, Nucl. Phys. A **552**, 323 (1993).
24. M. S. Antony, J. Britz, and A. Pape, At. Data Nucl. Data Tables **66**, 1 (1997).
25. B. Ya. Guzhovskiĭ *et al.*, Yad. Fiz. **21**, 930 (1975) [Sov. J. Nucl. Phys. **21**, 478 (1975)].
26. P. Richard *et al.*, Phys. Rev. **145**, 971 (1966); J. L. Foster *et al.*, Phys. Rev. **175**, 1498 (1968).
27. B. Ya. Guzhovskiĭ *et al.*, Yad. Fiz. **20**, 449 (1974) [Sov. J. Nucl. Phys. **20**, 242 (1975)].
28. N. Auerbach and A. Klein, Nucl. Phys. A **395**, 77 (1983).
29. V. A. Rodin and M. H. Urin, Contribution to the International Conference on Giant Resonances, Osaka, 2000.

Translated by A. Isaakyan

Physics of Atomic Nuclei, Vol. 64, No. 3, 2001, pp. 516–524. Translated from Yadernaya Fizika, Vol. 64, No. 3, 2001, pp. 570–578.

90th ANNIVERSARY OF A.B. MIGDAL'S BIRTHDAY
NUCLEI

Variations on the Deuteron Theme

I. B. Khriplovich*

Budker Institute of Nuclear Physics, Siberian Division, Russian Academy of Sciences, Novosibirsk, 630090 Russia, and Novosibirsk State University, Novosibirsk, Russia

Received July 27, 2000

Abstract—Several problems concerning the deuteron and having simple analytic solutions are considered. The relation between the electric quadrupole moment of the deuteron and the *np* scattering amplitude is established. The degree of the circular polarization of the photon emitted in the radiative capture of longitudinally polarized thermal neutrons is found. The anapole, electric dipole, and magnetic quadrupole moments of the deuteron are calculated. © *2001 MAIK "Nauka/Interperiodica".*

Dedicated to the memory of Arkadiĭ Benediktovich Migdal, the teacher of my teachers.

1. INTRODUCTION

Let us recall the classical question of Fermi: "What plays the role of the hydrogen atom in this problem?" In what is concerned with nuclear physics, this is of course the deuteron.

It is surprising how many nontrivial problems associated with the deuteron can be solved by means of sufficiently simple, sometimes quite elementary, analytic calculations. This is because the deuteron binding energy of $\varepsilon = 2.23$ MeV is anomalously small on the nuclear scale. As a result, the deuteron wave function decreases very slowly beyond the range of nuclear forces. At large distances, the asymptotic behavior of this wave function can be described as $e^{-\kappa r}$, where the parameter κ is small, $\kappa = \sqrt{m_p \varepsilon} = 45.7$ MeV (m_p is the proton mass). Accordingly, the typical length over which the wave function dies out is large, $\kappa^{-1} = 4.3$ fm; it is much larger than the range of nuclear forces, $r_0 \sim 1$ fm. This enables us to use the deuteron wave function in the so-called zero-range (with respect to nuclear forces) approximation, where it assumes the form of its asymptotic expression

$$\psi_d = \sqrt{\frac{\kappa}{2\pi}}\frac{e^{-\kappa r}}{r}, \qquad (1)$$

the factor $\sqrt{\kappa/2\pi}$ ensuring fulfillment of the standard normalization condition $\int d\mathbf{r}\,\psi_d^2 = 1$.

This article presents some results recently obtained on the basis of the zero-range approximation. Although the problems that will be considered here are associated with the deuteron, they have some bearing on various realms, including traditional nuclear physics and the problem of *P* and *T* nonconservation.

It is convenient, however, to begin by briefly discussing a few well-known problems that have long since been included in textbooks or even belong to physics folklore. The deuteron ground state involves, in addition to the $^3S_1$ wave, a small admixture of the $^3D_1$ wave, which can be disregarded, however, in many particular cases. In the low-energy limit, the wave function of the $^3S_1$ triplet state of the continuous spectrum of the neutron–proton system can be represented as

$$\psi_{St} = 1 - \frac{\alpha_t}{r}, \qquad (2)$$

where $\alpha_t = 5.42$ fm is the triplet scattering length. The analogous expression for the $^1S_0$ singlet wave function of the continuous spectrum has the form

$$\psi_{Ss} = 1 - \frac{\alpha_s}{r}. \qquad (3)$$

The singlet scattering length is negative and very large in magnitude, $\alpha_s = -23.7$ fm. Hereafter, the subscript *S* on the wave function indicates the *S* wave, while the subscripts *t* and *s* label quantities referring to the triplet and the singlet state, respectively. Somewhat more precise expressions for the wave functions of the *S*-wave state of the continuous spectrum—those that take into account the relative momentum *p* of scattered particles, which is small in relation to $1/r_0$, but which is not small in relation to $1/\alpha_{t,s}$—can be written as [1]

$$\psi_{St,Ss} = \frac{\sin pr}{pr} - \frac{\alpha_{t,s}}{1 + ip\alpha_{t,s}}\frac{e^{ipr}}{r}. \qquad (4)$$

The simplest of the aforementioned classical results concerns the relation between the deuteron binding energy and the triplet scattering length. From the

*e-mail: khriplovich@inp.nsk.su

orthogonality of the triplet wave functions (1) and (2) corresponding to different energy values, it immediately follows that

$$\alpha_t = \frac{1}{\kappa}, \quad \text{or} \quad \alpha_t = \frac{1}{\sqrt{m_p \varepsilon}}. \tag{5}$$

This relation is correct to within 20%.

Let us further consider the cross section for the deuteron-photodisintegration process $\gamma d \longrightarrow np$. It is natural to begin by discussing the contribution of the $E1$ transition [2, 3]. The relevant matrix element is

$$\langle {}^3P|\mathbf{r}|{}^3S\rangle = -4\sqrt{\frac{2\pi\kappa}{1-\kappa r_t}}\,\frac{\mathbf{p}}{(\kappa^2+p^2)^2}. \tag{6}$$

The corresponding contribution to the cross section is

$$\sigma_{E1} = \frac{8\pi\alpha}{3}\frac{\kappa p^3}{(1-\kappa r_t)(\kappa^2+p^2)^3}, \tag{7}$$

where $\alpha = 1/137$ is the fine-structure constant. The result of a straightforward calculation with the wave function (1) was supplemented here with the correction factors $(1-\kappa r_t)^{-1/2}$ in the matrix element (6) and the corresponding correction factor $(1-\kappa r_t)^{-1}$ in the cross section (7), where $r_t = 1.76$ fm is the so-called effective interaction range. The origin of this correction, which is in fact not small ($1-\kappa r_t = 0.59$), is the following. The matrix element (6) is dominated by the contribution of large distances, where the inclusion of the effective range modifies the asymptotic behavior of the deuteron wave function precisely in this way [3, 4]. As usual, the cross section for the $E1$ transition near the threshold is proportional to p^3.

At the same time, the $M1$ contribution to the deuteron-photodisintegration cross section decreases in proportion to first power of p in the threshold region, so that it is dominant in the immediate neighborhood of the threshold [5]. We now consider this contribution. Since the orbital angular momentum of the nucleons in the deuteron is zero (we neglect here the admixture of the D wave), the magnetic-moment operator reduces to the purely spin one,

$$\mathbf{M} = \frac{e}{2m_p}(\mu_p\boldsymbol{\sigma}_p + \mu_n\boldsymbol{\sigma}_n).$$

Here, $\boldsymbol{\sigma}_p$ and $\boldsymbol{\sigma}_n$ are the proton and the neutron spin operator, respectively, and $\mu_p = 2.79$ and $\mu_n = -1.91$ are the corresponding magnetic moments. Since the deuteron wave function is orthogonal to the wave function of the ${}^3S_1$ positive-energy state, the $M1$ transition proceeds to the ${}^1S_0$ singlet state of the continuous spectrum. A simple calculation yields [3, 5]

$$\langle {}^1S_0|(\mu_p\sigma_p + \mu_n\sigma_n)_z|{}^3S_1\rangle = \frac{2\sqrt{2\pi\kappa}(\mu_p-\mu_n)(1-\kappa\alpha_s)}{(\kappa^2+p^2)(1-ip\alpha_s)}. \tag{8}$$

Accordingly, we have

$$\sigma_{M1} = \frac{2\pi\alpha}{3}\frac{\kappa p(\mu_p-\mu_n)^2(1-\kappa\alpha_s)^2}{m_p^2(\kappa^2+p^2)(1+p^2\alpha_s^2)}. \tag{9}$$

Although this contribution to the cross section is enhanced by the large numerical factors of $\mu_p - \mu_n = 4.7$ and $1 - \kappa\alpha_s = 6.5$, it is dominant only within the region of 0.2 MeV above the threshold.

Having completed this rather lengthy introduction, we now proceed to put forth the basic matters of this review article.

2. AMPLITUDE FOR *np* SCATTERING AND DEUTERON QUADRUPOLE MOMENT

In just the same way as the triplet scattering length α_t is related to the asymptotic behavior of the ${}^3S_1$ deuteron wave function for $r \longrightarrow \infty$—that is, with the parameter κ [see Eq. (5)]—the limiting threshold values of the spin-dependent invariant amplitudes are related to the asymptotic value of the ${}^3D_1$ admixture in the deuteron wave function [6].

We proceed from the *np*-scattering amplitude as given by a standard expression that is valid if P and T invariance are not violated and if nuclear forces are independent of charge (see [7]). Specifically, we have

$$\begin{aligned} f(\mathbf{p}',\mathbf{p}) = {} & a + b(\boldsymbol{\sigma}_1\cdot\mathbf{n})(\boldsymbol{\sigma}_2\cdot\mathbf{n}) + c(\boldsymbol{\sigma}_1+\boldsymbol{\sigma}_2)\cdot\mathbf{n} \\ & + (g+h)(\boldsymbol{\sigma}_1\cdot\mathbf{n}_+)(\boldsymbol{\sigma}_2\cdot\mathbf{n}_+) \\ & + (g-h)(\boldsymbol{\sigma}_1\cdot\mathbf{n}_-)(\boldsymbol{\sigma}_2\cdot\mathbf{n}_-), \end{aligned} \tag{10}$$

where $\mathbf{p}$ and $\mathbf{p}'$ are, respectively, the initial and the final relative momentum of the nucleons in the c.m. frame; $\boldsymbol{\sigma}_1$ and $\boldsymbol{\sigma}_2$ are the nucleon spin operators; and

$$\mathbf{n}_\pm = \frac{\mathbf{p}\pm\mathbf{p}'}{|\mathbf{p}\pm\mathbf{p}'|}, \quad \mathbf{n} = \frac{\mathbf{p}\times\mathbf{p}'}{|\mathbf{p}\times\mathbf{p}'|}.$$

With the aid of the obvious relation $(\boldsymbol{\sigma}_1\cdot\mathbf{n})(\boldsymbol{\sigma}_2\cdot\mathbf{n}) = \boldsymbol{\sigma}_1\cdot\boldsymbol{\sigma}_2 - (\boldsymbol{\sigma}_1\cdot\mathbf{n}_+)(\boldsymbol{\sigma}_2\cdot\mathbf{n}_+) - (\boldsymbol{\sigma}_1\cdot\mathbf{n}_-)(\boldsymbol{\sigma}_2\cdot\mathbf{n}_-)$, we can eliminate the structure $(\boldsymbol{\sigma}_1\cdot\mathbf{n})(\boldsymbol{\sigma}_2\cdot\mathbf{n})$ from (10). We further use the momenta $\mathbf{p}$ and $\mathbf{p}'$ instead of the unit vectors $\mathbf{n}_\pm$ and go over from the operators $\boldsymbol{\sigma}_1$ and $\boldsymbol{\sigma}_2$ to the total-spin operator $\mathbf{S} = \frac{1}{2}(\boldsymbol{\sigma}_1+\boldsymbol{\sigma}_2)$ (the latter is done since we are interested in triplet scattering). As a result, the triplet *np* scattering amplitude assumes the form

$$\begin{aligned} f(\mathbf{p}',\mathbf{p}) = {} & -\alpha_t + \frac{1}{m_p^2}\{c'\mathbf{S}\cdot[\mathbf{p}'\times\mathbf{p}] \\ & + g_1(\mathbf{S}\cdot(\mathbf{p}'+\mathbf{p}))^2 + g_2(\mathbf{S}\cdot(\mathbf{p}'-\mathbf{p}))^2\}, \end{aligned} \tag{11}$$

where the triplet scattering length is related to the parameters in (10) by the equation $\alpha_t = -(a+b)$, while

the constants

$$c' = \frac{2cm_p^2}{p^2\sin\theta}, \quad g_1 = \frac{(g-b+h)m_p^2}{2p^2\cos^2(\theta/2)},$$
$$g_2 = \frac{(g-b-h)m_p^2}{2p^2\sin^2(\theta/2)}$$

are independent of the scattering angle θ, in just the same way as α_t. As a matter of fact, expression (11) represents the momentum expansion of the scattering amplitude, where only spin-dependent higher order terms are retained along with α_t.

We now proceed to construct the deuteron wave function at large r, allowing for the D-wave admixture. We begin by determining the effective delta-function potential (pseudopotential) $U(\mathrm{r})$ that reproduces the scattering amplitude (11) in the Born approximation (see [8]). Taking into account the relation

$$p_i'p_j' \longrightarrow -\nabla_i\nabla_j\delta(\mathbf{r}), \quad p_i'p_j \longrightarrow -\nabla_i\delta(\mathbf{r})\nabla_j,$$
$$p_ip_j \longrightarrow -\delta(\mathbf{r})\nabla_i\nabla_j,$$

we obtain

$$U(\mathbf{r}) = \frac{4\pi}{m_p}\left\{\alpha_t\delta(\mathbf{r}) + \frac{c'}{m_p^2}\varepsilon_{ijk}S_i\nabla_j\delta(\mathbf{r})\nabla_k\right.$$
$$+\frac{1}{2m_p^2}S_{ij}[(g_1+g_2)(\nabla_i\nabla_j\delta(\mathbf{r})+\delta(\mathbf{r})\nabla_i\nabla_j) \qquad (12)$$
$$\left.+(g_1-g_2)(\nabla_i\delta(\mathbf{r})\nabla_j+\nabla_j\delta(\mathbf{r})\nabla_i)]\right\},$$

where

$$S_{ij} = S_iS_j + S_jS_i - \frac{4}{3}\delta_{ij}.$$

In the wave function for the scattering problem, the diverging spherical wave can be represented as

$$-\frac{m_p}{4\pi}\int d\mathbf{r}'\frac{e^{ip|\mathbf{r}-\mathbf{r}'|}}{|\mathbf{r}-\mathbf{r}'|}U(\mathbf{r}')\Psi_0(\mathbf{r}'). \qquad (13)$$

The unperturbed solution Ψ_0 is assumed to be the S-wave one. In this case, expression (13) can be reduced to the form

$$-\left(\alpha_t + \frac{g_1+g_2}{2m_p^2}S_{ij}\nabla_i\nabla_j\right)\frac{e^{ipr}}{r}. \qquad (14)$$

By constructing an analytic continuation of the wave function (14) to the point $p = i\kappa$ corresponding to the bound state, we find that, at large distances, the deuteron wave function assumes the form

$$\Psi_d = \sqrt{\frac{\kappa}{2\pi}}\left(1+\frac{g_1+g_2}{2\alpha_tm_p^2}S_{ij}\nabla_i\nabla_j\right)\frac{e^{-\kappa r}}{r}. \qquad (15)$$

The expectation value of the quadrupole-moment tensor for this state is

$$Q_{ij} = \frac{1}{4}\langle 3r_ir_j - r^2\delta_{ij}\rangle = \frac{g_1+g_2}{2\alpha_tm_p^2}S_{ij}. \qquad (16)$$

Consequently, the deuteron quadrupole moment is given by

$$Q = Q_{zz}|_{S_z=1} = \frac{g_1+g_2}{3\alpha_tm_p^2}. \qquad (17)$$

Since the main contribution to Q comes from distances $r \sim 1/\kappa$, it is not necessary to introduce the correction factors $(1-\kappa r_t)^{-1/2}$ and $(1-\kappa r_t)^{-1}$ in expressions (15) and (16), respectively.

An analysis of experimental data on elastic dp scattering and on the stripping reaction yields [6, 9]

$$g_1 + g_2 = 67 \text{ fm}. \qquad (18)$$

The corresponding value of the deuteron quadrupole moment is

$$Q_1 = 0.18 \text{ fm}^2. \qquad (19)$$

The phase-shift analysis of np scattering leads to somewhat larger values [10]:

$$Q_1 = 0.20\text{–}0.24 \text{ fm}^2. \qquad (20)$$

At least the last result, that in (20), is not very far from the data of a direct experimental measurement of the deuteron quadrupole moment,

$$Q = 0.286 \text{ fm}^2. \qquad (21)$$

Of course, the accuracy of the direct experimental result (21) for the deuteron quadrupole moment is much higher than that of approximations made to derive (17) and than that of the phase-shift analysis of the aforementioned elastic processes and of the stripping reaction. It follows that, apart from being of purely theoretical interest, the relations obtained here can also be used predominantly to test the phenomenological description of the these reactions.

3. CIRCULAR POLARIZATION OF PHOTONS IN THE REACTION $np \longrightarrow d\gamma$ INDUCED BY POLARIZED NEUTRONS

Deuteron photodisintegration at the threshold occurs into the $^1S_0$ wave of the continuous spectrum; likewise, the radiative capture of thermal neutrons through the process $np \longrightarrow d\gamma$ proceeds from the same $^1S_0$ state via an $M1$ transition. It is clear that, within this

approximation, the polarization of an initial particle cannot be transferred to the final particle since the initial state is a pure $^1S_0$ state, which possesses exact spherical symmetry. Owing to the *D*-wave admixture in the deuteron wave function and in the incident wave, the *M*1 transition can proceed, however, from the triplet initial state as well. Moreover, the magnetic dipole transition from the triplet initial state is also induced by corrections to the *M*1 operator that are responsible for the nonadditivity of the magnetic moments of the nucleons in the deuteron. Finally, the *D*-wave admixture opens the possibility for a *E*2 transition to occur in this case. All relevant effects are quite small, but an analysis of these effects may furnish information about some subtle details of the *np* interaction at low energies.

The circular polarization of the photons emitted in the radiative capture of polarized thermal neutrons by unpolarized protons, $np \longrightarrow d\gamma$, was first measured in [11]. The result obtained there,

$$P_\gamma = -(2.90 \pm 0.87) \times 10^{-3},$$

was significantly improved in a more recent study of the same group [12],

$$P_\gamma = -(1.5 \pm 0.3) \times 10^{-3}. \quad (22)$$

This problem was theoretically considered in [13–18]. The present review article follows predominantly [13, 16].

We begin by considering the magnetic-moment operator

$$\mathbf{M} = \frac{e}{2m_p}(\mathbf{l}_p + \mu_p\boldsymbol{\sigma}_p + \mu_n\boldsymbol{\sigma}_n).$$

The orbital angular momentum of the proton, $\mathbf{l}_p$, is related to the total orbital angular momentum $\mathbf{L}$ by the obvious equation $\mathbf{l}_p = (1/2)\mathbf{L}$. It is convenient to represent the above linear combination of $\mathbf{L}$ and $\boldsymbol{\sigma}_{p,n}$ in the form

$$\frac{1}{2}\mathbf{L} + \mu_p\boldsymbol{\sigma}_p + \mu_n\boldsymbol{\sigma}_n = \frac{1}{2}\left(\mathbf{L} + \frac{1}{2}\boldsymbol{\sigma}_p + \frac{1}{2}\boldsymbol{\sigma}_n\right) + \frac{1}{2}(\mu_p - \mu_n)(\boldsymbol{\sigma}_p - \boldsymbol{\sigma}_n) + \frac{1}{2}\left(\mu_p + \mu_n - \frac{1}{2}\right)(\boldsymbol{\sigma}_p + \boldsymbol{\sigma}_n). \quad (23)$$

The first term on the right-hand side of Eq. (23) is nothing but half of the total angular momentum $\mathbf{I}$; being an integral of the motion, it cannot induce any transitions. The second term is responsible for the ordinary *M*1 transition from the $^1S_0$ state of the continuous spectrum—that is, for the process inverse to deuteron photodisintegration at the threshold. The effective operator of this (dominant) *M*1 transition, the coordinate matrix element of the second term, has the form

$$\hat{\mathbf{M}}_0 = \frac{e}{2m_p}\frac{1}{2}(\mu_p - \mu_n)\sqrt{2\pi\kappa}\frac{1 - \kappa\alpha_s}{\kappa^2}(\boldsymbol{\sigma}_p - \boldsymbol{\sigma}_n). \quad (24)$$

As to the last term on the right-hand side of (23), its matrix element differs from zero owing, above all, to the $^3D_1$ admixture to the deuteron wave function and to the $^3S_1$ state of the continuous spectrum (ψ_d and ψ_{St}, respectively). In order to calculate this matrix element, we use the orthogonality of the total radial wave functions of the two states,

$$\int_0^\infty dr r^2(R_{d0}R_{t0} + R_{d2}R_{t2}) = 0. \quad (25)$$

Here, the subscripts 0 and 2 label the radial functions of the *S*- and *D*-wave components of the initial and the final state, respectively. Taking into account (25), we easily obtain the required matrix element. The result is

$$\frac{1}{2}\left(\mu_p + \mu_n - \frac{1}{2}\right)\langle\boldsymbol{\sigma}_p + \boldsymbol{\sigma}_n\rangle = -\frac{3}{2}\left(\mu_p + \mu_n - \frac{1}{2}\right)\mathbf{I}\int_0^\infty dr r^2 R_{d2}R_{t2}. \quad (26)$$

The remaining radial integral is dominated by the distances that are smaller than the range of nuclear forces. It is reasonable to assume [13] that, at these distances, the functions R_{d2} and R_{t2} differ by only a normalization factor; that is,

$$R_{t2} = -\alpha_t\sqrt{\frac{2\pi}{\kappa}}R_{d2}.$$

The matrix element (26) then reduces to

$$\frac{3}{2}\left(\mu_p + \mu_n - \frac{1}{2}\right)\alpha_t P_d\mathbf{I}, \quad (27)$$

where P_d is the weight of the *D* wave in the deuteron.

The deuteron magnetic moment μ_d is given by the well-known expression

$$\mu_d = \mu_p + \mu_n - \frac{3}{2}\left(\mu_p + \mu_n - \frac{1}{2}\right)P_d + \Delta\mu, \quad (28)$$

its numerical value being $\mu_d = 0.8574$. Along with the corrections for the *D*-wave admixture (term involving P_d), μ_d includes relativistic corrections represented by $\Delta\mu$. Naturally, the matrix elements of relevant operators are also dominated by small distances. Again, we assume that, at these distances, the wave function of the $^3S_1$ state of the continuous spectrum differs from the deuteron wave function only by a factor. The coordinate matrix element of the operator for the relevant triplet–triplet transition is then given by

$$-\alpha_t\sqrt{\frac{2\pi}{\kappa}}\Delta\mu\mathbf{I}.$$

The resulting total effective operator for the triplet–triplet *M*1 transition has the form

$$\hat{\mathbf{M}} = \frac{e}{2m_p}\left[\frac{3}{2}\left(\mu_p + \mu_n - \frac{1}{2}\right)P_d - \Delta\mu\right]\alpha_t\sqrt{\frac{2\pi}{\kappa}}\mathbf{I}. \quad (29)$$

By virtue of (28), it can be rearranged as

$$\hat{\mathbf{M}} = \frac{e}{2m_p}(\mu_p + \mu_n - \mu_d)\alpha_t\sqrt{\frac{2\pi}{\kappa}}\mathbf{I}. \quad (30)$$

For the $M1$ contribution to the degree of circular photon polarization, a standard calculation that employs expression (24) for the dominant transition yields

$$P_\gamma(M1) = -\frac{\mu_p + \mu_n - \mu_d}{\mu_p - \mu_n}\frac{\kappa\alpha_t}{1-\kappa\alpha_s} = -0.92\times 10^{-3}. \quad (31)$$

Yet another contribution to the circular polarization of product photons comes from the quadrupole transition. Here, the $E2$ operator has the form

$$V = -\frac{1}{8}er_m r_n \partial_m E_n .$$

Recall that the proton coordinate $\mathbf{r}_p$ and the argument $\mathbf{r}$ of the wave function are related by the equation $\mathbf{r}_p = \mathbf{r}/2$. For the quadrupole contribution to the circular polarization, the result of a standard calculation with the wave functions (14) and (15) is

$$P_\gamma(E2) = -\frac{2}{15}\frac{\kappa^3(g_1+g_2)}{m_p^2(1-\kappa\alpha_s)(\mu_p-\mu_n)} = -\frac{2}{5}\frac{\alpha_t\kappa^3 Q}{(1-\kappa\alpha_s)(\mu_p-\mu_n)} = -0.25\times 10^{-3}. \quad (32)$$

Our final result,

$$P_\gamma = P_\gamma(M1) + P_\gamma(E2) = -1.1\times 10^{-3}, \quad (33)$$

is in reasonable agreement with the experimental result in (22). Also, there is good agreement between (33) and the eventual results from [17, 18], although the present results for $P_\gamma(M1)$ and $P_\gamma(E2)$ taken separately differ considerably from the corresponding results in those articles.

4. *P*- AND *T*-ODD ELECTROMAGNETIC MOMENTS OF THE DEUTERON

4.1. Generalities on the Anapole Moments

The concept of the anapole moment was introduced by Vaks (who was then a postgraduate student of A.B. Migdal) and independently by Zeldovich [19]. The anapole moment is some electromagnetic feature peculiar to systems where parity is not conserved.

It is characteristic of the anapole moment that its interaction with a charged test particle is of a contact character (for a more detailed discussion, see, for example, [20]). It follows that, for example, the interaction between an electron and the nucleon anapole moment—it is of order αG (G is Fermi constant of weak interaction)—cannot be distinguished, in general, from other radiative corrections to weak electron–nucleon interaction. This has far-reaching consequences because, within the gauge theory of electroweak interactions, only the total scattering amplitude—that is, the sum of all diagrams of order αG—is a gauge-invariant quantity (specifically, a quantity that is independent of the choice of gauge for the heavy-vector-boson Green's function). Thus, the anapole moment of an elementary particle or a nucleus is not a gauge-invariant concept in general; therefore, it does not have direct physical meaning. Nevertheless, there are special cases where the anapole moment does have physical meaning. In contrast to ordinary radiative corrections, the anapole moment in heavy nuclei is enhanced in proportion to $A^{2/3}$ [21] (where A is the atomic number).[1)] Indeed, the anapole moment of the ^{133}Cs nucleus was discovered and measured to a good precision in the atomic experiment reported in [22]. The result of this experiment is in reasonable quantitative agreement with theoretical predictions first presented in [21, 23].

There exists yet another object, the deuteron, whose anapole moment could have physical meaning, provided that the P-odd πNN coupling constant is sufficiently large [23]. The problem of the deuteron anapole moment was phenomenologically considered in [1, 23–25]. Recently, the deuteron anapole moment induced by P-odd pion exchange has been calculated in [26] (see also [27]).

4.2. Calculation of the Nucleon Anapole Moment

It is convenient to begin by considering the nucleon anapole moment in the limit $m_\pi \longrightarrow 0$. It was calculated by Vainshtein and the present author in 1980. The same result,

$$\mathbf{a}_p = \mathbf{a}_n = -\frac{eg\bar{g}}{12m_p m_\pi}\left(1 - \frac{6}{\pi}\frac{m_\pi}{m_p}\ln\frac{m_p}{m_\pi}\right)\boldsymbol{\sigma} \quad (34)$$

($e > 0$ is assumed here), was obtained for the proton and for the neutron.

In the nucleon anapole moment, this is the only contribution that is singular in m_π; therefore, the result in (34) is gauge invariant. In this respect, it has physical meaning.

The corresponding contribution to the amplitude of electron–nucleon scattering is also singular in m_π, but it is unfortunately small numerically in relation to other radiative corrections to the weak scattering amplitude. Indeed, the radiative corrections to the effective constants $C_{2p,n}$ in the operators $G/\sqrt{2}\,C_{2p,n}\boldsymbol{\sigma}_{p,n}$ of the weak neutral currents for the proton and for the neutron are [28]

$$C_{2p}^r = -0.032 \pm 0.030, \quad C_{2n}^r = 0.018 \pm 0.030. \quad (35)$$

[1)] Among other things, this means that there exists an intrinsic limit of about $A^{2/3}$ on the relative accuracy to which one can determine the anapole moment of a heavy nucleus. In the ^{133}Cs case, which is of experimental interest, this limiting accuracy is some 4%.

In the same units of $G/\sqrt{2}$, the effective axial constants induced by the electromagnetic interaction with the anapole moments of the proton and the neutron [see (34)] are

$$C^a_{p,n} = -\alpha a_N(|e|G/\sqrt{2})^{-1} = 0.07\times 10^5\bar{g}.$$

At the "best value" of $\bar{g} = 3.3\times 10^{-7}$, we then obtain

$$C^a_{p,n} = 0.002. \quad (36)$$

Since this value is much less than those corresponding to the central points and than the errors in (35), it is meaningless to consider the anapole moment from the practical point of view. This is the reason why the result presented in (34) has never been published by the authors. It is quoted in the monograph [20] (without the logarithmic term) just as a theoretical curiosity. This result was also obtained in [29], while the logarithmic term in the nucleon anapole moment is discussed in [30].

As was indicated in [31], the *P*-odd $\pi\pi NN$ interaction also generates a $\ln m_\pi$ contribution to the nucleon anapole moment. The coupling constant for this *P*-odd $\pi\pi NN$ interaction is known only from purely theoretical estimations. According to those that Kaplan and Savage [31] consider to be relatively reliable, the contribution of the *P*-odd $\pi\pi NN$ interaction to the nucleon anapole moment is approximately an order of magnitude less than the result in (34).

However, the situation around the deuteron anapole moment is quite different not only in that the anapole moment here receives contributions from the proton and from the neutron but also in that the isoscalar part of the radiative corrections is much smaller than each of the individual contributions C^r_{2p} and C^r_{2n}; furthermore, it is calculated to a much higher precision [28],

$$C^r_{2d} = C^r_{2p} + C^r_{2n} = 0.014\pm 0.0030. \quad (37)$$

In addition, new large contributions that are proportional to m_π^{-1} and which are induced by *P*-odd π-meson exchange arise in the deuteron anapole moment. We now proceed to analyze these contributions.

4.3. P-odd π-Meson Exchange

The Lagrangians for strong and for weak *P*-odd πNN interaction (L_s and L_w, respectively) are given by

$$L_s = g[\sqrt{2}(\bar{p}i\gamma_5 n\pi^+ + \bar{n}i\gamma_5 p\pi^-) + (\bar{p}i\gamma_5 p - \bar{n}i\gamma_5 n)\pi^0], \quad (38)$$

$$L_w = \bar{g}\sqrt{2}i(\bar{p}n\pi^+ - \bar{n}p\pi^-), \quad (39)$$

where

$$\gamma_5 = \begin{pmatrix} 0 & -I \\ -I & 0 \end{pmatrix}. \quad (40)$$

The relation between the *P*-odd πNN coupling constant $\bar{g}$ used here and that used conventionally and denoted by $h^{(1)}_{\pi NN}$ is $\bar{g}\sqrt{2} = h^{(1)}_{\pi NN}$. We imply the conventional definition of signs for the coupling constants: $g = 13.45$ and $\bar{g} > 0$ for the region of values discussed in [32].

In the momentum representation, the effective nonrelativistic potential of the *P*-odd nucleon–nucleon interaction induced by π-meson exchange has the form

$$V(\mathbf{q}) = \frac{2g\bar{g}}{m_p}\frac{\mathbf{I}\cdot\mathbf{q}}{m_\pi^2+\mathbf{q}^2}(N_1^\dagger\tau_{1-}N_1)(N_2^\dagger\tau_{2+}N_2), \quad (41)$$

where $\mathbf{q} = \mathbf{p}_1' - \mathbf{p}_1 = -(\mathbf{p}_2' - \mathbf{p}_2) = \mathbf{p}_n' - \mathbf{p}_p = -(\mathbf{p}_p' - \mathbf{p}_n)$. This *P*-odd interaction conserves the total spin

$$\mathbf{I} = \frac{1}{2}(\boldsymbol{\sigma}_p + \boldsymbol{\sigma}_n),$$

but it does not conserve the isospin. In our problem, this interaction therefore mixes the $^3P_1$ state of the continuous spectrum with the deuteron ground state ($^3S_1$). It should be noted that, when applied to the initial state $a_p^\dagger(\mathbf{r}_1)a_n^\dagger(\mathbf{r}_2)|0\rangle$, the interaction potential (41), which interchanges the proton and the neutron, transforms this initial state into $a_n^\dagger(\mathbf{r}_1)a_p^\dagger(\mathbf{r}_2)|0\rangle = -a_p^\dagger(\mathbf{r}_2)a_n^\dagger(\mathbf{r}_1)|0\rangle$. On the other hand, the coordinate wave function of the admixed $^3P_1$ state is proportional to the relative coordinate $\mathbf{r}$ defined as $\mathbf{r}_p - \mathbf{r}_n$. Therefore, it also changes sign under the permutation $p \longleftrightarrow n$. Thus, we conclude that, in the coordinate representation, this *P*-odd potential for the deuteron can be written merely as a function of $\mathbf{r} = \mathbf{r}_p - \mathbf{r}_n$ without indicating isotopic variables,

$$V(\mathbf{r}) = \frac{g\bar{g}}{2\pi m_p}(-i\mathbf{I}\cdot\nabla)\frac{e^{-m_\pi r}}{r}. \quad (42)$$

The relevant direct and inverse imaginary matrix elements are related as $\langle^3P_1|V|^3S_1\rangle = -\langle^3S_1|V|^3P_1\rangle$; the sign in (42) corresponds to $\langle^3P_1|V|^3S_1\rangle$.

It is worth noting that the weak interaction (42) generates a contact current $\mathbf{j}^c$. In order to obtain an explicit expression for this current, we consider the *P*-odd interaction *V* in the presence of an electromagnetic field, in which case we have to shift the proton momentum as $\mathbf{p} \longrightarrow \mathbf{p} - e\mathbf{A}$ and make the substitution $\mathbf{q} \longrightarrow \mathbf{q} + e\mathbf{A}$ in the interaction potential (41). In the momentum representation, the contact current then assumes the form

$$\mathbf{j}^c(\mathbf{q}) = -\frac{\partial V(\mathbf{q})}{\partial\mathbf{A}} = -\frac{\partial}{\partial\mathbf{A}}\frac{2g\bar{g}}{m_p}\frac{\mathbf{I}\cdot(\mathbf{q}+e\mathbf{A})}{m_\pi^2+(\mathbf{q}+e\mathbf{A})^2} = -\frac{2eg\bar{g}}{m_p}\left\{\frac{\mathbf{I}}{m_\pi^2+\mathbf{q}^2} - \frac{2\mathbf{q}(\mathbf{I}\cdot\mathbf{q})}{(m_\pi^2+\mathbf{q}^2)^2}\right\}, \quad (43)$$

where we have neglected the **A** dependence. In the coordinate representation, the contact current is

$$\mathbf{j}^c(\mathbf{r}) = \frac{eg\bar{g}}{2\pi m_p}\mathbf{r}(\mathbf{I}\cdot\nabla)\frac{e^{-m_\pi r}}{r}. \quad (44)$$

4.4. Calculation of the Deuteron Anapole Moment

First, we will discuss the general structure of the deuteron anapole moment induced by the *P*-odd *np* interaction conserving the total spin, only assuming that the deuteron is a pure $^3S_1$ state bound by a spherically symmetric potential. In doing this, we follow essentially the arguments applied in [23] (see also [20]) to the problem of a proton in a spherically symmetric potential. In that case, the anapole-moment operator is [23]

$$\hat{\mathbf{a}} = \frac{\pi e}{m_p}\left\{\mu_p\mathbf{r}\times\boldsymbol{\sigma} - \frac{i}{3}[\mathbf{l}^2,\mathbf{r}]\right\} + \frac{2\pi}{3}\mathbf{r}\times[\mathbf{r}\times\mathbf{j}^c]. \quad (45)$$

The corresponding expression for the deuteron has the form

$$\hat{\mathbf{a}}_d = \frac{\pi e}{2m_p}\left\{\mathbf{r}\times(\mu_p\boldsymbol{\sigma}_p - \mu_n\boldsymbol{\sigma}_n) - \frac{i}{6}[\mathbf{l}^2,\mathbf{r}]\right\} + \frac{\pi}{6}\mathbf{r}\times[\mathbf{r}\times\mathbf{j}^c]. \quad (46)$$

The operators (45) and (46) are both orthogonal to **r** (neither commutes with **r**, so that the orthogonality means here that $\hat{\mathbf{a}}\cdot\mathbf{r} + \mathbf{r}\cdot\hat{\mathbf{a}} = 0$). Therefore, the contact current (44), which is generated by *P*-odd pion exchange and which is directed along **r**, does not contribute to the nuclear anapole moment.

Let us represent the wave function of the $^3S_1$ state of the deuteron in the form $\psi_0(r)\chi_t$. Since weak interaction conserves the total spin **I**, the $^3P_1$ *P*-odd admixture can be written as $\delta\psi_1(\mathbf{r}) = i(\mathbf{I}\cdot\mathbf{r}/r)\psi_1(r)\chi_t$, with the wave functions $\psi_0(r)$ and $\psi_1(r)$ being both spherically symmetric. After some simple algebra, we find that, in the absence of the contact-current contribution, the expectation value of operator (46) in the state with the wave function $[\psi_0(r) + i(\mathbf{I}\cdot\mathbf{r}/r)\psi_1(r)]\chi_t$ is

$$\mathbf{a}_d = \frac{\pi e}{3m_p}\left(\mu_p - \mu_n - \frac{1}{3}\right)\mathbf{I}\int d\mathbf{r}\psi_0(r)r\psi_1(r). \quad (47)$$

Thus, we conclude that, under the above assumptions, the deuteron anapole moment must depend on the universal combination $\mu_p - \mu_n - 1/3$.

The actual calculations will be performed in the zero-range approximation, where $\psi_0(r) = \psi_d(r)$ [see Eq. (1)] and where the wave functions of the *P* states are free. In applying time-independent perturbation theory, we can further take plane waves for intermediate states over which summation is performed, since the perturbation $V(\mathbf{r})$ [see Eq. (42)] will automatically select the *P* states from the plane waves. The correction to the wave function is given by

$$\delta\psi_1(\mathbf{r}) = \int\frac{d\mathbf{k}}{(2\pi)^3}\frac{e^{i\mathbf{k}\cdot\mathbf{r}}}{-\varepsilon - k^2/m_p}\int d\mathbf{r}' e^{-i\mathbf{k}\cdot\mathbf{r}'}V(\mathbf{r}')\psi_0(r'). \quad (48)$$

After rather lengthy calculations, we obtain the matrix element of the radius vector in the form

$$\int d\mathbf{r}\psi_d(r)\mathbf{r}\delta\psi_1(\mathbf{r}) = -i\frac{eg\bar{g}\mathbf{I}}{6\pi m_\pi}\frac{1+\xi}{(1+2\xi)^2}, \quad (49)$$

where $\xi = \kappa/m_\pi = 0.32$. Using this matrix element and the operator in (46), we can represent the deuteron anapole moment as

$$\mathbf{a}_d^{(0)} = -\frac{eg\bar{g}}{6m_pm_\pi}\frac{1+\xi}{(1+2\xi)^2}\left(\mu_p - \mu_n - \frac{1}{3}\right)\mathbf{I}, \quad (50)$$

in accordance with the general formula (47).

Actually, the range of the *P*-odd interaction (42) is commensurate with the range of ordinary nuclear forces. Therefore, it seems hazardous to use the naive wave function (1) without any further substantiation. Nevertheless, numerical calculations with a model wave function that has more realistic properties lead to a result that differs from the result in (50) by not more than 20%. As to sources of *P* violation other than pion exchange, their contribution to the deuteron anapole moment can be shown to be within 5% of that in (50) (at the "best value" of $\bar{g}$).

It seems reasonable to combine the potential contribution (50) with the sum of the proton and neutron anapole moments (34). In this way, we arrive at the final result for the deuteron anapole moment:

$$\mathbf{a}_d = -\frac{eg\bar{g}}{6m_pm_\pi}[0.49(\mu_p - \mu_n - 1/3) + 0.46]\mathbf{I} = -2.60\frac{eg\bar{g}}{6m_pm_\pi}\mathbf{I}. \quad (51)$$

This result includes all corrections to the *P*-odd amplitude of *ed* scattering that are singular in m_π; therefore, it is gauge-invariant and physically meaningful.

It only remains to compare the contribution of the anapole moment (51) with the *P*-odd *ed*-scattering amplitude induced by ordinary radiative corrections, which are nonsingular in m_π. For the "best value" of $\bar{g} = 3.3\times10^{-7}$ and a 20% estimate for the error, we obtain

$$C_{2d}^a = 0.014 \pm 0.003. \quad (52)$$

This value is commensurate with the contribution (37) of ordinary radiative corrections. Combined together, they amounts to

$$C_{2d} = C_{2d}^r + C_{2d}^a = 0.028 \pm 0.005. \quad (53)$$

Yet another contribution to C_{2d} arises from the admixture of strange quarks in the nucleon [33]. This contribution is extremely interesting, but it is very uncertain.

It is very difficult to measure the constant C_{2d}. In view of the high accuracy of the theoretical predictions, such an experiment would furnish, however, valuable information about the P-odd πNN coupling constant and about the strange-quark admixture in the nucleon.

4.5. P-odd, T-odd Electromagnetic Moments of the Deuteron

Previously, the P-odd, T-odd multipole moments of the deuteron—specifically, the electric dipole and the magnetic quadrupole moment—were considered phenomenologically [34]. In [26], these multipole moments were calculated within the same approach as the anapole moment.

It is convenient to classify three independent P-odd, T-odd effective πNN Lagrangians according to their isotopic properties,

$$\Delta T = 0,$$
$$L_0 = g_0[\sqrt{2}(\bar{p}n\pi^+ + \bar{n}p\pi^-) + (\bar{p}p - \bar{n}n)\pi^0]; \quad (54)$$

$$|\Delta T| = 1,$$
$$L_1 = g_1\bar{N}N\pi^0 = g_1(\bar{p}p + \bar{n}n)\pi^0; \quad (55)$$

$$|\Delta T| = 2,$$
$$L_2 = g_2(\bar{N}\tau N\pi - 3\bar{N}\tau^3 N\pi^0) \quad (56)$$
$$= g_2[\sqrt{2}(\bar{p}n\pi^+ \bar{n}p\pi^-) - 2(\bar{p}p - \bar{n}n)\pi^0)].$$

Since the isospin of two nucleons can assume only the values of $T = 0, 1$, the last Lagrangian, which is associated with $|\Delta T| = 2$, is not operative within our approach.

The effective P-odd, T-odd np interaction is derived in just the same way as the interaction in (42). In the momentum representation, it has the form

$$W(\mathbf{r}) = \frac{g}{8\pi m_p}[(3g_0 - g_1)\boldsymbol{\sigma}_p - (3g_0 + g_1)\boldsymbol{\sigma}_n] \cdot \nabla\frac{e^{-m_\pi r}}{r}. \quad (57)$$

The deuteron dipole moment (that is, the expectation value of $e\mathbf{r}_p = e\mathbf{r}/2$) can be calculated by means of a procedure similar to that adopted above for the anapole moment. As a result, we obtain

$$\mathbf{d} = -\frac{egg_1}{12\pi m_\pi}\frac{1+\xi}{(1+2\xi)^2}\mathbf{I}. \quad (58)$$

The magnetic-quadrupole-moment operator is expressed in terms of the current density $\mathbf{j}$ as (see, for example, [20, 35])

$$M_{mn} = (r_m\varepsilon_{nrs} + r_n\varepsilon_{mrs})r_r j_s. \quad (59)$$

This expression can be recast into the form

$$M_{mn} = \frac{e}{2m}\left\{3\mu\left[r_m\sigma_n + r_n\sigma_m - \frac{2}{3}(\boldsymbol{\sigma}\cdot\mathbf{r})\right] + 2q(r_m l_n + r_n l_m)\right\}, \quad (60)$$

where μ is the total magnetic moment of the particle being considered, while q is its charge in units of e.

In our case, the orbital contribution to M_{mn} vanishes because of the spherical symmetry of the unperturbed wave function. The contact current here is again directed along $\mathbf{r}$; therefore, it does not contribute to the magnetic quadrupole moment. Thus, the deuteron magnetic quadrupole moment is induced by the spin term in (60). It is a given by

$$\mathcal{M} = M_{zz}|_{I_z = I} = -\frac{eg}{12\pi m_p m_\pi}\frac{1+\xi}{(1+2\xi)^2} \times [(3g_0 + g_1)\mu_p + (3g_0 - g_1)\mu_n]. \quad (61)$$

In conclusion, it is worth noting that, presently, the possibility of searches for the deuteron dipole moment at a storage ring for polarized nuclei is being discussed by experimentalists rather seriously.

ACKNOWLEDGMENTS

This review article is based on results obtained together with A.V. Blinov, A.P. Burichenko, L.A. Kondratyuk, and R.V. Korkin.

The work was supported by the Leading Scientific Schools Foundation (grant no. 00-15-96811), the Ministry for Higher Education of the Russian Federation (grant no. 3N-224-98) and the Federal Program Integration-1998 (grant no. 274).

REFERENCES

1. A. I. Mikhaĭlov, A. N. Moskalev, R. N. Ryndin, and G. I. Frolov, Yad. Fiz. **35**, 887 (1982) [Sov. J. Nucl. Phys. **35**, 516 (1982)].
2. H. Bethe and R. Peierls, Proc. R. Soc. London, Ser. A **148**, 570 (1935).
3. V. B. Berestetskiĭ, E. M. Lifshitz, and L. P. Pitaevskiĭ, *Quantum Electrodynamics* (Nauka, Moscow, 1980; Pergamon, Oxford, 1982).
4. J. L. Friar and S. Fallieros, Phys. Rev. C **29**, 232 (1984).
5. E. Fermi, Phys. Rev. **48**, 570 (1935).
6. A. V. Blinov, L. A. Kondratyuk, and I. B. Khriplovich, Yad. Fiz. **47**, 604 (1988) [Sov. J. Nucl. Phys. **47**, 382 (1988)].
7. L. Wolfenstein and J. Ashkin, Phys. Rev. **85**, 947 (1952).
8. L. D. Landau and E. M. Lifshitz, *Quantum Mechanics: Non-Relativistic Theory* (Nauka, Moscow, 1974; Pergamon, New York, 1977).

9. T. E. O. Ericson and M. Rosa-Clot, Nucl. Phys. A **405**, 493 (1984).
10. R. A. Arndt *et al.*, Phys. Rev. D **28**, 97 (1983).
11. V. A. Vesna *et al.*, Nucl. Phys. A **352**, 181 (1981).
12. A. N. Bazhenov *et al.*, Phys. Lett. B **289**, 17 (1992).
13. G. S. Danilov, in *Proceedings of the XI LNPI Winter School, Leningrad, 1976*, Vol. 1, p. 203.
14. I. L. Grach and M. Zh. Shmatikov, Yad. Fiz. **40**, 440 (1984) [Sov. J. Nucl. Phys. **40**, 280 (1984)].
15. I. L. Grach and M. Zh. Shmatikov, Yad. Fiz. **45**, 933 (1987) [Sov. J. Nucl. Phys. **45**, 579 (1987)].
16. A. P. Burichenko and I. B. Khriplovich, Nucl. Phys. A **515**, 139 (1990).
17. J.-W. Chen, G. Rupak, and M. J. Savage, Phys. Lett. B **464**, 1 (1999); nucl-th/9905002.
18. T. S. Park, K. Kubodera, D. P. Min, and M. Rho, Phys. Lett. B **472**, 232 (2000); nucl-th/9906005.
19. Ya. B. Zel'dovich, Zh. Éksp. Teor. Fiz. **33**, 1531 (1957) (in this article, mention is made of the fact that similar results were obtained by V. G. Vaks) [Sov. Phys. JETP **6**, 1184 (1958)].
20. I. B. Khriplovich, *Nonconservation of Parity in Atomic Phenomena* (Nauka, Moscow, 1988).
21. V. V. Flambaum, I. B. Khriplovich, and O. P. Sushkov, Phys. Lett. B **146B**, 367 (1984).
22. C. S. Woods *et al.*, Science **275**, 1759 (1997).
23. V. V. Flambaum and I. B. Khriplovich, Zh. Éksp. Teor. Fiz. **79**, 1656 (1980) [Sov. Phys. JETP **52**, 835 (1980)].
24. E. M. Henley and W.-Y. P. Hwang, Phys. Rev. C **23**, 1001 (1981).
25. B. Desplanques, in *Contributions to the 9th International Conference on High Energy Physics and Nuclear Structure, Paris, 1981*.
26. I. B. Khriplovich and R. V. Korkin, Nucl. Phys. A **665**, 365 (2000); nucl-th/9904081.
27. M. J. Savage and R. P. Springer, Nucl. Phys. A **644**, 235 (1998); Erratum: **657**, 457 (1999); nucl-th/9807014.
28. W. J. Marciano and A. Sirlin, Phys. Rev. D **29**, 75 (1984).
29. M. J. Musolf and B. R. Holstein, Phys. Rev. D **43**, 2956 (1991).
30. W. C. Haxton, E. M. Henley, and M. J. Musolf, Phys. Rev. Lett. **63**, 949 (1989).
31. D. B. Kaplan and M. J. Savage, Nucl. Phys. A **556**, 653 (1993).
32. B. Desplanques, J. F. Donoghue, and B. R. Holstein, Ann. Phys. (N.Y.) **124**, 449 (1980).
33. B. A. Campbell, J. Ellis, and R. A. Flores, Phys. Lett. B **225**, 419 (1989).
34. O. P. Sushkov, V. V. Flambaum, and I. B. Khriplovich, Zh. Éksp. Teor. Fiz. **87**, 1521 (1984) [Sov. Phys. JETP **60**, 873 (1984)].
35. S. K. Lamoreaux and I. B. Khriplovich, *CP Violation without Strangeness* (Springer-Verlag, Berlin, 1997).

Translated by O. Chernavskaya

Physics of Atomic Nuclei, Vol. 64, No. 3, 2001, pp. 525–535. From Yadernaya Fizika, Vol. 64, No. 3, 2001, pp. 579–589.

90th ANNIVERSARY OF A.B. MIGDAL'S BIRTHDAY
NUCLEI

Do We Understand the Role of Incoherent Interactions in Many-body Physics?*

V. G. Zelevinsky, D. Mulhall, and A. Volya

Department of Physics and Astronomy and National Superconducting Cyclotron Laboratory, East Lansing, Michigan, USA

Received August 11, 2000

Abstract—Recent developments in many-body quantum chaos show that a quantum system with strong incoherent interactions can still be described with the aid of mean quasiparticle occupation numbers as in Fermi liquid theory. We use these ideas and the geometric chaoticity of angular momentum coupling to explain the predominance of ground states with zero spin and the maximum possible spin for a system of randomly interacting fermions in a rotationally invariant mean field (an analog of the Hund rule). We show that spin ordering coexists with the chaotic features of the ground-state wave functions. *© 2001 MAIK "Nauka/Interperiodica".*

1. INTRODUCTION

The standard description of quantum many-body systems is largely based on the concept of the mean field. The mean field determines the symmetry of the system and possible modes of elementary excitations, quasiparticles. The residual interaction of quasiparticles may lead both to collective motion and to collision-like processes responsible for relaxation phenomena and the finite lifetime of elementary excitations. This general picture works as a foundation for the Fermi liquid theory [1] for macroscopic systems. Being generalized by Migdal [2] for finite Fermi systems, such as atomic nuclei, various versions of this approach serve as a basis of nuclear structure theory recently used successfully also for atomic clusters and other mesoscopic systems.

The domain of validity of the Fermi liquid approach is frequently claimed to be restricted to the low-energy region of spectra where the quasiparticle collisions are suppressed by the Pauli exclusion principle and the quasiparticles have a large lifetime. The emergence of collective modes does not strongly destroy the quasiparticle picture because each individual quasiparticle excitation contributes only a small part to the total collective strength and, therefore, it is only weakly distorted. As excitation energy increases, the frequent collisions reduce the lifetime of the quasiparticles that seemingly invalidates the Fermi liquid approach because the response of the system to an external field should include complicated many-particle excitations.

During the last years, the extensive study of quantum chaos started to gradually change some features of the traditional paradigm of many-body physics. This is seen more clearly in the mesoscopic physics of small quantum many-body systems. Mesoscopic objects are sufficiently complicated to allow for a statistical description. On the other hand, they are sufficiently small to reveal, at least in particular situations, the properties of individual quantum states. A complex nucleus is a perfect example of such a system with the strong interaction between its constituents. At relatively high excitation energy, the description of the nuclear processes uses such statistical notions as level density, temperature, strength function, and so on. However even here, experiments are possible which deal practically with single wave functions of nearly stationary states as in the case of isolated neutron resonances [3]. Therefore, it is feasible to study simultaneously the global ("secular") behavior of nuclear properties along the spectrum and local correlations and fluctuations of energy levels and eigenfunctions.

The extreme limit of a chaotic local pattern is given by random matrix theory [4–6]. The Gaussian Orthogonal Ensemble (GOE) is appropriate for chaotic time-reversal invariant systems. The analyses of actual chaotic systems (quantum billiards, microwave cavities, acoustic waves in solids, quantum dots, complex atoms, molecules and nuclei, quantum fields), as well as of numerous models, show that the spectral statistics are universal and close to the GOE limit. The deviations from universality should be the most interesting, although quite difficult to analyze because of the necessity to have a large reliable body of data with a minimum of missing levels, and are the object of future studies. It is even harder to study the statistical properties of the eigenstates. However, we know that, in many-body systems, the eigenfunctions are extremely complicated superpositions of a large number N of independent particle configurations. This mixing and, consequently, degree of complexity are smooth functions of excitation energy [7, 8], as is needed for the successful application of the statistical approach. This is where one can bridge the gap between quantum chaos and thermodynamics [8, 9], preparing the way to the reformulation of the concepts of thermal equilib-

* This article was submitted by the authors in English.

rium, especially for small closed systems. Furthermore, it turns out that one can still characterize the macroscopic observables in terms of the single-particle occupancies even in the presence of strong residual interactions [8, 10]. This means that in fact the Fermi liquid theory has a much greater domain of validity than was previously considered.

Another topic of principal interest is the relationship between coherent and quasirandom parts of the residual interaction. The mean field itself is a result of averaging over very complicated intermediate states in the dynamics of the single-particle density matrix [11]. In a self-sustaining system, there are integrals of motion, such as total angular momentum J, that are not destroyed by chaotic interactions. Within a block of states with given J, the states can be strongly mixed. Nevertheless, the different blocks, being governed by the same original Hamiltonian, can still keep some correlations. For example, even at high excitation energy, an object can allow collective rotation, so that each block will include corresponding states which are very similar but differ by the value of J (collective rotation frequency). In this case, one would observe "compound rotational bands" with strong radiative transitions between the J members of the band [12].

Recent studies [13, 14] show that a random interaction can result in ordered energy levels which resemble the actual structure of nuclear spectra. The necessary condition is that the interaction being random in sign and magnitude still respects the symmetry of the system (rotational invariance in the case of a self-sustaining finite system). The appearance of such ordered spectra again confirms the correlation between the different classes of states governed by the same Hamiltonian. The mechanism responsible for the appearance of quasi-ordered spectra in a system with chaotic dynamics was not explained either in the original work [13] or in the subsequent publications [14–16], although the numerical results for various versions of the shell model and interacting boson model are quite convincing.

Below, we consider the problem of ordered spectra from random interactions and suggest an explanation based on the idea of geometric chaoticity [8, 17] which appears in a finite many-fermion system with complex interactions due to exact rotational invariance. In fact, this should be a generic feature of any self-sustaining drop of Fermi liquid. To clarify the arguments, we limit ourselves here to the simplest situation of a single-j level. The generalization to more realistic situations is straightforward.

2. THE MODEL

Let us consider a system of N identical fermions occupying certain orbitals in a common spherically symmetric field. For simplicity, we assume that all particles are confined to a single-j level so that the only quantum number characterizing a single-particle state is the angular momentum projection m. The complete degeneracy of all single-particle states ensures the most effective role of the residual interaction. The capacity of the level $\Omega = 2j + 1$ should be sufficiently large to give rise to the possibility of statistical regularities.

The most general residual interaction between the particles in this space can be written in the particle–particle pp channel as

$$H = \sum_{L\Lambda} V_L P^\dagger_{L\Lambda} P_{L\Lambda}, \tag{1}$$

where the creation, $P^\dagger_{L\Lambda}$, and annihilation, $P_{L\Lambda}$, operators for a pair with total spin L and its projection Λ are defined according to

$$\begin{aligned} P^\dagger_{L\Lambda} &= \frac{1}{\sqrt{2}} \sum_{mm'} C^{L\Lambda}_{mm'} a^\dagger_m a^\dagger_{m'}, \\ P_{L\Lambda} &= \frac{1}{\sqrt{2}} \sum_{mm'} C^{L\Lambda}_{mm'} a_m a_{m'}, \end{aligned} \tag{2}$$

where $C^{L\Lambda}_{mm'} \equiv \langle L\Lambda | jmjm' \rangle$ are the Clebsch–Gordan coefficients of vector coupling. Note that, due to the Fermi statistics (anticommutation of the single-particle operators) and the corresponding symmetry $C^{L\Lambda}_{mm'} = (-1)^{L+1} C^{L\Lambda}_{m'm}$ for a half-integer j, only even momenta $L = 0, 2, \ldots, 2j - 1 = \Omega - 2$ of pairs are allowed. The pair operators in Eq. (2) are defined in such a way that the normalized pair state with spin L is $P^\dagger_{L\Lambda}|0\rangle$, where $|0\rangle$ is the vacuum state with no particles.

The same Hamiltonian can be identically transformed to the particle–hole ph channel, where it is expressed as

$$H = \epsilon \hat{N} - \frac{1}{2} \sum_{K\kappa} \tilde{V}_K \mathcal{M}^\dagger_{K\kappa} \mathcal{M}_{K\kappa}. \tag{3}$$

Here, the multipole operators

$$\mathcal{M}_{K\kappa} = \sum_{mm'} (-1)^{j-m} \begin{pmatrix} j & K & j \\ -m & \kappa & m' \end{pmatrix} a^\dagger_{m'} a_m \tag{4}$$

are Hermitian $\mathcal{M}^\dagger_{K\kappa} = (-1)^\kappa \mathcal{M}_{K-\kappa}$. The effective single-particle energy in Eq. (3) is $\epsilon = (1/2)\sum_K \tilde{V}_K$, and the interaction matrix elements $\tilde{V}_K$ in the ph channel ($K = 0, 1, \ldots, 2j = \Omega - 1$ can be both even and odd) are related

to the original matrix elements V_L in the *pp* channel as

$$V_L = \sum_K \left\{ \begin{array}{ccc} j & j & L \\ j & j & K \end{array} \right\} \tilde{V}_K \quad (\text{even } L), \tag{5}$$

or, inversely,

$$\tilde{V}_K = (2K+1) \sum_{\text{even } L} (2L+1) \left\{ \begin{array}{ccc} j & j & K \\ j & j & L \end{array} \right\} V_L. \tag{6}$$

Among the multipoles $\mathcal{M}_{K\kappa}$, the exact constants of motion are the particle-number operator

$$\hat{N} = \sum_m a_m^\dagger a_m = \sqrt{\Omega}\mathcal{M}_{00} \tag{7}$$

and the angular-momentum spherical components

$$J_\kappa = \sqrt{\Omega \mathbf{j}^2}\mathcal{M}_{1\kappa}. \tag{8}$$

The transition between the *pp* and *ph* channels (the so-called Pandey transformation) was studied from the dynamical viewpoint by Belyaev [18]. The channels are complementary in the following sense: the lowest L components of the *pp* channel contribute mainly to the highest K components of the *ph* channel, and vice versa. The pairing part of the interaction, $L = 0$, corresponds to the sum of all multipole interactions,

$$V_0 = -\frac{1}{\Omega}\sum_K (-1)^K \tilde{V}_K. \tag{9}$$

This complementarity explains the success of the popular interpolating model "pairing + multipole–multipole interaction," where the effective interaction combines phenomenologically the lowest components in both channels.

3. RANDOM HAMILTONIAN

The analytic solution for the general single-*j* Hamiltonian is not known, although it can be found for specific cases [19] such as the pure pairing problem, $V_L = V_0\delta_{L0}$, when the quasispin $SU(2)$ algebra of the operators P_{00}, $P_{00}^\dagger$, and $\hat{N}$ provides the additional integral of motion, seniority [20]. However, the numerical solution is readily available for not very large values of N and Ω. The matrix diagonalization can be performed both on the basis of the *m*-scheme Slater determinants and with the preliminary projection of the many-body states with a certain value of the total angular momentum J (as it is done, for example, in the OXBASH code [21]) and separate diagonalization within the J blocks. The maximum spin available for given values of N and Ω is

$$J_{\max} = \frac{1}{2}N(\Omega - N), \tag{10}$$

and the corresponding state is unique so that no diagonalization is required. The dimensions $d(J)$ of other J blocks can be easily counted, and their statistical distribution can be approximately evaluated assuming the idea of random coupling of individual angular momenta similar to that used for deriving [22] the Fermi gas level density: $d(J) \propto (2J+1)\exp[-\text{const} \times J(J+1)]$. Here, the constant in the exponent is related to the effective statistical moment of inertia determined by the average value $\overline{m^2}$ for available single-particle orbitals. Large-scale shell-model calculations with realistic residual forces [23] agree on average with this statistical estimate. In particular, the value $J = 0$ never corresponds to the maximum statistical probability.

The empirical fact that even–even nuclei always have a ground-state spin $J_0 = 0$ is usually traced to the presence of strong attractive pairing forces, $V_0 < 0$. Surprisingly, it turns out [13] that such forces are not necessary. Even with randomly chosen interaction parameters V_L, the probability of having $J_0 = 0$ is an order of magnitude higher than the fraction of states $J = 0$ in the entire Hilbert space. Moreover, this result is quite robust and insensitive to the precise definition of the random ensemble [14, 15, 24]; it is valid as well for randomly interacting bosons [16].

The random quasiparticle ensemble (RQE) chosen in [13] considers V_L as uncorrelated Gaussian variables with zero mean and the variance scaled as $(2L+1)^{-1}$. The authors claimed that, under this choice, the interaction parameters V_L and $\tilde{V}_K$ in the *pp* and *ph* channels, respectively, have identical distribution functions, which would stress the idea of the randomness of the interaction. This statement would be correct only if one could neglect the limitation by even L values in the *pp* channel for the pairs formed at the same *j* level. Due to the Fermi statistics, the number of different $\tilde{V}_K$ is larger than the number of V_L so that $\tilde{V}_K$ cannot be statistically independent if the V_L are. However, discarding this motivation, we still have the RQE as one of many reasonable ensembles representing the random two-body interaction.

Below, we mainly use an even simpler ensemble with a uniform distribution of uncorrelated constants V_L between –1 and 1. As compared to the RQE, here the weight of high L components is emphasized, but the general conclusions are qualitatively the same.

4. GROUND-STATE SPIN FOR A SINGLE-*j* LEVEL MODEL

For $N = 2$ particles on a single-*j* level, only states with even J are allowed; they are unique, and the ground state in a trivial way corresponds to the value of J which is equal to L for the smallest value of V_L in a given copy of the random ensemble. However, already for $N = 4$ the results are not trivial, being in general

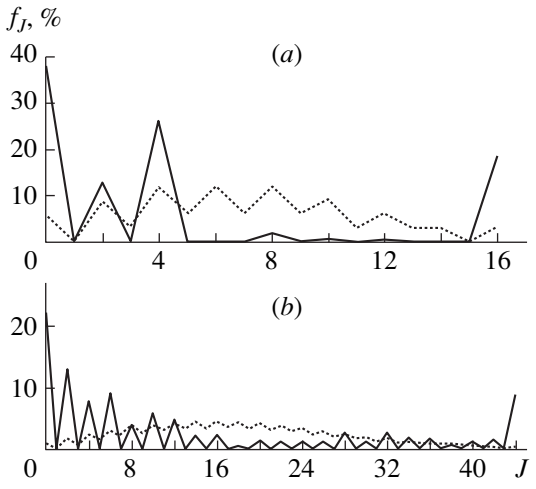

Fig. 1. The ground-state spin distribution f_J in the system of four fermions (solid line) with (*a*) $j = 11/2$ and (*b*) $j = 25/2$. The dotted line shows the statistical distribution of possible spins J for the system.

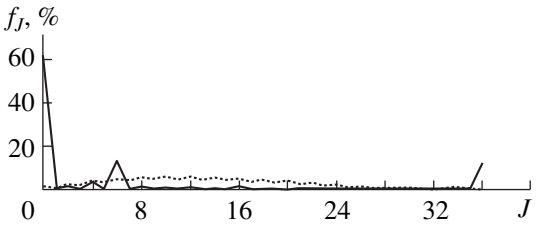

Fig. 2. As in Fig. 1, but for six fermions and $j = 17/2$.

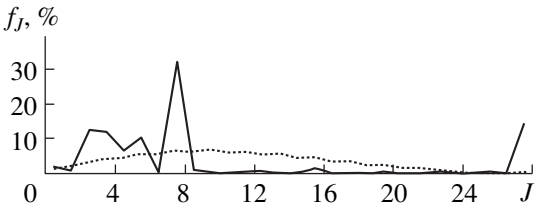

Fig. 3. As in Fig. 1, but for five fermions and $j = 15/2$.

agreement with the findings of [13, 14] for Gaussian ensembles. Below, we give only examples of a large body of our numerical data.

Figure 1 shows the distribution f_J of ground-state spins for a system of $N = 4$ particles on the (*a*) $j = 11/2$ and the (*b*) $j = 25/2$ level. The dotted line corresponds to the statistical distribution of possible spins in Hilbert space, while the solid lines show the actual distribution in the uniform ensemble. Figure 2 displays analogous results for $N = 6$ and $j = 17/2$. The generic pattern is characterized by a large excess of the probability f_0 for the zero ground-state spin. Frequently, f_0 exceeds 50%. The fluctuations of the distribution are smoothed for a larger particle number.

In the previous works [13–16, 24], only systems of even particle number were considered. Assuming the ground-state spin of an even system to be zero, one would expect the ground-state spin of an adjacent odd-N system to coincide with the level spin j. This is indeed the case as illustrated by Fig. 3, where, for the system of $N = 5$ and $j = 15/2$, we observe a peak of probability for $J = j = 15/2$.

Earlier [24], we noticed that the probability of the maximum possible spin $J_{\max}$ is also significantly enhanced, whereas it is vanishingly small for the statistical distribution since there is only one state with $J = J_{\max}$. This enhancement turns out to be a persistent feature as seen from Figs. 1–3. It was seen in the interacting boson model as well [16]: for a system of 16 *sd* bosons with a random two-body interaction, the unique state with $J = J_{\max} = 32$ turned out to be the ground state in 18.6% of all cases. The generic results of different models certainly call for a plausible physical explanation.

5. SEARCH FOR EXPLANATION

The authors of the original work [13] conjectured that the observed strong enhancement of the fraction f_0 is related to the effective pairing correlations which might appear even from random interaction, although a specific mechanism of pairing production was not presented. This aspect of the problem can be related to the more general question of the role of additional interactions in phenomena of superconductivity and superfluidity in Fermi systems.

In the classical BCS theory [25] of macroscopic superconductivity, it was usually assumed that the nonpairing parts of the interaction merely create a normal Fermi liquid dressing of original particles into quasiparticles. Large-scale nuclear shell-model calculations with an effective residual interaction [8, 26] show that this picture is incomplete, at least for small systems. In the model with pairing as the only residual interaction, one has a regular picture of families of states labeled by seniority. The spectrum for the total residual interaction smears these families and, therefore, removes large discontinuities of the level density. However, the pairing correlations, measured, for example, by the expectation value $\langle P^{\dagger}_{00} P_{00} \rangle$ for the individual eigenstates, show a significant excess (with respect to the normal Fermi gas) for the low-lying states. This excess rapidly decreases with excitation energy, revealing a similarity to the phase transition. It is important for us that, even with the pairing matrix elements removed from the residual interaction, one still sees a similar excess of the same quantity in the lowest states, although of a reduced magnitude. This means that other parts of the interaction still generate pairing correlations, supposedly through higher orders of perturbation theory. The whole picture scales with the angular momentum of the

states under consideration [23] in average agreement with the semiclassical consideration in [27].

To test the role of the pairing phenomena for the ground-state spin, we can compare the distribution f_J for the full random ensemble and for the ensemble with no pairing ($V_0 = 0$). As seen from the example of Fig. 4 for six particles on $j = 11/2$, the results are virtually unchanged after removal of the $L = 0$ component. On the other hand, the addition of regular attractive pairing, $V_0 = -1$, increases $f_{J=0}$ noticeably.

Another idea [15] was related to time-reversal invariance of the Hamiltonian which might support $J = 0$ for the role of the ground-state spin. As shown in [15], this is not the case, and the resulting picture does not change with the addition of a time-reversal-violating (but still Hermitian and rotationally invariant) Hamiltonian. This result could be expected since all imaginary effects are averaged out to zero by the construction of the Gaussian random ensemble.

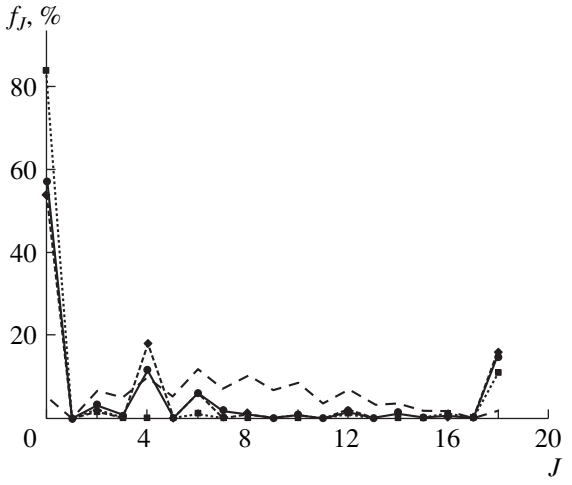

Fig. 4. The ground-state spin distribution f_J in the system of six fermions with $j = 11/2$; random ensemble (solid line), random ensemble with no pairing, $V_0 = 0$ (short-dashed line), random ensemble with regular attractive pairing, $V_0 = -1$ (dotted line), the statistical distribution of possible total spins J (long-dashed line).

6. BOSON APPROXIMATION

One of the approaches to the theory of collective motion in Fermi systems is related to the approximation of fermion pairs by bosons [28, 29]. This approximation served as a foundation of the interacting-boson models [30]. It is formally based on the simple algebraic properties of pair operators (2). Their commutation relations can be written as

$$[P_{L'\Lambda'}, P^\dagger_{L\Lambda}] = \delta_{L'L}\delta_{\Lambda'\Lambda} + 2\sum_{mm'm''} C^{L'\Lambda'}_{m'm''}C^{L\Lambda}_{m''m}a^\dagger_m a_{m'}. \quad (11)$$

The second term on the right-hand side of Eq. (11) is responsible for the nonbosonic kinematics of composite fermion pairs. With angular-momentum recoupling, this term can be presented as a sum of the multipole operators $\mathcal{M}_{K\kappa}$, Eq. (4). Then it is easy to see that the individual terms in the sum over K are of the order of N/Ω. Thus, the average value of Eq. (11) (monopole part, $K = 0$) gives a result similar to that for the quasispin algebra,

$$[P_{L'\Lambda'}, P^\dagger_{L\Lambda}]_{K=0} = \delta_{L'L}\delta_{\Lambda'\Lambda}\left(1 - 2\frac{\hat{N}}{\Omega}\right). \quad (12)$$

The nonbosonic correction is small for a small fermion number, as well as near the completed shell (due to the particle–hole symmetry, one only needs to interchange roles of the pair creation and pair annihilation operators). For the intermediate population of the shell, the correction is not small. However, the particle-number operator can then be approximated on average by a constant so that a simple renormalization leads again to Bose operators. The presence of many contributions with various values of K should not change the situation crucially in a system with random interactions since the multipoles $K = 0$ and $K = 1$ correspond to the constants of motion (see Section 2), while higher multipoles presumably will be averaged by random dynamics.

In the boson approximation for fermion pair operators, $P_{L\Lambda} \longrightarrow b_{L\Lambda}$, the Hamiltonian becomes the sum of random energies of independent bosons,

$$H \longrightarrow H^b = \sum_{L\Lambda}\omega_L b^\dagger_{L\Lambda}b_{L\Lambda} = \sum_{L\Lambda}\omega_L \hat{n}^b_{L\Lambda}. \quad (13)$$

Here, the energies ω_L are proportional to the original interaction parameters V_L. An example of the ground-state spin distribution f^b_J in the uniform ensemble for five bosons in space with allowed even values of L from 0 to 10 is given in Fig. 5, along with the corresponding statistical distribution (slightly different from that for fermions). We still see the pronounced effect of enhancement for $J = 0$, although it is smaller compared to typical results for fermions or for interacting bosons, but not for $J = J_{\max}$.

Now, we can argue that the bosonic approximation is not sufficient for explaining the effect of the enhancement. The source of the enhancement for spin zero in the bosonic system can be understood in the following way. In any realization of the random ensemble, one of the frequencies ω_L, let us say for $L = L_0$, takes the lowest value. The ground state of the Hamiltonian (12) corresponds to the condensation of all N bosons into the mode $L = L_0$. In the uniform ensemble, each value of L_0 can appear with the same probability $1/k$, where k is the number of allowed modes L. However, the results for the total spin J are different in the cases $L_0 = 0$ and $L_0 \neq 0$. In the first case, the ground state necessarily has the total spin $J = 0$. In the second case, the bosons with

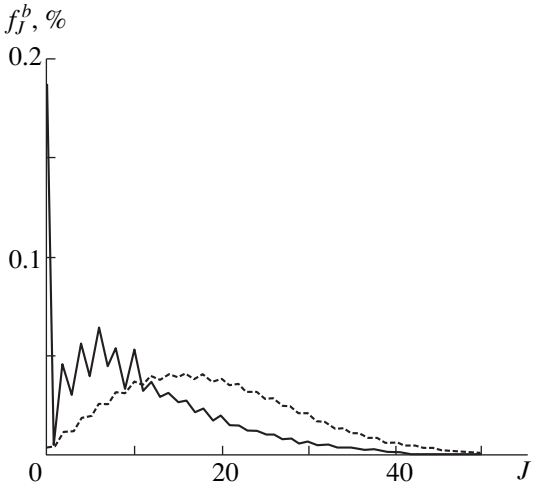

Fig. 5. The ground-state spin distribution f_J^b in the system of five independent bosons in the spin states $L = 0, 2, \ldots, 10$ (solid line) and the statistical distribution of total spins (dashed line).

$L = L_0$ still can couple to any total J allowed by the selection rules, so that the probability for any specific value of total spin is $\sim 1/k^2$ with all those states being degenerate in this approximation. This gives rise to the enhancement of $J_0 = 0$ and no enhancement for $J_0 = J_{\max}$. The fraction $f_0^b \sim 1/k$ is much smaller than that observed for a fermionic system. Moreover, it decreases as j increases because of the increase in the number of possible L values that contradicts the observations. Finally, the numerical experiment of Fig. 4 with pairing eliminated from the ensemble ($V_0 = 0$) shows no suppression of the fraction f_0, whereas in the bosonic case this would correspond to $\omega_0 = 0$, when the condensation to the $L = 0$ mode would be rather improbable. Indeed, the value $\omega_0 = 0$ would be the lowest frequency only for the realizations with all $\omega_{L\neq 0} > 0$, which happens with a small probability $\sim 2^{-(k-1)}$.

We can conclude that the deviations from the pure bosonic approximation associated with Fermi statistics are necessary for the manifestation of the enhancement effects. The kinematic and dynamic effects of pair interactions lift multiple degeneracies present in the bosonic picture and give preference to the limiting values of the total spin.

7. GEOMETRIC CHAOTICITY

The system with random interactions is expected to have eigenfunctions that are complicated "chaotic" superpositions of simple configurations of independent particles [8]. Two exact conservation laws, of the total particle number N and total spin J, divide the whole Hilbert space into classes. As mentioned in the Introduction, even the construction of correct linear combinations with a given value of J, for example, with the aid of the projection algorithm, leads to states of a high degree of complexity. This "geometric" chaoticity emerges as a consequence of the presence of multiple schemes of vector coupling of particle spins to the total spin J. Typically, one has to deal with nearly random angular-momentum coupling. High-j recoupling coefficients look almost as elements of random matrices, and the chains of the fractional parentage coefficients are close to random walks. The shell-model calculations invariably show that the angular-momentum projection is sufficient for obtaining the basis states $|k\rangle$ as combinations of the m-scheme Slater determinants (belonging to the same partition) with practically identical energy dispersion, or spreading width [8, 31].

The idea of geometric chaoticity can be used for developing approximations in the many-body problem that are not connected with the weakness of interactions. Instead, the contributions of the perturbation series can be classified in the degree of chaoticity related to angular-momentum coupling. This idea was utilized for the problems of fermions [32] or giant resonances [33] coupled to the soft-phonon field. The resulting technique is similar to the one used for disordered solids [34], and the most important graphs are rainbow ones which do not carry geometric chaoticity. It is known that the same graphs are the main ones in the diagrams for random matrix ensembles.

The notion of angular-momentum coupling as a random walk was used long ago in evaluation of the Fermi gas level density for a given value of J [22]. Roughly speaking, the result is equivalent to the thermal equilibrium of a rotating system with an average statistical moment of inertia. The analysis of chaotic eigenfunctions of the realistic shell model for nuclei [8] and atoms [10] shows that, in agreement with the concept of Fermi liquid, the mean-field orbitals are occupied by quasiparticles according to the Fermi–Dirac distribution. Combining these ideas, one could imagine that the average over the ensemble of random interactions should lead to the ensemble of ground states close to the thermal equilibrium of the rotating nucleus with the angular velocity corresponding to the angular momentum of the energetically favored configuration.

In the single-j model, the effective moment of inertia can be estimated directly from the rotational term, $K = 1$, of the Hamiltonian written in the *ph* form, Eq. (3). Using the explicit value of the corresponding 6j symbol in (6) and the angular-momentum operator (8), we obtain

$$H_{\rm rot} = A\mathbf{J}^2,$$
$$A = \frac{3}{4\Omega^2\mathbf{j}^4}\sum_{\text{even } L}(2L+1)V_L(\mathbf{L}^2 - 2\mathbf{j}^2). \tag{14}$$

The structure of this expression can be understood in simple physical terms. The contribution of the pair interaction for the pair spin L to the moment of inertia

changes its sign at $\mathbf{L}^2 = 2\mathbf{j}^2$, which corresponds to the absence of alignment of the partners (their spins are perpendicular to each other). At low L, pairs are antialigned, $\mathbf{L}^2 < 2\mathbf{j}^2$. If these pair states are attractive, $V_L < 0$, the contribution to the moment of inertia is positive, preferring a normal rotational spectrum with angular momentum increasing with excitation energy. Contrary to that, at high L, the pairs are aligned, $\mathbf{L}^2 > 2\mathbf{j}^2$, so that the attraction in such pairs leads to a negative contribution to the moment of inertia that favors the bands with an inverted spin sequence. The actual result is determined by the competition of all parts of the interaction. Being of a purely geometrical nature, the result (14) does not depend on the particle number, which enters only via restrictions on the allowed values of J. For small J, the rotational energy (14) is small as compared to the total energy found, for example, in the bosonic approximation. However, it plays an essential role in lifting the bosonic degeneracies. Another term in the *ph* Hamiltonian which corresponds to a constant of motion, namely, the particle number N, is that for $K = 0$,

$$H_0 = \frac{N^2}{2\Omega^2}\sum_L (2L+1)V_L. \tag{15}$$

However, being independent of the particle configuration, this term gives the energy reference point rather than the angular momentum splitting.

In what follows, we will have to establish an analog of the atomic physics Hund rule which decides on the ferromagnetic, $J_0 = J_{\max}$, or antiferromagnetic, $J_0 = 0$, character of the ground state. Even from this analogy, we can anticipate that these two possibilities, the lowest and the highest values of the ground-state spin, can be special and energetically favorable. For example, in the system of N identical interacting spins, the simplest Hamiltonian would be

$$H_{\rm sp} = \text{const} \times \sum_{a \neq b} \mathbf{s}_a \cdot \mathbf{s}_b = \text{const} \times [\mathbf{S}^2 - Ns(s+1)]. \tag{16}$$

The total ground-state spin S_0 will be zero for a positive constant, and $S_{\max} = Ns$ for a negative constant. If the constant has a random sign, the probabilities of the two extremes are 1/2. A similar situation takes place in any model with a rotational spectrum and an effective moment of inertia determined by a random interaction.

8. STATISTICAL APPROACH

Now, we can construct a simple statistical ensemble fulfilling the requirements of Fermi statistics and taking into account the constraints imposed by the conservation laws. We expect that the expectation values of physical quantities over the equilibrium state of the ensemble will be in approximate agreement with the average results for the ground state of the system governed by random interactions.

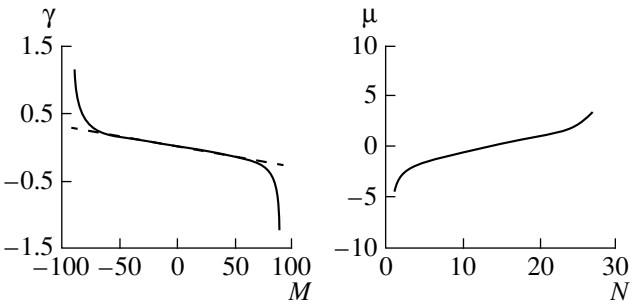

Fig. 6. $\gamma(N = 10, M)$ as a function of M and $\mu(N, M = 10)$ as a function of N for $j = 27/2$. The approximation with the Taylor expansion around $\gamma = 0$ is plotted with the dashed line; for μ this approximation is indistinguishable from the exact result.

In the presence of random interactions, the only direction which is singled out in the system is that of the total angular momentum. Therefore, the particle orbitals in the equivalent statistical ensemble are labeled by the projection quantum numbers m and are characterized by the mean occupancies n_m, so that the linear constraints for the particle number N and for the total angular momentum M are

$$N = \sum_m n_m, \quad M = \sum_m m n_m. \tag{17}$$

In the standard way, we are looking for the entropy maximum for the Fermi gas on a single-j level with the constraints (17). Introducing the Lagrange multipliers, μ of chemical potential and γ of effective angular frequency, we come to the Fermi–Dirac distribution

$$n_m = [e^{\gamma m - \mu} + 1]^{-1}. \tag{18}$$

This formulation is analogous to the cranking model description [3, 35] of the random coupling of individual spins with the cranking axis along the only available symmetry axis of the total spin [22, 36]. In contrast to the cranking model for collective rotation [3], where the rotational angular momentum is directed perpendicularly to the symmetry axis, here the total projection is equivalent to the K quantum number of the intrinsic spin of the nucleus. At the end, we orient our system in such a way that M is identified with the total spin J. The presence of the constraints creates an effective body-fixed frame and splits single-particle energies as $\epsilon_m = \gamma m$.

Figure 6 shows typical solutions for the Lagrange multipliers $\mu(N, M)$ and $\gamma(N, M)$. Time-reversal arguments require that μ and γ be even and odd functions of M, respectively. Therefore, $\gamma(N, 0) = 0$, and one can use the power-series expansion of Eq. (18) in the region around $M = 0$. As seen from Fig. 6, the dependence $\gamma(M)$ is close to linear, except for the very edge of max-

imum $|M|$. In the absence of cranking, $M = 0$, the distribution of occupancies is uniform,

$$n_m(N, 0) \longrightarrow n_m^0 = \bar{n} \equiv N/\Omega, \qquad \mu \longrightarrow \ln\frac{N}{\Omega - N}. \tag{19}$$

Taking into account the change of the chemical potential in the second order, we find the occupation numbers for the perturbational cranking:

$$n_m = \bar{n}\Big[1 - \gamma m(1-\bar{n}) + \frac{\gamma^2}{2}(m^2 - \overline{m^2})(1-\bar{n})(1-2\bar{n}) + \ldots\Big]. \tag{20}$$

Here, we have

$$\overline{m^2} = \frac{1}{\Omega}\sum_m m^2 = \frac{\mathbf{j}^2}{3}. \tag{21}$$

In the same approximation, the relation (17) between M and γ reads

$$M = -\gamma\bar{n}(1-\bar{n})\Omega\overline{m^2} = -\gamma\frac{2J_{\max}}{\Omega}\overline{m^2}, \tag{22}$$

where the maximum allowed spin $J_{\max}$ is given by Eq. (10). All corrections to the uniform occupation distribution in Eq. (20) are proportional to the intensity $\bar{n}(1-\bar{n})$ of fluctuations since the resulting total spin comes from the random coupling. The ratio M/γ is the statistical moment of inertia which determines the level density for given spin of the Fermi gas [22, 3]. It depends on the particle number and properties of single-particle space but not on the interaction parameters.

9. EQUILIBRIUM ENERGY

The expectation value of the Hamiltonian (1) in our statistical ensemble is given by Wick's theorem,

$$\langle H\rangle = \sum_L V_L \sum_{\Lambda m m'} \left|C_{mm'}^{L\Lambda}\right|^2 n_m n_{m'}. \tag{23}$$

Using the expansion (20) for the occupation numbers n_m, we come to the geometric sums of the Clebsch–Gordan coefficients squared with linear or bilinear expressions in m and m'. These sums can be easily calculated as the traces in space of states $|L\Lambda\rangle$ with fixed L. The remaining cranking parameter γ can now be expressed in terms of the total spin $M \longrightarrow J$. The final result up to the terms of the order J^4 is

$$\langle H\rangle_{N,J} = h_0 + h_2 J^2 + h_4 J^4, \tag{24}$$

where the coefficients h_p are sums of the contributions of all components of the interaction,

$$h_p = \sum_L (2L+1)V_L h_p(L), \tag{25}$$

and the geometric coefficients are

$$h_0(L) = \bar{n}^2, \tag{26}$$

$$h_2(L) = \frac{3}{2\Omega^2\mathbf{j}^4}(\mathbf{L}^2 - 2\mathbf{j}^2), \tag{27}$$

and

$$h_4(L) = \frac{9}{40}\frac{(1-2\bar{n})^2(3\mathbf{L}^4 + 3\mathbf{L}^2 - 12\mathbf{L}^2\mathbf{j}^2 - 6\mathbf{j}^2 + 8\mathbf{j}^4)}{(1-\bar{n})^2 N^2 \Omega^2 \mathbf{j}^8}. \tag{28}$$

We note that the coefficient $h_0(L)$, which in fact does not depend on L, and $h_2(L)$ coincide, up to a factor 2 coming from the correct inclusion of the exchange interactions, with the scalar part of the Hamiltonian H_0, Eq. (15), and the rotational part $H_{\rm rot}$, Eq. (14), respectively. We also see that the coefficients in high order rotational corrections are quite small.

The ground-state spin J_0 in a given realization of the ensemble of the interaction constants V_L is determined mostly by the sign of the rotational term h_2 with a possible correction from h_4. For a negative value of h_2, the energy minimum corresponds to the ground state with nonzero spin. If $h_2 \geq 0$ and $h_4 > 0$, the ground state has spin $J_0 = 0$. If, for a positive h_2, the fourth-order correction is negative, the zero spin still defines the local energy minimum. This minimum will be absolute if at the opposite edge, $J \longrightarrow J_{\max}$, the sum $h_2 + h_4 J_{\max}^2$ is still positive. Thus, in this approximation, the probability f_0 of having the ground-state spin equal to zero is typically close to 1/2 due to the smallness of h_4. More precisely,

$$f_0 = \int\limits_{S(h_2,h_4)} dh_2 dh_4 \mathcal{P}(h_2, h_4), \tag{29}$$

where the probability distribution $\mathcal{P}(h_2, h_4)$ is determined by the ensemble of V_L according to Eqs. (27) and (28), while the region S is the part of the positive h_2 half-plane where $h_4 > -(h_2/J_{\max}^2)$. For example, for a Gaussian ensemble of the parameters V_L with zero mean and variances σ_L, the linear combinations h_p are again Gaussian variables, and Eq. (29) gives a result close to 1/2,

$$f_0 = \frac{1}{4} + \frac{1}{2\pi}\arctan\left[\frac{Z + (X/J_{\max}^2)}{(XY - Z^2)^{1/2}}\right], \tag{30}$$

where the elements of the variance matrix in the (h_2, h_4) plane are

$$X = \sum_L [h_2(L)]^2 \sigma_L^2, \quad Y = \sum_L [h_4(L)]^2 \sigma_L^2,$$
$$Z = \sum_L h_2(L) h_4(L) \sigma_L^2. \tag{31}$$

In Fig. 7*a*, the dashed line shows the smooth behavior of the probability f_0 as a function of j for $N = 4$ particles. The solid line gives the results of the exact numerical diagonalization. Of course, the simple statistical theory cannot explain the observed staggering effects.

It would be premature to conclude from (24) that the remaining 50% of cases should reveal the maximum ground-state spin. Indeed, the expansion used in the derivation is not valid for large angular momenta. However, the wave functions for the largest possible spins are unique and can be constructed explicitly, irrespective of the interaction parameters. Their energies can be compared to the energies of lower spins. In this way, we improve slightly the results obtained above for spin $J_0 = 0$ (this is taken into account in plotting Fig. 7*a*) and extract the upper boundary for the probability of the maximum ground-state spin $J_{\max}$ (Fig. 7*b*). The consistency of the statistical approach is confirmed by the analysis of actual sets of random parameters V_L which lead to $J_0 = J_{\max}$. The average values V_L of this set found in the numerical data coincide (Fig. 8) with those found in the statistical model for $h_2 < 0$.

Thus, the statistical approach provides a natural qualitative explanation and reasonable quantitative estimate for the dominance of ground spin states $J_0 = 0$ and $J_0 = J_{\max}$. Additional small corrections can be introduced [16] by taking into account the difference of the widths of the energy distribution $\langle H^2 \rangle$ for different values of J. The remaining details of the picture, especially the nonmonotonic changes, require a more subtle approach.

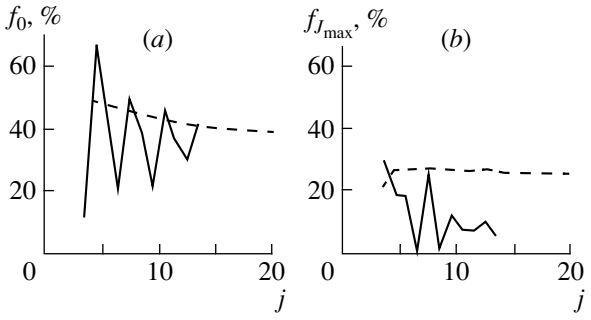

Fig. 7. (*a*) The fraction f_0 of ground-state spins $J_0 = 0$ as a function of (half integer) j: (solid line) numerical results and (dashed line) statistical theory; (*b*) the same for the maximum ground-state spin $J_{\max}$; here, the dashed line shows the upper boundary in the statistical theory.

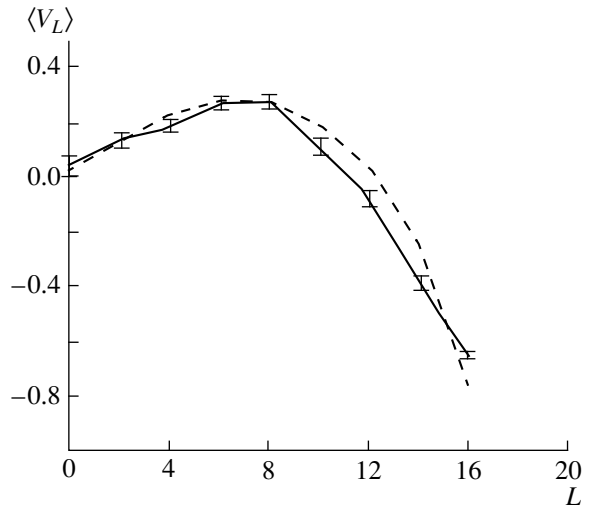

Fig. 8. The average values of the random parameters V_L as a function of L for the case where the ground-state spin $J_0 = J_{\max}$ with the statistical errors (solid line); the results of the statistical model for $h_2 < 0$ are plotted with the dashed line.

10. EIGENFUNCTIONS OF THE RANDOM HAMILTONIAN

If the apparent ordered signatures of the ground state, be it ferromagnetic or antiferromagnetic, are due to the random spin coupling, we could expect that the structure of the corresponding wave functions is close to that characteristic of chaotic dynamics [24]. For the zero ground-state spin, the appropriate reference function is that of the fully paired state $|0, p\rangle$ of seniority zero which would be the ground state for the pure pairing attractive interaction in our degenerate model (a particular choice of the parameters $V_0 = -1$, $V_{L \neq 0} = 0$). For any set of parameters from the random interaction ensemble, which leads to the zero ground-state spin, we calculate the overlap

$$x = |\langle J = 0, \text{g.s.} | 0, p \rangle|^2. \tag{32}$$

The histogram of the distribution $\mathcal{P}(x)$ is presented in Fig. 9*b* for the case of six particles on the $j = 11/2$ level. Clearly, the overlap is very low.

In the extreme chaotic limit, the eigenfunctions are expected to be nearly random superpositions of the basis states $|k\rangle$ with the uncorrelated amplitudes C_k constrained only by the orthonormality requirements. The distribution function of the (real) components of a given eigenfunction is the same as that of a multidimensional vector uniformly spread over a unit sphere, $\mathcal{P}(\{C_k\}) \propto \delta(\sum_k C_k^2 - 1)$. For the dimension d, this leads to the distribution function of any given compo-

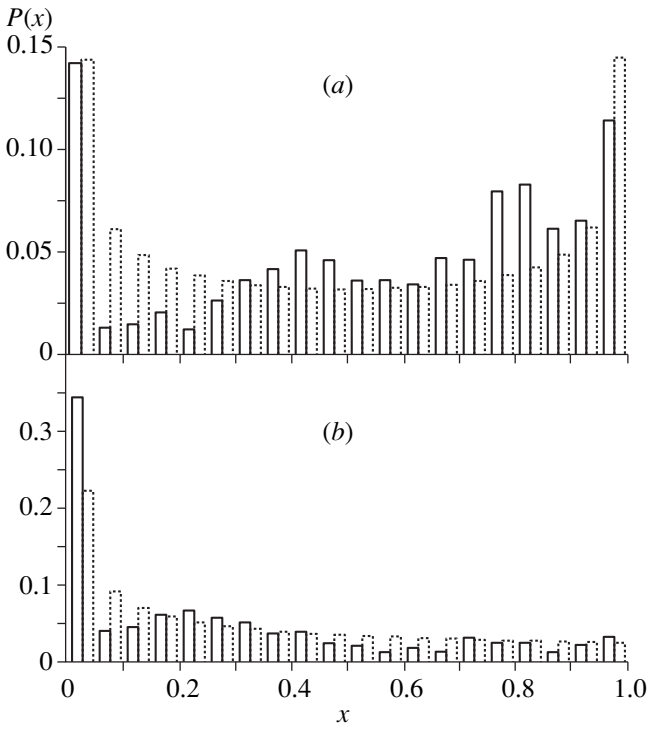

Fig. 9. The distribution of overlaps (solid histograms), Eq. (32), of ground states with $J_0 = 0$ with fully paired (seniority zero) state (*a*) for the ensemble with random $V_{L\neq 0}$ and regular pairing, $V_{L=0} = -1$, and (*b*) for the ensemble with all V_L random. The dashed histograms show the predictions for chaotic wave functions of dimension $d =$ (*a*) 2 and (*b*) 3.

nent C (a projection of the eigenvector onto a specified direction in Hilbert space)

$$\mathcal{P}(C) = \frac{\Gamma(d/2)}{\sqrt{\pi}\Gamma[(d-1)/2]}(1-C^2)^{(d-3)/2}\Theta(1-C^2). \quad (33)$$

In the limit of $d \gg 1$, Eq. (33) gives the Gaussian distribution with $\langle C^2\rangle = 1/d$, while the weights $x = C^2$ are distributed according to the Porter–Thomas law. Complicated nuclear shell-model wave functions obtained in realistic calculations with no random parameters are close to the chaotic limit. The typical d dependence can be unfolded [37] into a regular scheme of approximations, the so-called N scaling, which allows one to classify various processes going through the compound nucleus stage. The statistical enhancement of weak interaction effects observed via parity nonconservation in neutron resonances [38] is one of the most convincing illustration of statistical regularities seen on the level of individual wave functions.

In our examples, the dimensions d are typically not very large, but the statistical features are brought in by random interactions. We can look at the distribution of overlaps (32) as the representative of the distribution of components of eigenvectors along the pairing basis vector $|0, p\rangle$. Six particles on a $j = 11/2$ level give rise to $d = 3$ states of spin $J = 0$. In the chaotic limit, this would lead to $\mathcal{P}(C) =$ const, and, therefore,

$$\mathcal{P}_{d=3}(x) = \frac{1}{2\sqrt{x}}, \quad 0 < x \le 1 \quad (34)$$

(this distribution appears in the problem of pion multiplicity from a disordered chiral condensate [39, 40]). This prediction (the dashed histogram in Fig. 9*b*) is in agreement with the numerical results. Another situation is shown in Fig. 9*a*, where the data, the solid histogram, are taken for the ensemble which contains regular attractive pairing, $V_0 = -1$, plus uniformly random interactions in all channels with $L > 0$. The presence of pairing generates a significant probability for the paired ground state, a peak at $x = 1$. However, it is possible to show that there exists an "antipaired" state with $J = 0$ but with a vanishingly small probability of being a ground state, so that the space of the candidates for the ground-state position is effectively two-dimensional. For $d = 2$,

$$\mathcal{P}_{d=2}(x) = \frac{1}{\pi\sqrt{x(1-x)}}, \quad 0 < x \le 1, \quad (35)$$

which agrees qualitatively with the data, Fig. 9*a*.

11. CONCLUSION

We have taken the first steps towards an understanding of the role of random interactions in the structure of a small fermion system. Although only the simplest model with degenerate single-particle orbitals was considered, we hope that the results correctly emphasize the important functions of geometric chaoticity which inevitably appears in a many-fermion system as a consequence of rotational invariance. In fact, the system behaves as a Fermi liquid of quasiparticles with randomly coupled individual spins. The resulting ordering of total spins possible in the system is controlled by the interaction. If all components of interaction are random, the lowest and the maximum possible total spins are preferred for the ground state. In practice, this should happen if the two-body matrix elements of residual forces are incoherent. Then, the interaction induces mainly collision-like scattering processes which equilibrate the system, keeping, in general, the geometric (ferromagnetic or antiferromagnetic) spin ordering. We see here an example of a clear correlation between the classes of states with different exact quantum numbers but governed by the same Hamiltonian. In spite of the apparently ordered features of the energy spectra, the corresponding wave functions within a given class are close to those expected for chaotic dynamics (in the extreme limit, to the predictions of the GOE). In this sense, we would expect the even–even nuclei to have the ground-state spin $J = 0$ without strong pairing forces. The coherent components of the interaction should be sufficiently strong to introduce the dynamical energetic structure.

The numerical data contain more information than we explained. We did not discuss the statistical probabilities for sequences of ordered states as rotational or vibrational bands which seem to appear with an enhanced probability, in particular, in the randomly interacting boson model [16], perhaps because of a sharp dependence of the IBM eigenvectors on the parameters. Many specific features of the numerical results, such as, for example, odd–even staggering of the distribution function f_J, are related to more subtle physical aspects and cannot be understood without detailed studies of the vector coupling schemes in the given spaces along with the dynamical equations of motion. In general, the physics of the relationship between geometric chaoticity and pure dynamic effects in finite many-body systems is a promising subject for future studies.

The results of this paper were partly presented in [24] and [41].

ACKNOWLEDGMENTS

The question of the bosonic approximation was studied together with P. Cejnar during his visit to the NSCL. The authors are grateful to G.F. Bertsch, R.A. Broglia, B.A. Brown, V. Cerovski, V.V. Flambaum, M. Horoi, F.M. Izrailev, D. Kusnezov, and H.A. Weidenmüller for constructive discussions.

The support from the US National Science Foundation, grant nos. 96-05207 and 00-70911, is highly appreciated.

REFERENCES

1. L. D. Landau, Zh. Éksp. Teor. Fiz. **30**, 1058 (1956) [Sov. Phys. JETP **3**, 920 (1956)].
2. A. B. Migdal, *Theory of Finite Fermi Systems and Applications to Atomic Nuclei* (Interscience, New York, 1967; Nauka, Moscow, 1983).
3. A. Bohr and B. M. Mottelson, *Nuclear Structure* (Benjamin, New York, 1969, 1974; Mir, Moscow, 1981), Vols. 1, 2.
4. M. L. Mehta, *Random Matrices* (Academic, Boston, 1991).
5. T. A. Brody, J. Flores, J. B. French, *et al.*, Rev. Mod. Phys. **53**, 385 (1981).
6. T. Guhr, A. Müller-Groeling, and H. A. Weidenmüller, Phys. Rep. **299**, 189 (1998).
7. V. Zelevinsky, M. Horoi, and B. A. Brown, Phys. Lett. B **350**, 141 (1995).
8. V. Zelevinsky, B. A. Brown, N. Frazier, and M. Horoi, Phys. Rep. **276**, 85 (1996).
9. M. Horoi, B. A. Brown, and V. Zelevinsky, Phys. Rev. Lett. **74**, 5194 (1995).
10. V. V. Flambaum and F. M. Izrailev, Phys. Rev. E **53**, 5729 (1996).
11. V. G. Zelevinsky, Nucl. Phys. A **555**, 109 (1993).
12. T. Døssing *et al.*, Phys. Rep. **268**, 1 (1996).
13. C. W. Johnson, G. F. Bertsch, and D. J. Dean, Phys. Rev. Lett. **80**, 2749 (1998).
14. C. W. Johnson, G. F. Bertsch, D. J. Dean, and I. Talmi, Phys. Rev. C **61**, 014311 (2000).
15. R. Bijker, A. Frank, and S. Pittel, Phys. Rev. C **60**, 021302 (1999).
16. R. Bijker and A. Frank, Phys. Rev. Lett. **84**, 420 (2000); nucl-th/0004002.
17. V. Zelevinsky, Annu. Rev. Nucl. Part. Sci. **46**, 237 (1996).
18. S. T. Belyaev, Zh. Éksp. Teor. Fiz. **39**, 1387 (1961) [Sov. Phys. JETP **12**, 968 (1961)].
19. I. Talmi, *Simple Models of Complex Nuclei* (Harwood, New York, 1993).
20. G. Racah, Phys. Rev. **78**, 622 (1950).
21. B. A. Brown *et al.*, OXBASH code, MSUCL-524 (1988).
22. T. Ericson, Adv. Phys. **9**, 425 (1960).
23. M. Horoi and V. Zelevinsky, Bull. Am. Phys. Soc. **44** (1), 397 (1999); M. Horoi, J. Kaiser, and V. Zelevinsky, Bull. Am. Phys. Soc. **45** (1), 78 (2000).
24. M. Horoi, B. A. Brown, D. Mulhall, and V. Zelevinsky, Bull. Am. Phys. Soc. **44** (5), 45 (1999).
25. J. Bardeen, L. N. Cooper, and J. R. Schrieffer, Phys. Rev. **108**, 1175 (1957).
26. V. Zelevinsky, B. A. Brown, and M. Horoi, Bull. Am. Phys. Soc. **41**, 860 (1996).
27. Yu. T. Grin' and A. I. Larkin, Yad. Fiz. **2**, 40 (1966) [Sov. J. Nucl. Phys. **2**, 27 (1966)].
28. S. T. Belyaev and V. G. Zelevinsky, Zh. Éksp. Teor. Fiz. **42**, 582 (1962) [Sov. Phys. JETP **15**, 1104 (1962)]; Nucl. Phys. **39**, 582 (1962).
29. A. Klein and E. R. Marshalek, Rev. Mod. Phys. **63**, 375 (1991).
30. A. Arima and F. Iachello, *The Interacting Boson Model* (Cambridge Univ. Press, Cambridge, 1987).
31. N. Frazier, B. A. Brown, and V. Zelevinsky, Phys. Rev. C **54**, 1665 (1996).
32. S. T. Belyaev and V. G. Zelevinsky, Yad. Fiz. **2**, 615 (1965) [Sov. J. Nucl. Phys. **2**, 442 (1966)].
33. V. V. Samoilov and M. G. Urin, Nucl. Phys. A **567**, 237 (1994).
34. S. F. Edwards, Philos. Mag. **3**, 1020 (1958).
35. R. K. Bhaduri and S. Das Gupta, Nucl. Phys. A **212**, 18 (1973).
36. A. L. Goodman, Nucl. Phys. A **592**, 151 (1995).
37. V. V. Flambaum and O. P. Sushkov, Nucl. Phys. A **412**, 13 (1984).
38. V. V. Flambaum, Phys. Scr. T **46**, 198 (1993).
39. A. A. Anselm, Phys. Lett. B **217**, 169 (1989).
40. A. Volya, S. Pratt, and V. Zelevinsky, Nucl. Phys. A **671**, 617 (2000).
41. D. Mulhall, A. Volya, and V. Zelevinsky, Phys. Rev. Lett. **85**, 4016 (2000).

Physics of Atomic Nuclei, Vol. 64, No. 3, 2001, pp. 536–539. Translated from Yadernaya Fizika, Vol. 64, No. 3, 2001, pp. 590–593.

90th ANNIVERSARY OF A.B. MIGDAL'S BIRTHDAY
ELEMENTARY PARTICLES AND FIELDS

Relation between Energy and Mass in Bohr's Essay on His Debate with Einstein

L. B. Okun*

Institute of Theoretical and Experimental Physics, Bol'shaya Cheremushkinskaya ul. 25, Moscow, 117259 Russia

Received July 12, 2000

Abstract—The famous debate between Einstein and Bohr on the (in)consistency of quantum mechanics was described in detail by Bohr in his essay of 1949. The present article comments not on the main subject of the debate but only on the terminology that is relevant to the notions of the theory of relativity and which was used by the participants. In particular, their statement on the equivalence of mass and energy should not be taken literally. In fact, the rest energy is meant here. The authority of the two great physicists should not be misused to preserve the confusing terminology. *© 2001 MAIK "Nauka/Interperiodica".*

1. INTRODUCTION

The debate between Einstein and Bohr on quantum mechanics achieved a culmination point at the Sixth Solvay Congress in October 1930. In this debate, the former tried to prove the intrinsic inconsistency of quantum mechanics, while the latter aimed at showing that the gedanken experiments proposed by Einstein do not lead to such contradictions. This controversy was skillfully described in Bohr's article [1] published in 1949 and dedicated to Einstein's 70th birthday.

Bohr's article stimulated a wealth of contradictory responses from physicists, historians of physics, and philosophers. These include (in chronological order) M. Born, V. Fock, K. Popper, Y. Aharonov, D. Bohm, L. Rosenfeld, J. Holton, M. Klein, K. von Weizsäcker, M. Jammer, and A. Pais. A separate chapter of Jammer's monograph [2] is devoted to these responses. Articles on this theme have appeared in succeeding years as well (see, for example, [3, 4]). The latest of these was published in February 2000.

Various aspects of the debate between Bohr and Einstein and further development of the ideas stated in it are described in the miscellanea *Quantum Theory and Measurement* (over 800 pages) [5], which contains original articles and comments by the main participants and other eminent physicists.

2. EINSTEIN'S GEDANKEN EXPERIMENT

In the gedanken experiment proposed by Einstein in October 1930, there was a box filled with photons and hung by a spring balance, so that its vertical translation could be measured with a special scale. Thus, variations in the box mass could be measured by weighing.

In a lateral wall of the box, there was a small hole closed by a shutter that was controlled by a clock placed within the box. The clock opened the hole for a very short time interval, so that the instant at which a single photon escaped from the box could be determined to a precision as high as was desired.

On the other hand—as Bohr wrote [1]—the general energy–mass relation expressed by Einstein's famous formula

$$E = mc^2$$

made it possible to measure the photon energy, to any desired precision, by weighing the whole box prior to and after this event. According to Einstein's idea, this resulted in a contradiction with the known uncertainty relation

$$\Delta E \Delta T > h,$$

where ΔE is the uncertainty in the photon energy, ΔT is the uncertainty in the instant of its escape, and h is the Planck constant. Since the aforesaid suggested that both ΔE and ΔT could be arbitrarily small, their product could also be arbitrarily small in the gedanken experiment being discussed.

3. FAMOUS FORMULA $E = mc^2$

Prior to considering the way in which Bohr refuted Einstein's arguments, it is worth emphasizing that, in referring to Einstein's famous formula $E = mc^2$, Bohr did not specify the definitions of energy and mass. In [1], Bohr wrote that the discovery of induced radioactivity provided the most direct test of Einstein's fundamental law of mass–energy equivalence.

From these statements of Bohr, a reader that is insufficiently conversant with these matters could deduce that a photon with energy E has the mass $m = E/c^2$, and so does any particle or body.

This false interpretation of Einstein's famous formula is widespread in the popular-science literature

* e-mail: okun@heron.itep.ru

despite attempts at stamping it out (see, for example, [6–9]). Within the theory of relativity, it inevitably entails the completely superfluous notion of the rest mass and the use of nonrelativistic notions like the inertia mass and the gravitational mass (which were mentioned by Bohr in connection with the formula $E = mc^2$).

The phrase "equivalence of mass and energy" is repeated in the monograph [2] and in the articles [3, 4], where it is stated that energy has a weight. In [4], m is defined either as a "mass" or as a "rest mass."

4. E OR E_0? 1905–1921

Possibly, there would have been no reason for that inexact interpretation if Bohr had explained in more detail that E in Einstein's formula was the energy inherent in a body of mass m at rest, or, in other words, the rest energy of the body. It was just this meaning that was assigned to it by Einstein when he was deducing his formula in 1905 [10]. This follows from the fact that, in this article, he considered a body at rest that had emitted two oppositely directed light waves carrying away energy but not momentum, so that the body remained at rest after the emission event.

Einstein's discovery was as follows: if a body emits energy L in the form of radiation, then the mass of the body decreases by L/V^2. Obviously, it is of no importance in this case that the energy emitted by the body is converted directly into radiant energy. Owing to this, we arrive at the more general conclusion that the mass of a body is a measure of its energy content: if the energy changes by L, the mass changes accordingly by $L/(9\times10^{20})$, the energy and the mass being measured in ergs and in grams, respectively.

Obviously, V is the speed of light. It is interesting to note that there was no special symbol for mass in [10]. In present-day notation, L/V^2 is the right-hand side of the equation

$$\Delta m = \Delta E_0/c^2,$$

where E_0 is the rest energy. This notation dates back to Einstein's monograph *The Meaning of Relativity* [11], where Eq. (44) has the form

$$E_0 = mc^2$$

and where E_0 is referred to as the energy of a body at rest.

It should be emphasized that Einstein was not consistent in the period between the publication of the article [10] and the publication of the monograph [11]; occasionally, he interpreted E in his famous formula as the total energy of a body and wrote on mass–energy equivalence. It is possible that this inconsistency helped him to predict the effect of the gravitational red shift (1907), the deviation of a light ray by the Sun (1911),[1)] and eventually to create the general theory of relativity (1916). However, this inconsistency gave rise to the terminological confusion that has existed to date.

5. E OR E_0? 1921–1955

An interchange of the correct and incorrect formulations of the mass–energy relation in Einstein's articles published in the 1920s–1940s contributed greatly to this confusion. This can easily be seen in the second of the four volumes of his collected works.[2)] He mentions the equivalence of energy and inertial mass in his report [12]. The title of the lecture [13] is "Elementary Derivation of the Equivalence of Mass and Energy." At the same time, it is the rest energy, and not energy in general, that is mentioned in the main body of this lecture, where he writes that, here, it is natural to assign the rest energy m (mc^2 in standard units) to a particle at rest and that the supposed mass–energy equivalence exists as well; a further statement is that the relation $E_0 = m$ proves the equivalence of the inertia mass and the rest energy.

In the minor note [14], however, which has the same title "Elementary Derivation of the Equivalence of Mass and Energy," the term rest energy is absent, and the last paragraph says that this relation expresses the law of energy–mass equivalence. The increase of E in energy is associated with the increase of E/c^2 in mass. Since the definition of energy usually admits arbitrariness in an additive constant, one can choose this constant in such a way that $E = Mc^2$.

The first phrase of the next article, "$E = mc^2$: An Urgent Problem of Our Time" [15], comments on the principle of mass–energy equivalence. Two pages later, we can find the statement that the equivalence of mass and energy is usually expressed (although this is not quite correct) by the formula $E = mc^2$, where c is the speed of light equal to about 186000 miles per second, E is the energy content of a body at rest, and m is its mass.

In the article [16], which was written for an encyclopedia, Einstein omits the term "rest energy" once again. Summarizing the basic results of the special theory of relativity, he states that this demonstrates the equivalence of mass and energy.

These "terminological oscillations" are a real psychological puzzle. It seems impossible that Einstein was annoyed to pinpoint each time that he meant the rest energy E_0. He rather tried to proceed on equal terms with the reader, who had got used to "the famous formula $E = mc^2$" from his school days. Possibly, Einstein tried to emphasize the philosophical aspect of the problem: it is important that mass is related to energy, but it is not so important to which energy specifically. Only one thing is doubtless: from 1921 to the end of his life (1955), Einstein had spoken and written either explic-

[1)] The angle of deviation as calculated in 1911 was one-half as large as the correct value predicted by Einstein on the basis of the general theory of relativity.

[2)] Translated and published in Russian.

itly or implicitly about the equivalence of the mass of a body and its rest energy.

6. BOHR'S COUNTERARGUMENT

Bohr did not sleep all night long, thinking over Einstein's arguments contra the relation $\Delta T\Delta E > h$ (see, for example, [2]). In the morning, he disproved these arguments using Einstein's theory of general relativity. Bohr described it himself as follows [1]. In order to discuss the problem, it appeared to be necessary to consider the consequences of identifying the inertia mass with the gravitational mass that are caused by the use of the relation $E = mc^2$. It was especially necessary to take into account the relation between the rate of the clock and its position in the gravitational field. This relation, which is well known from the red shift of the lines of the Sun spectrum, follows from Einstein's principle of equivalence of effects of gravity and phenomena observed in accelerated frames of reference.

Suppose that measurement of the box weight by a spring balance to a precision Δm requires estimating its vertical translation to a precision Δq. According to the relation $\Delta q\Delta p \approx h$, this generates an uncertainty Δp in the box momentum. This uncertainty in turn must be smaller than the total momentum that body of mass Δm can acquire over the weighing period T owing to the effect of the gravitational field; that is,

$$\frac{h}{\Delta q} \approx \Delta p < Tg\Delta m,$$

where g is the acceleration due to gravity.

The position of the clock that is fixed rigidly within the box and which controls the shutter must also have the uncertainty Δq. But according to the general theory of relativity, a vertical translation of the clock changes its rate in such a way that

$$\frac{\Delta T}{T} = \frac{g\Delta q}{c^2}.$$

From the last two relations, it follows that

$$\Delta T > \frac{h}{c^2\Delta m}.$$

By using the "famous formula" in the form $\Delta E = \Delta mc^2$, Bohr obtained the required relation

$$\Delta T\Delta E > h.$$

Jammer writes that, after the Sixth Solvay Congress, Einstein concentrated on attempts at proving the incompleteness of quantum mechanics rather than on attempts at proving its inconsistency (see [2]).

7. ADDITIONAL COMMENTS ON TERMINOLOGY

Many authors who critically analyzed Bohr's proof mentioned above discussed various details of time measurement (so-called internal and external measurement) and the interpretation of the relation $\Delta T\Delta E > h$. However, I am unaware of any critical comment on energy–mass equivalence or on the identity of the inertia mass and the gravitational mass. Moreover, some authors wrote about weighing energy or stated that energy has a weight.

It is absolutely obvious that, in order to describe Einstein–Bohr's gedanken experiment unequivocally, it is necessary and sufficient to substitute the clause "rest energy" for the word "energy." The same concerns the weight of energy. As to identifying the inertia mass with the gravitational mass, these terms, as well as their identification, belong to the notions of Newtonian nonrelativistic theory. After all, it is widely known that the inertial properties of relativistic particles are controlled by their energy and that the gravitational properties are determined by the energy–momentum tensor, and not by the mass.

It should be emphasized that Bohr was absolutely right to explain the red shift of the spectral lines in a static gravitational field by the variation of the clock rate—that is, by the shift of atomic levels—and not by the photon weight. (A comparison of these two alternative explanations is drawn in [17, 18], where it is explained in detail that the second is wrong).

8. CONCLUSION

In summary, Bohr's analysis in [1] does not lead to the conclusion, despite some terminological faults, that the photon with energy E has the mass $m = E/c^2$.

ACKNOWLEDGMENTS

I am grateful to V.L. Telegdi and V.B. Braginsky, who called my attention to the articles [1] and [4], respectively, in connection with the problem of mass–energy equivalence and to A.Yu. Morozov and K.G. Selivanov for stimulating discussions.

This work was supported by the Russian Foundation for Basic Research (project no. 00-15-96562) and in part by A. von Humboldt Foundation.

POSTSCRIPT

When I got acquainted with A.B. Migdal fifty years ago, problems of history and philosophy of physics were of small interest to him, since he was fascinated by solving specific scientific problems and taught his pupils, me among them, to do that. In the late 1970s, the focus of his interests shifted drastically. He kept studying the articles by Bohr, Einstein, and other classical scientists. He lectured on the history of physics and on the psychology of creative activity in science. His popular-science articles appeared one after another [19–23], and many of them were translated into foreign languages. He became the editor-in-chief of the *Encyclopedic Dictionary for the Young Physicist* [24]. I often

recollect A.B. Migdal with deep gratitude, and I thought about him very frequently when I was writing this note about the debate between Bohr and Einstein. I believe that he would have taken interest in this note.

REFERENCES

1. N. Bohr, in *Albert Einstein: Philosopher-Scientist*, Ed. by P. A. Schilpp (Library of Living Philosophers, Evanston, 1949), Vol. VII, p. 200.
2. M. Jammer, *The Philosophy of Quantum Mechanics: The Interpretations of Quantum Mechanics in Historical Perspective* (Wiley, New York, 1974), Chap. 5.
3. W. G. Unruh and G. I. Opat, Am. J. Phys. **47**, 743 (1979).
4. Y. Aharonov and B. Reznik, Phys. Rev. Lett. **84**, 1368 (2000).
5. *Quantum Theory and Measurement*, Ed. by J. A. Wheeler and W. H. Zurek (Princeton Univ. Press, Princeton, 1983).
6. E. Taylor and J. A. Wheeler, *Spacetime Physics* (Freeman, New York, 1992, 3rd ed.), pp. 258, 272.
7. L. B. Okun', Usp. Fiz. Nauk **158**, 511 (1989) [Sov. Phys. Usp. **32**, 629 (1989)].
8. L. B. Okun, Phys. Today **42**, 31 (1989); **43**, 13 (1990); **43**, 15 (1990); **43**, 115 (1990); **43**, 117 (1990).
9. L. B. Okun, Eur. J. Phys. **15**, 403 (1998).
10. A. Einstein, *Collection of Scientific Works in Four Volumes* (Nauka, Moscow, 1966), Vol. 1, p. 36.
11. A. Einstein, *Collection of Scientific Works in Four Volumes* (Nauka, Moscow, 1966), Vol. 2, p. 5.
12. A. Einstein, *Collection of Scientific Works in Four Volumes* (Nauka, Moscow, 1966), Vol. 2, p. 109.
13. A. Einstein, *Collection of Scientific Works in Four Volumes* (Nauka, Moscow, 1966), Vol. 2, p. 416.
14. A. Einstein, *Collection of Scientific Works in Four Volumes* (Nauka, Moscow, 1966), Vol. 2, p. 650.
15. A. Einstein, *Collection of Scientific Works in Four Volumes* (Nauka, Moscow, 1966), Vol. 2, p. 653.
16. A. Einstein, *Collection of Scientific Works in Four Volumes* (Nauka, Moscow, 1966), Vol. 2, p. 657.
17. L. B. Okun', K. G. Selivanov, and V. L. Telegdi, Usp. Fiz. Nauk **169**, 1141 (1999).
18. L. B. Okun, K. G. Selivanov, and V. L. Telegdi, Am. J. Phys. **68**, 115 (2000).
19. A. B. Migdal, *Subscription Popular Scientific Series "Physics,"* No. 7: *Search for Truth* (Znanie, Moscow, 1978).
20. A. B. Migdal, *Search for Truth* (Molodaya Gvardiya, Moscow, 1983).
21. A. B. Migdal, *How Physical Theories Occur* (Pedagogika, Moscow, 1984).
22. A. B. Migdal, *Subscription Popular Scientific Series "Physics,"* No. 3: *Quantum Physics and Niels Bohr* (Znanie, Moscow, 1987).
23. A. B. Migdal, *Library "Quantum,"* Vol. 75: *Quantum Physics for Grown-up and Youngs* (Nauka, Moscow, 1989).
24. *Encyclopedic Dictionary for the Young Physicist. For Older and Middle Age*, Ed. by A. B. Migdal (Pedagogika, Moscow, 1984).

Translated by E. Kozlovskiĭ

Physics of Atomic Nuclei, Vol. 64, No. 3, 2001, pp. 540–547. From Yadernaya Fizika, Vol. 64, No. 3, 2001, pp. 594–601.

90th ANNIVERSARY OF A.B. MIGDAL'S BIRTHDAY
ELEMENTARY PARTICLES AND FIELDS

String Theory as a Universal Language*

A. M. Polyakov

Joseph Henry Laboratories, Princeton University, New Jersey, USA

Received August 24, 2000

Abstract—Some new results and new speculations on various topics are submitted. They include discussion of open strings in the AdS space, unusual features of *D* branes, and conformal gauge theories in higher dimensions. The infrared screening of the cosmological constant and the "brane worlds" are also discussed. © *2001 MAIK "Nauka/Interperiodica".*

1. PREFACE

Forty years ago, Sasha Migdal introduced me to his father, the renowned theoretical physicist Arkady Benedictovich Migdal. That was one of the most important moments of my life. He became my mentor and friend.

A.B., as people called him, was at the center of a highly intensive, if not turbulent, scientific and social life. At that time, he had just completed a set of admirable papers which I have reread to this day with excitement and fascination. The first one was a precursor of the Fermi liquid theory. By the courageous use of completely novel methods of quantum field theory, he found a discontinuity in the distribution of interacting Fermi particles. That meant that the notion of a quasiparticle is well defined, even when the interaction is strong. This work is fundamental—it started the many-body theory in its modern form.

My other favorite is the work on electron–phonon interaction. I am still amazed how he managed to get through infinite sets of Feynman diagrams, integral equations, etc. It was like climbing Everest for the first time (I must say that the work on these topics by some great physicists like J. Schwinger, done at about the same time, brought much more modest results). However, A.B. remembered this work with some sadness. The reason was that he was actually looking for the mechanism of superconductivity. He developed this powerful apparatus, used it for the one-electron Green's functions, and planned to look at the two-electron Green's function next. At that moment, Bardeen, Cooper, and Schrieffer developed the theory of superconductivity in a simplified model without much formalism but with great physical intuition. A.B. told me this story, and it was a good lesson for me. There is some consolation in the fact that, in the modern refined description of superconductors, the methods developed by A.B. play a crucial role.

I learned many things about life and about physics from A.B. There was always an area of excitement surrounding him, whether he was talking about physics, showing his highly original sculptures, or camping in the mountains. It was interesting to see in the last case how professional alpinists, usually stern independent people, respected A.B. and considered him as a high authority in the problems of life. He was very generous in everything. Once he nominated me for some prize, and I said, quite correctly, that I didn't contribute enough to deserve it. "Doesn't matter, you will repay later" (*Nichevo, potom otdash*) replied A.B.

He lived in difficult times. It is quite amazing that by the sheer strength of personality he managed to create his own fascinating world, well isolated from the hostile environment. He included his friends in this world and in many cases managed to help and to protect them.

The article that follows this preface would probably displease A.B. because of its somewhat formal character. But his intuition (hopefully) would tell him that there is something there, and his critique would be moderate.

2. INTRODUCTION

String theory is a beautiful and dangerous subject. On the one hand, it is a top achievement of theoretical physics, exploiting the most advanced and daring methods. On the other hand, without guidance from experiments, it can easily degenerate into a collection of baroque curiosities, some kind of modern alchemy looking for a philosophers' stone.

This danger can be somewhat reduced if we try to study string theory in connection with some concrete physical problem and then extrapolate the experience gained to the Planck domain unreachable by experiments. This is a well-established strategy in theoretical physics. For example, one can learn about Cherenkov radiation while studying supersonic aerodynamics. And usually, there is the "back reaction": the technical progress at the frontier turns out to be helpful in solving the old problems. Thus, it is conceivable that string theory will provide us with the language for future theoretical physics.

* This article was submitted by the author in English.

1063-7788/01/6403-0540$21.00 © 2001 MAIK "Nauka/Interperiodica"

In this paper, I will examine a number of problems in which the language of string theory is appropriate and effective. We begin with the problem of quark confinement. The task here is to find the string description of the color-electric flux lines emerging in QCD. Recently, there has been considerable progress in this field. Various aspects of it have been reviewed in [1, 2]. I shall not review again these developments and instead shall concentrate on new results. After that, we will discuss some general features of D branes, conformal gauge theories in higher dimensions, and speculations concerning the cosmological constant.

3. THE IMAGE OF GLUONS AND ZIGZAG SYMMETRY

As was explained in the above-mentioned references, a string theory, needed to describe gauge fields in four dimensions, must be formulated in the $5d$ space with the metric

$$ds^2 = d\varphi^2 + a^2(\varphi)d\mathbf{x}^2. \quad (1)$$

This curved $5d$ space is a natural habitat for the color-electric flux lines. If, apart from the pure gauge fields, there are some matter fields in the theory, they must correspond to extra degrees of freedom on the world sheet. In some cases, these extra degrees of freedom can be balanced so that the field-theory β function is equal to zero. These cases are the easiest ones since the conformal symmetry of the field theory requires conformal symmetry of the string background and determines it completely as $a(\varphi) \sim e^{\alpha\varphi}$, where α is some constant. After an obvious change of variables, the metric takes the form

$$ds^2 = \sqrt{\lambda}y^{-2}(dy^2 + d\mathbf{x}^2), \quad (2)$$

where λ is related to the coupling constant of field theory. When $\lambda \gg 1$, the curvature of this $5d$ space is small and the $2d$ sigma model describing the string in the above background is weakly coupled. This greatly simplifies the analysis, and we will concentrate on this case. Our aim in this section will be to demonstrate that open strings in this background have some very unusual properties allowing us to identify them with gluons.

Before starting, let us recall that at present we have two possible approaches to the question of field–string correspondence. None of them is fully justified, but both have certain heuristic power. In the first approach, one begins with a stack of D branes describing a gauge theory and then replaces the stack by its gravitational background. In the second approach, one does not introduce D branes and starts directly with the sigma-model action, adjusting the background so that the boundary states of this string describe the gauge theory. The key principle here is the zigzag symmetry. This is a requirement that these boundary states consist of vector gluons (and matter fields, if present) and nothing else.

The situation is very unusual. Normally we have an infinite tower of states in both open and closed string sectors. Here, we need a string theory in which the closed string sector contains an infinite number of states, while the open sector has a finite number of field-theory states. Our first task will be to explore how this is possible.

To set the stage, let us remember how open strings are treated in the standard case [3]. One begins with the action

$$S = \frac{1}{2}\int_D (\partial x)^2 + i\int_{\partial D} A_\mu dx_\mu, \quad (3)$$

where D is a unit disk, ∂D is its boundary, and A_μ is the vector condensate of the open string states. The possible fields A_μ are determined from the condition that the functional integral

$$Z[A] = \int Dx e^{-S} \quad (4)$$

is conformally invariant. The explicit form of this condition is derived by the splitting

$$x = c + z, \quad (5)$$

where c is a slow variable, while z is fast, and integrating out z. Conformal invariance requires vanishing of the divergent counterterms and that restricts the background fields. It is convenient to integrate first the fields inside the disk with the fields at the boundary being fixed. That gives the standard boundary action

$$S_B = \frac{1}{2}\int \frac{du\,dv}{(u-v)^2}(x(u)-x(v))^2 + i\int A_\mu dx_\mu. \quad (6)$$

We see that x_μ are the Gaussian fields with the correlation function (in the momentum space)

$$\langle x_\mu(p)x_\nu(-p)\rangle \sim \delta_{\mu\nu}|p|^{-1}. \quad (7)$$

Expanding the second term in z, we obtain

$$S_B \approx \frac{1}{2}\sum |p|z(p)z(-p) + \int \nabla_\lambda F_{\sigma\mu}(c)\frac{dc_\mu}{ds}z_\lambda(s)z_\sigma(s)ds. \quad (8)$$

Using the fact that

$$\langle z_\lambda(s)z_\sigma(s)\rangle \sim \delta_{\lambda\sigma}\int^\Lambda \frac{dp}{|p|}, \quad (9)$$

where Λ is an ultraviolet cutoff, we obtain as a condition that the divergence cancels (in this approximation):

$$\nabla_\lambda F_{\lambda\mu} = 0. \quad (10)$$

This is the on-shell condition for the massless string mode. Qualitatively, the same treatment is applicable to the massive states as well. In this case, one perturbs S_B with the operator

$$\Delta S_B = \int ds \Psi(x(s))(\dot{x}^2(s)h^{-2}(s))^n h(s), \qquad (11)$$

where Ψ is the scalar massive mode at the level $2n$ and $h(s)$ is the boundary metric on the world sheet needed for the general covariance of this expression. Conformal invariance of this perturbation means that the $h(s)$ dependence must cancel. The cancellation occurs between the explicit h dependence in the above formula and the factors coming from the quantum fluctuations of $x(s)$. These factors appear because in the covariant theory the cutoff is always accompanied by the boundary metric

$$h(s)(\Delta s)^2_{\min} = a^2, \qquad (12)$$

$$\Lambda^2 = \frac{1}{(\Delta s)^2_{\min}} = \frac{1}{a^2}h(s), \qquad (13)$$

where a is an invariant cutoff.

In the one-loop approximation (which is not, strictly speaking, applicable here but gives a correct qualitative picture), we have

$$\partial^2\Psi - M_n^2\Psi = 0, \qquad (14)$$

$$M_n^2 \sim n. \qquad (15)$$

This is the on-shell condition for the massive string mode, and it was obtained, let us stress it again, from the cancellation between the classical and quantum $h(s)$ dependence.

Now, we are ready to attack the AdS case. Let us consider the string action in this background:

$$S = \sqrt{\lambda}\int_D \frac{(\partial x_\mu)^2 + (\partial y)^2}{y^2} + \ldots, \qquad (16)$$

where we dropped all fermionic and Ramond–Ramond (RR) terms. This is legitimate in the WKB limit $\lambda \gg 1$, which we will study in this section. To find the counterterms, we must calculate once again the boundary action and $\langle z_\lambda(s) z_\mu(s)\rangle$. It is not as easy as in the previous case, but this well-defined mathematical problem was solved in [4, 5]. The answer has the form

$$S_{\text{calc}} = \sqrt{\lambda}\int ds_1 ds_2 \kappa_{\mu\nu}(s_1, s_2) z_\mu(s_1) z_\nu(s_2). \qquad (17)$$

After introducing variables $s = (s_1 + s_2)/2$ and $\sigma = s_1 - s_2$ and taking the Fourier transform with respect to σ, we obtain the following asymptotic behavior for the kernel in the mixed representation:

$$\kappa_{\mu\nu}(p, s) \underset{p\to\infty}{\approx} \frac{|p|^3}{(c'(s))^2}\left[3\frac{c'_\mu c'_\nu}{(c')^2} - \delta_{\mu\nu}\right]. \qquad (18)$$

From this, it follows that

$$\langle z_\mu(s) z_\nu(s)\rangle \propto \int^\infty \frac{dp}{|p|^3} < \infty. \qquad (19)$$

The remarkable feature of this answer is that it implies that there is no quantum ultraviolet divergences on the world sheet. Hence, if we add to the action the background fields

$$\Delta S \sim \int A_\mu dx_\mu + \int \Psi(x(s))(x'(s))^2 (h(s))^{-1} ds + \ldots \qquad (20)$$

and treat it in the one-loop approximation, we come to the following conclusions. First of all, as far as the A term is concerned, it is finite for any $A_\mu(x)$ and, thus, describes the off-shell gluons. This situation is in sharp contrast to the standard case in which conformal invariance implied the on-shell condition.

Now, let us examine the massive mode (11). The only quantum dependence on the cutoff comes from

$$\langle z'_\mu(s) z'_\nu(s)\rangle \sim \int \frac{dp}{|p|}. \qquad (21)$$

As a result, we obtain the counterterm

$$\Delta S \sim \int \Psi(x(s))(x'(s))^2 \left(\frac{\log h(s)}{h(s)}\right) ds. \qquad (22)$$

We see that the only way to keep the theory conformally invariant in this approximation is to set $\Psi = 0$. There is also a possibility that, at some fixed value of λ, the $h(s)$ dependence will go away. However, it is impossible to cancel it by a suitable on-shell condition. All this happens because, due to (19), the kinetic energy for the Ψ term is not generated.

There is one more "massless mode" in the AdS string which requires a special treatment. Let us examine

$$\Delta S = \int \Phi(x(s))\partial_\perp y(s) ds, \qquad (23)$$

where $\partial_\perp$ is the normal derivative at the boundary of the world sheet (which lies at infinity of the AdS space). In the more general case of $AdS_p \times S_q$, we also have the perturbation

$$\Delta S = \int \Phi^i(x) n^i(s) \partial_\perp y ds. \qquad (24)$$

Here, we must remember that the string action is finite only if [5, 6]

$$(\partial_\perp y)^2 = (x')^2. \qquad (25)$$

It is easy to see that, when we substitute the decomposition (5) into this formula, we get the logarithmic divergence (21) once again. We come to the conclusion that the above perturbation is not conformal and must not be present at the boundary. However, in the case of (24), there is also a logarithmic term coming from the fluctuations of $n^i(s)$. In the presence of spacetime super-

symmetry, these two divergences must cancel since the masslessness of the scalar fields is protected by the supersymmetry. Otherwise, keeping the scalar fields massless requires a special fine tuning of the background. It would be interesting to clarify the corresponding mechanism.

Another interesting problem for the future is the fate of the open string tachyon in the AdS space. So far, we assumed that it is excluded by the Goddard–Sherk–Olive (GSO) projection. But in the purely bosonic string, it may lead to some interesting effects via the Sen mechanism [7].

We come to the following conclusion concerning the spectrum of the boundary states in the AdS-like background. It consists of a few modes which would have been massless in the flat case. The infinite tower of the massive states cannot reach the boundary. The above finite set of states must be associated with the fields of the field theory under consideration.

The full justification of this assertion requires the analysis of the Schwinger–Dyson equations of the Yang–Mills theory. It is still absent, and we give some heuristic arguments instead. The loop equation expressing the Schwinger–Dyson equations in terms of loops has the form

$$\hat{L}(s)W(C) = W * W, \tag{26}$$

where $W(C)$ is the Wilson loop and $\hat{L}$ is the loop Laplacian and the right-hand side comes from the self-intersecting contours. In recent papers [4, 5], we analyzed the action of the loop Laplacian in the AdS space. It was shown that, at least in the WKB approximation and in the four-dimensional spacetime, we have a highly nontrivial relation

$$\hat{L}s \sim T_{\perp\parallel}(s), \tag{27}$$

where $T_{\perp\parallel}(s)$ is a component of the world sheet energy–momentum tensor at the boundary. When substituted into the string functional integral, the energy–momentum tensor receives contributions from the degenerate metrics only. These metrics describe a pinched disk, that is, two disks joined at a point. The corresponding amplitude is saturated by the allowed boundary operators inserted at this point. That gives Eq. (26) provided that the boundary operators of the string are the same as the fields of the field theory. Much work is still needed to make this argument completely precise.

4. THE *D*-BRANE PICTURE

An alternative way to understand gauge field–string duality is based on the *D*-brane approach. It is less general than the sigma-model approach described above, but in the supersymmetric cases it provides us with an attractive visual picture. The logic of this method is based on the fundamental conjecture that *D* branes can be described as some particular solitons in the closed string sector. One of the strongest arguments in favor of this conjecture is that both *D* branes and solitons have the same symmetries and are sources of the same RR fields [8]. The gauge field–string duality then follows from the *D*-brane–soliton duality in the limit $\alpha' \longrightarrow 0$. On the *D*-brane side, only the massless gauge field modes of the open string survive in this limit. On the string theory side, we have a near-horizon limit [1] of the soliton metric [9] given by (1). These two theories must be equivalent if the basic *D*-brane conjecture is correct.

The connection with the sigma-model approach of the previous section results from the following argument. First of all, the closed string background is the same in both cases. As for the open strings, we placed their ends at the boundary of the AdS space, where $a^2(\varphi) \longrightarrow \infty$. That means that the effective slope of these strings behaves as

$$\alpha'_{\text{open}} \sim a^{-2}(\varphi) \longrightarrow 0 \tag{28}$$

and, thus, only the massless modes are present. We said that the *D*-brane approach is less general because in the nonsupersymmetric cases there could exist solitons with the required boundary behavior, which are not describable by any combination of *D* branes in the flat space.

This fact is related to another often overlooked subtlety. The 3-brane soliton has the metric [9]

$$ds^2 = H^{-1/2}(r)(dx)^2 + H^{1/2}(r)(dy)^2, \tag{29}$$

$$r^2 = y^2, \quad H(r) = 1 + \frac{L^4}{r^4}. \tag{30}$$

It is often assumed that this metric is an extremum of the action

$$S = S_{\text{bulk}} + S_{\text{BI}}, \tag{31}$$

where the first term contains the modes of the closed string, while the second is the Born–Infeld action localized on the brane. In the equations of motion, the second term will give the delta function of the transverse coordinates.

Would it be the case where the 3-brane is located? From (30), it is clear that the singularity of the metric is located in the complex domain $r^4 = -L^4$. Let us try to understand the significance of this fact from the string-theory point of view. Consider a string diagram describing the *D*-brane world volume in the arbitrary order in $\lambda = g_s N$. It is represented by a disk with an arbitrary number of holes. At each boundary, one imposes the Dirichlet conditions for the transverse coordinates. An important feature of this diagram is that it is finite. This follows from the fact that the only source of divergences in string theory are tadpoles and for 3-branes their contribution is proportional to the integral $\int d^6k/k^2$, where k is the transverse momentum. This

expression is infrared finite (which is of course very well known). Thus, *D* branes in the flat space are described by the well-defined string amplitudes. But that contradicts the common wisdom that one must determine the background from the action (31) because the flat space is not a solution once the Born–Infeld term is added. Moreover, if we try to deform the flat space, the above disk with holes will lose its conformal invariance.

Let us analyze this apparent paradox. It is related to the fact that conformal invariance on a sphere is equivalent to the absence of tadpoles since for any (1, 1) vertex operator we have $\langle V\rangle_{\text{sphere}} = 0$. However, this is not true on a disk; the conformal symmetry does not forbid the nonzero expectation values of vertex operators. On a disk, conformal symmetry and the absence of tadpoles are two different conditions. Which one should we use?

If we denote the bulk couplings by λ and the boundary couplings by μ, we can construct three different objects, the bulk central charge $c(\lambda)$, the "boundary entropy" [10] $b(\lambda, \mu)$, and the effective action generating the S matrix, $S(\lambda, \mu) = c(\lambda) + b(\lambda, \mu)$. To ensure conformal invariance, we must have

$$\frac{\partial c}{\partial \lambda} = 0, \tag{32}$$

$$\frac{\partial b}{\partial \mu} = 0. \tag{33}$$

This does not coincide in general with the "no-tadpole condition"

$$\frac{\partial S}{\partial \lambda} = \frac{\partial S}{\partial \mu} = 0. \tag{34}$$

In the case of 3-branes, the paradox is resolved in an interesting way. The metric (30) has a horizon at $r = 0$. When we go to the Euclidean signature, the horizon, as usual, shrinks to a nonsingular point. As a result, we have a metric which solves Eq. (32) and has no trace of the *D*-brane singularity in it! The paradox is pushed under the horizon.

The conclusion of this discussion is as follows. We have two dual and different descriptions of the *D*-brane amplitudes. In the first description, we calculate the amplitudes of a disk with holes in the flat space. In this description, it is simply inconsistent to introduce the background fields generated by *D* branes.

In the second description, we forget about the *D* branes and study a nonsingular closed string soliton. The *D*-brane conjecture implies that we must get the same answers in these two cases. The situation is analogous to the one we have in the sine-Gordon theory, which admits two dual descriptions, either in terms of solitons or in terms of elementary fermions, but not both.

Let us touch briefly on another consequence of these considerations. When minimizing the action (31), one can find a solution which is singular on the 3-brane and is AdS space outside of it [11]. These solutions are known to "localize" gravitons on the brane and are the basis of the popular "brane-world" scenarios. It is clear that for the string-theory branes this is not a physical solution because the world volume does not contain gravity (being described by the open strings). As we argued above, there must be a horizon not a singularity. Technically, this happens because in string theory the Born–Infeld action is corrected with the Einstein term $\sim\int R\sqrt{g}d^{p+1}x$ coming from the finite thickness of the brane. It can be shown that the coefficient of this term (which is fully determined by string theory) is tuned so that the localization is destroyed. There are no worlds on *D* branes. Of course, if one compactifies the ambient transverse space, the $4d$ graviton reappears by the Kaluza–Klein mechanism.

5. CONFORMAL GAUGE THEORIES IN HIGHER DIMENSIONS

Although our main goal is to find a string-theory description of the asymptotically free theories, conformal cases are not without interest. They are easier and can be used as a testing ground for the new methods. In this section, we briefly discuss conformal bosonic gauge theories in various dimensions [2]. The background in these cases is just the AdS space. We have to perform the nonchiral GSO projection in order to eliminate the boundary tachyon (it would add an instability to the field theory under consideration; we do not consider here an interesting possibility that this instability resolves itself in some new phase).

The GSO projection in the noncritical string is slightly unusual. Let us consider first $d = 5$ (corresponding to the $d = 4$ gauge theory). In this case, we have four standard Neveu–Schwartz–Ramond (NSR) fermions ψ_μ on the world sheet and also a partner of the Liouville field ψ_5. For the former, we can use the standard spin fields defined by the OPE

$$\psi_\mu \times \Sigma_A \sim (\gamma_\mu)_{AB}\Sigma_B, \tag{35}$$

where we use the usual 4×4 Dirac matrices. The spinor Σ_A can be split into spinors $\Sigma_A^{\pm}$ with positive and negative chiralities. It is easy to check that the OPE for them have the structure

$$\Sigma^{\pm}\times\Sigma^{\pm} \sim (\psi)^{[\text{even}]}, \tag{36}$$

$$\Sigma^{\pm}\times\Sigma^{\mp} \sim (\psi)^{[\text{odd}]}. \tag{37}$$

The symbols on the right-hand sides mean the products of an even/odd number of NSR fermions. Notice that this structure is the opposite to the one in ten dimensions. In order to obtain the spin operators in $5d$, we have to introduce the Ising order and disorder operators, σ and μ, related to ψ_5. These operators are non-

holomorphic and correspond to RR states. Their OPE have the structure

$$\sigma \times \sigma \sim (\psi_5)^{[\text{even}]}, \tag{38}$$

$$\sigma \times \mu \sim (\psi_5)^{[\text{odd}]}. \tag{39}$$

Using these relations, we obtain the following GSO-projected RR spin operator:

$$\Sigma = \begin{pmatrix} \sigma\Sigma^+\overline{\Sigma^+} & \mu\Sigma^+\overline{\Sigma^-} \\ \mu\Sigma^-\overline{\Sigma^+} & \sigma\Sigma^-\overline{\Sigma^-} \end{pmatrix}. \tag{40}$$

It has the property

$$\Sigma \times \Sigma \sim (\psi)^{[\text{even}]} \tag{41}$$

needed for the nonchiral GSO projection, which consists of dropping all operators with an odd number of fermions. Notice also that the nonchiral-picture-changing operator has an even number of fermions. The RR matrix Σ has 16 elements. We can now write down the full string action in the AdS_5 space. It has the form

$$S = S_B + S_F + S_{\text{RR}} + S_{\text{ghost}}, \tag{42}$$

where S_B is given by (16); S_F by

$$S_F = \int d^2\xi \left[\bar{\psi}_M \nabla \psi_M + \frac{1}{\sqrt{\lambda}} (\overline{\psi_M} \gamma_\mu \psi_N)^2 \right], \tag{43}$$

where $M = 1, \ldots, 5$; and one has to use the standard spin connection projected from AdS on the world sheet in the Dirac operator. So far, we are describing the usual action of the sigma model with $N = 1$ supersymmetry on the world sheet. The unusual part is the RR term given by

$$S_{\text{RR}} = f \int d^2\xi \, \text{tr}(\gamma_5 \Sigma) e^{-\phi/2}. \tag{44}$$

Here, $e^{-\phi/2}$ is the spin operator for the bosonic ghost [12], and f is the coupling constant (which is equal to unity in the one-loop approximation).

I believe that this model can be exactly solved, although it has not been done yet. A promising approach to this solution may be based on the non-Abelian bosonization [13] in which the fermions ψ_M are replaced by the orthogonal matrix Ω_{MN} with the WZNW Lagrangian. In this case, the RR term is simply the trace of this matrix in the spinor representation. This formalism lies in the middle between the NSR and the Green–Schwartz approaches and hopefully will be useful. Meanwhile, we will have to be content with the one-loop estimates, which are justified in some special cases listed below and help to get a qualitative picture in general. In this approach, one begins with the effective action

$$S = \int d^d x \sqrt{G} e^{\Phi} \left[\frac{d-10}{2} - R - (\nabla\Phi)^2 \right] + \int d^d x F_d^2 \sqrt{G}. \tag{45}$$

Here, F_d is the RR d form, and

$$F_d^2 = G^{A_1 A_1'} \ldots G^{A_d A_d'} F_{A_1 \ldots A_d} F_{A_1' \ldots A_d'};$$

the form F_d will be assumed to be proportional to the volume form. The dilaton field Φ is normalized so that $e^{\Phi} = g_s^{-2}$, where g_s is the string coupling constant. Conformal cases involve either constant curvature solutions of the equations of motion or the products of the manifolds with constant curvatures. The dilaton in these cases is also a constant. Such an ansatz is very easy to analyze. Let us begin with the single AdS_d space. Consider the variation of the metric which preserves the constancy of the curvature

$$\delta G_{AB} = \varepsilon G_{AB}, \tag{46}$$

$$\delta R = \delta(G^{AB} R_{AB}) = -\varepsilon R, \tag{47}$$

$$\delta\Phi = \text{const}. \tag{48}$$

That immediately gives the relations

$$\frac{d-10}{2} - R = 0, \tag{49}$$

$$e^{\Phi}\left(1 - \frac{d}{2}\right) R - \frac{d}{2} F_d^2 = 0. \tag{50}$$

If we assume that the flux of the RR field is equal to N, we get $F_d^2 = N^2$. If we introduce the coupling constant $\lambda = g_s N = g_{\text{YM}}^2 N$, we obtain the background AdS solution [2] with

$$|R| \sim \lambda^2 \sim 10 - d. \tag{51}$$

We can trust this solution if $d = 10 - \epsilon$; in this case, the curvatures and the RR fields are small and the above one-loop approximation is justified. According to the discussion in the preceding sections, this solution must describe the Yang–Mills theory, perhaps with one adjoint scalar, in the space with dimension $9 - \epsilon$. We conclude that this bosonic higher dimensional gauge theory has a conformally invariant fixed point! It may be worth mentioning that it is not atypical for nonrenormalizable theories to have such fixed points. For example, a nonlinear sigma model in dimension higher than two, where it is nonrenormalizable, does have a conformal critical point at which the phase transition to the ferromagnetic phase takes place. However, it is hard to say up to what values of ϵ we can extrapolate this result.

These considerations allow for several generalizations. First of all, we can consider products of spaces with constant curvatures by the same method. Take, for

example, the space $AdS_p \times S_q$ with curvatures R_1 and R_2 and $d = p + q$. To get the equations of motion in this case, it is sufficient to consider the variations

$$\delta G_{ab} = \varepsilon_1 G_{ab}, \tag{52}$$

$$\delta G_{ij} = \varepsilon_2 G_{ij}, \tag{53}$$

where the first part refers to AdS and the second, to the sphere. A simple calculation gives the equations

$$\frac{d-10}{2} - R_1 - R_2 = 0, \tag{54}$$

$$\left(1 - \frac{2}{p}\right)R_1 + \frac{10-d}{2} = -e^{-\Phi}F_d^2, \tag{55}$$

$$\left(1 - \frac{2}{q}\right)R_2 + \frac{10-d}{2} = e^{-\Phi}F_d^2, \tag{56}$$

$$F_d^2 = \lambda^2 R_2^q. \tag{57}$$

Here, we assume that the RR flux is permeating the AdS component of space only, being given by the volume form. The last equation follows from the normalization condition of this flux and the extra factor proportional to the volume of S_q in the action. Solving these equations, we get

$$R_1 = -\left(\frac{10-p-q}{2}\right)\frac{p(q+2)}{p-q}, \tag{58}$$

$$R_2 = \left(\frac{10-p-q}{2}\right)\frac{q(p+2)}{p-q}. \tag{59}$$

This solution describes bosonic gauge theories with $q + 1$ adjoint bosons; again it can be trusted if the curvatures are small. Another generalization is related to the fact that, strictly speaking, we must include the closed-string tachyon in our considerations. It was shown in [14] that there exists an interesting mechanism for the tachyon condensation, following from its couplings to the RR fields. It is easy to include the constant tachyon field in our action and to show that it does not change our results in the small curvature limit. According to [14], in the critical case $d = 10$, the tachyon leads to the running coupling constants. In the noncritical case, there is also a conformal option described above in which the tachyon condenses to a constant value.

Finally, let us describe the reasons to believe that the conformal solutions can be extrapolated to nonsmall curvatures and, thus, the sigma model (42) has a conformal fixed point. The first two terms in (45) are the expansion of the sigma-model central charge. When the couplings are not small, we have to replace

$$\frac{d-10}{2} - R \Rightarrow \frac{c(R)-10}{2}, \tag{60}$$

where $c(R)$ is the central charge of the $2d$ sigma model with the target space having a curvature R. It decreases, according to Zamolodchikov, along the renormalization-group trajectory. We can call this the second law of the renormalization group. Let us conjecture that there is also a third law

$$c(R) \longrightarrow 0 \quad (R \longrightarrow +\infty), \tag{61}$$

$$c(R) \longrightarrow \infty \quad (R \longrightarrow -\infty). \tag{62}$$

The first property follows from the fact that usually the sigma models with positive curvature develop a mass gap and, thus, there are no degrees of freedom contributing to the central charge. The second equation is harder to justify; we know only that $c(R)$ increases in the direction of negative curvature.

With these properties and with some general form of the RR terms, it is possible to see that the conformal solution to the equations of motion obtained by the variations (46) continues to exist when ϵ is not small. Of course, this is not a good way to explore these solutions. Instead, one must construct the conformal algebra for the sigma-model action (42). This has not been done yet.

6. INFRARED SCREENING OF THE COSMOLOGICAL CONSTANT AND OTHER SPECULATIONS

In this section, we will discuss some speculative approaches to the problems of vacuum energy and spacetime singularities. I shall try to revive some old ideas [15], adding some additional thoughts. The motivation to do that comes from the remarkable recent observational findings indicating that the cosmological constant is nonzero, and its scale is defined by the size of the Universe (meaning the Hubble constant). These results seem very natural from the point of view advocated in [15], according to which there is an almost complete screening of the cosmological constant due to the infrared fluctuations of the gravitational field. This phenomenon is analogous to the complete screening of electric charge in quantum electrodynamics found by Landau, Abrikosov, and Khalatnikov and nicknamed "Moscow zero." Here, we will try to argue in favor of another "zero" of this kind, that of the cosmological constant.

Let us consider first the Einstein action

$$S = -\int (R - 2\Lambda_0)\sqrt{g}d^4x. \tag{63}$$

Here, Λ_0 is a bare cosmological constant which is assumed to be defined by the Planck scale. It is clear from the form of the action that, if we consider the infrared fluctuations of the metric (with the wavelength much larger than the Planck scale), their interaction will be dominated by the second term in this formula since it does not contain derivatives. To obtain some

qualitative understanding of the phenomenon, let us consider conformally flat fluctuations of the metric

$$g_{\mu\nu} = \varphi^2 \delta_{\mu\nu}. \quad (64)$$

The action takes the form

$$S = -\int\left[\frac{1}{2}(\partial\varphi)^2 - \Lambda_0\varphi^4\right]d^4x. \quad (65)$$

It has the well-known feature of nonpositivity. The way to treat it was suggested in [16], and we will accept it, although it does not have good physical justification. To use S in the functional integral, we will simply analytically continue $\varphi \Rightarrow i\varphi$; after that the action takes the form

$$S = \int\left[\frac{1}{2}(\partial\varphi)^2 + \Lambda_0\varphi^4\right]d^4x. \quad (66)$$

The infrared fluctuations of φ are relevant and lead to the screening of Λ_0,

$$\Lambda \sim \frac{1}{\log(M_{\rm Pl}L)}, \quad (67)$$

where L is an infrared cutoff. More generally, we could represent the metric in the form

$$g_{\mu\nu} = \varphi^2 h_{\mu\nu}, \quad \det(h_{\mu\nu}) = 1. \quad (68)$$

It is not known how to treat the unimodular part of the metric. We can only hope that it will not undo the infrared screening, although we can change it. Also, the screening (67) with $L \sim H^{-1}$ (where H is the Hubble constant) is not strong enough to explain the fact that $\Lambda \sim H^2$. It is not impossible that the two problems cure each other. When we have several relevant degrees of freedom, the renormalization-group equations governing the L dependence of various coupling constants including Λ may have a power asymptotic behavior [in contrast to (67)]. Such examples exist, starting from the cases with two independent coupling constants. Thus, the infrared limit of the Einstein action (perhaps with the dilaton added) may be described by a conformal field theory giving the cosmological constant defined by the Hubble scale. The renormalization group should take us from Planck to Hubble.

Even if this fantasy is realized, we have to resolve another puzzle. It is certainly unacceptable to have a large cosmological constant in the early Universe since it will damage the theory of nucleosynthesis. At first glance, it seems to create a serious problem for the screening theory because, when the Universe is relatively small, the screening is small too and the cosmological constant is large. The way out of this problem is to conjecture that, in the radiation-dominated Universe, the infrared cutoff is provided by the curvature of spacetime, while in the matter-dominated era it begins to depend on other quantities characterizing the size of the Universe. If this is the case, in the early Universe, we get the screening law $\Lambda \sim R$ instead of $\Lambda \sim H^2$. Substituting it in the Einstein action, we find that at this stage the infrared mechanism simply renormalizes the Newton constant and, thus, is unobservable. In the matter-dominated era, the effective Λ begin to depend on other things (like the Friedmann warp factor a) and that can easily give the observed acceleration of the Universe. Thus, the change in the infrared screening must be related to the trace of the energy–momentum tensor. We can say that, in the correct theory, the cosmological constant vanishes without a trace. To be more precise, it is disguised as a Newton constant until the trace of the energy–momentum tensor reveals its true identity. The above picture has some remote resemblance to the scenario suggested recently in [17].

In spite of the obvious gaps in these arguments, they give a very natural way of relating the cosmological constant to the size of the Universe and thus are worth developing. Perhaps the AdS–CFT correspondence will be of some use for this purpose. The main technical problem in testing these ideas is the unusual φ-dependent kinetic energy of the h field.

We can also notice that the above scenario can explain the dimensionality of spacetime. Indeed, if this dimensionality is larger than four, the infrared effects are small, the cosmological constant is large, and we end up in the universe of Planck size, which is not much fun.

ACKNOWLEDGMENTS

This work was supported in part by the NSF, grant no. PHY9802484.

REFERENCES

1. O. Aharony, S. Gubser, J. Maldacena, and H. Ooguri, Phys. Rep. **323**, 183 (2000).
2. A. Polyakov, Int. J. Mod. Phys. A **14**, 645 (1999); hep-th/9809057.
3. C. Callan *et al.*, Nucl. Phys. B **308**, 221 (1988).
4. A. Polyakov and V. Rychkov, hep-th/0002106.
5. A. Polyakov and V. Rychkov, hep-th/0005173.
6. N. Drukker, D. Gross, and H. Ooguri, Phys. Rev. D **60**, 125006 (1999); hep-th/9904191.
7. A. Sen, JHEP 9912027; hep-th/9911116.
8. J. Polchinski, Phys. Rev. Lett. **75**, 4724 (1995); hep-th/9510017.
9. G. Horowitz and A. Strominger, Nucl. Phys. B **360**, 197 (1991).
10. I. Affleck and A. Ludwig, Phys. Rev. Lett. **67**, 161 (1991).
11. L. Randall and R. Sundrum, Phys. Rev. Lett. **83**, 4690 (1999).
12. D. Friedan, E. Martinec, and S. Shenker, Nucl. Phys. B **271**, 93 (1986).
13. E. Witten, Commun. Math. Phys. **92**, 455 (1984).
14. Ig. Klebanov and A. Tseytlin, Nucl. Phys. B **547**, 143 (1999); hep-th/9812089.
15. A. Polyakov, Usp. Fiz. Nauk **136**, 538 (1982) [Sov. Phys. Usp. **25**, 187 (1982)].
16. G. Gibbons and S. Hawking, Phys. Rev. D **15**, 2752 (1977).
17. C. Armendariz-Picon, V. Mukhanov, and P. Steinhardt, astro-ph/0004134.

Physics of Atomic Nuclei, Vol. 64, No. 3, 2001, pp. 548–553. From Yadernaya Fizika, Vol. 64, No. 3, 2001, pp. 602–607.

90th ANNIVERSARY OF A.B. MIGDAL'S BIRTHDAY
ELEMENTARY PARTICLES AND FIELDS

Effective Lagrangian and Equations for Valence Quark and Gluon Green's Functions*

Yu. A. Simonov

Institute of Theoretical and Experimental Physics, Bol'shaya Cheremushkinskaya ul. 25, Moscow, 117259 Russia

Received June 6, 2000

Abstract—Starting from the QCD Lagrangian and separating background and valence degrees of freedom, one arrives at the effective Lagrangian for valence quarks and gluons. Each term in the Lagrangian contains a product of valence quark and gluon operators acting at the end of the fundamental or adjoint string, made of the background field. A simple procedure is described how to obtain from the Lagrangian self-coupled equations for quark and gluon Green's function. © *2001 MAIK "Nauka/Interperiodica".*

Forty years ago, I had a privilege to attend the lectures of such masters like A.B. Migdal and I.Ya. Pomeranchuk and take lessons from them, as well as from Migdal's disciples S.T. Belyaev and V.I. Kogan. Later on, I was happy to meet Arkadiĭ Benediktovich frequently with our mutual friends and at seminars and to have many disputes with him. In A.B., as friends and colleagues called him, we liked the joy of living and talents not only for physics but also for many other things—his personality was the incarnation of homo ludens, and his very existence proved the affinity of creative bursts in science and art, in handicrafts, and in friendly practical jokes. At the same time, there was a note of raillery in the attitude to A.B. at the Institute of Theoretical and Experimental Physics, as often occurs in the convent midst toward a man of free arts. The ebullient energy of A.B. was aimed at many things (maybe too many), and in this did he differ profoundly from Pomeranchuk; but how we miss now both of them! Science, especially quantum chromodynamics, has recently become much more complicated, and physical intuition inherent in them to so great an extent would help it out of the present stagnant state.

1. INTRODUCTION

Quarks and gluons in QCD play two different roles and can be accordingly classified as two distinct kinds: valence quarks and gluons and background quarks and gluons. Here one should stress the difference between the latter. Whereas background quarks (known also as sea quarks) are a small admixture and have a destructive role in the vacuum (breaking fundamental string), background gluons are the essence of the vacuum, creating strings (confinement) and more than 99% of the mass of all visible matter in the Universe.

The distinction between background and valence gluons is difficult to define absolutely rigorously, since both strongly interact and transform into each other, and therefore one should start with some gauge-invariant formalism avoiding double-counting and obtain equations connecting the two species, as is done, e.g., in [1].

One can roughly define the bare background gluonic field as the field in the gluonic condensate and inside the string, and bare valence gluons as the gluons propagating at the ends of adjoint string in glueballs, and in the middle of fundamental string in hybrids [2]. Note, that this definition may differ from that accepted in DIS, since the string made of background gluons, when boosted, in the parton picture contributes to the gluon part of the momentum and may be regarded as valence gluons (as the Coulomb field is represented in the Williams–Weizsäcker approach by a cloud of incident "valence" photons).

Our first goal is to integrate out the gluon background field formally using the cluster expansion theorem and to consider the resulting set of vertices for valence operators.

When one exploits for the background field a contour gauge [3], the averaging over the background naturally produces strings attached to products of valence operators. Physically these strings should end up at another valence vertex, and dynamical degrees of freedom of strings should enter in the next approximations when the background field in strings interacts with valence gluons. However, in the lowest approximation, strings do not carry dynamical d.o.f. and can be found from the minimization of the Euclidean action (maximization of the Green's function).

It is clear then that infinite strings disappear because of infinite action and valence vertices will be connected by strings of minimal length.

Thus, the second step of our approach is the derivation of the effective Lagrangians for white hadron-like combinations.

At this point, one meets with a new unexpected situation. It appears that the QCD string can be made minimally of two elementary fluxes (two gluon operators A_μ expressed through $F_{\mu\nu}$ via contour integrals); there-

* This article was submitted by the author in English.

fore, the most elementary vertex with one string contains four quark operators. This can be considered as a creation and annihilation of a diquark at the end of the string.

This vertex is fully defined by the bilocal correlator $\langle F(x)F(y)\rangle$ and so is defined the dynamics of the diquark system.

The situation with valence gluons is different; here, one has two elementary vertices with the string: (i) gluon–gluon–string vertex describing propagation of a valence gluon at the end of the adjoint string and (ii) digluon–digluon–string vertex, which is similar to the diquark vertex discussed above. This set of vertices has important physical consequences for the structure of baryons and glueballs, since it produces new dynamical configurations in these systems with specific quantum numbers.

The final step of this paper is the formulation of Dyson–Schwinger-type equations for hadron states. Here, one can use, for simplicity reasons, the large-N_c limit and construct effective mass operators from elementary vertices and quark and gluon Green's function. In the simplest case of heavy–light systems, this was done in [4] for quarks and in [1] for gluons. Here, the mass operator, e.g., for the quark, is obtained by contracting two-quark operators in the diquark–diquark–string vertex and replacing the contracted pair by the full quark Green's function.

The same is done for gluons with the digluon–digluon–string vertex, but in contrast to the quark case here one has in addition the gluon–gluon–string vertex.

Now, for mesons, baryons, and glueballs, one can derive equations as was done in [5], writing the full Green's function in the lowest approximation as a direct product of heavy–light Green's functions, with one valence quark (or gluon) complemented by a static source. The common trajectory of these static sources is defined by the contour (surface) minimization and does not have its independent dynamical degree of freedom.

This is only the first approximation, since perturbative gluon exchanges violate the direct product structure of the full Green's function, and one obtains the Bethe–Salpeter-type equation, which is similar to the standard one, except for the fact that free one-body Green's functions S_0, G_0 should be replaced by heavy–light Green's functions S, G and the minimization of the contours should be done.

A preliminary analysis of the equations is performed at the end of the paper, and the interrelation of perturbative and nonperturbative solutions is briefly discussed.

2. GENERAL FORMALISM

One starts with the background gauge formalism [6, 7] in the Euclidean 4*d* space, representing the total gluonic field A_μ as a sum of the NP background B_μ and valence gluon vector potential a_μ, with prescribed gauge transformation properties

$$A_\mu = B_\mu + a_\mu, \quad B_\mu \longrightarrow U^+\left(B_\mu + \frac{i}{g}\partial_\mu\right)U, \qquad a_\mu \longrightarrow U^+ a_\mu U. \tag{1}$$

The QCD Lagrangian density $L(B + a)$ is a sum

$$L(B+a) = L(B) + L_{qB} + L_1(B,a) + L_2(B,a) + L_{\rm int} + L_q^{(0)} + L_{qa}, \tag{2}$$

where

$$L_{qB} = \int {}^f\psi^+(x) g\hat{B}(x) {}^f\psi(x) d^4x, \tag{3}$$

$$L_1(B,a) = -a_\nu^c D_\mu^{ca}(B) F_{\mu\nu}^a = -2\,{\rm tr}(a_\nu D_\mu F_{\mu\nu}), \tag{4}$$

$$L_2(B,a) = -\frac{1}{2} a_\nu^c [D_\lambda^{ca} D_\lambda^{ad}\delta_{\mu\nu} - D_\mu^{ca} D_\nu^{ad} - g f^{cad} F_{\mu\nu}^a] a_\mu^d, \tag{5}$$

$$L_q^{(0)} = -i\,{}^f\psi^+(x)(\hat{\partial} + m_f)\,{}^f\psi(x), \tag{6}$$

and $L_{\rm int}$ contains terms $O(a^3, a^4)$, while L_{qa} is obtained replacing $B_\mu \longrightarrow a_\mu$.

In (2)–(6), the following notation is used:

$$D_\lambda^{ca} = \partial_\lambda \delta_{ca} + g f^{cba} B_\lambda^b \equiv \hat{D}_\lambda, \qquad F_{\mu\nu}^a = \partial_\mu B_\nu^a - \partial_\nu B_\mu^a + g f^{abc} B_\mu^b B_\nu^c, \tag{7}$$

and ${}^f\psi_{a\alpha}$ is the quark operator with flavor *f*, color *a*, and Lorentz index α.

To proceed, we shall separate out the terms containing valence quark and gluons and the background vector potential $B_\mu(x)$, since we are interested in the effective action for valence partons attached to a string.

The appropriate terms are contained in (3) and (5) and in $L_{\rm int}$. From the terms in (5), one obtains terms of the form (we keep the notation of [1])

$$L^{(2,1)} = \frac{1}{2} g f^{ikc} a_\mu^i [2B_\lambda^c \partial_\lambda \delta_{\mu\nu} + \overleftarrow{\partial}_\mu B_\nu^c - B_\mu^c \partial_\nu] a_\nu^k, \tag{8}$$

$$L^{(2,2)} = \frac{1}{2}\chi^{ik,ab}(a_\mu^i a_\mu^k B_\lambda^a B_\lambda^b - a_\mu^i a_\nu^k B_\mu^a B_\nu^b), \tag{9}$$

$$L^{(F)} = g f^{ika} a_\mu^i a_\nu^k F_{\mu\nu}^a, \tag{10}$$

and from $L_{\rm int}$ one gets

$$L^{(3,1)} = \chi^{ik,ba} a_\mu^i a_\mu^k a_\nu^b B_\nu^a, \tag{11}$$

where $\chi^{ik,ab} \equiv g^2 f^{cia} f^{ckb}$.

Now to visualize the appearance of the string, one can choose the generalized contour gauge [3], express-

ing $B_\mu(x)$ through $F_{\mu\nu}(z)$,

$$B_\mu(x) = \int\limits_{C(x)} F_{\lambda\beta}(z)\frac{\partial z_\beta(x,s)}{\partial x_\mu}\frac{\partial z_\lambda(x,s)}{\partial s}ds, \qquad (12)$$

where the contour $C(x)$ starts at the point x and ends up at x_0, which may be at infinity.

The set of contours $\{C\}$ satisfies certain automorphic conditions [3].

As a special case, it is convenient to consider the gauge [8], where an infinite line is prescribed (one can call it $\mathbf{x} = 0, -\infty < x_4 < \infty$), and the contour $C(x)$ consists of a perpendicular from point x to the line, and then along the line to $x_4 = -\infty$.

The next step is the averaging over vacuum background fields, i.e., over the stochastic ensemble of $\{F_{\mu\nu}(x)\}$, which yields the effective action for valence quarks and gluons [1]

$$\left\langle e^{-\int L(B+a)d^4x}\right\rangle_B \equiv e^{-S_{\rm eff}(a)}. \qquad (13)$$

Using the cluster expansion theorem [9], one can express $S_{\rm eff}$ as a series of cumulants

$$S_{\rm eff}(a) = \int\langle L(B+a)\rangle_B d^4x - \frac{1}{2}\int d^4x\int d^4y\langle\langle L(x)L(y)\rangle\rangle + \ldots, \qquad (14)$$

where notation is used for a connected average (cumulant), e.g.,

$$\langle\langle LL\rangle\rangle = \langle LL\rangle - \langle L\rangle\langle L\rangle.$$

The series (14) generates an infinite set of vertices each containing several valence operators and field correlators of two different types

$$\text{(i)}\quad \langle\langle B_{\mu_1}(x_1)\ldots B_{\mu_n}(x_n)\rangle\rangle, \qquad (15)$$

$$\text{(ii)}\quad \langle\langle F_{\mu_1\nu_1}(x_1)\ldots F_{\mu_n\nu_n}(x_n)\rangle\rangle. \qquad (16)$$

In the last case, some of F's can be replaced by B_μ or by DF.

For the type (i), one can use (12) to express the cumulant (15) as the (multiple) integral of the average of the type (ii). The latter are known to be short-ranged [10], of the range $T_g^{(n)}$, and recent precise measurement in [11] can be unambigiously interpreted [12] as evidence in favor of fast convergence of the cumulant series and small value of $T_g^{(n)}$ for $n \geq 4$. Indeed, it was demonstrated in [12] on the basis of data in [11] that the contribution of quartic and higher cumulants to the string tension is less than one percent, when they are calculated on the minimal area surface.

Therefore, we shall consider only the effective vertices generated by the first two terms in (14).

Moreover, while the terms (ii) are short-ranged, the terms (i), being the integrals over contour C of $\langle\langle FF\rangle\rangle$, are long-ranged. Actually, the average

$$g^2\langle\langle B_\mu(x)B_\nu(y)\rangle\rangle \equiv J_{\mu\nu}(x,y) = g^2\int\limits_C dz_\lambda\int\limits_C dz'_\gamma\frac{\partial z_\beta}{\partial x_\mu}\frac{\partial z'_\delta}{\partial y_\nu}\langle\langle F_{\lambda\beta}(z)F_{\gamma\delta}(z')\rangle\rangle \qquad (17)$$

describes the creation of the string of the width $\sim T_g^{(2)} \equiv T_g$ along the contour C.

At this point, one should remark that the choice of the contour C and contribution of higher cumulants are physically interconnected.

The sum over all cumulants does not depend on the choice of the contour C, which implies that for the correct choice of contour C, coinciding with the actual position of the QCD string, the contribution of higher cumulants is minimal.

The situation here is similar to the choice of the mass scale μ in $\alpha_s(\mu)$ in the perturbation series; i.e., for the optimal choice of μ, related to the inverse size of the system, the contribution of the higher power terms is minimal.

As was discussed above, one can represent $S_{\rm eff}(a)$ as a sum of kinetic terms $S_0(a) + S_0(\psi)$, plus terms containing string $S_{\rm str}$, and, finally, short-range terms $S_{\rm loc}$ proportional to $\langle\langle F(x_1)\ldots F(x_n)\rangle\rangle$,

$$S_{\rm eff} = S_0(a) + S_0(\psi) + S_{4q} + S_{\rm str} + S_{\rm loc} + S_{\rm int}, \qquad (18)$$

where we have defined

$$S_0(a) = \frac{1}{2}\int a^i_\mu(-\partial^2_\lambda\delta_{\mu\nu} + \partial_\mu\partial_\nu)a^i_\nu d^4x, \qquad (19)$$

$$S_0(\psi) = \int d^4x L_q^{(0)}, \qquad (20)$$

$$S_{4q} = -\frac{1}{2}\int d^4x d^4y^f\psi^+(x)t^a\gamma_\mu{}^f\psi(x)^g\psi^+(y) \times t^b\gamma_\nu{}^g\psi(y)\langle B^a_\mu(x)B^b_\nu(y)\rangle_B, \qquad (21)$$

$$S_{\rm str} = S^{(2,2)} + S^{(4,2)} + S^{(5,2)} + S^{(6,2)}, \qquad (22)$$

$$S^{(2,2)} = \int d^4x\langle L^{(2,2)}\rangle_B, \qquad (23)$$

where $L^{(2,2)}$ is given in (9);

$$S^{(4,2)} = -\frac{g^2}{8}f^{ikc}f^{lmd}\int d^4x d^4y a^i_\mu(x)d_{\lambda\mu\nu}a^k_\nu(x)a^l_{\mu'}(y) \times d_{\lambda'\mu'\nu'}a^m_{\nu'}(y)\langle B^c_\lambda(x)B^d_{\lambda'}(y)\rangle_B, \qquad (24)$$

where $d_{\lambda\mu\nu} \equiv 2\partial_\lambda\delta_{\mu\nu} + \overleftarrow{\partial}_\mu\delta_{\nu\lambda} - \partial_\nu\delta_{\mu\lambda}$;

$$S^{(5,2)} = -\int\langle L^{(2,1)}(x)L^{(3,1)}(y)\rangle_B d^4x d^4y, \qquad (25)$$

$$S^{(6,2)} = -\frac{1}{2}\int \langle L^{(3,1)}(x)L^{(3,1)}(y)\rangle_B d^4x d^4y. \quad (26)$$

The term $S_{\rm loc}$ in (18) is obtained from $\langle (L_1(x) + L^{(F)}(x))(L_1(y) + L^{(F)}(y))\rangle$ and interference terms containing the average of the products $\langle B_\mu F_{\lambda\sigma}\rangle$; since these terms contain additional powers of T_g (as compared to the length of string), we shall disregard them in the first approximation.

3. ANALYSIS OF QUARK, GLUON, AND DIQUARK AND DIGLUON VERTICES

Analysis of the term S_{4q} was done in [4], where mostly its contracted form, with ${}^f\psi(x){}^g\psi^+(y) \longrightarrow \delta_{fg}\langle\psi(x)\psi^+(y)\rangle$, was investigated, while its diquark structure was not studied.

Following [4], we shall rewrite (21) displaying all color and Lorentz indices as follows:

$$S_{4q} = -\frac{1}{2N_c}\int d^4x d^4y ({}^f\psi_a^+(x)\gamma_\mu {}^f\psi_b(x)) \times ({}^g\psi_b^+(y)\gamma_\nu {}^g\psi_a(y)) J_{\mu\nu}(x,y) \quad (27)$$

with $J_{\mu\nu}$ given in (17), where one can keep in the correlator $\langle\langle FF\rangle\rangle$ only the dominant part, producing string tension [13]

$$g^2\langle\langle F_{\lambda\beta}(x)F_{\gamma\delta}(y)\rangle\rangle = (\delta_{\lambda\gamma}\delta_{\beta\delta} - \delta_{\lambda\delta}\delta_{\beta\gamma})D(x-y) + O(D_1), \quad (28)$$

and $O(D_1)$ is a full derivative not contributing to σ, while

$$\sigma = \frac{1}{2}\int D(x)d^2x. \quad (29)$$

The vertex (27) has the structure of diquark–diquark–flux vertex, where flux implies the kernel $J_{\mu\nu}(x, y)$ and, as will be seen, is not yet the string.

The term S_{4q} has two defects. First, it is $O(1/N_c)$, and second, it does not create the string by itself, since in the term $J_{\mu\nu}(x, y)$ (17) both coordinates $\mathbf{x}$, $\mathbf{y}$ are not correlated within the width of the string, but rather may be far from each other (see Appendix of the first reference of [4] for the properties of $J_{\mu\nu}(x, y)$).

Both defects are cured simultaneously when one contracts two-quark operators, as was done in [4],

$${}^f\psi_b(x){}^g\psi_b^+(y) \longrightarrow N_c\delta_{fg}G_q(x,y), \quad (30)$$

where G_q is the quark Green's function, which for large $|\mathbf{x}|$, $|\mathbf{y}|$ is proportional to $\delta^{(3)}(\mathbf{x}-\mathbf{y})$.

This property will be used in the next section, where the effective mass operators (interaction kernels) will be constructed.

However, in this operation (30), the diquark–diquark–flux vertex of (27) transforms into the $\bar{q}q$-string vertex and the diquark structure is lost. Therefore, in what follows, we shall consider the diquark correlation as it appears in the diquark Green's function due to the usual string-junction construction.

We turn now to the gluon vertices. The term $S^{(2,2)}$ (23) is the basic vertex for the gluon–gluon–string vertex (denoted as *gg* string), and here the string appears directly from $J_{\mu\nu}(x, x)$.

Now the term $S^{(4,2)}$ has exactly the same defects as the term S_{4q}; namely, the nonlocal flux operator $J_{\lambda\lambda'}(x, y)$ appearing in (24) is not yet the string and, for the latter, one should contract two of the gluon operators, $a_\mu(x)a_\nu(y) \longrightarrow G_{\mu\nu}(x, y)$, where $G_{\mu\nu}$ is the confined gluon operator; the resulting vertex is of *gg*-string type and will be considered in the next section.

Finally, we come to the term $S^{(5,2)}$ and $S^{(6,2)}$, (25) and (26), respectively. These terms are proportional to the nonlocal flux kernel $J_{\mu\nu}(x, y)$, and as in the previous case the string is still missing unless the contraction of gluon operators is made, which produces *ggg*-string and digluon–digluon–string vertices, considered in the next section.

4. INTERACTION KERNELS FOR QUARK AND GLUON GREEN'S FUNCTIONS

In this section, we shall use the vertices obtained in previous section and compute the effective mass operators (interaction kernels) for the quark and gluon operators.

All kernels are proportional to $J_{\mu\nu}(x, y)$ (17), which we shall write in the gauge [8] as

$$J_{ik}^{(\lambda\rho)}(x,y) = x_i y_k \int_0^1 d\alpha \alpha^{(\lambda)} \int_0^1 d\beta \beta^{(\rho)} (\delta_{ik}\delta_{\lambda\rho} - \delta_{i\rho}\delta_{k\lambda}) D(x-y), \quad (31)$$

where we have defined

$$\alpha^{(\lambda)}, \beta^{(\lambda)} = 1 \text{ for } \lambda = 4,$$
$$\alpha^{(\lambda)}, \beta^{(\lambda)} = \alpha, \beta \text{ for } \lambda = 1, 2, 3.$$

Note that $D(x, y)$, as in (28), is defined in the fundamental representation and is proportional to the Casimir operator C_2^f; therefore, the kernels for gluon operators are proportional to $(N_c/C_2^f)J_{\mu\nu}$.

Now we define quark and gluon Green's functions $G_q(x, y)$ and $G_{\mu\nu}(x, y)$,

$$\langle {}^f\psi_a(x){}^g\psi_b^+(y)\rangle_B = \delta_{fg}\delta_{ab}G_q(x,y), \quad (32)$$

$$\langle a_\mu^i(x)a_\nu^k(y)\rangle_{B,a} = \delta_{ik}G_{\mu\nu}(x,y). \quad (33)$$

Note that both G_q and $G_{\mu\nu}$ are actually gauge-invariant, since they are defined as in the presence of the static charge. (The Green's function of the latter reduces to the parallel transporter along the x_4 axis,

which is equal to unity in the assumed gauge [8]. They can be made explicitly gauge-invariant when multiplied with the combination of parallel transporters $\Phi(\mathbf{x}, x_4; 0, x_4)\Phi(0, x_4; 0, y_4)\Phi(0, y_4; \mathbf{y}, y_4)$ equal to unity in the gauge [8].)

Introducing (32) in S_{4q}, (21), one obtains the mass operator for the quark Green's function which was derived in [4]

$$iM_q(x,y) = \gamma_\mu G_q(x,y)\gamma_\nu(\delta_{\mu\nu}J_{ii}^{(\mu\nu)} - J_{ik}^{(ik)}\delta_{\mu k}\delta_{\nu i}). \tag{34}$$

For the one-gluon mass operator, one obtains from $S^{(2,2)}$, $S^{(4,2)}$, and $S^{(6,2)}$ the corresponding contributions to the string part of the mass,

$$M_g^{(\mathrm{str})}(x,y) = M_{\mu\nu}^{(2,2)}(x,y) + M_{\mu\nu}^{(4,2)}(x,y) + M_{\mu\nu}^{(6,2)}(x,y), \tag{35}$$

where $M_{\mu\nu}^{(2,2)}$ coincides with the term found earlier in [1],

$$M_{\mu\nu}^{(2,2)}(x,y) = \frac{N_c}{C_2^f}\delta^{(4)}(x-y)[J_{\lambda\lambda}(x,y)\delta_{\mu\nu} - J_{\mu\nu}(x,y)], \tag{36}$$

and two other terms are obtained from the corresponding $S^{(i,k)}$ contributions by insertion of (33),

$$M_{\mu\nu}^{(4,2)}(x,y) = -\frac{N_c}{C_2^f}J_{\lambda\lambda'}(x,y)G_{\rho\sigma}(x,y)N_{\lambda\rho\mu}(x)N_{\lambda'\rho\nu}(y), \tag{37}$$

where

$$N_{\lambda\rho\mu}(x) = \delta_{\mu\rho}(2\partial_\mu^G + \partial_\lambda^J) + \delta_{\lambda\rho}(\partial_\mu^J - \partial_\mu^G) - \delta_{\lambda\mu}(2\partial_\rho^J + \partial_\rho^G) \tag{38}$$

and ∂_λ^G and ∂_λ^J imply derivatives acting on G and J, respectively. Analogously, from (26), one obtains

$$M_{\mu\nu}^{(6,2)}(x,y) = -\frac{g^2N_c^2}{2C_2^f}[J_{\mu\nu}(x,y)G_{\lambda\lambda}(x,y)G_{\sigma\sigma} + \text{perm.}], \tag{39}$$

where "perm." denotes terms obtained by permutation of indices in JGG.

The total gluon mass operator contains, besides, (35) also nonstring terms, called local $M_g^{(\mathrm{loc})}$, proportional to correlators of L_1 and $L^{(F)}$:

$$M^{(g)}(x,y) = M_g^{(\mathrm{str})}(x,y) + M_g^{(\mathrm{loc})}. \tag{40}$$

Using (18) and (22), one obtains integral equations of the Dyson–Schwinger type for the quark and gluon Green's function. For example, for the gluon case, one has [1]

$$(-\partial_\lambda^2\delta_{\mu\rho} + \partial_\mu\partial_\rho)G_{\rho\nu}(x,y) + \int M_{\mu\rho}^{(g)}(x,z)G_{\rho\nu}(z,y)d^4z = \delta^{(4)}(x-y)\delta_{\mu\nu}, \tag{41}$$

where $M^{(g)}$ is given in (40) and (35)–(39); and for the quark Green's function the corresponding equation is [4]

$$(-i\hat{\partial} - im)G_q(x,y) - i\int M_q(x,z)G_q(z,y)d^4z = \delta^{(4)}(x-y), \tag{42}$$

where M_q is given in (34).

The kernel $M^{(g)}$ contains a local string piece (36) behaving as const $\times$ $|\mathbf{x}|$ at large distances, and the corresponding spectrum is that of the gluelump, which was studied also on the lattice [14] and in the QCD string model [15]. The ground-state solution of (42) with the kernel (36) was obtained in [1] with the eigenvalue $\omega = 1$ GeV.

We turn now to the digluon vertex, which is obtained from the term $S^{(6,2)}$ (26), by contracting one pair of gluon operators (in contrast to the term $M_{\mu\nu}^{(6,2)}$, where two pairs of gluons were contracted). In this way, one obtains in the exponent (13), exp(–*aaMaa*), where explicit form of the exponent is

$$a_\mu^i(x)a_\nu^k(x)M_{\mu\nu\rho\sigma}^{iklm}(x,y)a_\rho^l(y)a_\sigma^m(y) \tag{43}$$

and M is defined as

$$M_{\mu\nu\rho\sigma}^{iklm}(x,y) = -\frac{1}{2C_2^f}\{\delta_{\mu\nu}\delta_{\rho\sigma}J_{\alpha\beta}(x,y)G_{\alpha\beta}(x,y)\chi^{ik,ba}\chi^{lm,ba} + J_{\nu\sigma}(x,y)G_{\mu\rho}(x,y)\chi^{ib,ka}\chi^{lb,ma} + \text{perm.}\}, \tag{44}$$

where the explicit form of permutation terms denoted in (44) as perm. is obtained by interchanging the lower and upper indices in M (44). Denoting the Hermitian operators of octet digluon creation and annihilation

$$if^{eib}b_\mu^i(x)b_\nu^b(x) \equiv D_{\mu\nu}^e(x), \tag{45}$$

one can write the octet digluon mass operator corresponding to the second term on the right-hand side of (44) as

$$D_{\mu\nu}^i(x)M_{\mu\nu\rho\sigma}^{(\mathrm{octet})ik}(x,y)D_{\rho\sigma}^k(y). \tag{46}$$

5. DISCUSSION AND CONCLUSIONS

We have obtained equations for the one-gluon and one-quark Green's functions $G_{\mu\nu}$ and G_q, (41) and (42), respectively, and defined their kernels $M^{(g)}$ and M_q in the lowest order of background perturbation theory and in the Gaussian approximation of the background field averaging procedure.

The resulting equations are Lorentz-covariant and gauge-invariant; the latter property is due to the fact that, actually, $G_{\mu\nu}(G_q)$ describe propagation of the

gluon (quark) in the field of a static adjoint (fundamental) source, and the corresponding system can be made gauge-invariant with the help of parallel transporters.

The most important property of (41) and (42) is that they are nonlinear, and therefore the equations may have solutions of two types. The first one is a perturbative solution which starts with the free Green's function and contains all the next-order terms obtained by the interaction procedure (to this end also additional perturbative terms should be included in $M^{(g)}$ and M_q). In this case the string is absent, since in perturbation theory both confinement and chiral symmetry breaking are missing, and there is no mechanism for creation of the background component B_μ and the corresponding correlator $D(x)$. This is a trivial perturbation theory result.

There is, however, another type of solution, which essentially exploits the nonlinear character of (41) and (42). This solution, if it exists, cannot be expanded in a perturbation series. One example was given in [1] for the case of $G_{\mu\nu}$. At this point, one should stress that up to now only nonlinearity in terms of $G_{\mu\nu}$, G_q was discussed, while background field correlators $D(x)$, $D_1(x)$ were entered as an input. Now, one can go an essential step further and connect $D(x)$, $D_1(x)$ to the solutions $G_{\mu\nu}$. There are two possible justifications of this procedure. The first was suggested in [1] on the basis of large N_c. Namely, it was argued there that a valence gluon, having some fixed color index $a = 1, \ldots, N_c^2 - 1$, will keep this color index interacting with the string, since the string is a white object and does not influence the color of the valence gluon. Therefore, all the remaining $N_c^2 - 2$ gluons can be considered as a background; therefore, one obtains a connection of the form [1]

$$D_1(x) \sim \partial\partial G(x) + \text{perm.}, \tag{47}$$

$$\begin{aligned} D(x) &\sim \langle a_\mu(x) a_\nu(x) a_\mu(0) a_\nu(0)\rangle \\ &= \langle D^i_{\mu\nu}(x) D^i_{\mu\nu}(0)\rangle + O(G(x)G(x)) + \ldots. \end{aligned} \tag{48}$$

Here, $D^i_{\mu\nu}$ is the digluon operator (44), and one expects accuracy of this procedure to be $O(1/N_c^2)$.

Another argument in favor of connection (47) and (48) comes from the precise distinction between perturbative and nonperturbative regimes. Namely, connection (47) and (48) follows from the definition of the field operator $F_{\mu\nu}$ through the vector potential; the latter is represented through the sum of the specific solution of the nonlinear equation, called B_μ, and perturbative corrections to that solution, called a_μ. In this way, the self-consistent solution of nonlinear equation (41), where the kernel is nonlinear not only due to the appearance of $G_{\mu\nu}$ in $M_g^{(\mathrm{str})}$ (35)–(39), but also due to the dependence of D in $J_{\mu\nu}$ on $G_{\mu\nu}$, is logically separated into two pieces, nonperturbative due to B_μ and perturbative due to a_μ.

The first step in this direction was made in [1], where the self-constituent solution of (41) with the kernel (36) was obtained. In the next step, one should also use digluon operators as in (48) and digluon vertex (43), and the kernels (37), (39). This part is planned for a subsequent publication.

ACKNOWLEDGMENTS

The author is grateful to A.B. Kaidalov for useful discussions.

This work was supported in part by the Russian Foundation for Basic Research (project nos. 00-02-17836 and 00-15-96786).

REFERENCES

1. Yu. A. Simonov, Yad. Fiz. **61**, 941 (1998) [Phys. At. Nucl. **61**, 855 (1998)]; hep-ph/9712250.
2. Yu. A. Simonov, in *Proceedings of Hadron'93, Como, 1993*, p. 2629; *Lectures at the XVII International School of Physics, Lisbon, 1999*; hep-ph/9911237; Yu. S. Kalashnikova and Yu. B. Yufryakov, Phys. Lett. B **359**, 175 (1995).
3. V. I. Shevchenko and Yu. A. Simonov, Phys. Lett. B **437**, 146 (1998); hep-th/9807157.
4. Yu. A. Simonov, Yad. Fiz. **60**, 2252 (1997) [Phys. At. Nucl. **60**, 2069 (1997)]; hep-ph/9704301; Yu. A. Simonov and J. A. Tjon, Phys. Rev. D **62**, 014501 (2000); hep-ph/0001075.
5. Yu. A. Simonov, Yad. Fiz. **62**, 2087 (1999) [Phys. At. Nucl. **62**, 1932 (1999)]; hep-ph/9912383.
6. B. S. De Witt, Phys. Rev. **162**, 1195 (1967); **162**, 1239 (1967); J. Homerkamp, Nucl. Phys. B **48**, 269 (1972); G. 't Hooft, Nucl. Phys. B **62**, 44 (1973); Acta Univ. Wratislav. **368**, 345 (1976); L. F. Abbot, Nucl. Phys. B **185**, 189 (1981).
7. Yu. A. Simonov, Lect. Notes Phys. **479**, 139 (1996); Yad. Fiz. **58**, 113 (1995) [Phys. At. Nucl. **58**, 107 (1995)].
8. I. I. Balitsky, Nucl. Phys. B **254**, 166 (1985).
9. N. G. van Kampen, Phys. Rep. C **24**, 171 (1976); H. G. Dosch, Phys. Lett. B **190**, 177 (1987); H. G. Dosch and Yu. A. Simonov, Phys. Lett. B **205**, 339 (1988); Yu. A. Simonov, Nucl. Phys. B **307**, 512 (1988); Yad. Fiz. **48**, 1381 (1988) [Sov. J. Nucl. Phys. **48**, 878 (1988)]; Yad. Fiz. **50**, 213 (1989) [Sov. J. Nucl. Phys. **50**, 134 (1989)].
10. A. Di Giacomo and H. Panagopoulos, Phys. Lett. B **285**, 133 (1992); A. Di Giacomo, E. Meggiolaro, and H. Panagopoulos, Nucl. Phys. B **483**, 371 (1997); Nucl. Phys. B (Proc. Suppl.) **54**, 343 (1997).
11. G. S. Bali, hep-lat/9908021.
12. Yu. A. Simonov, Pis'ma Zh. Éksp. Teor. Fiz. **71**, 187 (2000) [JETP Lett. **71**, 127 (2000)]; hep-ph/0001244; V. I. Shevchenko and Yu. A. Simonov, hep-ph/0001299.
13. H. G. Dosch and Yu. A. Simonov, Phys. Lett. B **205**, 339 (1988).
14. M. Foster and C. Mochael, Phys. Rev. D **59**, 094509 (1999); hep-lat/9811010.
15. Yu. A. Simonov, hep-ph/0003114.

Physics of Atomic Nuclei, Vol. 64, No. 3, 2001, pp. 554–560. Translated from Yadernaya Fizika, Vol. 64, No. 3, 2001, pp. 608–614.

90th ANNIVERSARY OF A.B. MIGDAL'S BIRTHDAY
ELEMENTARY PARTICLES AND FIELDS

Chiral Thermodynamics in a Magnetic Field

N. O. Agasian*

Institute of Theoretical and Experimental Physics, Bol'shaya Cheremushkinskaya ul. 25, Moscow, 117259 Russia

Received July 12, 2000

Abstract—The phase structure of the QCD vacuum in a magnetic field H is investigated at low temperatures T. The free energy of the hadronic phase in a constant homogeneous magnetic field is calculated in the one-loop approximation of chiral perturbation theory. The quark and the gluon condensate are found as functions of temperature and the field strength. It is shown that the order parameter $\langle \bar{q}q \rangle$ for the chiral phase transition remains constant when the temperature T and the magnetic field H change in such a way that $H = \text{const} \times T^2$. © *2001 MAIK "Nauka/Interperiodica".*

1. INTRODUCTION

In recent years, the properties of the vacuum state under various external conditions have received much attention in quantum field theory. Within the theory of strong interactions (QCD), external conditions are determined by temperature and by the baryon-number density. At temperatures below the temperature of the chiral phase transition, $T < T_c$, quark confinement and a spontaneous breakdown of chiral symmetry are the most important dynamical features of the system. At low temperatures $T < T_c$, the partition function is dominated by the contribution of the lightest particles of the physical spectrum. The π meson, which is a Goldstone excitation over the chiral condensate, represents the lightest physical particle in QCD. For this reason, low-temperature physics (hadronic phase) can be adequately described in terms of effective chiral theory [1–3]. It is important to study the behavior of the order parameter for the chiral phase transition (quark condensate $\langle \bar{q}q \rangle$) with increasing temperature. In the ideal-gas approximation, the contribution of thermal pions to the quark condensate is of order T^2 [4, 5]. Within chiral perturbation theory (ChPT), the two-loop ($\sim T^4$) and three-loop ($\sim T^6$) contributions to $\langle \bar{q}q \rangle$ were calculated in [5] and [6], respectively.

The physics of the gluon condensate $\langle G^2 \rangle \equiv \langle (G^a_{\mu\nu})^2 \rangle$ is totally different. The gluon condensate appears to be something other than an order parameter for any phase transition. No spontaneous symmetry breaking is associated with the gluon condensate. At the quantum level, scale invariance is violated because of the anomaly in the trace of the energy–momentum tensor, with the result that there arises a nonzero value of $\langle G^2 \rangle$, but no Goldstone particle is generated. The mass of the lightest excited state (dilaton) in gluodynamics is directly related to the condensate, $m_D \propto (\langle G^2 \rangle)^{1/4}$. As a consequence, thermal glueball excitations are suppressed by the exponential Boltzmann factor $\sim \exp\{-m_{gl}/T\}$; therefore, their contribution to the shift of the gluon condensate is negligibly small ($\Delta\langle G^2 \rangle / \langle G^2 \rangle \sim 0.1\%$ at $T =$ 100 MeV) [7]. In the one-loop approximation of ChPT, pions in the chiral limit can be treated as a gas of noninteracting massless particles. Obviously, this system is scale-invariant, so that it does not contribute to the trace of the energy–momentum tensor and, hence, to $\langle G^2 \rangle$. It was shown in [8] that only in the three-loop approximation of ChPT does the gluon condensate become dependent on temperature in the chiral limit. The effect of thermal excitations of massive hadrons on the properties of the quark and the gluon condensate was first studied in [9, 10] within the generalized nonlinear σ model invariant under conformal transformations.

The phase structure of the vacuum in an external magnetic field H is another important subject of investigation. The magnetic-field dependence of the quark condensate was first investigated in [11] on the basis of the Nambu–Jona-Lasinio model. Within QCD, the one-loop result for the magnetic-field dependence of the quark condensate $\langle \bar{q}q \rangle$ was derived in [12]. In either case, the condensate was found to increase with H, in contrast to what we have in the case of conventional superconductivity, where the condensate of Cooper pairs is destroyed by a magnetic field. The behavior of the gluon condensate $\langle G^2 \rangle$ in an Abelian magnetic field is also nontrivial. Gluons have no electric charge, but they generate virtual quarks whose interaction with the magnetic field H leads to a shift of $\langle G^2 \rangle$. This phenomenon was investigated in [13, 14] on the basis of low-energy theorems. The phase structure of the QCD vacuum in an Abelian magnetic field at finite temperatures was studied in [15]. It should also be noted that long-wave chromomagnetic fields in the QCD vacuum are gluon fluctuations governing the nonperturbative dynamics of the QCD vacuum in the phase of temperature deconfinement [16–20].

* e-mail: agasyan@heron.itep.ru

Low-energy theorems are of crucial importance for understanding the properties of the vacuum in the quantum field theory. They (for example, the Low theorems [21]) were established concurrently with the application of the methods of quantum field theory to particle physics. Within QCD, low-energy theorems were proved in the early 1980s [22]. These theorems follow from general symmetry properties, so that they are unaffected by specific (and unknown) details of the confinement mechanism. For this reason, they sometimes furnish unique information about physical processes—that is, information that cannot be obtained by any other methods. Furthermore, these theorems provide physically plausible limitations successfully used in constructing effective field theories. An important advancement in using low-energy theorems was made in [23], where they were generalized to the case of QCD at finite temperatures. Low-energy theorems in the two-loop approximation of ChPT were deduced in [14], where the vacuum energy density and the condensates $\langle G^2\rangle$ and $\langle \bar{q}q\rangle$ were also calculated as functions of H in the same approximation.

In the present study, the free energy of the QCD vacuum in a magnetic field at finite temperatures is calculated within ChPT. The quark and the gluon condensate as functions of T and H are found on the basis of the general relations derived here. The freezing of the order parameter for the chiral phase transition by a magnetic field as the temperature increases is considered. The physics behind this new phenomenon is also discussed.

2. LOW-ENERGY THEOREMS FOR QCD IN A MAGNETIC FIELD AT FINITE TEMPERATURES

In the Euclidean formulation, the QCD partition function in an external Abelian field A_μ can be represented in the form ($T = 1/\beta$ is the temperature)

$$Z = \exp\left\{-\frac{1}{4e^2}\int_0^\beta dx_4\int_V d^3x F_{\mu\nu}^2\right\} \times \int [DB][D\bar{q}][Dq]\exp\left\{-\int_0^\beta dx_4\int_V d^3x\, \mathcal{L}\right\}, \quad (1)$$

where the QCD Lagrangian in the background field has the form

$$\mathcal{L} = \frac{1}{4g_0^2}(G_{\mu\nu}^a)^2 + \sum_{q=u,d}\bar{q}\left[\gamma_\mu\left(\partial_\mu - iQ_qA_\mu - i\frac{\lambda^a}{2}B_\mu^a\right) + m_q\right]q. \quad (2)$$

Here, Q_q is the charge matrix for the quarks of flavor $q = (u, d)$. The gauge-fixing and ghost terms are omitted in formula (2) for the sake of simplicity. The free-energy density is determined by the expression $\beta VF(T, H, m_q) = -\ln Z$. From (1), it follows that, in the chiral limit $m_q \longrightarrow 0$, the quark ($\langle\bar{q}q\rangle$) and the gluon ($\langle G^2\rangle$) condensates are given by

$$\langle\bar{q}q\rangle(T, H) = \left.\frac{\partial F(T, H, m_q)}{\partial m_q}\right|_{m_q = 0}, \quad (3)$$

$$\langle G^2\rangle(T, H) = 4\left.\frac{\partial F(T, H, m_q)}{\partial(1/g_0^2)}\right|_{m_q = 0}. \quad (4)$$

The dimensional-transmutation phenomenon gives rise to the nonperturbative dimensional parameter

$$\Lambda = M\exp\left\{\int_{\alpha_s(M)}^\infty \frac{d\alpha_s}{\beta(\alpha_s)}\right\}, \quad (5)$$

where M is the ultraviolet-cutoff mass, $\alpha_s = g_0^2/4\pi$, and $\beta(\alpha_s) = d\alpha_s(M)/d\ln M$ is the Gell-Mann–Low function. If the partition function of a system is given by (1), then this system can be described by three dimensional parameters (M, T, and H) in the chiral limit. Since the free-energy density is renormalization-invariant, its anomalous dimension is zero. For this reason, F has only the normal (canonical) dimension of 4. By using the renormalization invariance of Λ, we arrive at the general formula

$$F = \Lambda^4 f\left(\frac{T}{\Lambda}, \frac{H}{\Lambda^2}\right), \quad (6)$$

where f is an unknown function. From Eqs. (5) and (6), we obtain

$$\frac{\partial F}{\partial(1/g_0^2)} = \frac{\partial F}{\partial\Lambda^2}\frac{\partial\Lambda^2}{\partial(1/g_0^2)} = \frac{4\pi\alpha_s^2}{\beta(\alpha_s)}\left(4 - T\frac{\partial}{\partial T} - 2H\frac{\partial}{\partial H}\right)F. \quad (7)$$

Taking into account expression (4), we find that the gluon condensate can be represented as

$$\langle G^2\rangle(T, H) = \frac{16\pi\alpha_s^2}{\beta(\alpha_s)}\left(4 - T\frac{\partial}{\partial T} - 2H\frac{\partial}{\partial H}\right)F(T, H). \quad (8)$$

At $T = 0$ and $H = 0$, we arrive at the well-known expression for the nonperturbative vacuum energy density in the chiral limit. In the one-loop approximation ($\beta = -b_0\alpha_s^2/2\pi$, $b_0 = (11N_c - 2N_f)/3$), it assumes the form

$$\varepsilon_v = F(0, 0) = -\frac{b_0}{128\pi^2}\langle G^2\rangle. \quad (9)$$

Using the above relations, one can derive low-energy theorems for QCD at finite temperatures in a magnetic field. Strictly speaking, β depends on H, so

that the low-energy theorems could involve electromagnetic corrections of order e^4. Since the free energy is independent of the scale parameter M introduced to regularize ultraviolet divergences, we can take $M^2 \gg H$, T^2, Λ^2, in which case the electromagnetic corrections vanish for β evaluated in the leading order [$\beta(\alpha_s) = -b_0\alpha_s^2/2\pi$]. Taking the aforesaid into consideration, we introduce the field $\sigma(\tau = x_4, \mathbf{x})$ and the operator $\hat{D}$ as

$$\sigma(\tau, \mathbf{x}) = -\frac{b_0}{32\pi^2}(G^a_{\mu\nu}(\tau, \mathbf{x}))^2, \tag{10}$$

$$\hat{D} = 4 - T\frac{\partial}{\partial T} - 2H\frac{\partial}{\partial H}. \tag{11}$$

Differentiating expression (4) with respect to $(1/g_0^2)$ n times and taking into account Eqs. (7), (10), and (11), we arrive at

$$\hat{D}^{n+1}F = \hat{D}^n\langle\sigma(0, \mathbf{0})\rangle = \int d\tau_n d^3x_n \ldots \times \int d\tau_1 d^3x_1 \langle\sigma(\tau_n, \mathbf{x}_n)\ldots\sigma(\tau_1, \mathbf{x}_1)\sigma(0, \mathbf{0})\rangle_c. \tag{12}$$

The subscript c in expression (12) indicates that only the contribution of connected diagrams is included in the vacuum expectation value. A similar argument can be applied to an arbitrary operator $O(x)$ constructed from the quark and gluon fields, in which case we obtain

$$\left(T\frac{\partial}{\partial T} + 2H\frac{\partial}{\partial H} - d\right)^n\langle O\rangle = \int d\tau_n d^3x_n \ldots \times \int d\tau_1 d^3x_1 \langle\sigma(\tau_n, \mathbf{x}_n)\ldots\sigma(\tau_1, \mathbf{x}_1)O(0, \mathbf{0})\rangle_c, \tag{13}$$

where d is the canonical dimension of the operator O. If the operator O has an anomalous dimension as well, we must take into account the relevant γ function.

3. FREE ENERGY OF THE QCD VACUUM AT $H \neq 0$ AND $T \neq 0$

With the aid of the above formulas, the condensates can be determined as functions of T and H, provided that the free-energy density is known. Here, we compute the free-energy density within ChPT. At low temperatures $T < T_c$ (T_c being the temperature of the chiral phase transition) and weak magnetic fields,[1] $H < \mu^2_{\text{hadr}} \sim (4\pi F_\pi)^2$, typical momenta in vacuum loops are small, whence it follows that it is possible to formulate adequately the theory in question in terms of a low-energy effective Lagrangian L_{eff} [2, 3] that can be represented as a power series in momenta (derivatives) and masses:

$$L_{\text{eff}} = L^{(2)} + L^{(4)} + L^{(6)} + \ldots. \tag{14}$$

The leading term in (14) is similar to the Lagrangian of the nonlinear σ model in an external field V_μ and is given by

$$L^{(2)} = \frac{F_\pi^2}{4}\text{tr}(\nabla_\mu U^+\nabla_\mu U) + \Sigma\,\text{Re}\,\text{tr}(\hat{M}U^+), \qquad \nabla_\mu U = \partial_\mu U - i[U, V_\mu], \tag{15}$$

where U is the $SU(2)$ unitary matrix; $F_\pi = 93$ MeV is the pion decay constant; and the parameter Σ has the meaning of the quark condensate, $\Sigma = |\langle\bar{u}u\rangle| = |\langle\bar{d}d\rangle|$. The external Abelian magnetic field H directed along the z axis corresponds to $V_\mu(x) = (\tau^3/2)A_\mu(x)$, where the vector potential A_μ is chosen to be $A_\mu(x) = \delta_{\mu 2}Hx_1$. The Lagrangian L_{eff} involves only second-order and higher order terms in the mass difference between the u and d quarks. Since, in the chiral limit, the quark condensate can be expressed in terms of the first derivative with respect to the mass of one of the quarks, the above mass difference can be neglected, whereupon the quark mass matrix becomes diagonal, $\hat{M} = m\hat{I}$.

At $T < T_c$ and $H < \mu^2_{\text{hadr}}$, the QCD partition function (1) coincides with the partition function in the effective chiral theory:

$$Z_{\text{eff}}[T, H] = e^{-\beta V F_{\text{eff}}[T, H]} = Z_0[H]\int[DU]\exp\left\{-\int_0^\beta dx_4\int_V d^3x L_{\text{eff}}[U, A]\right\}. \tag{16}$$

In the one-loop approximation, it is sufficient to retain only second-order terms in the pion field when we use the expansion of the Lagrangian L_{eff}. For the exponential parametrization $U(x) = \exp\{i\tau^a\pi^a(x)/F_\pi\}$, we arrive at

$$L^{(2)} = \frac{1}{2}(\partial_\mu\pi^0) + \frac{1}{2}M_\pi^2(\pi^0)^2 + (\partial_\mu\pi^+ + iA_\mu\pi^+)(\partial_\mu\pi^- - iA_\mu\pi^-) + M_\pi^2\pi^+\pi^-, \tag{17}$$

where the fields of the charged and neutral mesons ($\pi^\pm$ and π^0, respectively) are defined as

$$\pi^\pm = (\pi^1 \pm i\pi^2)/\sqrt{2}, \quad \pi^0 = \pi^3. \tag{18}$$

Thus, expression (16) can be recast into the form[2]

[1] A transition to the chiral limit implies that $M_\pi^2 \ll H$. It was shown in [13, 14] that the parameter of the ChPT expansion in a magnetic field is $\xi = H/(4\pi F_\pi)^2$. Thus, the domain of ChPT validity in a magnetic field is $M_\pi^2/(4\pi F_\pi)^2 \ll \xi < 1$. In the chiral limit, the axial constant is $F_\pi(M_\pi \longrightarrow 0) \longrightarrow \text{const} \approx 80$ MeV; hence, we have $0 < \xi < 1$.

[2] The partition function Z^R_{eff} describes the Bose gas of charged ($\pi^\pm$) and neutral (π^0) mesons in a magnetic field. In terms of Bose–Einstein condensation and the Meissner effect, the gas of relativistic Bose particles at finite temperatures and a finite particle-number density was studied in [24–27].

$$Z^R_{\rm eff}[T,H] = Z^{-1}_{\rm PT}Z_0[H]\int[D\pi^0][D\pi^+][D\pi^-] \times\exp\left\{-\int_0^\beta dx_4\int_V d^3x L^{(2)}[\pi,A]\right\}, \quad (19)$$

where we removed the divergent expression for the partition function at $T=0$ and $H=0$:

$$Z_{\rm PT} = [\det(-\partial_\mu^2+M_\pi^2)]^{-3/2}. \quad (20)$$

Performing integration with respect to the pion fields in (19), we obtain

$$Z^R_{\rm eff} = Z^{-1}_{\rm PT}Z_0[H][\det{}_T(-\partial_\mu^2+M_\pi^2)]^{-1/2} \times[\det{}_T(-|D_\mu|^2+M_\pi^2)]^{-1}, \quad (21)$$

where $D_\mu=\partial_\mu - iA_\mu$ is the covariant derivative and where the symbol T indicates that the determinant is calculated at finite temperature T according to the conventional Matsubara technique. Rearranging the factors in (21) and taking into account (20), we reduce $Z^R_{\rm eff}$ to the form

$$Z^R_{\rm eff}[T,H] = Z_0[H]\left[\frac{\det_T(-\partial_\mu^2+M_\pi^2)}{\det(-\partial_\mu^2+M_\pi^2)}\right]^{-1/2} \times\left[\frac{\det(-|D_\mu|^2+M_\pi^2)}{\det(-\partial_\mu^2+M_\pi^2)}\right]^{-1}\left[\frac{\det_T(-|D_\mu|^2+M_\pi^2)}{\det(-|D_\mu|^2+M_\pi^2)}\right]^{-1}. \quad (22)$$

The effective free energy can then be represented as

$$F^R_{\rm eff}(T,H) = -\frac{1}{\beta V}\ln Z^R_{\rm eff} = \frac{H^2}{2e^2}+F_{\pi^0}(T)+F_{\pi^\pm}(H)+F_s(T,H), \quad (23)$$

where F_{π^0} is the free energy of the massive scalar boson,

$$F_{\pi^0}(T) = T\int\frac{d^3p}{(2\pi)^3}\ln(1-\exp(-\sqrt{\mathbf{p}^2+M_\pi^2}/T)); \quad (24)$$

$F_{\pi^\pm}$ is the Schwinger result for the density of the vacuum energy of charged scalar particles in a magnetic field,

$$F_{\pi^\pm}(H) = -\frac{1}{16\pi^2}\int_0^\infty\frac{ds}{s^3}e^{-M_\pi^2 s}\left[\frac{Hs}{\sinh(Hs)}-1\right]; \quad (25)$$

and

$$F_s(T,H) = \frac{HT}{\pi^2}\sum_{n=0}^\infty{}'\int_0^\infty dk\ln(1-\exp(-\omega_n/T)), \quad \omega_n = \sqrt{k^2+M_\pi^2+H(2n+1)}. \quad (26)$$

Here, ω_n are the Landau levels for the $\pi^\pm$ mesons in the constant magnetic field H.[3)]

4. QUARK AND GLUON CONDENSATES

The free energy $F^R_{\rm eff}$ determines the thermodynamic properties and the phase structure of the QCD vacuum in a magnetic field below the temperature of the chiral phase transition—that is, in the confining phase.

Equations (8) and (23) determine the condensate $\langle G^2\rangle$ as a function of T and H. Applying the operator $\hat D$ to $F^R_{\rm eff}$, we find that $\hat D F_{\pi^0}(T)=0$ because, in the chiral limit, $M_\pi^2\longrightarrow 0$, $F_{\pi^0}(T)\sim T^4$, and $(4-T\partial/\partial T)F_{\pi^0}(T)=0$. Further, a straightforward calculation yields $\hat D F_s(T,H)=0$. A nontrivial dependence of $\langle G^2\rangle$ on H is entirely due to the Schwinger term $F_{\pi^\pm}(H)$:

$$\langle G^2\rangle(T,H) = \langle G^2\rangle + \frac{\alpha_s^2}{3\pi\beta(\alpha_s)}H^2. \quad (27)$$

By virtue of asymptotic freedom in QCD, the β function is negative, $\beta(\alpha_s)=-b_0\alpha_s^2/2\pi+\ldots$; consequently, the gluon condensate decreases with increasing magnetic field H:

$$\langle G^2\rangle(T,H) = \langle G^2\rangle - \frac{2}{3b_0}H^2.$$

To determine the quark condensate as a function of T and H, we use the Gell-Mann–Oaks–Renner relation

$$F_\pi^2M_\pi^2 = -\frac{1}{2}(m_u+m_d)\langle\bar uu+\bar dd\rangle = 2m\Sigma. \quad (28)$$

Substituting expression (23) into (3), differentiating it with respect to M_π^2, and going over to the limit $M_\pi^2\longrightarrow 0$, we

[3)] The expression for the free energy $F=\frac{1}{2}\mathrm{tr}\ln(p_4^2+\omega_0^2(\mathbf{p}))$ for the vacuum at $H=0$ and $T=0$ can readily be extended to the case of $H\neq 0$ and $T\neq 0$. Without going into details, we merely indicate that this corresponds to the substitutions $p_4\longrightarrow\omega_k=2\pi kT$ ($k=0,\pm1,\ldots$), $\omega_0=\sqrt{\mathbf{p}^2+M_\pi^2}\longrightarrow\omega_n=\sqrt{p_z^2+M_\pi^2+H(2n+1)}$, and $\mathrm{tr}\longrightarrow\frac{HT}{2\pi}\sum_{n=0}^\infty{}'\sum_{k=-\infty}^{+\infty}\int_{-\infty}^{+\infty}\frac{dp_z}{2\pi}$, where the degeneracy multiplicity $H/2\pi$ of the Landau levels has been taken into account. Performing summation over the Matsubara frequencies, we arrive at (26).

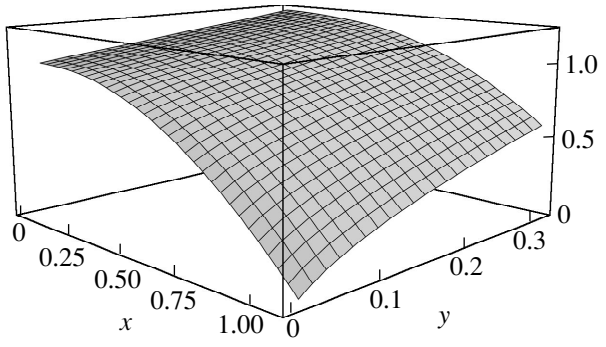

Quark condensate $\langle\bar{q}q\rangle(T, H)/\langle\bar{q}q\rangle$ as a function of $x = T/\sqrt{8}F_\pi$ and $y = H/(4\pi F_\pi)^2$.

obtain

$$\langle\bar{q}q\rangle(T, H) = \langle\bar{q}q\rangle\left(1 - \frac{T^2}{24F_\pi^2} + \frac{H}{(4\pi F_\pi)^2}\ln 2 - \frac{H}{2\pi^2 F_\pi^2}\varphi\left(\frac{\sqrt{H}}{T}\right)\right), \quad (29)$$

$$\varphi(\lambda) = \sum_{n=0}^{\infty}\int_0^\infty \frac{dx}{\omega_n(x)(\exp(\lambda\omega_n(x)) - 1)},$$

$$\omega_n(x) = \sqrt{x^2 + 2n + 1}.$$

Let us consider various limiting cases. In the strong-field case, $\sqrt{H} \gg T(\lambda \gg 1)$, the main contribution to (29) comes from the lowest Landau level ($n = 0$):

$$\varphi(\lambda \gg 1) = \sqrt{\frac{\pi}{2\lambda}}e^{-\lambda} + O(e^{-\sqrt{3}\lambda}). \quad (30)$$

In the weak-field limit, $\sqrt{H} \ll T(\lambda \ll 1)$, the sum in (29) can be evaluated, to a required precision, by means of the Euler–Maclaurin summation formula. Using the asymptotic expansion of the integral in (29) [28] for $\lambda \ll 1$, we obtain

$$\varphi(\lambda \ll 1) = \frac{\pi^2}{6}\frac{1}{\lambda^2} + \frac{7\pi}{24}\frac{1}{\lambda} + \frac{1}{4}\ln\lambda + C + \frac{\zeta(3)}{48\pi^2}\lambda^2 + O(\lambda^4), \quad (31)$$

where $C = \frac{1}{4}\left(\gamma - \ln 4\pi - \frac{1}{6}\right)$, $\gamma = 0.577\ldots$ is the Euler constant, and $\zeta(3) = 1.202$ is the Riemann zeta function. Thus, we find that the limiting expressions for the quark condensate in a magnetic field for $T \neq 0$ are given by

$$\frac{\langle\bar{q}q\rangle(T, H)}{\langle\bar{q}q\rangle} = 1 - \frac{T^2}{24F_\pi^2} + \frac{H}{(4\pi F_\pi)^2}\ln 2 - \frac{H^{3/4}T^{1/2}}{(2\pi)^{3/2}F_\pi^2}e^{-\sqrt{H}/T}, \quad (32)$$

$$\sqrt{H} \gg T;$$

$$\frac{\langle\bar{q}q\rangle(T, H)}{\langle\bar{q}q\rangle} = 1 - \frac{T^2}{8F_\pi^2} + \frac{H}{(4\pi F_\pi)^2}A - \frac{7\sqrt{H}T}{48\pi F_\pi^2} - \frac{H}{(4\pi F_\pi)^2}\ln\frac{H}{T^2}, \quad (33)$$

$$\sqrt{H} \ll T,$$

where $A = \ln 2 + 8C \simeq 4.93$.

Within ChPT, the quark condensate (29) at $H \neq 0$ and $T \neq 0$ is determined by three dimensionless parameters: $H/(4\pi F_\pi)^2$, T^2/F_π^2, and $\lambda = \sqrt{H}/T$. The quantity λ is a natural dimensionless parameter in the approximation used here. The motion of a particle (massless pion) in a field is characterized by the radius of curvature of its trajectory; in the magnetic field, this is the Larmor radius $R_L = 1/\sqrt{H}$. At the same time, another quantity having dimensions of length, $l_T = 1/T$, arises when $T \neq 0$. It is associated with the thermal motion of the particle. If the Larmor radius is much less than $l_T(\lambda \gg 1)$, the charged $\pi^\pm$ mesons in a work magnetic field acquire the effective mass $m_{\text{eff}} = \sqrt{H}$, which is determined by the lowest Landau level. The contribution from such mesons to the chiral condensate is exponentially suppressed by the Boltzmann factor $\exp\{-m_{\text{eff}}/T\}$. Within chiral thermodynamics, $\pi^\pm$ mesons in a weak magnetic field make a standard contribution to the quark condensate $\langle\bar{q}q\rangle$. Moreover, there arise some additional temperature and magnetic corrections. The contribution of the neutral pion to $\langle\bar{q}q\rangle(T, H)$ is calculated by considering that it is a massless scalar particle. The quark condensate $\langle\bar{q}q\rangle(T, H)/\langle\bar{q}q\rangle$ as a function of the variables $x = T/\sqrt{8}F_\pi$ and $y = H/(4\pi F_\pi)^2$ is shown in the figure.

The phase structure of the QCD vacuum under study shows an interesting effect. From expression (29), we can find a function $H(T)$ such that the quark condensate $\langle\bar{q}q\rangle(T, H)$ remains constant as the temperature T varies along with the magnetic field $H_* = H(T)$. The quantity H_* is determined as a solution to the equation $\langle\bar{q}q\rangle(T, H_*) - \langle\bar{q}q\rangle = 0$, where the first term on the left-

hand side is given by (29). Upon introducing the variable $\lambda = \sqrt{H}/T$, this equation takes the form

$$1 - \frac{3}{2\pi^2}\lambda^2 \ln 2 + \frac{12}{\pi^2}\lambda^2 \varphi(\lambda) = 0. \quad (34)$$

By numerically solving Eq. (34), we obtain $\lambda_* = 0.111\ldots$. Thus, the quark condensate $\langle \bar{q}q \rangle(T, H)$ remains unchanged when the temperature T and the magnetic field increase in such a way that $H = 0.013T^2$. It can be said that the order parameter $\langle \bar{q}q \rangle$ for the chiral phase transition is "frozen" by the magnetic field. At $T = T_c \simeq 150$ MeV, we have $H(T_c)/(4\pi F_\pi)^2 \simeq 2 \times 10^{-4} \ll 1$, so that the above relations remain valid up to the point of the chiral phase transition and, hence, to the point of the confinement–deconfinement phase transition. In the vicinity of T_c, the effective low-energy chiral Lagrangian can no longer describe the thermodynamic properties of the QCD vacuum adequately; strictly speaking, it is inapplicable there.

5. CONCLUSION

It has been demonstrated that the quark condensate is "frozen" by a magnetic field when the temperature T and the magnetic field H are related by the equation $H = \text{const} \times T^2$. This effect indicates that the QCD quark condensate bears no resemblance to the condensate in the theory of superconductivity. In Bardeen–Cooper–Schrieffer theory, both temperature and the magnetic field destroy the condensate of Cooper pairs. The freezing of the condensate can be understood on the basis of the general Le Chatelier's principle.[4)] The external field contributes $H^2/2$ to the energy density of the system. The system tends to compensate for this change and to reduce its free energy by increasing the absolute value of the quark condensate: $\Delta\varepsilon_v = -m|\Sigma(H) - \Sigma(0)| < 0$. On the other hand, an increase in temperature (say, owing to heating) gives rise to processes in which heat is absorbed via the reduction of the condensate. It is the competition between these two processes that leads to the freezing of $\Sigma(T, H)$. Since gluons have no electric charge, the magnetic field can affect the gluon sector of the QCD vacuum only through the quark sector. For this reason, Le Chatelier's principle cannot be applied directly to the gluon condensate. This may account for the nonlinear magnetic-field dependence of the decrease in the gluon condensate, $\Delta\langle G^2 \rangle \propto -H^2$; for the quark condensate, we have $\Delta\Sigma \propto H$.

In $N_f = 2$ QCD, the temperature phase transition restoring chiral $SU(2)_L \times SU(2)_R$ symmetry is a second-order phase transition. As the temperature is increased, the order parameter $\Sigma(T)$ decreases monotonically, vanishing at the critical point T_c. The existence of the jump $\Delta\Sigma(T_c) \neq 0$ would indicate the occurrence of a first-order phase transition. The order parameter at any nonzero magnetic field H is greater than that at $H = 0$; hence, $\Sigma(T, H) - \Sigma(T, H = 0) > 0$. Because of this, it may turn out that the chiral phase transition in a magnetic field becomes a first-order phase transition. In order to clarify the character of the phase transition, it is necessary to investigate the behavior of the system and of the order parameter in the fluctuation region near T_c; however, the effects of $\pi\pi$ interaction are substantial in this region. It follows that, within the approach used here, it is impossible to establish the change in the order of the transition, although this seems highly probable.[5)] This phenomenon may prove to be of use in investigating various cosmological scenarios after the Big Bang. For this reason, it would be interesting to continue studying the chiral phase transition in a magnetic field.

ACKNOWLEDGMENTS

I am grateful to B.L. Ioffe, V.A. Novikov, Yu.A. Simonov, and A.V. Smilga for discussions on the results presented here and for enlightening comments.

This work was supported in part by the Russian Foundation for Basic Research (project no. 00-02-17836).

REFERENCES

1. S. Weinberg, Physica A (Amsterdam) **96**, 327 (1979).
2. J. Gasser and H. Leutwyler, Ann. Phys. (N.Y.) **158**, 142 (1984).
3. J. Gasser and H. Leutwyler, Nucl. Phys. B **250**, 465 (1985).
4. P. Binétrui and M. K. Gaillard, Phys. Rev. D **32**, 931 (1985).
5. J. Gasser and H. Leutwyler, Phys. Lett. B **184**, 83 (1987); **188**, 477 (1987); H. Neuberger, Phys. Rev. Lett. **60**, 889 (1988).
6. H. Leutwyler, Nucl. Phys. B (Proc. Suppl.) **4**, 248 (1988); P. Gerber and H. Leutwyler, Nucl. Phys. B **321**, 387 (1989).
7. N. O. Agasyan, Pis'ma Zh. Éksp. Teor. Fiz. **57**, 200 (1993) [JETP Lett. **57**, 208 (1993)].
8. H. Leutwyler, Lecture given at the Workshop on Effective Field Theories, Dobogoko, Hungary, 1991; Preprint No. BUTP-91-43 (Bern Univ., 1991).
9. N. O. Agasian, D. Ebert, and E. M. Ilgenfritz, Nucl. Phys. A **637**, 135 (1998).
10. N. O. Agasian, D. Ebert, and E. M. Ilgenfritz, Talk given at 31st International Ahrenshoop Symposium on the Theory of Elementary Particles, Buckow, Germany, 1997, p. 195.
11. S. P. Klevansky and R. H. Lemmer, Phys. Rev. D **39**, 3478 (1989).
12. I. A. Shuspanov and A. V. Smilga, Phys. Lett. B **402**, 351 (1996).

[4)] When an external force is applied to a system at equilibrium, the system adjust so as to minimize the effect of the applied force.

[5)] The presence of an external field (not necessarily a magnetic field) transforms a second-order phase transition into a first-order phase transition [29].

13. N. O. Agasyan and I. A. Shushpanov, Pis'ma Zh. Éksp. Teor. Fiz. **70**, 711 (1999) [JETP Lett. **70**, 717 (1999)].
14. N. O. Agasian and I. A. Shuspanov, Phys. Lett. B **472**, 143 (2000).
15. N. O. Agasian, Phys. Lett. B **488**, 39 (2000).
16. E. L. Gubankova and Yu. A. Simonov, Phys. Lett. B **360**, 93 (1995).
17. H. G. Dosch, H. J. Pirner, and Yu. A. Simonov, Phys. Lett. B **349**, 335 (1995).
18. Yu. A. Simonov, in *Proceedings of the Enrico Fermi International School in Physics, Varenna, 1995*, pp. 319–337.
19. N. O. Agasyan, Pis'ma Zh. Éksp. Teor. Fiz. **71**, 65 (2000) [JETP Lett. **71**, 43 (2000)].
20. N. O. Agasian, B. O. Kerbikov, and V. I. Shevchenko, Phys. Rep. **320**, 131 (1999).
21. F. E. Low, Phys. Rev. **110,** 974 (1958).
22. V. A. Novikov, M. A. Shifman, A. I. Vainshtein, and V. I. Zakharov, Nucl. Phys. B **191**, 301 (1981); Fiz. Élem. Chastits At. Yadra **13**, 542 (1982) [Sov. J. Part. Nucl. **13**, 224 (1982)]; A. B. Migdal and M. A. Shifman, Phys. Lett. B **114B**, 445 (1982).
23. P. J. Ellis, J. I. Kapusta, and H.-B. Tang, Phys. Lett. B **443**, 63 (1998).
24. J. Daicic, N. E. Frankel, and V. Kowalenko, Phys. Rev. Lett. **71**, 1779 (1993).
25. D. J. Toms, Phys. Lett. B **343**, 259 (1995); Phys. Rev. D **55**, 7797 (1997); cond-mat/9612003.
26. P. Elmfors, P. Liljenberg, D. Persson, and Bo-S. Skagerstam, Phys. Lett. B **348**, 462 (1995).
27. H. P. Rojas, Phys. Lett. B **379**, 148 (1996).
28. J. I. Kapusta, *Finite Temperature Field Theory* (Cambridge Univ. Press, Cambridge, 1989).
29. L. D. Landau and E. M. Lifshitz, *Statistical Physics* (Nauka, Moscow, 1976; Pergamon, Oxford, 1980).

Translated by R. Rogalyov

Physics of Atomic Nuclei, Vol. 64, No. 3, 2001, pp. 561–573. From Yadernaya Fizika, Vol. 64, No. 3, 2001, pp. 615–627.

90th ANNIVERSARY OF A.B. MIGDAL'S BIRTHDAY
ELEMENTARY PARTICLES AND FIELDS

Magnetic Monopoles, Alive*

M. N. Chernodub[1], F. V. Gubarev[1, 2], M. I. Polikarpov[1], and V. I. Zakharov[2]

Received July 25, 2000

Abstract—We review recent developments in understanding the physics of the magnetic monopoles in unbroken non-Abelian gauge theories. Since numerical data on the monopoles are accumulated in lattice simulations, the continuum theory is understood as the limiting case of the lattice formulation. We emphasize physical effects related to the monopoles. In particular, we discuss the monopole–antimonopole potential at short and larger distances as well as a dual formulation of the gluodynamics, relevant to the physics of the confinement.

1. GENERALITIES

1.1. Introduction

Magnetic monopoles are undoubtedly a fascinating subject. Not a new one, though. The Dirac magnetic monopole will soon be 70 years old [1]. And the first 50 years of development of the theory of the magnetic monopoles were summarized in an illuminating review by Coleman [2]. Thus, the question may arise why it is instructive to come back to the monopoles now.

The main development since Coleman's review is that monopoles were copiously observed (for review and further references see, e.g., [3]) and the theory can be now confronted with the data. True, the monopoles observed are not exactly those introduced by Dirac, but rather their close kin, that is, monopoles of non-Abelian gauge theories (moreover, for the sake of definiteness we concentrate on the simplest gauge group, that is, $SU(2)$). Also true, the data are mostly numerical and obtained on the lattice, so that their interpretation in terms of the continuum theory may not be so straightforward. Nevertheless, it is a direct challenge to theory to explain the ample data on the magnetic monopoles which have already been accumulated in the lattice simulations.

Moreover, the issue of the so-to-say lattice monopoles is very rich and varied by itself. Let us mention here three topics:

(a) The numerical data refer mostly to the monopoles with a double magnetic charge, $|Q_m| = 2$, where the units are fixed by the Dirac quantization condition for the gluons. Classically, there are no stable solutions with $|Q_m| = 2$ [4], and, therefore, quantum effects seem to be absolutely crucial even to introduce such monopoles. As a result, the theory of these monopoles is in its infancy.

(b) There are recent measurements of the interaction potential between the fundamental monopoles with $|Q_m| = 1$ on the lattice [5], which are introduced through the so-called 't Hooft loop [6]. Unlike the case of the $|Q_m| = 2$ monopoles, the interaction of the fundamental monopoles is in fact quite well understood, a fact that might not be well appreciated by the community.

(c) There exists a surprisingly simple phenomenological description of the properties of the $|Q_m| = 2$ monopoles, which are so poorly understood on the purely theoretical side. We mean here models like the Abelian Higgs model which provide quantitative support to the old idea of the dual-superconductor mechanism [7] and work surprisingly well at least in some cases (for a review and further references see [3, 8]).

In this minireview, we will emphasize some new points related to each of the items (a)–(c) listed above and based mostly on the original papers [9–11]. The new points, although they refer to various topics, are unified by a common approach. The starting point is that we consider monopoles within the fundamental gluodynamics, while the more traditional approach is to introduce monopoles within an effective theory intended to mimic QCD in the infrared region [3, 8]. Also, we understand the continuum gluodynamics rather as the limiting case of the lattice formulation. As a result, one allows for certain singular gauge transformations which are not included in more traditional frameworks.

1.2. Dirac Monopole and Dirac String

The Dirac monopole, by definition, is associated with a radial magnetic field similar to the electric field of a pointlike charge, $\mathbf{H} = \frac{Q_m}{4\pi}\frac{\mathbf{r}}{r^3}$. One can easily construct a corresponding vector potential:

$$A_r = A_\theta = 0, \quad A_\phi = \frac{Q_m}{4\pi}\frac{(1+\cos\theta)}{r\sin\theta}. \qquad (1)$$

The analogy between the electric and magnetic charges is somewhat formal, however. Namely, because of the

* This article was submitted by the authors in English.

[1] Institute of Theoretical and Experimental Physics, Bol'shaya Cheremushkinskaya ul. 25, Moscow, 117259 Russia.
[2] Max-Planck-Institut für Physik, München, Germany.

conservation of the magnetic flux, the radial magnetic field of the monopole should be supplemented by the magnetic field of a string which brings in the flux spread out uniformly by the radial component of the field. Thus, we actually have

$$\mathbf{H} = \mathbf{H}_{\rm rad} + \mathbf{H}_{\rm string}. \quad (2)$$

The presence of the string is exhibited, in particular, by the explicit expression for the potential **A** above.

The Dirac string is unphysical and there is a number of constraints imposed on the theory to ensure that the string does not produce any physical effect. First, there is the Dirac veto, which forbids any direct interaction with the string. The best known constraint is the Dirac quantization condition, which ensures the absence of the Aharonov–Bohm effect for the electrons scattered on the string:

$$Q_e \oint\limits_{\rm string} \mathbf{A} d\mathbf{x} = Q_e Q_m = 2\pi k, \quad (3)$$

where Q_e is the electric charge of the electron and k is an integer number. Let us also emphasize that naively the energy of the string is infinite in the ultraviolet:

$$\epsilon_{\rm string} \sim \int (\mathbf{H}_{\rm string})^2 d^3 r \sim \frac{(\text{Length})}{(\text{Area})} \sim \Lambda_{\rm UV}^2 (\text{Length}), \quad (4)$$

where we used the fact that the magnetic flux is quantized (see above) and that the cross section of the string denoted by (Area) should tend to zero at the end of the calculation. Thus, we replaced $(\text{Area})^{-1}$ by $\Lambda_{\rm UV}^2$.

The radial part of the magnetic field is also associated with an infinite energy:

$$\epsilon_{\rm rad} \sim \int (\mathbf{H}_{\rm rad})^2 d^3 r \sim \frac{1}{r_0} \sim \Lambda_{\rm UV}. \quad (5)$$

Note that this ultraviolet divergence is linear, i.e., somewhat weaker than the divergence due to the string [see Eq. (4)].

The infinite magnetic field of the string may have more subtle manifestations as well. Consider interaction of two magnetic monopoles with magnetic charge $\pm Q_m$ placed at distance R from each other. Then, by the analogy with the case of two electric charges, we would like to have the following expression for the interaction energy:

$$\epsilon_{\rm int} = \int \mathbf{H}_{1,\,\rm rad} \cdot \mathbf{H}_{2,\,\rm rad} d^3 r = -\frac{Q_m^2}{4\pi} \frac{1}{R}. \quad (6)$$

Note, however, that if we substitute the sum of the radial and string fields for $\mathbf{H}_{1,\,2}$, then we would have an extra term in the interaction energy:

$$\tilde{\epsilon}_{\rm int} = \int (\mathbf{H}_{1,\,\rm rad} \cdot \mathbf{H}_{2,\,\rm string} + \mathbf{H}_{1,\,\rm string} \cdot \mathbf{H}_{2,\,\rm rad}) d^3 r = +2\frac{Q_m^2}{4\pi} \frac{1}{R}. \quad (7)$$

In other words, the account of the string field would flip the sign of the interaction energy! This contribution, although it looks absolutely finite, is of course a manifestation of the singular nature of the string magnetic field, $|\mathbf{H}_{\rm string}| \sim (\text{Flux})/(\text{Area})$. Note that the integral in (7) does not depend on the shape of the string.

To maintain the unphysical nature of the Dirac string, we should use a regularization scheme which would allow to get rid of these singularities.

1.3. Lattice Regularization

Since the monopoles naively have divergent energy (or action) in the ultraviolet, the regularization is a crucial issue. Moreover, we would like to follow the lattice formulation since the monopoles are observed on the lattice.

Consider first the $U(1)$ case. As is emphasized in [12], the lattice formulation implies that the Dirac string, which produces no Aharonov–Bohm scattering, costs no action as well. The reason is very simple. The lattice action is written originally in terms of the contour integrals like (3) rather than field strength $F_{\mu\nu}$:

$$S = \sum_p \mathrm{Re} \exp\left\{ i Q_e \oint\limits_{\partial p} A_\mu dx^\mu \right\}, \quad (8)$$

where the sum is taken over all the plaquettes p. Thus, the condition (3) means absence of both the Aharonov–Bohm effect and the quadratic divergence (4) in the lattice regularization. Moreover, it is straightforward to see that the interference term (7) also vanishes. Later, we will also discuss the case of the Dirac string which in the limit $g \longrightarrow 0$ corresponds to negative plaquettes in the lattice formulation. Its energy is infinite in the continuum limit, in agreement with the naive estimate (4). The interference term (7), however, disappears in the lattice formulation in this case as well.

Moreover, the lattice formulation naturally leads to the monopole–antimonopole potential (6) without the unphysical string contribution (7).

The radial field, $\mathbf{H}_{\rm rad}$, may also cause problems with infinite energy [see (5)]. The lattice regularization is not very specific in that case, however. The role of r_0 is simply played by the lattice spacing a. Thus, the probability to find a monopole on the lattice is suppressed by the action as

$$e^{-S} \sim \exp(-\text{const} \times Q_e^{-2} L/a), \quad (9)$$

where L is the length of the monopole trajectory, and the Q_e^{-2} factor appears because of the Dirac quantization condition (3), which relates the magnetic charge Q_m to the inverse electric charge.

Although Eq. (9), at first sight, rules out monopoles as physically significant excitations, the fate of the monopoles in the $U(1)$ case depends in fact on the value of the charge Q_e. The point is that the entropy factor

grows also exponentially with the length of the monopole trajectory:

$$(\text{Entropy}) \sim \exp(+\text{const}' \times L/a), \tag{10}$$

where the const' is a pure geometric factor, not related to any coupling constant like Q_e. As a result, for $Q_e \sim 1$, there is a phase transition corresponding to the condensation of the monopoles. This phase transition, which is well studied on the lattice, is the first and striking example of importance of the UV regularization in the nonperturbative sector. Indeed, once the UV divergence (4) is removed by the lattice regularization, the monopoles can modify the physics completely (for further comments see [13]).

1.4. Classification of Monopoles in Non-Abelian Theories

From now on, we will discuss monopoles in unbroken non-Abelian gauge theories, having in mind primarily gluodynamics, i.e., quantum chromodynamics without dynamical quarks. Moreover, for the sake of simplicity, we will consider only the $SU(2)$ gauge group.

A natural starting point to consider monopoles in non-Abelian theories is their classification. There are actually a few approaches to the monopole classification, and it is important to realize both similarities and differences between them.

The dynamical, or $U(1)$ classification. Within this approach [14], one looks for monopole-like solutions of the classical Yang–Mills equations. Here, by "monopole-like" solutions, one understands potentials which fall off as $1/r$ at large r [see Eq. (1)]. The basic finding is that there are no specific non-Abelian solutions and all the monopoles can be viewed as Abelian-like embedded into the $SU(2)$ group. Moreover, using the gauge invariance, one can always choose the corresponding $U(1)$ group as, say, the rotation group around the third direction in the color space. According to this classification, the monopoles are characterized by their charge with respect to a $U(1)$ group and may have, therefore, charges,

$$|Q_m| = 0, 1, 2, \ldots . \tag{11}$$

The topological, or Z_2 classification. The Z_2 classification [15] is based entirely on topological arguments. Namely, independent types of monopoles can be enumerated by considering the first homotopy group of the gauge group. The $SU(2)$ gauge group is trivial since $\pi_1(SU(2)) = 0$, while in the case of the $SO(3)$, however,

$$\pi_1(SU(2)/Z_2) = Z_2 \tag{12}$$

and there exists a single nontrivial topological monopole. We will denote the magnetic charge of such monopoles as $|Q_m| = 1$. Note, however, that the charges $Q_m = \pm 1$ are indistinguishable in fact. As for the charges $Q_m = 2$, they are equivalent, from this point of view, to no magnetic charge at all.

The topological classification (12) is readily understood if one tries to enumerate various types of the Dirac strings whose end points represent monopoles under consideration. Then, there is only one nontrivial string, that is, the one for which Eq. (3) is satisfied for gluons but not for quarks. Namely, because the $U(1)$ charge associated with gluons is twice as big as that of the particles in the fundamental representation (quarks), we may have

$$\exp\{ig\oint A_\mu dx^\mu\} = -1 \tag{13}$$

and such a string is not visible for the isospin-one particles. On the other hand, the standard plaquette action is based on the phase factor evaluated for particles in the fundamental representation. This means, in turn, that the Dirac string pierces the negative plaquettes. This observation is the basis for introducing the $|Q_m| = 1$ monopoles via the 't Hooft loop: one changes the sign of β ($\beta \equiv 4/g^2$) on a world sheet. The boundary of this sheet corresponds to the end points of the Dirac string, or the monopole trajectory.

1.5. Z_2 Monopoles

In principle, the $U(1)$ and Z_2 classifications are different. Indeed, while the $U(1)$ classification allows for any integer charge, the Z_2 classification leaves space only for a single nontrivial charge:

$$Q_m = 0, 1. \tag{14}$$

The reconciliation of the two classifications is that the $U(1)$ solutions with $|Q_m| \geq 2$ are in fact unstable because of the presence of massless charged vector particles (gluons) [4]. The instability of the solutions implies that, even if the external sources with $|Q_m| \geq 2$ were introduced into the vacuum state of the gluodynamics, charged gluons would fall onto the center because of the strong magnetic interactions. Moreover, one can imagine that, as the result of this instability, the charged fields $A^\pm$ are built up as well.

In a somewhat related way, one can demonstrate the apparent irrelevance of the $|Q_m| = 2$ monopoles by producing an explicit non-Abelian field configuration which looks like a $|Q_m| = 2$ monopole in its Abelian part but has no $SU(2)$ action at all [9]. This field configuration is a Dirac string with open ends, which correspond to the monopole–antimonopole pair separated by the distance R. In more detail, such a configuration is generated from the vacuum by the following gauge rotation matrix:

$$\Omega = \begin{pmatrix} e^{i\varphi}\sqrt{A_D} & \sqrt{1-A_D} \\ -\sqrt{1-A_D} & e^{-i\varphi}\sqrt{A_D} \end{pmatrix}, \tag{15}$$

where φ is the angle of rotation around the axis connecting the monopoles and A_D is the $U(1)$ potential representing pure Abelian monopole pair:

$$A_\mu dx_\mu = \frac{1}{2}\left(\frac{z_+}{r_+} - \frac{z_-}{r_-}\right)d\varphi \equiv A_D(z, \rho)d\varphi, \qquad (16)$$

where $z_\pm = z \pm R/2$, $\rho^2 = x^2 + y^2$, and $r_\pm^2 = z_\pm^2 + \rho^2$. Note that the action associated with the Dirac string is considered in this case zero, in accordance with the lattice version of the theory (for details see [9]).

In this example, the monopoles with $|Q_m| = 2$ are a kind of pure gauge field configurations carrying no action. Note that the Abelian flux is still transported along the Dirac string and is still conserved for the radial field. What is lost, however, is the relation between the Abelian flux and action. In the Abelian case, nonvanishing flux means nonvanishing magnetic field and nonvanishing action since the action density is simply $\mathbf{H}^2$. Now, the action is $(F_{\mu\nu}^2)^2$ and the Abelian part of the $F_{\mu\nu}^3$ can be canceled by the commutator term. This is exactly what happens in the example (15) above.

It is somewhat more difficult to visualize dynamically the equivalence of the $Q_m = \pm 1$ monopoles, also implied by the Z_2 classification. The mechanism mixing the $Q_m = \pm 1$ solutions seems to be the following. Imagine that we start with, say, the $Q_m = +1$ solution. Then, a Dirac string carrying the flux corresponding to the $Q_m = -2$ can be superimposed on this solution. It is important at this point that such a Dirac string costs no action (or energy). Then, the radial magnetic field can also change its direction since it does not contradict the flux conservation any longer. In a related language, one could say that the $|Q_m| = 2$ monopoles are condensed in the vacuum and that is why the magnetic charge can be changed freely by two units.

As far as interaction of two $|Q_m| = 1$ monopoles is concerned, one might expect that they would behave as a monopole–antimonopole pair. Indeed the monopole and antimonopole would attract each other and thus represent the lowest energy state of the system.

1.6. Conclusions 1

Thus, the physics of the monopoles in the first approximation turns out to be very simple.

Namely, there exist only monopoles with $|Q_m| = 1 \equiv 2\pi/g$, where g is the coupling constant of the non-Abelian $SU(2)$ theory. The monopoles are infinitely heavy and can be introduced only as an external object through the 't Hooft loop. Their interaction is Abelian-like:

$$V_{m\bar{m}} = -\frac{Q_m^2}{4\pi R} = -\frac{\pi}{g^2 R}, \qquad (17)$$

where R is the separation between the monopoles.

Clearly enough, this first, or classical, approximation falls far short of an adequate description of the empirical data on the monopoles (see Introduction). Thus, we are invited to go into more advanced approaches which we would try to introduce step by step.

2. LAGRANGIAN APPROACH

2.1. The Zwanziger Lagrangian

There is a long standing interest in constructing the dual gluodynamics (for a review and further references see [8]). The dual gluon, by definition, interacts with monopoles. The motivation is to realize in the field theoretical language the dual superconductor model of the quark confinement [7] according to which the quarks are connected at large distances by an Abrikosov-type vortex [16]. The key element is the construction of the non-Abelian monopoles, which are usually modeled after the 't Hooft–Polyakov solution. Namely, one introduces first non-Abelian dual gluons interacting with Higgs fields and then assumes condensation of the Higgs fields, which mimics the condensation of the monopoles. In the realistic case of the $SU(3)$ gauge group, one needs an octet of dual gluons and three octets of the Higgs fields, all of them understood in terms of effective field theory valid in the infrared region.

While such a construction might be viable as an effective theory, we need in fact tools to describe interaction of non-Abelian monopoles at arbitrary short distances as well [9]. Indeed, in the lattice version of the theory, external monopoles can be introduced via the 't Hooft loop operator [6], and in the continuum limit these monopoles are pointlike. Thus, we are encouraged to consider the dual gluodynamics at short distances, or at the fundamental level.

It is natural to try a Lagrangian approach to the dual gluodynamics. Indeed, in the case of the same 't Hooft loop operator, it is known that its expectation value depends only on the boundary and not on the shape of the Dirac string. Thus, it seems natural to introduce a dual gluon which would interact directly with pointlike monopoles. In the context of electrodynamics, the idea is of course very old and goes back to papers in [17]. There are successes and problems inherent to this approach (for a review see [18]).

A well-known example of a Lagrangian which describes interaction of $U(1)$ gauge fields with Abelian pointlike monopoles is due to Zwanziger [17]:

$$L_{Zw}(A, B) = \frac{1}{2}(m \cdot [\partial \wedge A])^2 + \frac{1}{2}(m \cdot [\partial \wedge B])^2 + \frac{i}{2}(m \cdot [\partial \wedge A])(m \cdot *[\partial \wedge B]) \qquad (18)$$
$$- \frac{i}{2}(m \cdot [\partial \wedge B])(m \cdot *[\partial \wedge A]) + i j_e A + i j_m B,$$

where j_e and j_m are electric and magnetic currents, respectively; m_μ is a constant vector; $m^2 = 1$; and

$$[A \wedge B]_{\mu\nu} = A_\mu B_\nu - A_\nu B_\mu,$$
$$(m \cdot [A \wedge B])_\mu = m_\nu [A \wedge B]_{\mu\nu},$$
$$*[A \wedge B]_{\mu\nu} = \frac{1}{2}\varepsilon_{\mu\nu\lambda\rho}[A \wedge B]_{\lambda\rho}.$$

At first sight, we have introduced two different vector fields, A and B, to describe interaction with electric and magnetic charges, respectively. If it were so, however, we would have solved a wrong problem because we need to have a single photon interacting with both electric and magnetic charges. And this is what is achieved by the construct (18). Indeed, the action (18) is not diagonal in the A and B fields and one can convince oneself that the form of the bilinear in A and B interference terms in (18) is such that the field strength tensors constructed on the potentials A and B are in fact related to each other:

$$F_{\mu\nu}(A) = *F_{\mu\nu}(B). \tag{19}$$

This means in turn that there are only two physical degrees of freedom corresponding to the transverse photons which can be described either in terms of the potential A or B. Topological excitations, however, can be different in terms of A and B.

The physical content of (18) is revealed by the propagators for the fields A and B. In the α gauge, one can derive

$$\langle A_\mu A_\nu \rangle = \langle B_\mu B_\nu \rangle = \frac{1}{k^2}\left(\delta_{\mu\nu} - (1-\alpha)\frac{k_\mu k_\nu}{k^2}\right),$$
$$\langle A_\mu B_\nu \rangle = -\langle B_\mu A_\nu \rangle = \frac{i}{k^2(km)} *[m \wedge k]_{\mu\nu}. \tag{20}$$

The propagators should reproduce, as usual, the classical solutions. And indeed, the $\langle AA \rangle$ and $\langle BB \rangle$ propagators describe the Coulomb-like interaction of two charges and magnetic monopoles, respectively, while the $\langle AB \rangle$ propagator reproduces interaction of the magnetic field of a monopole with a moving electric charge. The appearance of the poles in $k \cdot m$ is a manifestation of the Dirac strings.

To summarize, the Zwanziger Lagrangian in electrodynamics [17] reproduces the classical interaction of monopoles and charges. Upon the quantization, it describes the correct number of the degrees of freedom associated with the photon.

2.2. Dual Gluon as an Abelian Vector Field

Now, if we approach the problem of constructing a Zwanziger-type Lagrangian for the dual gluodynamics, we immediately come to a paradoxical conclusion that the dual field, if any, is Abelian. Indeed, monopoles associated with, say, $SU(N)$ gauge group are classified according to $U(1)^{N-1}$ subgroups [14] and might be realized as a pure Abelian objects. Thus, there is no place for a non-Abelian dual gluon because the monopoles do not constitute representations of the non-Abelian group.

The function of the classical Lagrangian is, first of all, to reproduce the classical interactions of the monopoles and charges. It is rather obvious that the potential (17) can be derived in the classical approximation from the Lagrangian:

$$L_{\text{dual}}(A^a, B) = \frac{1}{4}(F^a_{\mu\nu})^2 + \frac{1}{2}(m \cdot [\partial \wedge B - i*G])^2 + ij_m B + ij^a_e A^a, \tag{21}$$

where $a = 1, 2, 3$ is the color index; j_m is the magnetic current; and $F^a_{\mu\nu}$ is the non-Abelian field strength tensor. The Lagrangian (21) also contains vector field n^a, $n^2 = 1$ in the adjoint representation, and the antisymmetric tensor $G_{\mu\nu}$ is the 't Hooft tensor [19]:

$$G_{\mu\nu} = n^a F^a_{\mu\nu} - \varepsilon^{abc} n^a (D_\mu n)^b (D_\nu n)^c. \tag{22}$$

Let us add a few comments on the meaning and rules of using the Lagrangian (21).

(a) First, if the magnetic current is vanishing, $j_m = 0$, then the integration over the field B reproduces the standard Lagrangian of the gluodynamics.

(b) As far as the quantization is concerned, the Lagrangian (21) reproduces the correct degrees of freedom of the free gluons. Indeed, in the limit $g \longrightarrow 0$ and for $n^a = \delta^{a,3}$, the Lagrangian (21) becomes

$$L_{\text{dual}}(A^a, B) = \frac{1}{4}[\partial \wedge A^1]^2 + \frac{1}{4}[\partial \wedge A^2]^2 + ij_m B + ij^a_e A^a + \frac{1}{2}(m \cdot [\partial \wedge A^3])^2 + \frac{1}{2}(m \cdot [\partial \wedge B])^2 + \frac{i}{2}(m \cdot [\partial \wedge A^3])(m \cdot *[\partial \wedge B]) - \frac{i}{2}(m \cdot *[\partial \wedge A^3])(m \cdot [\partial \wedge B]), \tag{23}$$

which is essentially the Zwanziger Lagrangian (18). Quantization at this point is the same as in the case of a single photon.

(c) Already in the Zwanziger example (18), we have seen that the fields that are mixed up in the Lagrangian have a common source. Namely, in case of the electrodynamics, $\partial *F(A) = \partial F(B) = j_m$. Since it is known [19] that the monopoles in non-Abelian theories serve as a source for the 't Hooft tensor (22), one expects from the very beginning that in the case of the gluodynamics the (dual) field strength tensor built up on the dual gluon field B is mixed up with the 't Hooft tensor constructed in terms of the gluon filed A. And, indeed, this is true for (21).

(d) The emergence of the vector n^a is of crucial importance in the Lagrangian (21). The point is that the origin of the vector n^a goes back to choosing the color orientation of the monopoles. As is emphasized above, the monopole solutions are Abelian in nature, which means, in particular, that they can be rotated to any direction in the color space by gauge transformations. Thus, picking up a particular n^a is nothing else but using the gauge fixing freedom. Therefore, we can either average over the directions of n^a or fix n^a but evaluate only gauge invariant quantities, like the Wilson loop (note somewhat similar remarks in [20]).

(e) The Z_2 nature of the monopoles is manifested in the freedom of changing $n^a \longrightarrow -n^a$, $B_\mu \longrightarrow -B_\mu$. Indeed, under such transformation, the monopole with the charge $Q_m = +1$ is transformed into a monopole with $Q_m = -1$ and vice versa. In the language we used above, such a transformation corresponds to adding a Dirac string with a double magnetic flux. We see that the averaging over $\pm n^a$ is a part of the overall averaging over all possible embedding of the $U(1)$ into the $SU(2)$ gauge group.

An apparent application of (21) would be evaluating the running of the coupling g in the expression (17). And, indeed, exploiting the Lagrangian (21), one can approach the problem of the running of the coupling in a way similar to the case of pure electrodynamics (for a review and further references, see [18]). We comment on this approach below.

2.3. Radiative Corrections

We will consider now the radiative corrections to the Coulomb-like interaction (17) at short distances. Obviously enough, one would expect that the radiative corrections result in the standard, non-Abelian running of the coupling g^2. This is indeed our main conclusion. Moreover, since for a constant vector n^a the non-Abelian monopole essentially coincides with the Dirac monopole, there is not much specific about the derivation of the running of the coupling. And, indeed, our considerations overlap to a great extent with those given in the original papers [21, 22] and in the reviews [2, 18]. Still, we feel that it is useful to present the arguments, maybe in a new sequence, to emphasize the points crucial for our purposes.

Let us emphasize from the very beginning that the evaluation of the radiative corrections addresses in fact two different, although closely related, problems—that is, running of the coupling and stability of the classical solutions. Both aspects are unified, of course, into evaluation of a single loop in the classical background. However, the running of the coupling can be clarified by keeping track of the ultraviolet logs, $\ln\Lambda_{UV}$ alone, and is universal since in the ultraviolet all the external fields can be neglected. Therefore, the coefficient in front of $\ln\Lambda_{UV}$ can be found by evaluating the loop graph with two external legs, i.e., the graph corresponding to the standard polarization operator in perturbation theory. This is true despite the fact that the monopole field is strong (i.e., the product of the magnetic and electric coupling is of order of unity). On the other hand, the stability of the classical solution is decided by the physics in the infrared. Here, one needs to consider the particular dynamical system, monopoles in our case, and the fact that the magnetic charge is of order $1/g$ can be crucial.

Consider first the running of the coupling. Moreover, for the sake of definiteness, we concentrate on the Dirac monopole with the minimal magnetic charge interacting with electrons and in the one-loop approximation [18, 21–23]. The crucial point here is that only loops with insertion of two external (i.e., monopole) fields can be considered despite the fact that there is no perturbative expansion at all. Indeed, considering more insertions makes the graphs infrared sensitive, with no possibility for $\ln\Lambda_{UV}$ to emerge.

Then, the evaluation of, say, first radiative correction to the propagator $\langle B_\mu B_\nu\rangle$ in the Zwanziger formalism (20) seems very straightforward and reduces to taking a product of two $\langle AB\rangle$ propagators and inserting in between the standard polarization operator of two electromagnetic currents. The result is [23]

$$\langle B_\mu B_\nu\rangle(k) = \frac{\delta_{\mu\nu}}{k^2}(1-L) + \frac{1}{(k\cdot m)^2}(\delta_{\mu\nu} - m_\mu m_\nu)L, \qquad L = \frac{\alpha_{el}}{6}\ln\Lambda_{UV}^2/k^2, \tag{24}$$

and we neglect the electron masses so that the infrared cutoff is provided, in the logarithmic approximation, by the momentum k.

At first sight, there is nothing disturbing about the result (24). Indeed, we have a renormalization of the original propagator, which is to be absorbed into the running coupling, and a new structure with the factor $(k\cdot m)^{-2}$, which is nonvanishing, however, only on the Dirac string. The latter term would correspond to renormalization of the Dirac string self-energy, which we do not follow in any case since it is included in the self-energy of the external monopoles. What is actually disturbing is that according to (24) the magnetic coupling would run exactly the same as the electric charge,

$$\langle A_\mu A_\nu\rangle(k) = (1-L)\frac{\delta_{\mu\nu}}{k^2},$$

violating the Dirac quantization condition.

The origin of the trouble is not difficult to figure out. Indeed, using the propagator $\langle AB\rangle$ while evaluating the radiative corrections is equivalent, of course, to using the full potential corresponding to the Dirac monopole A_D^{cl}. Then, switching on the interaction with electrons would bring terms like $A_D^{cl}\bar\psi\gamma\psi$. Since A_D includes the potential of the string, electrons do interact with the

Dirac string and we are violating the Dirac "veto," which forbids any direct interaction with the string.

Let us demonstrate that, indeed, the incorrect treatment of the Dirac string changes the sign of the radiative correction. This can be done in fact in an amusingly simple way. First, let us note that it is much simpler to remove the string if one works in terms of the field strength tensor, not the potential. Indeed, we have $\mathbf{H} = \mathbf{H}_{\rm rad} + \mathbf{H}_{\rm string}$, while in terms of the potential $\mathbf{A}$ any separation of the string would be ambiguous (see Eq. (1)).

Thus, we start with relating the potential, or energy, to the interference term in the $\mathbf{H}^2$ field:

$$V_{m\bar{m}} = \int \mathbf{H}_1 \cdot \mathbf{H}_2 d^3 r. \tag{25}$$

Now, it is not absolutely trivial how we should understand the product $\mathbf{H}_1 \cdot \mathbf{H}_2$. Indeed, we emphasized in Subsection 1.2 that the string field is to be removed from this interference term [see Eq. (7)]. Thus, in the zero, or classical, approximation we have

$$\mathbf{H}_1 \cdot \mathbf{H}_2 \equiv \mathbf{H}_{1,\,\rm rad} \cdot \mathbf{H}_{2,\,\rm rad}. \tag{26}$$

However, if we use the standard technique of an external field,

$$A_\mu = A_\mu^{\rm cl} + a_\mu, \tag{27}$$

and substitute (1) as the classical background, then the first radiative correction would yield the product of the total $\mathbf{H}_1 \cdot \mathbf{H}_2$, which also includes the string contribution.[3)] Indeed, the result in the logarithmic approximation would be as follows:

$$\begin{aligned}\delta(\mathbf{H}_1 \cdot \mathbf{H}_2) &= L(\mathbf{H}_{1,\,\rm string} + \mathbf{H}_{1,\,\rm rad}) \cdot (\mathbf{H}_{2,\,\rm string} + \mathbf{H}_{2,\,\rm rad}) \\ &= -L\mathbf{H}_{1,\,\rm rad} \cdot \mathbf{H}_{2,\,\rm rad},\end{aligned} \tag{28}$$

where at the last step we have used the observation (7).

Now, it is clear how we could ameliorate the situation. Namely, to keep the Dirac string unphysical, we should remove the string field from the expression (28), which arises automatically if we use the propagators (20) following from the Zwanziger Lagrangian. Thus, we introduce

$$(\mathbf{H}_1 \cdot \mathbf{H}_2)' \equiv \mathbf{H}_{1,\,\rm rad} \cdot \mathbf{H}_{2,\,\rm rad} \tag{29}$$

and change $\mathbf{H}_1 \cdot \mathbf{H}_2$ in the expression (28) into (29), so to say, by hand. The justification is that we should remove the effect of the string field from any observable.

Then, we reverse the sign of the radiative correction, and the final result is

$$(V_{m\bar{m}})_{\rm cl} \equiv -\frac{\pi}{g_0^2}\,\frac{1}{R} \longrightarrow -\frac{\pi}{g^2(R)}\,\frac{1}{R}. \tag{30}$$

[3)]At this point, we assume in fact that $\Lambda_{\rm UV}$ is smaller than the inverse size of the string, which is convenient for our purposes here. Other limiting procedures could be considered as well, however.

One might wonder how it happens that the couplings in the electric and magnetic potential run in opposite ways. Indeed, now we reduced the product $\mathbf{H}_1 \cdot \mathbf{H}_2$ to exactly the same form as the product $\mathbf{E}_1 \cdot \mathbf{E}_2$ in the case of two electric charges (since the radial magnetic and electric fields are the same, up to a change of the overall constants). The resolution of the paradox is that the renormalization of the electric and magnetic fields are indeed similar in the language of the Lagrangian. However, the small corrections to the Lagrangian and Hamiltonian are related as

$$\delta L = -\delta H. \tag{31}$$

Since $\mathbf{E}^2$ and $\mathbf{H}^2$ enter with the same sign into the expression for the Hamiltonian and with the opposite signs into the Lagrangian, Eq. (31) implies that the runnings of the couplings in the electric V_e and magnetic V_m potentials are opposite in sign. This is, of course, in full agreement with expectations since $V_e \sim g^2$ and $V_m \sim g^{-2}$.

Thus, it is not difficult to derive the running of the magnetic coupling following only the ultraviolet logarithm, $\ln\Lambda_{\rm UV}$. Note, however, that the same arguments would go through without change if we started with, say, monopoles with $Q_m = 2$. But such monopoles are unstable [4], and this is a much more drastic effect than the would-be running of the coupling. There are also more subtle mechanisms which can be brought in by radiative corrections. In case of the same Dirac monopole interacting with electrons [24], consideration of the modes reveals that the Hamiltonian is in fact non-Hermitian. As a result, the classical field approximation is not adequate, and one should consider the corresponding field theory, or the monopole catalysis [25].

Thus, to investigate the stability of the classical solution one has, generally speaking, to consider all orders in $g_e g_m \sim 1$. It is known that single monopoles with $Q_m = 1$ are stable. The stability of the monopole–antimonopole system, which we are interested in, has never been investigated analytically in detail because of the complexity of the problem. However, there is no known mechanism which could cause instability of the classical monopole–antimonopole solution. Moreover, we checked numerically that the classical solution is indeed stable [9].

2.4. Why the "Right Way" Is Correct

Thus, our exercise with evaluating the running of the magnetic coupling has brought mixed results. On one hand, we were able to derive that the product of electric and magnetic coupling constants is not renormalized, as one would expect. On the other hand, to derive this, we had to go actually beyond the Lagrangian approach and remove the effect of the magnetic field of the string. Now we ask the next question, why this removal was the correct procedure.

Let us reexamine the grounds for the Lagrangian approach, in their generality. Any monopole involves

also a Dirac string and, as a result, a world sheet, not just particle trajectories. If we stop here, then the conclusion would be that there is no Lagrangian approach to the problem. However, we are aware that the 't Hooft loop operator depends only on its boundary, which is the monopoles' trajectory, j_m. And this is the real basis for the hopes for the Lagrangian formulation. Now, we see that the Dirac veto is not respected by the Lagrangian formulation and, therefore, the possibility arises that the world sheet swept by the Dirac string is still somehow important. Thus, we will outline in this subsection an approach [9] which is based on derivation of a continuum analog of the lattice 't Hooft loop operator and avoids any direct use of Lagrangians.

The general one-plaquette action of $SU(2)$ lattice gauge theory (LGT) can be represented as

$$S_{\rm lat}(U) = \frac{4}{g^2}\sum_p S_p\left(1-\frac{1}{2}{\rm tr}\, U[\partial p]\right), \qquad (32)$$

where g is the bare coupling, ∂p is the boundary of an elementary plaquette p, the sum is taken over all p, and $U[\partial p]$ is the ordered product of link variables U_l along ∂p. In particular, if $S_p(x) = x$, then (32) is the standard Wilson action. The exponent of the lattice field strength tensor F_p is defined in terms of $U[\partial p]$:

$$U[\partial p] = e^{i\hat{F}_p} = \cos\left[\frac{1}{2}|F_p|\right] + i\tau^a n^a \sin\left[\frac{1}{2}|F_p|\right], \qquad (33)$$

where $\hat{F} = F^a\tau^a/2$, $|F| = \sqrt{F^aF^a}$, and we define $n_p^a = F_p^a/|F_p|$ for $|F_p| \neq 0$, while n_p^a is an arbitrary unit vector for $|F_p| = 0$.

The lattice action (32) depends only on $\cos[1/2|F_p|]$. Therefore, the action of the $SU(2)$ LGT possesses not only the usual gauge symmetry, but allows also for the gauge transformations which shift the field strength tensor by $4\pi k$, $|F_p| \longrightarrow |F_p| + 4\pi k$, $k \in Z$:

$$e^{i\hat{F}_p} = \exp\{i|F_p|\hat{n}_p\}$$
$$= \exp\{i(|F_p| + 4\pi)\hat{n}_p\} = \exp\{i(F_p^a + 4\pi n_p^a)\tau^a/2\}. \qquad (34)$$

Thus, the symmetry inherent to the lattice formulation can be represented as

$$F_p^a \longrightarrow F_p^a + 4\pi n_p^a, \quad \mathbf{F}_p \times \mathbf{n}_p = 0, \quad n_p^2 = 1. \qquad (35)$$

The symmetry (35) is absent in the conventional continuum limit, $\int (F_{\mu\nu}^a)^2\, d^4x$. Note that in the continuum limit, n_p^a becomes a singular two-dimensional structure ${}^*\Sigma_{\mu\nu}^a$, which represents the Dirac string world sheet.

So far, we discussed an invisible Dirac string, which is nothing else but a generalized (or singular) gauge transformation. The Dirac string corresponding to the fundamental monopole corresponds to the phase factor –1, and we can obtain, therefore, an expression for a continuum analog of the 't Hooft loop by substituting

$$F_{\mu\nu}^a \longrightarrow F_{\mu\nu}^a + 2\pi {}^*\Sigma_{\mu\nu}^a. \qquad (36)$$

In this way, we come to the following definition of the 't Hooft loop operator in the continuum:

$$H(\Sigma_{\mathscr{C}}) = \exp\left\{\frac{1}{4g^2}\int d^4x[(F_{\mu\nu}^a)^2 - (F_{\mu\nu}^a + 2\pi {}^*\Sigma_{\mathscr{C}\mu\nu}^a)^2]\right\}, \qquad (37)$$

$$\Sigma_{\mathscr{C}\mu\nu}^a = \int d^2\sigma_{\mu\nu} n^a(\sigma)\delta^{(4)}(x - \tilde{x}(\sigma)), \qquad (38)$$

where the surface $\Sigma_{\mathscr{C}}^a$ spanned on the contour $\mathscr{C}$ is assumed to be nonintersecting. The unit three-dimensional vector field $n^a(\sigma)$, $n^2 = 1$ is defined on the world sheet:

$$n^a(\sigma) = (t\cdot {}^*F^a)[(t\cdot {}^*F^b)^2]^{-1/2}, \quad (t\cdot F^a) = t_{\mu\nu}(\sigma)F_{\mu\nu}^a(\tilde{x}), \qquad (39)$$

$$t_{\mu\nu}(\sigma) = \frac{1}{\sqrt{g}}\varepsilon^{\alpha\beta}\partial_\alpha\tilde{x}_\mu\partial_\beta\tilde{x}_\nu, \quad t_{\mu\nu}^2 = 2, \quad g(\sigma) = {\rm Det}[\partial_\alpha\tilde{x}_\mu\partial_\beta\tilde{x}_\mu]. \qquad (40)$$

Therefore, $n^a(\sigma)$ is not an independent variable; it is completely determined by the components of the field strength tensor $F_{\mu\nu}^a$. On the set of points where $t\cdot {}^*F^a = 0$, the direction of $n^a(\sigma)$ is arbitrary. It can be shown [10] that Eqs. (37)–(40) define the correct 't Hooft loop operator, the expectation value of which depends only on the contour $\mathscr{C}$, not on the particular position of the surface $\Sigma_{\mathscr{C}}$.

Consider now the equations of motion in the presence of the 't Hooft loop operator:

$$D_\nu(F_{\mu\nu}(A) + 2\pi {}^*\Sigma_{\mu\nu}) = 0, \qquad (41)$$

which should be supplemented by the Bianchi identities:

$$D_\nu {}^*F_{\mu\nu} = 0. \qquad (42)$$

To appreciate the meaning of the equation of motion (41), let us choose the gauge such that $\Sigma_{\mu\nu}^a$ has a constant color orientation characterized by the vector n_0^a. A particular solution of (41) may be found within the anzatz $A_\mu^a = n_0^a A_\mu$, for which Eq. (41) reduces to

$$\partial_\nu(\partial_{[\mu}A_{\nu]}) = -2\pi\partial_\nu {}^*\Sigma_{\mu\nu}. \qquad (43)$$

The solution of this equation in the Landau gauge,

$$A_\mu^a = -n_0^a \cdot 2\pi\frac{1}{\Delta}\partial_\nu {}^*\Sigma_{\mu\nu}, \qquad (44)$$

corresponds to the gauge potential of an Abelian monopole current $\partial\Sigma$ embedded into the $SU(2)$ group. Thus, $\Sigma_{\mu\nu}$ is the Dirac world sheet.

Derivation of the classical equations of motion (43) is the first step in deriving the interaction of the fundamental monopoles outside any Lagrangian framework.

One could consider along these lines also the radiative corrections [11]. We will not go into detail here, but let us mention how it comes about that the "Dirac veto" is observed and virtual particles do not interact with the Dirac string. We will substantiate this point here on the example of the spin interaction. Since the Yang–Mills quanta possess spin, there exists an interaction which is a generalization of the nonrelativistic expression $\boldsymbol{\sigma}\cdot\mathbf{H}$. In particular, if there exists a classical field directed in third direction in the color space, $(F^3_{\mu\nu})_{\rm cl}$, then its interaction with the quantum charged fields $a^{\pm}_{\mu}$ contains the term

$$g(F^3_{\mu\nu})_{\rm cl}a^{+}_{\mu}a^{-}_{\nu}. \qquad (45)$$

In the Zwanziger formalism, the $(F^3_{\mu\nu})_{\rm cl}$ means the whole magnetic field, including the field of the string. Then, the interaction (45) brings the term $\mathbf{H}_{1,\,\rm string}\cdot\mathbf{H}_{2,\,\rm rad}$ on the level of the quantum corrections. As we emphasized in Subsection 1.2, this term is actually proportional to $\mathbf{H}_{1,\,\rm rad}\cdot\mathbf{H}_{2,\,\rm rad}$, which is responsible for the coupling running. In this way, the term $\mathbf{H}_{1,\,\rm string}\cdot\mathbf{H}_{2,\,\rm rad}$, if it arises, brings in a "wrong" sign of the radiative correction.

On the other hand, in our formulation of the continuum analog of the 't Hooft loop operator [see Eq. (37)], there is no spin interaction of the virtual particles with the string magnetic field. It is crucial to prove [11] that the coupling governing the monopole–antimonopole interaction indeed runs as g^{-2}.

2.5. Conclusions 2

We considered in fact two different points. First, we argued that the dual gluon is a $U(1)$ gauge boson. The $SU(2)$ invariance is to be maintained either by integrating over all the possible embedding of the (dual) $U(1)$ into $SU(2)$ or by constraining calculations to gauge invariant quantities, like the Wilson loops.

Second, we discussed how far one can go with a Lagrangian formulation of the dual gluodynamics a la Zwanziger. To test the Lagrangian approach, we evaluated the running of the coupling in the monopole–antimonopole potential. The conclusion is that one can get the correct running of the coupling by imposing the Dirac veto, which forbids the interaction of virtual particles with the Dirac string. This requirement is not inherent to the Lagrangian approach (the same is true for the Zwanziger Lagrangian in the $U(1)$ case), however. It can be derived by studying the continuum analog of the 't Hooft loop operator.

3. MONOPOLES WITH $Q_m = 2$

3.1. $Q_m = 2$ Monopoles as Quantum Objects

So far, we discussed the fundamental monopoles $|Q_m| = 1$, which can be visualized as classical infinitely heavy objects. Because of infinite mass, they can be used only as probes of the QCD vacuum but play no dynamical role by themselves. The monopoles with the double charge $|Q_m| = 2$ are very different. As discussed above, they do not exist on the classical level. On the other hand, there exist very simple arguments that they can play dynamical role on the quantum level. As far as the fundamental Lagrangian is concerned, the only role of the quantum corrections is the running of the non-Abelian coupling. In particular, if we consider a lattice coarse enough, then $g_{SU(2)}$ becomes of order unity. Obviously, the same coupling governs the physics associated with any $U(1)$ subgroup of the $SU(2)$. However, if the coupling $g_{U(1)}$ becomes of order unity, then there is a phase transition associated with the monopole condensation [12]. Thus, one can argue that the running will be stopped by the monopole condensation, if not by something else already at smaller values of $g_{SU(2)}$.

Thus, it is very natural to assume that the monopole condensation also occurs in QCD since the running of the coupling allows one to scan the physics at all the values of $g_{SU(2)}$ until one runs into a phase transition.

However, even if one accepts such speculations, there remains a very important unresolved question. Namely, it is not clear which $U(1)$ subgroup of the full non-Abelian group is to be selected as the classification group for the monopoles. The most common approach here is to rely on the empirical data. In a way, it is forced on us since the phase transition is expected to happen at $g^2_{SU(2)} \sim 1$, where analytic approaches are hardly possible. From the lattice simulations, it is known that the monopoles in the Maximal Abelian projection appear to be the most relevant (see [3] for a review and further references).

Instead of reviewing this material once more—which would take us far beyond the scope of the present article—we will highlight some features of a new kind of monopoles introduced in [10]. The basic idea behind this construction is to make monopoles look like geometric objects as much as possible.

3.2. "Geometric" Monopoles

The construction of the new kind monopoles is done in few steps, which we will briefly outline now.

(i) The usual starting point to introduce monopoles is to fix some $U(1)$ for the whole lattice and then look for the Dirac strings and monopoles with respect to this $U(1)$. The starting point of [10] is somewhat different. Namely, it is the observation that each Wilson loop defines in a natural way its own $U(1)$. Indeed, turn back to the expression (33) for the plaquette action, which is actually true for any Wilson loop. Then, it is clear that

each Wilson loop defines the vector $\hat{F}_p$ and the "natural" $U(1)$ is the group of rotation around this vector (in the color space). In this way, one can define a $U(1)$ group for each plaquette. The definition of the $U(1)$ subgroup varies from one plaquette to another, emphasizing the non-Abelian nature of the underlying theory.

(ii) The plaquette action is $1/2\cos\phi$ and is invariant under $\phi_p \longrightarrow \phi_p + 2\pi k$, as is emphasized in Subsection 1.3. Now to detect the Dirac strings we should be able to somehow define the integer k. For a plaquette, the natural decomposition is

$$\phi_p = \phi_1 + \phi_2 + \phi_3 + \phi_4, \tag{46}$$

where the phases ϕ_i ($i = 1, \ldots, 4$) are associated with the corresponding links. The decomposition (46) comes about naturally in the basis of the coherent states. Indeed, for a particular coherent state, the whole evolution may be reduced to a phase factor:

$$|\psi(t)\rangle = e^{i\phi(t)}|\psi(0)\rangle. \tag{47}$$

Moreover, the coherent states can be explicitly constructed in terms of the link matrices (for details and further references see [10]). As a result, for any given lattice fields configuration, one can determine k and detect the Dirac strings in this way. The monopoles are defined then as the end points of the strings.

(iii) The phase $\phi(t)$ can in fact be decomposed into the dynamical and Berry phase. It is useful for this purpose to introduce a single-valued state vector $|\tilde{\psi}\rangle$ defined as

$$|\tilde{\psi}(T)\rangle = |\tilde{\psi}(0)\rangle, \tag{48}$$

where T is the period of the motion so that at $t = T$ the system comes back to the same point in the parameter space as at the moment $t = 0$. Then,

$$\begin{aligned}\phi(T) &= \delta + \gamma \\ &= -\int_0^T \langle\tilde{\psi}|H|\tilde{\psi}\rangle + i\int_C \left\langle \tilde{\psi}\left|\frac{\partial}{\partial\lambda_i}\right|\tilde{\psi}\right\rangle d\lambda^i,\end{aligned} \tag{49}$$

where λ_i are parameters, $\lambda_i(T) = \lambda_i(0)$, and C is a closed contour in the parameter space.

3.3. Choice of the Gauge and the Numerical Results

The steps (i)–(iii) described above fully determine monopoles as geometric objects. As a mathematical construct, it certainly appears very appealing. However, from the physical point of view, the crucial observation is the gauge dependence of the monopoles constructed in this way. As a result, the monopoles are devoid, generally speaking, of any physical meaning. It is amusing that one can actually specify the conditions for the monopoles to be physical objects. In particular, the monopole density ρ should satisfy the renormalization-group equation:

$$\rho = \text{const} \times \beta^{153/121} \exp\left(-\frac{9\pi^2}{11}\beta\right), \tag{50}$$

where $\beta \equiv 4/g^2$. The condition (50) is a very strong constraint, and there is not much surprise that the monopoles defined according to the procedure outlined in the preceding subsection, generally speaking, do not satisfy (50).

To continue with the physics, we need a physically motivated choice of the gauge. At first sight, such a choice is impossible. However, one can argue [10, 26] that the Lorentz gauge is a proper gauge. The Lorentz gauge on the lattice is defined by the requirement that the functional

$$R = \sum_l \left(1 - \frac{1}{2}\text{tr}\, U_l\right) \tag{51}$$

is minimal on the gauge orbit (U_l denote the link matrices). In the naive continuum limit, (51) reduces to $R = 1/4\int (A^a_\mu)^2$.

The logic behind the choice of (51) is as follows. In the continuum limit, both the Dirac strings and monopoles correspond to singular gauge potentials A^a_μ. It is easy to imagine, therefore, that one can generate an arbitrary number of spurious strings and monopoles by going to arbitrary large potentials A, so to say, inflated by the gauge transformations. On the other hand, by minimizing potentials, one may hope to squeeze the number of the topological defects to its minimum and these topological defects may be physically significant.

And, indeed, the numerical simulations indicate that the geometric monopoles defined in the Lorentz gauge are physical objects; i.e., their density satisfies the condition (50). There are also other indications that the geometric monopoles are physical [10]. For example, there is an excess of the non-Abelian action associated with them.

3.4. Conclusions 3

Monopoles with $Q_m = 2$ unify properties of field-theoretical and statistical objects. Namely, on one hand, the monopoles are defined locally in terms of the link matrices. However, the link matrices are gauge dependent, and existence or nonexistence of a monopole at a particular point is devoid of physical meaning for this reason. On the other hand, if one introduces gauge fixing in a physically reasonable way, the statistical properties of the monopoles, such as their density, satisfy very nontrivial renormalization-group constraints and demonstrate their physical significance.

4. PHENOMENOLOGICAL APPLICATIONS

4.1. The Effective Lagrangian and the Casimir Scaling

The standard way to develop a phenomenology is to assume that the monopoles condense. We will follow suit and modify the Zwanziger Lagrangian (21) by add-

ing the effective Higgs interaction where the role of the Higgs field is played by the monopole field ϕ_m:

$$S_{\text{eff}} = S_{\text{dual}}(A^a, B) + S_{\text{Higgs}}(B, \phi_m), \quad (52)$$

where S_{Higgs} is the standard action of the Abelian Higgs model. The vacuum expectation value of the Higgs, or monopole, field is, of course, of order Λ_{QCD}.

Despite its apparent simplicity, Eq. (52) is highly speculative. Namely, it unifies, so to say, fundamental gluons, A^a; their dual counterpart B, which is an Abelian gauge boson; and ϕ_m, which is presumably an effective scalar field. One may justify the use of (52) by assuming that the effective size of the monopoles with $Q_m = 2$ is in fact numerically small, although generically it is of order Λ_{QCD}. While in our presentation here we follow mostly the lines of [9, 11, 27], let us note that similar consequences arise within the models [28, 29] also introducing a new mass scale.

What is also specific about the Lagrangian (52) is that the dual gluon is a $U(1)$ gauge boson. The color symmetry is maintained by averaging over all possible embeddings of the (dual) $U(1)$ into $SU(2)$ (see the discussion in Subsection 2.2). The confinement mechanism inherent to (52) is the formation of the Abrikosov–Nielsen–Olesen string, which can be considered on the classical level. More generally, the Lagrangian (52) exhibits the Abelian dominance in the confining region which is the dominance of Abelian-like field configurations in the full non-Abelian theory. This dominance is common to all the realizations of the dual-superconductor model of confinement [7] and is strongly supported by the lattice data [3]. What we avoid, however, is the breaking of $SU(2)$ to $U(1)$ which is inherent to the models [8] which start with the dual gluons in the adjoint representation and then add effective-isospin-one Higgs fields. Such models have well-known principal difficulties with, say, describing interaction of the adjoint sources (see, e.g., [30]).

On the contrary, the model (52) can be applied to consider the static interaction of the sources belonging to various representations of $SU(2)$. One of the basic facts here, established through the numerical simulations on the lattice [31], is the so-called Casimir scaling. The phenomenon of the Casimir scaling is that the static potential is described by a sum of the Coulomb-like and linear terms:

$$V_j(r) \approx -j(j+1)\frac{\alpha_s}{\pi r} + j(j+1)\sigma r, \quad (53)$$

where j labels the representation (we consider the $SU(2)$ case) and σ is independent of j. Note that at large distances one expects qualitatively different behavior of the potential for integer and half-integer spins j because of the string breaking in case of the integer representations. However, at presently measured distances, Eq. (53) turns to be a very good approximation to the potential.

The potential of the type (53) does arise in the classical approximation in the model (52) because there are classical string solutions. However, the tension of the string is now a dynamical quantity which can be found as a function of the parameters of the model, that is, vector and Higgs masses:

$$\sigma = \sigma_j(m_H/m_V). \quad (54)$$

In particular, the Casimir scaling holds in the London limit,

$$\frac{\sigma_{j_1}}{\sigma_{j_2}} = \frac{j_1(j_1+1)}{j_2(j_2+1)}, \quad \text{if} \quad m_H \gg m_V. \quad (55)$$

Thus, the model (52) can incorporate the Casimir scaling.

However, the description of the profile of the confining string is the best if $m_H \approx m_V$ [32]. Thus, there is a mismatch with (55). Since the functions of m_H/m_V involved in the fits are rather smooth, it is possible to get a compromise description which is valid in both cases, say, with 20% accuracy. This is not bad at all, keeping in mind that we use a classical approximation. Nevertheless, the fact that the Casimir scaling works at a percent level [31] remains a kind of unexplained mystery in the classical approximation. Further analysis of this point might be needed.

4.2. Unconventional Power Corrections

We introduced (52) as an effective Lagrangian. Now, we will describe a rather paradoxical situation that this Lagrangian seems to provide with better phenomenology of the power corrections to the parton approximation than the conventional QCD approach. Namely, there are novel $1/Q^2$ corrections inherent to Higgs models [27, 28] which are absent in the standard considerations.[4)] Moreover, these corrections seem to fit the data at all the distances measured so far, that is, $r \geq 0.1$ fm. An example of this type was found in [27, 33]. Further support came from instanton physics [28]. We have already reviewed the unconventional power corrections in [13] and will be brief here.

In the standard approach, the power corrections are given by matrix elements of various operators constructed on the quark and gluon fields [34]. For our setup, the central point is that for the vacuum state the simplest matrix element had dimension $d = 4$,

$$\langle 0|\alpha_s(G^a_{\mu\nu})^2|0\rangle \sim \Lambda^4_{\text{QCD}}, \quad (56)$$

and, as a result, there are no $\Lambda^2_{\text{QCD}}/Q^2$ corrections [34]. On the other hand, the Higgs model has a mass parameter built it. This mass parameter can thought of as the mass of the vector particle, m_V^2. Let us list a few examples where the two approaches lead to different predictions:

[4)] Literally, the model (52), which introduces averaging over all the embedding of the Abelian dual gluon into $SU(2)$, has never been discussed so far. However, as far as the power corrections are concerned, there is no difference from the cases considered in [27, 28, 33].

(i) First, within the Higgs model, the dual gluon acquires mass and the monopole potential becomes the Yukawa type:

$$V_{m\bar{m}} \longrightarrow \frac{\pi}{g^2 r} e^{-m_V r}. \quad (57)$$

The prediction has already been confirmed by the data [5]. In the conventional approach, one should have to remove at least the term $-m^2 r$ at short distances. The quality of the data might not be so good as to rule this out, but the possibility looks quite bizarre.

(ii) Since the dual and "ordinary" gluons are in fact the same particles (see discussion in Section 2), one would assume that the massiveness of the dual gluon implies the massiveness of the gluon interacting with the color. But this is not true [27]! There is no analyticity in this sense. And the reason is again problems with the Dirac veto, which we already had a chance to discuss in connection with the radiative corrections (see Subsection 2.3). Namely, as far as we discuss only the "dual world," one can forget about the Dirac strings. However, if we introduce color sources $Q\bar{Q}$ into the vacuum with $\langle\phi_m\rangle \neq 0$, we should respect the Dirac veto. The ordinary operator product expansion or perturbative expansion in m_V^2/Q^2 does not respect this veto—as ordinary perturbation theory does not do this either (see Subsection 2.1). The correct treatment demonstrates that there is a linear correction to the quark potential at short distances:

$$\delta V_{Q\bar{Q}} = \sigma_0 r, \quad (58)$$

where σ_0 is calculable function of m_H and m_V. Within the standard approach, there is no such term (for explanations and further references, see [13]). The data do support the presence of the linear term. Amusingly enough, the data refer exclusively to the nonperturbative potential, and there is no need for painful separation of (small) power corrections against the perturbative "background."

(iii) The linear term (58) can be rephrased as the statement that the gluon has a tachyonic mass. Indeed, the ordinary mass would give a negative σ_0, as seen from the expansion of the Yukawa potential at short distances. The introduction of a tachyonic gluon mass in the framework of the QCD sum rules allows one to resolve in an absolutely natural way long-standing problems with the phenomenology based on the QCD sum rules [35].

(iv) The last, but not least, point in our discussion concerns the instanton density [28]. The conventional approach predicts that the deviations from the 't Hooft instanton density due to nontrivial background vacuum fields are of the fourth order in the instanton size ρ:

$$dn(\rho) = dn_{\rm pert}(\rho)\left(1 + \frac{\pi^4\rho^4}{2g^4}\langle 0|g^2(G^a_{\mu\nu})^2|0\rangle + \ldots\right). \quad (59)$$

The data, on the other hand, are beautifully fitted by a quadratic correction, inherent to (52). Note however, that the coefficient in front of the quadratic term has been fitted rather than calculated from (52) so far.

4.3. Conclusions 4

We have proposed in this section a phenomenological Lagrangian (52) which unifies the Higgs mechanism for the Abelian dual gluon with full $SU(2)$ symmetry of the ordinary gluodynamics. The full study of the consequences from this formulation is still awaiting its time to come.

However, it seems promising that the color $SU(2)$ is not broken at any step despite the Higgs mechanism. This allows one to broaden applications of the effective Lagrangian and incorporate, to certain accuracy, the Casimir scaling.

Also, emergence of the mass of the dual gluon in the effective Lagrangian approach provides a natural framework to introduce the novel $1/Q^2$ corrections. Phenomenologically, these corrections bring crucial improvements to the existing phenomenology. Moreover, generically the corrections are of the same type as those associated with ultraviolet renormalons (see, e.g., [36]). However, within the effective Lagrangian approach, these corrections should disappear in the limit of infinite Q^2, which is not true for the ultraviolet renormalons and has not been supported by any data so far.

5. CONCLUSIONS

In this review, we considered various effects related to the monopoles in unbroken non-Abelian gauge theories. In conclusion, let us reiterate the main points (see also conclusions to Sections 1–4):

(i) Fundamental monopoles with the magnetic charge $|Q_m| = 1$ are introduced as external objects via the 't Hooft loop. The corresponding intermonopole potential $V_{m\bar{m}}(r)$ can be evaluated at short distances from first principles. In the Lagrangian approach similar to that of Zwanziger, the dual gluon interacting with pointlike external monopoles appears as an Abelian gauge field (see Section 2 and [9, 11] for details).

(ii) Monopoles with the magnetic charge $|Q_m| = 2$ are pure quantum objects which can be studied so far only numerically. We discussed briefly the newly introduced [10] geometric monopoles which appear to be physical objects.

(iii) The effective Lagrangian which assumes condensation of the monopoles incorporates the Abelian dominance at distances where the effects of confinement are crucial, without breaking $SU(2)$ to $U(1)$. In the London limit, it reproduces the Casimir scaling phenomenon. There are further phenomenological consequences, in particular, the evaluation of the potential

$V_{m\bar{m}}(r)$ at larger distances (see Section 4 and [9, 11] for details).

ACKNOWLEDGMENTS

The review is based to a large extent on talks presented by the authors on various conferences this year. The authors are grateful to the organizers for the invitations. We are grateful to V.A. Shevchenko, Yu.A. Simonov, L. Stodolsky, T. Suzuki, and V.A. Rubakov for valuable discussions. M.N.Ch. and M.I.P. acknowledge the kind hospitality of the staff of the Max-Planck-Institut für Physik (München), where the work was initiated.

The work of M.N.C., F.V.G., and M.I.P. was supported in part by the Russian Foundation for Basic Research (project no. 99-01230a) and INTAS (grant no. 96-370); M.N.Ch. and M.I.P. were supported by Monbushu grant and CRDF award RP1-2103.

REFERENCES

1. P. A. M. Dirac, Proc. R. Soc. London, Ser. A **133**, 60 (1931).
2. S. Coleman, in *The Unity of the Fundamental Interactions, Erice Lectures, 1981*, Ed. by A. Zichichi (Plenum, London, 1983), p. 21.
3. T. Suzuki, Nucl. Phys. B (Proc. Suppl.) **30**, 176 (1993); M. N. Chernodub, F. V. Gubarev, M. I. Polikarpov, and A. I. Veselov, Prog. Theor. Phys. Suppl. **131**, 309 (1998); hep-lat/9802036; H. Suganuma, H. Ichie, A. Tanaka, and K. Amemiya, Prog. Theor. Phys. Suppl. **131**, 559 (1998); A. Di Giacomo, Prog. Theor. Phys. Suppl. **131**, 161 (1998); L. Del Debbio, M. Faber, J. Greensite, and S. Olejnik, in *Zakopane 1997, New Developments in Quantum Field Theory*, p. 47; hep-lat/9708023; R. W. Haymaker, Phys. Rep. **315**, 153 (1999).
4. R. A. Brandt and F. Neri, Nucl. Phys. B **161**, 253 (1979).
5. C. Hoelbling, C. Rebbi, and V. A. Rubakov, hep-lat/0003010; Nucl. Phys. B (Proc. Suppl.) **83-84**, 485 (2000); **73**, 527 (1999).
6. G. 't Hooft, Nucl. Phys. B **138**, 1 (1978).
7. Y. Nambu, Phys. Rev. D **10**, 4262 (1974); G. 't Hooft, in *High Energy Physics* (Editorice Compositori, Bologna, 1975); S. Mandelstam, Phys. Rep. C **23**, 516 (1976).
8. M. Baker, J. S. Ball, and F. Zachariasen, Phys. Rep. **209**, 73 (1991); Phys. Rev. D **51**, 1968 (1995).
9. M. N. Chernodub, F. V. Gubarev, M. I. Polikarpov, and V. I. Zakharov, hep-th/0003138.
10. F. V. Gubarev and V. I. Zakharov, hep-th/0004012.
11. M. N. Chernodub, F. V. Gubarev, M. I. Polikarpov, and V. I. Zakharov, Preprint No. ITEP-TH-28/00, ITÉF (Institute of Theoretical and Experimental Physics, Moscow, 2000).
12. A. M. Polyakov, Phys. Lett. B **59B**, 82 (1975).
13. F. V. Gubarev, M. I. Polikarpov, and V. I. Zakharov, hep-ph/9908292.
14. P. Goddard, J. Nuyts, and D. Olive, Nucl. Phys. B **125**, 1 (1977).
15. E. Lubkin, Ann. Phys. (N.Y.) **23**, 233 (1963).
16. A. A. Abrikosov, Zh. Éksp. Teor. Fiz. **32**, 1442 (1957) [Sov. Phys. JETP **5**, 1174 (1957)]; H. B. Nielsen and P. Olesen, Nucl. Phys. B **61**, 45 (1973).
17. D. Zwanziger, Phys. Rev. D **3**, 343 (1971); R. A. Brandt, F. Neri, and D. Zwanziger, Phys. Rev. D **19**, 1153 (1979).
18. M. Blagojevic and P. Senjanovic, Phys. Rep. **157**, 233 (1988).
19. G. 't Hooft, Nucl. Phys. B **79**, 276 (1974).
20. C. Korthals-Altes and A. Kovner, hep-ph/0004052.
21. G. Calucci and R. Iengo, Nucl. Phys. B **223**, 501 (1983).
22. G. J. Goebel and M. T. Thomas, Phys. Rev. D **30**, 823 (1984).
23. J. Schwinger, Phys. Rev. **144**, 1087 (1966); **151**, 1048 (1966); **151**, 1055 (1966); **173**, 1536 (1968); W. Deans, Nucl. Phys. B **197**, 307 (1982); C. Panagiotakopoulos, J. Phys. A **16**, 133 (1983).
24. Y. Kazama, C. N. Yang, and A. S. Goldhaber, Phys. Rev. D **15**, 2287 (1977).
25. V. A. Rubakov, Pis'ma Zh. Éksp. Teor. Fiz. **33**, 658 (1981) [JETP Lett. **33**, 644 (1981)]; C. G. Callan, Phys. Rev. D **26**, 2058 (1982).
26. F. V. Gubarev, L. Stodolsky, and V. I. Zakharov, unpublished.
27. F. V. Gubarev, M. I. Polikarpov, and V. I. Zakharov, Mod. Phys. Lett. A **14**, 2039 (1999); Phys. Lett. B **438**, 147 (1998).
28. E. V. Shuryak, hep-ph/9911244.
29. S. J. Huber, M. Reuter, and M. G. Schmidt, Phys. Lett. B **462**, 158 (1999).
30. A. Di Giacomo, Nucl. Phys. B (Proc. Suppl.) **64**, 322 (1998).
31. G. S. Bali, Nucl. Phys. B (Proc. Suppl.) **83-84**, 422 (2000); hep-lat/9908021.
32. F. V. Gubarev, E. M. Ilgenfritz, M. I. Polikarpov, and T. Suzuki, Phys. Lett. B **468**, 134 (1999).
33. K. G. Chetyrkin, S. Narison, and V. I. Zakharov, Nucl. Phys. B **550**, 353 (1999).
34. M. A. Shifman, A. I. Vainshtein, and V. I. Zakharov, Nucl. Phys. B **147**, 385 (1979); **147**, 448 (1979).
35. V. A. Novikov, M. A. Shifman, A. I. Vainshtein, and V. I. Zakharov, Nucl. Phys. B **191**, 301 (1981).
36. R. Akhoury and V. I. Zakharov, Nucl. Phys. B **465**, 295 (1996); Phys. Lett. B **357**, 646 (1995); hep-ph/9705318.

Physics of Atomic Nuclei, Vol. 64, No. 3, 2001, pp. 574–578. From Yadernaya Fizika, Vol. 64, No. 3, 2001, pp. 628–632.

90th ANNIVERSARY OF A.B. MIGDAL'S BIRTHDAY
ELEMENTARY PARTICLES AND FIELDS

QCD at Finite Density and Color Superconductivity

E. V. Shuryak

Department of Physics and Astronomy, SUNY Stony Brook, USA

Received July 27, 2000

Abstract—The paper contains a brief review of recent applications of many-body theory to quark matter. We discuss the progress in theory of dense quark matter during the last two years, especially color superconductivity. We emphasize that there are two basic dynamical reasons for it: short-range forces induced by instantons and long-range ones mediated by exchanges of magnetic gluons. For quark matter which is supposed to be found in neutron stars, both lead to superconducting gaps on the order of 100 MeV. The most surprising facts are the rather impressive richness of different phases and their robustness in respect to variation of the fundamental interaction. © *2001 MAIK "Nauka/Interperiodica".*

1. BRIEF HISTORY

Methods of quantum field theory had been generalized to finite temperature and density by the late 1950s, and A.B. Migdal was among the pioneers who enthusiastically applied it to many problems, especially to finite nuclei. The nucleon pairing, leading to superfluidity and superconductivity of nuclear matter, was one of his favorite subjects. The pion condensation (basically what we would call today a chiral crystal) was another one. Very similar ideas to be discussed below are under intense studies today, but for the next level of matter—quark matter of high density.

So let me start by attempting to answer a question (which I would probably get from A.B. right away): Why did it take so long, about a quarter of a century counting from the early days of QCD in the 1970s, to figure out all these phases? Aren't they more or less a variation of what was worked out in the 1950s and 1960s for condensed matter and nuclei?

Yes, they are, but the internal logic of science is not often easy to explain, and the path toward the results is never a straight line. In the 1970s, the first QCD-based calculations showed that, in spite of "antiscreening" (asymptotic freedom) in vacuum, for finite T and/or density we have Debye screening and other plasma-type phenomena as in QED, so this phase of matter was called quark–gluon plasma (QGP) [1]. Its studies are actively going on in nuclear high-energy collisions, with RHIC in Brookhaven taking its first data right now. However, collisions always produce entropy, thus relatively high temperatures: the part of the phase diagram with cold dense quark matter was not really studied much.

Early ideas about Color Superconductivity (CSC) [2] were based on simple observation: unlike electrons, quarks of different colors are attracted to each other even by Coulomb forces. Due to Cooper instability, any small attraction is enough: however, the superconducting gap was estimated to be only $\Delta \sim 1$ MeV, and applicability of perturbative QCD was in doubt. In addition to that, gluoelectric exchanges in matter are Debye screened, and gluomagnetic ones were much more difficult to account for. Not much work was done on it in the 1980s.

At that time, the interest of many people shifted from applications of perturbative methods to nonperturbative effects. The 1980s were the prime time of lattice simulations, development of the main ideas about instanton-induced effects, and continuing attempts to understand confinement and chiral symmetry breaking.

My own work was devoted to development of the so-called interacting instanton liquid model (IILM), which eventually included 't Hooft effective interaction to all orders and was able to describe wide range of phenomena, starting from chiral symmetry breaking in vacuum (both $SU(N_f)$ and $U(1)_A$) and ending in quantitative reproduction of the correlation and wave function of all major hadronic channels, known from data and lattice. The finite T-phase transition into QGP has also been understood in this model, with good agreement with related lattice works. This work has been reviewed in [3], and I will not describe it here.

The road to dense matter started from the following observation: not only the lowest baryons were shown to be bound states in IILM,[1)] but there was correct splitting between octet (N, …) and decuplet (Δ, …) baryons. It was then traced down to finding [4] that in the instanton liquid model the *ud* scalar diquarks are very deeply bound,[2)] by the amount of 200–300 MeV. It is comparable to the constituent quark mass itself, $M_{\rm eff} \sim 400$ MeV. This fact should not be surprising: its dynamical roots are the same as for basic dynamics of the "supercon-

* This article was submitted by the author in English.

[1)] There is no confinement in this model.

[2)] Discussion of phenomenological manifestations of scalar diquarks can be found in [5].

1063-7788/01/6403-0574$21.00 © 2001 MAIK "Nauka/Interperiodica"

ductivity" of the QCD vacuum, the chiral (χ) symmetry breaking. The forces are microscopically described by the same 't Hooft Lagrangian—simply Fierz-transformed from the $\bar{q}q$ to the qq channel. These spin-isospin-zero diquarks are therefore related to pions, which are even deeper bound, by $-2M_{\rm eff}$ as compared to "normal" s-wave mesons like ρ and ω.

Further refinement of the argument for deeply bound diquarks comes from bicolor ($N_c = 2$) theory: in it the scalar diquark is degenerate with pions. By continuity from $N_c = 2$ to 3, a trace of it should exist in real QCD.[3)]

Explicit calculations with instanton-induced forces for $N_f = 2$, $N_c = 3$ QCD have been made in two simultaneous[4)] papers [6, 7]. Indeed, very robust Cooper pairs and gaps $\Delta \sim 100$ MeV were found. From then on, the field has been booming.

This phase (called CSC2) has the same symmetries as discussed before [2]: the χ symmetry is restored, but color group is broken by the diquark condensate, acting like Higgs VEV of the Standard Model. A new variety of color superconductor, CSC3 with color–flavor locking exists for three or more light flavors $N_f = 3$ (see Section 5). At asymptotically high densities, the perturbation theory must become right (see Section 6). Finally, we will discuss some more recent findings.

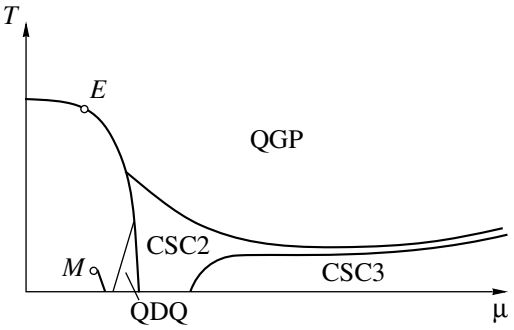

Fig. 1. QCD phase diagram at the μ–T plane, baryonic chemical potential–temperature.

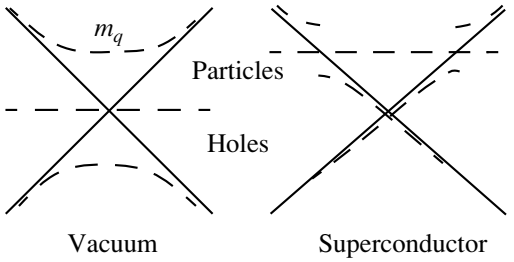

Fig. 2. Pairing in vacuum (left) and in dense quark matter (right).

2. PHYSICS OVERVIEW

The QCD phase diagram, as we understand it today, is shown in Fig. 1. At small T and μ, there is ordinary hadronic matter with broken chiral symmetry. The point M (from "multifragmentation") is the endpoint of the nuclear liquid–gas phase transition. At the (hypothetical) critical point E, the first-order line either continues as second-order (for m_u, $m_d = 0$) or disappears (for finite masses): according to recent a proposal [8], it can be found in real heavy-ion collisions. QDQ (quark–diquark) phase is hypothetical [9]: I will not discuss it here. The main point is the relative locations of the two superconducting phases, CSC2 and CSC3. At $T = 0$ going to large μ, the χ symmetry seems to be first recovered in CSC2 and then broken again in CSC3.

Let me then explain a few major physics points. Why is there a transition from particle–hole to particle–particle pairing? Figure 2 (dispersion curves $\omega(k)$ for quarks in vacuum and superconductor) explains it: it is better to have a gap at the surface of the Fermi sphere rather than the Dirac sea.

Why instantons? The reasons are the following: (i) They are the strongest nonperturbative effect known. (ii) Unlike one-gluon exchange (OGE), they do explain quantitatively χ-symmetry breaking in a vacuum. (iii) The anomaly cannot be eliminated by finite density, so tunneling leads to level crossing at the surface of the Fermi sphere as well.

Note the following amusing triality: There are three attractive channels which compete: (i) the instanton-induced attraction in the $\bar{q}q$ channel leading to χ-symmetry breaking; (ii) the instanton-induced attraction in qq which leads to color superconductivity; (iii) the light-quark-induced attraction of $\bar{I}I$, which leads to pairing of instantons into "molecules" in the QGP phase without any condensates.

How are the calculations actually done? Analytically, mostly in the mean field approximation, similar to the original BCS theory in Gorkov formulation. Total thermodynamical potential consists of "kinetic energy" of the quark Fermi gas, including mass operators of two types (shown in Fig. 3, upper part). The "potential energy" in such an approximation is the interaction Lagrangian convoluted with all possible condensates. For example, the instanton-induced one with $N_f = 3$ leads to two types of diagrams shown in Fig. 3 (lower part), with $\langle\bar{q}q\rangle^3$ and $\langle qq\rangle^2\langle\bar{q}q\rangle$. Then, one minimizes the potential over all condensates and gets gap equations: the algebra may be involved because masses/condensates are color–flavor matrices.

3. TWO COLORS: A VERY SPECIAL THEORY

One reason it is special is well known to the lattice community: its fermionic determinant is real even for

[3)]Instanton-induced interaction strength in the diquark channel is $1/(N_c - 1)$ of that for $\bar{q}\gamma_5 q$ one. It is the same at $N_c = 2$, zero for large N_c, and is exactly in between for $N_c = 3$.

[4)]Submitted to hep-ph on the same day.

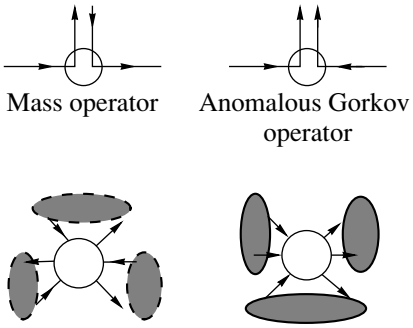

Fig. 3. Green's functions with ordinary and anomalous mass insertions (upper part) and the "potential energy" (lower part). The circle in the center is an instanton, with six quark lines because it is written for the case of three massless quark flavors.

nonzero μ, which makes simulations possible. Early works by Karsch, Dagotto, *et al.* (of the mid-1980s!) showed very strong diquark condensate, but these papers make sense only now.

The major interest to this theory is related to the so-called Pauli–Gursey symmetry, due to which diquarks are degenerate with mesons. The χ-symmetry breaking is $SU(2N_f) \longrightarrow Sp(2N_f)$; for $N_f = 2$, the coset $K = SU(4)/Sp(4) = SO(6)/SO(5) = S^5$. Those five massless modes are pions plus scalar diquark S and its antiparticle $\bar{S}$. The corresponding sigma model was worked out in [6]: for further development see [10]. As argued in [6], in this theory the critical value of transition to CSC is simply $\mu = m_\pi/2$, the diquark condensate is just a rotated $\langle \bar{q}q \rangle$ one, and the gap is the constituent quark mass. Recent lattice works [11] and instanton liquid simulation [12] display it in great detail, building confidence for other cases.

4. TWO-FLAVOR QCD

In Fig. 4, the phase diagram [13] is a rare example of the calculated T–μ one: the first-order line is dashed, and the second-order ones are solid lines. Most studies of this theory [6, 7, 14] are at $T = 0$. In all these works, one more possible phase (intermediate between vacuum and CSC2), Fermi gas of constituent quarks, with both $M, \Delta \neq 0$, was unstable. However, in the last more refined calculation [9], it obtains a small window, as shown by the long-dashed line in Fig. 5. Its features are amusingly close to those of nuclear matter: but it isn't, of course: to get nucleons one should go outside the mean field. The first attempt to do so in [9] was for another cluster—the $\bar{I}I$ molecules. At $T = 0$ it is, however, only a 10% correction to previous results, but is dominant as T grows.

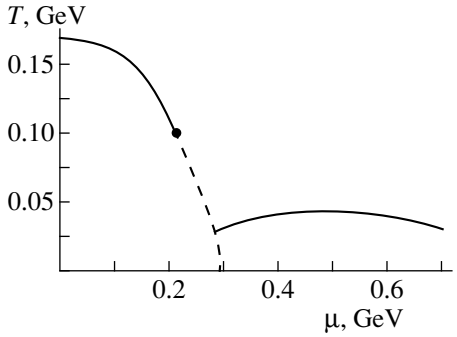

Fig. 4. The phase diagram at μ–T plane.

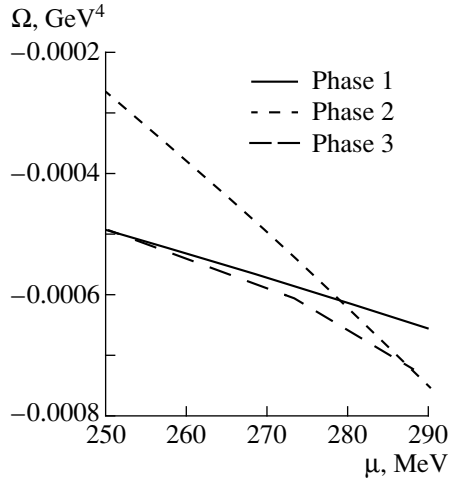

Fig. 5. The thermodynamical potential versus chemical potential: the phase 2 appears in the window between phase 1 (chirally asymmetric vacuum) and phase 3 (chirally symmetric color superconductor) and has both condensates. It is as close as we can get to nuclear matter in the mean-field approximation.

5. THE $N_f = 3$ QCD: COLOR–FLAVOR LOCKING

The color–flavor locking phenomenon [15] means that diquark condensate has the structure $\langle q_i^a C q_j^b \rangle = \bar{\Delta}_1 \delta_{ia}\delta_{bj} + \bar{\Delta}_2 \delta_{ib}\delta_{ja}$, where i, j are color and a, b are flavor indices. It is very symmetric, reducing $SU(3)_c SU(3)_f \longrightarrow SU(3)_{\text{diagonal}}$. It was verified in [15] for the OGE interaction, and for the instanton-induced one in [9]: probably it is always true for that theory. Gaps δ_i and masses σ_i, following from instanton-based calculation [9], are shown as a function of μ in Fig. 6.

Two-plus-strange flavor QCD ($m_s \neq 0$) was studied in several papers [9, 16]. Just kinematically, *us* and *ds* Cooper pairs with zero momentum are difficult to make: for $\mu_{u,d} = \mu_s$, the momenta $p^F_{u,d} \neq p^F_s$. Instantons also generate the dynamical operator $m_s(\bar{u}\bar{d})(ud)$. The resulting behavior is as shown in Fig. 1.

Finally, if this is the phase of color superconductor, it allows for kaon (K^-) condensation [17], even for a

tiny (few MeV) electron chemical potential. It is very similar to Migdal's pion condensate, except that, in the perverse high-density phase, kaons are lighter than pions (because strange quark can be traded into a condensate).

6. ASYMPTOTICALLY LARGE DENSITIES

Above, we have used forces normalized to what we know in the QCD vacuum: we argued that those are mostly due to instantons. However, at high densities ($\mu > 1$ GeV), instantons are Debye-screened [18]. So are the electric OGE Coulomb forces. As a result, magnetic gluons should be considered as the leading interaction. As shown in [19] and subsequent papers, magnetically bound Cooper pairs are possible: however, in order to describe them properly, one has to take care of time delay effects, using the so-called Eliashberg gap equation rather than the BCS one. The angular integral leads to a second log in the gap equation, leading to an unusual answer: $\Delta \sim \mu \exp(-3\pi^2/\sqrt{2}\, g)$, which implies that the gap grows indefinitely with μ[5)] and pQCD becomes finally justified. However, it is the case for huge densities, with $\mu > 10$ GeV or so.

7. THE HADRON–QUARK CONTINUITY

As it was pointed out in [21], the CSC3 phase not only has the same symmetries as hadronic matter (such as broken χ symmetry), but also has very similar excitations. The original eight gluons become eight massive vector mesons, and 3×3 quarks become $8 + 1$ baryons. The eight massless pions remain massless.[6)] Can these phases be separated by symmetries, and if not, should there be any phase transition between nuclear and quark matter in the theory with three massless quarks ($N_f = 3$)?

Furthermore, the photon and one of the gluons are recombined into a massless γ_{inside} and massive (Meissner effect) new gluon, quite the same thing as a Z boson and new photon in the Weinberg–Salam Standard Model of weak interactions.

Is it then a superconductor, after all? For example, if one puts a piece of CSC3 into an ordinary magnet, the field is decomposed on the boundary into these two components. One, γ_{inside}, goes through without the Meissner effect (see [23] for details), but another is expelled by some currents. So, in principle, it may still levitate in the magnet, etc.

8. CHIRAL CRYSTAL?

There is one more possible structure of quark matter, which is now under study [24]. Superconductivity is not the only way to minimize energy of the Fermi gas: the famous Overhauser effect in solids [25] is another option, leading to a spin density waves. Similarly, one may minimize energy by making the chiral condensate waves. (It differs from Migdal's pion condensate, as it is a σ field which is oscillating here.)

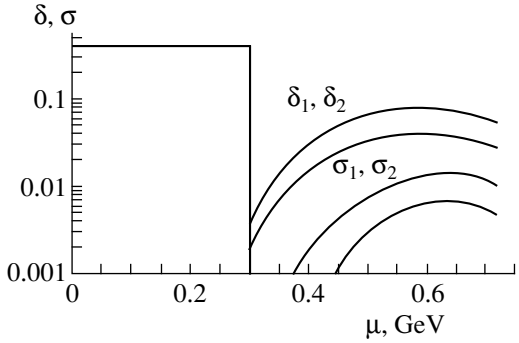

Fig. 6. Calculated gaps [9] due to $\langle qq \rangle$ are called δ and to $\langle \bar{q}q \rangle$ called σ (in GeV). Superconducting and mass gaps take two values each, which follows from diagonalization of the appropriate color–flavor matrices. The gap in the low-density phase, about 400 MeV, is the constituent-quark mass.

In the context of QCD in 3 + 1 dimensions, it has been shown by Deryagin *et al.* [26] that, if we use OGE at high densities, the Overhauser pairing prevails over the BCS instability in the $N_c \longrightarrow \infty$ limit. This is based on the fact that BCS pairing, being a color nonsinglet, is $1/N_c$ suppressed as compared to the (colorless) Overhauser bound states. A condensate of the latter acquires a spatial dependence induced by the finite "wave" vector Q of the pair, which, in the case of the considered scalar–isoscalar channel [26], represents a chiral density wave. More recently, Shuster and Son [27] revisited this issue for finite N_c including Debye screening in the OGE. As a result, the *p–h* instability only develops for a very large number of colors. In Nambu–Jona-Lasinio or instanton-induced interactions, the coupling strength in the scalar–isoscalar *p–h* channel is augmented by a factor of $(N_c - 1)$ over the (most attractive) scalar diquark channel. We find a natural window for it to be at intermediate densities, i.e., large enough for the system to be in the quark phase, but small enough to render nonperturbative forces applicable. This should roughly correspond to chemical potentials in the range of $\mu_q \simeq 0.4$–0.6 GeV.

At finite densities, the formation of a condensate carrying nonzero total momentum Q is associated with nontrivial spatial structures, i.e., crystals, with lattice spacing $a = 2\pi/Q$. In three dimensions, a more complete description thus calls for the inclusion of additional "wave" vectors. In general, the *p–h* pairing gap can be written as

$$\langle \bar{q}q \rangle(\mathbf{r}) = \sum_j \sum_{n=-\infty}^{+\infty} \sigma_{j,n} e^{in\mathbf{Q}_j \cdot \mathbf{r}}, \qquad (1)$$

[5)] Numerical details for all densities can be found in recent work [20].

[6)] Very exotic three-dimensional objects, "superqualitons" [22], the skyrmions made of pions are among the excitations.

where the $\mathbf{Q}_j$ correspond to the (finite) number of fundamental waves, and the summation over $|n| > 1$ accounts for higher harmonics in the Fourier series. The matrix propagator formalism allows for the treatment of multiple waves through a straightforward expansion of the basis states. It was considered up to $n_w = 6$ waves in three orthogonal directions with $Q_x = Q_y = Q_z$ and $n = \pm 1$, characterizing a cubic crystal through three standing waves with the fundamental modes (for simplicity, we will also assume the magnitude of the various Overhauser condensates to be equal, i.e., $\sigma_j \equiv \sigma$). The energy found (from standard but rather tedious calculation) is very close to that of the BCS 2-flavor superconductor with the same forces. Since the accuracy of the mean-field and other approximations (like cubic crystal only) are worse than the difference (few percent), we are not able to tell with confidence which phase wins.

Furthermore, in the reality of neutron stars, the densities (and their Fermi momenta) of *u*, *d*, and *s* quarks are different. They negatively affect the instanton-induced pairing (which is always flavor-asymmetric, like *ud*, *ds*, and *us* pairs) but not so much the chiral crystal phase. Although no calculations for asymmetric matter have been made so far, we think there would be a window for the chiral crystal phase.

9. CONCLUDING REMARKS

Early realization by Migdal and others that nuclear matter is both superfluid and superconducting had profound consequences for nuclear structure, and it also changed forever the physics of neutron stars.

A similar development is now on the way for quark matter: people calculate how the quark core of the star should react to rotation, magnetic fields, etc. Phenomena similar to nuclear backbending have been discussed, with a recent claim [28] that, when an old star speeds up by accretion, it should be "stuck" at a particular frequency, about 250 Hz, because of disappearance of quark matter. Remarkably enough, of about 20 x-ray sources with millisecond beats found in the last two years, all are peaked exactly in this window of frequencies!

Superconductivity of the quark core should dramatically change neutrino cooling and propagation [29], as well as simply specific heat of the core, see [30].

A recent paper by Son and Stephanov [31] has indicated that matter with very high isospin (such as that made of, say, *u* quarks and *d* antiquarks) should have pion condensate, at practically all densities, including infinitely large ones!

I can only repeat in the conclusion: quantum many-body theory is alive and well, and at the quark level there are many exciting things still waiting to be discovered. It is a pity we do not have A.B., with his intuition and enthusiasm, to share these findings with him.

ACKNOWLEDGMENTS

This work was supported in part by the US Department of Energy under grant no. DE-FG02-88ER40388.

REFERENCES

1. E. V. Shuryak, Phys. Rep. **61**, 71 (1980).
2. S. C. Frautschi, in *Proceedings of Workshop on Hadron Matter, Erice, 1978*, p. 18; F. Barrois, Nucl. Phys. B **129**, 390 (1977); D. Bailin and A. Love, Phys. Rep. **107**, 325 (1984).
3. T. Schäfer and E. V. Shuryak, Rev. Mod. Phys. **70**, 323 (1998).
4. T. Schäfer, E. V. Shuryak, and J. Verbaarschot, Nucl. Phys. B **412**, 143 (1994).
5. M. Anselmino *et al.*, Rev. Mod. Phys. **65**, 1199 (1993).
6. R. Rapp, T. Schäfer, E. V. Shuryak, and M. Velkovsky, Phys. Rev. Lett. **81**, 53 (1998).
7. M. Alford, K. Rajagopal, and F. Wilczek, Phys. Lett. B **422**, 247 (1998).
8. M. Stephanov, K. Rajagopal, and E. V. Shuryak, Phys. Rev. Lett. **81**, 4816 (1998); hep-ph/9806219.
9. R. Rapp, T. Schäfer, E. V. Shuryak, and M. Velkovsky, hep-ph/9904353; Ann. Phys. (New York) (in press).
10. J. B. Kogut, M. A. Stephanov, and D. Toublan, hep-ph/9906346.
11. S. Hands, J. B. Kogut, M.-P. Lombardo, and S. E. Morrison, hep-lat/9902034; M.-P. Lombardo, hep-lat/9907025.
12. T. Schäfer, Phys. Rev. D **57**, 3950 (1998).
13. J. Berges and K. Rajagopal, Nucl. Phys. B **538**, 215 (1999); hep-ph/9804233.
14. G. W. Carter and D. I. Diakonov, hep-ph/9812445.
15. M. Alford, K. Rajagopal, and F. Wilczek, hep-ph/9804403.
16. T. Schäfer and F. Wilczek, hep-ph/9903503; M. Alford, J. Berges, and K. Rajagopal, hep-ph/9903502.
17. T. Schäfer, SUNY-NTG-00-14.
18. E. V. Shuryak, Phys. Lett. B **79B**, 135 (1978); Nucl. Phys. B **203**, 140 (1982).
19. D. T. Son, Phys. Rev. D **59**, 094019 (1999); hep-ph/9812287.
20. T. Schäfer and F. Wilczek, hep-ph/9906512.
21. T. Schäfer and F. Wilczek, Phys. Rev. Lett. **82**, 3956 (1999); hep-ph/9811473.
22. Deog Ki Hong, M. Rho, and I. Zahed, hep-ph/9906551.
23. M. Alford, J. Berges, and K. Rajagopal, Nucl. Phys. B **571**, 269 (2000); hep-ph/9910254.
24. R. Rapp, E. Shuryak, and I. Zahed, *Chiral Crystal Phase of High Density QCD* (in progress).
25. A. W. Overhauser, Adv. Phys. **27**, 343 (1978).
26. D. V. Deryagin, D. Y. Grigoriev, and V. A. Rubakov, Int. J. Mod. Phys. A **7**, 659 (1992).
27. E. Shuster and D. T. Son, hep-ph/9905448.
28. N. K. Glendenning and F. Weber, astro-ph/0003426.
29. G. W. Carter and S. Reddy, hep-ph/0005228.
30. D. Page, M. Prakash, J. M. Lattimer, and A. Steiner, hep-ph/0005094.
31. D. T. Son and M. A. Stephanov, hep-ph/0005225.

Physics of Atomic Nuclei, Vol. 64, No. 3, 2001, pp. 579–584. From Yadernaya Fizika, Vol. 64, No. 3, 2001, pp. 633–638.

90th ANNIVERSARY OF A.B. MIGDAL'S BIRTHDAY
ELEMENTARY PARTICLES AND FIELDS

On the Migdal–Watson Approach to FSI Effects in Meson Production in *NN* Collisions*

V. V. Baru[1), 2)], A. M. Gasparian[1), 2)], J. Haidenbauer[1)], A. E. Kudryavtsev[2)], and J. Speth[1)]

Received July 3, 2000

Abstract—The influence of the nucleon–nucleon final-state interaction (FSI) on properties of the meson-production amplitude near threshold is discussed. For nucleon–nucleon interaction, a simple Yamaguchi potential and realistic potential models are considered. It is shown that FSI effects cannot be factorized from the production amplitude. The absolute magnitude of FSI effects depends on the momentum transfer (or on the mass of the produced meson) and hence is not universal. Only in the case of the production of rather heavy mesons like η' or φ FSI do effects become universal. The Jost function approach to FSI effects is critically examined. © *2001 MAIK "Nauka/Interperiodica"*.

1. INTRODUCTION

Back in the 1950s, Watson [1] and Migdal [2] showed that the energy dependence for meson production reactions $NN \longrightarrow NNx$ near threshold is predominantly determined by the strong *NN* interaction in the final state. Their arguments have been used for justifying a rather simple treatment of effects from the final-state interaction (FSI) (see, e.g., [3–6]). It consists in simply multiplying the basic production amplitude with the on-shell *NN T* matrix, i.e.,

$$\mathcal{M} = -NA^{\text{on}}_{\text{prod}}\frac{e^{i\delta}\sin\delta}{ka_{NN}}, \tag{1}$$

where $\delta = \delta(k)$ is the *NN* phase shift, a_{NN} the *NN* scattering length, $A^{\text{on}}_{\text{prod}}$ the on-shell meson-production amplitude, and *N* a normalization factor. This expression suggests that the FSI effect is universal, i.e., does not depend on the specific meson emitted.

Recently, some aspects of FSI effects in the reaction $NN \longrightarrow NNx$ were investigated by Hanhart and Nakayama [7] and Niskanen [8]. In particular, these authors pointed out that the evaluation of the total reaction amplitude by just multiplying the production amplitude by the on-shell *NN T* matrix is not acceptable for obtaining quantitative predictions. In the present paper, we want to study those FSI effects in more detail. Specifically, we want to shed some light on the validity of the multiplication prescription (1). We examine the influence of the *NN* FSI on the absolute value of the reaction amplitude by employing realistic models of the *NN* interaction. Furthermore, we investigate the dependence of the FSI effects on the mass of the produced meson. For that purpose, we will vary the mass of *x* and adopt values corresponding to those of the π, η, and η' mesons.

In general, the total amplitude for the reaction $pp \longrightarrow ppx$ can be determined from the DWBA expression

$$\mathcal{M} = A^{\text{on}}_{\text{prod}} + A^{\text{off}}_{\text{prod}}G_0T_{NN}, \tag{2}$$

where the second term on the right-hand side implies an integration over the off-shell production amplitude and the off-shell *NN T* matrix. Equation (2) corresponds to the sum of the two diagrams shown in Fig. 1. Meson production in *NN* collisions requires a large momentum transfer between the initial and final nucleons, which is typically of the order of $\sqrt{mm_x}$, where *m* is the nucleon mass and m_x the mass of the produced meson. Thus, the range of the production interaction will be much smaller than the characteristic range of the *NN* interaction in the final state. Goldberger and Watson argued that in such a case the meson can be considered to be produced practically from a pointlike region, so that the production amplitude can be factored out of the integral [9], i.e.,

$$\begin{aligned}\mathcal{M} &= A^{\text{on}}_{\text{prod}} + A^{\text{off}}_{\text{prod}}G_0T_{NN} \approx A^{\text{on}}_{\text{prod}}[1 + G_0T_{NN}]\\ &= A^{(\text{on})}_{\text{prod}}\psi^{(-)*}_k(0).\end{aligned} \tag{3}$$

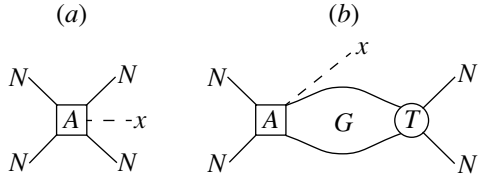

Fig. 1. Diagrammatic representation of the DWBA expression (2). *A* is the elementary meson-production amplitude and *T* is the *NN T* matrix.

* This article was submitted by the authors in English.

1) Institut für Kernphysik, Forschungszentrum Jülich, Germany.
2) Institute of Theoretical and Experimental Physics, Bol'shaya Cheremushkinskaya ul. 25, Moscow, 117259 Russia.

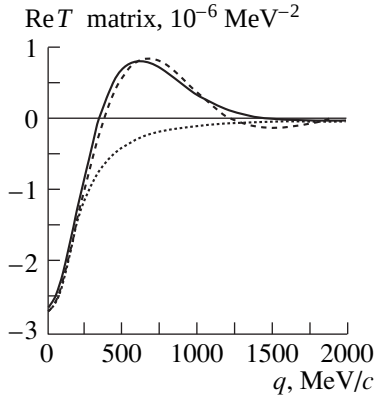

Fig. 2. Real part of the NN $^1S_0$ T matrix as a function of the off-shell momentum q calculated at the fixed on-shell momentum k = 10 MeV/c. The solid, dashed, and dotted curves are the results for the Paris [15], Bonn [16], and Yamaguchi potentials, respectively.

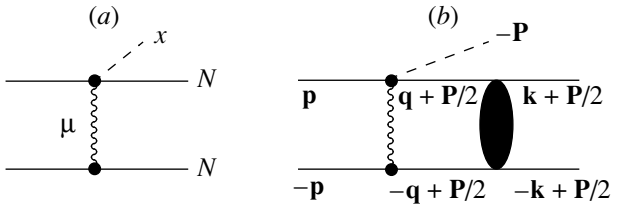

Fig. 3. Contributions to the total reaction amplitude $\mathcal{M}$: (*a*) Born term A; (*b*) loop diagram including the final-state interaction.

Here $\psi_k^{(-)}(\mathbf{r})$ is the (suitably normalized) NN wave function in the continuum [9], where $\psi_k^{(-)}(0)$ is related to the Jost function $\Im$ via $\psi_k^{(-)*}(0) = \Im^{-1}(-k)$ [9].

Clearly, also in this case, one arrives at results where the FSI effects are reduced to a mere multiplicative factor $|\psi_k^{(-)*}(0)|^2$ (commonly referred to as an enhancement factor).

The prescription described by (3) has been utilized by several authors [10–14] in their studies of meson production. Its validity has been examined by an explicit calculation of the loop diagram in [10] employing an OBE model for the production amplitude. However, one has to keep in mind that this investigation is based on a simple separable Yamaguchi potential for the NN FSI. It is well known that the off-shell behavior of the T matrix for the Yamaguchi potential is rather different from the one resulting from realistic models of the NN force. This can be seen from Fig. 2, where we compare the off-shell properties of the Paris [15] and (one version of) the Bonn [16] NN models with the one of the Yamaguchi potential for the $^1S_0$ partial wave. The most striking difference is definitely the zero crossing by the T matrix that occurs for realistic potential models at off-shell momenta $q \approx 350$ MeV/c, whereas the one of the Yamaguchi potential never changes sign. As we will show below, this specific feature has a strong and important influence on the result for the FSI effects.

The paper is structured in the following way. In Section 2, we present our formalism. We specify the meson-production amplitude that we use in the present investigation and we give the explicit expression for the loop diagram of Fig. 1*b*. In Section 3, we present and discuss our results. Specifically, we show calculations for the effects of the FSI considering different NN models and the production of mesons with different masses. Furthermore, we take a look at the energy dependence of the FSI effects and examine the validity of some commonly used approximations. The paper ends with a short summary.

2. LOOP-DIAGRAM CALCULUS

For the calculation of the loop diagram of Fig. 1*b* with off-shell amplitudes of realistic NN interactions, we need to specify a model for the production amplitude. We assume that it has the form

$$A_{\text{prod}} = \frac{gA_{\mu N\to xN}}{t-m_\mu^2}, \tag{4}$$

which corresponds to the exchange of a scalar meson μ of mass m_μ in the t channel followed by the production of a meson x in a rescattering process. The corresponding diagram is shown in Fig. 3*a*. The coupling g at the $NN\mu$ vertex and the amplitude $A_{\mu N\to xN}$ are assumed to be constants. For m_μ, we take the value of the pion mass, i.e., m_μ = 135 MeV. Furthermore, for simplicity reasons, we use nonrelativistic kinematics for the intermediate nucleons. The total reaction amplitude for this production model is then given by the sum of the two diagrams of Fig. 3, i.e.,

$$\mathcal{M} = -\frac{mg}{E}\frac{A_{\mu N\to xN}}{\left(\mathbf{k}-\mathbf{P}/2+\frac{m}{E}\mathbf{p}\right)^2+\lambda^2}\Psi(\mathbf{k}), \tag{5}$$

where

$$E = \sqrt{m^2+p^2}, \quad \lambda^2 = \frac{m}{E}m_\mu^2+\frac{m^2}{E^2}\tau^2,$$

with $\tau = E - m$. $\Psi(\mathbf{k})$ is given by the expression

$$\Psi(\mathbf{k}) = 1-\frac{m\pi\left[\left(\mathbf{k}-\mathbf{P}/2+\frac{m}{E}\mathbf{p}\right)^2+\lambda^2\right]}{r} \times\int_0^\infty \frac{dqqT_{NN}(q,k)}{q^2-k^2-i0}\ln\left[\frac{(q+r)^2+\lambda^2}{(q-r)^2+\lambda^2}\right], \tag{6}$$

where

$$r = \left|\frac{m}{E}\mathbf{p} - \mathbf{P}/2\right|.$$

$T_{NN}(q, k)$ is the NN half-off-shell T matrix in the $^1S_0$ partial wave. The function $F_{NN}(k) = |\Psi(\mathbf{k})|^2$ can be considered as a generalization of the FSI enhancement factor $|\psi_k^{(-)*}(0)|^2$ that follows from the factorization assumption (3). We would like to emphasize, however, that [contrary to $\psi_k^{(-)*}(0)$ in (3)] $\Psi(\mathbf{k})$ does also contain information on the production mechanism and not only on the NN FSI.

In the actual calculations, we want to include the Coulomb interaction between the outgoing protons. Therefore, we have to replace the NN half-off-shell T matrix in (6) by the quantity $T^{\rm cs}$, i.e., the Coulomb-distorted hadronic T matrix. This quantity is obtained by the prescription introduced in [17], namely via

$$T^{\rm cs}(q, k) = \frac{C(\gamma_q)}{C(\gamma_k)}\frac{T_{NN}(q, k)}{T_{NN}(k, k)}T^{\rm cs}(k, k), \qquad (7)$$

where k and q denote the on-shell and off-shell momentum, respectively. $T_{NN}(k, k)$ and $T_{NN}(q, k)$ are the on-shell and half-off-shell T matrices for the strong interaction alone. The Coulomb penetration factor C is given by

$$C^2(\gamma_q) = \frac{2\pi\gamma_k}{e^{2\pi\gamma_k} - 1}; \quad \gamma_k = \frac{m}{2}\frac{1}{\alpha k}, \qquad (8)$$

with α the fine-structure constant. Furthermore, the first term on the left-hand side of (6) (the "1") has to be replaced by $C(\gamma_k)$.

3. DISCUSSION

First, we want to discuss the dependence of $\Psi(k)$ on the mass of the produced meson. For that purpose, we start out from a somewhat simpler expression for Ψ which follows from (6) for the kinematics at the production threshold:

$$\Psi(k) = C(\gamma_k) - \frac{m\pi[mm_x + m_\mu^2]}{\sqrt{mm_x + m_x^2/4}}\int_0^\infty \frac{dqqT^{\rm cs}(q, k)}{q^2 - k^2 - i0} \times \ln\left[\frac{(q + \tilde{r})^2 + \tilde{\lambda}^2}{(q - \tilde{r})^2 + \tilde{\lambda}^2}\right], \qquad (9)$$

where

$$\tilde{r} = \frac{m}{m + m_x/2}\sqrt{mm_x + m_x^2/4},$$

$$\tilde{\lambda}^2 = \frac{m^2}{(m + m_x/2)^2}\frac{m_x^2}{4} + \frac{m}{m + m_x/2}m_\mu^2.$$

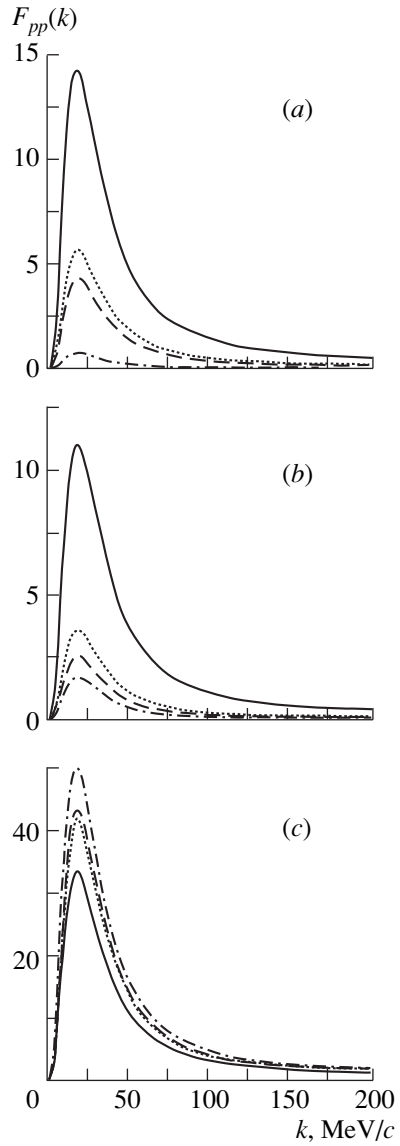

Fig. 4. The FSI factor $F_{pp} = |\Psi(k)|^2$ [cf. (9)] for the Paris (*a*), Bonn (*b*), and Yamaguchi (*c*) potentials and the production of the π (solid curve), η (dotted curve), and η' (dashed curve) mesons. The dash-dotted curves are the results based on the factorization assumption (3), i.e., $F_{pp}(k) = |\Im(-k)|^{-2}$. Note that different scales are used for each NN model!

For the production of a light meson, $m_x \ll m$, we get $\tilde{r} \approx \sqrt{mm_x}$, $\tilde{\lambda}^2 = m_\mu^2 + m_x^2/4$, so that there is a dependence of the integral on the right-hand side of (9) on m_x. In the case of a heavy meson, $m_x \gg m$, it follows that $\tilde{r} \approx m$, $\tilde{\lambda}^2 \approx m^2$ and, consequently, $\Psi(k)$ does not depend on the mass of the emitted meson x. In other words, we expect that FSI effects become universal for the production of heavy mesons via an OBE-type production mechanism leading to the amplitude (4).

Let us now come to the results for the FSI factor $F_{NN} = |\Psi(k)|^2$. In Fig. 4, we show calculations for differ-

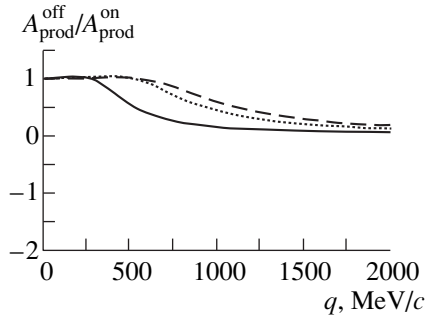

Fig. 5. Ratio $A^{off}_{prod}/A^{on}_{prod}$ of the production amplitude as a function of the off-shell momentum q calculated at the fixed on-shell momentum $k = 0$. The solid, dotted, and dashed curves correspond to the production of the π, η, and η' mesons, respectively.

ent *NN* models and for some typical masses of the emitted meson *x*. It can be seen from those figures that the magnitudes of F_{NN} resulting for the Bonn and the Paris potentials are fairly similar, whereas the one for the separable Yamaguchi potential is quite different. (Note that different scales are used for each *NN* model!) This result can be understood qualitatively from the features of the corresponding off-shell *T* matrices shown in Fig. 2. The *T* matrices for the Bonn and Paris potentials are very similar. In particular, for both models, there is a change of sign at an off-shell momentum of $q \approx 350$ MeV/*c*. Because of this change of sign, cancellations occur in the integral for $\Psi(k)$ [cf. (6)]. The off-shell *T* matrix of the Yamaguchi potential does not change sign. Therefore, no such cancellations take place in the integration, and, as a consequence, the FSI factor F_{NN} is significantly larger than the ones for the realistic interaction models (cf. Fig. 4).

There is also a striking difference in the results with regard to the mass of the emitted meson. For the Paris and Bonn potentials, the FSI factor decreases with increasing mass of the produced meson. However, for the Yamaguchi potential, we observe the opposite effect. Here, $F_{NN}(k)$ becomes larger with the mass of the produced meson increased. These features can again be understood in terms of the *NN* off-shell properties. However, now the off-shell behavior of the production amplitude, which enters into the integral (6) as well, also becomes relevant. With increasing mass of the produced meson, the required momentum transfer *t* increases as well and, accordingly, the production mechanism becomes more and more short-ranged. As a consequence, the production amplitude remains constant over a larger (off-shell) momentum range, as can be seen in Fig. 5. This feature enhances the cancellation effects for the Bonn and Paris *NN T* matrices discussed above and therefore leads to a reduction of F_{NN} for larger meson masses. In case of the Yamaguchi potential, no such cancellations can occur, and therefore the FSI factor turns out to be almost independent of the mass of the produced meson.

Nevertheless, we see that also for realistic *NN* potentials the FSI factors become more and more similar with increasing mass of the produced meson, i.e., for high momentum transfers. This is expected. It simply reflects the universality of FSI effects for the production of heavy mesons as discussed above. We would like to emphasize that the universality of FSI effects at large *t* should set in not only for the particular production amplitude used in the present investigation [cf. (4)], but is expected to occur in general. Actually, we examined the behavior of F_{NN} for the OBE-type production amplitude (4) with inclusion of form factors of monopole and dipole type at the *NN*μ vertex. Corresponding numerical calculations clearly indicate that the qualitative behavior of the FSI factors remains basically unchanged.

However, it is important to realize that the actual values for the FSI factors do, of course, depend on the particular production amplitude. Thus, the results presented in Fig. 4 are by no means absolute predictions that can be taken from this paper and used blindly for FSI corrections in any other study of meson production. Our results demonstrate rather that if one wants to obtain reliable quantitative predictions, FSI effects have to be calculated always explicitly by utilizing the respective production amplitudes and a proper *NN* off-shell *T* matrix. (In this context, we would also like to draw attention to the requirement of a consistent treatment of both the *NN* scattering and production amplitudes as discussed in the Appendix of [18].) Specifically, this means that the apparent universality of the FSI effects for large meson masses does not imply that one can use the prescription applied in the studies [10, 12–14], i.e., take the production amplitude out of the integral in (9). Even though the factor $\Psi(k)$ becomes independent of the mass of the produced meson, its actual magnitude is still determined by the off-shell properties of the *NN T* matrix as well as by the production amplitude. In order to demonstrate this, we also show results based on the factorization assumption, (3) (dash-dotted curves in Fig. 4). In this case, the FSI factor is simply given by the enhancement factor $F_{NN}(k) = |\mathfrak{J}(-k)|^{-2}$. It is really startling how strongly the results for the Yamaguchi potential and for realistic *NN*-interaction models differ. For the former potential, the enhancement factor based on the Jost function is larger than the FSI factor obtained from (2), whereas for the latter models it turns out to be much smaller than the DWBA values. Clearly, these results suggest that it is rather questionable to use the Jost function of some arbitrary potentials for the evaluation of FSI effects in meson-production reactions [10, 12–14].

Finally, let us make a remark on the differences between the results for realistic *NN* models. Obviously, these are small (about 20%) for the pion-production case. But for the η' meson, the Paris result is nearly

twice as large as that for the Bonn model. This is not too surprising because for the production of heavier mesons a larger momentum transfer is required and therefore the features of the *NN* interaction at shorter distances (or larger off-shell momenta) become more and more important in the actual calculations. As we can see in Fig. 2, there are fairly large differences in the off-shell properties of these two models for large off-shell momenta. Note that such a sensitivity to the off-shell behavior of realistic *NN* models at large off-shell momenta has been also seen, e.g., in proton–proton bremsstrahlung producing hard photons [19].

By all the variations we see in the magnitudes of the FSI factors presented in Fig. 4, we would like to point out that their energy dependence is basically the same for all the different potentials and for the different meson masses. If we normalize them to the same value for small k (e.g., at the peak of F_{NN} at $k \approx 20$ MeV/c), all curves would lie essentially on top of each other. This means that the energy dependence of the FSI factors is really primarily determined by the on-shell *NN T* matrix. Consequently, the on-shell prescription (1) is indeed a fairly good approximation, at least for energies near the production threshold. In order to demonstrate this, let us compare one of the curves based on the Paris potential with the result corresponding to (1) (normalized to the Paris curve at $k \approx 20$ MeV/c) (cf. Fig. 6). Nonetheless, we do observe an increasing difference between these two curves for $k \geq 50$ MeV/c, which corresponds to excess (cms) energies $Q \geq 3$ MeV. For $k =$ 100 MeV/c ($Q \approx 10$ MeV), the curves differ already by a factor of around 2. It is interesting to see that the Jost function approach (3) deviates even more strongly from the correct results than the on-shell approximation in the energy range $k \leq 100$ MeV/c.

Let us now investigate the origin of those discrepancies in more detail. For that purpose, we rewrite the amplitude $\mathcal{M}$ (2) in the form given in [7],

$$\mathcal{M} = -A_{\text{prod}}^{\text{on}} \frac{e^{i\delta}\sin\delta}{k a_{pp}} [P(k) - a_{pp} k \cot\delta]$$
$$= -A_{\text{prod}}^{\text{on}} \frac{e^{i\delta}\sin\delta}{k a_{pp}} [P(k) + 1 - 1/2 a_{pp} r_0 k^2 + O(k^4) + \ldots]. \quad (10)$$

Here, $P(k)$ is proportional to the principal value of the loop integral (cf. Fig. 3*b*) and contains information on the off-shell behavior of both A_{prod} and T_{NN}. [Note that we have neglected corrections coming from the Coulomb interaction in (10) for simplicity reasons. Those terms do not play a role anymore at the energies where the discrepancies discussed above occur.]

Evidently, corrections to the simple on-shell prescription (1) come from the energy dependence of the function $P(k)$ as well as from the $\cot\delta$ term. Actual calculations with the *NN* potentials utilized in the present study revealed that the value of $P(k)$ at $k = 0$ is positive and about 3 to 5 units larger, which makes it the dominant piece of the terms in the brackets of (10). Furthermore, $P(k)$ slowly decreases with k. The k^2 term slowly increases with k (note that a_{pp} is negative for the $^1S_0$ partial wave!), so that there is a compensation in the energy dependence of the terms in the brackets of (10). This circumstance is certainly partly responsible for the fact that (1) works relatively well.

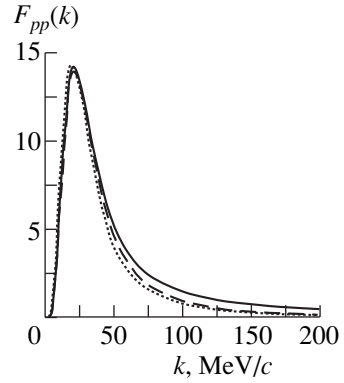

Fig. 6. The FSI factor $F_{pp} = |\Psi(k)|^2$ for the Paris *NN* potential and for pion production (solid curve) in comparison to results based on the approximations (1) (dashed curve) and (3) (dotted curve). The latter two curves are normalized to the one of the Paris potential at the peak ($k \approx 20$ MeV/c).

As already mentioned above, the value at $P(k = 0)$ is positive and fairly large (cf. also the comments in [7]). Note that, in order to get (1) with the normalization N set to one, as chosen in [5, 6], we have to assume that $P(k) \equiv 0$ and omit all the terms proportional to k^2, k^4, etc., in the square brackets on the right-hand side of (10). Therefore, this particular normalization can only be obtained under very specific conditions (cf. the discussion in the Appendix of [18]).

4. SUMMARY

In the present paper, we have studied some aspects of effects from the final-state interaction in the meson-production reaction $NN \longrightarrow NNx$ near the threshold. Specifically, we have demonstrated that the nucleon–nucleon FSI cannot be factorized from the production amplitude if one wants to obtain reliable quantitative predictions. This conclusion confirms the arguments given in paper [7]. Furthermore, we have demonstrated that the absolute value of the FSI factor depends on the momentum transfer, i.e., on the mass of the produced meson. It is not universal! Only for large momentum transfers, i.e., for the production of heavy mesons, does the FSI factor become independent of the mass of the produced meson. Finally, we have shown that the use of the Jost function of some arbitrary potentials for the evaluation of FSI effects is rather questionable and may lead to a considerable overestimation of those FSI effects.

ACKNOWLEDGMENTS

The authors are grateful to C. Hanhart and K. Nakayama for stimulating discussions and careful reading of the manuscript. A.E.K. acknowledges the hospitality of the Institute für Kernphysik, Forschungszentrum Jülich.

The work of A.E.K. and V.V.B. was supported in part by the Russian Foundation for Basic Research (project no. 98-02-17618).

REFERENCES

1. K. M. Watson, Phys. Rev. **88**, 1163 (1952).
2. A. B. Migdal, Zh. Éksp. Teor. Fiz. **28**, 3 (1955) [Sov. Phys. JETP **1**, 2 (1955)].
3. A. Moalem, E. Gedalin, L. Razdolskaja, and Z. Shorer, Nucl. Phys. A **589**, 649 (1995).
4. E. Gedalin, A. Moalem, and L. Razdolskaja, Nucl. Phys. A **634**, 368 (1998).
5. V. Bernard, N. Kaiser, and Ulf-G. Meißner, Eur. Phys. J. A **4**, 259 (1999).
6. N. Kaiser, Phys. Rev. C **60**, 057001 (1999).
7. C. Hanhart and K. Nakayama, Phys. Lett. B **454**, 176 (1999).
8. J. A. Niskanen, Phys. Lett. B **456**, 107 (1999).
9. M. L. Goldberger and K. M. Watson, *Collision Theory* (Wiley, New York, 1964; Mir, Moscow, 1967), Chap. 9.3.
10. B. L. Druzhinin, A. E. Kudryavtsev, and V. E. Tarasov, Z. Phys. A **359**, 205 (1997).
11. G. Fäldt and C. Wilkin, Phys. Lett. B **382**, 209 (1996).
12. R. Shyam and U. Mosel, Phys. Lett. B **426**, 1 (1998).
13. A. Sibirtsev and W. Cassing, nucl-th/9904046; Eur. Phys. J. A **2**, 333 (1998).
14. A. I. Titov, B. Kämpfer, and B. L. Reznik, Eur. Phys. J. A **7**, 543 (2000).
15. M. Lacombe *et al.*, Phys. Rev. C **21**, 861 (1980).
16. J. Haidenbauer, K. Holinde, and M. B. Johnson, Phys. Rev. C **48**, 2190 (1993).
17. C. Hanhart, J. Haidenbauer, A. Reuber, *et al.*, Phys. Lett. B **358**, 21 (1995).
18. Cf. the Appendix of C. Hanhart and K. Nakayama, nucl-th/9809059.
19. V. Hermann, K. Nakayama, O. Scholten, and H. Arellano, Nucl. Phys. A **582**, 568 (1995).